ANALYSIS OF FOOTINGS ON UPPER SURFACE OF SLOPES UNDER ECCENTRIC INCLINED LOADS

A THESIS

Submitted in partial fulfilment of the requirements for the award of the degree of

DOCTOR OF PHILOSOPHY

in

CIVIL ENGINEERING

by

TRILOCHAN SAHU

DEPARTMENT OF CIVIL ENGINEERING
INDIAN INSTITUTE OF TECHNOLOGY ROORKEE
ROORKEE - 247 667 (INDIA)

APRIL, 2009

INDIAN INSTITUTE OF TECHNOLOGY ROORKEE

ROORKEE

CANDIDATE'S DECLARATION

I hereby certify that the work which is being presented in the thesis entitled "**ANALYSIS OF FOOTINGS ON UPPER SURFACE OF SLOPES UNDER ECCENTRIC INCLINED LOADS**" in partial fulfilment of the requirements for the award of the Degree of DOCTOR OF PHILOSOPHY and submitted in the Department of Civil Engineering of the Indian Institute of Technology Roorkee, Roorkee, India is an authentic record of my own work carried out during the period from July 2005 to April 2009 under the supervision of Dr. M. N. Viladkar, Professor, Department of Civil Engineering and Prof. Swami Saran, Emeritus Fellow, Department of Earthquake Engineering, Indian Institute of Technology Roorkee, Roorkee, India.

The matter presented in this thesis has not been submitted by me for the award of any other degree of this or any other institute/university.

Trilochan Sahu

(TRILOCHAN SAHU)

This is to certify that the above statement made by the candidate is correct to the best of our knowledge.

Saran

(SWAMI SARAN)
Supervisor
Date:

M.N. Viladkar 08/4/09

(M. N. VILADKAR)
Supervisor
Date:

The Ph.D. viva- voce examination of **Mr. Trilochan Sahu**, Research Scholar has been held on Sept. 30, 2009.

Saran M.N. Viladkar 30/9

Signature of Supervisors

P. Bandhar 30/09/2009

Signature of External Examiner

ABSTRACT

Shallow footings on or upper surface of slopes are often encountered in many engineering structures such as bridge abutments, highway and railway overpass structures, retaining walls, transmission towers, structures placed on benches cut into the slopes, buildings situated close to the open section of underground railways etc. Footings of such structures are generally subjected to eccentric- inclined loads. In such situations, the major problem is that of obtaining the ultimate bearing capacity of the foundation from i) local foundation failure consideration, ii) the settlement and tilt of the footing and iii) the overall stability of the slope.

Several theories are available to compute the ultimate bearing capacity of a footing on or upper surface of a slope subjected to central vertical load. Various investigators have solved the problem by applying i) slip line method (Sokolovski, 1960; Siva Reddy and Mogaliah, 1975; Graham et al., 1988; Cheng and Au, 2005), ii) limit equilibrium approach (Meyerhof, 1957; Mizuno et al., 1960; Siva Reddy and Mogaliah, 1976; Bowles, 1977; Myslivec and Kysela, 1978; Saran et al., 1989), iii) limit analysis (Chen, 1975; Kusakabe et al., 1981; Saran et al., 1989; Xiao et al., 2007) and iv) finite element (Arduino et al., 1994,1998; Liu et al., 2006).

Many investigators have conducted model tests to study the behaviour of footings on slopes. Most of these tests were conducted on footings on slopes subjected to central vertical loads. Peynircioglu (1948), Shields et al. (1977), Saran et al. (1989) have reported the results of experiments to measure the ultimate bearing capacity of footings placed at various locations within and on the top of granular slopes. Kusakabe, Kimura et al. (1981) have reported the results of model tests on a c- ϕ soil slope.

Very few investigators have studied the problem of a footing on or upper surface of a slope and subjected to an eccentric-inclined load. Jao et al. (2001, 2008) studied the effect of eccentric vertical load on the bearing capacity and settlement of a footing placed on upper surface of a slope using finite element method. Shields et al. (1981) have conducted some experiments on footings placed on and upper surface of slopes with central inclined loads. Marechal et al. (1999) reported the results of centrifuge tests for

footings on upper surface of slopes and subjected to eccentric-inclined loads. However, no rational method has been reported to determine the bearing capacity, settlement and tilt of a footing placed on the upper surface of a slope and subjected to eccentric-inclined load. So the need was felt to take up this problem for study.

In the present investigation the ultimate bearing capacity has been obtained by limit equilibrium approach. It is assumed that failure occurs on the side of the slope and the rupture surface is a log-spiral. The eccentricity and obliquity of the load is assumed towards the slope. The resistance mobilised on this side is full passive and that on the other side of the slope is partial and characterised with a mobilization factor, m, which is less than unity. Expressions for bearing capacity factors have been developed by considering the equilibrium of a triangular elastic wedge below the strip footing. The mobilised passive earth pressures corresponding to the maximum value of m satisfying all the three conditions of equilibrium have been adopted in computing the bearing capacity factors. Non-dimensional bearing capacity factors N_c, N_q and N_γ have been obtained considering three cases separately i.e. i) $c = q = 0$, ii) $\gamma = c = 0$, iii) $\gamma = q = 0$, and the bearing capacity is expressed as

$$q_u = \frac{1}{2}\gamma B N_\gamma + \gamma D_f N_q + c N_c \qquad (1)$$

These bearing capacity factors depend on angle internal friction of the soil mass (ϕ), slope angle (β), edge distance to width ratio (D_e /B), depth to width ratio (D_f /B), eccentricity to width ratio (e/B) and the load inclination (i), and are presented in the form of design charts convenient for use in design.

It has been observed that the values of these bearing capacity factors increase with increase in the edge distance and after a certain distance; this value becomes independent of the slope. These factors reduce with the increase in eccentricity and obliquity of the load, though the rate of increase or decrease is different for the three bearing capacity factors.

The values of N_γ factor for central vertical load on slope have been computed and compared with the work of earlier investigators. It is observed that the N_γ values from the present analysis are less than Graham's (1988) and Saran's (1989) values, but higher than Meyerhof's (1957), Cheng's (2005) and Xiao's (2007) values. The difference may

be attributed to the difference in the nature of rupture surface adopted in the methodology for estimating the N_γ values. The reduction in the factor N_γ for different values of eccentricity and inclination of load for a footing on a level ground have been calculated from the present analysis and then compared with earlier investigators (Meyerhof, 1963, Hansen,1970, Vesic, 1975, Saran & Agrawal (1986). It has been observed that the proposed reduction in N_γ values tallies reasonably well with the earlier investigators.

For comparing the N_q factor, $q_u/\gamma B$ values have been obtained from the present analysis for a footing on a cohesionless slope and subjected to central vertical loads and then compared with those given by earlier investigators. It has been observed that the $q_u/\gamma B$ values from the present analysis are higher as compared to those by Cheng (2005), but less than Graham (1988) and Saran (1989) values.

The N_c values obtained for footings on slopes from the present investigation for central vertical load have been compared with those given by the earlier investigators. It has been observed that the values from the present analysis are less than Saran's (1989) values, but higher than Hansen's (1970) and Xiao's (2007) values. The reduction in the factor N_c for different inclination and eccentricity of the load have been obtained from the present analysis for level ground and compared with those given by the earlier investigators. The reduction factors compare well with Saran & Agrawal (1991) values, but are higher than Meyerhof's (1963) values.

Pressure-settlement and pressure-tilt relationships are essentially functions of non-linear constitutive laws of soil. In this investigation a methodology has been proposed to predict the pressure-settlement and pressure-tilt characteristics of a rigid strip footing placed on the upper surface of a slope and subjected to an eccentric-inclined load using non-linear constitutive laws of soil. Firstly, the analysis has been developed for a flexible footing subjected to an eccentric-inclined load. The contact pressure distribution is assumed to be i) uniform for central loading, ii) trapezoidal, when eccentricity to width ratio, (e/B) is less than 1/6, and iii) triangular when eccentricity to width ratio, (e/B) is greater than 1/6. The soil below the footing has been divided into thin strips upto a significant depth. For the assumed contact pressure on the base of the footing, the vertical stresses, horizontal stresses and shear stresses have been obtained at the centre of different strips along vertical sections using theory of elasticity. Presently no method is

available to calculate the stresses due to footing load on a soil mass which is restricted by a slope on one side. Hence, a new method is proposed for finding the stresses due to a footing load placed on a slope. Using these stresses, principal stresses and their directions are evaluated. Principal strains and strains in the vertical directions have been obtained using non-linear constitutive laws. The vertical settlement of any layer along a vertical section is computed by multiplying the strain with the thickness of each layer. The total settlement along any vertical section is computed by adding the settlement of all the layers along the vertical section and thus the settlement below various points of the footing have been determined. This settlement pattern of the flexible footing is compared with that of a rigid footing. Since the settlement of a rigid footing will be linear, having maximum settlement on one side (S_{max}) and minimum on the other side (S_{min}), these settlements are obtained by applying the following principles.

i) The area of the settlement diagram of the flexible footing is equal to the area of the settlement diagram of the rigid footing.

ii) The distance of the centre of settlement diagram of the flexible footing from one edge of footing is equal to the distance of centre of settlement diagram of the rigid footing from the same edge of the footing.

Knowing the values of S_{max} and S_{min}, average settlement (S_{av}) and tilt (t) are computed as follows:

$$S_{av} = \frac{S_{max} + S_{min}}{2} \tag{2}$$

$$t = \frac{S_{max} - S_{min}}{B} \tag{3}$$

This was repeated for different footing loads and complete pressure-settlement and pressure-tilt characteristics of the footing have been predicted. The validity of this type of approach has already been shown by Sharan (1977), Amir (1992) and Agrawal (1986).

The above method was adopted to predict the pressure-settlement and pressure-tilt characteristics of footings placed on upper surface of a cohesionless soil slope of Ranipur sand. Stress-strain characteristics of Ranipur sand at 70% relative density were obtained by performing triaxial compression tests at different confining pressures. From these test

data, Kondner's (1963) hyperbolic constant a and b were obtained and used to obtain the pressure-settlement and pressure-tilt characteristics.

To verify the analytical solutions, model tests were conducted on strip footings of size 150 mm × 600 mm in a tank, 3000 mm long, 601 mm wide and 900 mm deep containing sand deposited at a desired relative density. The tests were conducted on Ranipur sand at relative density of 70 percent. The footings were tested at two slope angles (β = 30° and 26.56°), four edge distance to width ratios (D_e/B = 0, 1, 2 and 3), three eccentricity to width ratios (e/B = 0, 0.1, 0.2) and three load inclinations (i = 0, 10°, 20°). In each case, the footing was loaded upto failure and its pressure-settlement and pressure-tilt characteristics were obtained.

The values of ultimate bearing capacity obtained from the present theory and the model tests were compared. The failure load has been taken as the peak load. It was observed that the values of ultimate bearing capacity obtained from the model tests data compare well with the corresponding values obtained from the proposed theory.

The pressure-settlement characteristics predicted from the proposed theory were compared with those obtained from the model tests. It is observed that the two curves are similar in nature and upto about 50% of the failure pressure, the tally between predicted and experimental values is reasonable. From the point of view of design, the settlements are usually obtained corresponding to a pressure equal to one-third of the failure pressure. For this pressure, the present methodology gives the estimate of settlement almost precisely.

ACKNOWLEDGEMENT

The author wishes to offer his profound and sincere gratitude to Dr. Swami Saran, Emeritus Fellow, Department of Earthquake Engineering and Dr. M.N.Viladkar, Professor, Department of Civil Engineering, Indian Institute of Technology Roorkee, Roorkee for their inspiring guidance, valuable suggestions and substantial encouragement throughout the course of this research work. Words would fail to record the invaluable help which the author was privileged to receive from them on numerous occasions.

The author is grateful to Prof. N.K. Samadhiya, Prof. Pradeep Bhargava, and Dr. Priti Maheswari, Assistant Professor, Department of Civil Engineering, IIT Roorkee, for their generous support and useful suggestions during the course of this work.

The author owes his sincere thanks to the Head and other faculty members of the Department for extending the facilities and resources whenever needed.

Thanks are due to Sri Atma Ram, Sri Dipak Raj Saxena, Sri Pitambar Singh, Sri Om Veer, Sri Suresh Chand and other staff members of the Geotechnical Engineering Laboratory for the help rendered by them during the experimental investigations.

The financial support received from the All India Council for Technical Education, New Delhi, under Quality Improvement Programme, is gratefully acknowledged.

The author would like to place on record his sincere thanks to the authorities of the Orissa Engineering College, Bhubaneswar for deputing him to carry out the research work at IIT Roorkee.

The author wishes to record his appreciation for his wife, Mamata and daughters, Soumyamitra and Saranya, for their constant encouragement and whole hearted support throughout this work.

The author recognises with warm appreciation the moral support and ever-growing blessings of his parents.

The author wishes to express his heartfelt thanks to his friends Mr. Mohd. Yousuf Shah, Mr. Kranti Borgaonkar, Mr. Dipak Kumar Sahoo and Mr. Abdesh Kumar Sinha for their constant moral support and companionship during the entire period of this work.

Last, but not the least, the author wishes to thank numerous well wishers and friends who have contributed in making this work a success.

Trilochan Sahu

(TRILOCHAN SAHU)

CONTENTS

LIST OF FIGURES

LIST OF TABLES

NOTATIONS

Symbol	Description
A	Area of failure surface on the level ground side
A_s	Area of the failure surface on the slope side
$a,\ b$	Hyperbolic constants
B	Width of the footing
B'	Effective width of the footing
C	Cohesion force along arc ED
C_a	Cohesion force along BE
Ca'	Cohesion force along $A'E$
c	Unit cohesion
c_H	Cohesion in horizontal direction
c_v	Cohesion in vertical direction at any point
c_{vs}	Cohesion in vertical direction at top of slope
D_e	Distance of the edge of the footing from the crest of slope
D_f	Depth of foundation
D_r	Relative density
E_i	Initial tangent modulus
E_s	Secant modulus
E_t	Tangent modulus
e	Eccentricity
e_l	Effective eccenticity
e_γ	Reduction factor for N_γ due to load eccentricity
e_q	Reduction factor for N_c due to load eccentricity
e_c	Reduction factor for N_c due to load eccentricity

F	A factor
H	Height of slope
i	Load inclination with vertical
i_e	Reduction factor for bearing capacity due to load eccentricity
i_δ	Reduction factor for bearing capacity due to load inclination
i_β	Reduction factor for bearing capacity due to slope
$i_{e\delta\beta}$	Combined reduction factor due to load eccentricity, load inclination and slope angle
i_γ	Reduction factor for N_γ due to load inclination
i_q	Reduction factor for N_q due to load inclination
i_c	Reduction factor for N_c due to load inclination
K_o	Coefficient of earth pressure at rest
k	Coefficient of anisotropy
L	Length of the foundation
L_s	Length of failure surface for footing on slopes
L'	Length of failure surface for footing on level ground
M	Applied moment
M_γ	Moment of weight force
M_q	Moment of surcharge force
M_c	Moment of cohesive force
m	Mobilisation factor
N_s	Stability factor
N_γ	Bearing capacity factor for weight part
N_q	Bearing capacity factor for surcharge part
N_c	Bearing capacity factor for cohesion part
$N_{\gamma q}$	Bearing capacity factor for weight and surcharge
N_{cq}	Bearing capacity factor for cohesion and surcharge

P_p	Passive earth pressure
P_m	Passive earth pressure at partial mobilisation
$P_{p\gamma}$	Passive pressure for weight part
P_{pq}	Passive pressure for surcharge part
P_{pc}	Passive pressure for cohesive part
$P_{m\gamma}$	Mobilised passive pressure for weight part
P_{mq}	Mobilised passive pressure for surcharge part
P_{mc}	Mobilised passive pressure for cohesion part
Q_d	Total load
$Q_{d\gamma}$	Load due to weight part
Q_{dq}	Load due to surcharge part
Q_{dc}	Load due to cohesion part
q	Load intensity
q_u	Ultimate bearing pressure
q_v	Vertical contact pressure distribution
q_h	Horizontal contact pressure distribution
R_f	Ratio of failure stress and ultimate stress in triaxial test
r_o	Initial radius of log spiral (i.e BE)
S	Total settlement along a vertical section
S_e	Settlement of any layer along a vertical section
S_{max}	Maximum settlement of rigid footing
S_{min}	Minimum settlement of rigid footing
S_{av}	Average settlement of rigid footing
t	Tilt of rigid footing
x_1	Ratio of effective width and full width of footing
z	Vertical distance from the surface
α_1, α_2	Wedge angles

β	Slope angle
γ	Unit weight of soil
ϕ	Angle of internal friction of soil
ϕ_m	Mobilised angle of internal friction
σ	Normal stress
σ_x	Stress in x-direction
σ_z	Stress in z-direction
σ_u	Ultimate deviatoric stress in hyperbolic representation
σ_1	Major principal stress
σ_3	Minor principal stress
τ_{xz}	Shear stress
θ	Angle
θ_1	Log spiral angle on the slope side
θ_2	Log spiral angle on the level side
θ'_1	Inclination of major principal stress w.r.t. vertical axis
θ'_3	Inclination of minor principal stress w.r.t. vertical axis
ε_1	Major principal strain
ε_3	Minor principal strain
ε_z	Strain in z-direction
μ	Poisson's ratio
μ_1, μ_2	Ratio

CHAPTER-I

INTRODUCTION

1.1 GENERAL

Shallow footings on or upper surface of slopes are often encountered in case of many engineering structures such as bridges, flyovers, retaining walls, transmission towers, structures placed on benches cut into the slopes, etc. Many highway and railway overpass structures and abutments of river bridges are built on approach embankments. Buildings and retaining structures are sometimes constructed adjacent to a ravine. Foundations of buildings situated close to the open section of underground railways are very frequent in crowded metros.

In general, a foundation is subjected quite often to vertical and horizontal loads and moment as well. The resultant of these forces may be expressed as an equivalent eccentric-inclined load on the foundation, Fig.1.1. When a footing is placed close to the crest of a slope, its bearing capacity is reduced as compared to a footing placed on a level ground; and it is further reduced if the applied loads are either eccentric, inclined or any combination thereof.

For the design of a footing on a level ground under the action of eccentric-inclined load, the important design criteria considered are: i) the ultimate bearing capacity due to shear failure and ii) the failure due to excessive settlement and the tilt of the structure. When such a footing is placed on upper surface of a slope, the overall stability of the slope should also be checked. In case of non-cohesive soils, the bearing capacity of the footings will always be governed by the foundation failure, while the bearing capacity of footings on cohesive soils may be limited by the overall stability of the whole slope.

1.2 FOOTINGS ON UPPER SURFACE OF SLOPES AND SUBJECTED TO CENTRAL VERTICAL LOADS

Several theories are available for computation of the bearing capacity of footings on or upper surface of slopes and subjected to central vertical loads. Various investigators have attempted the problem by applying: i) slip line method, ii) limit analysis method, iii) limit equilibrium method and iv) finite element method.

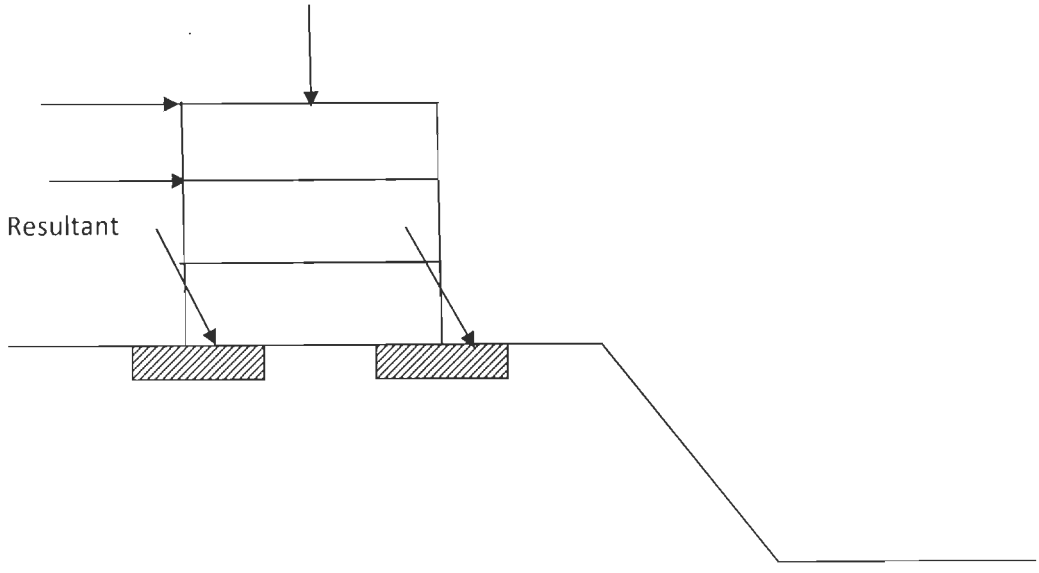

(a) Portal Frame Structure on the Bench Cut on a Slope or Near an Excavation

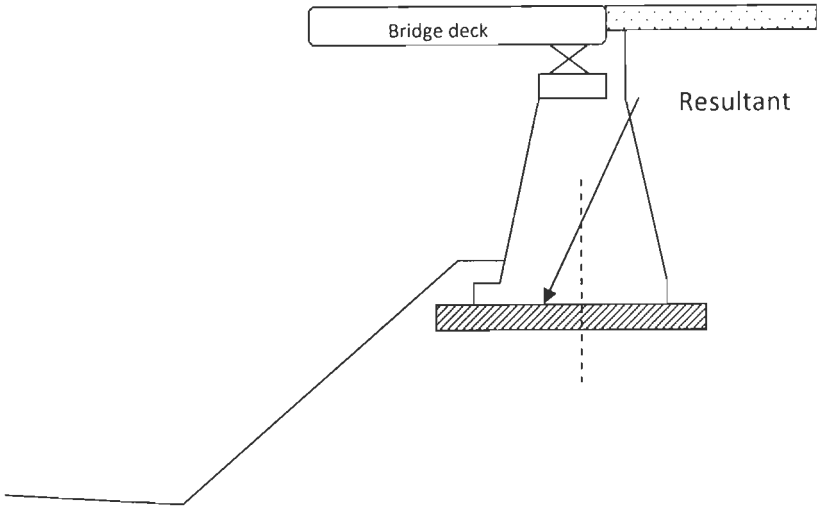

(b) Bridge Abutment on the Top of a Slope

Fig. 1.1 Structures on Top of Slopes with Eccentric-Inclined Load

Meyerhof (1957) was the first to study the problem of ultimate bearing capacity of a footing placed on or near the edge of slopes and subjected to central vertical loads. Meyerhof extended his classical theory of bearing capacity of foundations on a level ground and combined it with the theory of stability of slopes to cover the

stability of foundations on slopes. The slip lines were constructed by taking into account the slope angle, the distance from the edge of the slope and the angle of shearing resistance of the slope material.

Using the theory of plasticity, Sokolovski (1960) obtained the magnitude of uniform pressure which can be applied on the top of a slope. Mizuno et al. (1960) investigated the performance of footings resting on the crest of cohesionless soil slopes using limit equilibrium approach. Chen (1975) investigated the problem by limit analysis and solved it by taking the same failure surface as that of Meyerhof (1957). Kusakabe et al. (1981) also attempted the problem using limit analysis approach incorporating the effect of the footing location from the crest of the slope. Graham et al. (1988) approached the problem by applying the method of stress characteristics for cohesionless soil. The nonfailing zone of soil immediately beneath the footing was assumed asymmetric. Saran et al. (1989) developed analytical solutions for obtaining the ultimate bearing capacity of footings on upper surface of slopes using limit equilibrium and limit analysis methods. One sided rupture failure on the side of the slope was assumed and partial mobilisation was considered on the side of the flat ground. Arduino et al. (1994, 1998) analysed the problem of bearing capacity of a footing placed on top of a slope subjected to central vertical loads by finite element method and obtained both the ultimate bearing capacity and the settlement. Cheng and Au (2005) derived the expressions for bearing capacity factors N_q and N_γ for the case of a footing resting on a sloping ground and under the action of a central vertical load based on the slip line method and verified it by using the finite difference analysis. Yang et al. (2007) applied energy dissipation method to determine the bearing capacity of footings on a sloping ground. The soil failure was assumed to be governed by a linear Mohr-Coulomb yield criterion.

Few investigators have conducted model tests for investigating the behaviour of footings on or upper surface of slopes. Peynircioglu (1948) performed series of model tests on cohesionless slopes. Shields et al. (1977) reported the results of experiments for footings located at various locations within a granular slope. The footings were placed both on and upper surface of the slopes. The primary conclusion of the investigation was that the theory proposed by Meyerhof (1957) did not predict correctly the magnitude of the bearing capacity of a footing for its various locations. Saran et al. (1989) conducted tests to study the behaviour of footings on slopes and

compared the results with the theoretically predicted results from different available theories. Some investigators have also conducted centrifuge model tests for footings on slopes. Garnier et al. (1994) reported the results of a series of centrifuge tests to study the bearing capacity of a footing on upper surface of the slopes and subjected to central vertical loads and proposed an equation for reduction factor in bearing capacity due to nearness of a footing to the edge of a slope.

1.3 FOOTINGS ON UPPER SURFACE OF SLOPES UNDER ECCENTRIC-INCLINED LOADS

Jao et al. (2001, 2008) investigated analytically the performance of strip footings placed on upper surface of a slope and subjected to eccentric vertical loads using a two dimensional plane-strain elasto-plastic finite element method.

Shields et al. (1981) reported the results of experiments for footings placed at various locations within a granular slope. The loading on the footings was central inclined in some experiments. Marechal et al. (1999) reported the results of centrifuge model tests for footings on or upper surface of slopes and subjected to eccentric-inclined load and expressed the bearing capacity reduction due to the presence of a slope and due to eccentricity and obliquity of the load.

1.4 SCOPE OF WORK

The literature reveals that there is no rational method available for the estimation of bearing capacity, settlement and the tilt of a footing placed on upper surface of a slope and subjected to eccentric-inclined load. Except one finite element study and one centrifuge model study, no other study has been reported in this area. Thus, it becomes essential to develop a simplified procedure for estimation of the bearing capacity, settlement and tilt of a foundation placed on upper surface of a slope and subjected to eccentric-inclined load.

To study the behaviour of footings placed on upper surface of a slope and subjected to eccentric-inclined loads, the following investigations have been proposed:

a) To obtain the ultimate bearing capacity of footings by limit equilibrium approach.

b) To develop an analytical procedure for evaluating pressure-settlement and pressure-tilt characteristics of foundations using constitutive laws of soil.

c) To conduct model tests for verification of the analytical results.

1.5 ORGANISATION OF THESIS

The relevant literature on the subject has been critically reviewed and presented in Chapter II. The review of the literature mainly covers the following aspects:

i) Ultimate bearing capacity

ii) Constitutive laws

iii) Model tests

Chapter III deals with the assumptions made and the theoretical formulation proposed for obtaining the ultimate bearing capacity by the limit equilibrium method.

An analytical procedure to predict pressure-settlement and pressure-tilt characteristics of a footing placed on upper surface of a slope under eccentric-inclined load using the constitutive laws is presented in Chapter IV.

Chapter V includes constitutive relations obtained for Ranipur sand and description of model tests in detail.

Interpretations of analytical investigations and model test data have been presented in Chapter VI. Finally, the summary of the work, the conclusions and the scope of future work have been given at the end of the thesis in Chapter VII.

CHAPTER-II

REVIEW OF LITERATURE

2.1 GENERAL

In this chapter, a detail review of literature related to the behaviour of footings founded on or upper surface of slopes is presented. Firstly, the analytical solutions of the problem of determining the ultimate bearing capacity of footings on or upper surface slopes and subjected to different types of loadings are reviewed. Thereafter, constitutive laws for soils, factors affecting them, various constitutive models and the methods for predicting the settlement and tilt are discussed. Lastly, the experimental model studies and the centrifuge model studies of foundations placed on and upper surface of the slopes are discussed.

2.2 ULTIMATE BEARING CAPACITY

The well known techniques used in the solution for ultimate bearing capacity can be divided into four groups, namely,

i) Slip Line method

ii) Limit Equilibrium Analysis

iii) Limit Analysis

iv) Finite Element Method

After discussing the salient features of each method, detailed review of literature with special reference to footings on or near the slope has been presented.

2.2.1 Slip-Line Method

In a slip line solution, soil mass near the footing is assumed to be in the state of plastic equilibrium. The solution consists of constructing a slip line field in the region, which satisfies all the stress boundary conditions that directly concern the region, as well as the equilibrium and the yield conditions at every point in the region.

Plastic flow of soil occurs when a sufficiently large region beneath the footing is stressed to its limiting or yield condition, resulting in an unrestricted plastic flow of the soil. At the instant of impending plastic flow, both equilibrium and the yield conditions are satisfied in the region near the footing. For soils, Mohr-Coulomb criterion has been widely used as the yield condition. Combining Mohr-Coulomb

criterion with equations of equilibrium, a set of differential equations of plastic equilibrium in this region are obtained. Together with the stress boundary condition, this set of differential equations can be solved to obtain the stresses in the soil beneath the footing at the instant of impending plastic flow. In order to solve specific problems, the set of equations are generally transformed to a curvilinear co-ordinate system, whose direction at every point in the yield region coincides with the direction of the failure or the slip plane. These slip directions are known as slip lines and the network is called as the slip-line field.

Kotter (1903) was the first to derive these slip line equations for the case of plane deformation. Prandtl (1920) obtained an analytical closed form solution to these equations for a footing on a weightless soil. These results were subsequently applied by Reissner (1924) to some specific problems of bearing capacity of footings on a weightless soil, when the slip lines of at least one family are straight and the solutions have a closed form. Sokolovski (1960) adopted a numerical procedure based on a finite difference approximation of the slip line equations and obtained solutions of number of problems related to bearing capacity of footings, for which it was impossible to find the closed form solutions.

Sokolovski (1960) presented a solution to the problem of a slope of c–ϕ soil making an angle, β with the horizontal and predicted the maximum vertical load that can be applied along x-axis (Fig. 2.1) such that limiting equilibrium can be maintained.

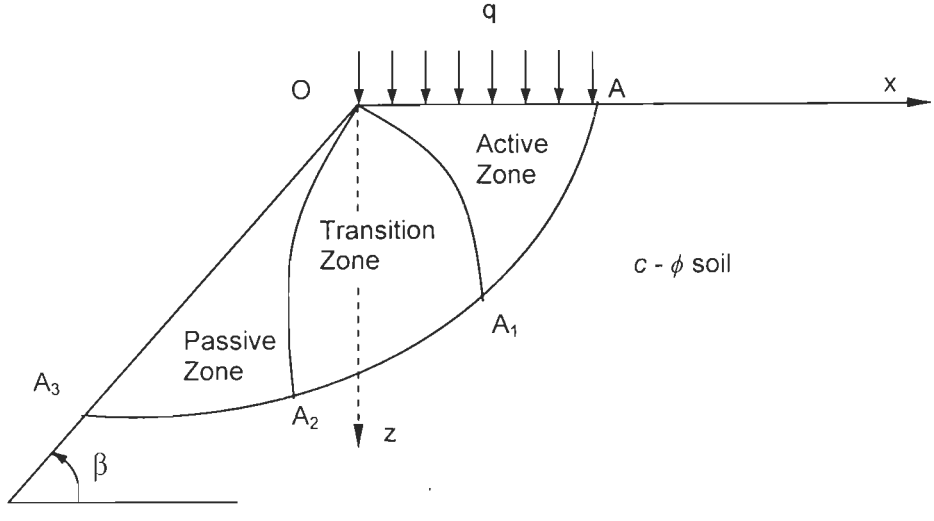

Fig. 2.1 Rupture Surface (Sokolovski, 1960)

The soil below the loading area was divided into three zones, an active zone AOA_1, passive zone A_2OA_3 and a transition zone A_1OA_2. Sokolovski presented the values of maximum load, σ_z/c along the x-axis (in units of γ/c) for a range of ϕ and β values as given in Table 2.1.

Table 2.1 Values of (σ_z/c) for Different Values of ϕ and β (Sokolovski, 1960)

	ϕ=20°			ϕ= 40°			
β / x	0	10°	20°	10°	20°	30°	40°
0	14.8	12.7	10.9	55.9	41.4	30.6	22.5
2.0	25.4	19.9	15.0	186.0	115.0	68.4	38.1
4.0	34.0	25.8	18.3	299.0	179.0	101.0	50.4
6.0	41.8	31.4	21.4	409.0	241.0	132.0	61.7

Siva Reddy and Mogaliah (1975) have studied the effect of anisotropy and non-homogeneity of soil on the ultimate bearing capacity of foundations on slopes for the case of central vertical loads using Sokolovski's (1960) method of characteristics. The variation of cohesion in any direction was given by -

$$c = c_H\left[1+(k-1)\sin^2\psi\right] \tag{2.1}$$

where c = cohesion corresponding to any value of ψ,

ψ = angle made with the horizontal, by the bisector of the angle between the failure planes at a point,

c_H = cohesion in horizontal direction, corresponding to $\psi = 0$ and

k = coefficient of anisotropy

The variation of cohesion with depth was expressed by the following equation:

$$c_v = c_{vs} + \alpha(D_f + Z) \tag{2.2}$$

where c_v = cohesion in vertical direction at any point,

c_{vs} = cohesion in vertical direction at top of slope,

α = rate of increase of c_v with z, and

D_f = depth of foundation

The rupture surface was taken similar to that of Meyerhof (1957) as shown in Fig. 2.2.

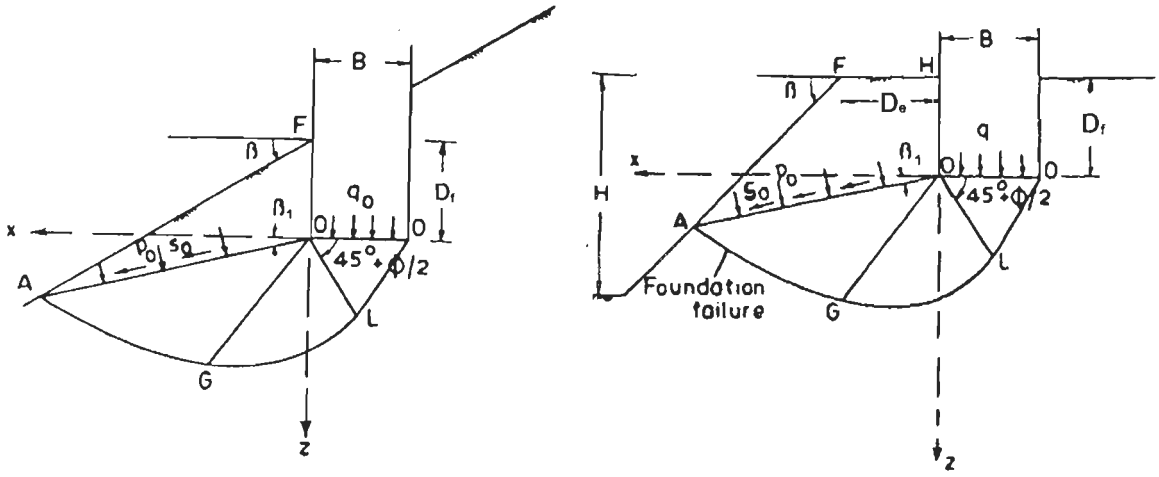

(a) (b)

Fig. 2.2 Plastic Zone and Slip Surfaces below a Strip Footing (a) on Face of Slope, (b) on Top of Slope (Siva Reddy and Mogaliah, 1975)

The ultimate bearing capacity was expressed as,

$$q_u = N_c + p_o N_q + \frac{1}{2}\frac{\gamma l}{c_{vs}} B'_f N_\gamma \qquad (2.3)$$

where N_c, N_q and N_γ are non dimensional bearing capacity factors.

The values of p_o and s_o, the stresses on the equivalent free surface were calculated from the assumed value of α, D'_f, β and D'_e. All the quantities with primes are dimensionless. The non dimensional stresses and distances were obtained by dividing the stresses and distances by the characteristic stress, c_{vs} and the characteristic length, $l = c_{vs}/\gamma$. The values of N_c corresponding to $k=1$ and $\alpha.l/c_{vs} = 0$ (for homogeneous and isotropic soils) were obtained by the investigators and compared with those of Meyerhof (1957) as presented in Table 2.2. It can be observed from the table that the calculated values of N_c were, in general, in good agreement with the values given by Meyerhof (1957). The other bearing capacity factor, $N_{\gamma q}$ corresponding to $k=1$ and $\alpha.l/c_{vs} = 0$ was calculated and compared with the results of Meyerhof (1957) and given in Table 2.3. It can be observed that the values obtained by the investigators were higher than those given by Meyerhof (1957). The footing loads were central vertical and the effect of eccentricity and inclination of the loads were not incorporated in the analysis.

Table 2.2 Comparison of N_c Values Given by Siva Reddy and Mogaliah (1975) with those by Meyerhof (1957)

$\phi°$	$\beta°$	D_e/B	D_f/B	N_c Siva Reddy, Mogaliah(1975)	N_c Meyerhof (1957)
0	15	0	0.23	5.04	5.08
0	45	0	0.648	4.41	4.48
0	30	0.8	0.102	5.03	5.10
0	60	0.97	0.121	5.03	4.90
10	15	0	0	7.11	7.10
20	15	0	0	11.78	11.80
30	15	0	0	21.82	21.90
30	30	0	0	15.68	15.70
30	45	0	0	11.14	11.20

Table 2.3 Comparison of $N_{\gamma q}$ Values Given by Siva Reddy and Mogaliah (1975) with those by Meyerhof (1957)

$\phi°$	$\beta°$	D_e/B	D_f/B	$N_{\gamma q}$ Siva Reddy, Mogaliah (1975)	$N_{\gamma q}$ Meyerhof (1957)
30	15	0	0	13.76	10.0
30	30	0	0	5.01	3.10
30	15	0	0.681	33.60	30.0
30	15	0	0.308	20.10	17.0
30	15	1.42	0.236	28.10	24.50

Graham et al. (1988) employed the method of stress characteristics to solve the problem of bearing capacity of foundation on slopes for central vertical loads. The difference with the earlier methods was that the method has been used to solve the problem for purely cohesionless soil and took particular account of the stress conditions immediately beneath the footing. The nonfailing zone of soil immediately beneath the footing has been assumed as asymmetric as shown in the Fig. 2.3. The problem was solved numerically and the bearing capacity was expressed as

$$q_u = 0.5\gamma B N_{\gamma q} \tag{2.4}$$

The authors have developed charts for the bearing capacity factor, $N_{\gamma q}$ as a function of slope angle, β for different values of edge distance and depth of footing. The charts have been reproduced in Figs. 2.4 and 2.5. The results were compared with the results of earlier investigators as shown in Fig. 2.6. It can be observed from Fig. 2.6 that the results of Graham et al. (1988) gives values of $N_{\gamma q}$ which lie above those given by the previous investigators.

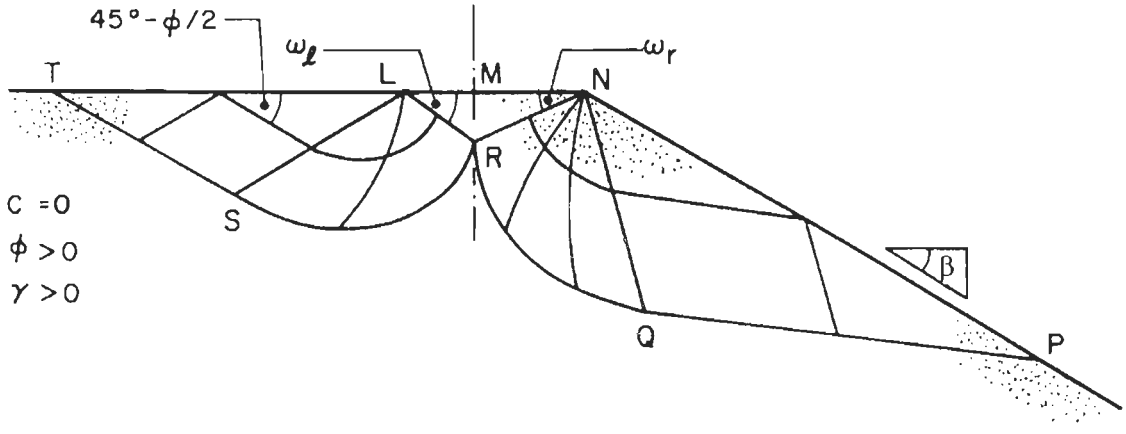

Fig. 2.3 Schematic Diagram of Failure Zone for Footing at Crest of Slope (Graham et al., 1988)

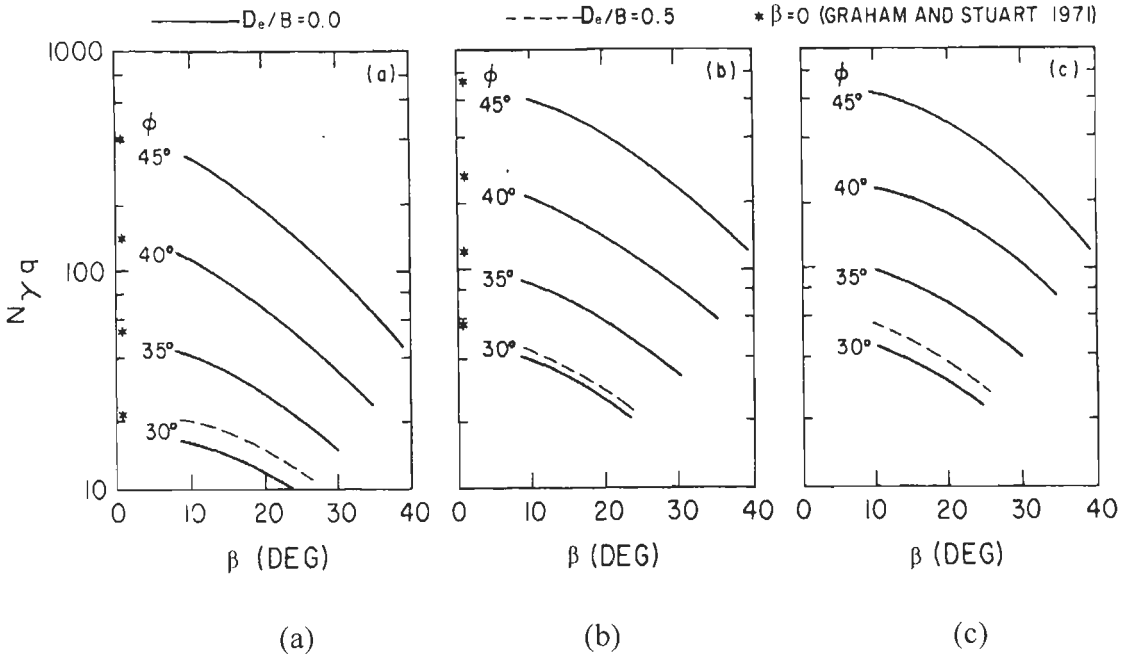

Fig. 2. 4 Charts for Bearing Capacity Factor, $N_{\gamma q}$ (Graham et al., 1988) (a) D_f/B=0; (b) D_f/B=0.5; (c) D_f/B=1.0 (D_e/B=0.0, 0.5)

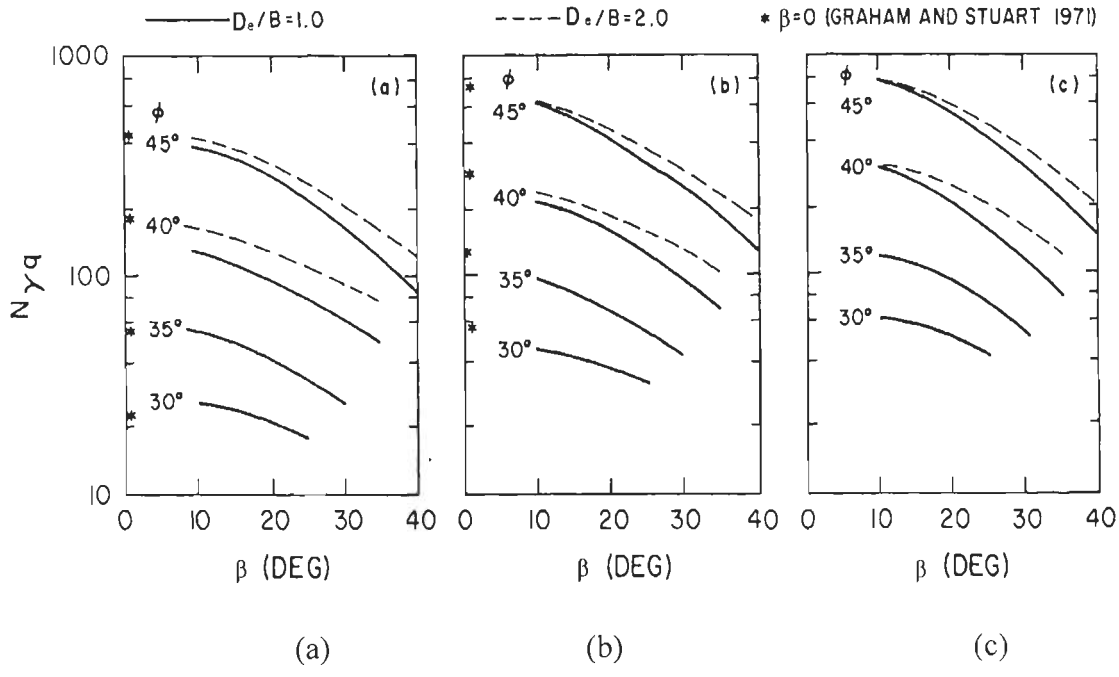

Fig. 2.5 Charts for Bearing Capacity Factor, $N_{\gamma q}$ (Graham et al., 1988)
(a) D_f/B=0; (b) D_f/B=0.5; (c) D_f/B=1.0 (D_e/B=1.0, 2.0)

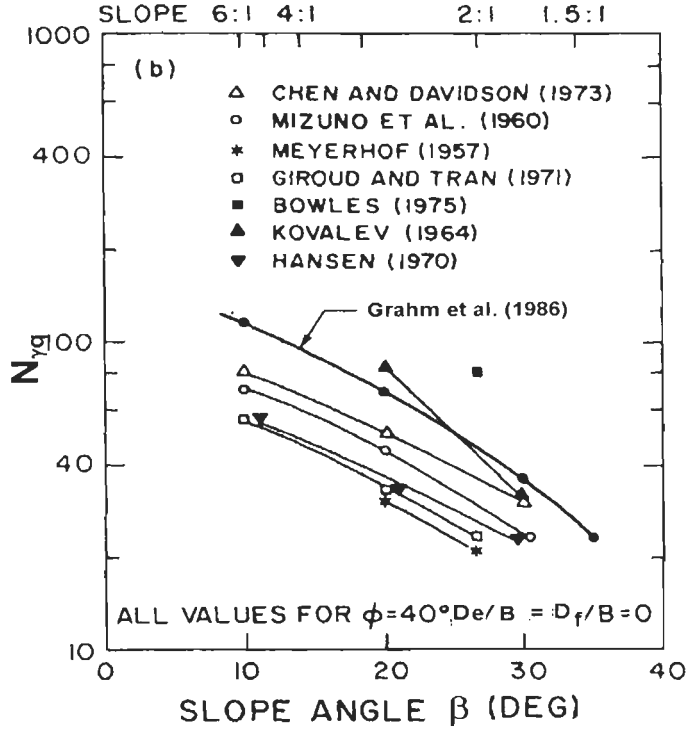

Fig. 2. 6 Comparison of $N_{\gamma q}$ Values of Graham et al. (1988) with other Investigators

Cheng and Au (2005) derived the expression for the bearing capacity factor, N_q for a footing on sloping ground for the case of central vertical load based on slip line method and verified it by using the finite difference analysis. The bearing capacity factor, N_γ for the case of a sloping ground was also obtained by an iterative finite difference method which gave the solution of the slip line equations. The values of N_γ obtained from slip line analysis were found to be in close agreement with those of Vesic (1973) and Hansen (1970), but the values of Graham et al. (1988) were much larger than the values given by all other methods as shown in Table 2.4. The investigators proposed design charts for the bearing capacity factors as a function of the slope angle, β as shown in Figs. 2.7 and 2.8.

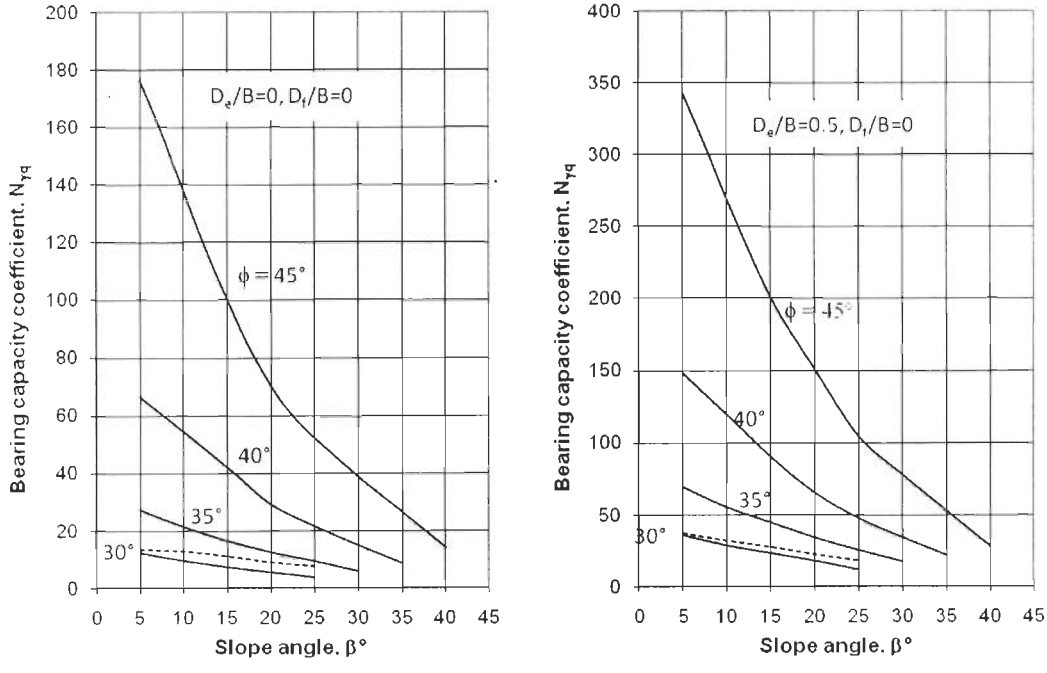

Fig. 2.7 Charts for Bearing Capacity Factor, $N_{\gamma q}$ (Cheng and Au, 2005)

Table 2.4 Comparison of N_γ Values from Different Methods of Analysis with those by Cheng and Au (2005) Values for ϕ=35°

β°	Cheng & Au (2005)	Vesic (1973)	Hansen (1970)	Graham et al. (1988)
10	22.50	32.59	21.38	40.0
20	14.90	19.43	12.42	25.0
30	9.70	8.58	6.18	10.0
35	0.00	4.32	3.90	0.00

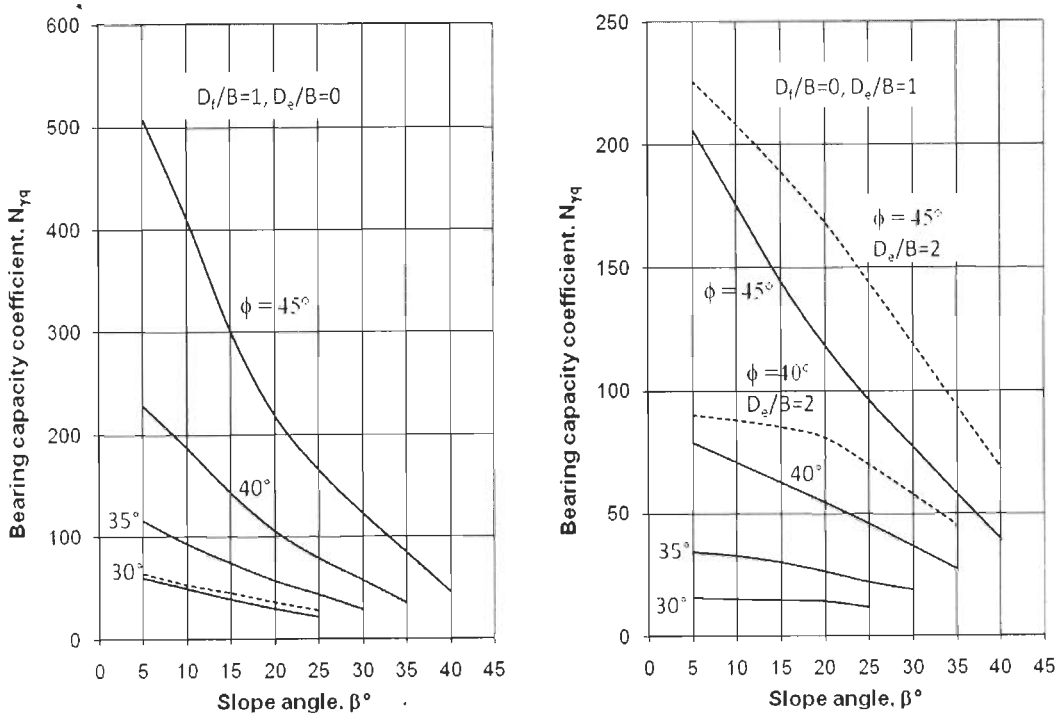

Fig. 2.8 Charts for Bearing Capacity Factor, $N_{\gamma q}$ (Cheng and Au, 2005)

2.2.2 Limit Equilibrium Method

The limit equilibrium method is the most commonly used method for obtaining an approximate solution for the stability problems which include: i) ultimate bearing capacity of the footings, ii) lateral earth pressure on retaining walls, and iii) stability of slopes. The method generally assumes a failure surface of simple shape – planar, circular, log spiral, or a combination of these, based on experience and experimental results. Some simplified assumptions regarding the stress distribution along the failure surface are made so that over all equations of equilibrium, in terms of stress resultants can be written for the given problem. With these assumptions, each stability problem is reduced to finding the most critical position of the failure or slip surface of the shape chosen, which may not be particularly well defined, but quite often gives fairly good results. Therefore, this simplified approach makes it possible to solve various problems by employing simple statics.

Common assumptions made in limit equilibrium method are as follows:

i) The soil mass follows the Mohr-Coulomb failure criterion,

$$\tau = c + \sigma \tan \phi \tag{2.5}$$

where τ represents the shear stress, c, the cohesion, σ, the normal stress on the failure plane and ϕ, the angle of internal friction.

ii) A failure surface of simple shape, e.g. planar, circular, log spiral or combination of these is assumed,

iii) The distribution of stress along the failure surface is also assumed,

iv) The general shape of various regions in the failure zone remains unchanged (straight slip lines remaining straight) irrespective of the consideration of the weight, and

v) Principle of superposition holds good. The three important factors – the weight of the soil and the effect of the strength parameters of the soil are assessed separately on the basis of a conservative mechanism and the three, in turn, provide a conservative estimate.

Terzaghi (1943) followed the limit equilibrium method and presented his classical theory for obtaining the bearing capacity of both rough and smooth shallow foundations on a level ground. Terzaghi chose the model of the failure mechanism similar to that chosen by Prandtl (1920) for the penetration of punches into the metal, replaced the soil above the base of the footing by a uniform surcharge and presented the results in terms of non-dimensional bearing capacity factors N_c, N_q and N_γ. Meyerhof (1951) extended the work of Terzaghi (1943) to both shallow and deep foundations. Meyerhof assumed the yield surfaces which extend right up to the ground surface, and the resistance which acts along the whole yield surface. Brinch Hansen (1961), starting from the basic equation of Terzaghi, accounted for the influence of depth of foundation, shape of the foundation and inclination of the load. Many other investigators have also employed the limit equilibrium analysis by using different rupture surfaces to find the bearing capacity of foundations on a level ground.

Meyerhof (1957) was the first to use the limit equilibrium analysis for finding the ultimate bearing capacity of a footing placed on or near the slopes and subjected to central vertical loads by extending his classical bearing capacity theory (Meyerhof, 1951) of foundation on level ground and combined it with the theory of the stability of slopes to cover the stability of foundations on slopes. Meyerhof considered the following two cases, namely

Case I: Strip Foundation on the slope face

Case II: Strip foundation on top of the slope

The failure surfaces considered for both the cases are reproduced in Figs. 2.9 a, b respectively.

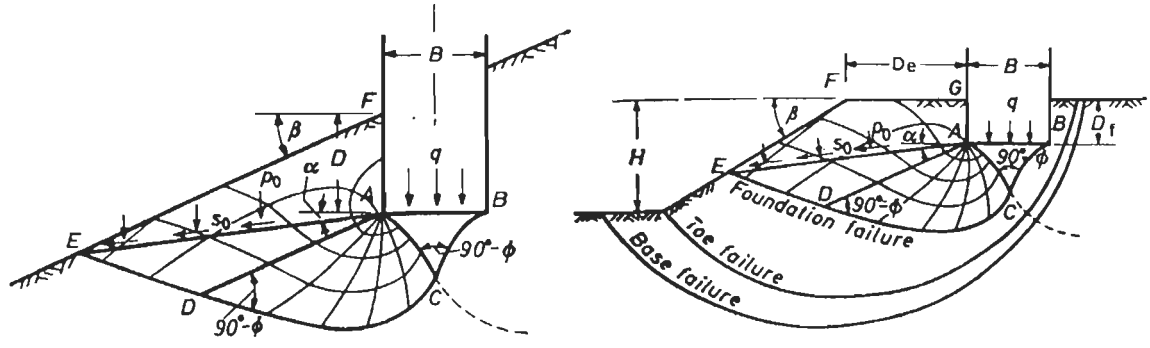

(a) (b)

Fig. 2.9 Plastic Zone and Slip Surfaces for a Strip Footing (a) on Face of Slope, (b) on Top of Slope (Meyerhof, 1957)

The region above the failure surface of a shallow rough strip foundation was assumed to be divided into a central elastic zone *ABC*, a radial shear zone *ACD* and a mixed shear zone *ADEF* for the case of footing on a slope or zone *ADEFG* for the case of footing on top of a slope and at a distance, D_e from the edge of the slope. The stresses in zones of plastic equilibrium were computed by replacing the weight of soil wedge *AEF* (case I) or *AEFG* (case II) by equivalent stresses p_0 and s_0, the normal and tangential respectively to the plane AE inclined at an angle α to the horizontal. The bearing capacity of a foundation on slope having a slope angle, β has been given by the following equation

$$q_u = cN_{cq} + \frac{1}{2}\gamma B N_{\gamma q} \tag{2.6}$$

where c is the cohesion of soil, γ, the unit weight of soil, and B is the width of foundation. N_{cq} and $N_{\gamma q}$ are the bearing capacity factors depending on slope angle, β, angle of shearing resistance of the soil, ϕ, the depth/width ratio, D_f/B and in addition a ratio of distance from edge of the slope to the footing width, D_e/B in case of footing on the top of slope and stability number N_s ($N_s = \gamma H / c$; H = height of the slope) in case of purely cohesive soil.

In case of a strip foundation on the face of the slope, charts for bearing capacity factors are presented in Figs. 2.10 a and b for purely cohesive (ϕ =0) and cohesionless (c = 0) materials, respectively. The factors decrease with greater inclination of the slope to minimum for $\beta=90°$ in case of purely cohesive material and for $\beta=\phi$ in case of cohesionless soil, when the slope becomes unstable. For cohesive material with a small or no angle of shearing resistance, Meyerhof combined his theory with the theory of slope stability, since in this case; the bearing capacity of a foundation can be limited by the stability of the whole slope.

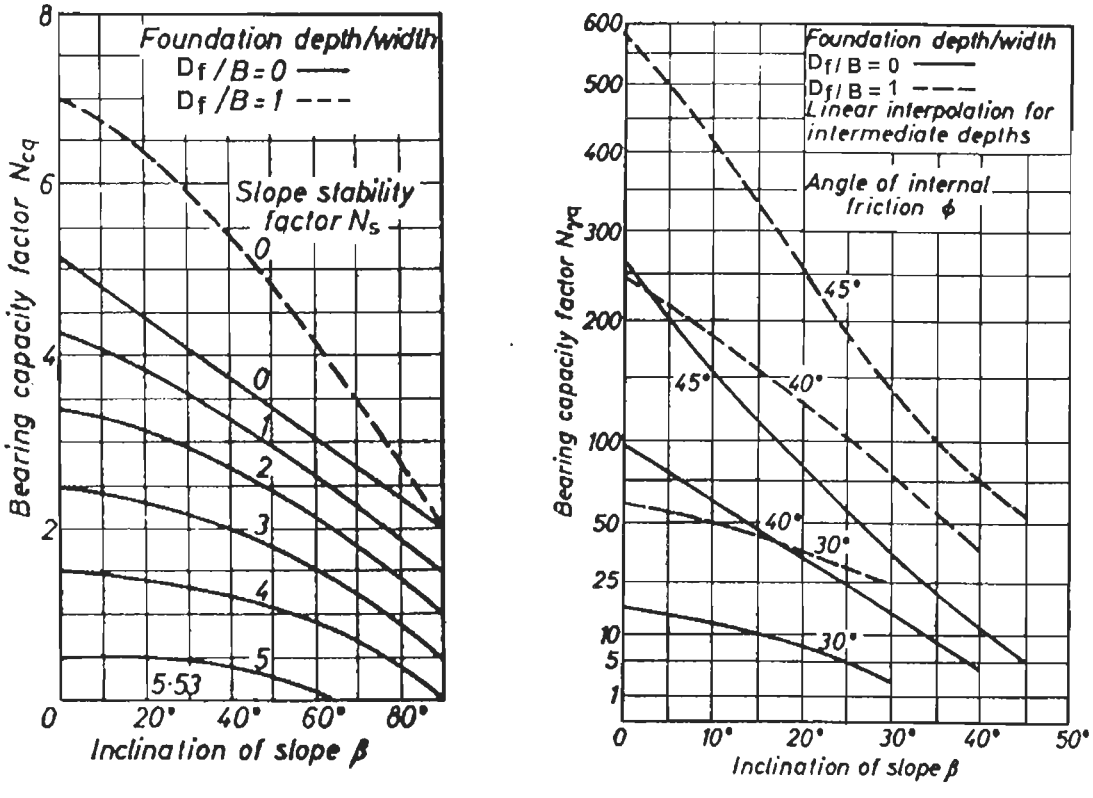

(a) (b)

Fig. 2.10 Bearing Capacity Factors for a Strip Foundation on Face of Slope for (a) Purely Cohesive and (b) Cohesionless Soil (Meyerhof, 1957)

In case of strip foundation on top of the slopes, charts for the bearing capacity factors have been reproduced in Figs. 2.11a and b for purely cohesive (ϕ =0) and cohesionless (c = 0) materials, respectively. While the N_{cq} and $N_{\gamma q}$ factors decrease with greater inclination of the slope, they have been found to increase rapidly with greater foundation distance from the edge of the slope. Beyond a distance of about 2 to 6 times the foundation width (depending upon ϕ and D_f/B), the bearing capacity

has been found to be independent of the inclination of slope and becomes the same as that of a foundation on an extensive horizontal ground surface. For slopes on cohesive soil, Meyerhof performed an analysis for the case of slope failure (through toe or base) under a foundation load on the assumption of a cylindrical slip surface as for unloaded slopes (Fellenius, 1927), and the average load over the whole foundation area was replaced by a uniform surcharge.

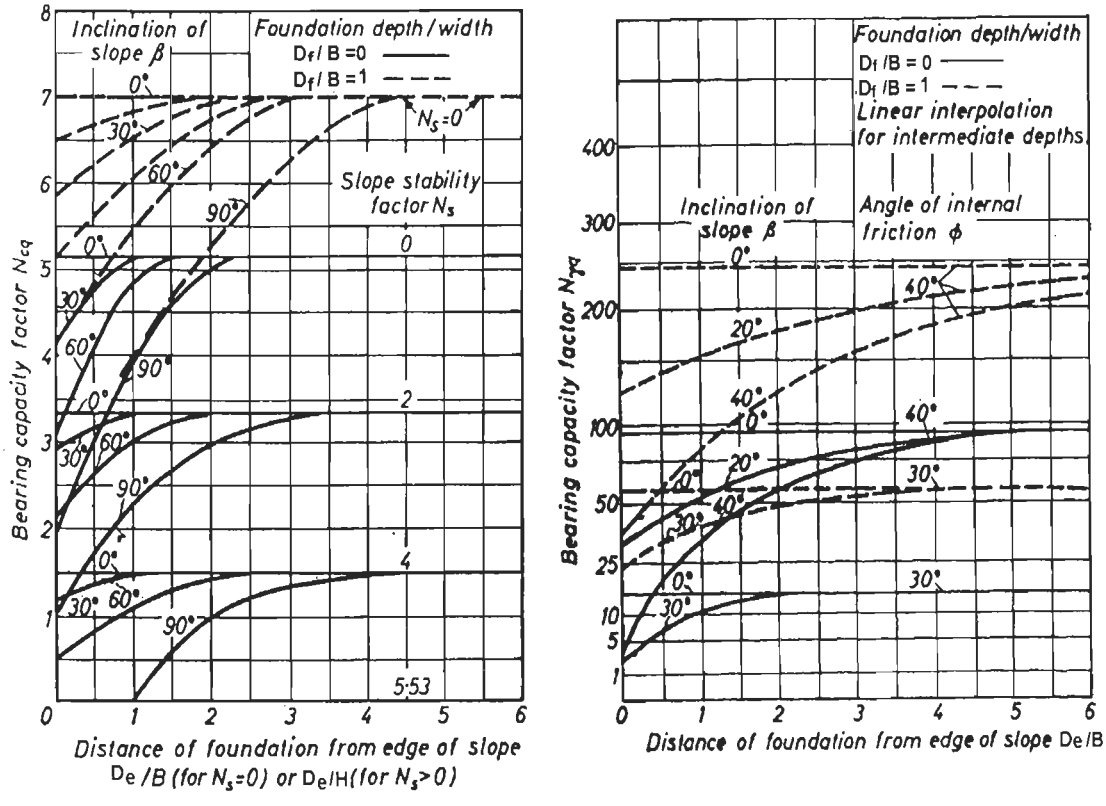

(a) (b)

Fig. 2.11 Bearing Capacity Factors for a Strip Foundation on Top of Slope for (a) Purely Cohesive and (b) Cohesionless Soil (Meyerhof, 1957)

For a surcharge on the whole horizontal top surface of the slope, a solution of the slope stability was obtained on the basis of dimensionless parameters (Janbu, 1954) and the bearing capacity was represented by the following equation:

$$q_u = cN_{cq} + \gamma D \tag{2.7}$$

where the bearing capacity factor, N_{cq} depends on D_e/B as well as β and the stability factor of the slope, N_s. It can be observed from Fig. 2.11a that the bearing capacity of foundations on top of a slope is governed by the foundation failure for a small slope height (N_s approaches zero) and by the overall slope failure for greater heights.

Mizuno et al. (1960) proposed limit equilibrium method to predict the sliding surface as well as bearing capacity of a slope of cohesionless soil under vertical central load acting on its horizontal top or berm. The sliding surface was divided into an active pressure region, a transition region and a passive pressure region as shown in Fig. 2.12. The stresses in the state of limit equilibrium at a point at a vertical depth below the sloping surface *BE*, within the passive region has been assumed as conjugate and the stresses were calculated by Mohr stress circle method. The transition region between the two zones has been divided into a number of small wedges. For these wedges, force equilibrium condition was applied successively and at the same time, the sliding surface was drawn by taking into account the sliding condition, the stress components being found by means of Mohr stress circle and the bearing capacity was determined. The relation between the slope angle, β and bearing capacity factor, $(2q/\gamma B)$ was obtained for various values of angles of internal friction, ϕ and are reproduced in Fig. 2.13 in the form of a chart. In this analysis, distance of the foundation from the edge of the slope has not been taken into account. The values of factor, N_γ given by this method are on the higher side as compared to the values given by Meyerhof (1957). The N_γ values for ϕ=40° and β=20° are 30 (Meyerhof, 1957) and 44 (Mizuno et al., 1960), respectively.

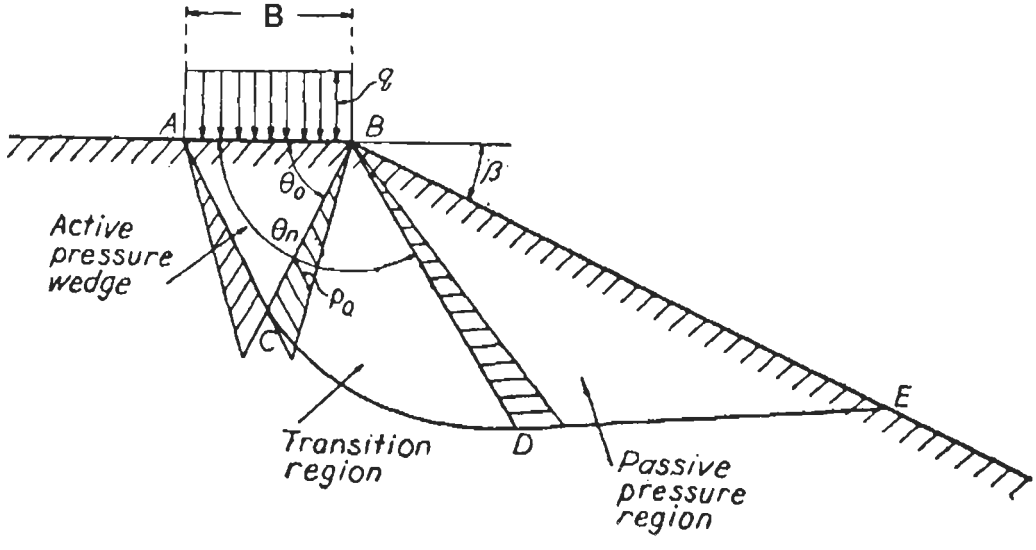

Fig. 2.12 Plastic Zone and Slip Surface (Mizuno et al., 1960)

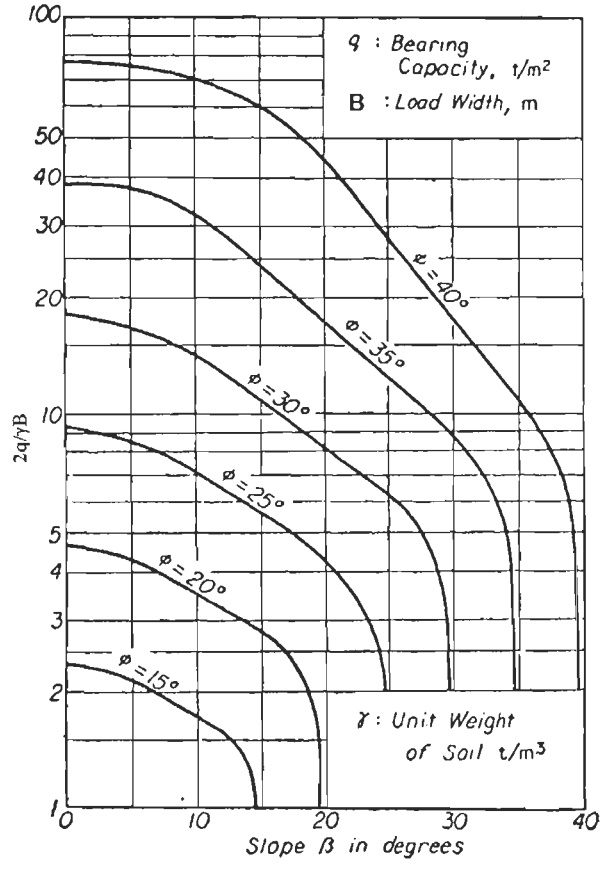

Fig. 2.13 Bearing Capacity Factors for Footing with Central Vertical Load on Top of Berm (Mizuno et al., 1960)

Siva Reddy and Mogaliah (1976) analysed the problem of a foundation on a slope from the point of view of the overall stability of the slope. The authors considered the slope failure through the toe or base under a foundation load using the friction circle method (Taylor, 1937) for c-ϕ soils possessing anisotropy and non-homogeneity in cohesion. Figure 2.14 shows the schematic diagram for the case of slope failure under a foundation load, q acting over a width, B as considered by the authors. The variation of cohesion with depth and direction were given in Eqs. 2.1 and 2.2. The authors presented the values of bearing capacity factor, N_c for purely cohesive soil (ϕ=0) for different values of N_s and compared with those given by Meyerhof (1957) as shown in Table 2.5. It is observed from this table that the values of N_c are higher than those of Meyerhof (1957), since Meyerhof's values correspond to a foundation of infinite width, while in this investigation, foundations are of finite width.

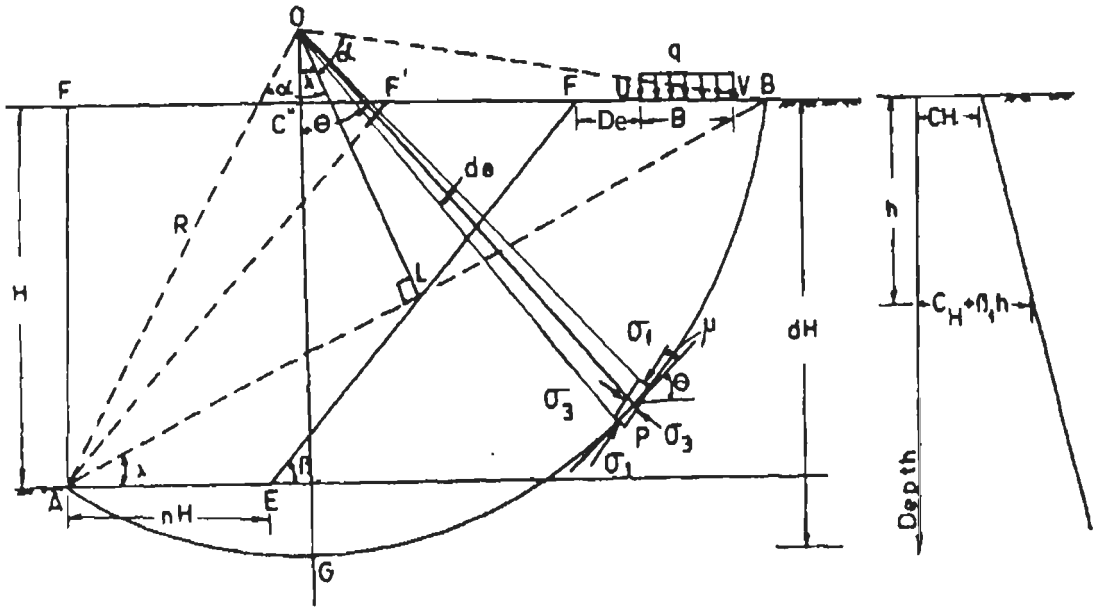

Fig. 2.14 Schematic Diagram Showing Slope Failure under a Foundation Load (Siva Reddy and Mogaliah, 1976)

Table 2.5 Comparison of N_c Values by Siva Reddy and Mogaliah (1976) and Meyerhof (1957)

$\beta°$	N_s	Siva Reddy and Mogaliah (1976)		Meyerhof (1957)
		B/H	N_c	N_c
15	5.0	0.25	0.53	0.52
60	5.0	0.25	0.67	0.1
60	4.5	0.25	1.52	0.5
75	4.5	0.25	0.18	0.0
75	4.0	0.25	1.28	0.50
75	3.5	0.25	2.10	0.75

Bowles (1977) presented tables of reduced values of bearing capacity factors N_c and N_q for estimation of bearing capacity of footings on or upper surface of slopes for central vertical loads on the basis of reduced length/area of failure envelope as compared to a flat ground. The failure surface is shown in Figs. 2.15a and b.

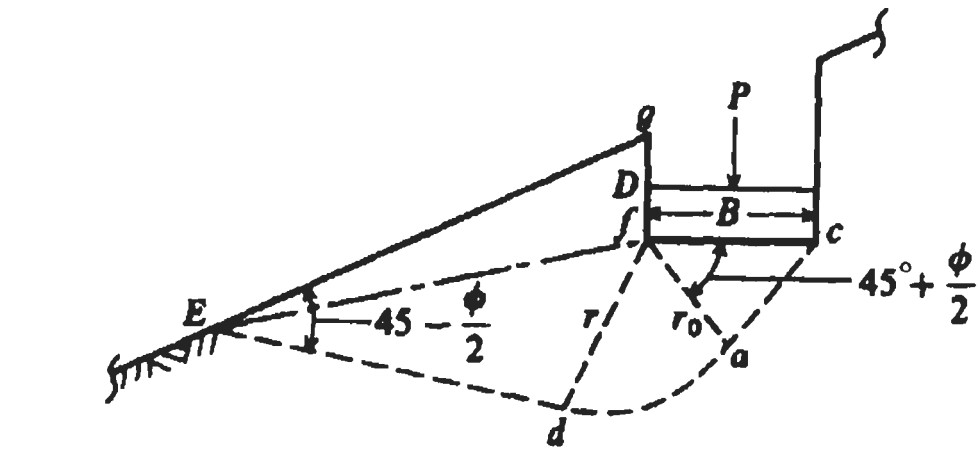

(a)

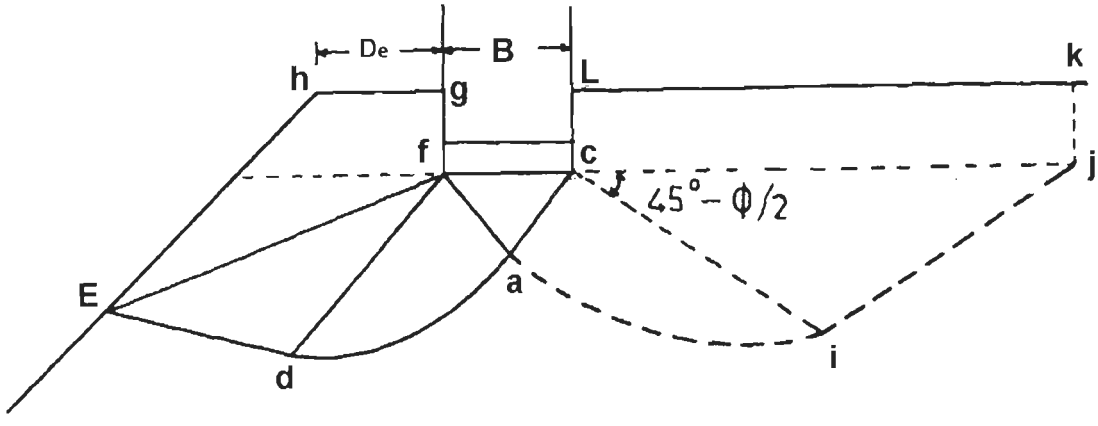

(b)

Fig.2.15 Failure Surface for Footing on Face of Slope or Upper surface of Slope (Bowles, 1977)

The angle of exit was taken as (45°-ϕ/2), since the slope line is a principal line. The value of factor, N_c has been reduced proportional to the reduction in length of the failure surface and expressed as:

$$N_c' = N_c \frac{L_s}{L'} \tag{2.8}$$

where L_s = length of failure surface for footing on slopes,

L' = length of failure surface for footing on level ground.

Similarly, factor, N_q was reduced on the basis of area under the failure envelope and expressed as-

$$N_q' = N_q \frac{A_s}{A} \tag{2.9}$$

where A_s = area *Efg*, Fig. 2.15a and area *Efgh*, Fig. 2.15b for failure surface of footing on or upper surface of slope and

A = area *cjkL*, Fig. 2.15b for footing on level ground

The other bearing capacity factor, N_γ was adjusted to N_γ' to account for the reduction in passive pressure on the slope side of the wedge, *caf* when the base is either within $D_e/B<2$ on top of slope or when $D_e/B = 0$ and expressed as-

$$N_\gamma' = \frac{N_\gamma}{2} + \frac{N_\gamma}{2}\left[R + \frac{D_e}{2B}(1-R)\right] \tag{2.10}$$

where $R = \dfrac{K_{min}}{K_{max}}$ (2.10a)

K_{min} = coefficient of Coulomb passive earth pressure on side, *af* of the slope side

K_{max} = coefficient of Coulomb passive earth pressure on side, *ca* on the flat side

Myslivec and Kysela (1978) used the graphical solution as proposed by Przedechi - Rossinski et al. (1961) for prediction of the ultimate bearing capacity of a foundation subjected to central vertical load and influenced by a slope in a c-ϕ soil.

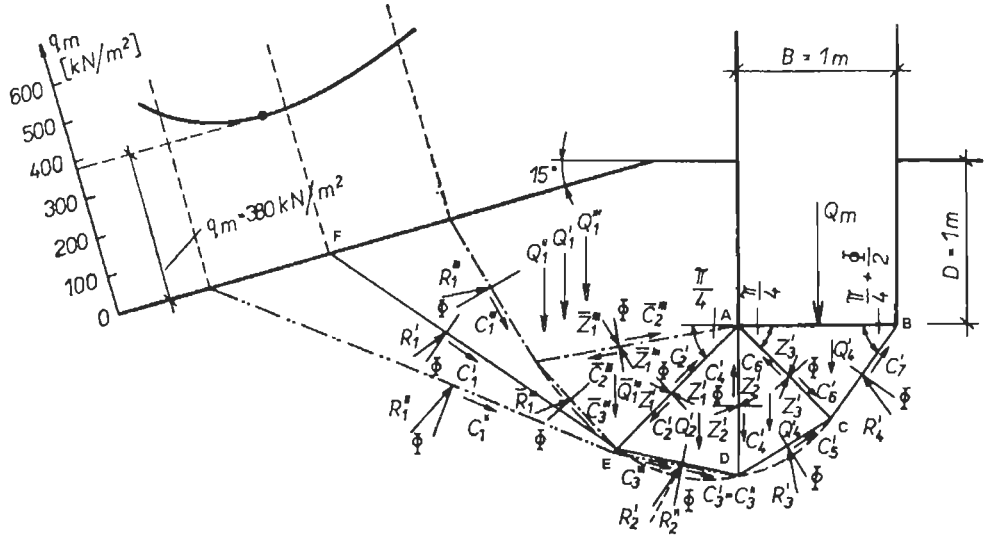

Fig. 2.16 Graphical Solution for Bearing Capacity (Myslivec and Kysela, 1978)

The solution for the ultimate bearing capacity of a foundation of width B = 1 m, D_f = 1 m and D_e/B = 0.5 and for a slope angle, β= 15° has been obtained for a soil having ϕ =20°, c = 10 kN/m^2 and γ = 20 kN/m^3 (Figure 2.16). The ultimate bearing capacity works out to be 380 kPa while Meyerhof's (1957) method predicts the value of 310 kPa, which is 23% less than the bearing capacity obtained by the graphical solution.

Saran et al. (1989) developed analytical solutions for obtaining bearing capacity of footings on upper surface of a slope for central vertical loads by applying limit equilibrium method. One sided failure was assumed to occur along the surface, *DEI* as shown in Fig. 2.17.

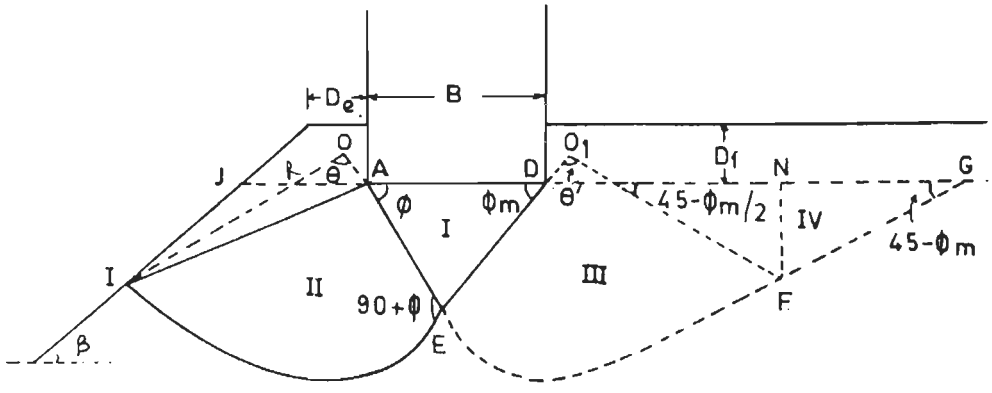

Fig. 2.17 Rapture Surface in Limit Equilibrium and Limit Analysis Approaches (Saran et al., 1989)

The failure region was divided into two zones, Zone I - an elastic region and Zone II - a combination of radial and passive shear bounded by a logarithmic spiral, *EI*. The soil on the side of the flat ground was assumed to be partially mobilized and to compute the partial resistance offered by this side, a rupture surface shown by dotted lines was considered. Bearing capacity expressions were then developed by considering the equilibrium of the elastic wedge *ADE* (Figs. 2.17 and 2.18). The forces acting on the wedge included earth pressure on the sides *AE* and *DE*, vertical load and cohesion on side *AE* and *DE*. The bearing capacity was expressed in terms of bearing capacity factors N_c, N_q and N_γ by the following expression:

$$Q_u = B\left(\frac{1}{2}\gamma B N_\gamma + \gamma D_f N_q + cN_c\right) \tag{2.11}$$

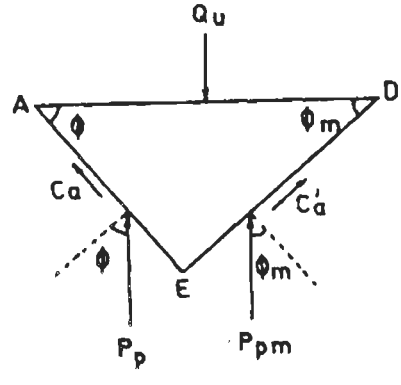

Fig.2. 18 Forces on Elastic Wedge *ADE* (Saran et al., 1989)

2.2.3 Limit Analysis Method

In contrast to slip line and limit equilibrium methods, limit analysis method considers the stress-strain relationship of soil in an idealised manner. This idealisation, termed as normality principle (or the plastic flow rule), establishes the limit theorems on which limit analysis is based. The plastic limit theorems of Drucker et al. (1952) are conveniently used to obtain the upper and the lower bounds of the collapse load. The two theorems are:

i) **Lower Bound Theorem:** If a safe and statically admissible state of stress exists for a given loading, failure does not occur under this loading. A safe and statically admissible state of stress is one in which the stress distribution satisfies the equilibrium condition under the given loads, and in which the stresses are less than the yield stress at every point. The lower bound technique considers only the equilibrium and the yield. It gives no consideration to soil kinematics.

ii) **Upper Bound Theorem:** If a kinematically admissible failure state can be found for any loading, failure must impend or must have taken place already. The loads are determined by equating the external rate of work to the internal rate of dissipation of energy in an assumed deformation mode (or velocity field) that satisfies: a) velocity boundary conditions and b) strain and velocity conditions which are not less than the actual collapse load. The dissipation of energy during plastic flow associated with such a field can be computed from the idealised stress-strain rate relation. A velocity field satisfying the above conditions has been termed as a kinematically admissible velocity field. The upper bound technique considers only the velocity or failure modes and energy dissipation. The stress distribution need not be in equilibrium and is only defined in the deforming regions of the mode.

Many stability problems have been solved using this method by many investigators such as Drucker and Prager (1952), Finn (1967), Chen (1975). Chen (1975) has used Prandtl type of failure mechanism to calculate the bearing capacity factor, N_γ by limit analysis for footings on slopes with central vertical loads. The chart giving the values of N_γ computed for slope angle varying from 0 - 30° and friction angle, ϕ ranging from 10° to 45° has been reproduced in Fig. 2.19. The difference between this upper bound limit analysis and Meyerhof (1957) method ranges from 1.5 to 45 percent.

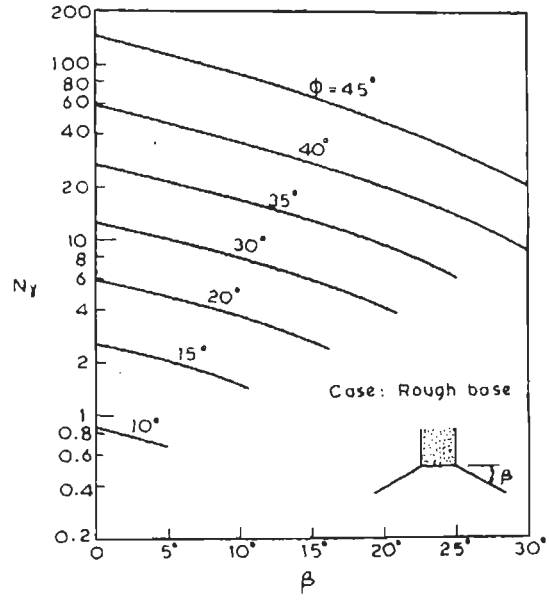

Fig. 2.19 Bearing Capacity Factors N_γ (Chen, 1975)

Kusakabe et al. (1981) calculated the bearing capacities of slopes loaded with central vertical loads on top surfaces by using the upper bound theorem of limit analysis. The authors considered the failure mechanism consisting of a triangular active wedge, *DCE*, a logarithmic spiral, *BC* and a straight line, *AB* joining the log spiral smoothly and intersecting the inclined surface of the slope at point, A (Fig. 2.20). Equating the rate of internal energy dissipation to the rate of external work, the investigators obtained the following equation:

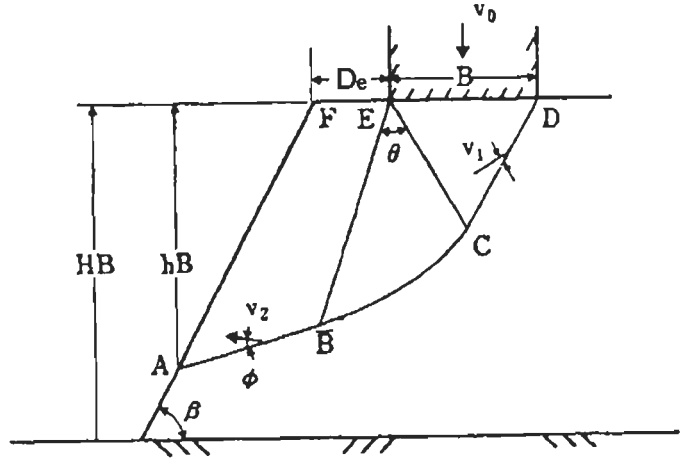

Fig. 2.20 Failure Mechanism (Kusakabe et al., 1981)

$$q_u = cN_c + \frac{\gamma B}{2} N_\gamma \qquad (2.12)$$

where

$$N_c = \frac{1}{2\cos\left(\frac{\pi}{4}+\frac{\phi}{2}\right)\sin\left(\frac{\pi}{4}-\frac{\phi}{2}\right)} \times \{\cos\phi + \cot\phi(\exp(2\theta_0 \tan\phi) - 1)\} + \frac{\overline{AB}\cos\phi\exp(\theta_0 \tan\phi)}{B\sin\left(\frac{\pi}{4}-\frac{\phi}{2}\right)} \tag{2.13}$$

$$N_\gamma = -\frac{1}{2}\tan\left(\frac{\pi}{4}+\frac{\phi}{2}\right) - \frac{2\cos\left(\frac{\pi}{4}+\frac{\phi}{2}+\theta_0\right)\exp(\theta_0 \tan\phi)S}{B^2\sin\left(\frac{\pi}{4}-\frac{\phi}{2}\right)} - \frac{1}{4\cos^2\left(\frac{\pi}{4}+\frac{\phi}{2}\right)\sin\left(\frac{\pi}{4}-\frac{\phi}{2}\right)(9\tan^2\phi+1)} \times \left\{ \begin{array}{l} \exp(3\theta_0 \tan\phi)\left(3\tan\phi\cos\left(\frac{\pi}{4}+\frac{\phi}{2}+\theta_0\right)+\sin\left(\frac{\pi}{4}+\frac{\phi}{2}+\theta_0\right)\right) \\ -\left(3\tan\phi\cos\left(\frac{\pi}{4}+\frac{\phi}{2}\right)+\sin\left(\frac{\pi}{4}+\frac{\phi}{2}\right)\right) \end{array} \right\} \tag{2.14}$$

where S is the area of the quadrilateral $ABEF$. The solution to this problem was obtained by the authors numerically. The bearing capacity normalized with respect to γB was plotted against the normalized height as shown in the Fig. 2.21 and the curve yielding the minimum value was taken as an upper bound solution. The authors presented the comparison of values of bearing capacity thus obtained with those by other investigators as presented in Table 2.5.

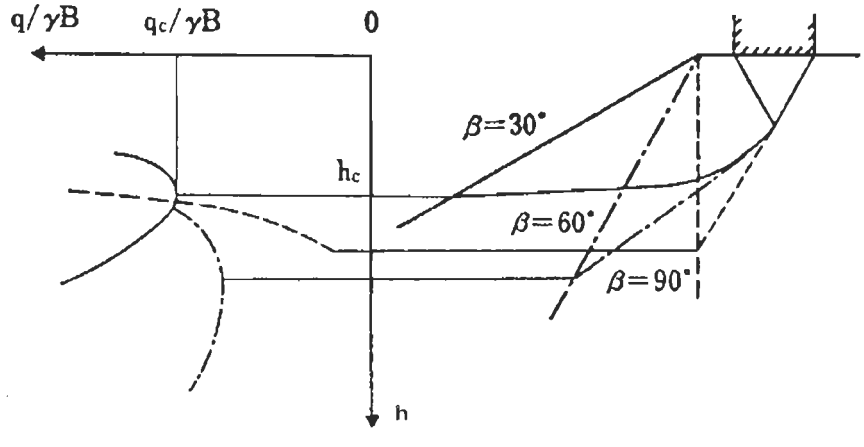

Fig. 2.21 Critical Values of ($q/\gamma B$) and Failure Surface for Various Slope Inclinations (Kasukabe et al., 1981)

Table 2.6 Comparison of Bearing Capacity Obtained by Kasukabe et al. (1981) with other Investigators

D_e/B	ϕ in degree	$c/\gamma B$	$q/\gamma B$				
			Kusakabe (1981)	**Bishop (1955)**	**Fellenius (1927)**	Kotter **(1903)**	**Lower Bound**
0	0	25.0	102.0	103.0	103.0	102.0	89.58
0	0	5.0	20.2	20.5	20.5	20.4	17.82
0	0	1.0	3.84	3.95	3.95	3.98	3.61
0	0	0.5	1.78	1.42	1.42	----	1.68
0	30	25.0	395.0	439.0	276.0	----	159.2
0	30	5.0	81.0	88.0	58.3	81.2	32.11
0	30	1.0	18.3	17.1	12.9	18.2	6.86
0	30	0.5	10.3	11.3	7.45	10.2	3.84
0.4	30	1.0	20.7	20.4	14.0	----	8.72
0.8	30	1.0	23.2	27.9	16.3	----	8.85
1.0	30	1.0	24.4	28.3	16.5	----	9.2
2.0	30	1.0	30.0	32.0	19.5	----	12.12

It is observed from the Table 2.6 that the bearing capacity values given by Kotter's and Bishop's slice method compares well with the values predicted by Kusakabe et al. (1981), while Fellenius method gives values less than those of upper bound theory.

Saran et al. (1989) developed analytical solutions for obtaining the bearing capacity of a footing on upper surface of the slope by applying limit analysis method for central vertical loads. The bearing capacity equation was obtained by equating the total rate of energy dissipated to the total rate of work done and expressed as:

$$q_u = \frac{1}{2}\gamma B N_\gamma + \gamma D_f N_q + cN_c \qquad (2.15)$$

where N_c, N_q and N_γ are the bearing capacity factors which depend upon the slope angle, β, friction angle, ϕ, distance of the foundation from the edge of the slope, D_e and the depth of the foundation, D_f. The authors have developed design charts for these factors which are reproduced in Figs. 2.22 a, b and c respectively.

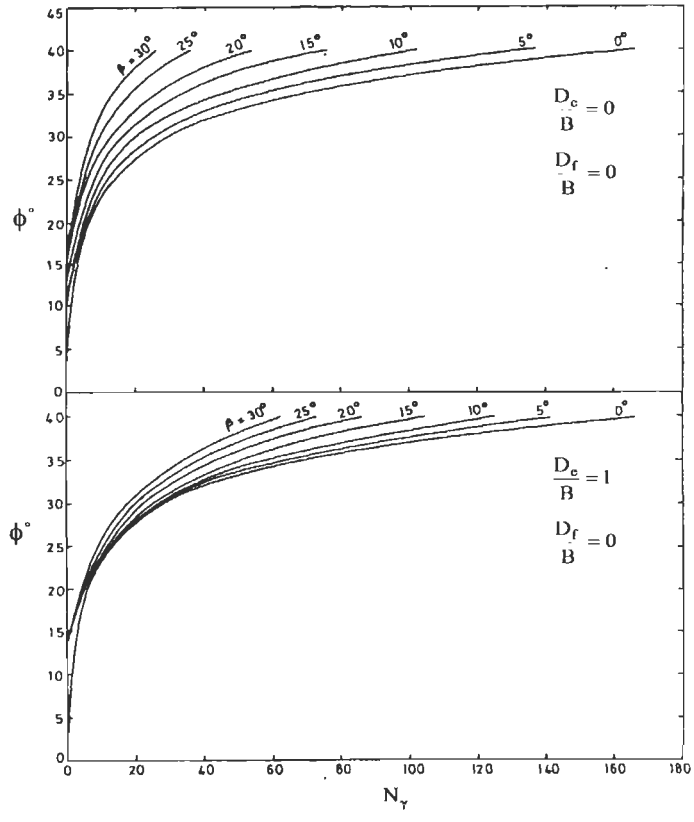

Fig. 2.22 a Design Chart for N_γ for $D_f/B = 0$ and $D_e/B = 0$, 1.0 (Saran et al., 1989)

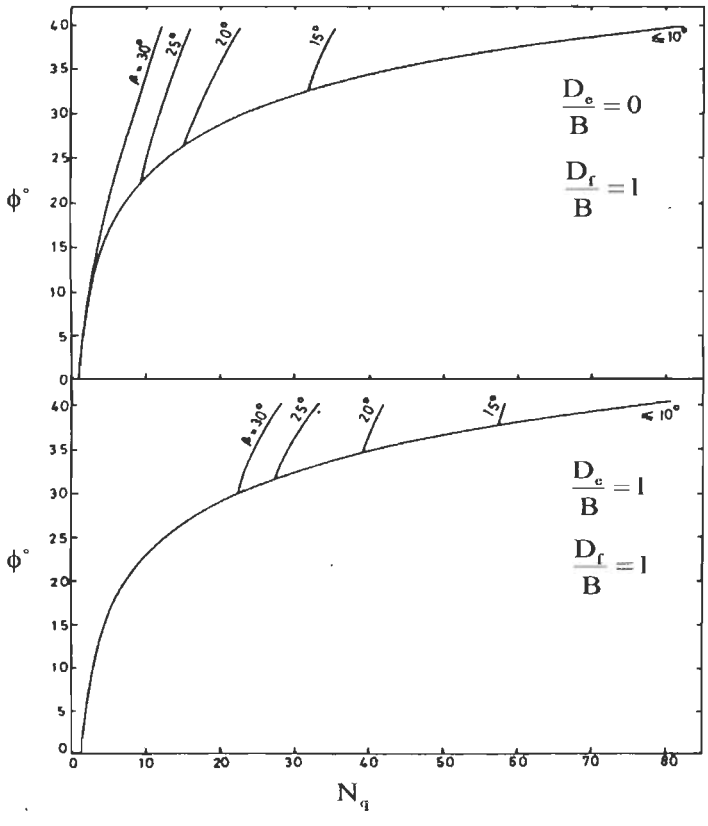

Fig. 2.22b Design Chart for N_q for D_f/B =1.0 and $D_e/B = 0$, 1.0 (Saran et al., 1989)

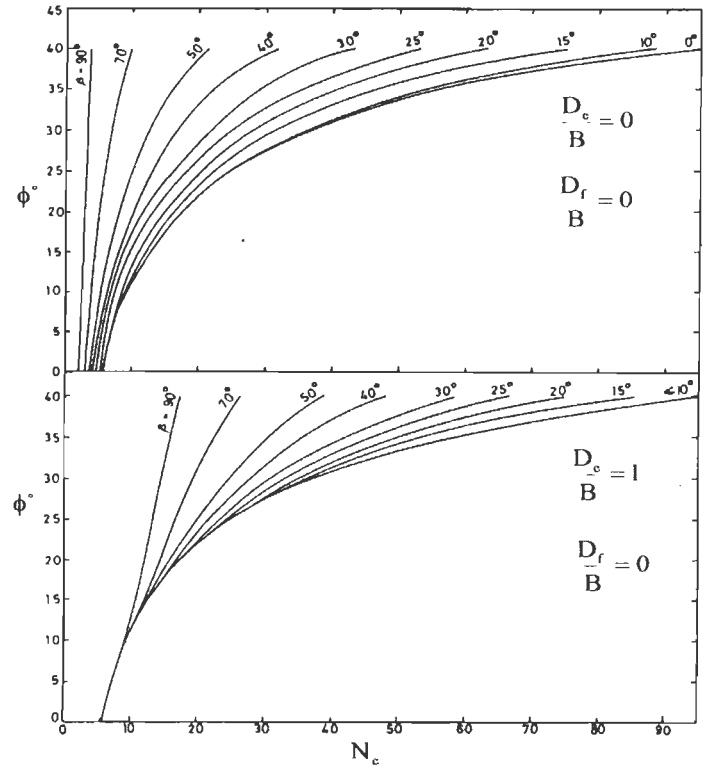

Fig. 2.22 c Design Chart for N_c for D_f/B=0.0 and D_e/B = 0, 1.0 (Saran et al., 1989)

A comparison of the values of N_γ obtained by the authors with earlier investigators is presented in Table 2.7. It can be observed that values predicted by the authors are, in most cases, higher than the values of the earlier investigators.

Table 2.7 Comparison of N_γ Values of Saran et al. (1989) with other Investigators

ϕ	β	D_e/B	D_f/B	Meyerhof (1957)	Mizuno (1960)	Siva Reddy & Mogaliah (1975)	Chen (1975)	Saran et al. (1989)
40°	30°	0.0	0.0	20.	17.0	-	19.5	25.37
40°	30°	1.0	0.0	40.0	--	-	-	62.20
40°	20°	0.0	0.0	34.0	44.0	-	55.0	53.47
40°	20°	1.0	0.0	55.0	-	-	-	85.98
40°	20°	2.0	0.0	70.0	-	-	-	121.22
40°	20°	0.0	1.0	125.0	-	-	-	168.00
30°	30°	0.0	0.0	3.1	-	5.01	-	6.14
30°	20°	0.0	0.0	7.5	8.0	-	10.	11.61
30°	15°	0.0	0.0	10.0	11.0	13.76	12.0	15.25
30°	15°	0.0	0.68	30.0	-	33.60	-	32.20

Xiao et al. (2007) used energy dissipation method to obtain the bearing capacity of footings on a sloping ground for vertical central load. A multi wedge failure mechanism as shown in Fig. 2.23 was used to calculate the bearing capacity factors of a strip footing. The potential sliding soil mass was divided into a number of triangular wedges using a series of inclined straight lines and each triangular wedge was assumed to move as a rigid wedge. Equating the work done by the external load to the rate of internal energy dissipation, the bearing capacity was calculated and expressed as:

$$q_u = cN_c + q_0 N_q + 0.5\gamma BN\gamma \tag{2.16}$$

where N_c, N_q and N_γ are bearing capacity factors which depend on slope angle, β and soil friction angle, ϕ. The investigators developed design charts for these factors which are presented in Figures 2.24 a, b, and c. In this analysis, the distance of the foundation from the edge of the slope was not taken into consideration and it is applicable to situations with central vertical loads only.

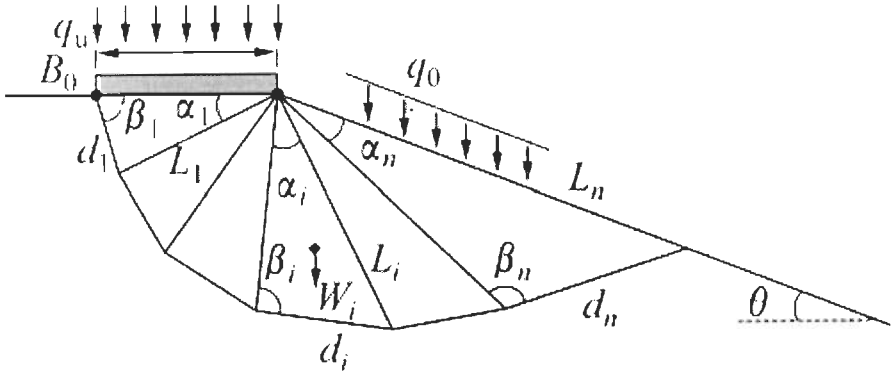

Fig. 2.23 Failure Mechanism (Xiao et al., 2007)

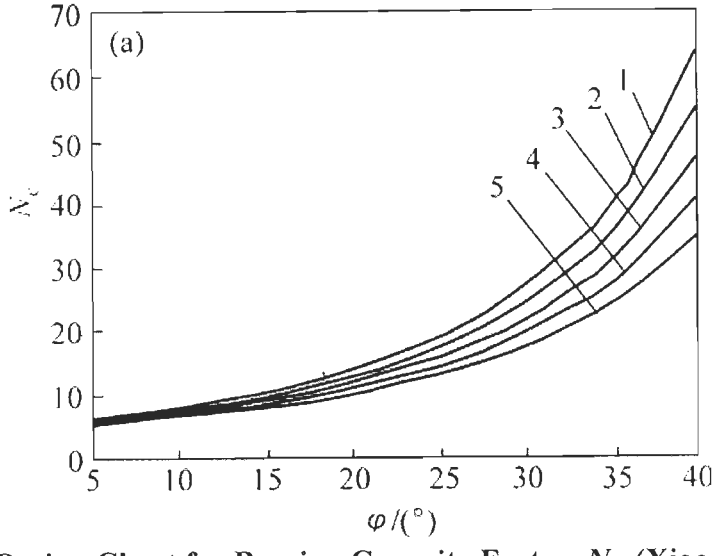

Fig. 2.24 a Design Chart for Bearing Capacity Factor, N_c (Xiao et al., 2007)

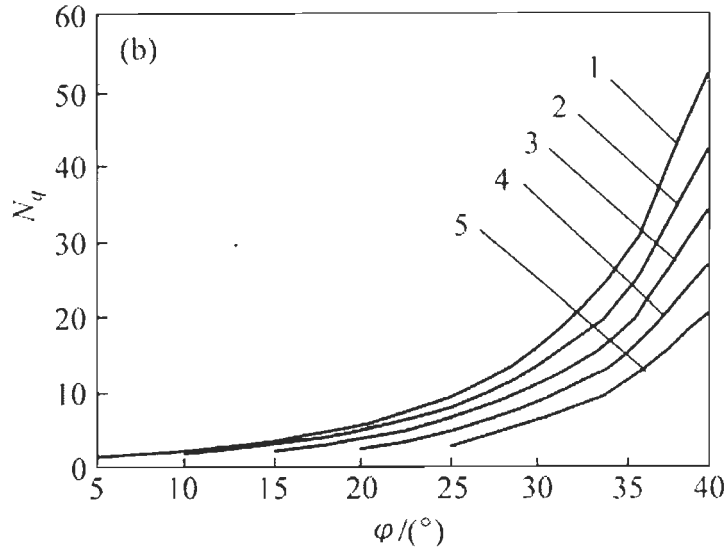

Fig. 2.24 b Design Chart for Bearing Capacity Factor, N_q (Xiao et al., 2007)

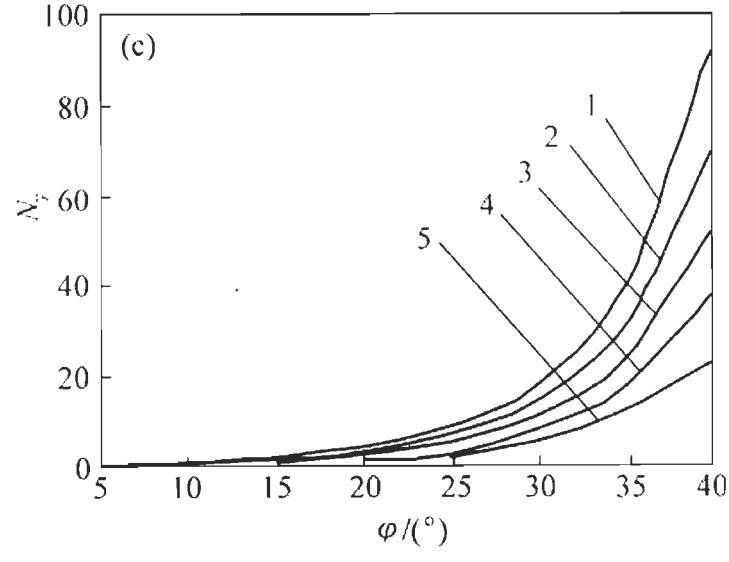

Fig. 2.24 c Design Chart for Bearing Capacity Factor, N_γ (Xiao et al., 2007)
Slope Angle θ °: 1 -5°, 2 – 10°, 3 -15°, 4 – 20°, 5 – 25°

2.2.4 Finite Element Method

Arduino et al. (1994,1998) analysed the problem of the bearing capacity of footings on slopes subjected to central vertical load only by finite element method and compared the results with those of classical bearing capacity theories and centrifuge model tests. To simulate the non-linear characteristics of the granular material, the authors proposed a new constitutive model namely MRS-Lade model. This model was pressure sensitive, three stress invariants dependent, cone-cap elasto-plastic model. The material parameters were obtained by physical calibration by using

conventional triaxial compression test data from three tests and one isotropic compression test data. The selected prototype slope geometry (Fig. 2.25 a) and load conditions were simulated by an appropriate finite element discretization with 9-noded isoparametric finite elements as shown in Figures 2.25 b and c. From the analysis, the ultimate bearing capacity was predicted as 1044.46 kPa and the same from the centrifuge model test was obtained as 1072.92 kPa. The authors concluded that since the finite element method gave both the ultimate bearing capacity and the settlement, it is a better method.

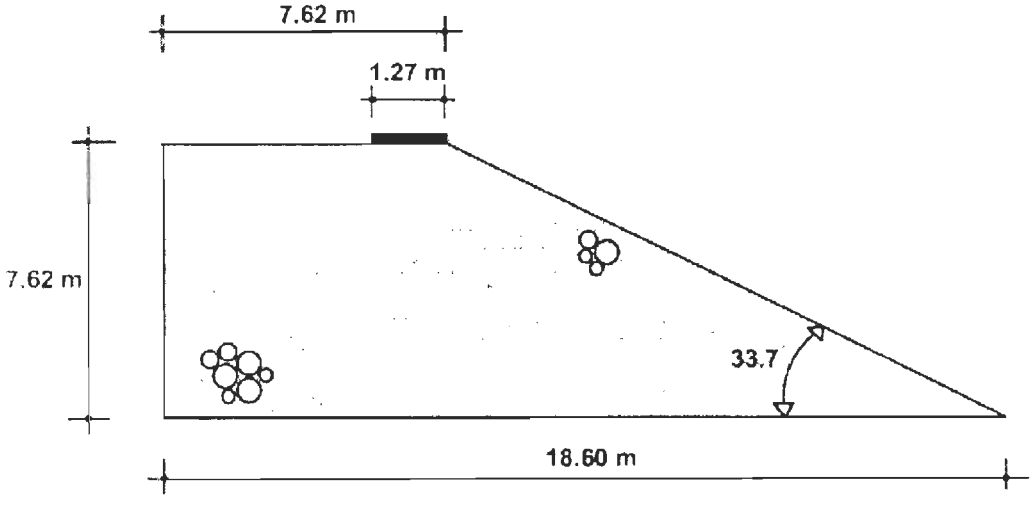

(a)

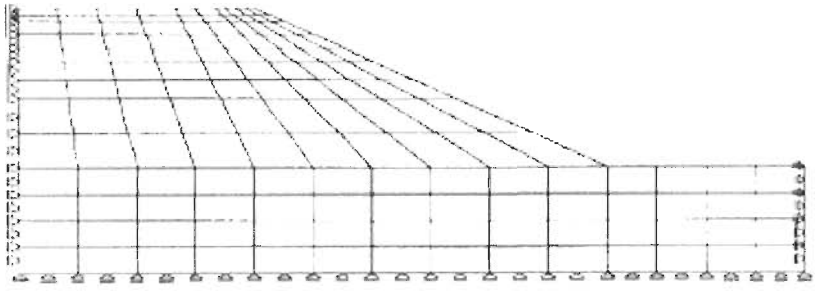

(b)

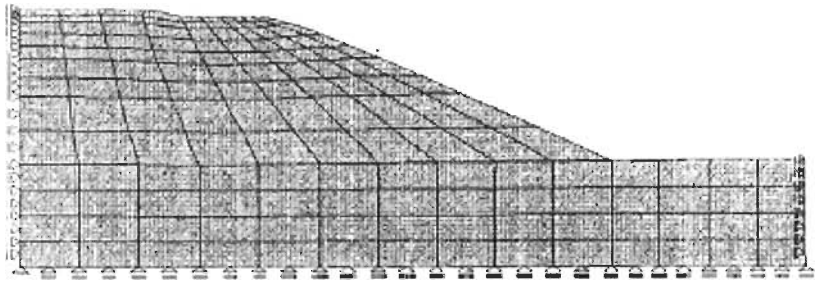

(c)

Fig.2.25 a) Prototype Slope, b) Undeformed and c) Deformed Mesh Showing Slope and Boundary Conditions (Pedro Arduino et al., 1994, 1998)

Jao et al. (2001, 2008) studied the performance of strip footings situated on top of a slope and subjected to central vertical or eccentric vertical loading using a two dimensional plane-strain elasto-plastic finite element method. In the analysis, the foundation soil was idealised as an elastic-perfectly plastic material. Within the elastic range, Duncan-Chang hyperbolic stress-strain law was used whereas, Drucker-Prager yield criterion was employed to model the plastic behaviour. The slopes analysed were i) 18.4° (3H: 1V), ii) 26.6° (2H: 1V), and iii) 45° (1H: 1V) with a height of 7.3m. The strip footing was parallel to the slope with its centre located at 1.4, 2.3, 3.2, 4.1, 5 and 5.9 m from the slope crest. The computer analyses were performed for three loading conditions, i.e., e = 0, -*B*/6 (on the slope side) and +*B*/6 (off the slope side). The finite element mesh adopted for analysis and the growth of the yield zone are shown in Figs. 2.26 a and b.

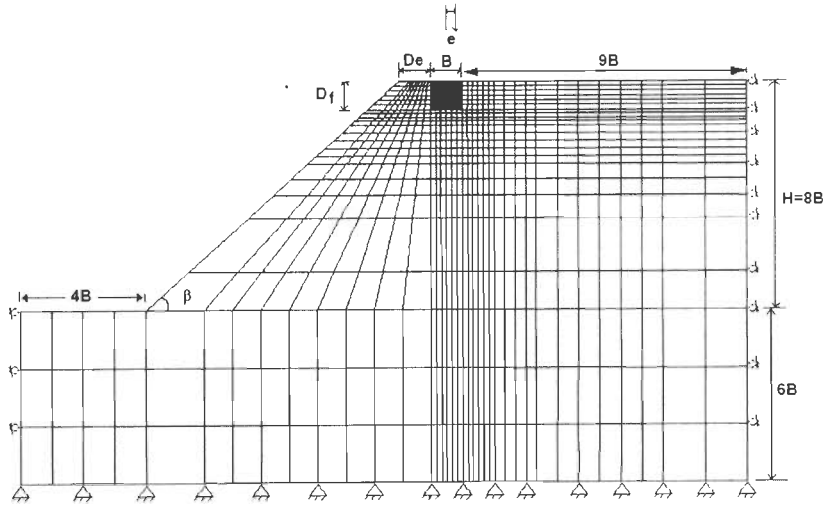

(a)

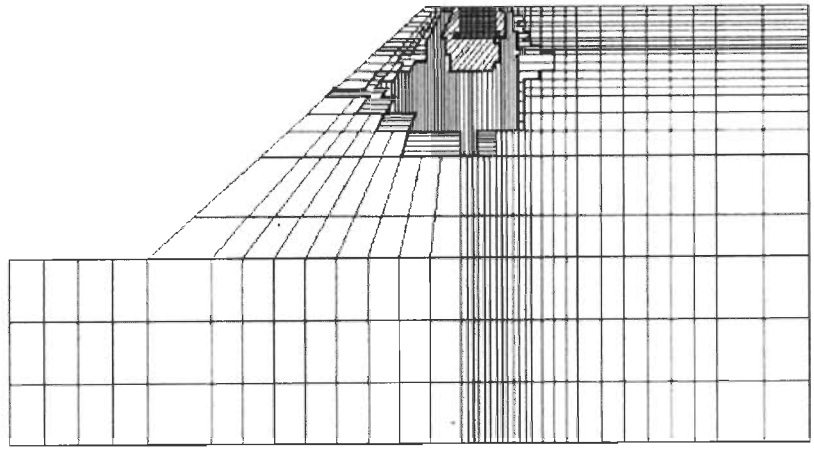

(b)

Fig.2.26 a) Undeformed Mesh and b) Growth of the Yield Zone for Strip Footings on a Slope (Jao et al. 2001, 2008)

In this study, the ultimate bearing capacity was taken as the smaller of the following two values:

i) On the curve relating footing pressure to the area of yielded soil elements, the pressure beyond which the slope of the curve attains a minimum constant value; it is a criterion proposed by Wang et al. (1994).

ii) The pressure under which the yielding soil spreads to the face of slope as illustrated in Fig. 2.26b.

The variation of bearing capacity thus obtained with change in the distance from the crest of slope and the change in the slope angle are reproduced here in Figs. 2.27a and b respectively. The results of analysis show that both progressive soil yielding and the ultimate bearing capacity are greatly affected by the load eccentricity. The ultimate bearing capacity is significantly greater for the load that acts on the slope side than on the other side of the footing centre. Furthermore, for a 2(H): 1(V) slope in silty clay, the influence of slope on the footing behaviour decreases with increasing distance between the footing centre and the slope crest, and disappears when the distance reaches about 5-times the footing width.

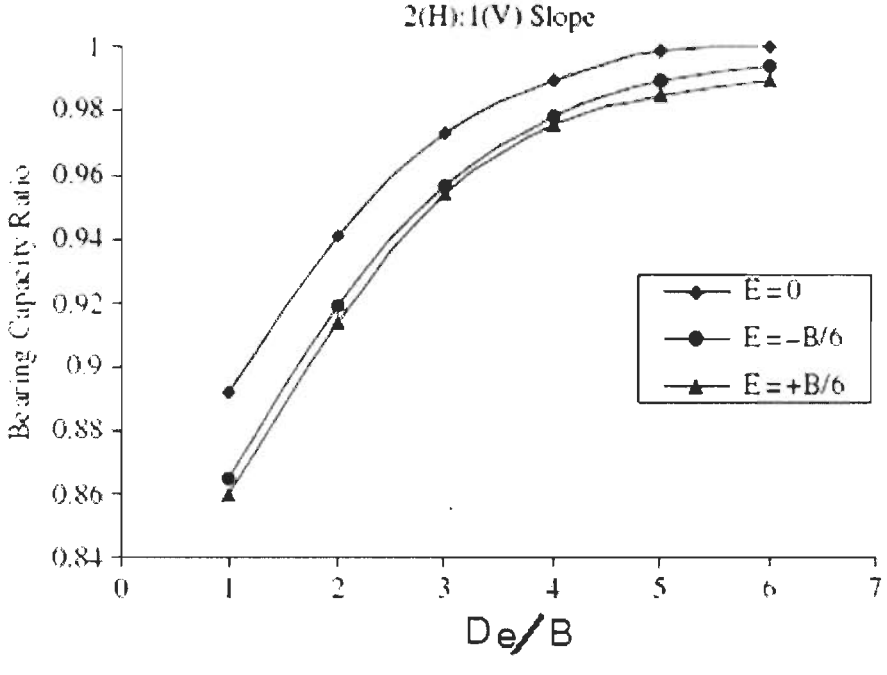

Fig. 2.27 a Variation of Bearing Capacity Ratio with D_e/B (Jao et al. 2008)

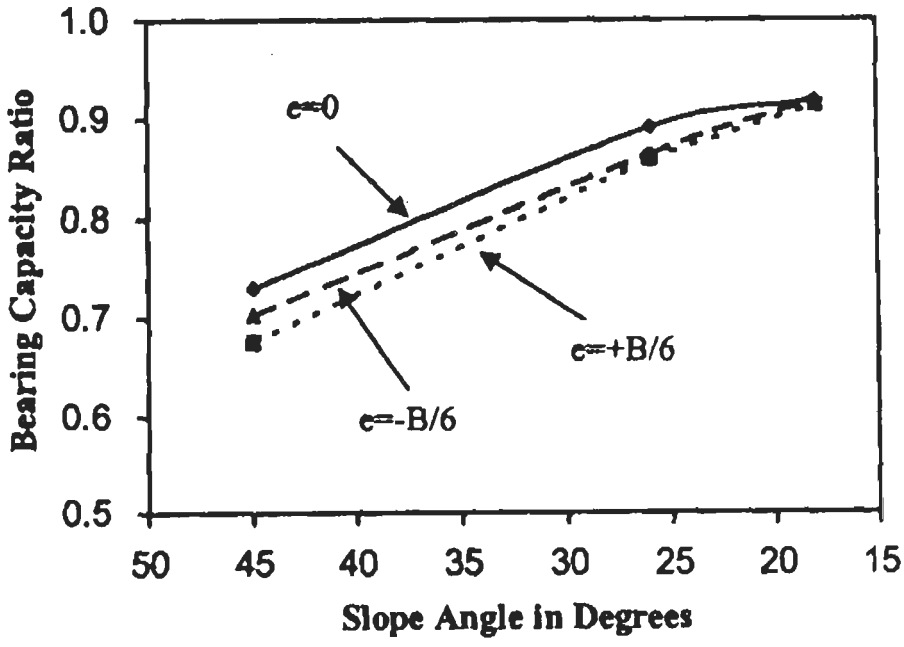

Fig. 2.27b Variation of Bearing Capacity Ratio with Slope Angle (Jao et al. 2001)

Liu et al. (2006) simulated the problem of bearing capacity and deformation behaviour of a strip footing on sand slope subjected to central vertical load by finite element method. Figure 2.28 shows the mesh and boundary conditions of the slope model.

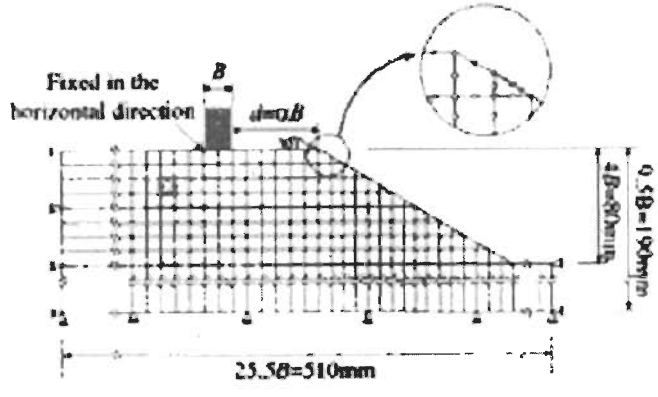

Fig.2.28 Mesh and Boundary Condition (Liu et al., 2006)

An eight-noded isoparametric quadrilateral element with reduced two-point Gaussian integration was employed. A newly developed constitutive model, the MMX- model, which was based on a double yield surface theory, was used. The investigators compared the analytical results with experimental model tests and concluded that the relationship between bearing capacity and settlement of slope obtained through finite element analysis agreed well with experimental data. The bearing capacity became

independent of the slope when the footing was placed far away i.e more than 10B from the crest of the slope.

2.3 CONSTITUTIVE LAWS FOR SOILS

The behaviour of soils over a wide range of stresses is non-linear, inelastic and dependent upon the magnitude of the confining pressure. To estimate the settlement of soils under a foundation load, it is essential to represent accurately the laboratory or field stress-strain curves in a form suitable for easy incorporation in the analysis. Constitutive laws of soil define the relation between the physical quantities such as stress, strain and time. Various factors influencing the constitutive laws of soil include physical properties of soils, sample size, moisture content and density, confining pressure, intermediate principal stress, rate of strain and stress history, and it is difficult to establish a general law which takes into account all these factors. Therefore, laboratory testing under simulated field conditions is done to establish the constitutive laws for a given foundation soil. Various but limited simplified mathematical models which take into account the non-linearity, stress dependency and inelasticity have been described below:

i) Bilinear and Multi-linear Models

The simplest type of nonlinear model is the bilinear one. The material has initial Young's modulus until the stresses reach a yield value, after which the modulus is changed. The non-linear curve can also be divided into a number of linear curves known as multi-linear or piecewise linear models.

ii) Hyperbolic Functions

Kondner (1963) and Kondner and Zelasko (1963) have found that the non-linear stress-strain curve of both clay and sand obtained in a triaxial test can be represented by hyperbolae of the following form:

$$\frac{\varepsilon}{\sigma_1 - \sigma_3} = a + b\varepsilon \tag{2.17}$$

or $$\varepsilon = \frac{a(\sigma_1 - \sigma_3)}{1 - b(\sigma_1 - \sigma_3)} \tag{2.18}$$

where ε = axial strain

a, b = constants of hyperbola

The plot of $\varepsilon/(\sigma_1-\sigma_3)$ versus ε gives a straight line, where a is the intercept on the Y axis and b is the slope of the line. At a very small strain,

$$\sigma_1-\sigma_3=\frac{\varepsilon}{a} \tag{2.19}$$

so that $\frac{1}{a}$ represents the initial tangent modulus E_i. At very large strains, the relation becomes

$$\sigma_1-\sigma_3=\frac{1}{b} \tag{2.20}$$

so that $\frac{1}{b}$ is the ultimate deviatoric strength which is larger than the failure strength. This is expected since the failure compressive strength at all finite values of strain will be reached before the curve becomes asymptotic.

Duncan and Chang (1970) have used hyperbolic form of functions to simulate stress-strain curves in terms of shear strength and initial tangent modulus as given below:

$$E_t=E_i\left[1-\frac{R_f(\sigma_1-\sigma_3)(1-\sin\phi)}{2\sigma_3\sin\phi+2c.\cos\phi}\right]^2 \tag{2.21}$$

where E_t = tangent modulus and R_f is the failure ratio given by-

$$R_f=\frac{(\sigma_1-\sigma_3)_f}{\sigma_u} \tag{2.22}$$

The initial tangent modulus, E_i has been found to vary with the confining pressure according to the following expression (Janbu, 1963):

$$E_i=k.P_a\left(\frac{\sigma_3}{P_a}\right)^n \tag{2.23}$$

where P_a is atmospheric pressure. The values of constants, k and n can be readily determined. The main limitation of the hyperbolic simulation is that it is valid only for stress below the peak stress-strain curve, usually for monotonically increasing loads.

iii) Parabolic Functions

Hansen (1963) proposed two functional representations of stress-strain relationships.

$$(\sigma_1-\sigma_3)=\left(\frac{\varepsilon}{a+b}\right)^{1/2} \tag{2.24}$$

$$(\sigma_1 - \sigma_3) = \frac{\varepsilon^{1/2}}{a + b} \qquad (2.25)$$

The first equation accounts for the possibility of parabolic variation of stress-strain curves at small strains. The second equation is an alternative form to account for the parabolic variation and possesses the property of giving a maximum value of $(\sigma_1 - \sigma_3)$ for finite strain. Hansen (1963) used one of the data from Kondner (1963) and compared the stresses obtained from the above equations and found that if the stress-strain curve is initially parabolic, Eq. 2.24 is better and if it shows work softening, Eq.2.25 should be used.

iv) Spline Functions

Desai (1971) used cubic spline functions to define analytically the curve drawn through a number of data points. A spline function approximates a given stress-strain, non-linear curve by a number of polynomials of a given degree spanning a number of nodes or data points.

Many other constitutive models have been developed by different investigators for use in finite element or finite difference calculations. Some of the important models are: Modified Drucker-Prager/Cap Model (Drucker et al., 1957), Modified Cam-Clay model (Burland, 1965), Single Hardening model (Lade et al., 1988), Plaxis Soft Soil model (Brinkgreve and Vermeer, 1977), Plaxis Hardening model (Brinkgreve and Vermeer, 1977) etc.

No soil can be accurately modelled by any stress strain law, partly because of the complexity of its behaviour and partly because of its variability in the ground (Naylor, 1978). In the present investigation, a simple and an acceptable model as proposed by Kondner (1963) has been adopted for predicting the settlement behaviour of footings.

2.4 MODEL TESTS

Many investigators have conducted model tests for studying the behaviour of foundations on slopes. Most of these tests were for foundations on slopes subjected to central vertical loads. Peynircioglu (1948) performed series of model tests in a box measuring 550×330×260 mm, the size of the test plate was 256×75 mm and the main conclusions were

i) Almost in all the tests, the formation of the sliding wedge occurred on one side of the fill.

ii) The observed values of the angle of triangular wedge were found to lie between ϕ and $(45°+\phi/2)$

iii) The surface of sliding in a uniform sand mass produced by a strip load consisted of a curved part and a straight part. The observed curved part coincided practically either with an arc of a circle or a logarithmic spiral.

Shields et al. (1977, 1981).reported the results of experiments conducted to measure the ultimate bearing capacity of footings placed at various locations within a granular slope. The authors also studied the scale effect and the influence of load inclination on the bearing capacity of footing on slopes. The tests were conducted in a sand box measuring 15 m in length, 2 m in width and 2.2 m in height. The tests were performed on a 0.3 m wide footing stretching across the 2 m width of the box to create a two dimensional loading case. Few tests were also conducted with a 0.6 m wide footing to study the scale effects. The sand used in the test series consisted of a specially crushed uniformly graded quartz material. The sand was deposited in an air dry condition by means of a rotating drum spreader. Tests were conducted at relative densities of 70% and 90% and on a standard slope of 2 horizontal to 1 vertical. The bearing capacity factor, $N_{\gamma q}$ was back calculated from the experimental data by the following equation and then compared with Meyerhof's (1957) theoretical values:

$$N_{\gamma q} = \frac{2q_{ult}}{\gamma B} \tag{2.26}$$

The authors concluded that Meyerhof's (1957) theory in general gives higher value of bearing capacity as compared to experimental results. However, at shallow depths close to the crest of the slope, the theory is closer to the actual bearing capacity. For a footing with an inclined load, the experimental results were compared with the inclination factor as suggested by Meyerhof (1963) namely,

$$i_\gamma = \left(1 - \frac{i}{\phi}\right)^2 \tag{2.27}$$

where i = angle of load inclination from vertical and ϕ, the angle of frictional resistance.

On an average, inclination factors from the experimental results were 0.28 and 0.53 for 300 mm and 600 mm wide footings respectively. The same factor when

computed using Meyerhof's (1963) theory works out to be 0.44, which falls between the two experimental average values.

Kusakabe et al. (1981) carried out model tests to study the applicability of their theory. A steel container of size 500 mm long, 125 mm wide and 300 mm high was used for the experiments. Load was applied to the model through a 50 mm wide rigid loading plate using a manually operated loading jack. Soil used was a c- ϕ soil having the following properties:

Specific gravity	= 2.86
Liquid limit	= 87.0%
Plastic limit	= 37.5%
Apparent cohesion in terms of effective stress	= 1.5kN/m^2
Angle of shear resistance in terms of effective stress	= 30.3°

The undrained strength of the c–ϕ soil as measured was in the range of 8 kN/m^2 to 10 kN/m^2. The load tests were performed under the plane strain condition by applying the settlement at a rate of 1 mm per minute until the total settlement reached 10 mm. The experimental values of bearing capacity were in general about 30% higher than the theoretically predicted values. The difference in the values was explained on the basis of the fact that the loading tests were conducted under plane strain condition, while the values of undrained shear strength were obtained from the unconfined compression tests under axi-symmetrical condition and the existence of friction between the sample and the wall of the container.

Saran et al. (1989) conducted tests to study the behaviour of footings on slopes. The tests were performed in a sand box, 3 m long, 0.6 m wide and 0.9 m high. Dry Ranipur sand at two relative densities of 84% and 72% was used. The angles of shearing resistance of sand at the two relative densities were obtained by performing drained triaxial tests, and the corresponding values were 39° and 37.5° respectively. A box type footing, 120 mm wide and 600 mm long was used and the tests were conducted on three slopes with angles of 30°, 26.56° and 20° and at seven different edge distances. Pressure-settlement characteristic of the footing was obtained in each test and failure pressure was then computed using intersection tangent method. The authors compared these results with their theoretically predicted values and concluded that there was a good agreement among them.

Borthakur et. al. (1988) reported the results of the experimental work conducted with a strip footing placed on the top of a non-cohesive soil slope with varying slope inclination and footing placed at various edge distances. A test box measuring 1.21m x 0.6 m x 0.5 m with Perspex sheet as side wall was used for the experiments. The test bed was prepared by placing local sand at a density of 15.20 kN/m^3. Two model footings of size, 71 mm × 580 mm and 58 mm × 472 mm were used for conducting the tests. Load tests were carried out with slope angles of 0°, 10°, 15°, 25° and 30° and varying the edge distance from $1B$ to $5B$. It was observed that the experimental values of bearing capacity were higher as compared to Meyerhof's (1963) theoretical values. The authors have concluded that for all the slope inclinations, the bearing capacity becomes independent of the slope when the foundations are placed at an edge distance of $5B$.

Bransby and Davidson (2008) conducted a series of model tests to examine the response of shallow foundations on upper surface of a slope and subjected to a vertical load. They investigated the effect of fixity of a foundation on bearing capacity and load settlement response of a footing placed on upper surface of a slope. The tests were conducted on slopes of slope angle, β= 0°, 10° and 20° for three different fixity conditions: i) horizontal displacement, h, and rotation, t, prevented – 'fully fixed'; ii) horizontal displacement only prevented –'pinned'; iii) neither h nor t constrained – 'free'. Model testing was carried out in the laboratory under plane strain testing conditions. Soil was contained within an aluminium box of internal dimensions 670 mm wide, 500 mm broad and 500 mm deep. The box had a Perspex front face which allowed digital photography of the soil and foundation movements as the tests proceeded. The soil was prepared by spot pluviation to give a relative density, $D_r \approx$ 65%. The authors concluded that: i) Both angle of the slope and the fixity of the foundation affected the bearing capacity of the foundation. ii) When the foundation was fully free to rotate and slide the vertical bearing capacity of the foundation next to the slope was found to be in good agreement with previous recommendations of Vesic (1973) and Hansen(1970).

2.5 CENTRIFUGE MODEL STUDIES

Some investigators have carried out model studies in geotechnical centrifuge for footings on slopes and subjected to central vertical and eccentric-inclined loads.

Kimura et al. (1985) conducted experiments for foundations on slopes subjected to central vertical loads. The following four parameters were varied: the width of the footing, the height of the slope, the distance of the footing from the crest of the slope and the slope angle. Toyoura sand was poured into a container from a hopper through two sieves to form a sand deposit with uniform density. Subsequently a slope former assembled and attached to the container and the slope was made by sucking in sand particles with a vacuum pump. The relative density was 90±1.5 % and the angle of shearing resistance in plane strain condition was 49°. The observed effect of the edge distance and the slope angle was presented in terms of a ratio of N_γ on slope and N_γ on level ground as shown in Fig. 2.29.

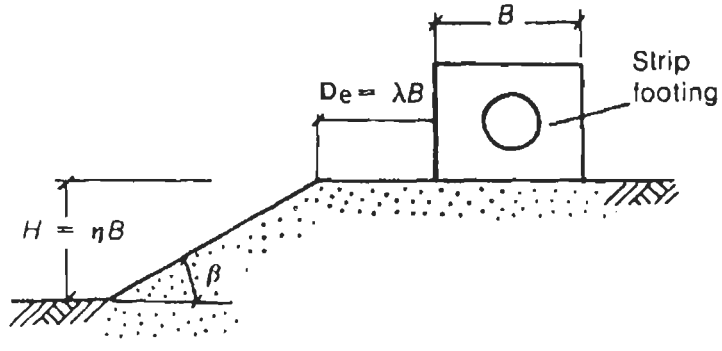

(a)

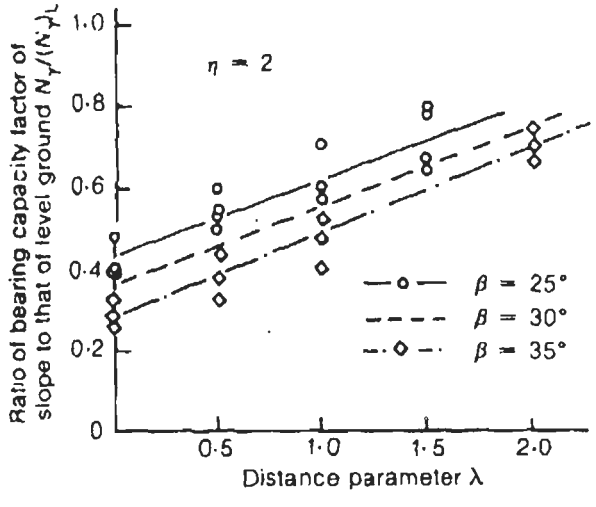

(b)

Fig.2.29 Reduction in Bearing Capacity with Variation in Slope Angle and Distance from Crest of Slope (Kimura et al., 1985)

Gemperline (1988) reported the results of 215 centrifuge tests on model footings located at the top of a slope of cohesionless sand. Based on the outcome of these experiments, the author proposed an equation for determining the bearing capacity factor, $N_{\gamma q}$ that can be used in Meyerhof's (1957) bearing capacity equation

$$q = 0.5\gamma B N_{\gamma q} \tag{2.28}$$

where

$$N_{\gamma q} = f_{(\varphi)} \times f_{(B)} \times f_{(B/L)} \times f_{(D_f/B,B/L)} \times f_{(\beta,/D_e B)} \times f_{(\beta,b/B,D_e/B)} \times f_{(\beta,D_e/B,B/L)} \tag{2.28a}$$

$$f_{(\phi)} = 10^{(0.1159\phi - 2.386)};\ f_{(B)} = 10^{(0.34 - 0.2 log_{10} B)};\ f_{(D_e/B)} = 1 + 0.65(D_f/B); \tag{2.28b}$$

$$f_{(B/L)} = 1 - 0.27(B/L);\ f_{(D_f/B,B/L)} = 1 + 0.39(D_f/L); \tag{2.28c}$$

$$f_{(\beta,b/B)} = 1 - 0.8\left[1 - (1 - tan\beta)^2\right]\left\{2/\left[2 + (D_e/B)^2 tan\beta\right]\right\}; \tag{2.28d}$$

$$f_{(\beta,b/B,B/L)} = 1 + 0.6(B/L)\left[1 - (1 - tan\beta)^2\right]\left\{2/\left[2 + (D_e/B)^2 tan\beta\right]\right\}; \tag{2.28e}$$

$$f_{(\beta,b/B,D/B)} = 1 + 0.33(D_f/B)tan\beta\left\{2/\left[2 + (D_e/B)^2 tan\beta\right]\right\} \tag{2.28f}$$

where L = length of the foundation. Various terms related to the geometrical dimensions are explained in Fig. 2.30.

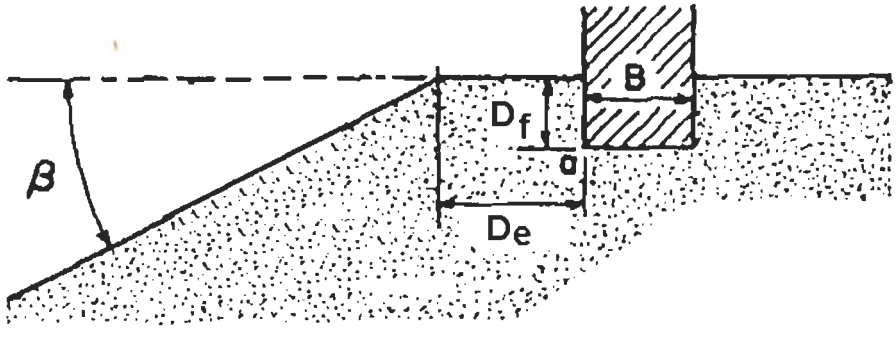

Fig.2.30 Definition of Terms (Gemperline, 1988)

Garnier et al. (1994) reported the results of a series of centrifuge tests to study the bearing capacity of footings near the slopes and subjected to central vertical loads. The sand was deposited by pluviation. The relative density and bulk unit weight were 80% and 16.1±0.2 kN/m^3 respectively and the angle of friction was 40.5±1.5°. The results were presented in terms of reduction factor which is the ratio of bearing capacity on slope and bearing capacity on level ground as shown in Fig.

2.31. Analysis of the test data led to development of an equation for reduction factor for bearing capacity as expressed below:

$$i_\beta = 1 - \left[1.8\tan\beta - 0.9(\tan\beta)^2\right]\left[1 - D_e / 6B\right]^2 \qquad for\ D_e / B < 6$$
$$i_\beta = 1 \qquad for\ D_e / B > 6 \qquad (2.29)$$

where i_β is the reduction factor, β the slope angle and D_e is the distance of the footing from the edge of the slope

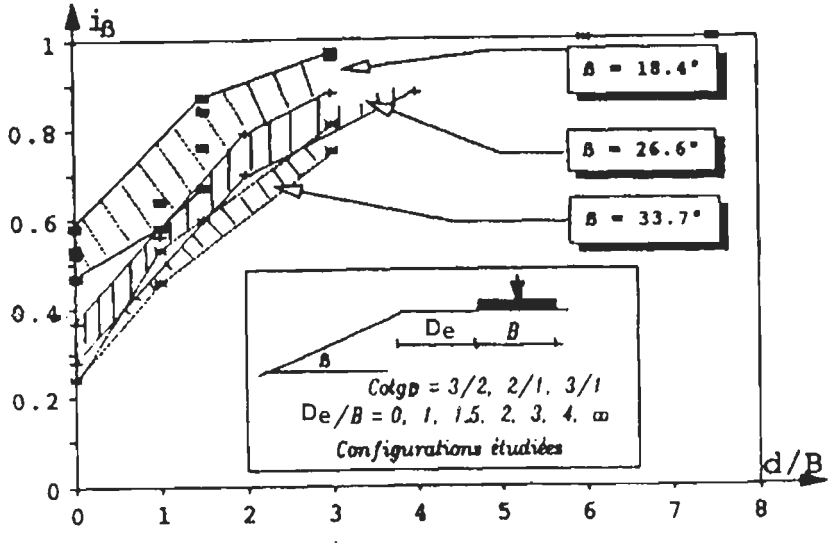

Fig.2.31 Reduction Factor for Bearing Capacity for Different Slope Angles, (Garnier et al., 1994)

Marechal et al. (1999) reported the results of centrifuge tests for footings on or near the slopes subjected to inclined and eccentric load. The reduction in bearing capacity of the footing on slope with reference to the bearing capacity on level ground were expressed in terms of coefficients, i_e for load eccentricity, i_δ for load inclination and i_β for slope angle. The combined effect of these three factors was represented by a coefficient, $i_{e\delta\beta}$ and expressed as

$$i_{e\delta\beta} = i_e \times i_\delta \times i_\beta \qquad (2.30)$$

Tests were conducted for studying the effect of the individual parameters and then for the combined parameter. The density of sand attained was 16.1 kN/m^3 at a relative density of 70%. The centrifuge tests were conducted at 50g on a strip footing, 40 mm wide (2 m in prototype scale) and L/B = 7. Figure 2.32 shows various notations of geometry used in the experiments. Different parametric values considered for the investigation and the results of the tests are presented in Table 2.8 and Table 2.9

respectively. It was concluded that the values of global combined reduction coefficient, $i_{e\delta\beta}$ were close to the product of the basic coefficients, $i_e \times i_\delta \times i_\beta$.

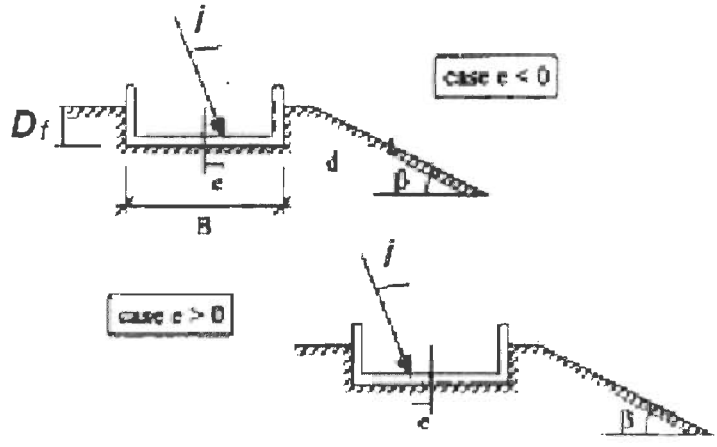

Fig. 2.32 Notations Used in the Experiments (Marechal et al., 1999)

Table 2.8 Experimental Conditions (Marechal et al., 1999)

Test No.	*tanβ*	D_f/B	D_e/B	*e/B*	*i*
1-3	½	0	1	+1/8	15^0
4-5	½	0	1	+1/8	20^0
6	½	3/8	1	-1/8	15^0
7	½	0	2	-1/8	15^0
8	½	1/2	2	-1/8	15^0

Table 2.9 Bearing Capacity Reduction Coefficients (Marechal et al., 1999)

Test No.	q_{ref}(kPa)	i_e	i_δ	i_β	$i_{e\delta\beta}$	$i_e \times i_\delta \times i_\beta$
1	2016	0.85	0.47	0.67	0.27	0.27
2	1776	0.83	0.52	0.64	0.31	0.28
3	1768	0.82	0.5	0.67	0.28	0.28
4	1779	0.75	0.34	0.66	0.23	0.17
5	1941	0.75	0.28	0.64	0.18	0.13
6	2246	0.82	0.54	0.55	0.2	0.24
7	1573	0.84	0.56	0.84	0.34	0.40
8	2596	0.79	0.57	0.6	0.31	0.27

2.6 CONCLUDING REMARKS

Various methods to determine the ultimate bearing capacity of foundations on and upper surface of slopes have been discussed. In all these methods, the loading considered is central vertical. No rational analytical method is available to calculate the bearing capacity of foundations on slopes subjected to eccentric-vertical, central-inclined and eccentric-inclined loads. Most of the model tests for foundations on slopes reported were also for central vertical loads only.

From the above discussions, it appears that enough literature is available to compute the ultimate bearing capacity of footings on slopes subjected to central vertical loads. However, no rational method has been proposed as yet to obtain the ultimate bearing capacity of footings on slopes subjected to eccentric-inclined loads.

CHAPTER-III

ULTIMATE BEARING CAPACITY BY LIMIT EQUILIBRIUM APPROACH

3.1 GENERAL

In this chapter, an analytical solution for determining the ultimate bearing capacity of a footing placed near the top edge of a slope and subjected to an eccentric-inclined load has been presented. The solution makes use of the limiting equilibrium method. For critical state, the eccentricity and inclination of the applied load are taken towards the slope side. At failure, the resistance offered by the soil on the side of the slope will be smaller than the resistance offered by the soil on the other side. Due to this reason, the soil on the slope side attains the state of plastic equilibrium earlier and hence a rupture surface develops on the slope side only. The shear strength of soil on the other side will not be fully mobilised.

3.2 ASSUMPTIONS

For the development of the analytical solution, following assumptions have been made:

i) The footing considered for analysis is a shallow strip footing having a rough base.

ii) The weight of the soil above the base of the footing is replaced by an equivalent surcharge.

iii) One sided failure of soil is assumed to occur along the surface *AED* (Figure 3.1a). The failure region is divided into two zones. Zone I represents an elastic region and Zone II is a combination of radial and passive shear bounded by a log spiral *ED*. The centre of the log spiral is assumed to be at the edge of the footing *B*, (Saran, 1970). The log spiral is represented by the equation,

$$r = r_0 e^{\theta \tan \phi} \tag{3.1}$$

where r_0 = initial radius of the log spiral equal to *BE*,

r = radius of the log spiral at an angle θ and

ϕ = angle of internal friction of soil mass

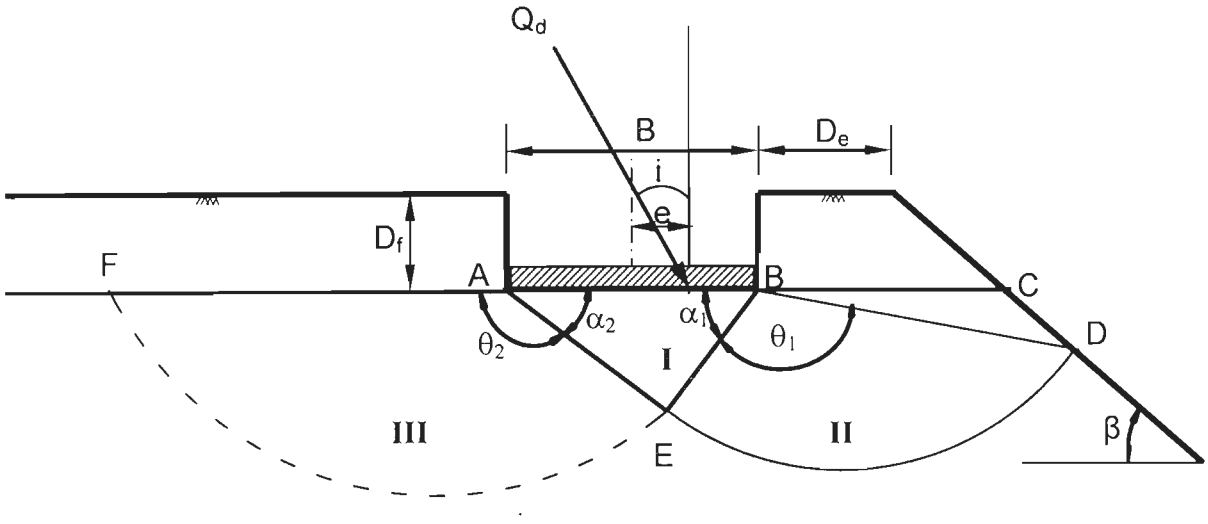

(a) Full Contact

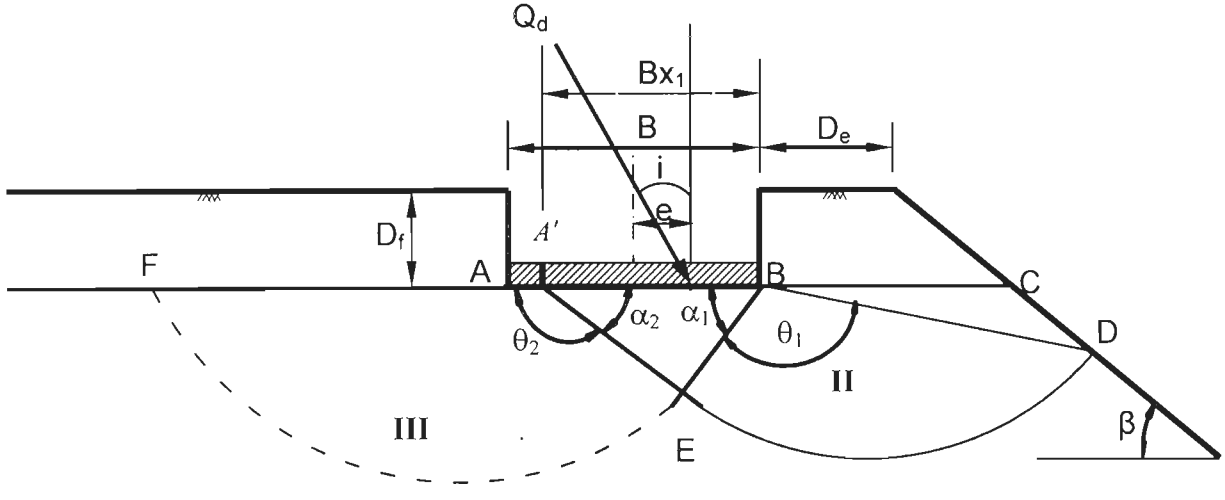

(b) Partial Contact

Fig.3.1 Boundaries of Zone of Plastic Equilibrium after Failure of Soil beneath a Strip Footing Placed on Top Surface of Slope

The sides of the elastic soil wedge are inclined at angles α_1 and α_2 with the horizontal.

iv) A similar rupture surface is considered when the footing loses its contact with the soil due to excessive eccentricity. The rupture surface starts from A' instead of A (Fig. 3.1 b). The effective width is represented by $B \cdot x_1$, where x_1 is the ratio of contact width to the total width of the footing.

v) The shear strength of soil on the left side of the failure plane, AE or $A'E$ is assumed to be partially mobilised and this is characterised by a mobilisation factor, m. Shear strength of the soil is then expressed as-

$$\tau = m(c + \sigma \tan\phi) \tag{3.2}$$

To compute the partial resistance offered by the soil on the left side of $A'E$, a rupture surface as shown by the dashed line is considered which is a combination of radial and passive shear bounded by a log spiral EF.

vi) Method of superposition holds good.

3.3 ANALYTICAL SOLUTION

An analytical solution to the problem of ultimate bearing capacity of a strip footing with eccentric-inclined load has been obtained using the following steps:

i) Geometry of the failure wedge (Fig. 3.1) has been expressed in terms of footing width, B, angle of internal friction, ϕ, log spiral angle, θ_1 and θ_2, wedge angles, α_1 and α_2, slope angle, β, distance of the footing from the slope edge, D_e, depth of the footing, D_f and contact width factor, x_1.

ii) Bearing capacity expression has been then developed by considering the equilibrium of the wedge $A'BE$ (Fig. 3.2). The forces acting on the wedge include passive pressures on the sides BE and $A'E$, vertical and horizontal components of the eccentric-inclined load, Cohesion C_a on side BE and C'_a on side $A'E$.

The earth pressure consists of three components, computed separately and representing the contribution of: a) friction of the material possessing weight and carrying no surcharge, b) friction of a weightless material upon addition of a surcharge, q on the ground surface and c) the cohesion and friction of a weightless material carrying no surcharge.

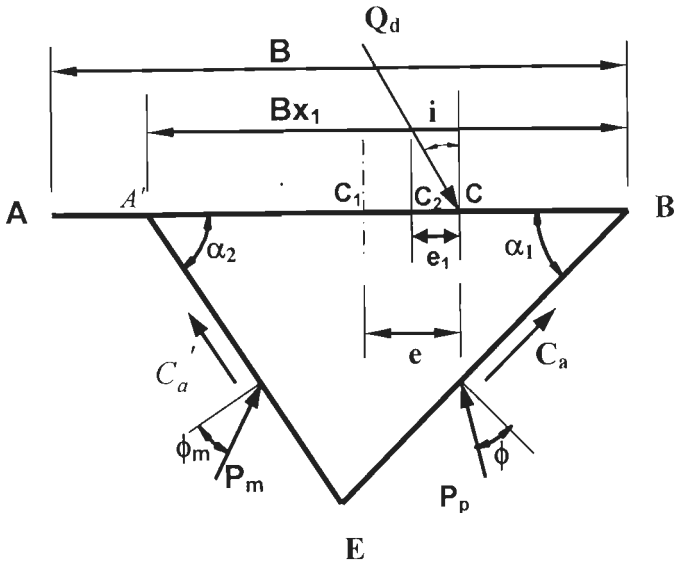

Fig. 3.2 Forces on Elastic Wedge *A'BE*

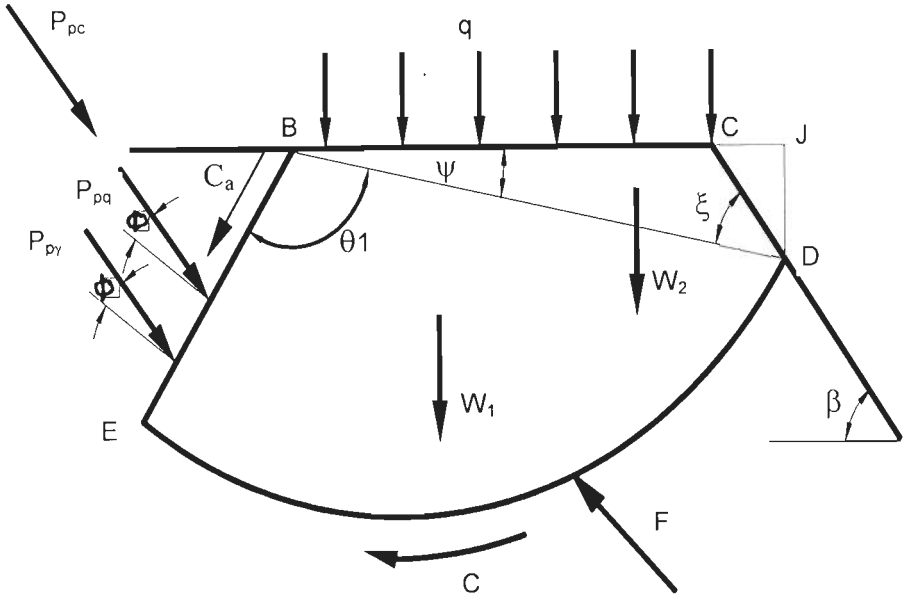

Fig.3.3 Forces on Soil Mass *BEDC*

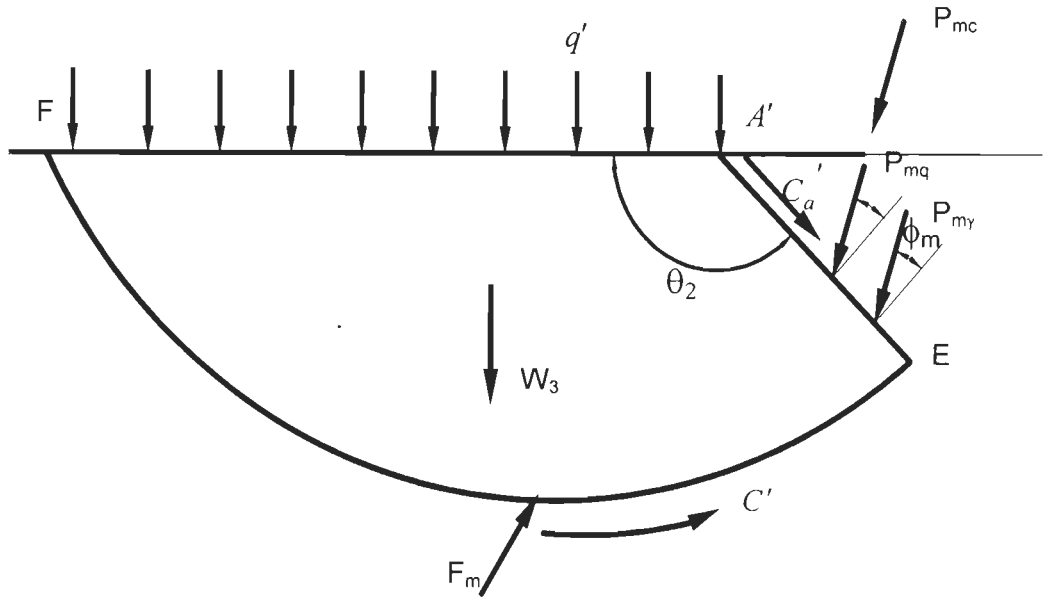

Fig. 3.4 Forces on Soil Mass $A'EF$

iii) Expressions for the passive earth pressure on the side, BE have been developed by considering the equilibrium of the soil mass, $BEDC$ (Fig. 3.3).

iv) Expressions for the mobilized earth pressures on the side, $A'E$ have been developed by considering the equilibrium of the soil mass, $A'EF$ and taking the mobilization factor, m (Fig. 3.4).

v) Relationship between wedge angles, α_1 and α_2 has been derived by solving the three equilibrium equations obtained by statics of the wedge, $A'BE$ (Fig. 3.2). The ultimate bearing capacity has been evaluated for the case when a) all the three equilibrium conditions are satisfied and b) the mobilization factor, m attains the maximum value.

3.3.1 Geometry of the Failure Surface

Equations have been developed for a general case when the footing has lost part of its contact with the soil below. The contact width, $A'B$ has been assumed as $B \cdot x_1$.

For full contact width, $Bx_1 = B$ i.e. $x_1 = 1.0$. In Fig. 3.2, from triangle, $A'BE$

$$\frac{A'B}{Sin(\alpha_1 + \alpha_2)} = \frac{BE}{Sin\alpha_2} = \frac{A'E}{Sin\alpha_1} \tag{3.3}$$

Therefore, $BE = \dfrac{A'B\,Sin\alpha_2}{Sin(\alpha_1 + \alpha_2)}$

Substituting $A'B = Bx_1$

$$BE == \frac{B\,x_1\,Sin\alpha_2}{Sin(\alpha_1+\alpha_2)} = B{\cdot}x_1{\cdot}x \qquad (3.4)$$

$$\text{where } x = \frac{Sin\alpha_2}{Sin(\alpha_1+\alpha_2)} \qquad (3.5)$$

$$\text{Also, } A'E = \frac{A'B\ Sin\alpha_1}{Sin(\alpha_1+\alpha_2)} = \frac{B\,x_1 Sin\alpha_1}{Sin(\alpha_1+\alpha_2)} = B{\cdot}x_1{\cdot}y \qquad (3.6)$$

$$\text{where } y = \frac{Sin\alpha_1}{Sin(\alpha_1+\alpha_2)} \qquad (3.7)$$

The log spiral angle on the side of partial mobilisation is

$$\theta_2 = 180-\alpha_2 \qquad (3.8)$$

$$\text{Then} \quad A'F = A'E\cdot e^{\theta_2 \tan\phi_m} = B\cdot x_1\cdot y\cdot e^{\theta_2 \tan\phi_m} \qquad (3.9)$$

The log spiral angle, θ_1 on the side of the full mobilisation on the slope side is unknown. This angle has been determined by trial and error as below.

Consider the triangle BCD (Fig. 3.3)

$$BC = D_e + \frac{D_f}{tan\,\beta} \qquad (3.10)$$

$$\frac{BC}{Sin\xi} = \frac{BD}{Sin\beta}, \qquad \text{where } \xi = \beta+\alpha_1+\theta_1\text{-}180° \qquad (3.11)$$

$$BD = \frac{BC\,Sin\beta}{Sin\xi} = \frac{\left(D_e + D_f/\tan\beta\right)Sin\beta}{Sin\xi} \qquad (3.12)$$

From the log spiral

$$BD = BE\ e^{\theta_1 \tan\phi} = B{\cdot}x_1{\cdot}x\,e^{\theta_1 \tan\phi} \qquad (3.13)$$

$$\frac{\left(D_e + D_f/\tan\beta\right)Sin\beta}{Sin\xi} = B{\cdot}x_1{\cdot}x\,e^{\theta_1 \tan\phi}$$

$$\frac{\left(D_e/B + D_f/B\tan\beta\right)Sin\beta}{Sin\xi} = x_1{\cdot}x{\cdot}e^{\theta_1 \tan\phi} \qquad (3.14)$$

θ_1 can be obtained by trial from the above expression.

3.3.2 Expression for Bearing Capacity

At failure, the following forces act on the wedge, $A'BE$ (Fig. 3.2).

i) Passive earth pressure, P_p acting on the face, BE at an angle, ϕ with the normal at that point.

ii) Passive earth pressure, P_m at partial mobilisation, acting on the face, $A'E$ at an angle, ϕ_m with the normal at that point, where ϕ_m is given by the following relation:

$$\phi_m = \tan^{-1}(m \tan\phi) \tag{3.15}$$

iii) Cohesive force, C_a acting along the face, BE.

iv) Cohesive force, C'_a acting along the face, $A'E$

v) Eccentric-inclined load, Q_d at point, C at a distance, e from the centre of the footing, C_l.

Neglecting the weight of the wedge $A'BE$, the equilibrium of the footing requires that $\sum V = 0$

$$Q_d\, Cos\, i = P_p Cos(\alpha_1 - \phi) + P_m Cos(\alpha_2 - \phi_m) + C_a Sin\alpha_1 + C'_a Sin\alpha_2 \tag{3.16}$$

If c is the unit cohesion, then

$$C_a = c \cdot BE = c \cdot B \cdot x_1 \frac{Sin\alpha_2}{Sin(\alpha_1 + \alpha_2)} \tag{3.17}$$

$$C'_a = m \cdot c \cdot B \cdot x_1 \frac{Sin\alpha_1}{Sin(\alpha_1 + \alpha_2)} \tag{3.18}$$

Substituting for C_a and C'_a from Eqs. 3.17 and 3.18 in Eq. 3.16 gives-

$$Q_d\, Cos\, i = P_p Cos(\alpha_1 - \phi) + P_m Cos(\alpha_2 - \phi_m) + \frac{c \cdot B \cdot x_1 \cdot Sin\alpha_2 \cdot Sin\alpha_1}{Sin(\alpha_1 + \alpha_2)} + \frac{m \cdot c \cdot B \cdot x_1 \cdot Sin\alpha_2 \cdot Sin\alpha_1}{Sin(\alpha_1 + \alpha_2)}$$

$$\text{or} \quad Q_d\, Cos\, i = P_p Cos(\alpha_1 - \phi) + P_m Cos(\alpha_2 - \phi_m) + \frac{(1+m)\, c \cdot B \cdot x_1 \cdot Sin\alpha_2 \cdot Sin\alpha_1}{Sin(\alpha_1 + \alpha_2)} \tag{3.19}$$

The passive earth pressure, P_p can be divided in to three parts $P_{p\gamma}$, P_{pq} and P_{pc}. The pressure, $P_{p\gamma}$ represents the resistance due to the weight of the soil mass $BEDC$ (Figure 3.3). The point of application of $P_{p\gamma}$ is located at lower one third of BE. The forces, P_{pq} and P_{pc} represent the resistance due to surcharge and cohesion respectively. Since both the pressures, P_{pq} and P_{pc} are uniformly distributed, their

point of application is located at the midpoint of BE. Similarly the earth pressure, P_m at partial mobilisation, m can be divided into three parts $P_{m\gamma}$, P_{mq} and P_{mc}, representing the forces due to weight, surcharge and cohesion respectively of the soil mass $A'EF$ (Fig. 3.4).

The expression for bearing capacity can be evaluated by substituting the expressions for P_p and P_m in Eq. 3.19 as $(P_{p\gamma} + P_{pq} + P_{pc})$ and $(P_{m\gamma} + P_{mq} + P_{mc})$ respectively.

$$Q_d Cos\, i = (P_{p\gamma} + P_{pq} + P_{pc}) Cos(\alpha_1 - \phi) + (P_{m\gamma} + P_{mq} + P_{mc}) Cos(\alpha_2 - \phi_m) + \frac{(1+m)\, c \cdot B \cdot x_1 \cdot Sin\alpha_2 \cdot Sin\alpha_1}{Sin(\alpha_1 + \alpha_2)} \quad (3.20)$$

The surcharge intensity, q on the side of the slope (Figure 3.1) can be expressed as-

$$q = \frac{D_e \gamma D_f + \frac{1}{2}\gamma D_f^{\,2} / tan\beta}{D_e + D_f / tan\beta} \quad (3.21)$$

The surcharge intensity, q' on the side without slope can be expressed as-

$$q' = \gamma D_f \quad (3.22)$$

By introducing N_γ, N_q and N_c factors as-

$$N_\gamma = \frac{2\left[P_{p\gamma} Cos(\alpha_1 - \phi) + P_{m\gamma} Cos(\alpha_2 - \phi_m)\right]}{\gamma B^2 Cos\, i} \quad (3.23)$$

$$N_q = \frac{2\left[P_{pq} Cos(\alpha_1 - \phi) + P_{mq} Cos(\alpha_2 - \phi_m)\right]}{\gamma D_f B Cos\, i} \quad (3.24)$$

$$N_c = \frac{2\left[P_{pc} Cos(\alpha_1 - \phi) + P_{mc} Cos(\alpha_2 - \phi_m)\right]}{c B Cos\, i} + \frac{(1+m)\, x_1 Sin\alpha_1 Sin\alpha_2}{Sin(\alpha_1 + \alpha_2) Cos\, i} \quad (3.25)$$

and substituting these factors in Eq. 3.20, the bearing capacity can be expressed as-

$$Q_d = B\left[\frac{1}{2}\gamma B N_\gamma + \gamma D_f N_q + c N_c\right] \quad (3.26)$$

The quantities N_γ, N_q and N_c are referred to as the bearing capacity factors. These are non-dimensional quantities which depend upon $\phi, \beta, D_e / B, D_f / B$, e/B and i only.

3.3.3 Computation of Passive Earth Pressures $P_{p\gamma}$, P_{pq} and P_{pc}

The equilibrium of the soil mass *BEDC* has been considered to express the components of passive earth pressures, $P_{p\gamma}$, P_{pq} and P_{pc}, (Fig. 3.3). The forces, which have been considered to determine these passive earth pressures, are listed below:

i) Weight, W of the soil mass *BEDC* which acts vertically downward through the centre of gravity of the soil mass.

ii) Surcharge weight, q acting on side *BC*. This surcharge is assumed to be uniformly distributed along *BC*.

iii) Cohesive force, C acting along the log spiral, *DE*.

iv) Cohesive force, C_a acting along the face, *BE*.

v) Passive earth pressure, $P_{p\gamma}$ acting on the face *BE*. It acts at lower one third point of *BE* and it makes an angle, ϕ with the normal at that point.

vi) Passive earth pressure, P_{pq} acting on the face *BE*. It acts at mid point of *BE* and makes an angle, ϕ with the normal at that point.

vii) Passive earth pressure, P_{pc} acting on the face *BE*. It acts at the mid point of *BE* and makes an angle, ϕ with the normal at that point.

viii) Resultant, F of the normal and frictional forces acting along the log spiral. It will pass through the centre of the log spiral, since it makes an angle, ϕ with the normal at the point of application.

The passive earth pressures namely, $P_{p\gamma}$, P_{pq} and P_{pc} have been determined by taking moment of all the forces about the centre of the log spiral, which is at the edge of the footing, *B*. The moment due to the force, F becomes zero as it passes through the centre of the log spiral. The moments of the other forces are listed below in the same order:

i) Moment of the soil wedge, *BEDC* (Fig. 3.5):

M'_{γ} = Moment of wedge, *BED* + Moment of wedge, *BDC*

Moment of wedge *BED* (Fig.3.5),

$$M'_{\gamma}(1) = \int_0^{\theta_1} \frac{1}{2}\gamma r^2 d\theta \ \frac{2}{3} r \, Sin(\theta - \eta')$$

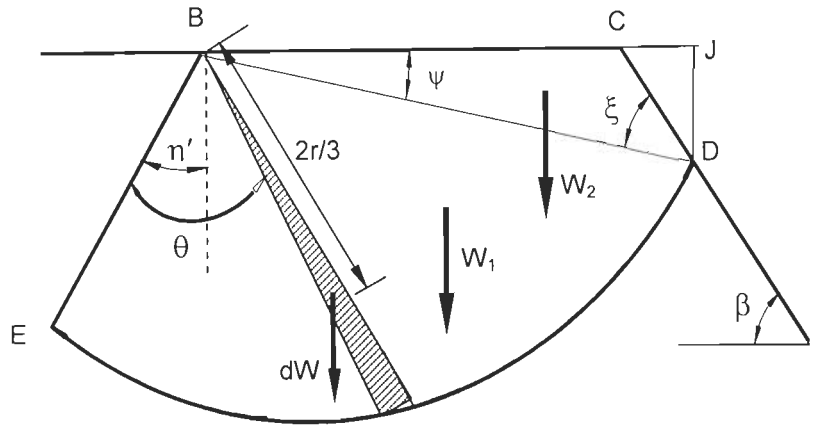

Fig. 3.5 Method for Computing Moment of Soil Wedge *BED*

$$\text{or}\quad \frac{M'_{\gamma}(1)}{\gamma B^3} = \frac{1}{3}\frac{x_1^{\,3}x^3}{(9\tan^2\phi+1)}\left[\begin{array}{r} e^{3\theta_1\tan\phi}\{3\tan\phi\, Sin(\theta_1-\eta')-Cos(\theta_1-\eta')\} \\ +\cos\eta'+3\tan\phi\, Sin\eta' \end{array}\right] \tag{3.27}$$

Moment of wedge *BDC*,

$M'_{\gamma}(2)$ = Moment of wedge *BJD* – Moment of wedge *CJD*

$$= \frac{1}{2}\gamma(BD)Sin\psi(BD)Cos\psi\ \frac{2}{3}(BD)Cos\psi$$

$$-\frac{1}{2}\gamma(CD)Sin\beta(CD)Cos\beta\left[(BC)+\frac{2}{3}(CD)Cos\beta\right]$$

$$\text{or}\quad \frac{M'_{\gamma}(2)}{\gamma B^3} = \frac{1}{3}x_1^{\,3}\,x^3 Sin\psi\, Cos^2\psi\, e^{3\theta_1\tan\phi}$$

$$-\frac{1}{2}x_1^{\,3}\,x^3 e^{3\theta_1\tan\phi}\,Cos\beta\frac{Sin^2\psi}{Sin\beta}\left[\frac{Sin\xi}{Sin\beta}+\frac{2}{3}\frac{Sin\psi\,Cos\beta}{Sin\beta}\right] \tag{3.28}$$

$$M'_{\gamma} = M'_{\gamma}(1)+M'_{\gamma}(2) \tag{3.29}$$

ii) Moment due to surcharge weight acting on *BC*:

$$M'_{q} = q(BC)\frac{BC}{2}$$

$$= \frac{1}{2}\frac{D_e\gamma D_f+\frac{1}{2}\gamma D_f^{\,2}/\tan\beta}{D_e+D_f/\tan\beta}\cdot(D_e+D_f/\tan\beta)^2$$

or $$\frac{M^1{}_q}{\gamma D_f B^2} = \frac{1}{2}\left(\frac{D_e}{B} + \frac{1}{2}\frac{D_f}{B}\frac{1}{\tan\beta}\right)\left(\frac{D_e}{B} + \frac{D_f}{B}\frac{1}{\tan\beta}\right) \tag{3.30}$$

iii) Moment of cohesive force, C acting along the log spiral, DE:

$$M^1{}_c = \int_0^{\theta_1} c\, r^2\, d\theta = c r_0^{\,2} \int_0^{\theta_1} e^{2\theta\tan\phi}\, d\theta = c\, B\, x_1^{\,2} x^2 \frac{(e^{2\theta_1\tan\phi} - 1)}{2\tan\phi}$$

or $$\frac{M^1{}_c}{cB^2} = x_1^{\,2} x^2 \frac{(e^{2\theta_1\tan\phi} - 1)}{2\tan\phi} \tag{3.31}$$

iv) Moment of the cohesive force, C_a acting along BE about B will be zero

v) Moment of the passive earth pressure, $P_{p\gamma}$:

$$M_\gamma = P_{p\gamma}\, Cos\phi \frac{2}{3}(BE)$$

Substituting the expression for BE from Eq. 3.4,

$$M_\gamma = \frac{2}{3} P_{p\gamma} B\, Cos\phi\, x_1 x = P_{p\gamma}\, B\, \tau_1 \tag{3.32}$$

where $\tau_1 = \frac{2}{3}\cos\phi\, x_1 x$

vi) Moment of the passive earth pressure, P_{pq}:

$$M_q = P_{pq} Cos\phi \frac{1}{2}(BE) = P_{pq} Cos\phi \frac{1}{2} B x_1 x$$

$$= P_{pq}\, B\, \tau_2 \tag{3.33}$$

where $\tau_2 = \frac{1}{2}\cos\phi\, x_1\, x$

vii) Moment of the passive earth pressure, P_{pc}:

$$M_c = P_{pc}\, Cos\phi \frac{1}{2}(BE) = P_{pc}\, Cos\phi \frac{1}{2} B\, x_1 x$$

$$= P_{pc} B \tau_2 \tag{3.34}$$

viii) Moment of the force F about B will be zero

For equilibrium of the soil mass $BEDC$,

$\sum M = 0$

or $M^1{}_\gamma + M^1{}_q + M^1{}_c = P_{p\gamma} B\tau_1 + P_{pq} B\tau_2 + P_{pc} B\tau_2$

or $$N_{p\gamma}\, \gamma B^3 + N_{pq}\, \gamma D_f\, B^2 + N_{pc}\, c B^2 = P_{p\gamma} B\tau_1 + P_{pq} B\tau_2 + P_{pc} B\tau_2 \tag{3.35}$$

where

$$N_{p\gamma} = \frac{M^1{}_{\gamma}}{\gamma B^3} \tag{3.36}$$

$$N_{pq} = \frac{M^1{}_{q}}{\gamma D_f B^2} \tag{3.37}$$

$$N_{pc} = \frac{M^1{}_{c}}{c B^2} \tag{3.38}$$

Eq. 3.35 has been solved by considering three independent cases, namely,

Case 1: For soil having weight only, without surcharge i.e. $c = 0$, $q = 0$,

$$N_{p\gamma}\,\gamma B^3 = P_{p\gamma} B \tau_1$$

$$P_{p\gamma} = \frac{N_{p\gamma}}{\tau_1}\gamma B^2 \tag{3.39}$$

Case 2: For weightless soil whose ability to sustain a surface stress depends on the presence of surcharge only i.e. $\gamma = c = 0$,

$$N_{pq}\,\gamma D_f B^2 = P_{pq} B \tau_2$$

$$P_{pq} = \frac{N_{pq}}{\tau_2}\gamma D_f B \tag{3.40}$$

Case 3: For weightless soil with no surcharge, but possessing cohesion, i.e. $\gamma = q = 0$,

$$N_{pc}\,c B^2 = P_{pc} B \tau_2$$

$$P_{pc} = \frac{N_{pc}}{\tau_2} c B \tag{3.41}$$

3.3.4 Computation of Passive Earth Pressures $P_{m\gamma}$, P_{mq} and P_{mc}

The passive earth pressures, $P_{m\gamma}$, P_{mq} and P_{mc} at the mobilisation factor, m can be determined by considering the rupture surface $A'EF$ as shown in the Fig. 3.1. For the determination of the passive earth pressures, the equilibrium of soil mass, $A'EF$ (Fig. 3.4) has been considered. The forces, which have been considered for the determination of the passive earth pressures, are listed below:

i) Weight W_3, of the soil wedge, $A'EF$ which acts vertically through the centre of gravity of the wedge.

ii) Surcharge, q' acting on $A'F$ uniformly.

iii) Cohesive force, C' acting along the log spiral EF.

iv) Cohesive force, C'_a acting along $A'E$.

v) Passive earth pressure, $P_{m\gamma}$ acting on the face $A'E$. It acts at lower one third point of $A'E$ and makes an angle, ϕ_m to the normal at that point.

vi) Passive earth pressure, P_{mq} acting on the face $A'E$. It acts at mid point of $A'E$ and makes an angle, ϕ_m to the normal at that point.

vii) Passive earth pressure, P_{mc} acting on the face $A'E$. It acts at mid point of $A'E$ and makes an angle, ϕ_m to the normal at that point.

viii) Resultant, F_m, of the normal and the frictional force along the log spiral, EF. It passes through the centre of the log spiral.

The passive earth pressures, $P_{m\gamma}$, P_{mq} and P_{mc} have been determined by taking the moments of all the forces about the centre of the log spiral, which is at the edge of the footing A'. Expressions for moments of all the forces are given below in the same order as the forces are listed above:

i) Moment of the weight of the soil wedge, $A'EF$ (Fig. 3.6):

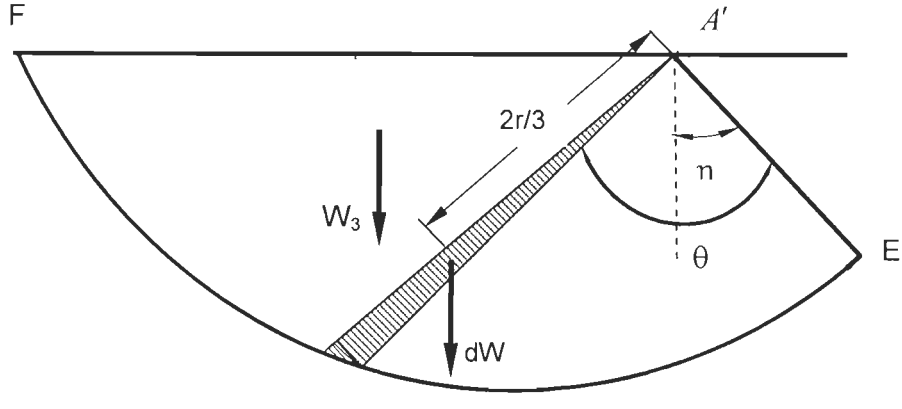

Fig. 3.6 Method for Computing Moment of Soil Wedge $A'EF$

$M'_{m\gamma}$ = Moment of wedge $A'EF$

$$= \int_0^{\theta_2} \frac{1}{2} \gamma r^2 \, d\theta \frac{2}{3} r \, Sin(\theta - \eta)$$

$$\text{or } \frac{M'_{m\gamma}}{\gamma B^3} = \frac{1}{3} \frac{x_1^3 y^3}{(9\tan^2 \phi_m + 1)} \left[e^{3\theta_2 \tan\phi_m} \{3\tan\phi_m \, Sin(\theta_2 - \eta) - Cos(\theta_2 - \eta)\} + \cos\eta + 3\tan\phi_m \, Sin\eta \right] \quad (3.42)$$

ii) Moment of the surcharge, q' acting on $A'F$:

$$M'_{mq} = q'(A'F)\left(\frac{A'F}{2}\right) = \frac{1}{2}\gamma D_f B^2 x_1^2 y^2 e^{2\theta_2 \tan\phi_m}$$

$$\frac{M'_{mq}}{\gamma D_f B^2} = \frac{1}{2} x_1^2 y^2 e^{2\theta_2 \tan\phi_m} \qquad (3.43)$$

iii) Moment of mobilised cohesive force C' acting along the log spiral, EF:

$$M'_{mc} = \int_0^{\theta_2} mc\, r\, d\theta\, r = mc \int_0^{\theta_2} r_0^2 e^{2\theta \tan\phi_m} d\theta$$

$$= mcB^2 x_1^2 y^2 \frac{(e^{2\theta_2 \tan\phi_m} - 1)}{2\tan\phi_m}$$

$$\frac{M'_{mc}}{c\,B^2} = \frac{m}{2tan\varphi_m} x_1^2 y^2 (e^{2\theta_2 tan\varphi_m} - 1) \qquad (3.44)$$

iv) Moment of the cohesive force, C'_a about A' will be zero.

v) Moment of passive earth pressure, $P_{m\gamma}$:

$$M_{m\gamma} = P_{m\gamma} Cos\phi_m \frac{2}{3}(A'E) = P_{m\gamma} Cos\phi_m \frac{2}{3} Bx_1 y = P_{m\gamma} B\tau_3 \qquad (3.45)$$

where $\tau_3 = \frac{2}{3} Cos\phi_m x_1 y$

vi) Moment of passive earth pressure, P_{mq}:

$$M_{mq} = P_{mq} Cos\phi_m \frac{1}{2}(A'E) = P_{mq} Cos\phi_m \frac{1}{2} Bx_1 y = P_{mq} B\tau_4 \qquad (3.46)$$

where $\tau_4 = \frac{1}{2} Cos\phi_m x_1 y$

vii) Moment of passive earth pressure, P_{mc}:

$$M_{mc} = P_{mc} Cos\phi_m \frac{1}{2}(A'E) = P_{mc} Cos\phi_m \frac{1}{2} Bx_1 y = P_{mc} B\tau_4 \qquad (3.47)$$

(viii) Moment of resultant F_m will be zero as it passes through the centre of the log spiral.

For equilibrium of the soil mass, $A'EF$,

$\sum M = 0$

$$M'_{m\gamma} + M'_{mq} + M'_{mc} = P_{m\gamma} B\tau_3 + P_{mq} B\tau_4 + P_{mc} B\tau_4$$

or $$N_{m\gamma}\,\gamma B^3 + N_{mq}\,\gamma D_f B^2 + N_{mc}\,cB^2 = P_{m\gamma}\,B\tau_3 + P_{mq}B\tau_4 + P_{mc}B\tau_4 \quad (3.48)$$

where

$$N_{m\gamma} = \frac{M'_{m\gamma}}{\gamma B^3} \quad (3.49)$$

$$N_{mq} = \frac{M'_{mq}}{\gamma D_f B^2} \quad (3.50)$$

$$N_{mc} = \frac{M'_{mc}}{cB^2} \quad (3.51)$$

Equation 3.48 has been solved by considering three independent cases.

Case 1: For soil having weight only, without surcharge i.e. $c = q = 0$,

$$N_{m\gamma}\,\gamma B^3 = P_{m\gamma} B\tau_3$$

or $$P_{m\gamma} = \frac{N_{m\gamma}}{\tau_3}\gamma B^2 \quad (3.52)$$

Case 2: For weightless soil whose ability to sustain a surface stress depends on the presence of surcharge only i.e. $\gamma = c = 0$

$$N_{mq}\,\gamma D_f\,B^2 = P_{mq}\,B\tau_4$$

or $$P_{mq} = \frac{N_{mq}}{\tau_4}\gamma D_f\,B \quad (3.53)$$

Case 3: For weightless soil with no surcharge, but possessing cohesion, i.e. $\gamma = q = 0$

$$N_{mc}\,c\,B^2 = P_{mc}B\,\tau_4$$

or $$P_{mc} = \frac{N_{mc}}{\tau_4}c\,B \quad (3.54)$$

The expressions for $P_{p\gamma}$, P_{pq}, P_{pc} and $P_{m\gamma}$, P_{mq}, P_{mc} thus obtained have been used in Eqs. 3.23, 3.24 and 3.25 to calculate the bearing capacity factors. But these values cannot be calculated unless the wedge angles α_1 and α_2 are known. The values of α_1 and α_2 have been determined by considering the equilibrium of the wedge, $A'BE$ separately for soils having weight only, cohesion only and surcharge only.

3.3.5 Wedge Angle Relation

i) For soil having weight only ($c = q = 0$)

By considering the static equilibrium of the wedge $A'BE$ (Fig. 3.7), three equilibrium equations have been obtained to determine the wedge angle relationship, α_1 and α_2 for a particular inclination of load and eccentricity/width ratio. In Fig. 3.7, e represents the eccentricity of the load $Q_{d\gamma}$ from the centre of the footing C_1, whereas e_1 represents the effective eccentricity, which is the distance of the load from the centre C_2 of the contact width $B.x_1$.

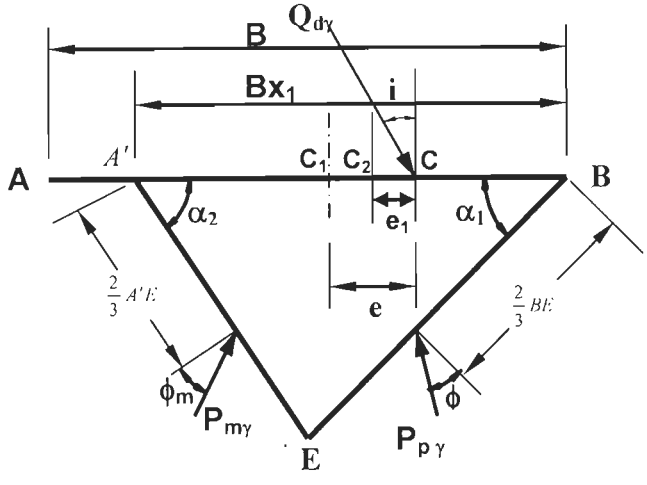

Fig.3.7 Forces on Soil Wedge $A'BE$ for $c = q = 0$

From the Fig. 3.7,

$$e_1 = \frac{B \cdot x_1}{2} - \left(\frac{B}{2} - e\right) = \frac{B \cdot x_1}{2} - \frac{B}{2} + e$$

Dividing by Bx_1, one gets

$$\frac{e_1}{B \cdot x_1} = \frac{1}{2} - \frac{1}{2x_1} + \frac{e}{B \cdot x_1} \tag{3.55}$$

Applying the equations of equilibrium,

$$\sum V = 0$$

$$P_{p\gamma} \cos(\alpha_1 - \phi) + P_{m\gamma} \cos(\alpha_2 - \phi_m) = Q_{d\gamma} \cos i \tag{3.56}$$

$$\sum H = 0$$

$$P_{p\gamma} \sin(\alpha_1 - \phi) - P_{m\gamma} \cos(\alpha_2 - \phi_m) = Q_{d\gamma} \sin i \tag{3.57}$$

$$\sum M_{A'} = 0$$

$$P_{m\gamma}\cos\phi_m \times \frac{2}{3}A'E + P_{p\gamma}\cos\phi\left[\frac{1}{3}BE + A'E\cdot\cos(\alpha_1+\alpha_2)\right] + P_{p\gamma}\sin\phi\cdot A'E\cdot\sin(\alpha_1+\alpha_2)$$

$$= Q_{d\gamma}\cos i\left(\frac{Bx_1}{2}+e_1\right)$$

Substituting the expressions for BE and $A'E$ from Eqs. 3.4 and 3.6

$$\frac{2}{3}P_{m\gamma}\cos\phi_m\frac{Bx_1\sin\alpha_1}{\sin(\alpha_1+\alpha_2)} + P_{p\gamma}\cos\phi\left[\frac{1}{3}\frac{Bx_1\sin\alpha_2}{\sin(\alpha_1+\alpha_2)} + \frac{Bx_1\sin\alpha_1}{\sin(\alpha_1+\alpha_2)}\cos(\alpha_1+\alpha_2)\right]$$

$$+ P_{p\gamma}\sin\phi\frac{Bx_1\sin\alpha_1}{\sin(\alpha_1+\alpha_2)}\sin(\alpha_1+\alpha_2) = Q_{d\gamma}\cos i\left(\frac{Bx_1}{2}+e_1\right)$$

or $$\frac{2}{3}P_{m\gamma}\cos\phi_m + P_{p\gamma}\cos\phi\left[\frac{1}{3}\frac{\sin\alpha_2}{\sin\alpha_1}+\cos(\alpha_1+\alpha_2)\right] + P_{p\gamma}\sin\phi\sin(\alpha_1+\alpha_2)$$

$$= Q_{d\gamma}\cos i\frac{\sin(\alpha_1+\alpha_2)}{\sin\alpha_1}\left(\frac{1}{2}+\frac{e_1}{Bx_1}\right) \quad (3.58)$$

Solving the above three equations of equilibrium i.e. Eqs. 3.56, 3.57 and 3.58, the wedge angle relations α_1 and α_2 have been obtained in terms of ϕ, ϕ_m , e/B, i and x_1.

From Eqs. 3.56 and 3.57, one gets,

$$P_{m\gamma} = \frac{Q_{d\gamma}\sin(\alpha_1-\phi-i)}{\sin(\alpha_1+\alpha_2-\phi-\phi_m)} \quad (3.59)$$

and $$P_{p\gamma} = \frac{Q_{d\gamma}\sin(\alpha_2-\phi_m+i)}{\sin(\alpha_1+\alpha_2-\phi-\phi_m)} \quad (3.60)$$

Substituting these expressions of $P_{m\gamma}$ and $P_{p\gamma}$ from Eqs. 3.59 and 3.60 and expression for $\frac{e_1}{Bx_1}$ from Eq. 3.55 in Eq. 3.58, one gets,

$$\frac{2}{3}\frac{\sin(\alpha_1-\phi-i)}{\sin(\alpha_1+\alpha_2-\phi-\phi_m)}\cos\phi_m + \frac{\sin(\alpha_2-\phi_m+i)}{\sin(\alpha_1+\alpha_2-\phi-\phi_m)}\left[\frac{\cos\phi\sin\alpha_2}{3\sin\alpha_1}+\cos(\alpha_1+\alpha_2-\phi)\right]$$

$$= \cos i\frac{\sin(\alpha_1+\alpha_2)}{\sin\alpha_1}\left(1+\frac{e}{Bx_1}-\frac{1}{2x_1}\right) \quad (3.61)$$

Equation 3.61 has been simplified and expressed as a quadratic equation in terms of $\tan\alpha_2$ as given below.

$$A_\gamma\tan^2\alpha_2 + B_\gamma\tan\alpha_2 + C_\gamma = 0$$

or $$\tan\alpha_2 = \frac{-B_\gamma \pm \sqrt{B_\gamma^{\,2} - 4A_\gamma C_\gamma}}{2A_\gamma} \qquad (3.62)$$

where

$$A_\gamma = \cos\phi\cos(\phi_m - i) + 2\sin\alpha_1\cos\phi_m\sin(\alpha_1 - \phi - i) - 3\sin\alpha_1\cos(\phi_m - i)\sin(\alpha_1 - \phi)$$
$$-3\cos i\cos\alpha_1\cos(\alpha_1 - \phi - \phi_m)\left(1 + \frac{e}{Bx_1} - \frac{1}{2x_1}\right) \qquad (3.63)$$

$$B_\gamma = 3\sin\alpha_1\cos(\alpha_1 - \phi - \phi_m + i) - \cos\phi\sin(\phi_m - i)$$
$$-3\cos i\sin(2\alpha_1 - \phi - \phi_m)\left(1 + \frac{e}{Bx_1} - \frac{1}{2x_1}\right) \qquad (3.64)$$

$$C_\gamma = 2\sin\alpha_1\cos\phi_m\sin(\alpha_1 - \phi - i) - 3\sin\alpha_1\cos(\alpha_1 - \phi)\sin(\phi_m - i)$$
$$-3\sin\alpha_1\cos i\sin(\alpha_1 - \phi - \phi_m)\left(1 + \frac{e}{Bx_1} - \frac{1}{2x_1}\right) \qquad (3.65)$$

ii) For soil having surcharge only ***($\gamma = c = 0$)***

Figure 3.8 shows the forces acting on the wedge, $A'BE$.

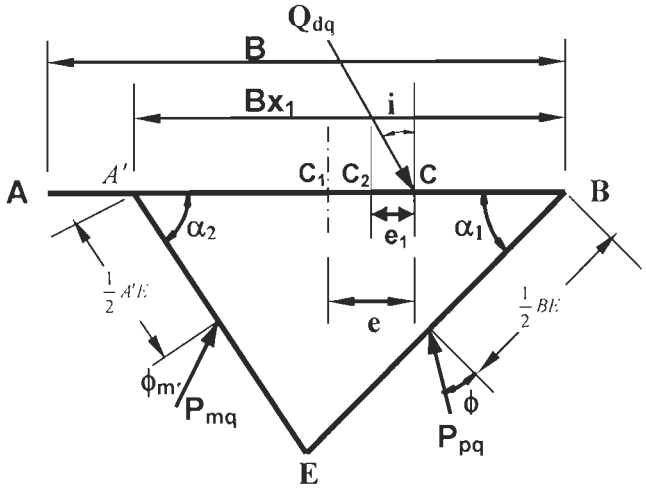

Fig.3.8 Forces Acting on Wedge $A'BE$ **for** $\gamma = c = 0$

Applying the equations of equilibrium, one gets,

$$\sum V = 0$$

$$P_{pq}\cos(\alpha_1 - \phi) + P_{mq}\cos(\alpha_2 - \phi_m) = Q_{dq}\cos i \qquad (3.66)$$

$$\sum H = 0$$

$$P_{pq}\sin(\alpha_1 - \phi) - P_{mq}\sin(\alpha_2 - \phi_m) = Q_{dq}\sin i \tag{3.67}$$

$$\sum M_{A'} = 0$$

$$P_{mq}\cos\phi_m \times \frac{1}{2}A'E + P_{pq}\cos\phi\left[\frac{1}{2}BE + A'E\cdot\cos(\alpha_1+\alpha_2)\right] + P_{pq}\sin\phi\cdot A'E\cdot\sin(\alpha_1+\alpha_2)$$

$$= Q_{dq}\cos i\left(\frac{Bx_1}{2} + e_1\right)$$

Substituting the expression for BE and $A'E$ from Eqs. 3.4 and 3.6, the above equation reduces to

$$\frac{1}{2}P_{mq}\cos\phi_m + P_{pq}\left[\frac{\sin\alpha_2\cos\phi}{2\sin\alpha_1} + \cos(\alpha_1+\alpha_2-\phi)\right] =$$

$$Q_{dq}\cos i\frac{\sin(\alpha_1+\alpha_2)}{\sin\alpha_1}\left(\frac{1}{2} + \frac{e_1}{Bx_1}\right) \tag{3.68}$$

From Eqs. 3.66 and 3.67, one gets,

$$P_{mq} = \frac{Q_{dq}\sin(\alpha_1 - \phi - i)}{\sin(\alpha_1+\alpha_2-\phi-\phi_m)} \tag{3.69}$$

and $$P_{pq} = \frac{Q_{dq}\sin(\alpha_2 - \phi_m + i)}{\sin(\alpha_1+\alpha_2-\phi-\phi_m)} \tag{3.70}$$

Substituting these expressions for P_{mq} and P_{dq} from Eqs. 3.69 and 3.70 and expression for $\frac{e_1}{Bx_1}$ from Eq. 3.55 in Eq. 3.68, one gets,

$$\frac{1}{2}\frac{\sin(\alpha_1-\phi-i)}{\sin(\alpha_1+\alpha_2-\phi-\phi_m)}\cos\phi_m + \frac{\sin(\alpha_2-\phi_m+i)}{\sin(\alpha_1+\alpha_2-\phi-\phi_m)}\left[\frac{\cos\phi\sin\alpha_2}{2\sin\alpha_1} + \cos(\alpha_1+\alpha_2-\phi)\right]$$

$$= \cos i\frac{\sin(\alpha_1+\alpha_2)}{\sin\alpha_1}\left(1 + \frac{e}{Bx_1} - \frac{1}{2x_1}\right) \tag{3.71}$$

The above equation can be simplified and expressed as a quadratic equation as,

$$A_q\tan^2\alpha_2 + B_q\tan\alpha_2 + C_q = 0$$

or $$\tan\alpha_2 = \frac{-B_q \pm \sqrt{B_q^{\,2} - 4A_qC_q}}{2A_q} \qquad (3.72)$$

where

$$A_q = \cos\phi\cos(\phi_m - i) + \sin\alpha_1\cos\phi_m\sin(\alpha_1 - \phi - i) - 2\sin\alpha_1\cos(\phi_m - i)\sin(\alpha_1 - \phi)$$
$$- 2\cos i\cos\alpha_1\cos(\alpha_1 - \phi - \phi_m)\left(1 + \frac{e}{Bx_1} - \frac{1}{2x_1}\right) \qquad (3.73)$$

$$B_q = 2\sin\alpha_1\cos(\alpha_1 - \phi - \phi_m + i) - \cos\phi\sin(\phi_m - i)$$
$$- 2\cos i\sin(2\alpha_1 - \phi - \phi_m)\left(1 + \frac{e}{Bx_1} - \frac{1}{2x_1}\right) \qquad (3.74)$$

$$C_q = \sin\alpha_1\cos\phi_m\sin(\alpha_1 - \phi - i) - 2\sin\alpha_1\cos(\alpha_1 - \phi)\sin(\phi_m - i)$$
$$- 2\sin\alpha_1\cos i\sin(\alpha_1 - \phi - \phi_m)\left(1 + \frac{e}{Bx_1} - \frac{1}{2x_1}\right) \qquad (3.75)$$

iii) For soil having cohesion only (q = γ = 0)

Figure 3.9 shows the forces acting on the wedge $A'BE$.

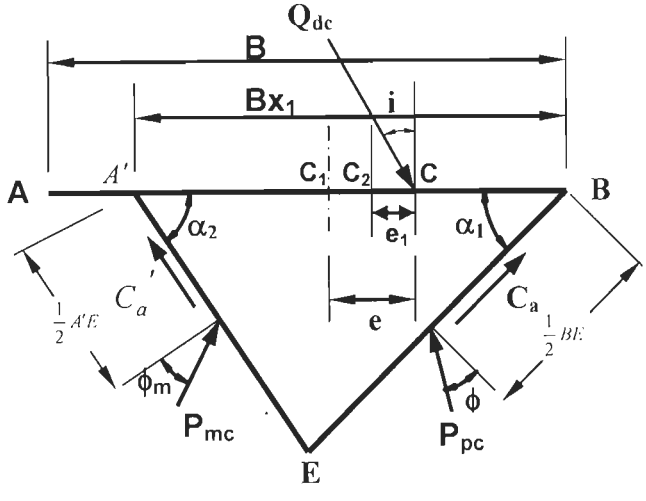

Fig.3.9 Forces Acting on Wedge $A'BE$ for $q = \gamma = 0$

Applying the equations of equilibrium, we get,

$$\sum V = 0$$

$$P_{pc}\cos(\alpha_1 - \phi) + P_{mc}\cos(\alpha_2 - \phi_m) + C_a\sin\alpha_1 + C_a'\sin\alpha_2 = Q_{dc}\cos i$$

Substituting the expressions for C_a and C_a' from Eqs. 3.17 and 3.18, one gets,

$$P_{pc}\cos(\alpha_1-\phi)+P_{mc}\cos(\alpha_2-\phi_m)+\frac{(1+m)\,c\,B\,x_1\sin\alpha_1\sin\alpha_2}{\sin(\alpha_1+\alpha_2)}=Q_{dc}\cos i \qquad (3.76)$$

$\sum H=0$

$$P_{pc}\sin(\alpha_1-\phi)-P_{mc}\sin(\alpha_2-\phi_m)+m.c.A'E.\cos\alpha_2-c.BE.\cos\alpha_1=Q_{dc}\sin i$$

Substituting the values of BE and $A'E$ from Eqs. 3.4 and 3.6 and after simplification, one gets,

$$P_{pc}\sin(\alpha_1-\phi)-P_{mc}\sin(\alpha_2-\phi_m)+\frac{c\,B\,x_1(m\sin\alpha_1\cos\alpha_2-\cos\alpha_1\sin\alpha_2)}{\sin(\alpha_1+\alpha_2)}$$

$$=Q_{dc}\,sini \qquad (3.77)$$

$\sum M_{A'}=0$

$$P_{mc}\cos\phi_m\frac{1}{2}A'E+P_{pc}\cos\phi\left[\frac{1}{2}BE+A'E.\cos(\alpha_1+\alpha_2)\right]+P_{pc}\sin\phi.A'E\sin(\alpha_1+\alpha_2)$$

$$+c.BE.A'E.sin(\alpha_1+\alpha_2)=Q_{dc}\,cosi\left(e_1+\frac{Bx_1}{2}\right)$$

Substituting the expressions for BE and $A'E$ from Eqs. 3.4 and 3.6, expression for $\frac{e_1}{Bx_1}$ from Eq. 3.55 and simplifying, one gets,

$$\frac{1}{2}P_{mc}\cos\phi_m+P_{pc}\left[\frac{\cos\phi\sin\alpha_2}{2\sin\alpha_1}+\cos(\alpha_1+\alpha_2-\phi)\right]+c.Bx_1.\sin\alpha_2$$

$$=Q_{dc}\,cos\,i\,\frac{sin(\alpha_1+\alpha_2)}{sin\,\alpha_2}\left(1+\frac{e}{Bx_1}-\frac{1}{2x_1}\right) \qquad (3.78)$$

The equilibrium equations (Eqs. 3.76, 3.77 and 3.78) are non-homogeneous. The quantities P_{pc}, P_{mc} and Q_{dc} cannot be eliminated as it was possible in cases i) when soil is having weight only ($c = q = 0$) and ii) when soil is weightless having surcharge

only($\gamma = c = 0$). To obtain the relation between α_1 and α_2 for a particular value of ϕ, ϕ_m, e/B and i, trial and error method has been used. This method is explained below:

i) Assume a value of wedge angle, α_1 for a given set of values of ϕ, ϕ_m, e/B, i, D_e/B, D_f/B and β.

ii) For the above values of parameters, assume a value of α_2. Find the value of θ_1 by trial using Eq. 3.14. Compute the value of P_{pc}/cB, P_{mc}/cB using Eqs. 3.41 and 3.54.

iii) Substitute the values of P_{pc}/cB, P_{mc}/cB in Eq. 3.76 and calculate the value of Q_{dc}/cB.

iv) Substitute the values of P_{pc}/cB, P_{mc}/cB and Q_{dc}/cB in Eq. 3.78 and obtain the value of $\sum M$.

v) If $\sum M \neq 0$, then select another value of α_2 and repeat the steps from ii) to iv), till $\sum M = 0$.

vi) For $\sum M = 0$, pick up that set of values of α_1 and α_2 for the given set of values of ϕ, ϕ_m, e/B, i, D_e/B, D_f/B and β and substitute in Eq. 3.77 to satisfy $\sum H = 0$.

vii) If $\sum H = 0$, then pick up α_1, α_2 for the given set of values of ϕ, ϕ_m, e/B, i, D_e/B, D_f/B and β. If $\sum H \neq 0$, then assume another value of α_1 for the same given values of parameters and repeat steps from i) to vi) till $\sum H = 0$ condition is satisfied.

In this way, the wedge angle relation between α_1 and α_2 for the given set of parameters can be determined.

3.4 COMPUTATIONS AND RESULTS

As indicated earlier, computations for bearing capacity were carried out separately for three different cases, namely- i) for soils considering its weight only, without surcharge and cohesion, ii) for weightless and cohesionless soil having surcharge only and iii) for soils having cohesion only but without weight and surcharge, so as to evaluate the bearing capacity factors N_γ, N_q and N_c respectively.

The following steps were followed to find the values of N_γ for a given value of angle of internal friction, ϕ, slope angle, β, depth factor, D_f/B, edge distance, D_e/B, eccentricity, e and inclination of the load, i:

i) A value of mobilisation factor, m is assumed.

ii) The value of ϕ_m is calculated using Eq. 3.15.

iii) The value of α_1 is assumed.

iv) The value of α_2 is obtained from the wedge angle relationship developed in Eq. 3.62.

v) The value of angle θ_1 is calculated by trial using Eq. 3.14.

vi) The passive earth pressures, $P_{p\gamma}/\gamma B^2$ and $P_{m\gamma}/\gamma B^2$ are obtained by using Eqs. 3.39 and 3.52.

vii) The above computed values of passive earth pressures satisfy the two equations of equilibrium, namely $\sum V = 0$ and $\sum M = 0$ simultaneously as the former is used for determining the bearing capacity, Q_d and later is used for developing the wedge angle relationship. The equilibrium equation, $\sum H = 0$ remains only to be satisfied.

viii) Substitute the values of earth pressures obtained in step vi) in Eq. 3.57. If this equation $\sum H = 0$ is satisfied, then pick up the value of α_1 and α_2. Otherwise assume another value of α_1 and repeat the steps iv) to vii).

ix) Repeat the steps ii) to vii) for different values of mobilization factor, m. The passive earth pressures corresponding to the maximum value of m satisfying all the three conditions of equilibrium are adopted in computing the bearing capacity factor, N_γ.

x) The passive earth pressures and wedge angles for the maximum value of mobilization factor, m which satisfies all the conditions of equilibrium are substituted in Eq. 3.23 to obtain bearing capacity factor, N_γ.

The maximum value of m was adopted because for failure, the soil must develop maximum possible resistance compatible with stability. The corresponding bearing capacity factor is the smallest in this case. Computations for N_γ were carried out for range of values of ϕ, β, D_f/B, D_e/B, e/B *and* i and presented in the form of

charts in Figs. 3.10 a, b, c, d for parametric values, i=0°, D_f/B=0, e/B=0.0, 0.1, 0.2 and 0.3, and D_e/B varied between 0 to 5.0 and for values of slope angles, β varied between 0° to 40°. Charts for N_γ values are presented in Figs. 3.11 a, b, c, d for load inclination, i=10° and in Figs. 3.12 a, b, c, d for load inclination i=20°. Similar charts for N_γ have also been presented for D_f/B=0.5 and D_f/B=1.0 in Appendix-I. It is to be noted that for cohesion less soil, N_γ value is to be taken only when angle of friction ϕ is greater than the slope angle, β, or otherwise the slope becomes unstable and this analysis cannot be applied.

The same procedure as given above for N_γ has been followed for the evaluation of bearing capacity factor N_q and the computations were carried out and presented in the form of charts in Figs. 3.13 a, b, c, d for parametric values, i=0°, D_f/B=0, e/B=0.0, 0.1, 0.2 and 0.3, and D_e/B varied between 0 to 5.0. Charts for N_q values are presented in Figs. 3.14 a, b, c, d for load inclination, i=10° and in Figs. 3.15 a, b, c, d for load inclination i=20°. The N_q values for surface footing (D_f/B = 0) have been found to be independent of slope angle β. Similar charts for N_q have also been presented for D_f/B=0.5 and D_f/B=1.0 in Appendix-II. While using these tables for cohesionless soils, N_q values will be picked up only when slope angle β is less than friction angle ϕ.

The procedure for computation of bearing capacity factor, N_c is different. Here the earth pressures, P_{pc}/cB, P_{mc}/cB, determined during calculations of the wedge angles α_1 and α_2, satisfy all the three conditions of equilibrium. So these values are substituted in Eq. 3.25 to calculate the bearing capacity factor, N_c. These values of N_c are presented in the form of charts in Figs. 3.16 a, b, c, d for parametric values, i=0°, D_f/B=0, e/B=0.0, 0.1, 0.2 and 0.3, and D_e/B varied between 0 to 6.0 and for values of slope angle, β varied between 0° to 50°. Similar charts for N_c have been presented in Figs. 3.17 a, b, c, d for load inclination, i=10° and in Figs. 3.18 a, b, c, d for load inclination i=20° . Similar charts for N_γ have also been presented for D_f/B=0.5 and D_f/B=1.0 in Appendix-III.

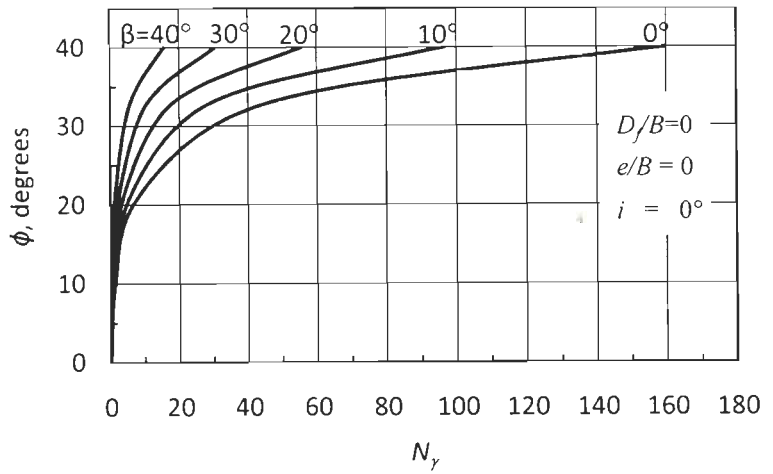

Fig. 3.10 a (i) N_γ versus ϕ for, D_e/B=0

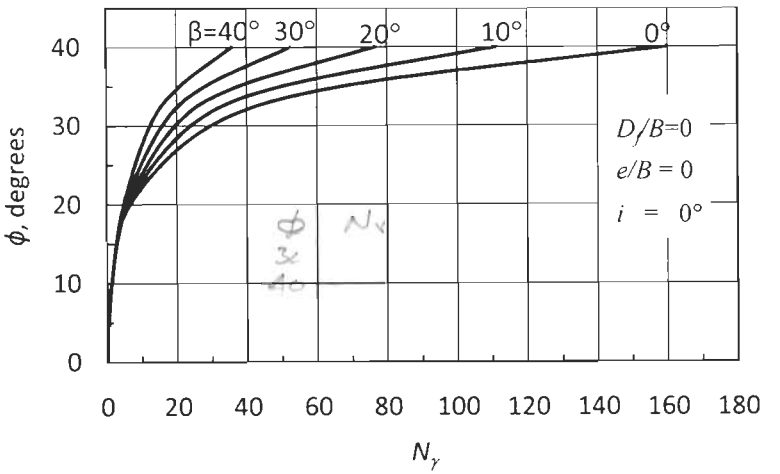

Fig. 3.10 a (ii) N_γ versus ϕ for, D_e/B=1.0

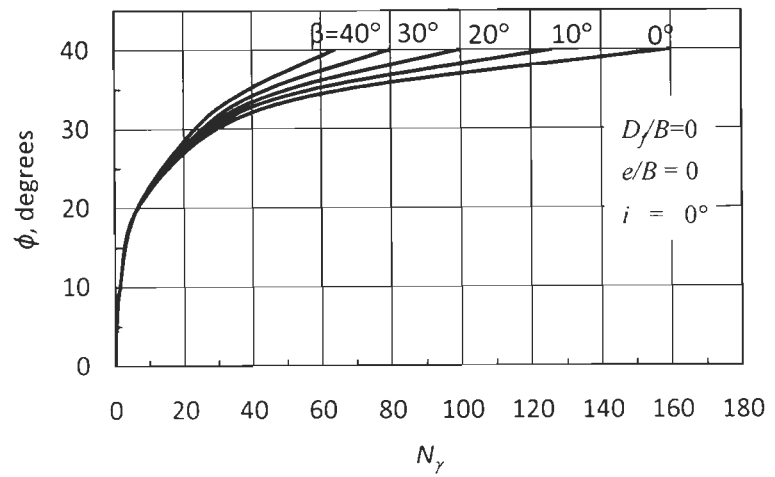

Fig. 3.10 a (iii) N_γ versus ϕ for D_e/B=2.0

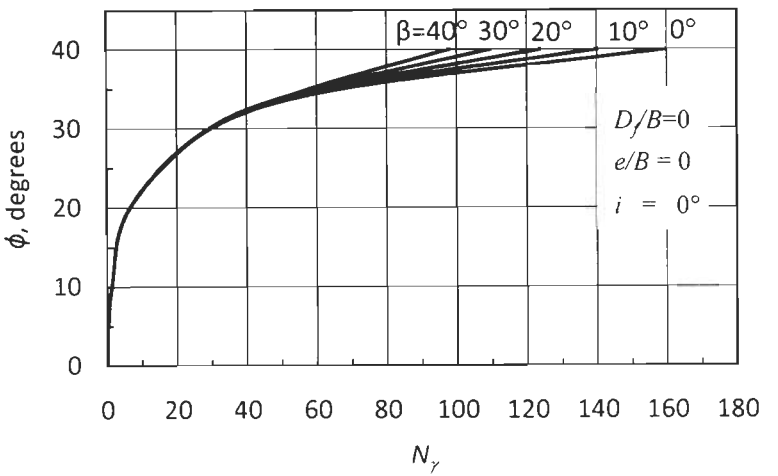

Fig. 3.10 a (iv) N_γ versus ϕ for D_e/B=3.0

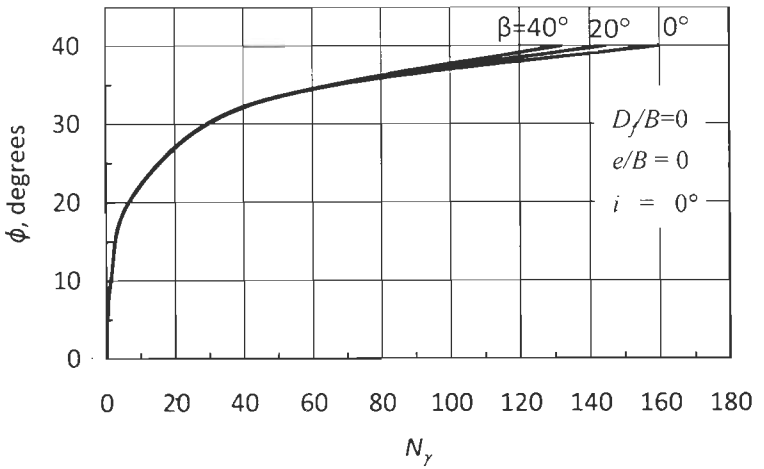

Fig. 3.10 a (v) N_γ versus ϕ for D_e/B=4.0

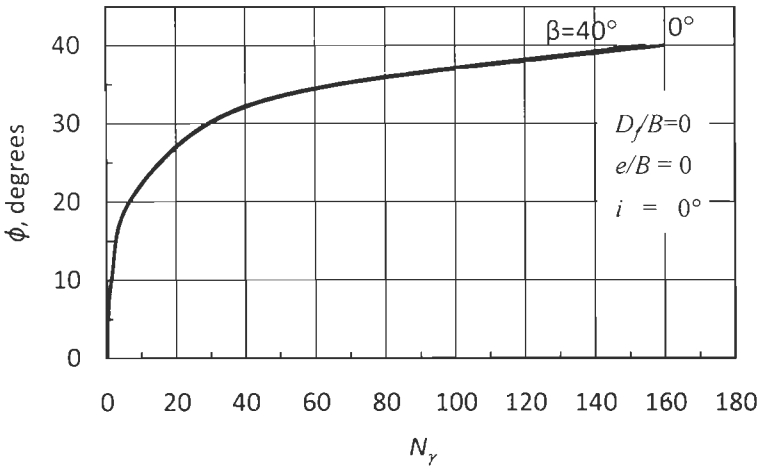

Fig. 3.10 a (vi) N_γ versus ϕ for D_e/B=5.0

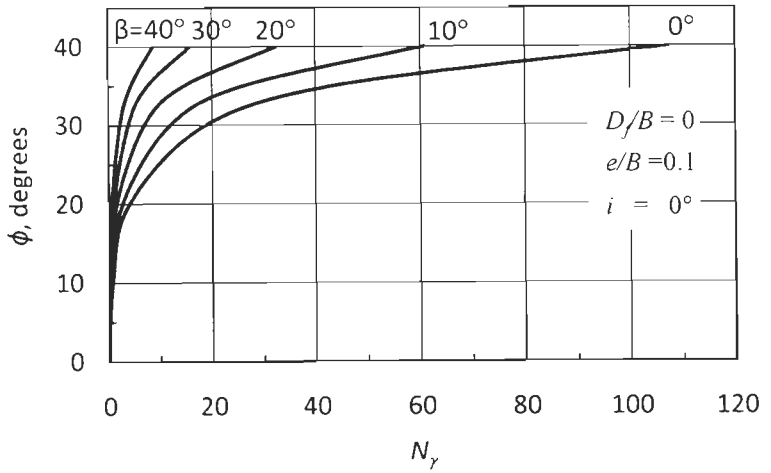

Fig. 3.10 b (i) N_γ versus ϕ D_e/B=0

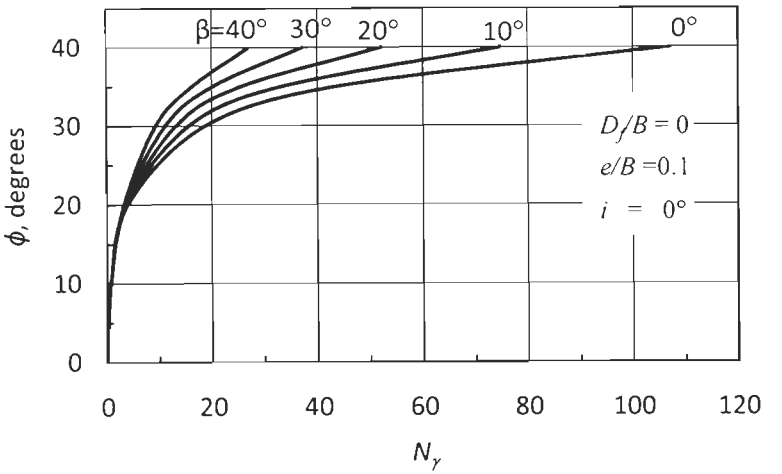

Fig. 3.10 b (ii) N_γ versus ϕ for D_e/B=1.0

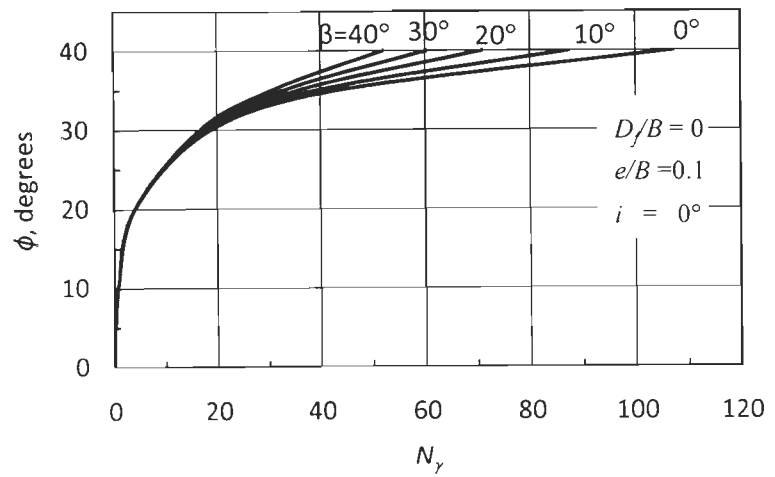

Fig. 3.10 b (iii) N_γ versus ϕ for D_e/B=2.0

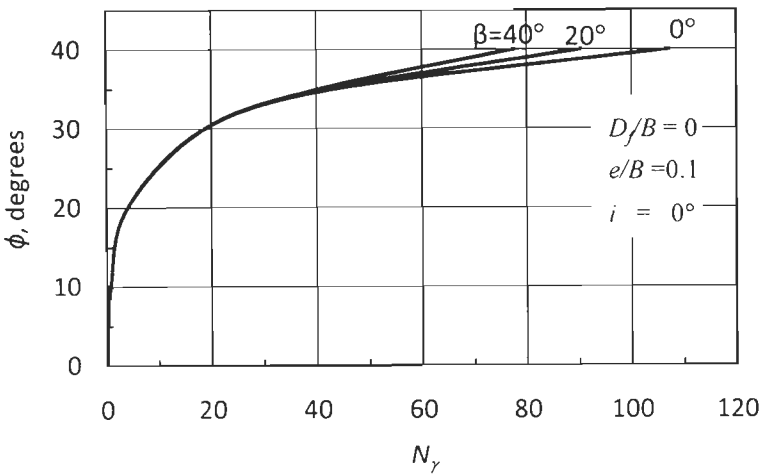

Fig. 3.10 b (iv) N_γ versus ϕ for D_e/B=3.0

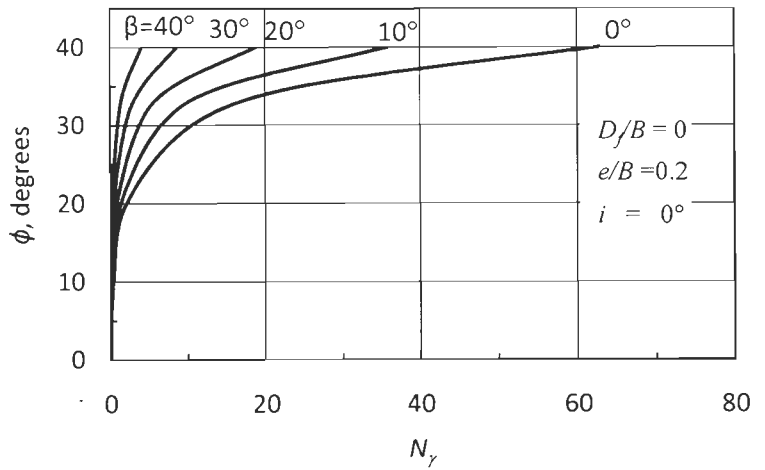

Fig. 3.10 c (i) N_γ versus ϕ for D_e/B=0

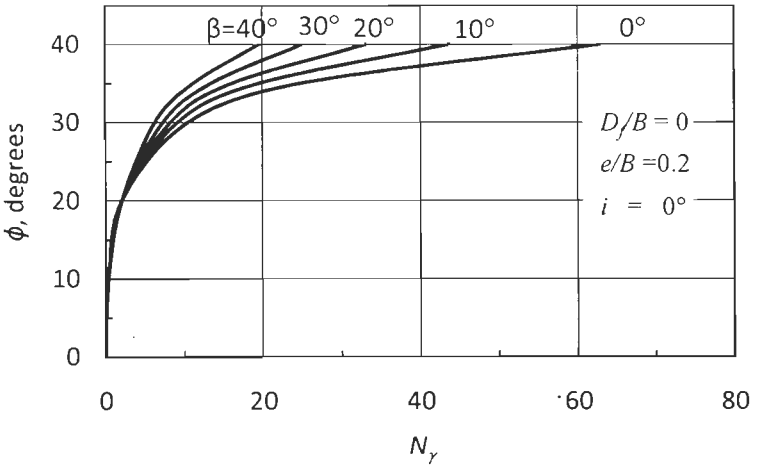

Fig. 3.10 c (ii) N_γ versus ϕ for D_e/B=1.0

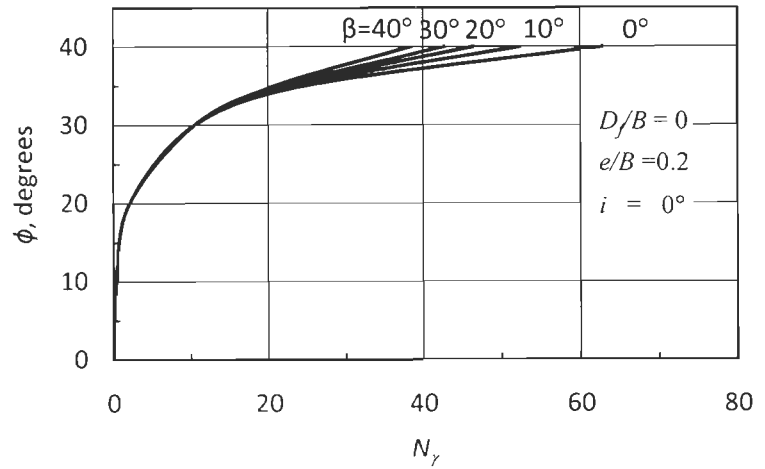

Fig. 3.10 c (iii) N_γ versus ϕ for D_e/B=2.0

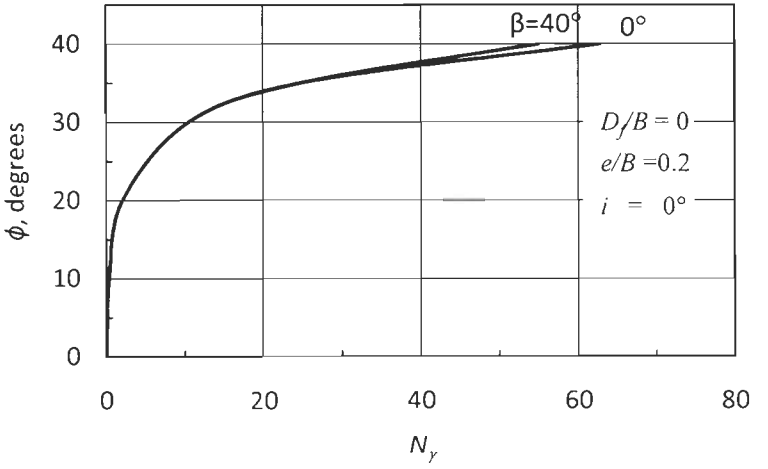

Fig. 3.10 c (iv) N_γ versus ϕ for D_e/B=3.0

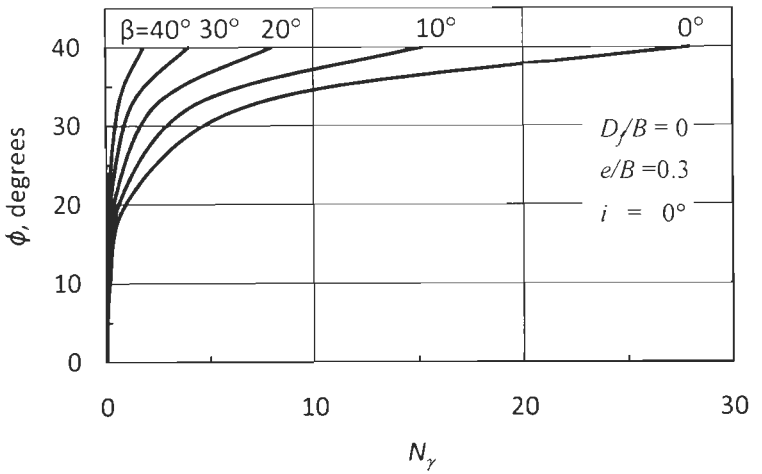

Fig. 3.10 d (i) N_γ versus ϕ for D_e/B=0

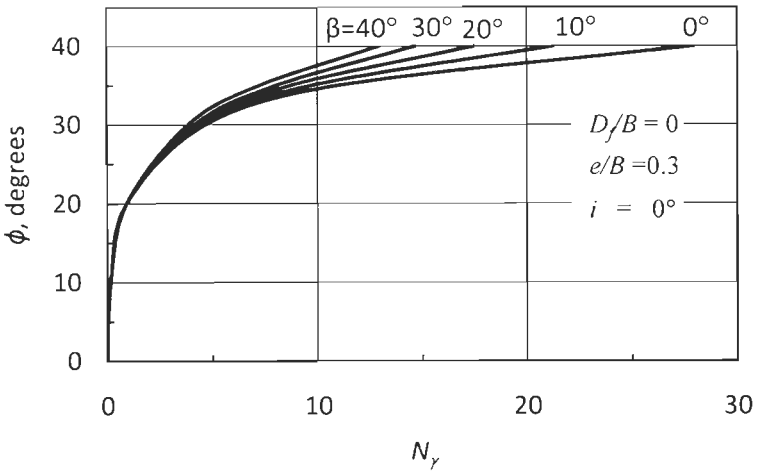

Fig. 3.10 d (ii) N_γ versus ϕ for D_e/B=1.0

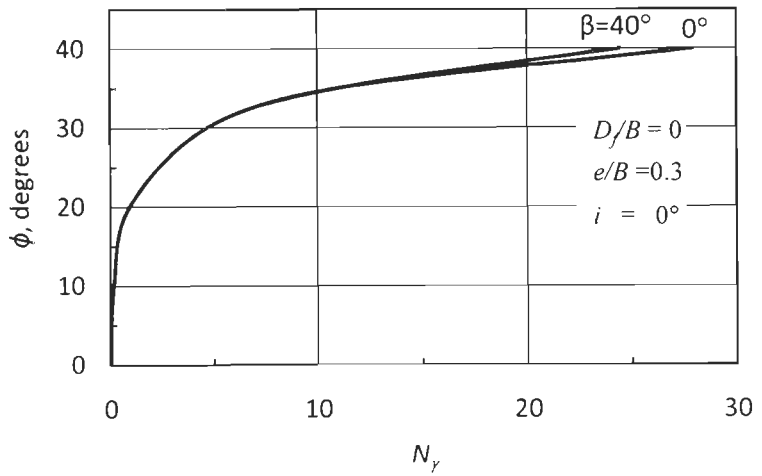

Fig. 3.10 d (iii) N_γ versus ϕ for D_e/B=2.0

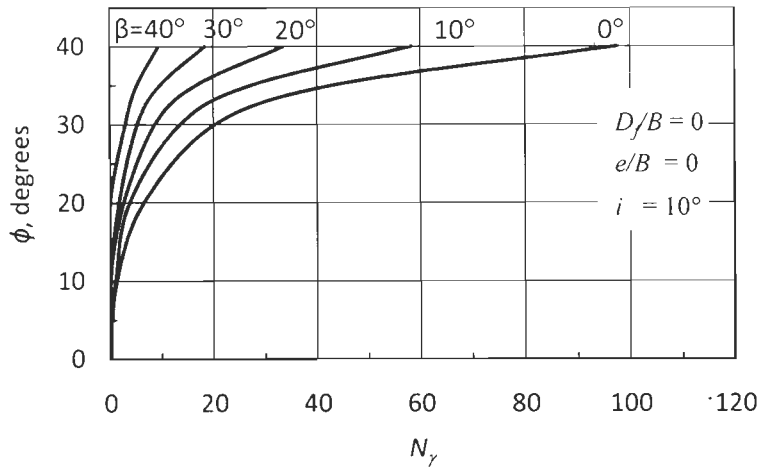

Fig. 3.11 a (i) N_γ versus ϕ for D_e/B=0

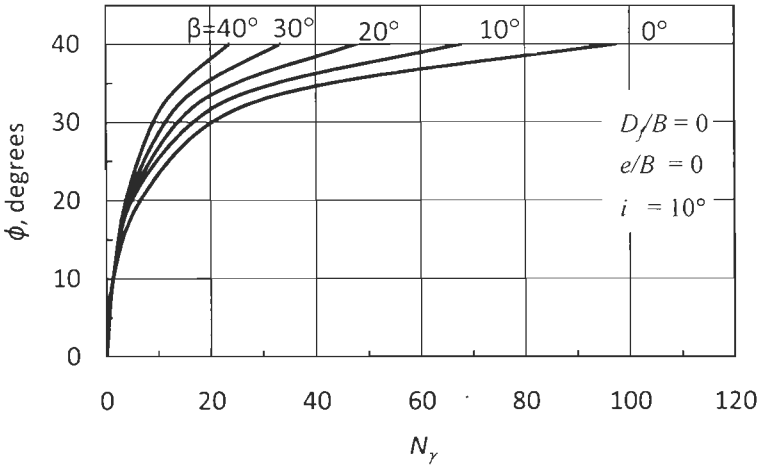

Fig. 3.11 a (ii) N_γ versus ϕ for D_e/B=1.0

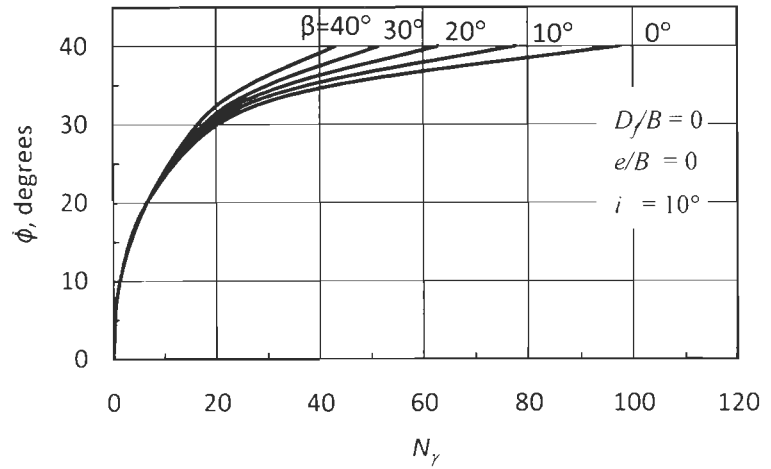

Fig. 3.11 a (iii) N_γ versus ϕ for D_e/B=2.0

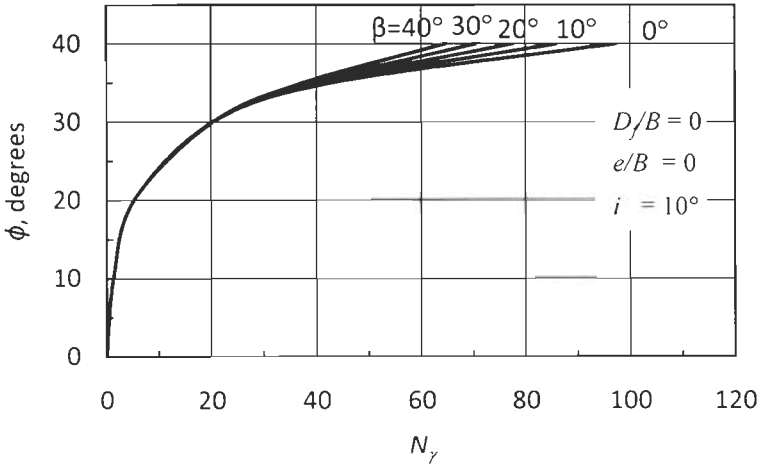

Fig. 3.11 a (iv) N_γ versus ϕ for D_e/B=3.0

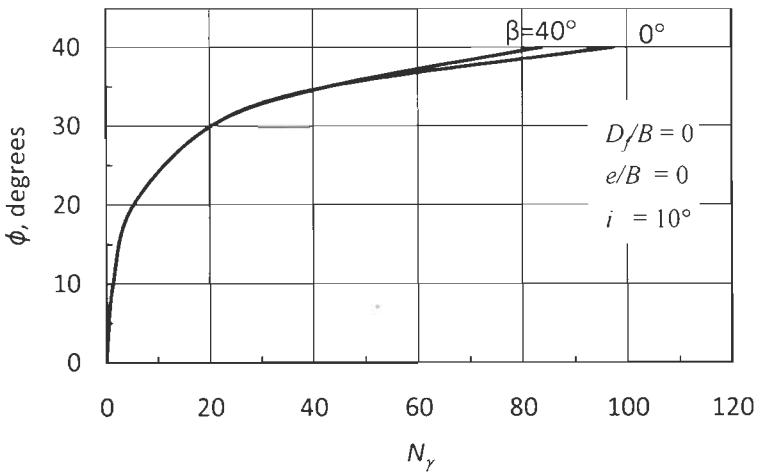

Fig. 3.11 a (v) N_γ versus ϕ for D_e/B=4.0

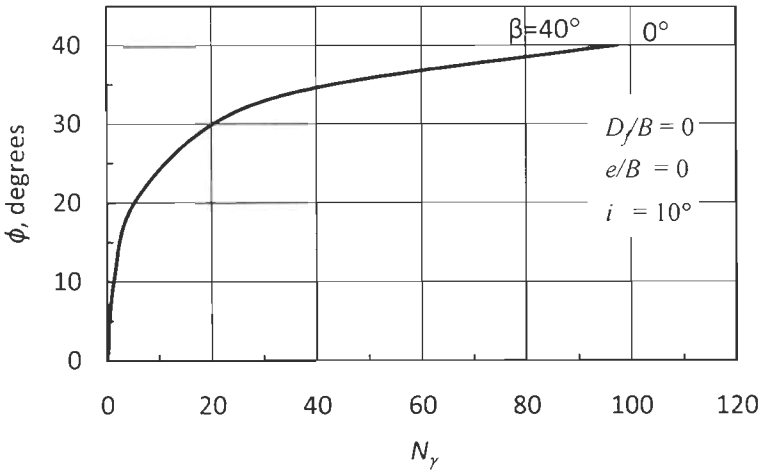

Fig. 3.11 a (vi) N_γ versus ϕ for D_e/B=5.5

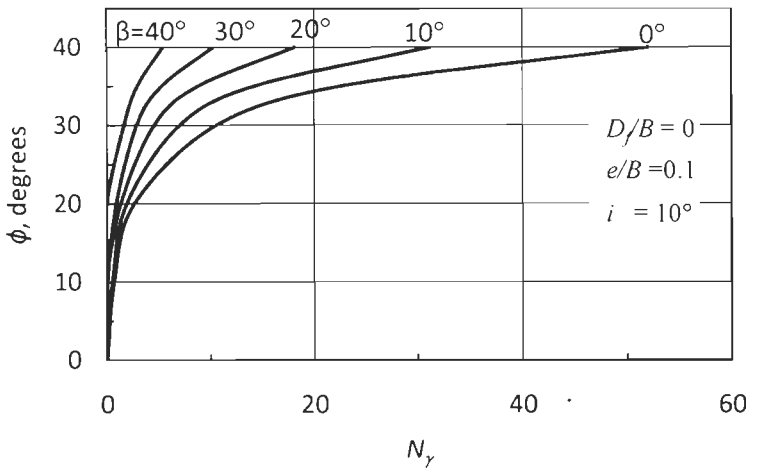

Fig. 3.11 b (i) N_γ versus ϕ for D_e/B=0

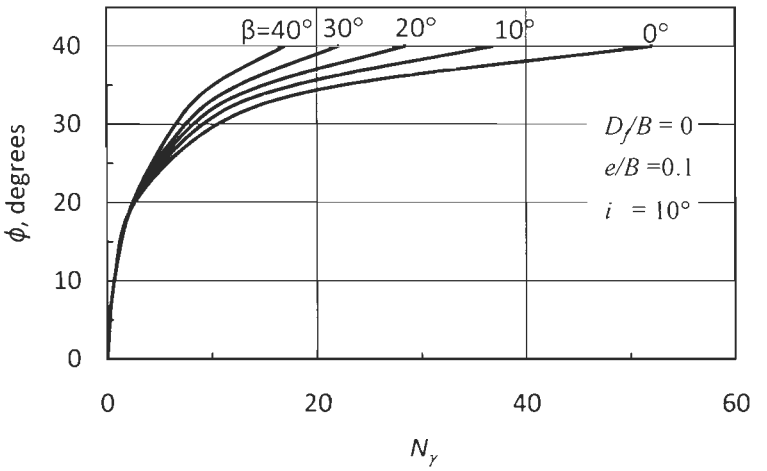

Fig. 3.11 b (ii) N_γ versus ϕ for D_e/B=1.0

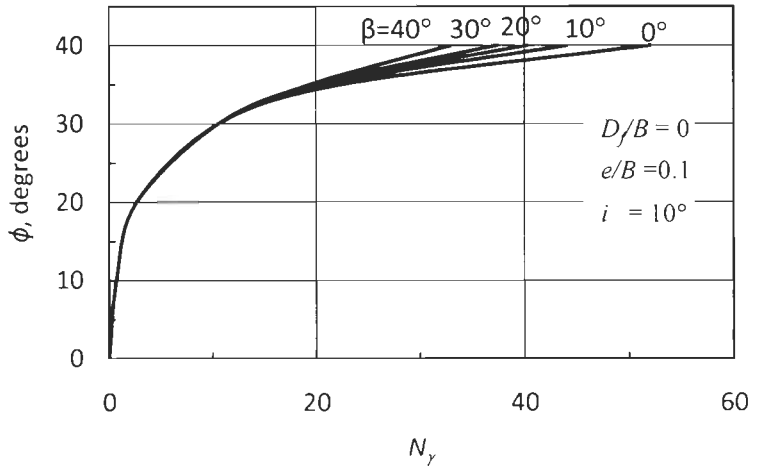

Fig. 3.11 b (iii) N_γ versus ϕ for D_e/B=2.0

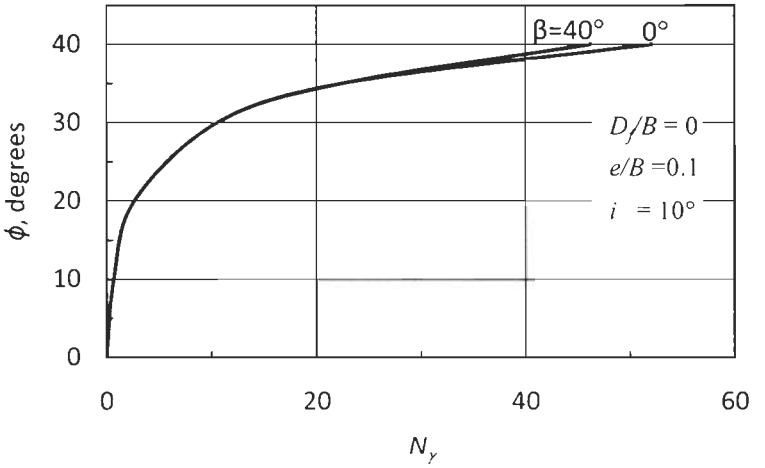

Fig. 3.11 b (iv) N_γ versus ϕ for D_e/B=3.0

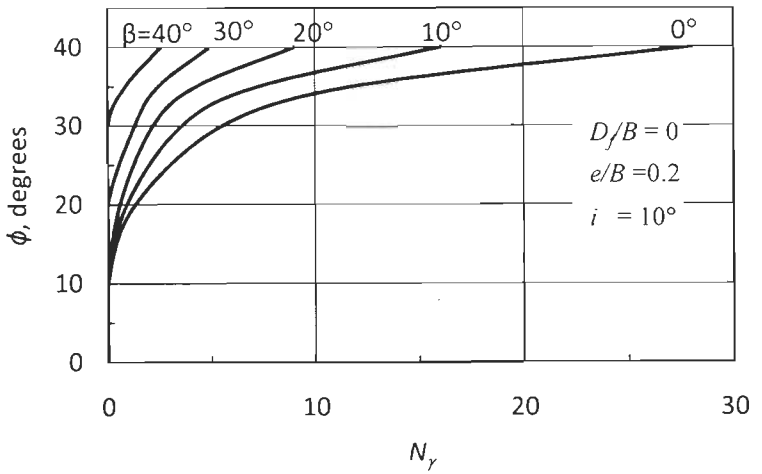

Fig. 3.11 c (i) N_γ versus ϕ for D_e/B=0

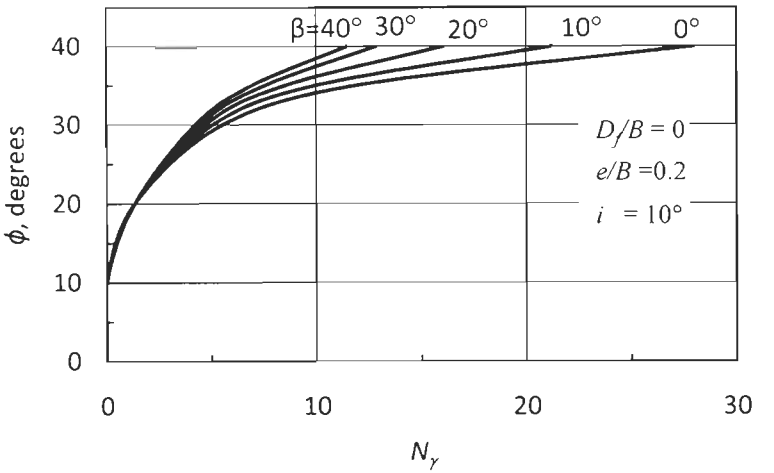

Fig. 3.11 c (ii) N_γ versus ϕ for D_e/B=1.0

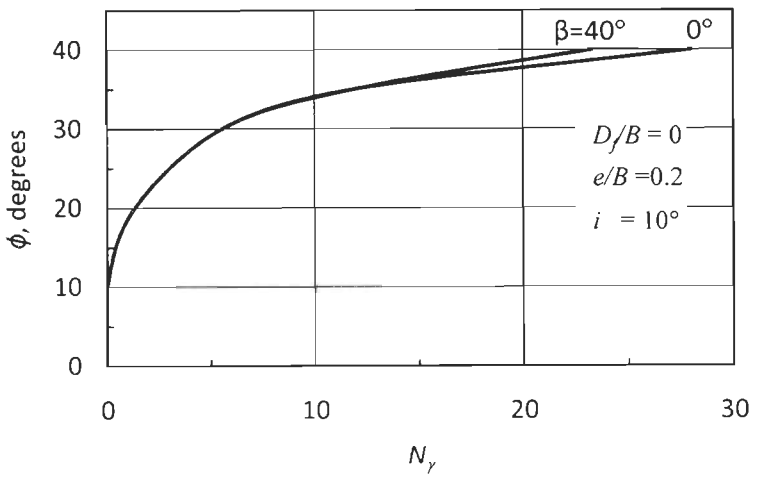

Fig. 3.11 c (iii) N_γ versus ϕ for D_e/B=2.0

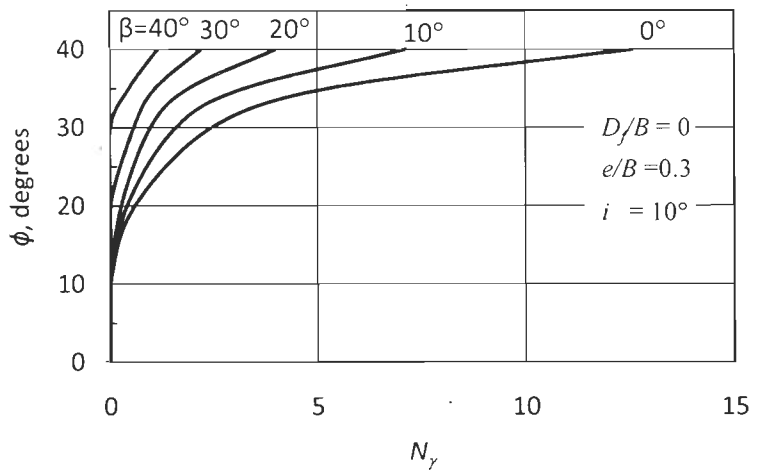

Fig. 3.11 d (i) N_γ versus ϕ for D_e/B=0

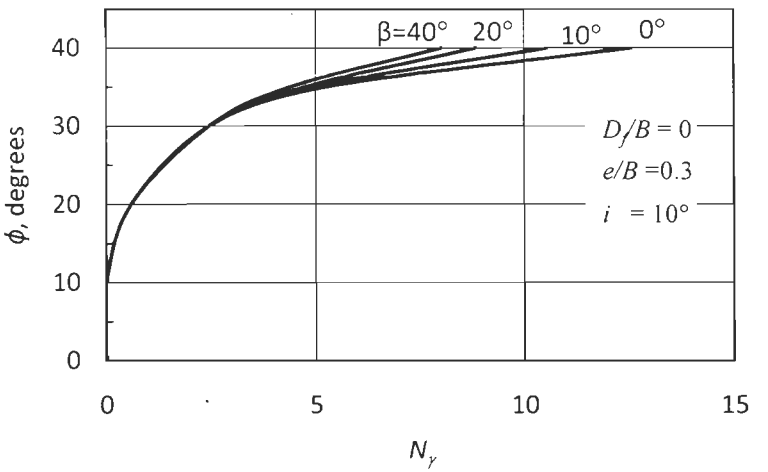

Fig. 3.11 d (ii) N_γ versus ϕ for D_e/B=1.0

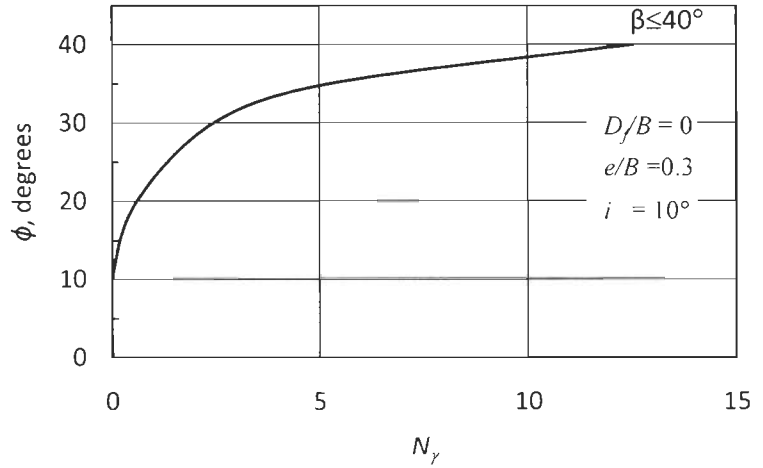

Fig. 3.11 d (iii) N_γ versus ϕ for D_e/B=2.0

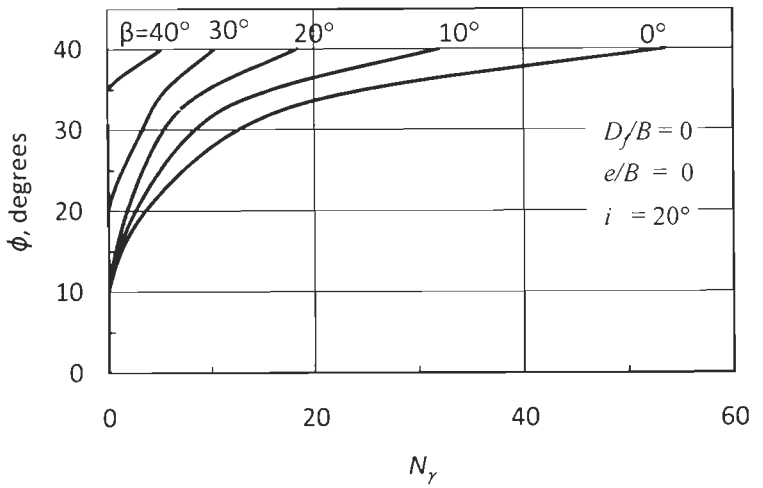

Fig. 3.12 a N_γ versus ϕ for D_e/B=0

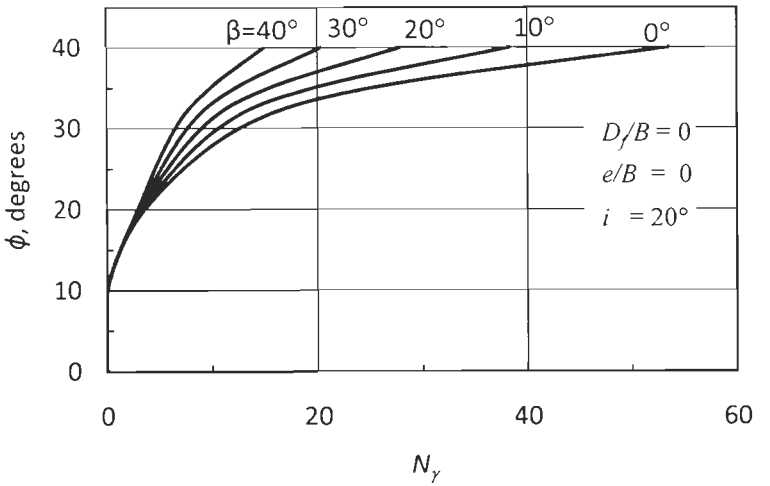

Fig. 3.12 a (ii) N_γ versus ϕ for D_e/B=1.0

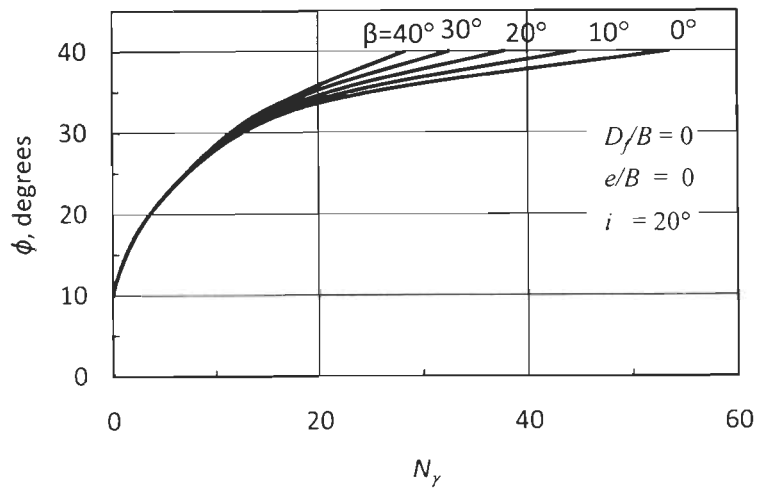

Fig. 3.12 a (iii) N_γ versus ϕ for D_e/B=2.0

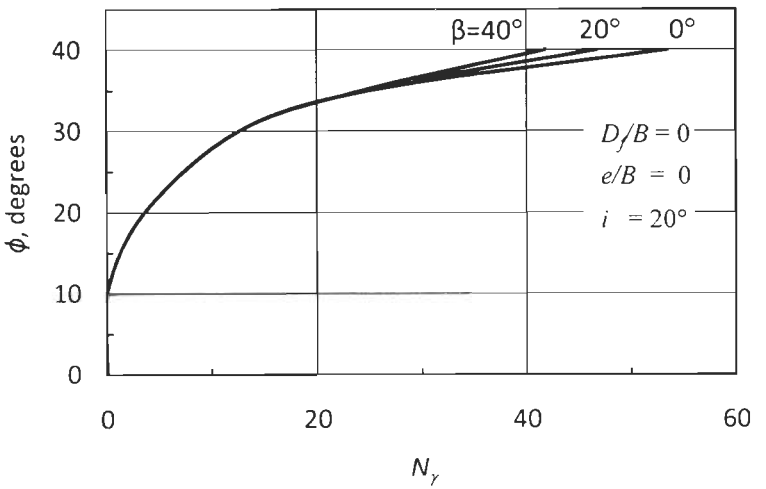

Fig. 3.12 a (iv) N_γ versus ϕ for D_e/B=3.0

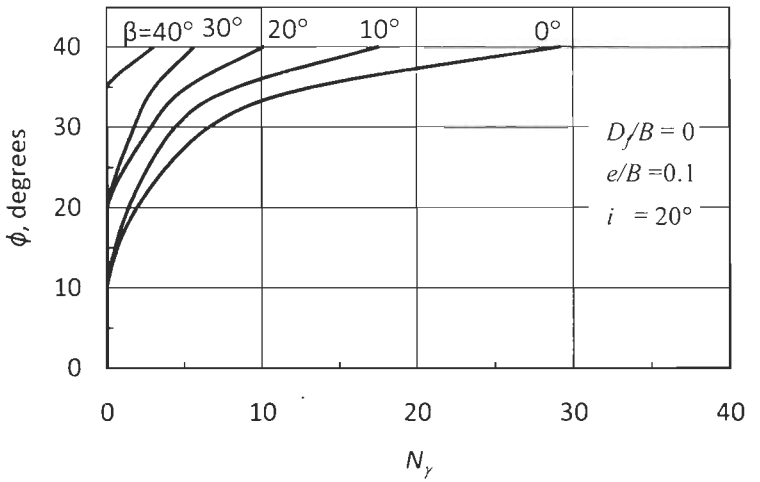

Fig. 3.12 b (i) N_γ versus ϕ for D_e/B=0

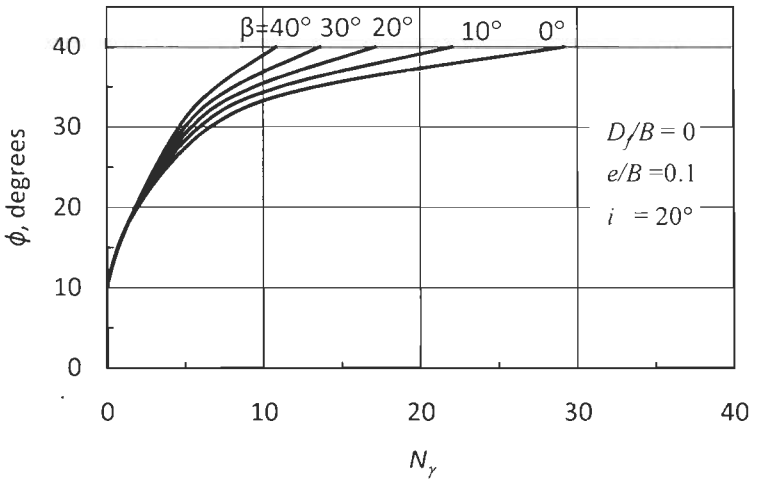

Fig. 3.12 b (ii) N_γ versus ϕ for D_e/B=1.0

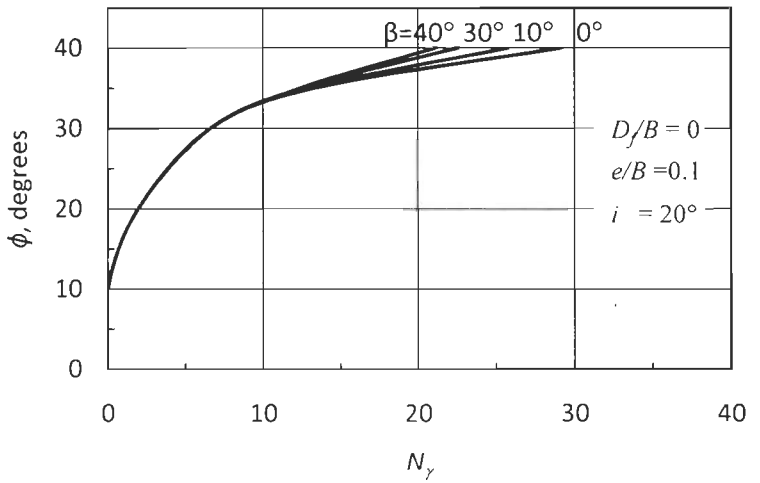

Fig. 3.12 b (iii) N_γ versus ϕ for D_e/B=2.0

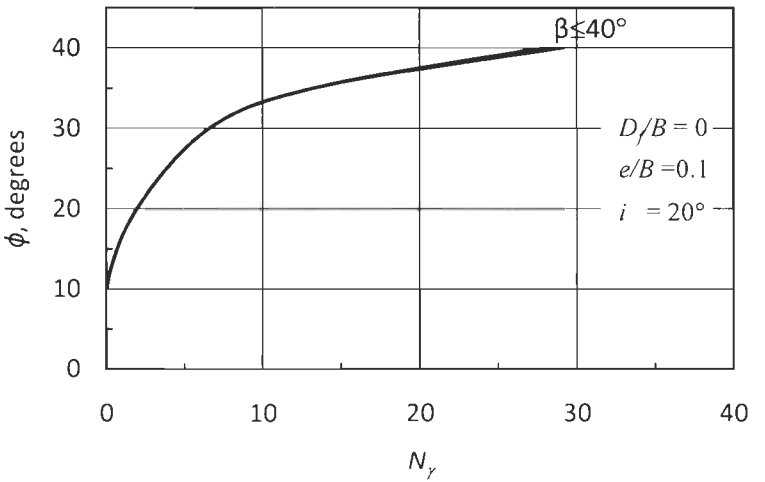

Fig. 3.12 b (iv) N_γ versus ϕ for D_e/B=3.0

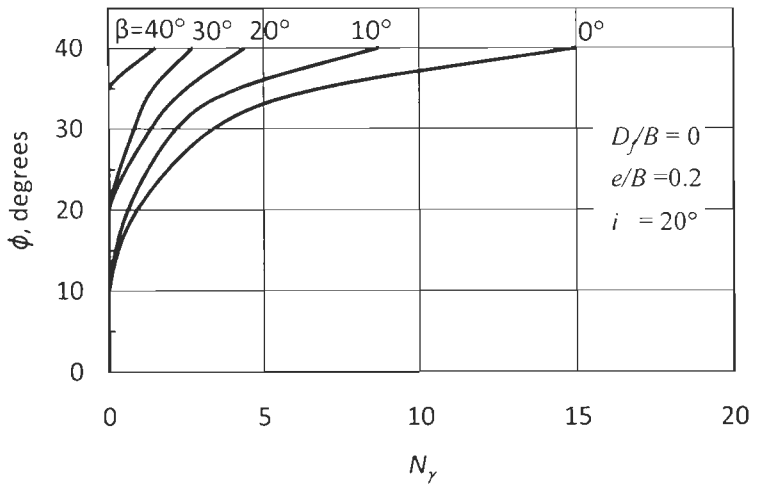

Fig. 3.12 c (i) N_γ versus ϕ for D_e/B=0

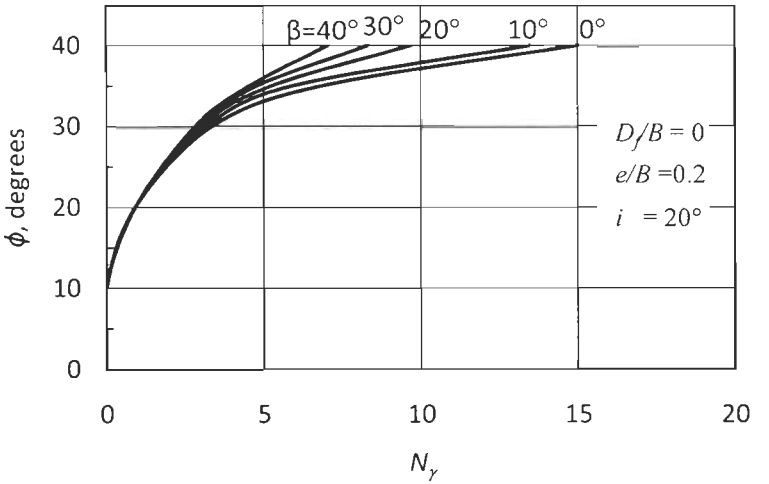

Fig. 3.12 c (ii) N_γ versus ϕ for D_e/B=1.0

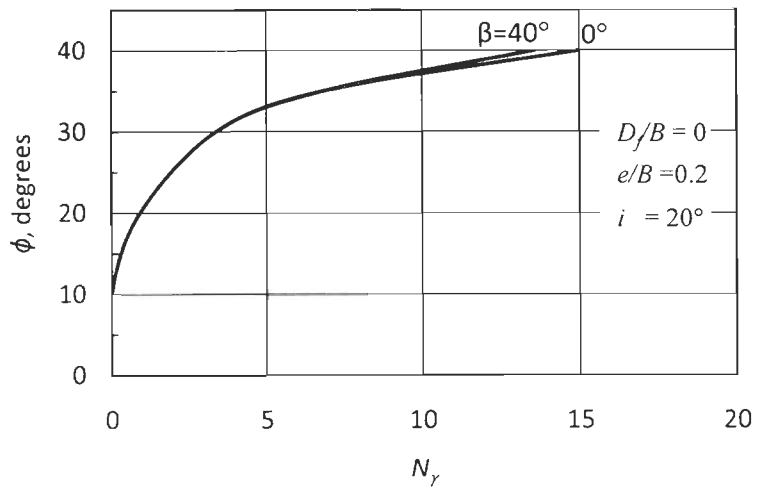

Fig. 3.12 c (iii) N_γ versus ϕ for D_e/B=2.0

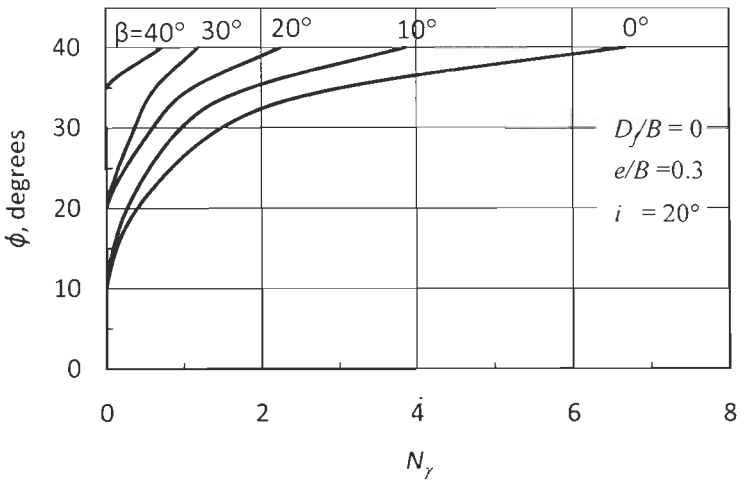

Fig. 3.12 d (i) N_γ versus ϕ for D_e/B=0

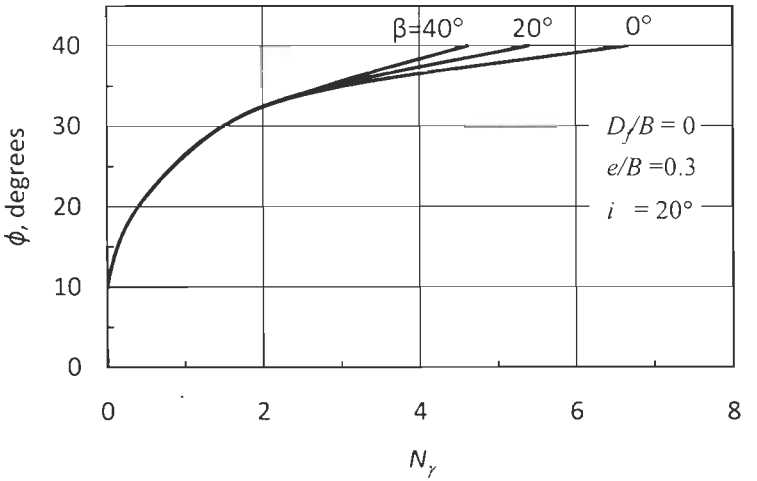

Fig. 3.12 d (ii) N_γ versus ϕ for D_e/B=1.0

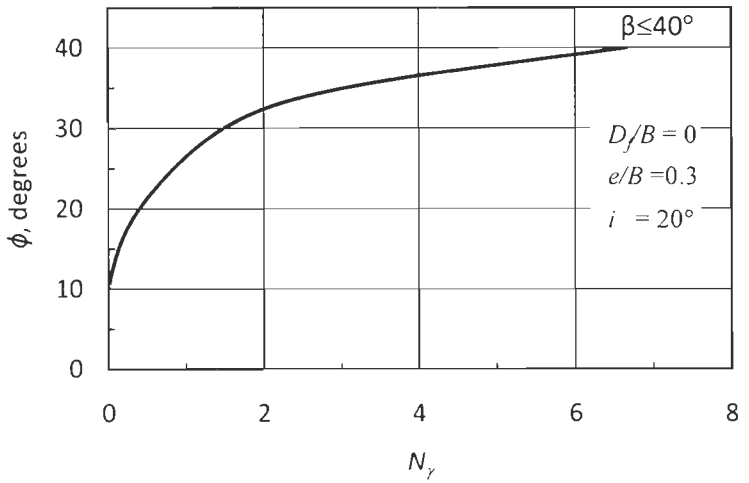

Fig. 3.12 d (iii) N_γ versus ϕ for D_e/B=2.0

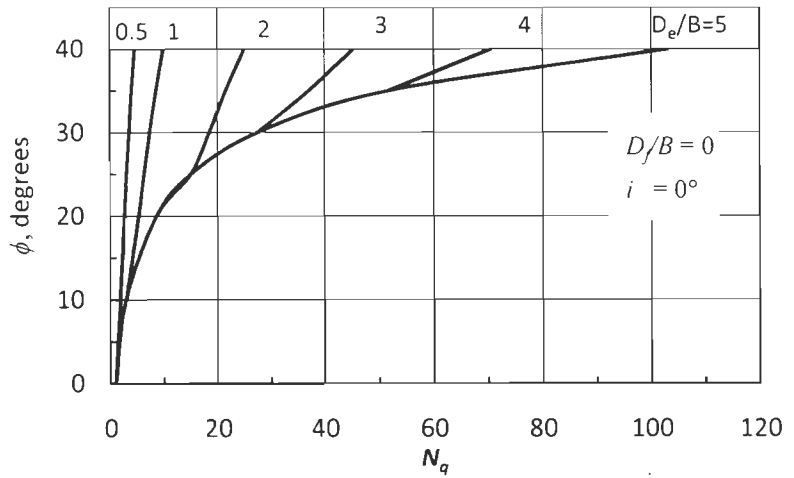

Fig. 3.13 a N_q versus ϕ for e/B=0

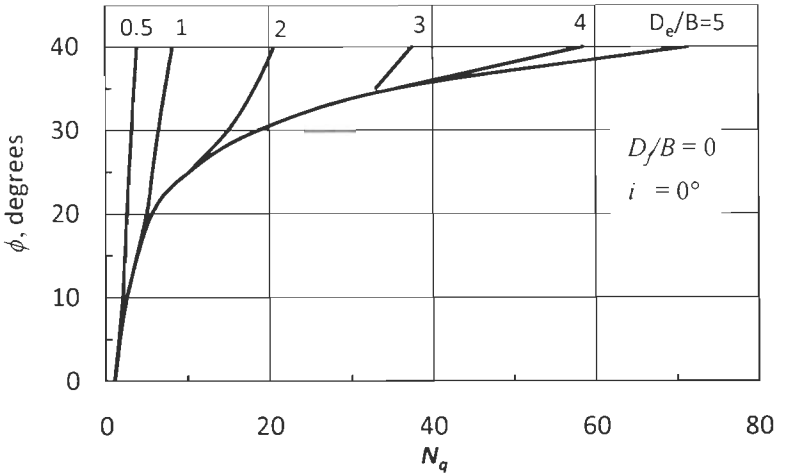

Fig. 3.13 b N_q versus ϕ for e/B=0.1

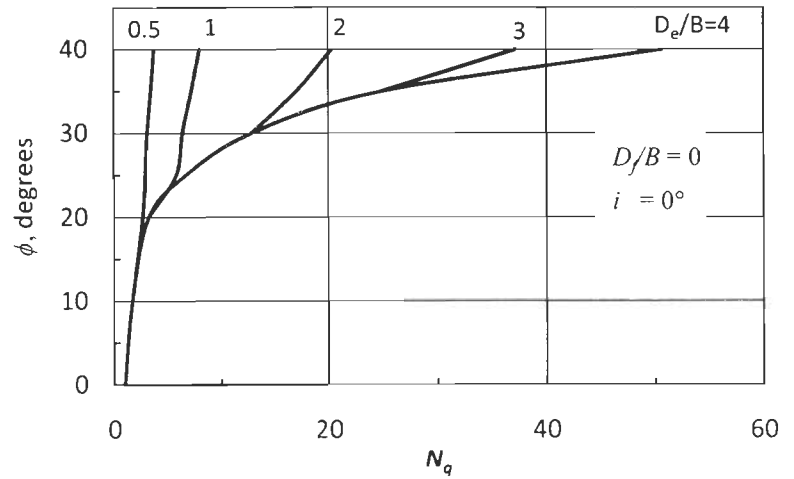

Fig. 3.13 c N_q versus ϕ for e/B=0.2

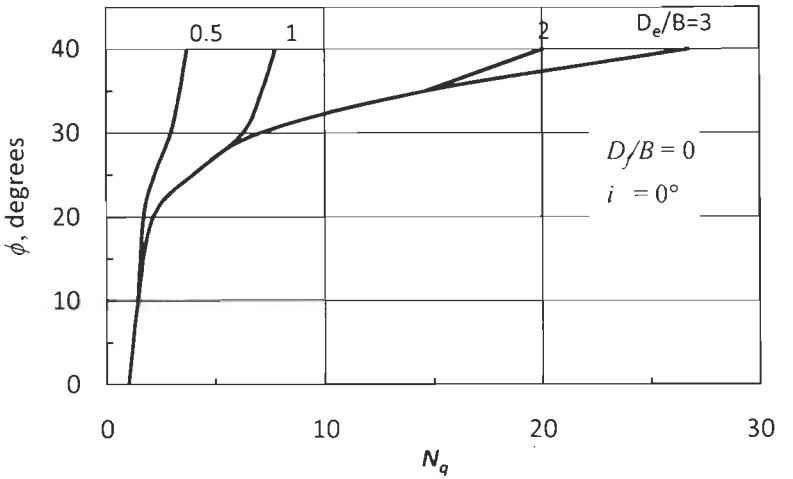

Fig. 3.13 d N_q versus ϕ for e/B=0.3

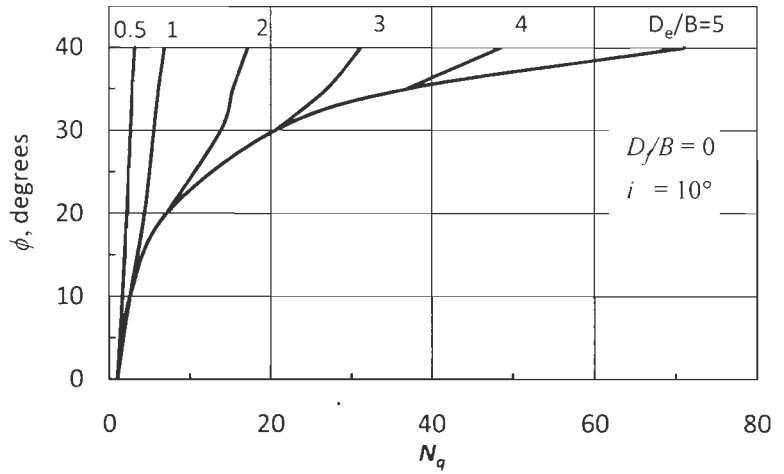

Fig. 3.14 a N_q versus ϕ for e/B=0

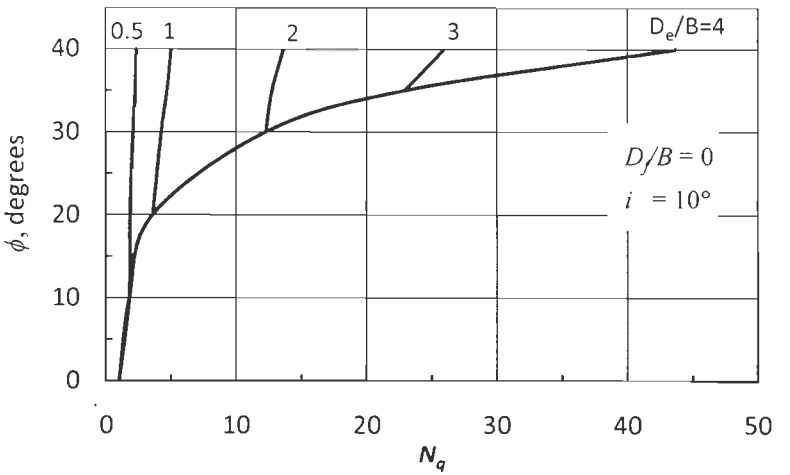

Fig. 3.14 b N_q versus ϕ for e/B=0.1

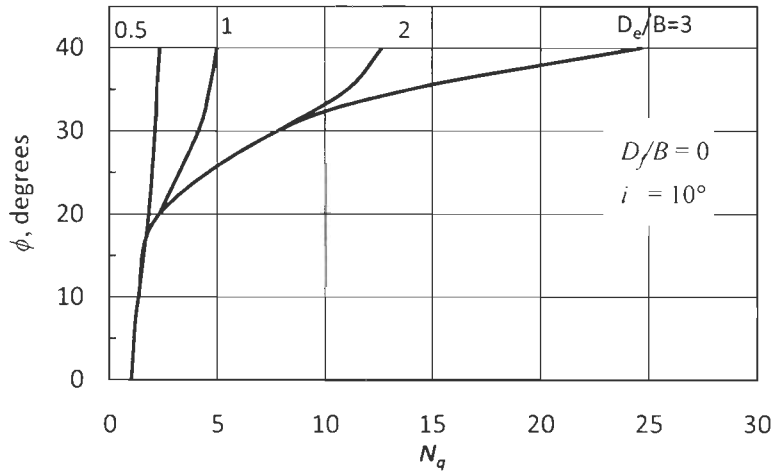

Fig. 3.14 c N_q versus ϕ for e/B=0.2

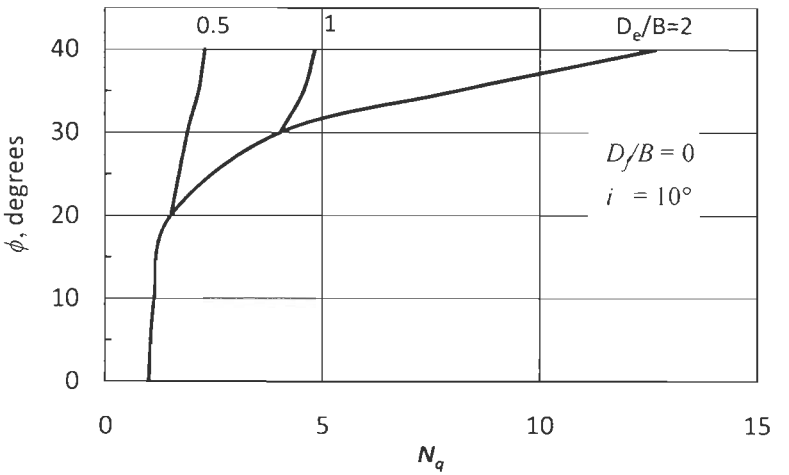

Fig. 3.14 d N_q versus ϕ for e/B=0.3

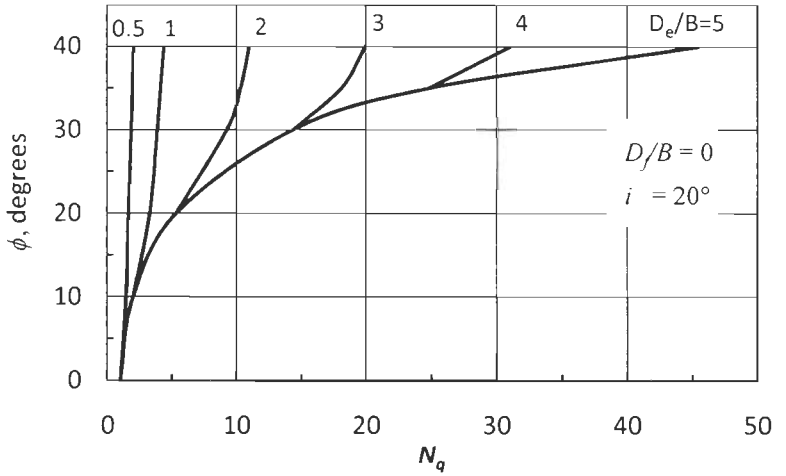

Fig. 3.15 a N_q versus ϕ for e/B=0

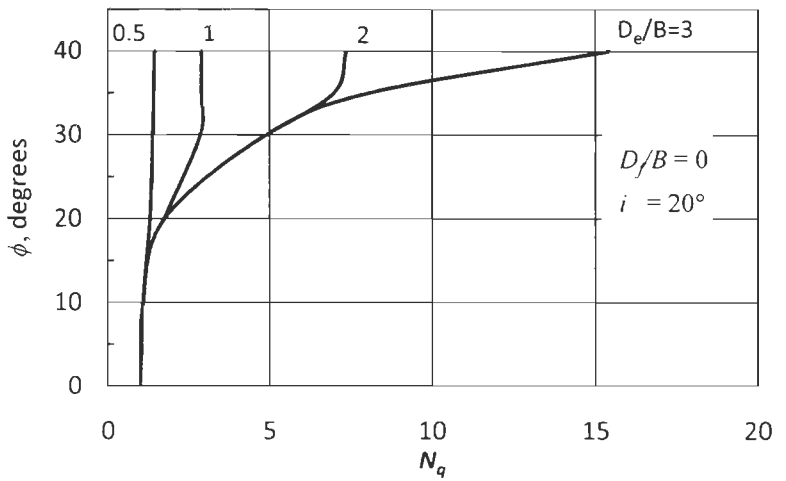

Fig. 3.15 c N_q versus ϕ for e/B=0.2

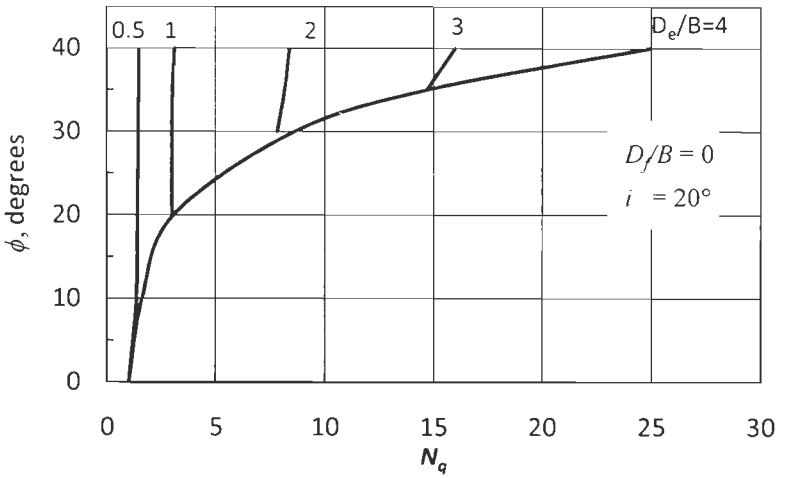

Fig. 3.15 c N_q versus ϕ for e/B=0.1

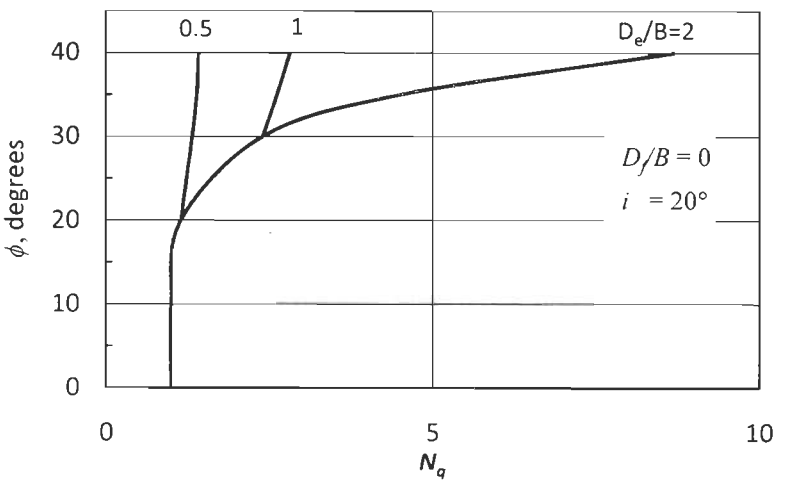

Fig. 3.15 d N_q versus ϕ for e/B=0.3

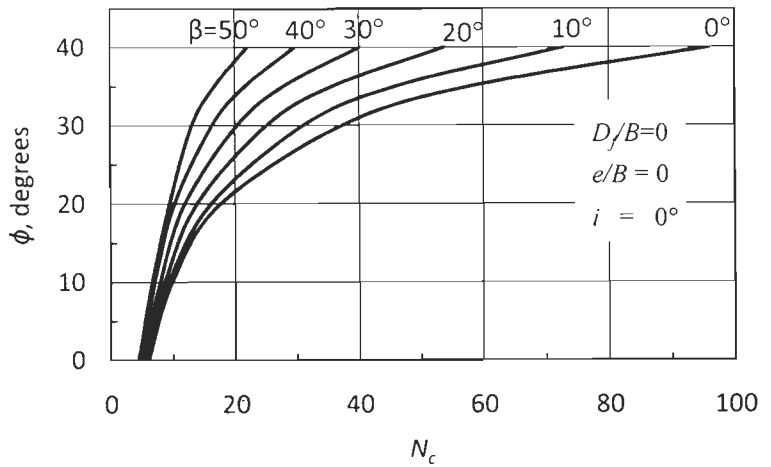

Fig. 3.16 a (i) N_c versus ϕ for D_e/B=0

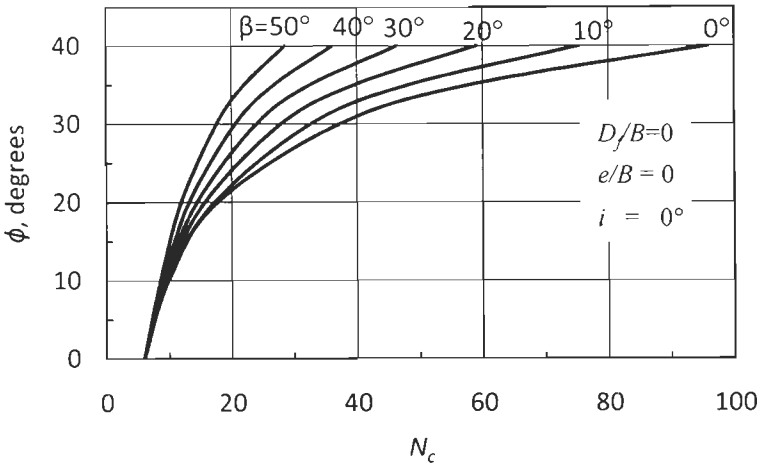

Fig. 3.16 a (ii) N_c versus ϕ for D_e/B=1.0

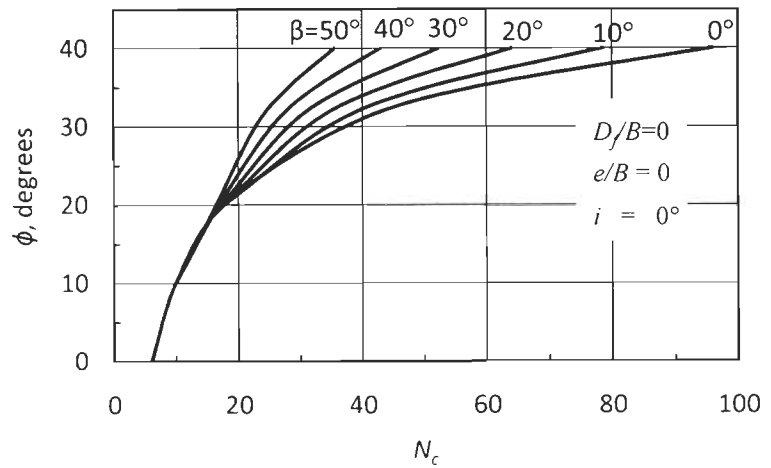

Fig. 3.16 a (iii) N_c versus ϕ for D_e/B=2.0

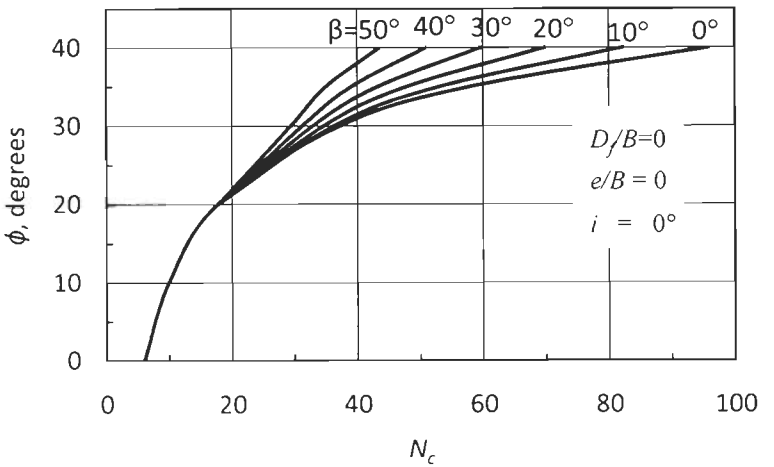

Fig. 3.16 a (iv) N_c versus ϕ for D_e/B=3.0

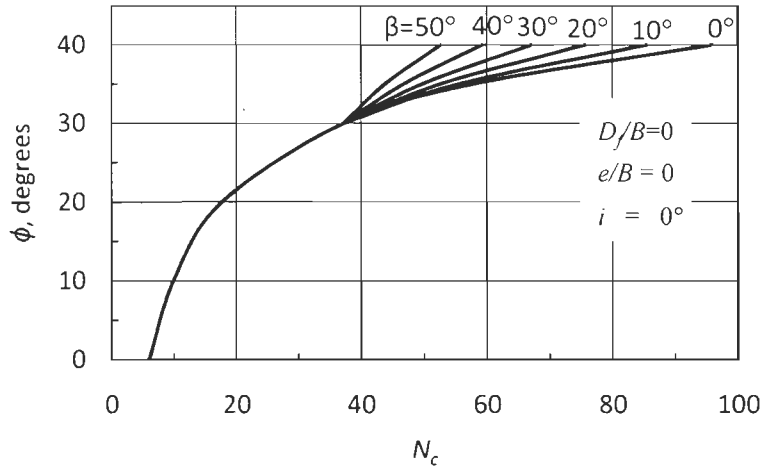

Fig. 3.16 a (v) N_c versus ϕ for D_e/B=4.0

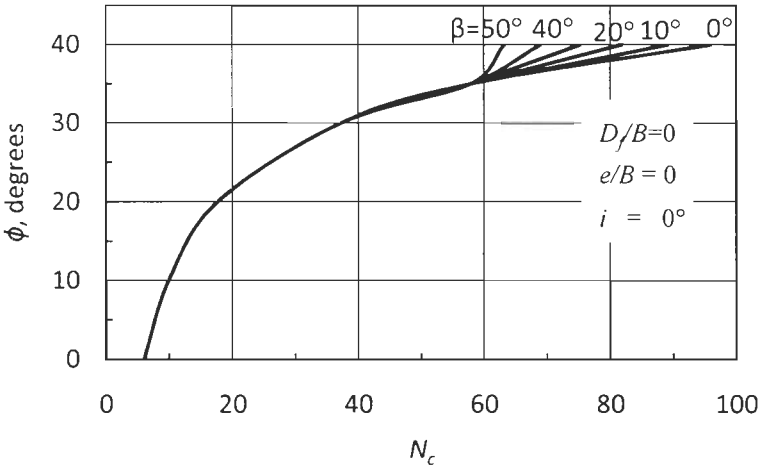

Fig. 3.16 a (vi) N_c versus ϕ for D_e/B=5.0

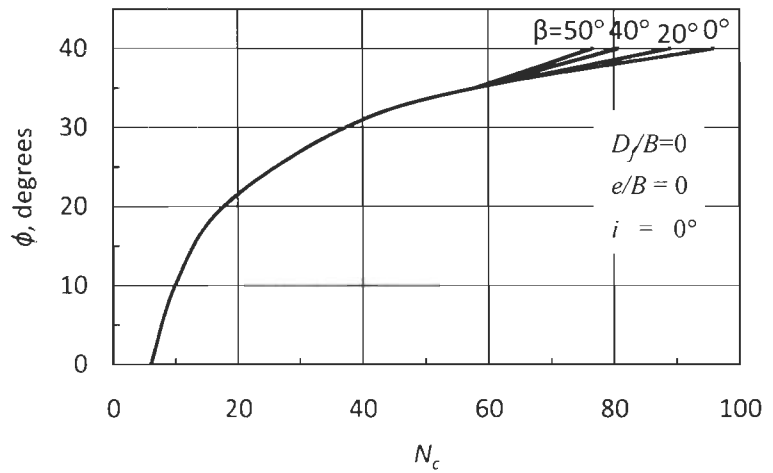

Fig. 3.16 a (vii) N_c versus ϕ for D_e/B=6.0

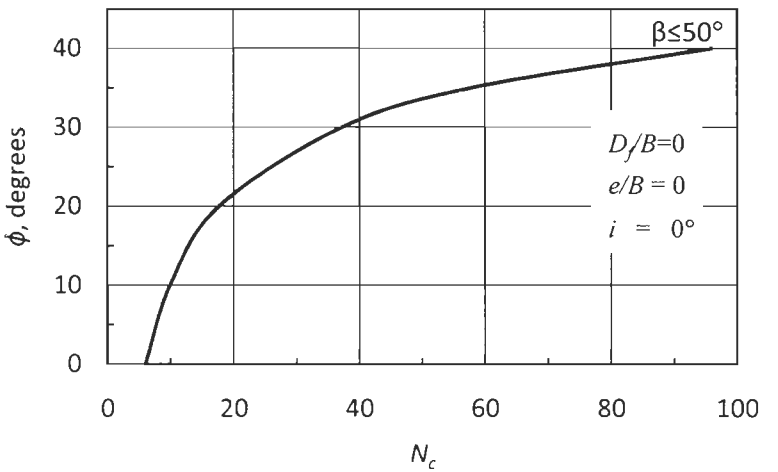

Fig. 3.16 a (viii) N_c versus ϕ for D_e/B=7.0

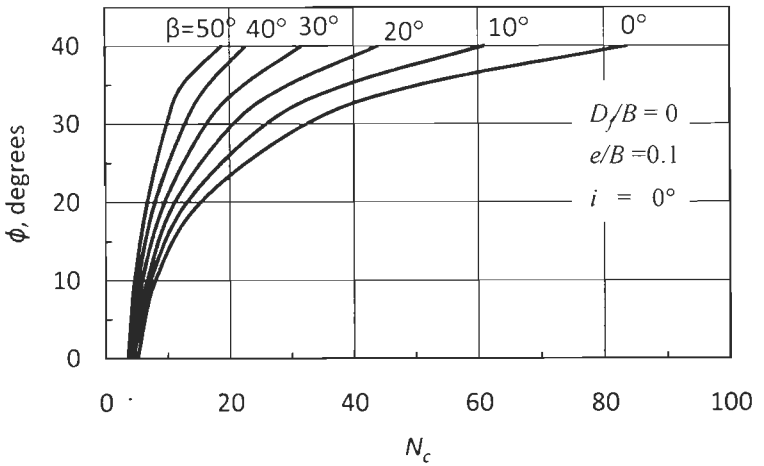

Fig. 3.16 b (i) N_c versus ϕ for D_e/B=0

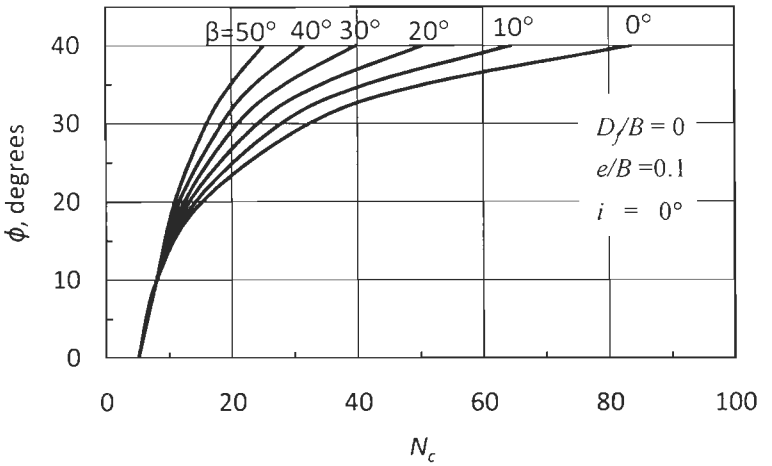

Fig. 3.16 b (ii) N_c versus ϕ for D_e/B=1.0

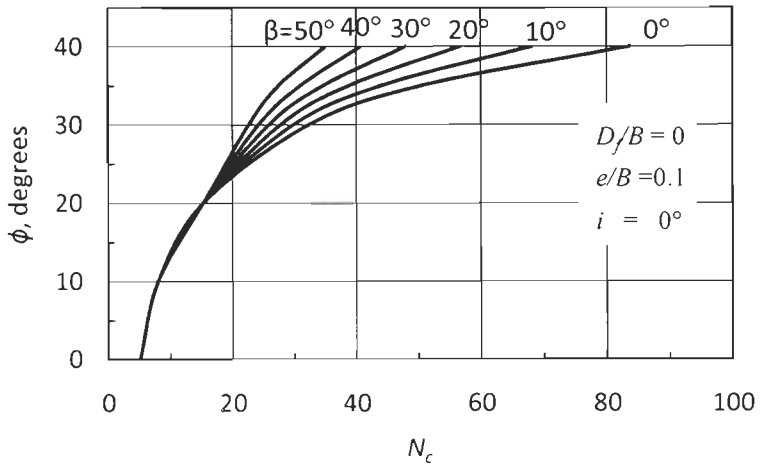

Fig. 3.16 b (iii) N_c versus ϕ for D_e/B=2.0

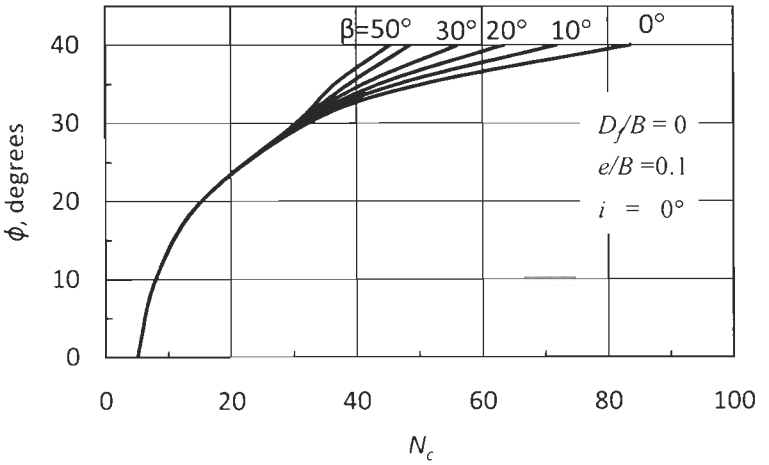

Fig. 3.16 b (iv) N_c versus ϕ for D_e/B=3.0

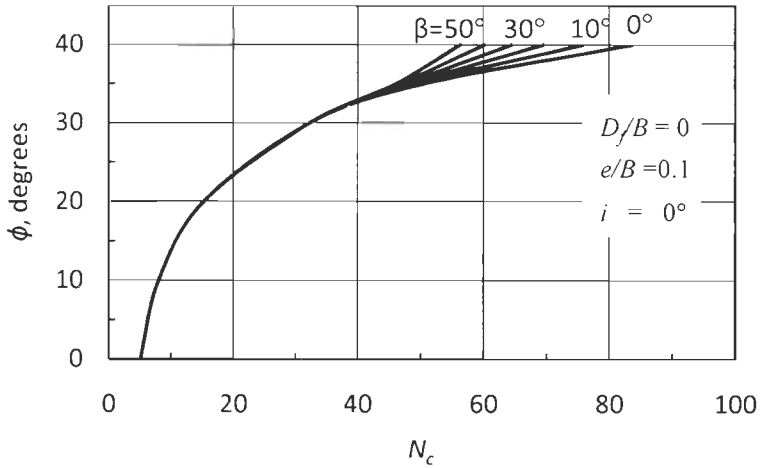

Fig. 3.16 b (v) N_c versus ϕ for D_e/B=4.0

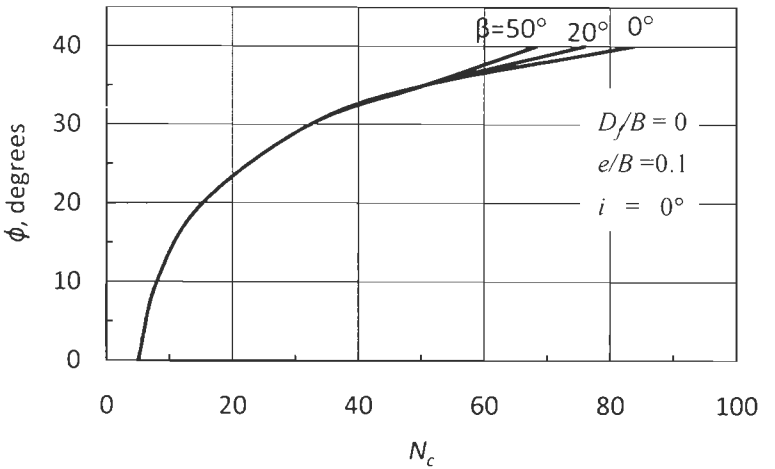

Fig. 3.16 b (vi) N_c versus ϕ for D_e/B=5.0

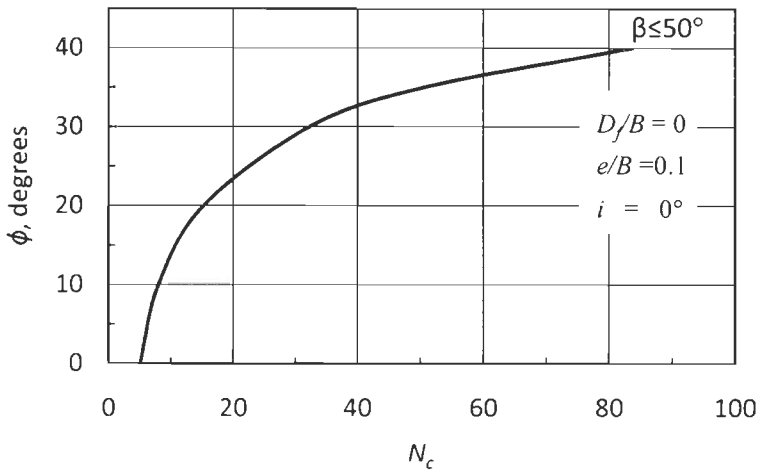

Fig. 3.16 b (vii) N_c versus ϕ for D_e/B=6.0

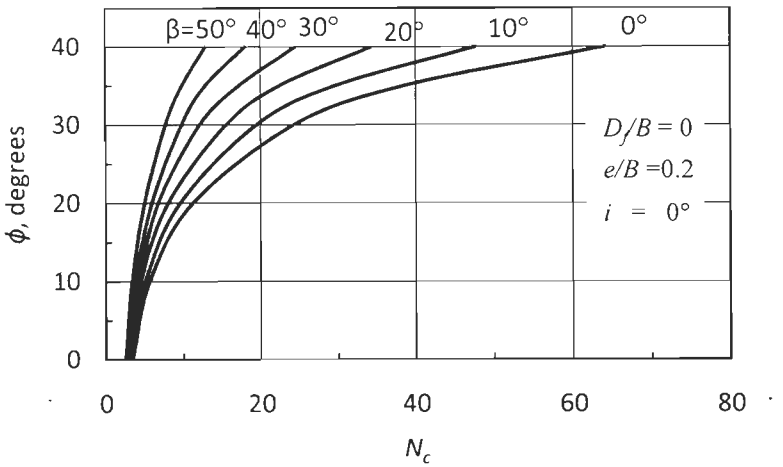

Fig. 3.16 c (i) N_c versus ϕ for D_e/B=0

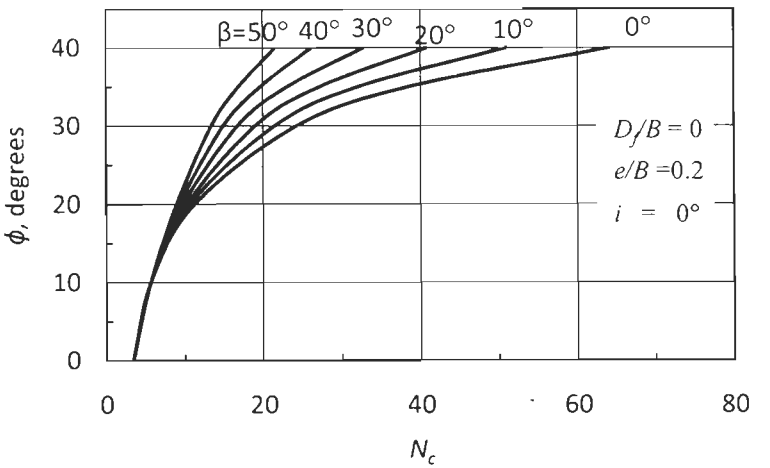

Fig. 3.16 c (ii) N_c versus ϕ for D_e/B=1.0

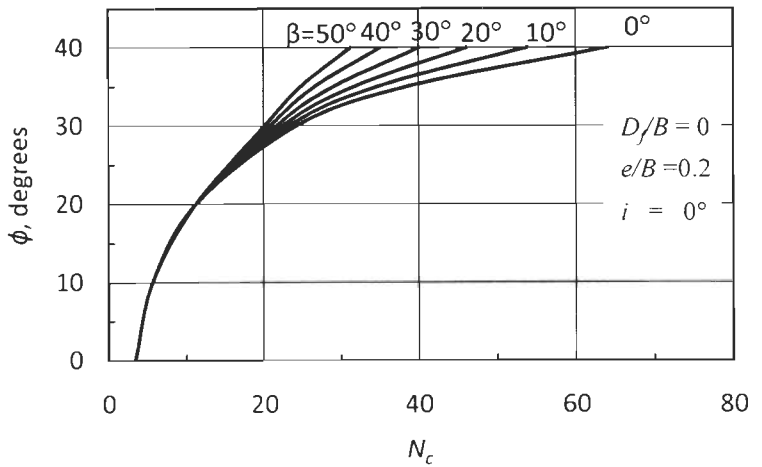

Fig. 3.16 c (iii) N_c versus ϕ for D_e/B=2.0

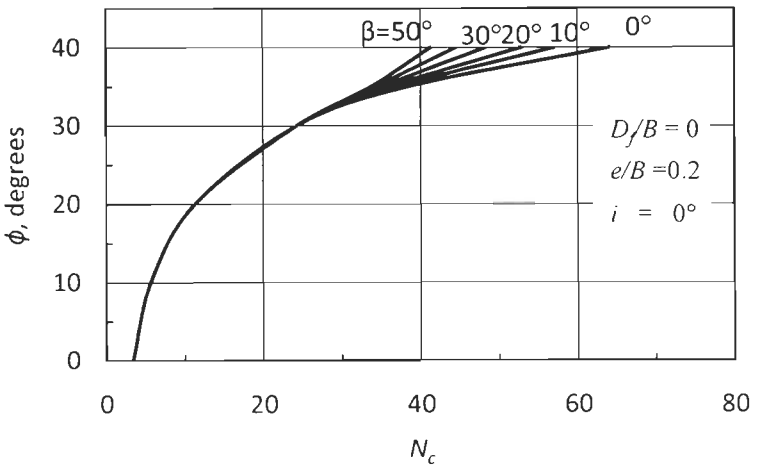

Fig. 3.16 c (iv) N_q versus ϕ for D_e/B=3.0

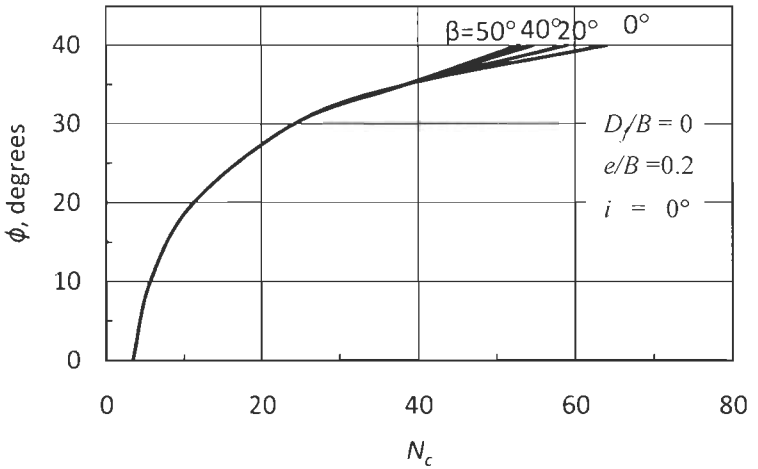

Fig. 3.16 c (v) N_c versus ϕ for D_e/B=4.0

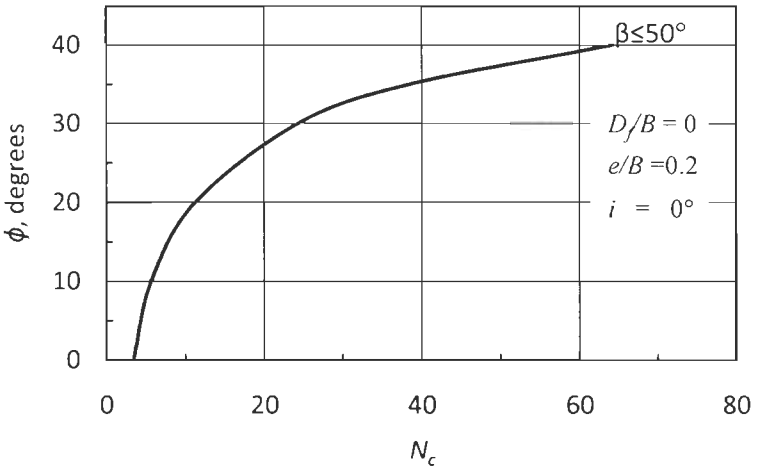

Fig. 3.16 c (vi) N_c versus ϕ for D_e/B=5.0

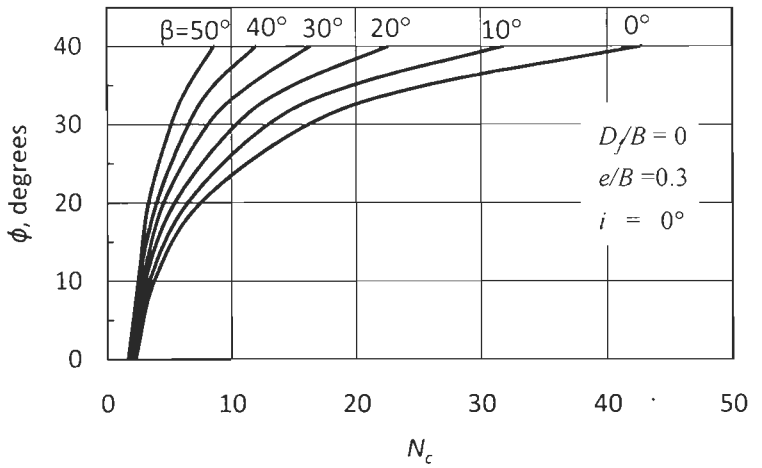

Fig. 3.16 d (i) N_c versus ϕ for D_e/B=0

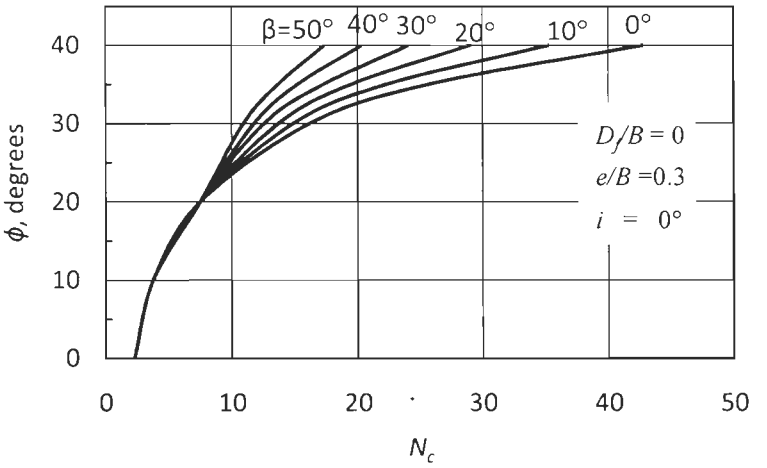

Fig. 3.16 d (ii) N_c versus ϕ for D_e/B=1.0

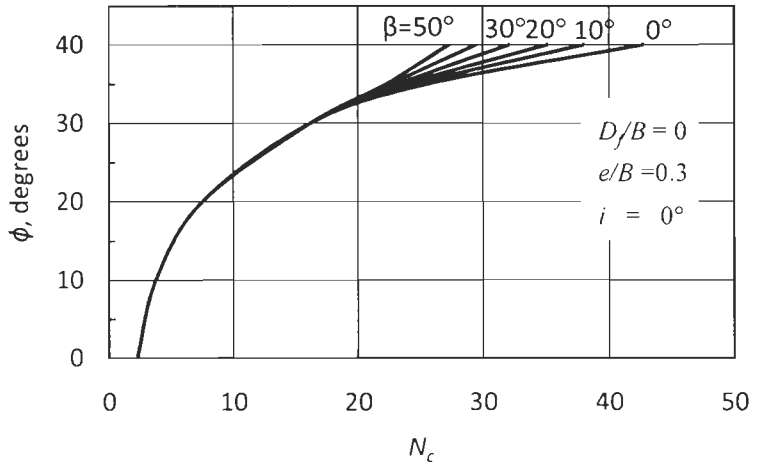

Fig. 3.16 d (iii) N_c versus ϕ for D_e/B=2.0

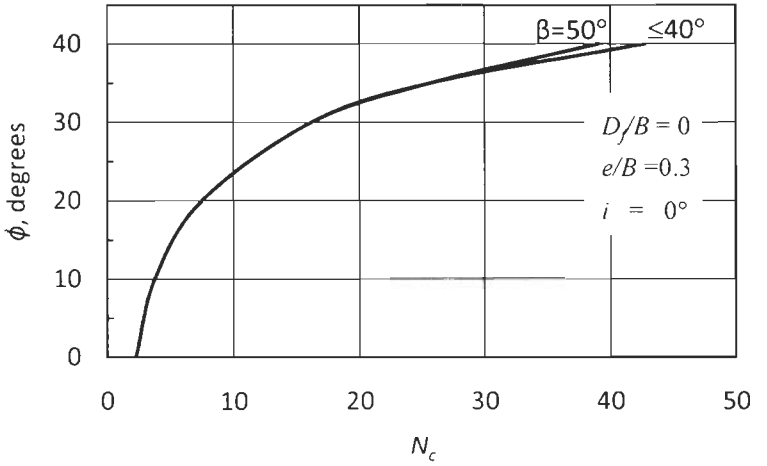

Fig. 3.16 d (iv) N_c versus ϕ for D_e/B=3.0

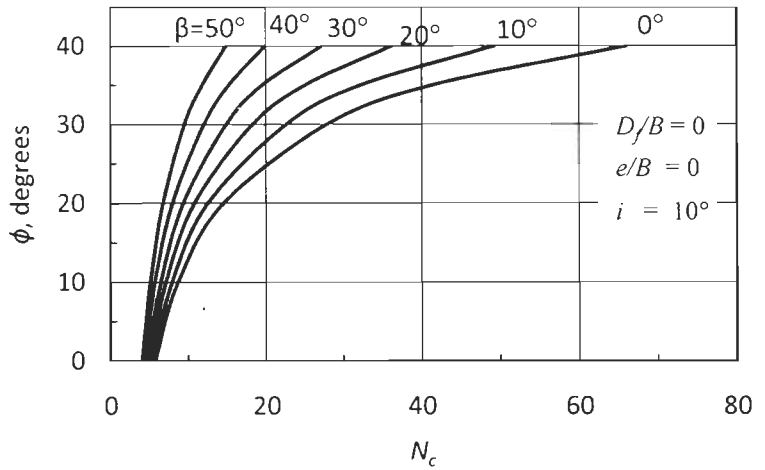

Fig. 3.17 a (i) N_c versus ϕ for D_e/B=0

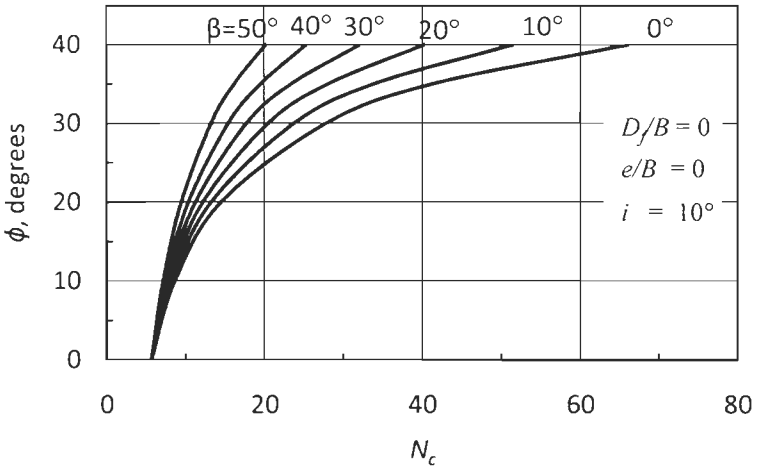

Fig. 3.17 a (ii) N_c versus ϕ for D_e/B=1.0

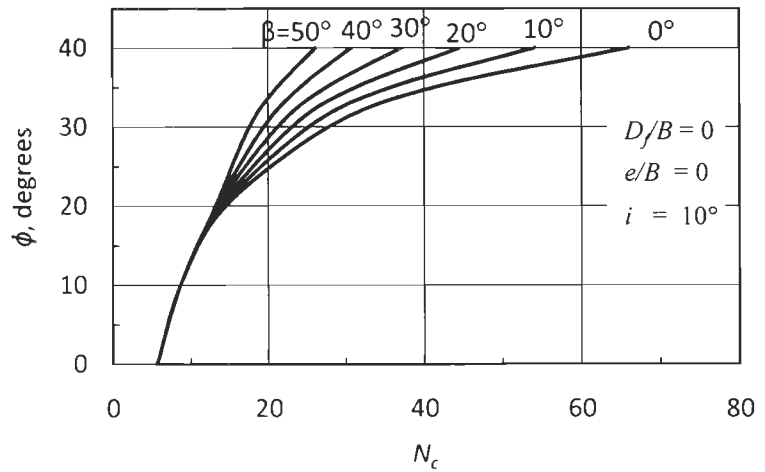

Fig. 3.17 a (iii) N_c versus ϕ for D_e/B=2.0

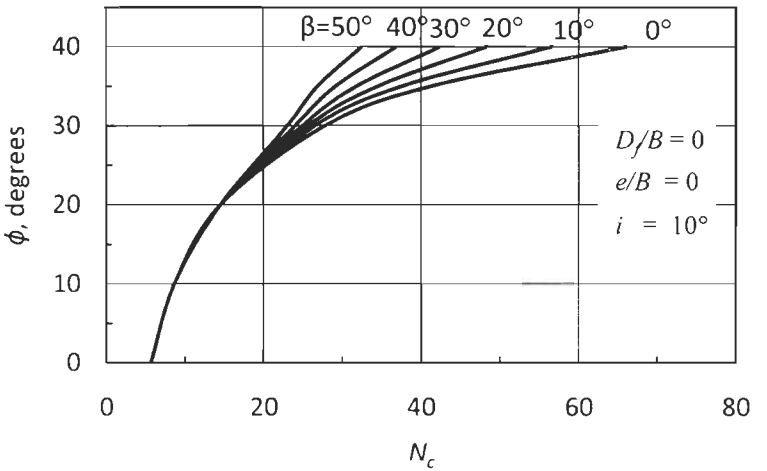

Fig. 3.17 a (iv) N_c versus ϕ for D_e/B=3.0

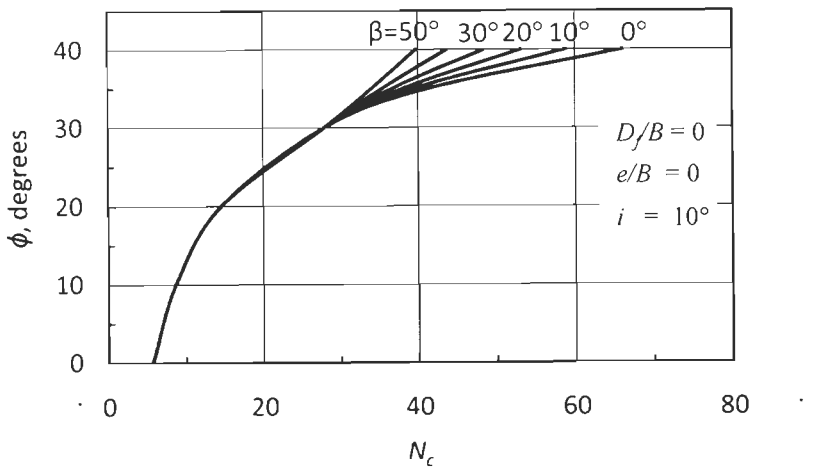

Fig. 3.17 a (v) N_c versus ϕ for D_e/B=4.0

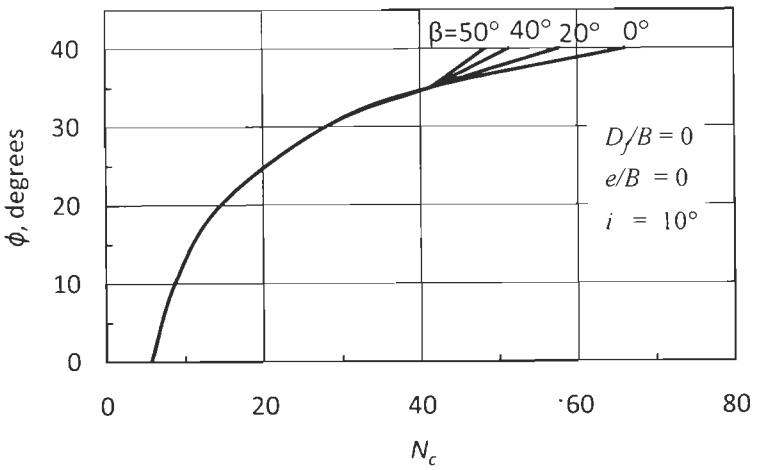

Fig. 3.17 a (vi) N_c versus ϕ for D_e/B=5.0

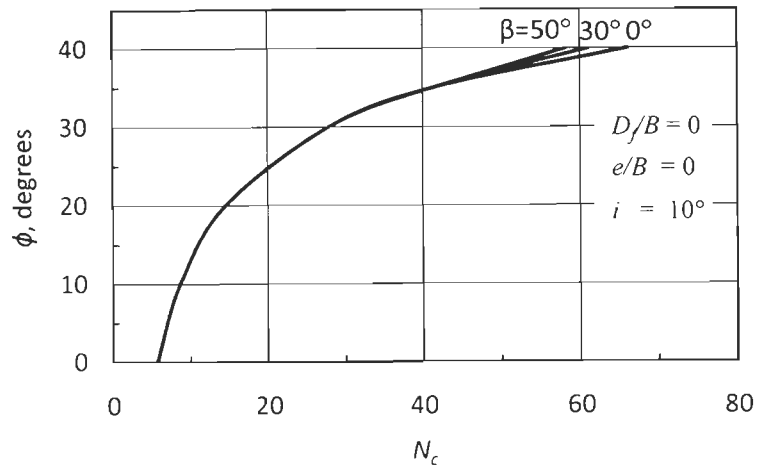

Fig. 3.17 a (vii) N_c versus ϕ for D_e/B=6.0

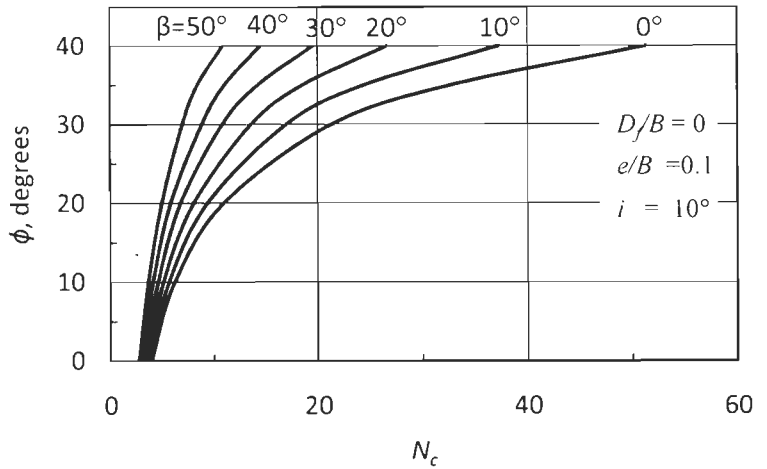

Fig. 3.17 b (i) N_c versus ϕ for D_e/B=0

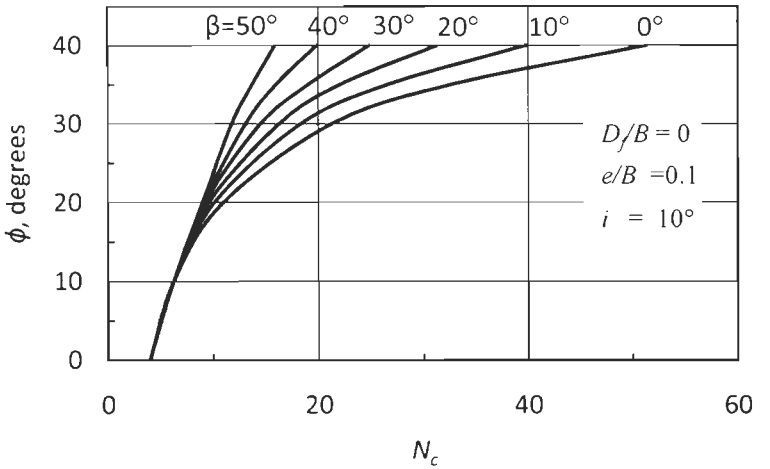

Fig. 3.17 b (ii) N_c versus ϕ for D_e/B=1.0

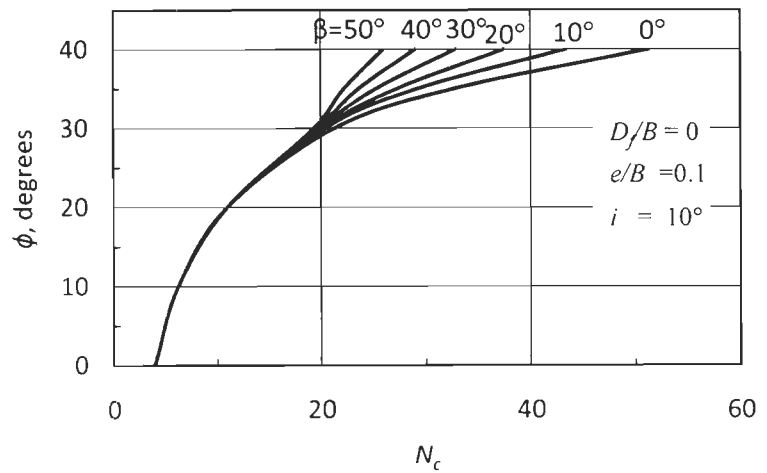

Fig. 3.17 b (iii) N_c versus ϕ for D_e/B=2.0

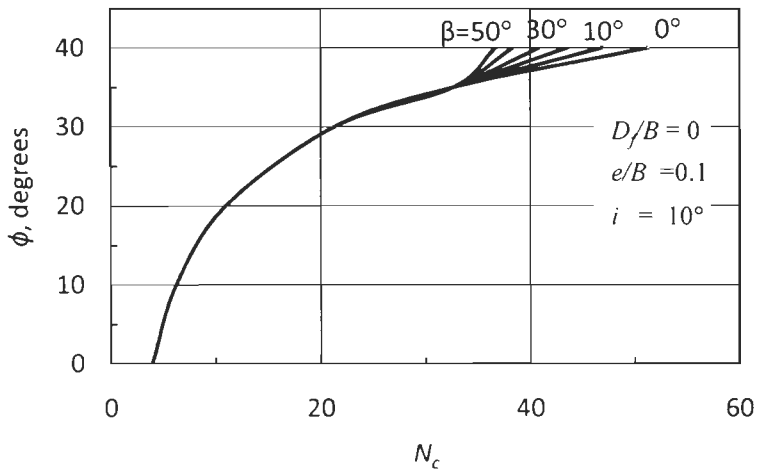

Fig. 3.17 b (iv) N_c versus ϕ for D_e/B=3.0

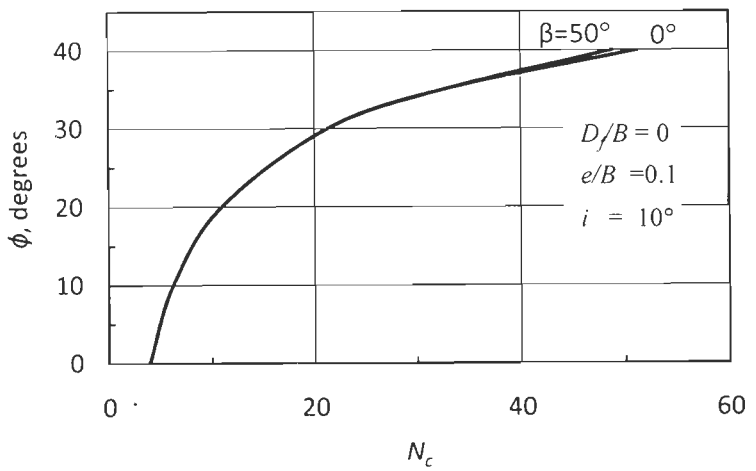

Fig. 3.17 b (v) N_c versus ϕ for D_e/B=4.0

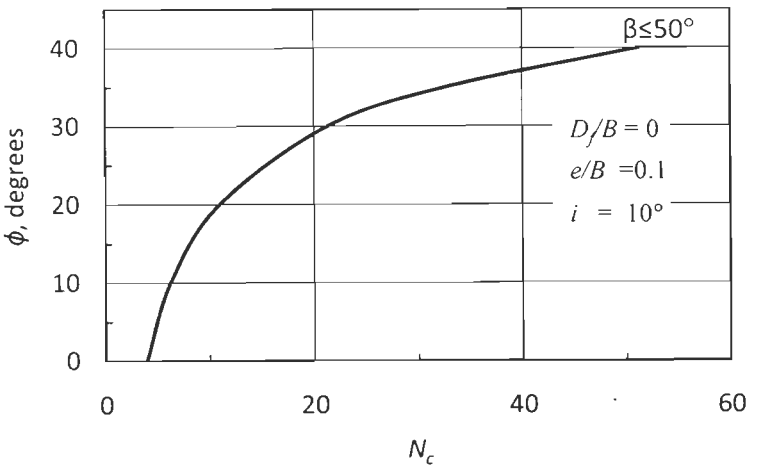

Fig. 3.17 b (vi) N_c versus ϕ for D_e/B=5.0

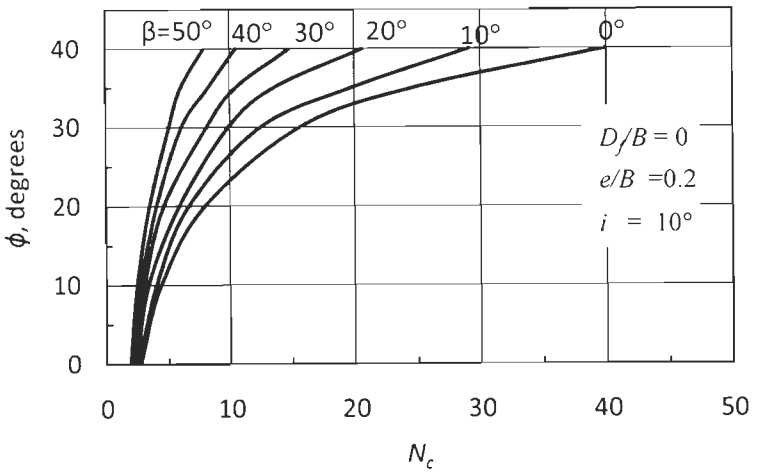

Fig. 3.17 c (i) N_c versus ϕ for D_e/B=0

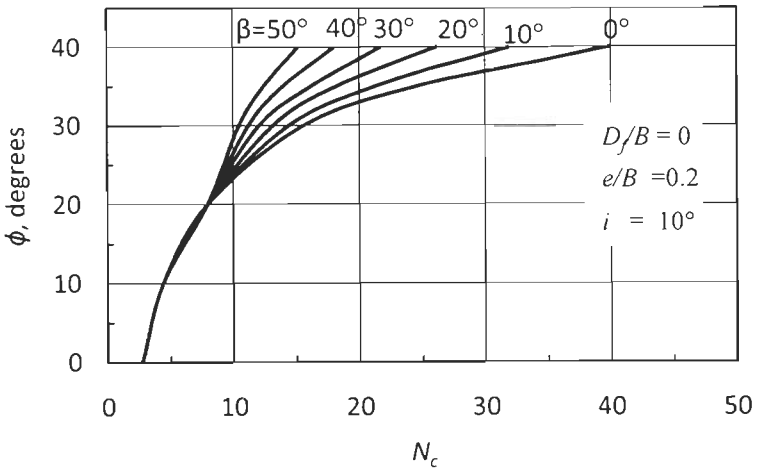

Fig. 3.17 c (ii) N_c versus ϕ for D_e/B=1.0

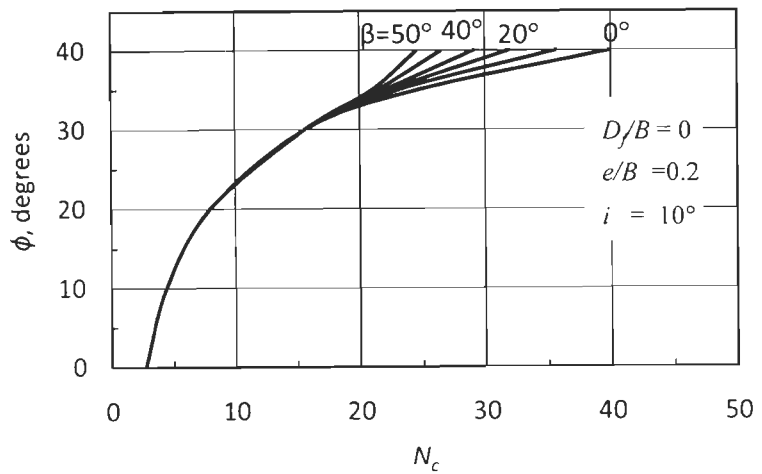

Fig. 3.17 c (iii) N_c versus ϕ for D_e/B=2.0

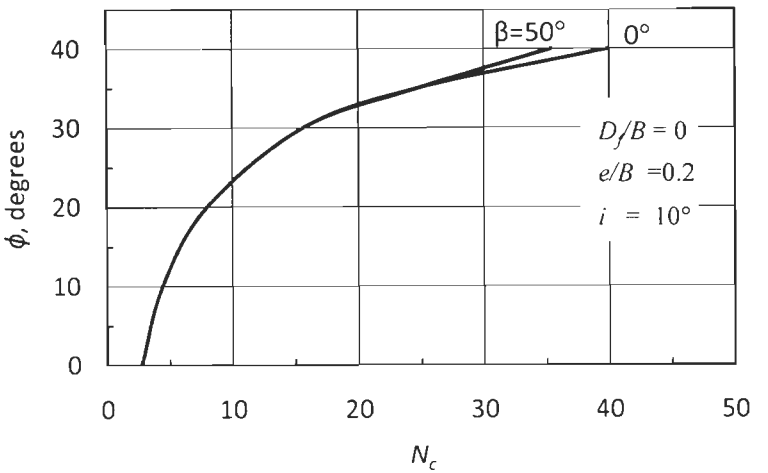

Fig. 3.17 c (iv) N_c versus ϕ for D_e/B=3.0

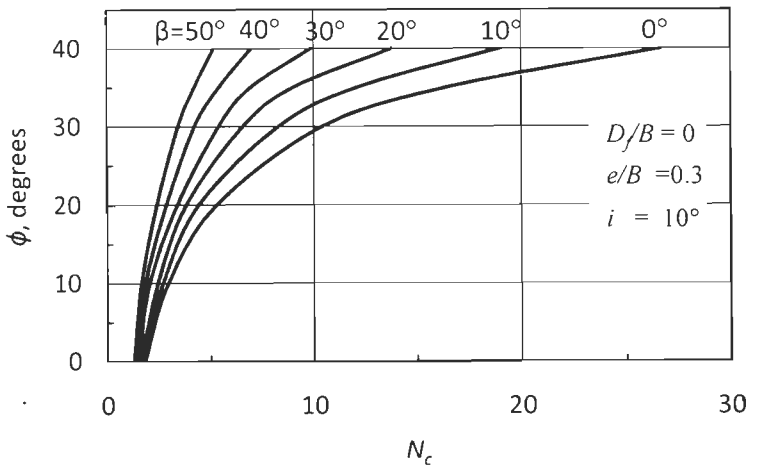

Fig. 3.17 d (i) N_c versus ϕ for D_e/B=0

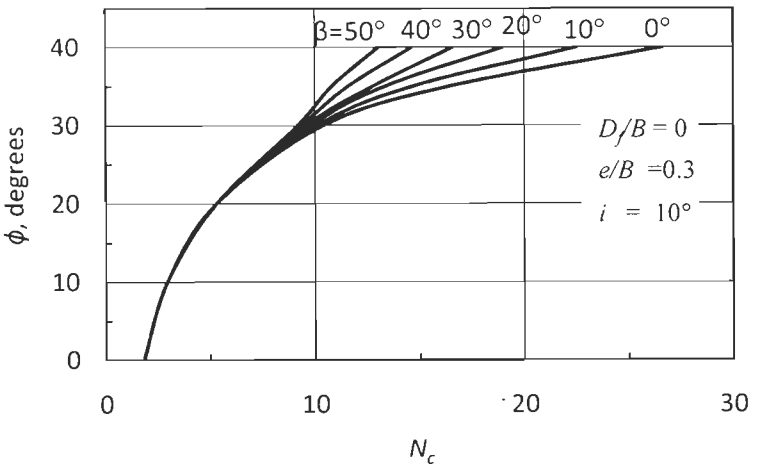

Fig. 3.17 d (ii) N_c versus ϕ for D_e/B=1.0

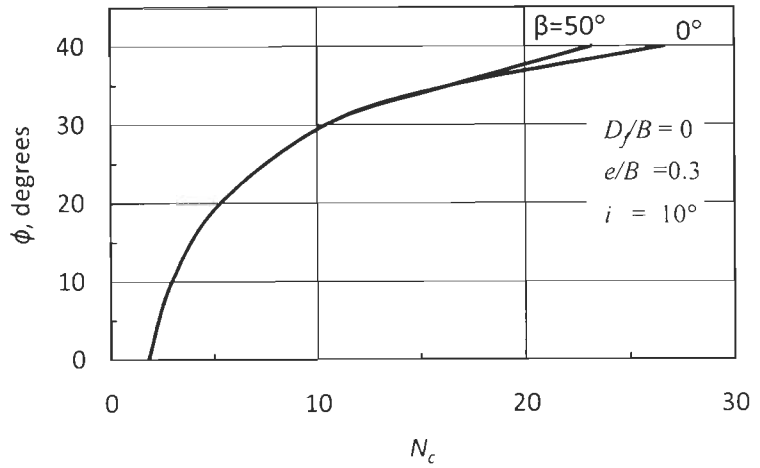

Fig. 3.17 d (iii) N_c versus ϕ for D_e/B=2.0

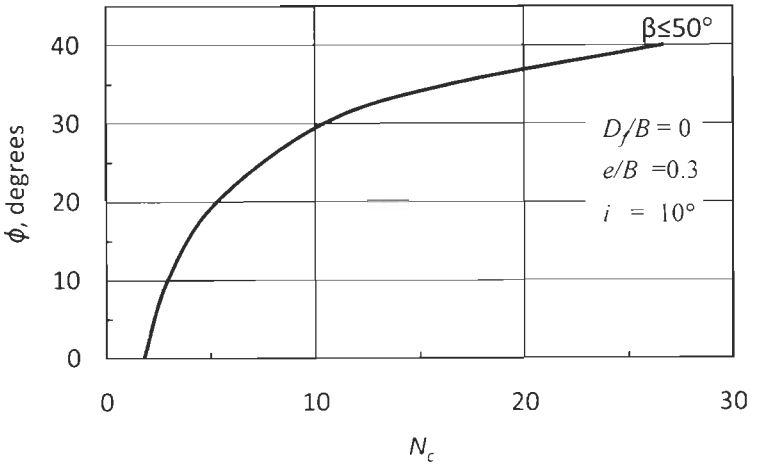

Fig. 3.17 d (iv) N_c versus ϕ for D_e/B=3.0

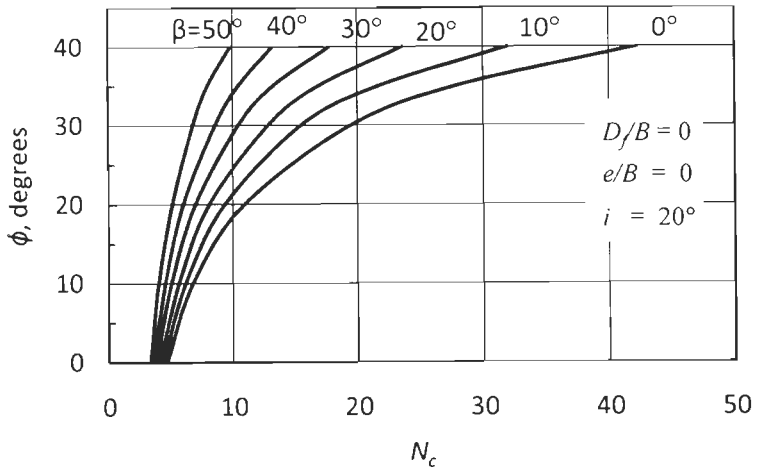

Fig. 3.18 a (i) N_c versus ϕ for D_e/B=0

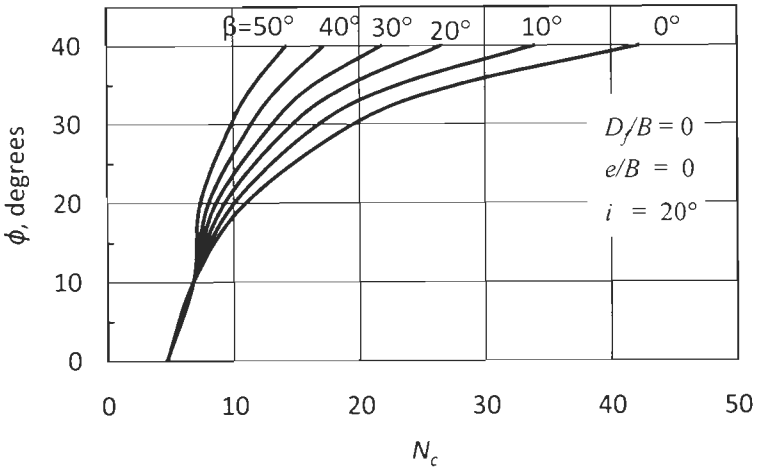

Fig. 3.18 a (ii) N_c versus ϕ for D_e/B=1.0

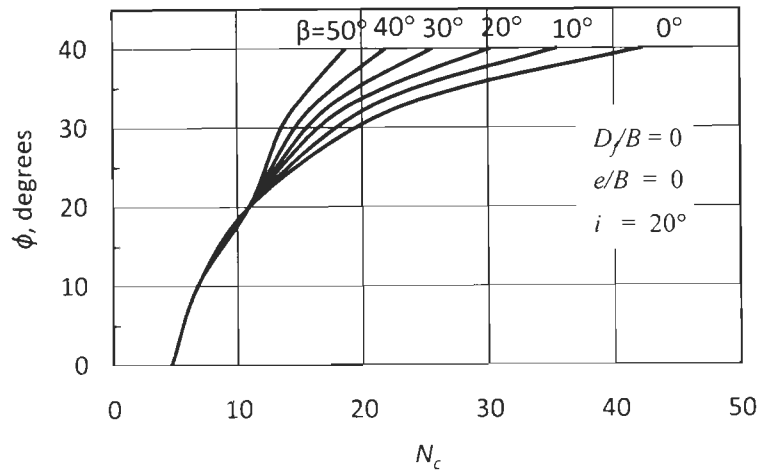

Fig. 3.18 a (iii) N_c versus ϕ for D_e/B=2.0

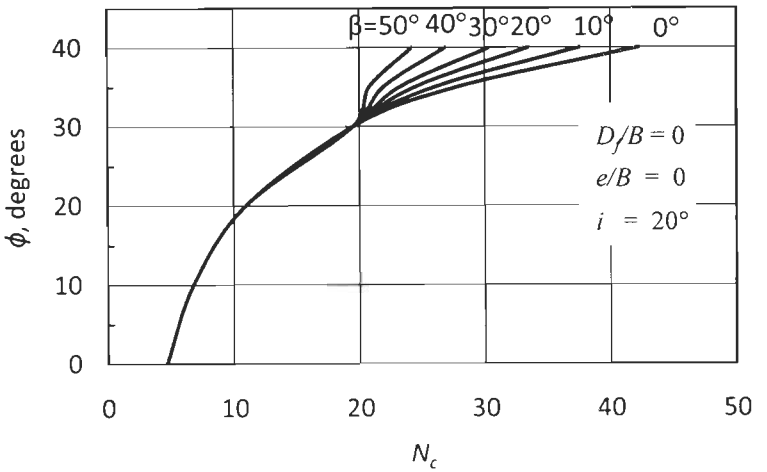

Fig. 3.18 a (iv) N_c versus ϕ for D_e/B=3.0

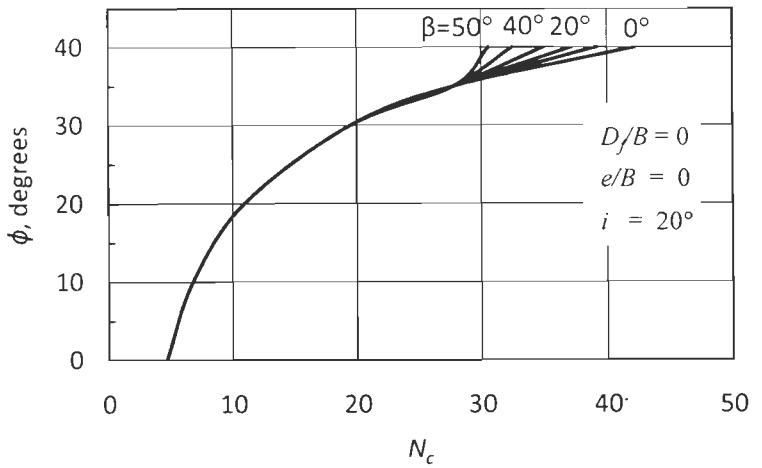

Fig. 3.18 a (v) N_c versus ϕ for D_e/B=4.0

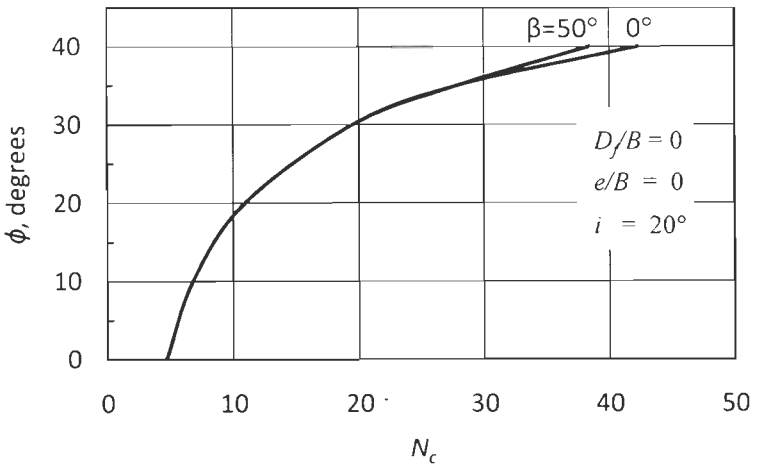

Fig. 3.18 a (vi) N_c versus ϕ for D_e/B=5.0

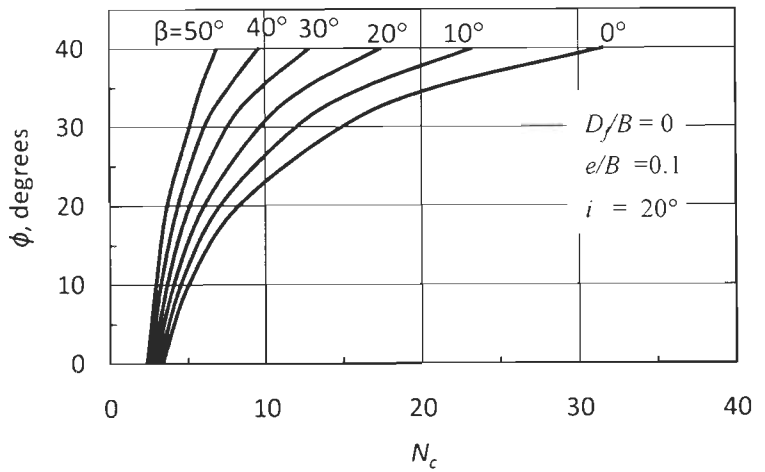

Fig. 3.18 b (i) N_c versus ϕ for D_e/B=0

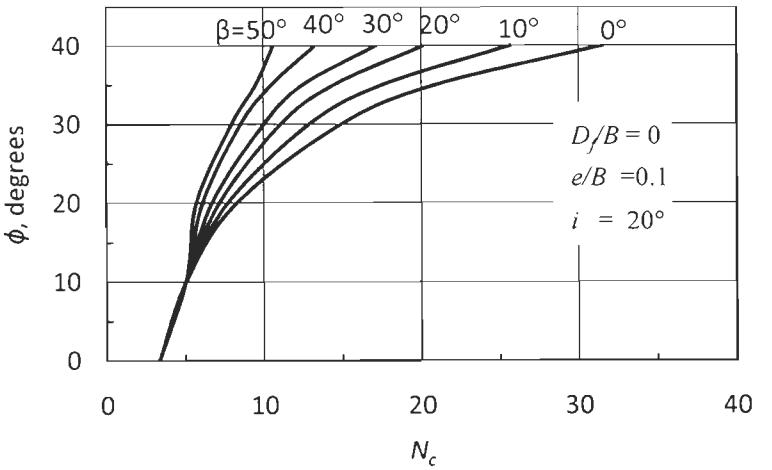

Fig. 3.18 b (ii) N_c versus ϕ for D_e/B=1.0

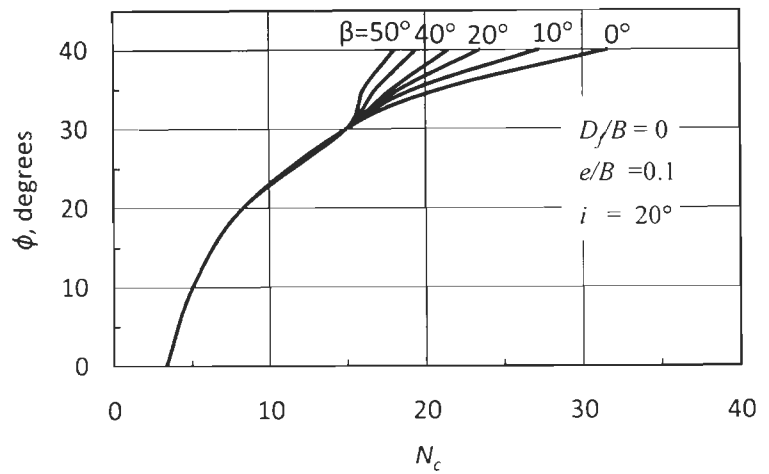

Fig. 3.18 b (iii) N_c versus ϕ for D_e/B=2.0

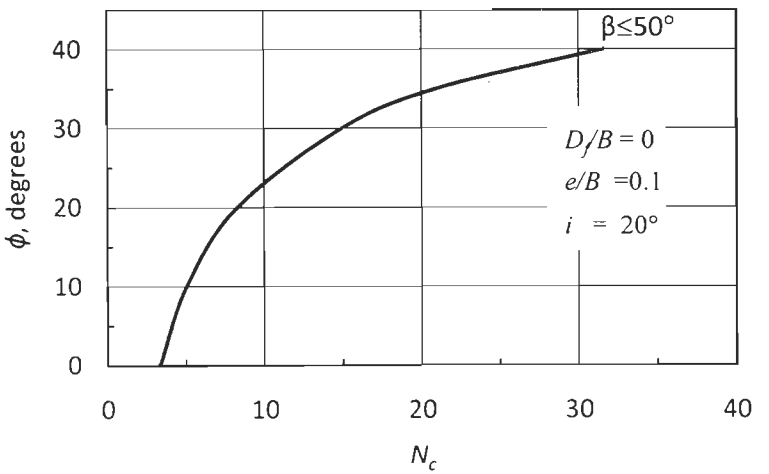

Fig. 3.18 b (iv) N_c versus ϕ for D_e/B=3.0

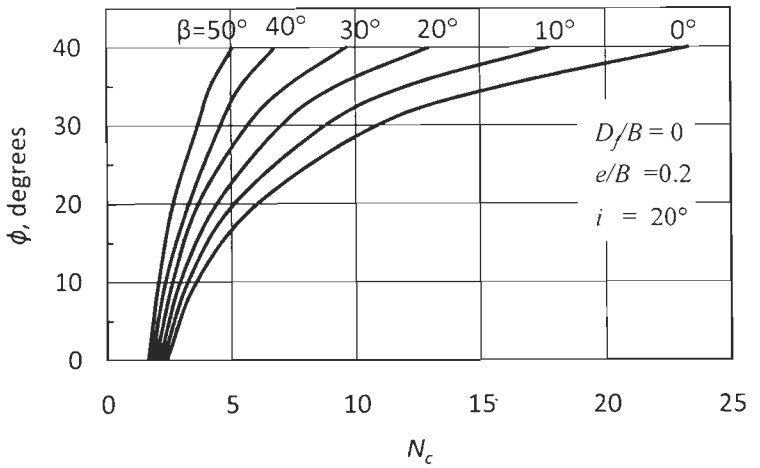

Fig. 3.18 c (i) N_c versus ϕ for D_e/B=0

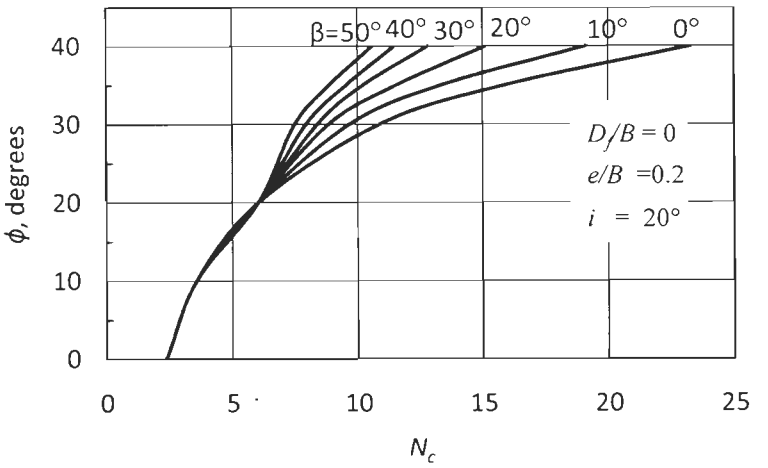

Fig. 3.18 c (ii) N_c versus ϕ for D_e/B=1.0

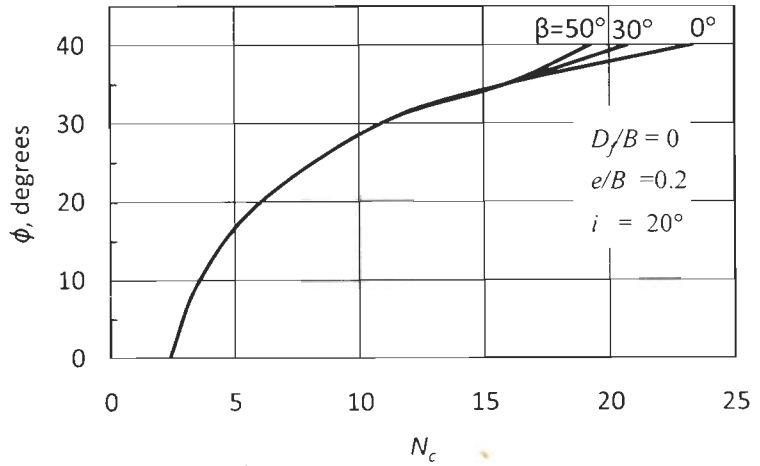

Fig. 3.18 c (iii) N_c versus ϕ for D_e/B=2.0

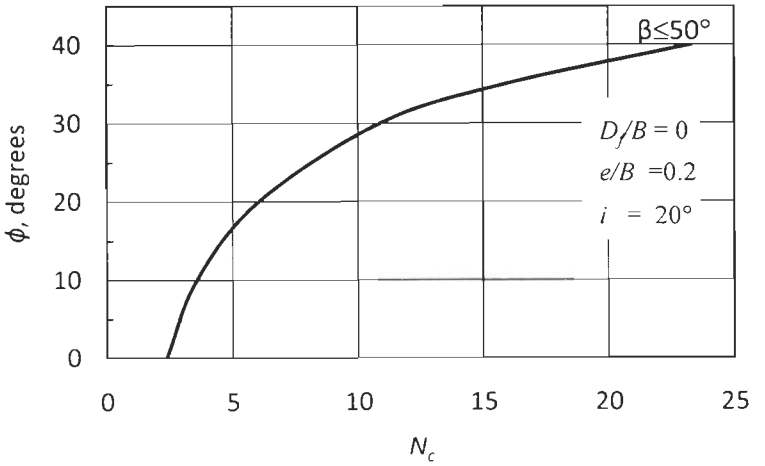

Fig. 3.18 c (iv) N_c versus ϕ for D_e/B=3.0

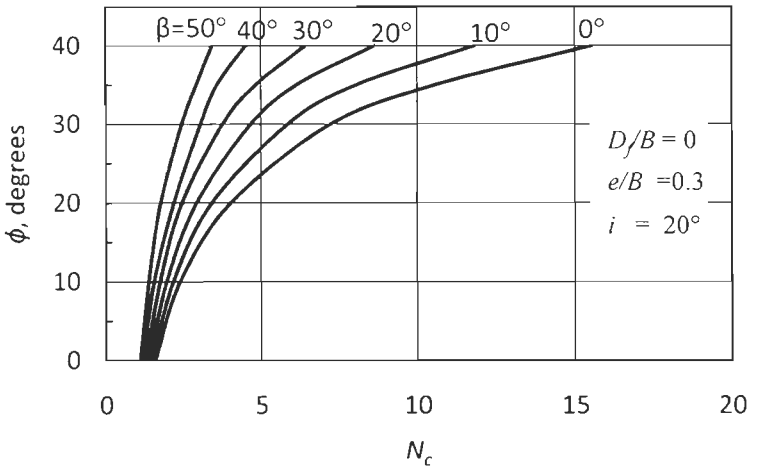

Fig. 3.18 d (i) N_c versus ϕ for D_e/B=0

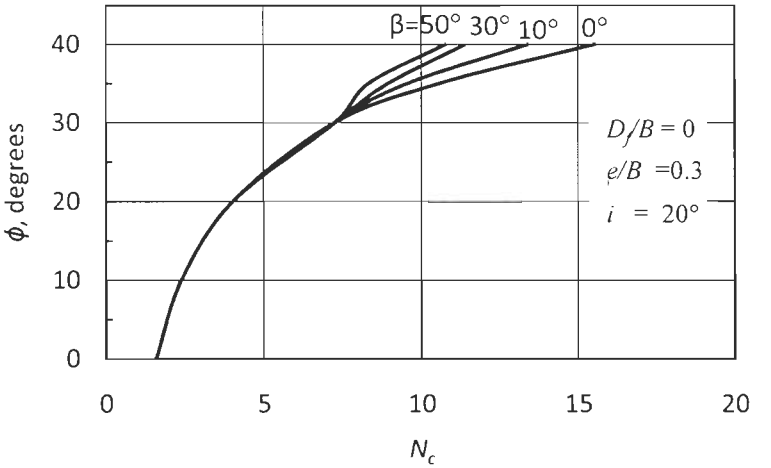

Fig. 3.18 d (ii) N_c versus ϕ for D_e/B=1.0

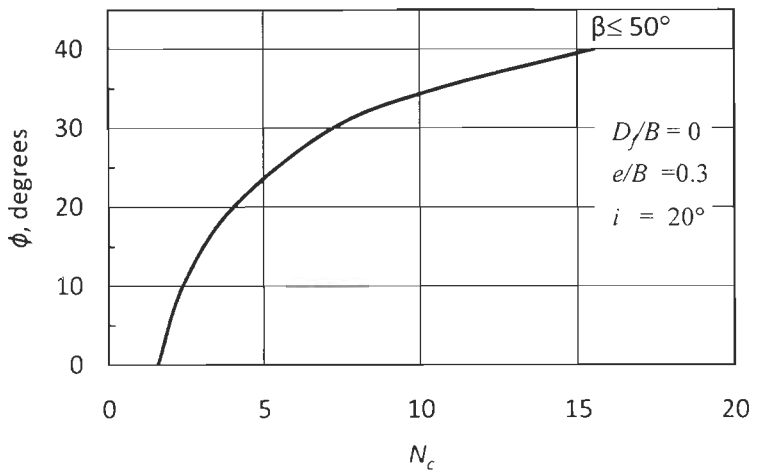

Fig. 3.18 d (iii) N_c versus ϕ for D_e/B=2.0

CHAPTER-IV

PRESSURE-SETTLEMENT CHARACTERISTICS OF FOOTINGS ON UPPER SURFACE OF SLOPES

4.1 GENERAL

In this chapter, a methodology has been presented to predict the pressure-settlement and pressure-tilt characteristics of a footing placed near the edge of a slope and subjected to eccentric-inclined load using the constitutive laws of soil.

Sharan (1977) studied the behaviour of a footing resting on both clay and sand surfaces using non-linear constitutive laws and the footing was considered to be subjected to central vertical load. One of the important findings of this study was that the pressure versus average settlement response of a flexible footing is very close to the pressure versus settlement response of a rigid footing. For a given pressure intensity, the maximum difference between the average settlement of a flexible footing and the settlement of a rigid footing was found to be less than 3.5%. Advantage of this concept has been taken in the present study. Initially, the footing is analysed considering it to be a flexible footing, and then the results are interpreted for the case of a rigid footing. The method makes use of theory of elasticity only for stress calculation; the stress-strain relations needed for the subsequent phase of calculation are taken from the results of triaxial tests performed on actual soil specimens. Since the method takes care of the non-linearity of a real soil obtained from experiments, a good agreement can be obtained between the calculated and actual settlements.

4.2 STRESS EQUATIONS

Soil, in general, is a non-homogeneous and anisotropic material. In sands, Young's modulus, E is dependent on the confining pressure. However, E is independent of confining pressure in fully saturated over consolidated clays. Presently, there is no method available in which variation of E with confining pressure can be considered for computing the stresses in soil. The equations which are available for calculating the stresses in a soil mass due to different load conditions are derived from Boussinesq's equation, which assumes the soil to be elastic, isotropic

and homogeneous. Further, these equations are applicable to the footing load applied on a surface of a level ground. No method is yet available for calculating the stresses due to footing load on a soil mass which is restricted by a slope on one side. Hence, a new method is proposed for finding the stresses due to a footing load placed on a slope. In the first step, the stresses are calculated considering the footing placed on a level surface *ABE* as shown in Fig. 4.1.

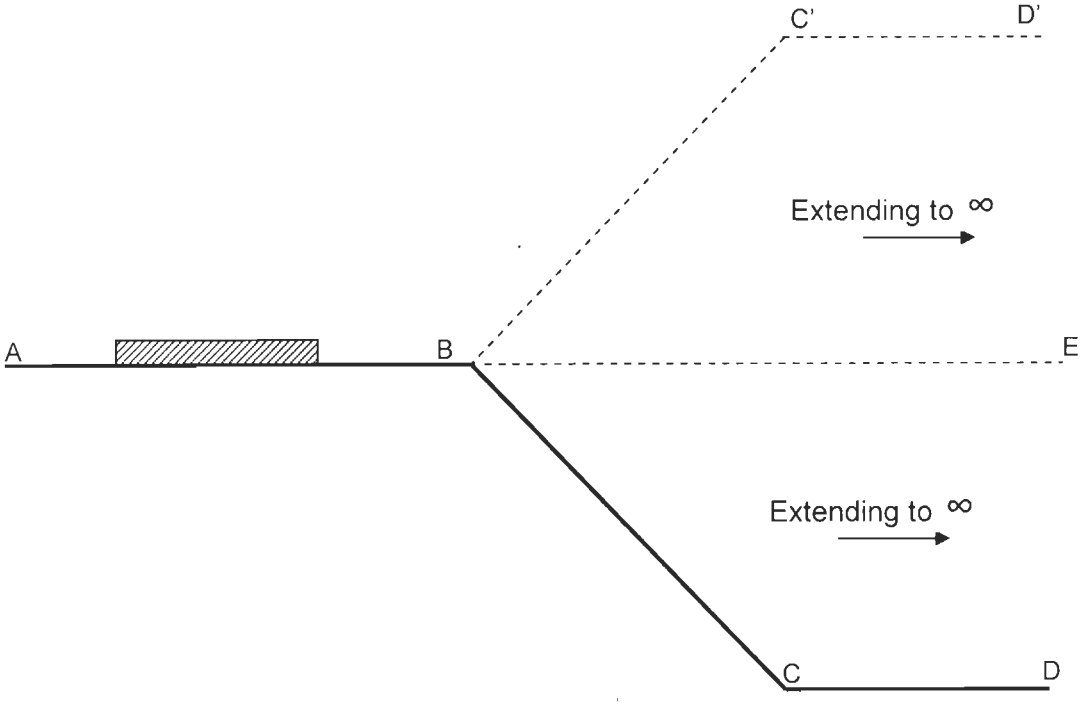

Fig. 4.1 Calculation of Stress due to Loading on the Top of a Slope

Then the soil is loaded with an imaginary embankment loading, *BC'D'E* which is exactly opposite to the wedge *BCDE* and the stresses are calculated due to this loading. These stresses are then deducted from the previous stresses computed in the first step so as to get the stresses due to a footing load on a sloping surface.

This concept of calculating the stress at any point is verified by comparing with the experimental results reported by Bathurst et.al. (2003) and reproduced in Fig. 4.2. It can be observed from this figure that the calculated stresses match very well with the experimental stress values.

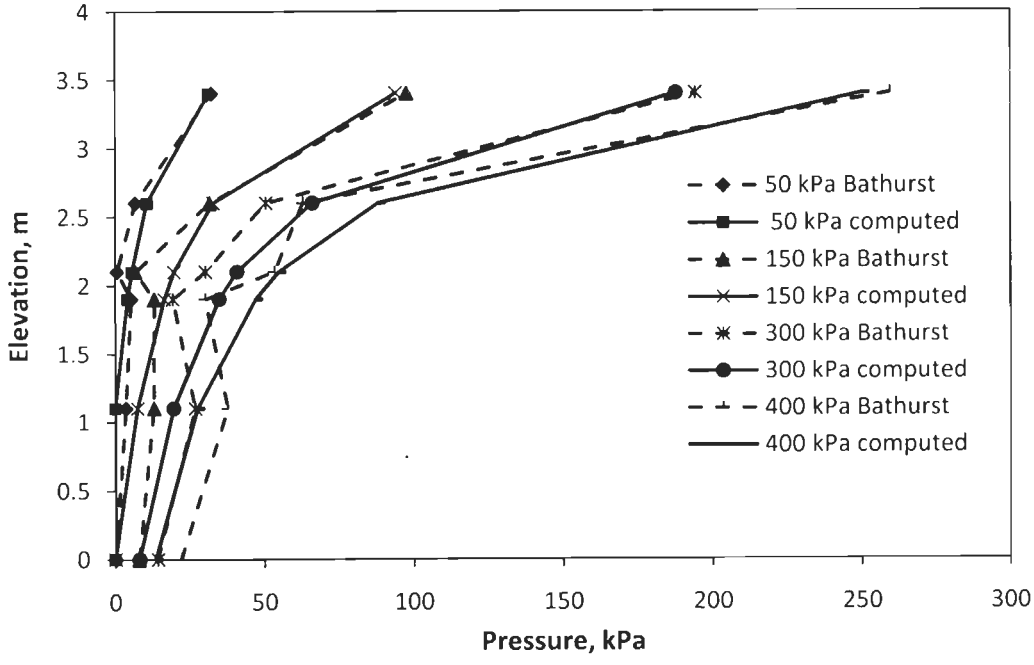

Fig. 4.2 Comparison of Calculated and Experimental Stresses (Bathurst et.al. (2003)

Different available stress equations used in the present study are reproduced below:

i) Uniform vertical loading (Fig. 4.3)

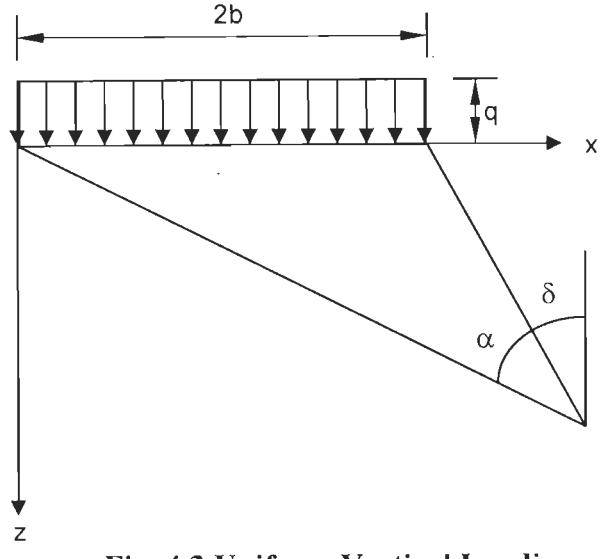

Fig. 4.3 Uniform Vertical Loading

Inplane stresses σ_x, σ_y and τ_{xz} are given by-

$$\sigma_z = \frac{q}{\pi}\left[\alpha + \sin\alpha \cdot \cos(\alpha + 2\delta)\right] \tag{4.1}$$

$$\sigma_x = \frac{q}{\pi}\left[\alpha - \sin\alpha \cdot \cos(\alpha + 2\delta)\right] \tag{4.2}$$

$$\tau_{xz} = \frac{q}{\pi}\sin\alpha \cdot \sin(\alpha + 2\delta) \tag{4.3}$$

ii) Uniform horizontal loading (Fig. 4.4)

$$\sigma_z = \frac{q}{\pi}\sin\alpha \cdot \sin(\alpha + 2\delta) \tag{4.4}$$

$$\sigma_x = \frac{q}{\pi}\left[\log_e \frac{R_1^2}{R_2^2} - \sin\alpha.\sin(\alpha + 2\delta)\right] \tag{4.5}$$

$$\tau_{xz} = \frac{q}{\pi}\left[\alpha - \sin\alpha \cdot \cos(\alpha + 2\delta)\right] \tag{4.6}$$

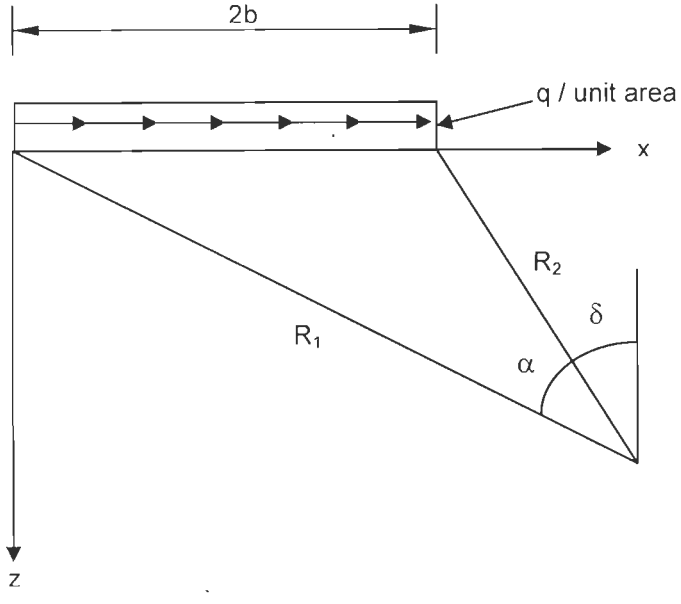

Fig. 4.4 Uniform Horizontal Loading

iii) Vertical loading increasing linearly along footing width (Fig. 4.5)

$$\sigma_z = \frac{q}{2\pi}\left[\frac{x}{b}\alpha - \sin 2\delta\right] \tag{4.7}$$

$$\sigma_x = \frac{q}{2\pi}\left[\frac{x}{b}\alpha - \frac{x}{b}\log_e \frac{R_1^2}{R_2^2} + \sin 2\delta\right] \tag{4.8}$$

$$\tau_{xz} = \frac{q}{2\pi}\left[1 + \cos 2\delta - \frac{z\alpha}{b}\right] \tag{4.9}$$

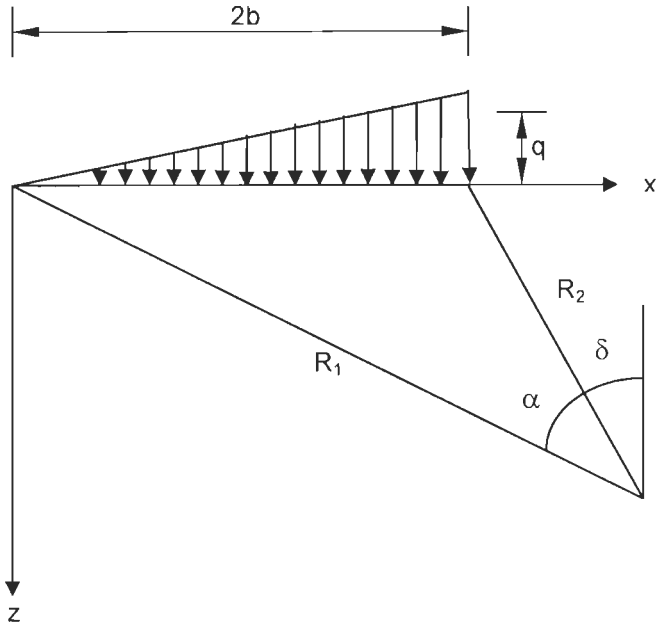

Fig. 4.5 Vertical Loading Increasing Linearly along Footing Width

iv) Horizontal loading increasing linearly along footing width (Fig.4.6)

$$\sigma_z = \frac{q}{2\pi}\left[1 + \cos 2\delta - \frac{z\alpha}{b}\right] \tag{4.10}$$

$$\sigma_x = \frac{q}{2\pi}\left[\frac{3z\alpha}{b} - \frac{x}{b}\log_e \frac{R_1^2}{R_2^2} - \cos 2\delta - 5\right] \tag{4.11}$$

$$\tau_{xz} = \frac{q}{2\pi}\left[\frac{x}{b}\alpha - \frac{z}{b}\log_e \frac{R_1^2}{R_2^2} + \sin 2\delta\right] \tag{4.12}$$

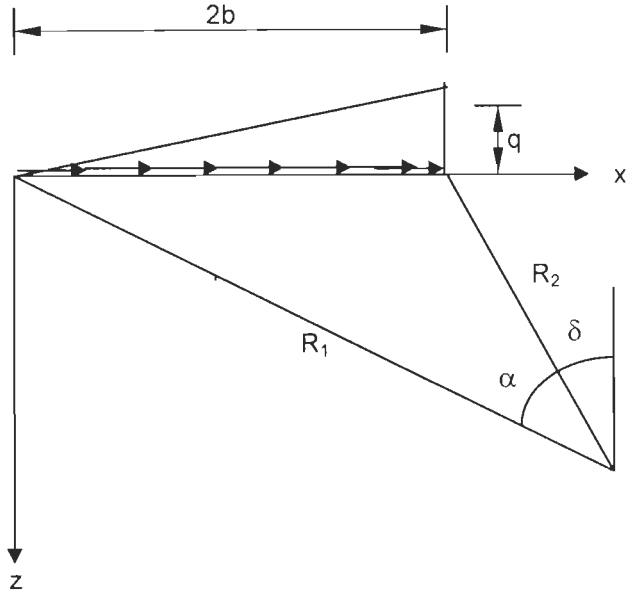

Fig. 4.6 Horizontal Loading Increasing Linearly along Footing Width

(v) Embankment loading (Fig. 4.7)

$$\sigma_z = \frac{p}{\pi a}[a\delta + x\alpha] \tag{4.13}$$

$$\sigma_x = \frac{p}{\pi a}\left[a\delta + x\alpha + 2z\log_e \frac{R_2}{R_1}\right] \tag{4.14}$$

$$\tau_{xz} = -\frac{p}{\pi a} z\alpha \tag{4.15}$$

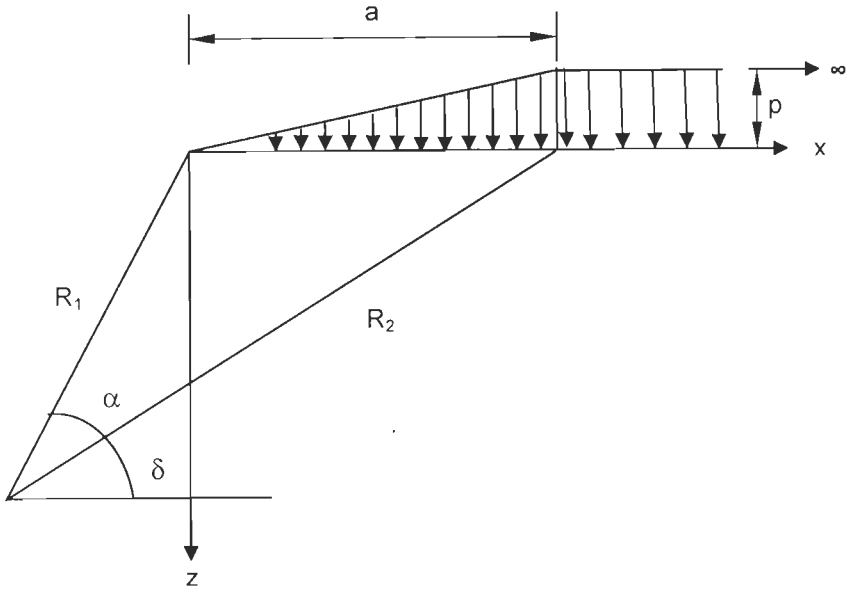

Fig. 4.7 Embankment Loading

where

σ_x = normal stress along horizontal direction

σ_z = normal stress along vertical direction

τ_{xz} = shear stress

other notations are shown in respective figures

4.3 ASSUMPTIONS

Following assumptions have been made in the analysis:

i) The footing has been assumed as flexible and the contact pressure distribution as uniform for central vertical loading. The contact pressure distribution for central vertical load is shown in Fig. 4.8 a, eccentric vertical load in Figs. 4.8 b, c, for central inclined load in Fig. 4.8 d and for eccentric- inclined load in Figs. 4.8 e and f respectively.

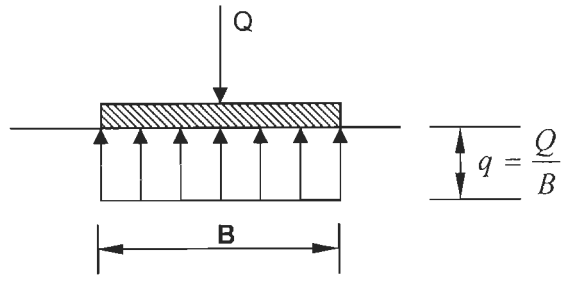

Fig. 4.8 a Contact Pressure Distribution for Central Vertical Loading

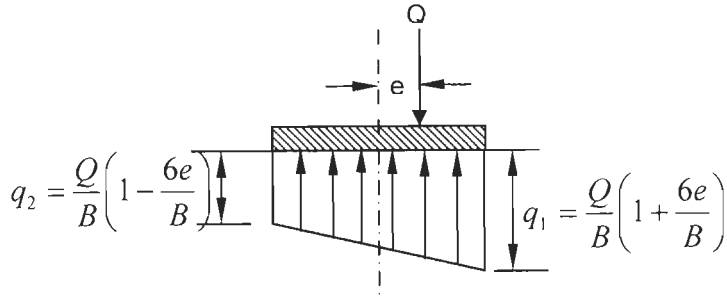

Fig. 4.8 b Contact Pressure Distribution for Eccentric Vertical Loading for e/B<1/6

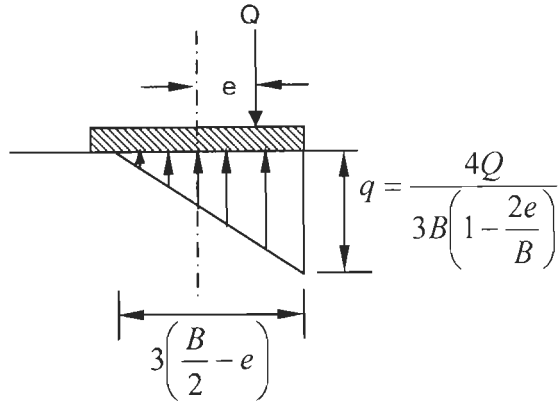

Fig. 4.8 c Contact Pressure Distribution for Eccentric Vertical Loading for e/B≥1/6

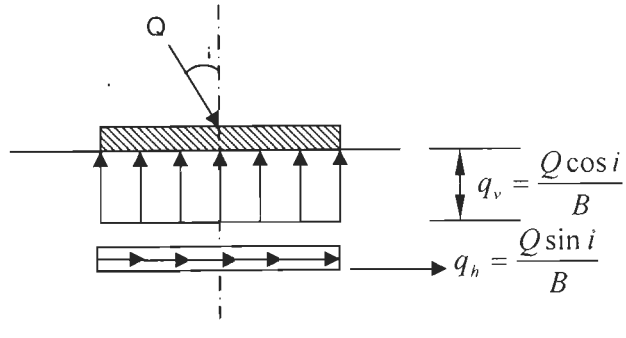

Fig. 4.8 d Contact Pressure Distribution for Central Inclined Loading

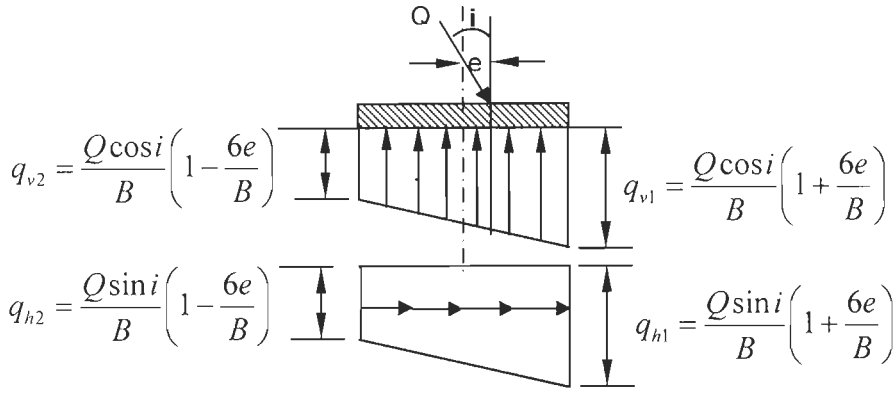

Fig. 4.8 e Contact Pressure Distribution for Eccentric Inclined Loading for e/B<1/6

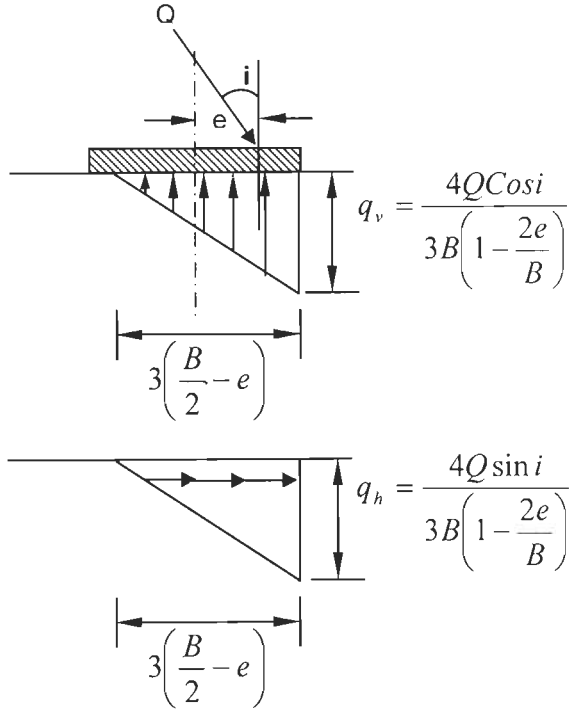

Fig. 4.8 f Contact Pressure Distribution for Eccentric Inclined Loading for e/B≥1/6

ii) The whole soil mass below the footing has been divided into large number of thin horizontal strips.

iii) There is no slippage at the interface between the layers of the soil mass.

iv) The effect of weight of the soil mass has been added in the determination of stresses in soil mass.

v) A coefficient, F has been introduced such that at all the stress levels, the following relationship is satisfied:

$$\frac{q_u}{q} = \frac{\sigma_u}{\sigma_1 - \sigma_3} = F \tag{4.16}$$

where

q_u = ultimate bearing capacity

q = intensity of load less than ultimate bearing capacity

σ_u = ultimate stress from hyperbola relationship of Kondner(1963) and is equal to $1/b$

σ_1 and σ_3 = major and minor stresses in the soil due to load, q and weight of soil

4.4 VERTICAL SETTLEMENT AND TILT

Procedure adopted for obtaining pressure-settlement and pressure-tilt characteristics under different loading conditions are given in the following steps:

Step 1. Evaluation of contact pressure

For a given eccentric-inclined load, the vertical and horizontal contact pressure distribution (q_v, q_h) is calculated according to art. 4.3.

Step 2. Evaluation of stresses

The soil mass supporting the footing has been divided into a large number of thin layers (say n layers) up to a depth at which the pressure intensity is less than $0.05q$.

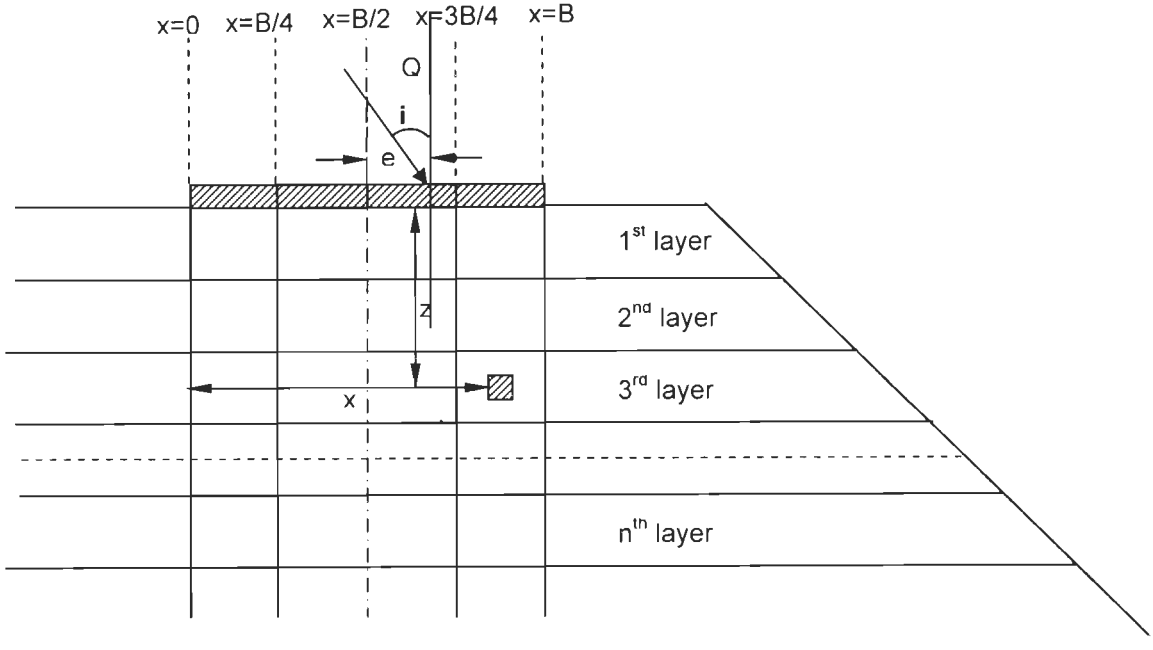

Fig.4.9 Soil Mass Divided into *n* Layers and the Vertical Sections where Stresses and Settlement are Calculated

The stresses in each layer of the soil mass at five vertical sections (Fig. 4.9) due to q_v, q_h and weight of soil are obtained separately and the corresponding stresses are added. Vertical stress due to weight of the soil has been taken as γz, where γ is the unit weight of soil and z is the depth of soil layer from the top surface. The horizontal stress due to soil weight has been taken as $k_0 \gamma z$, where k_0 is the coefficient earth pressure at rest. The stresses due the embankment loading are calculated by applying Eqs.4.13-4.15 and subtracted from the above stresses which give the stresses due to different loadings on a sloped surface.

Step 3. Evaluation of principal stresses

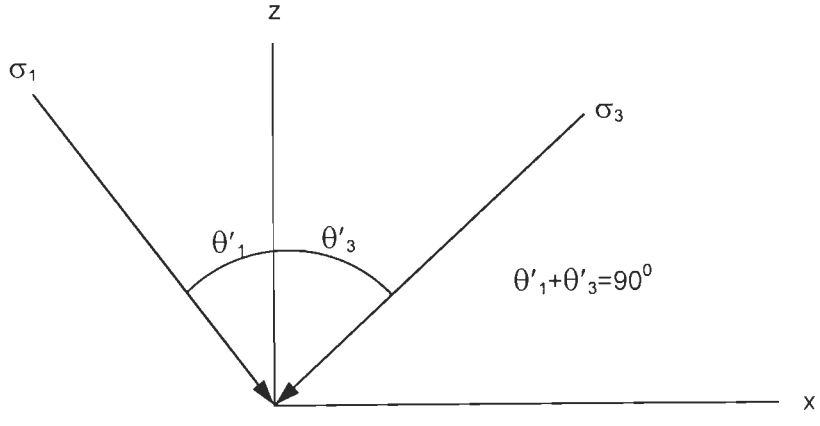

Fig.4.10 Principal Stresses at a Point and their Directions

The principal stresses and their directions with respect to the vertical axis (Fig. 4.10) are computed using the following equations:

$$\sigma_1 = \frac{\sigma_z + \sigma_x}{2} + \sqrt{\left(\frac{\sigma_z - \sigma_x}{2}\right)^2 + \tau_{xz}^2} \tag{4.17}$$

$$\sigma_3 = \frac{\sigma_z + \sigma_x}{2} - \sqrt{\left(\frac{\sigma_z - \sigma_x}{2}\right)^2 + \tau_{xz}^2} \tag{4.18}$$

$$tan2\theta = \frac{2\tau_{xz}}{\sigma_z - \sigma_x} \tag{4.19}$$

Positive value of θ is measured in counter clockwise with direction of σ_z.

where σ_1, the major principal stresses; σ_3, the minor principal stresses; σ_z, the stress in z direction; σ_x, the stress in x direction and τ_{xz} represents the shear stress.

Step 4. Evaluation of principal strain using constitutive laws of soil

Kondner (1963) has shown that non-linear stress strain curve for soil may be closely approximated by a hyperbola (Fig. 4.11 a), and the relation between stress and strain is given by the following relationship:

$$\sigma_1 - \sigma_3 = \frac{\varepsilon_1}{a + b\varepsilon_1} \tag{4.20}$$

where σ_1 and σ_3 are the major and minor principal stresses and ε_1 is the axial strain.

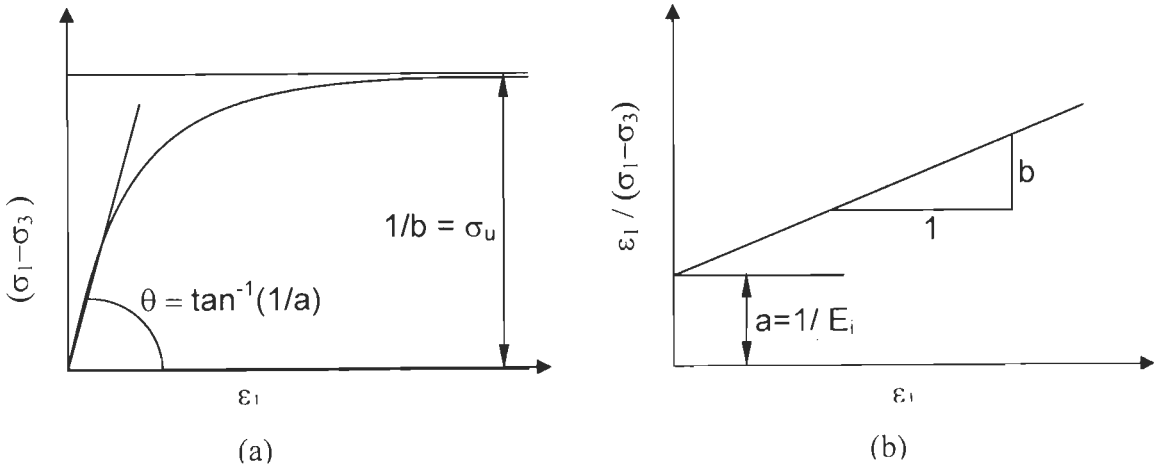

Fig.4.11 Hyperbolic Stress Strain Representation (Kondner, 1963)

As shown in Fig. 4.11b, parameter a is the reciprocal of the initial tangent modulus, E_i and b is the reciprocal of the asymptotic value of deviatoric stress, $(\sigma_1 - \sigma_3)_{ult}$ i.e. the value at which the stress-strain curve becomes asymptotic. The values of a and b can be readily determined if the stress-strain data is plotted on the transformed axis as shown in Fig. 3.11b and the above equation can be written as:

$$\frac{\varepsilon_1}{\sigma_1 - \sigma_3} = a + b\varepsilon_1 \tag{4.21}$$

$$\text{or} \quad \varepsilon_1 = \frac{a(\sigma_1 - \sigma_3)}{1 - b(\sigma_1 - \sigma_3)} \tag{4.22}$$

The ultimate bearing capacity (q_u) for the given eccentric inclined load is calculated by applying the principles of chapter III. To calculate the settlement at any pressure intensity q, coefficient, F is determined from Eq. 4.16.

$$F = \frac{q_u}{q}$$

$$\therefore \sigma_1 - \sigma_3 = \frac{\sigma_u}{F}$$

Then Eq. 4.22 can be modified as:

$$\varepsilon_1 = \frac{a(\sigma_u / F)}{1 - b(\sigma_u / F)} \tag{4.23}$$

The modulus of elasticity (E_s) at any stress level (σ_u/F) (Fig. 4.12) and the strain (ε_1) in each layer in the direction of major principal stress are then calculated by applying the following relations:

$$E_s = \frac{Stress}{Strain} = \frac{1 - b(\sigma_u / F)}{a} \tag{4.24}$$

$$\varepsilon_1 = \frac{\sigma_1 - \sigma_3}{E_s} \tag{4.25}$$

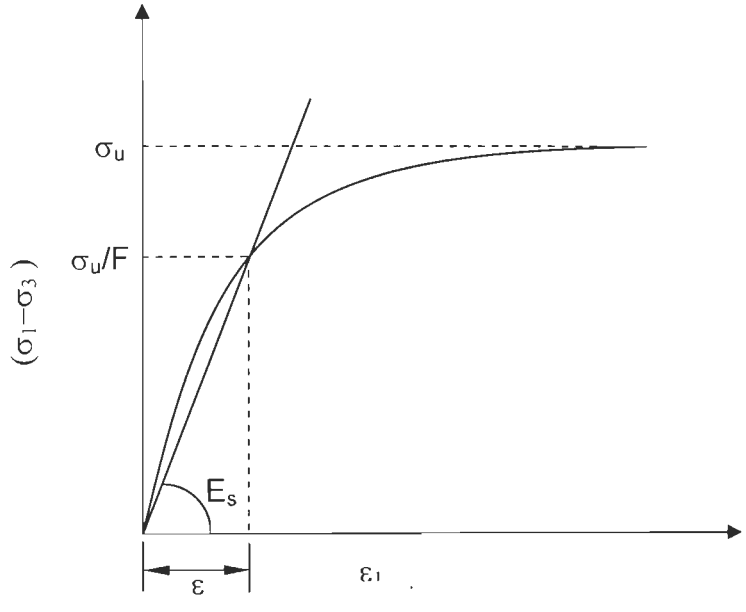

Fig.4.12 Determination of E_s from Hyperbolic Stress Strain Relation

Step 5. Evaluation of lateral strain

The strain, ε_2 in the direction of intermediate principal stress, σ_2 is equal to zero in plain strain condition. Therefore from theory of elasticity

$$\varepsilon_2 = \frac{1}{E}[\sigma_2 - \mu(\sigma_1 + \sigma_3)] = 0 \tag{4.26}$$

or $$\sigma_2 = \mu(\sigma_1 + \sigma_3)$$

and $$\varepsilon_1 = \frac{1-\mu^2}{E}\left[\sigma_1 - \frac{\mu}{1-\mu}\sigma_3\right] \tag{4.27}$$

$$\varepsilon_3 = \frac{1-\mu^2}{E}\left[\sigma_3 - \frac{\mu}{1-\mu}\sigma_1\right] \tag{4.28}$$

Assuming

$\mu_1 = \frac{\mu}{1-\mu}$ and $E_1 = \frac{E}{1-\mu^2}$, from Eq. 4.27 and 4.28 one gets,

$$\varepsilon_1 = \frac{1}{E_1}\left[\sigma_1 - \mu_1 \sigma_3\right] \tag{4.29}$$

$$\varepsilon_3 = \frac{1}{E_1}\left[\sigma_3 - \mu_1 \sigma_1\right] \tag{4.30}$$

Dividing Eqn. 4.30 with Eqn.4.29, one gets,

$$\frac{\varepsilon_3}{\varepsilon_1} = \frac{\sigma_3 - \mu_1\sigma_1}{\sigma_1 - \mu_1\sigma_3} \tag{4.31}$$

Let $$\frac{\varepsilon_3}{\varepsilon_1} = -\mu_2 \tag{4.32}$$

Then $$\mu_2 = \frac{-\sigma_3 + \mu_1\sigma_1}{\sigma_1 - \mu_1\sigma_3} \tag{4.33}$$

So the strain in the direction of minor principal stress is calculated using Eq.4.32 as

$$\varepsilon_3 = -\mu_2\varepsilon_1 \tag{4.34}$$

Step 6. Evaluation of vertical strain

The strain in the vertical direction, ε_z in each layer along vertical sections is computed using the following relation:

$$\varepsilon_z = \varepsilon_1 \cos^2\theta_1' + \varepsilon_3 \cos^2\theta_3' \tag{4.35}$$

where θ'_1 and θ'_3 are the directions of the principal strain with respect to vertical axis (Fig. 4.10)

Step 7. Evaluation of settlement

The vertical settlement (S_e) of any layer along a vertical section is computed by multiplying the strain, ε_z with the thickness of each layer, δz as -

$$S_e = \varepsilon_z\, \delta z \tag{4.36}$$

The total settlement S along any vertical section is computed by adding the settlement of all the layers along the vertical section.

$$S = \sum \varepsilon_z \delta z \qquad (4.37)$$

The total settlement is computed along all vertical sections for each pressure intensity. The settlement pattern of a flexible footing will be as shown in Fig. 4.13.

Step 8. Evaluation of settlement and tilt of rigid footing

A rigid footing will follow the settlement pattern as shown in Fig.4.14. The values of S_{max} and S_{min} of a rigid footing (Fig. 4.14) are obtained using the following concept from the settlement diagram of the flexible footing (i.e. Fig. 4.13)

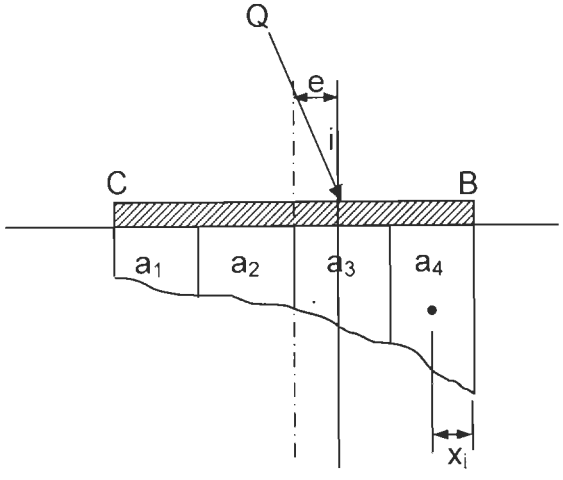

Fig. 4.13 Settlement of Flexible Footing

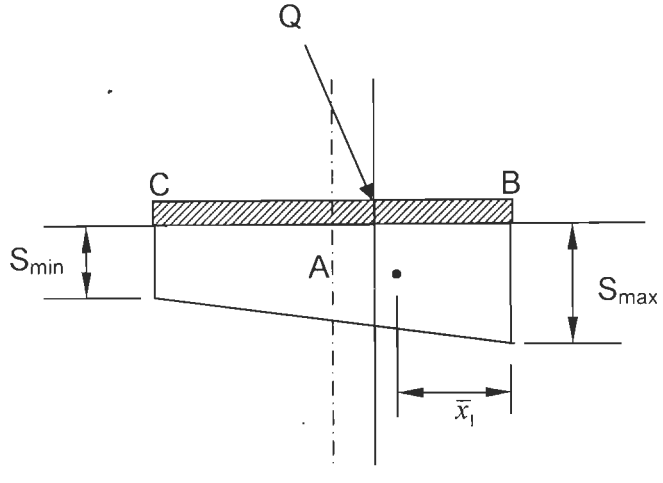

Fig.4.14 Settlement of Rigid Footing

i) The area of the settlement diagram of Figure 4.14 is equal to the area of the settlement diagram of Fig. 4.13 (Σa_i) and

ii) The distance of centre of settlement diagram of Fig.4.13 from edge of footing, point B i.e. $\bar{x}_1$ is equal to the distance of centre of settlement diagram of

Fig.4.14 from the edge of the footing point B. Values of Σa_i and $\bar{x}_1 \left(= \frac{\sum a_i x_i}{\sum a_i} \right)$ may be obtained using the numerical integration technique. Then,

$$\sum a_i = \frac{S_{max} + S_{min}}{2} \times B \tag{4.38}$$

$$\text{and } \bar{x}_1 = \frac{2S_{max} + S_{min}}{S_{max} + S_{min}} \times \frac{B}{3} \tag{4.39}$$

where

S_{max} = Maximum settlement of the footing edge on the side of eccentricity

S_{min} = Minimum settlement of the footing edge away from the eccentricity

Knowing the values of S_{max} and S_{min}, average settlement (S_{av}) and tilt (t) are computed as follows:

$$S_{av} = \frac{S_{max} + S_{min}}{2} \tag{4.40}$$

$$\text{and } t = \frac{S_{max} - S_{min}}{B} \tag{4.41}$$

Step 9. The average settlement and tilt for various pressure intensities on footings are computed by repeating steps 1 to 8 and the pressure versus settlement and pressure versus tilt curves are drawn.

CHAPTER-V

EXPERIMENTAL PROGRAMME

5.1 GENERAL

In any geotechnical engineering problem, field tests on prototype foundations give realistic results. However, economical considerations and other practical difficulties either eliminate prototype tests completely or restrict their scope to a large extent. Under such circumstances, model tests, if carefully conducted, could be used with good confidence. Model studies normally are less expensive and also have the flexibility of varying the parameters envisaged to influence the particular behaviour under controlled conditions. In model studies, it is possible to set some of the influencing parameters as constant and the effect of other parameters can be studied. Model tests thus provide useful qualitative data, which can subsequently be used to study the influence of important variables through prototype tests.

In the present study, model tests were conducted under plane strain conditions for predicting the ultimate bearing capacity and pressure-settlement as well as pressure-tilt behaviour of a strip footing resting on upper surface of a sand slope and subjected to an eccentric-inclined load. The purpose of the model tests conducted in this study was to examine the validity of the proposed theoretical analysis. Triaxial tests were also conducted to develop the constitutive law of the soil used in the model tests.

5.2 SOIL USED

The soil used in this investigation was dry Ranipur sand. The particle size distribution curve of the sand is shown in Fig. 5.1. According to Indian Standard (IS 1498-1970) on soil classification for general engineering purpose; the sand used in the investigation was classified as poorly graded sand (SP). The other engineering properties of sand as determined in the laboratory according to Indian Standard Code IS: 2720 are presented in Table 5.1. The mechanical property affecting the bearing capacity of sand is its shearing resistance. Shear strength of sand is a function of angle of internal friction, ϕ . Model tests were conducted on Ranipur sand at a relative density of 70% and the angle of internal friction corresponding to this relative density

was determined by triaxial compression tests. Triaxial tests were performed on oven dry sand samples under confining pressures of 25, 50, 100 and 150 and 200 kN/m^2. These test results yielded value of angle of internal friction, ϕ as 39.5°.

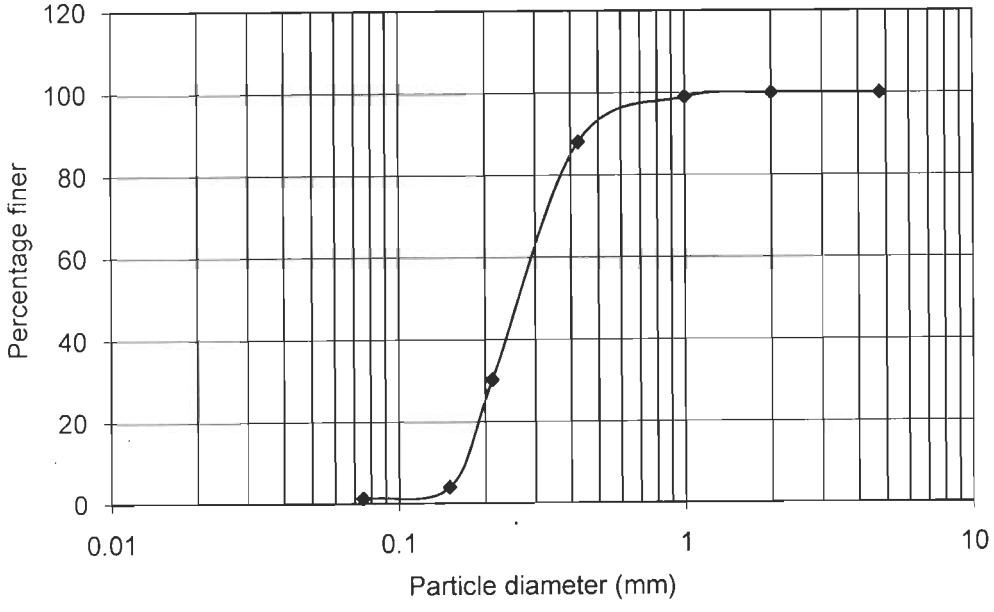

Fig. 5.1 Grain Size Distribution of Ranipur Sand

Table 5.1 Physical Properties of Ranipur Sand

S. No.	Property	Value
1	Soil type	SP
2	Effective size (D_{10})	0.16
3	Uniformity coefficient (C_u)	1.84
4	Coefficient of curvature (C_c)	0.93
5	Mean specific gravity, G	2.60
6	Maximum dry density $\gamma_{d\,max}$ (kN/m^3)	17.4
7	Minimum dry density $\gamma_{d\,min}$ (kN/m^3)	14.1
8	Relative density, D_r	70%
9	Unit weight of sand at 70% D_r (kN/m^3)	16.6

5.3 EVALUATION OF CONSTITUTIVE PROPERTIES

For obtaining the constitutive relationships of Ranipur sand, triaxial compression tests were performed with confining pressure varying from 25 kN/m^2 to 200 kN/m^2 and at relative density of 70%. The stress-strain curves thus obtained are presented in Fig. 5.2. The transformed hyperbolic stress-strain relationships have been plotted in Fig. 5.3. It is observed that hyperbolic equation (Kondner, 1963) can be used to represent these stress–strain relationships. The parameters, '*a*' and '*b*' of the hyperbola were correlated with confining pressures and are plotted in Fig. 5.4 and Fig. 5.5. respectively.

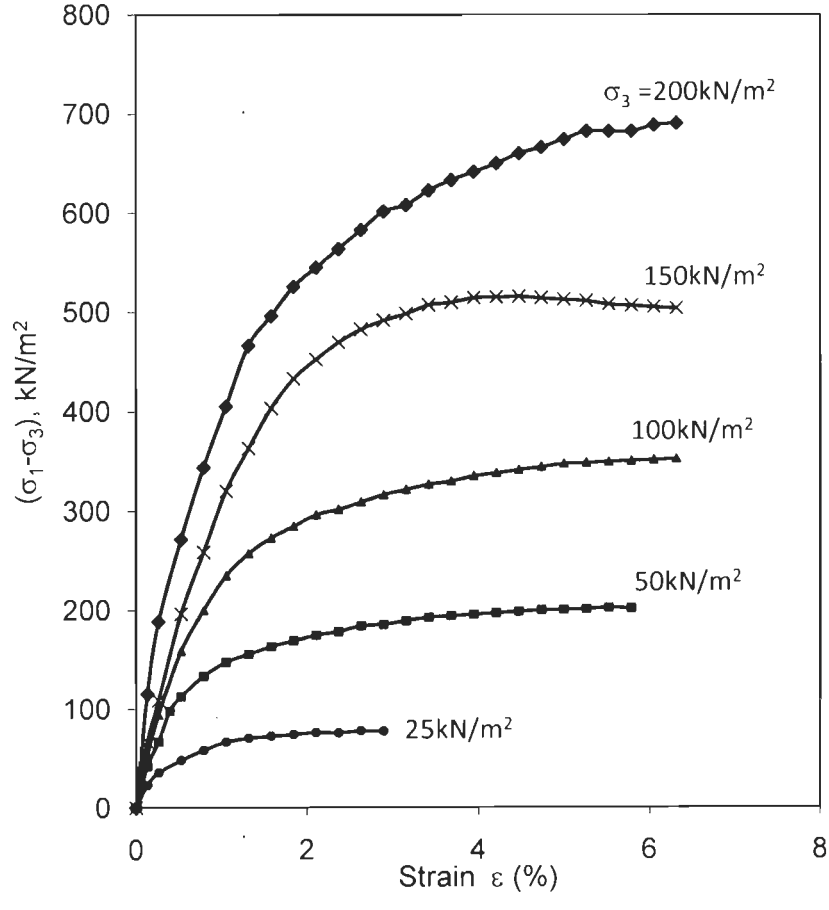

Fig. 5.2 Stress-Strain Plots of Ranipur Sand for Different Confining Pressures

The following relationships hold good for tests performed on Ranipur sand.

$$\frac{1}{a} = k_1 + A_1\sigma_3 \tag{5.1}$$

$$\frac{1}{b} = k_2\sigma_3 \tag{5.2}$$

k_1, A_1 and k_2 are constants obtained from analysis of triaxial tests data whose values are presented in Table 5.2; σ_3 is the confining pressure in kN/m^2 and $1/a$ and $1/b$ represent respectively initial tangent modulus E_i, and ultimate deviator stress, $(\sigma_1-\sigma_3)_u$ in kN/m^2 .

Table 5.2 Parameters of Constitutive Laws

D_r	k_1	A_1	k_2
70%	11595	398	4.0

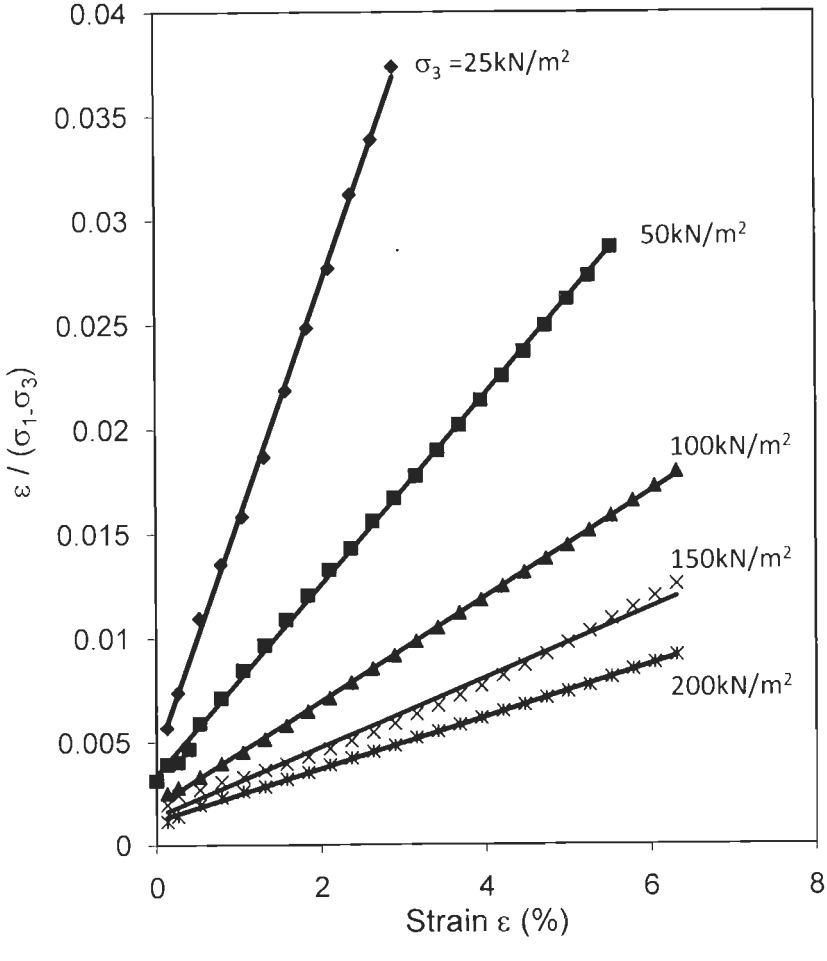

Fig. 5.3 Transformed Stress–Strain Response of Ranipur Sand

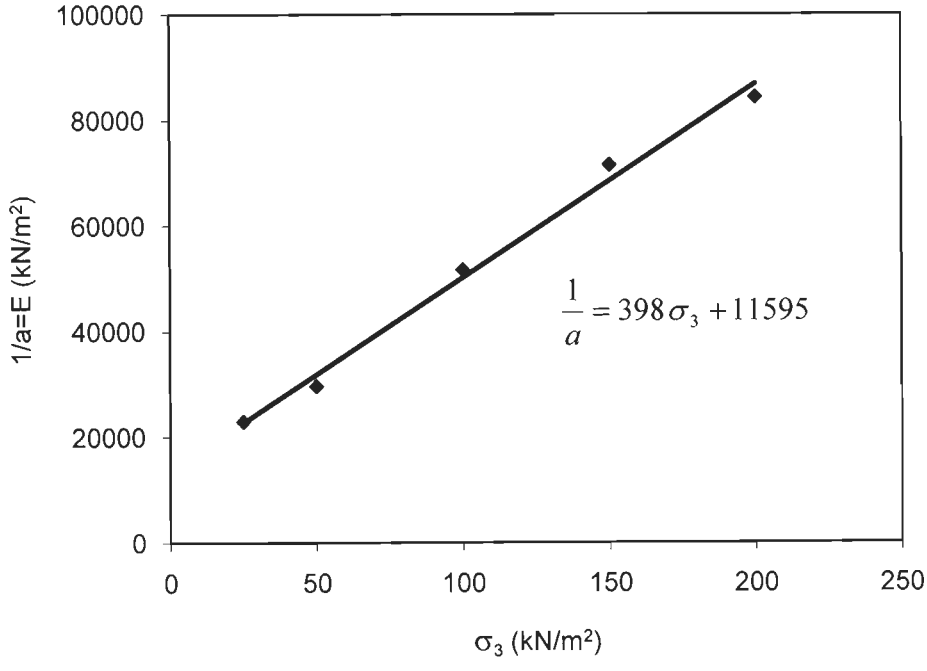

Fig. 5.4 Variation of 1/a (E_i) with Confining Pressure

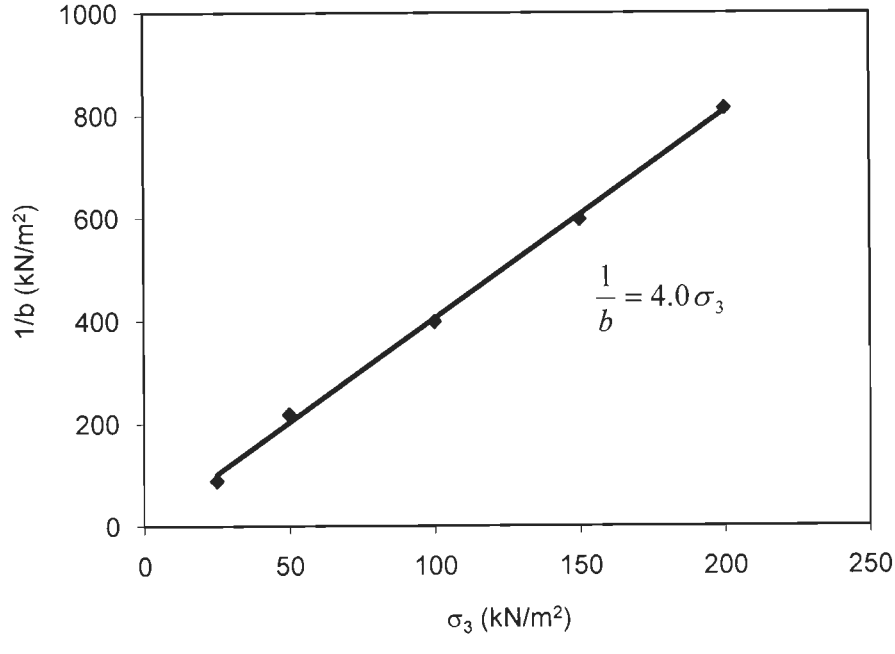

Fig. 5.5 Variation of 1/b with Confining Pressure

5.4 MODEL TESTS

Model tests were performed in which Ranipur sand was used at a relative density of 70%. The physical properties of sand have already been presented in Table 5.1. The experimental setup used in the study is shown in Fig. 5.6.

Fig. 5.6 View of the Experimental Setup

5.4.1 Footing

A 25 mm thick steel plate was used as the model strip footing. The footing was 150 mm wide and 600 mm long. The length of the footing was almost equal to the width of the tank so as to maintain the plane strain condition. To ensure the rough base of footing, a sand paper was attached to the bottom of the steel footing plate. The footing was provided with small grooves so as to position the loading plunger either centrally or at some eccentricity.

5.4.2 Tank

The inside dimensions of the tank used were 601mm in width, 3000 mm in length and 900 mm in height, built of angle iron frame. The two consecutive sidewalls of the tank were constructed using well-polished wooden planks, 20 mm thick and the other two consecutive walls were constructed using transparent Perspex sheets (25

mm thick) for the ease of observing the failure mechanism during testing. On one side of the tank, the perspex sheet was fixed in a groove so that it could be removed to open this side for removal of sand so as to make a slope at a desired angle. Horizontal steel stiffeners were provided for strengthening the side walls. In order to prevent the effect of friction with the inside walls of the tank constructed of wooden planks, a smooth polythene sheet was pasted over their surfaces. Line markings were made on the longer sides of the tank for preparing slopes of 30° and 26.56°.

5.4.3 Loading Device

Inclined load on the footing was applied by using inclined loading device developed by Murthy (1967). It consists of two arcs of mild steel plates, 20 mm thick, making an angle of 50° at the centre (Figure 5.7). The two plates separated by a web, were cut at the top and bottom in V-grooves to facilitate the ball bearings over which a cast iron block of 100 mm ×89 mm× 165 mm size slides. A screw jack with a capacity of 30 kN was inserted into the cast iron block. The plate was marked with graduations from 0° to 35° so that the inclination of the applied load can be directly read. The screw jack was fitted to a calibrated proving ring and in turn, to a rod tapered at the end. The whole assembly was fixed to a beam with supports across the whole tank. The view of the loading device is shown in Fig. 5.7.

Fig.5.7 View of the Loading Device

5.4.4 Measuring Device for Vertical Settlement and Horizontal Displacement

To measure the vertical settlement and horizontal displacement of the point of load application, a steel plate (250 mm long and 30 mm wide) was fixed in between the proving ring and the plunger as shown in Fig. 5.6. This plate remains always normal to the plunger. Two dial gauges were fixed normal to this plate, which measure the displacement of the point of application of load along the direction of movement of the plunger. For a given inclined load, knowing the displacement along the plunger and the inclination of the plunger, vertical settlement and horizontal displacement can be calculated as shown in the Fig. 5.8.

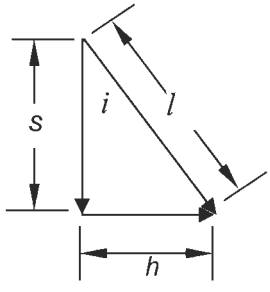

$s = l \cos i$

$h = l \sin i$

where l = displacement along the plunger

s = vertical settlement

h = horizontal displacement

Fig. 5.8 Determination of Vertical Settlement and Horizontal Displacement

5.4.5 Measurement of Tilt

Tilts were measured with specially designed tilt meters. Tilt meters were provided with a micrometer screw, with help of which tilt upto an accuracy of 0.001radian can be measured. For each footing, two tilt meters were fixed along the two edges of the footing. A view of the footing plate with the tilt meters fixed on it is shown in Fig. 5.9.

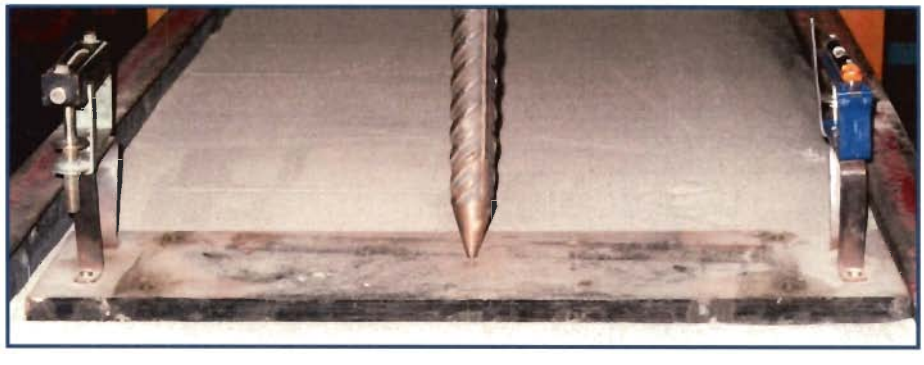

Fig.5.9 View of Footing Plate with Tilt Meters

5.4.6 Sand Filling

The inner faces of the walls of the tank were marked with lines at 50 mm intervals to facilitate accurate preparation of sand bed in layers with desired relative density of sand. Sand was deposited in weighed quantity in layers of 50 mm each and compacted to achieve a relative density of 70%. Every layer was compacted uniformly so as to obtain a uniform density.

5.4.7 Slope Formation

Sand was first placed uniformly up to the same level over the entire length of the tank at the desired density. The Perspex sheet was then removed from the end where the slope was to be constructed. From the marked line of the slope at top, sand was slowly removed downwards with the help of a plane edge. The whole of the extra sand above the desired slope line was removed from the tank. The view of the completed slope is shown in the Fig. 5.10.

Fig.5.10 View of Completed Slope

5.5 TEST PROCEDURE

Sand surface in the tank was first levelled and the slope was formed. The footing was positioned at the desired location with respect to the edge distance of the footing from the crest of slope in the tank, taking care that the gap between the footing sides and the tank is uniform on either side. The loading frame was then

moved above the footing and the loading device was adjusted at the desired angle of load application. The proving ring and the plunger were fixed in between the screw jack and the footing. In all the tests, load was applied by means of the hand-operated screw jack. Increments of load were applied when the settlement under any given applied load increment becomes reasonably constant i.e. less than 0.01mm in ten minutes. The displacements along the plunger were recorded with the help of two dial gauges and the average of these two readings was recorded. Similarly, the tilts were measured with the help of the two tilt meters placed along the edge of the footing and the average of these two was recorded. Several tests were repeated to confirm the reproducibility of the test data.

5.6 TESTS PERFORMED

In all, 39 tests were performed for a footing on sloping ground and 9 tests on level ground. Details of these model tests are presented in Table 5.3 and the notations used to represent different geometric parameters are illustrated in Figs. 5.11 and 5.12. The pressure versus settlement and pressure versus tilt characteristics obtained for various cases under consideration are presented in Figs. 5.13 through 5.42. The results of these tests and their interpretation have been discussed in the next chapter.

Table 5.3 Parametric Values for Laboratory Model Tests

Flat ground, $\beta = 0$	***e/B***		***i***
	0, 0.1, 0.2		0, 10°, 20°
Slope angle $\beta = 30°$	D_e/B	***e/B***	***i***
	1.0, 2.0, 3.0	0, 0.1, 0.2	0, 10°, 20°
Slope angle $\beta = 26.56°$	2.0	0, 0.1, 0.2	0, 10°, 20°
	0, 0.5, 1.0	0	0

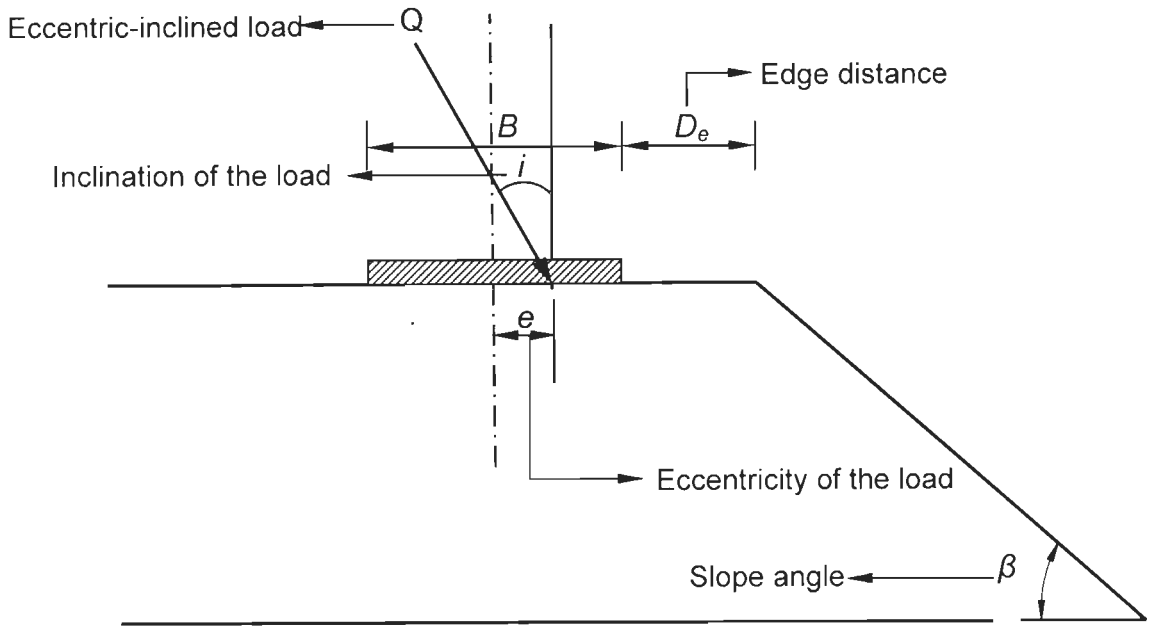

Fig. 5.11 Geometric Parameters used in Various Tests

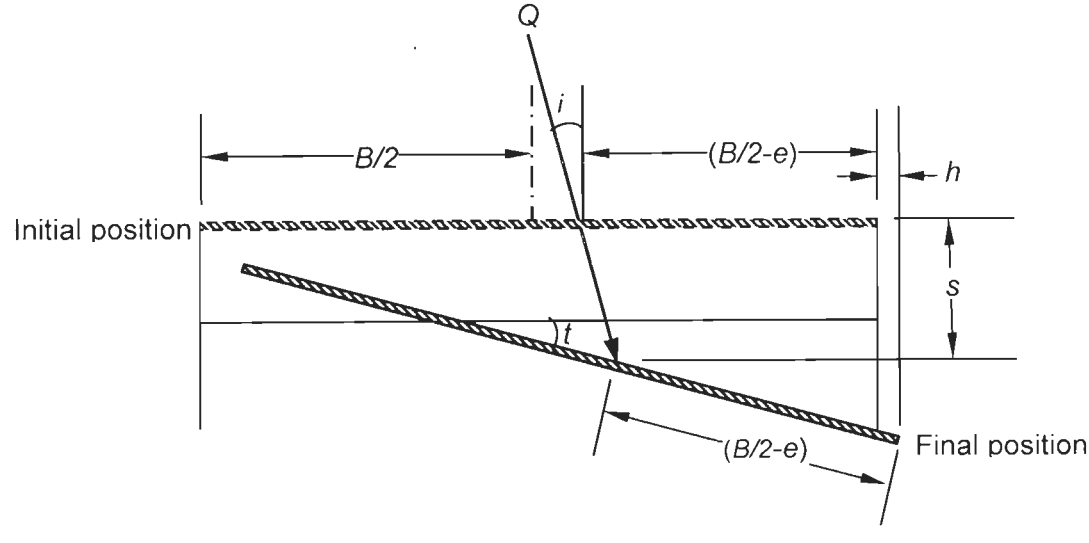

Fig. 5.12 Settlement and Tilt of a Footing with Eccentric-Inclined Load

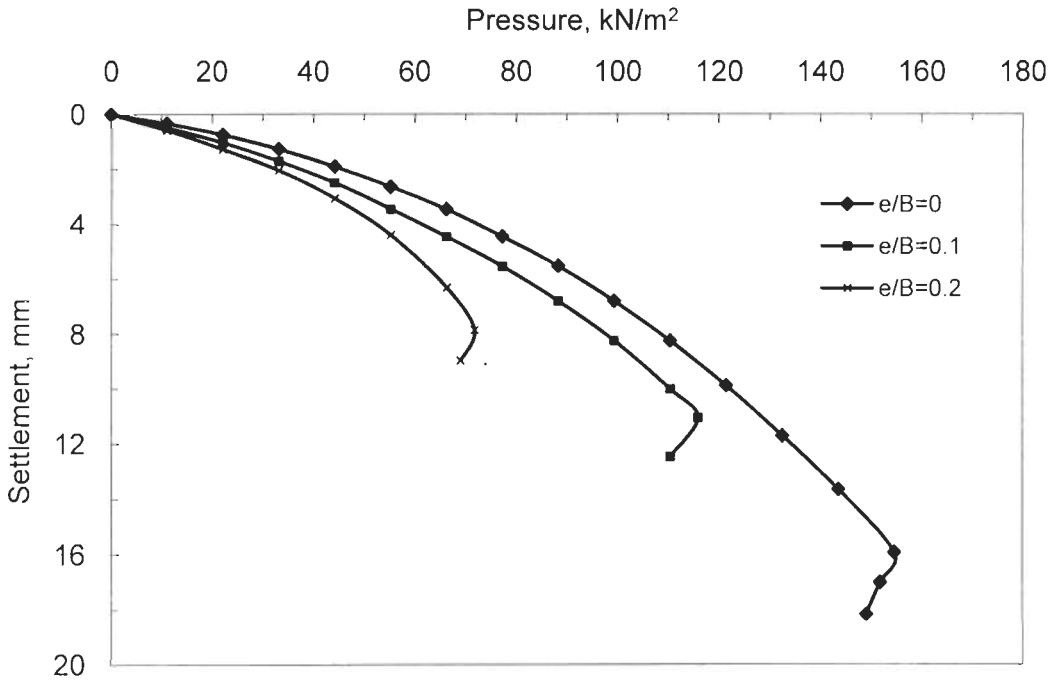

Fig. 5.13 Pressure versus Vertical Settlement Curves for Footing on Level Ground ($i = 0°$)

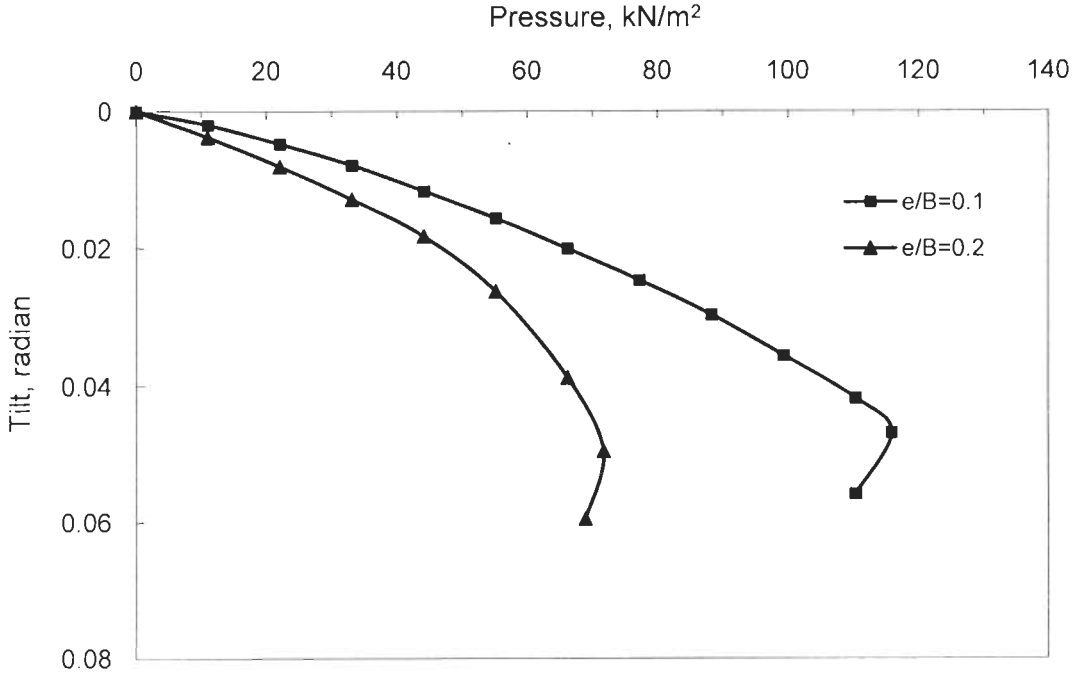

Fig. 5.14 Pressure versus Tilt Curves for Footing on Level Ground ($i = 0°$)

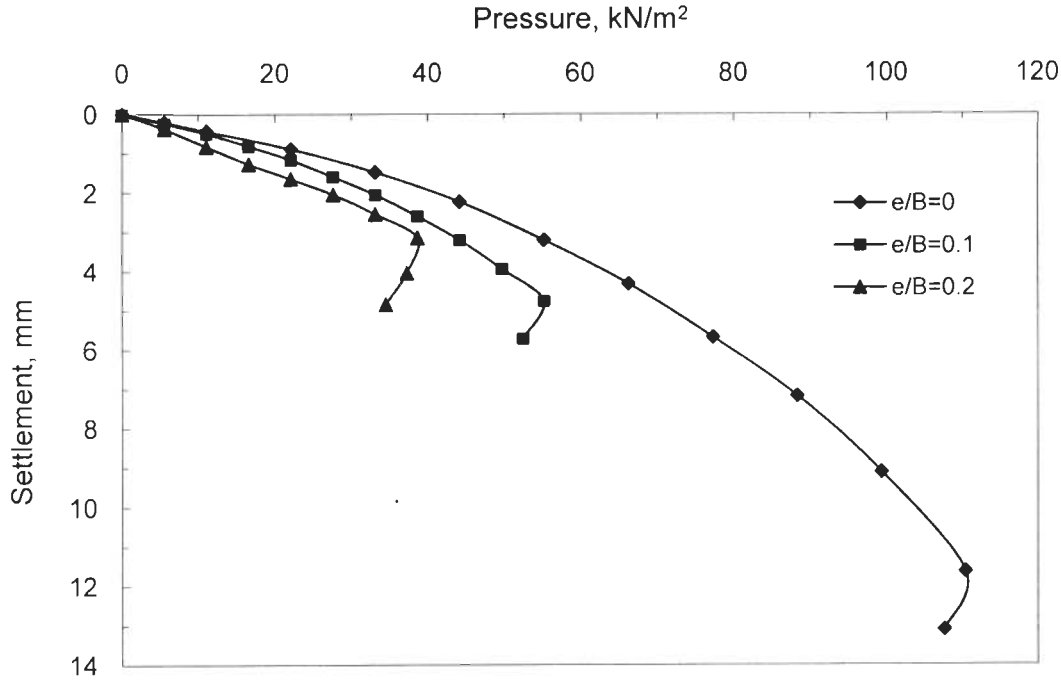

Fig. 5.15 Pressure versus Vertical Settlement Curves for Footing on Level Ground (i =10°)

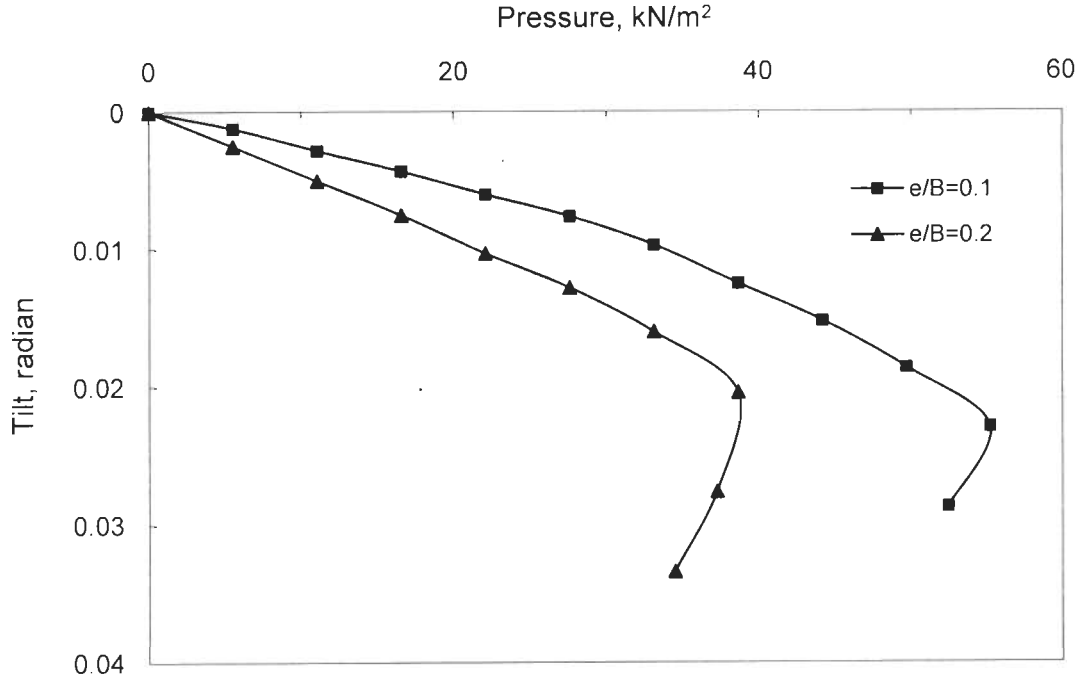

Fig. 5.16 Pressure versus Tilt Curves for Footing on Level Ground (i = 10°)

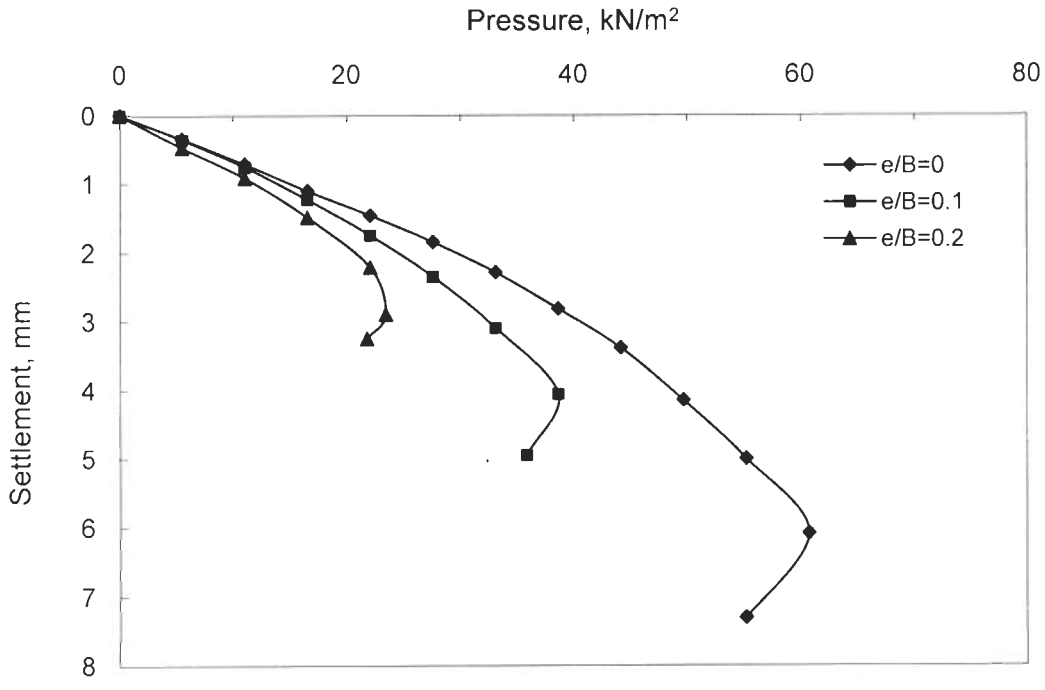

Fig. 5.17 Pressure versus Vertical Settlement Curves for Footing on Level Ground (i=20°)

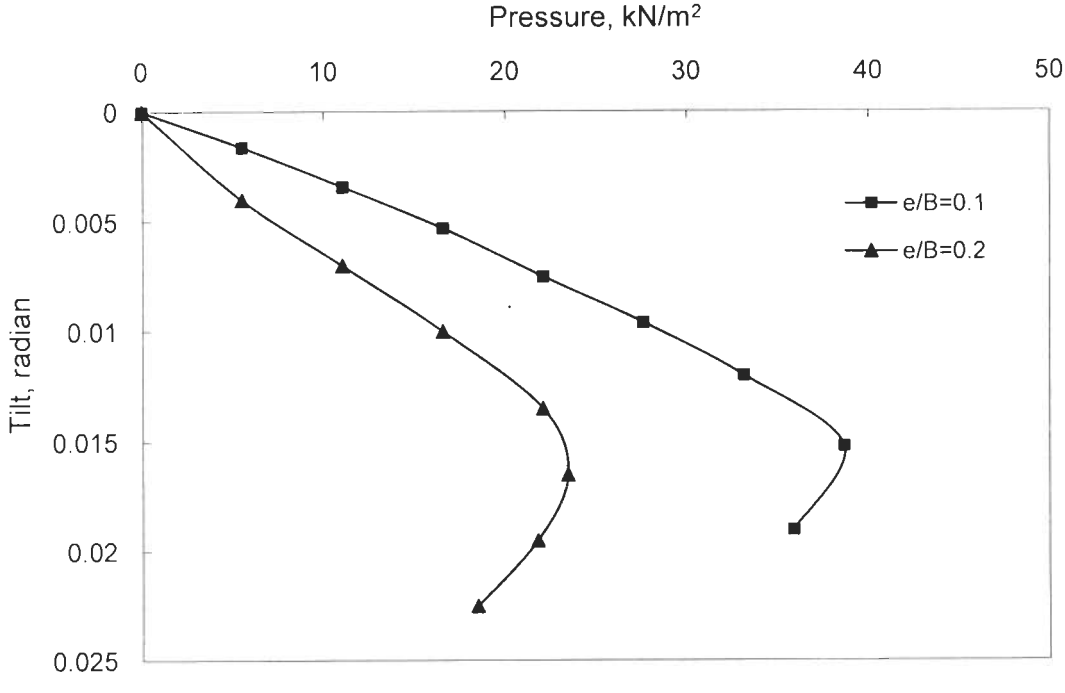

Fig. 5.18 Pressure versus Tilt Curves for Footing on Level Ground (i=20°)

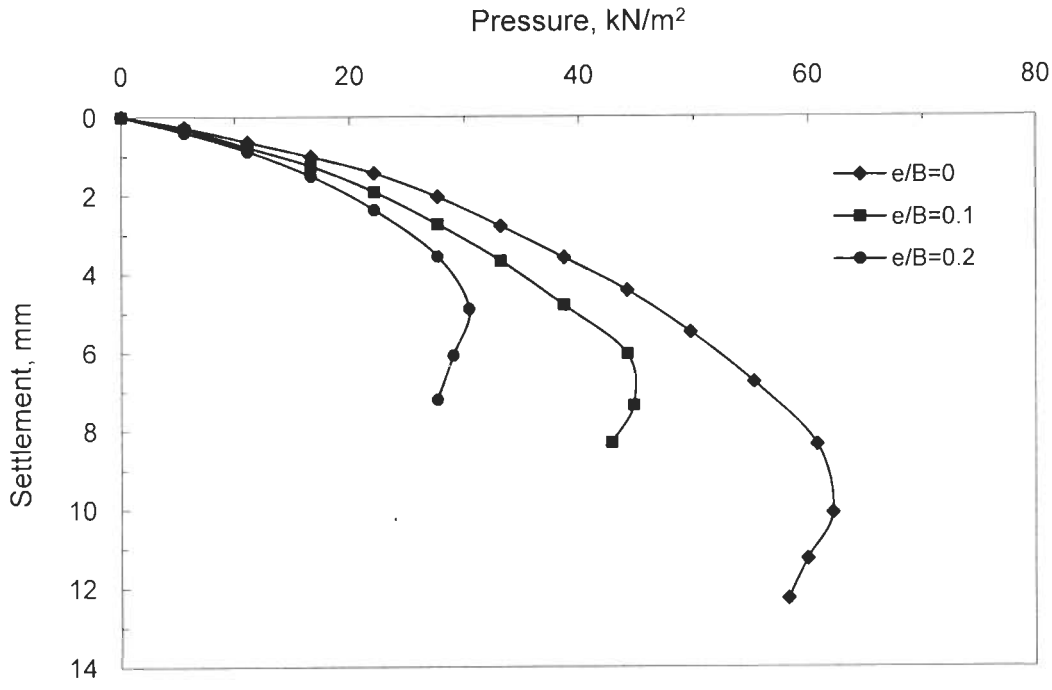

Fig. 5.19 Pressure versus Vertical Settlement Curves for Footing on a Slope (β =30° , *De/B*=1.0, i =0°)

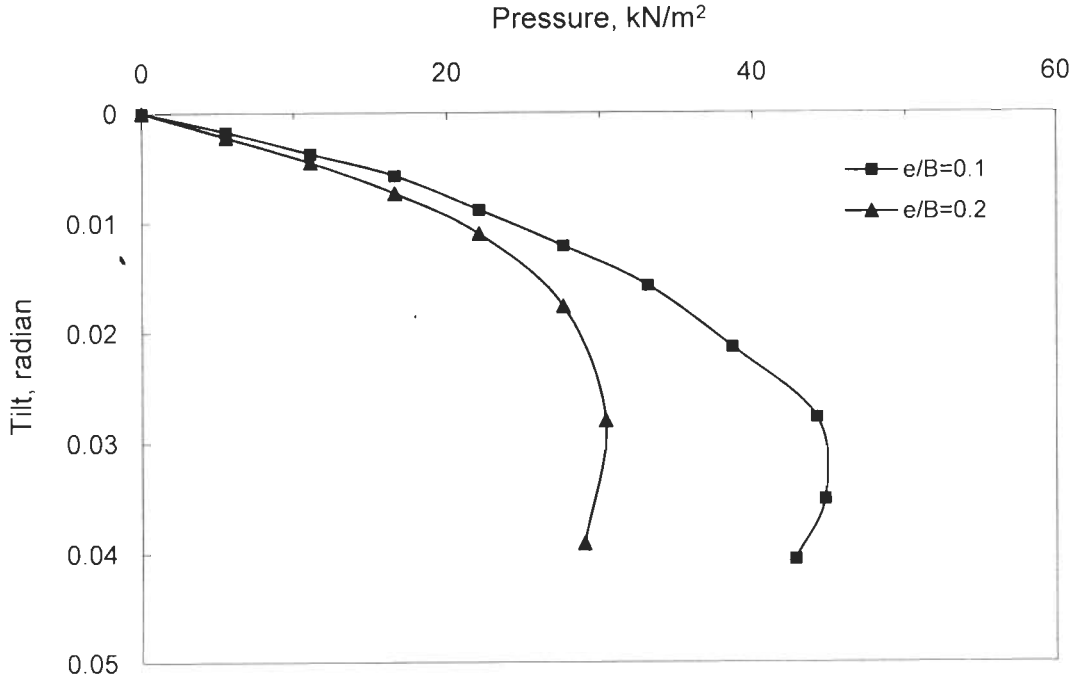

Fig. 5.20 Pressure versus Tilt Curves for Footing on a Slope (β =30° , *De/B*=1.0, i=0°)

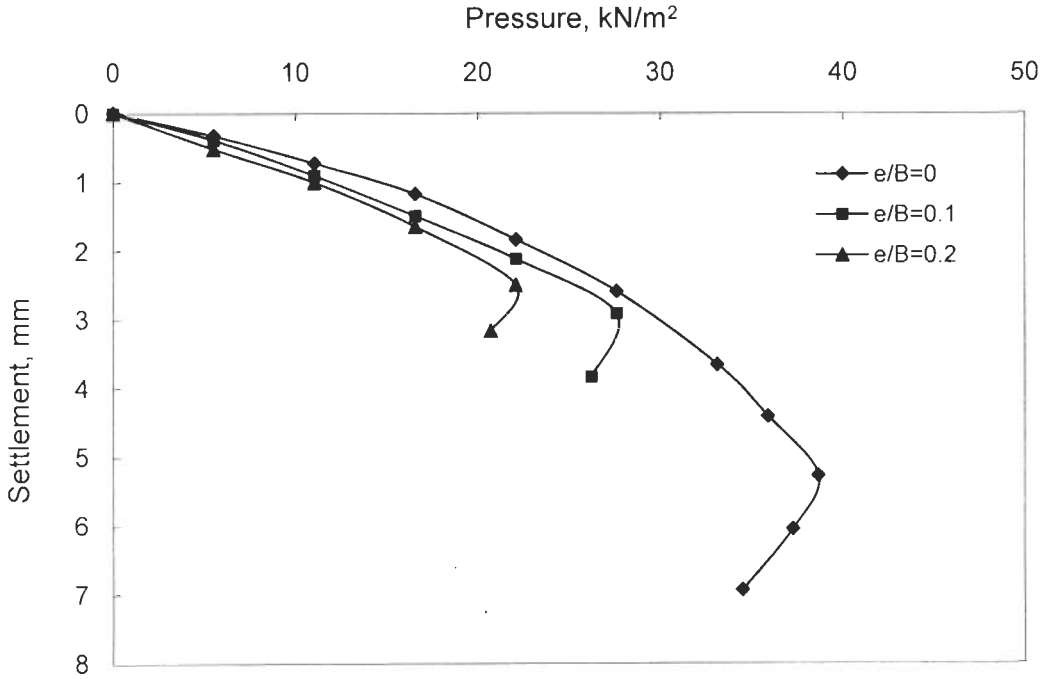

Fig. 5.21 Pressure versus Vertical Settlement Curves for Footing on a Slope (β =30°, *De/B*=1.0, *i*=10°)

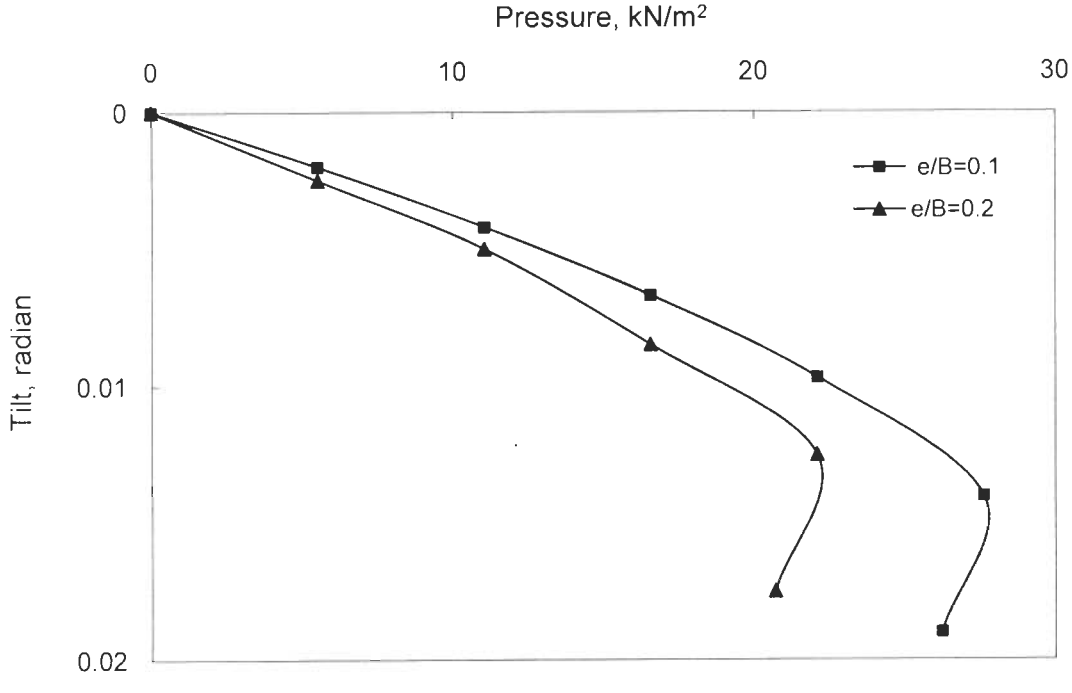

Fig. 5.22 Pressure versus Tilt Curves for Footing on a Slope (β =30° , *De/B*=1.0, *i*=10°)

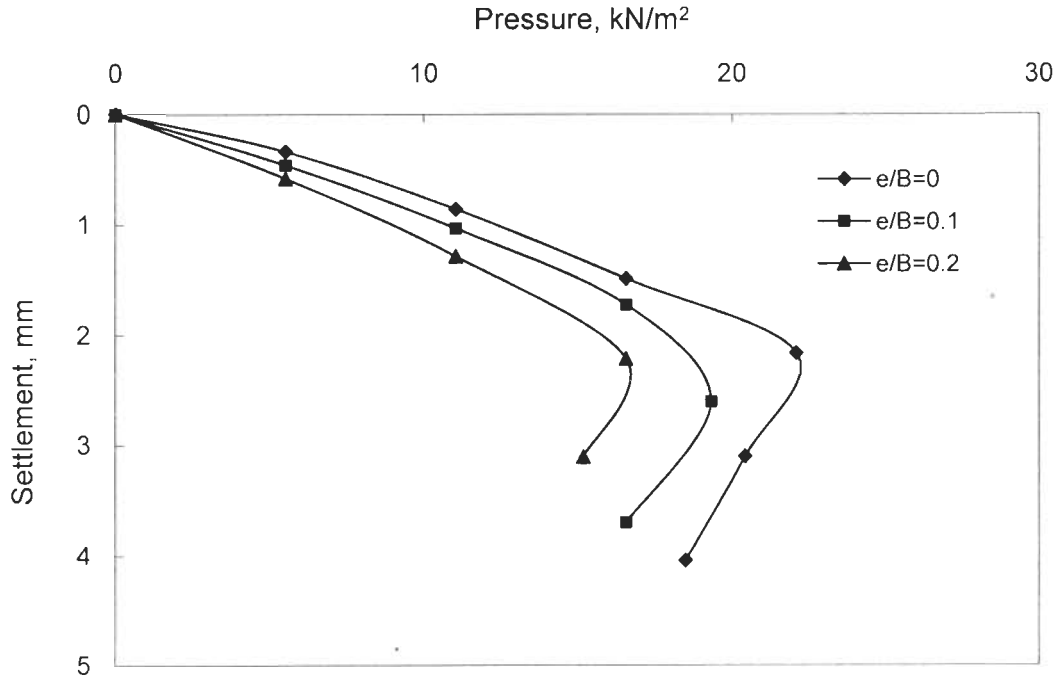

Fig. 5.23 Pressure versus Vertical Settlement Curves for Footing on a Slope (β =30°, *De/B*=1.0, *i*=20°)

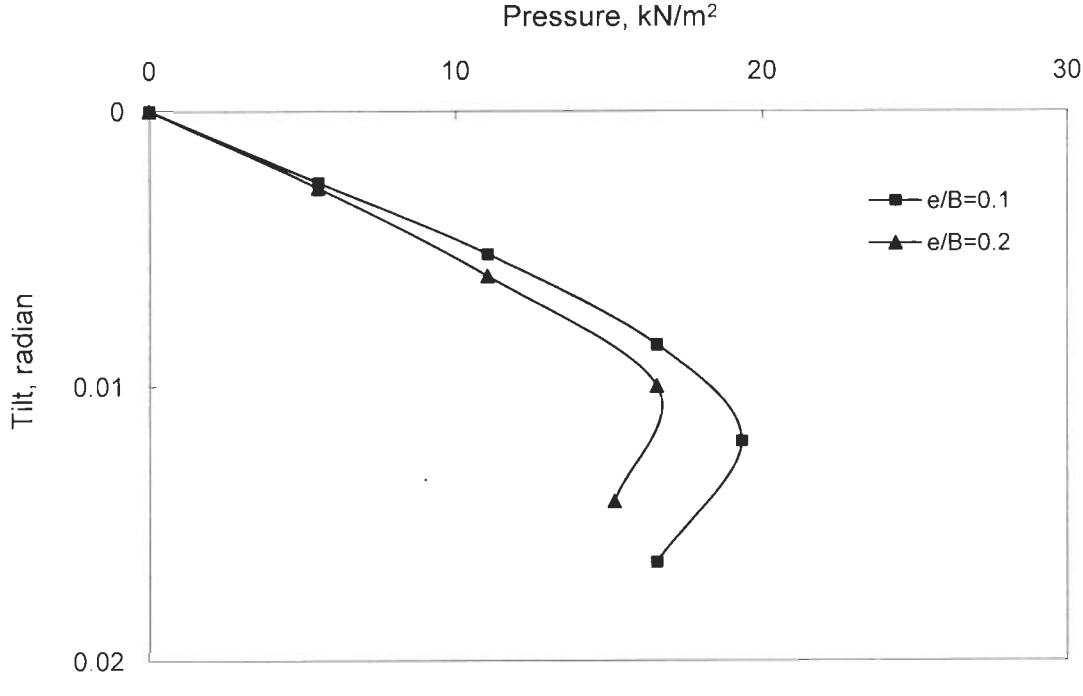

Fig. 5.24 Pressure versus Tilt Curves for Footing on a Slope (β =30° , *De/B*=1.0, *i* =20°)

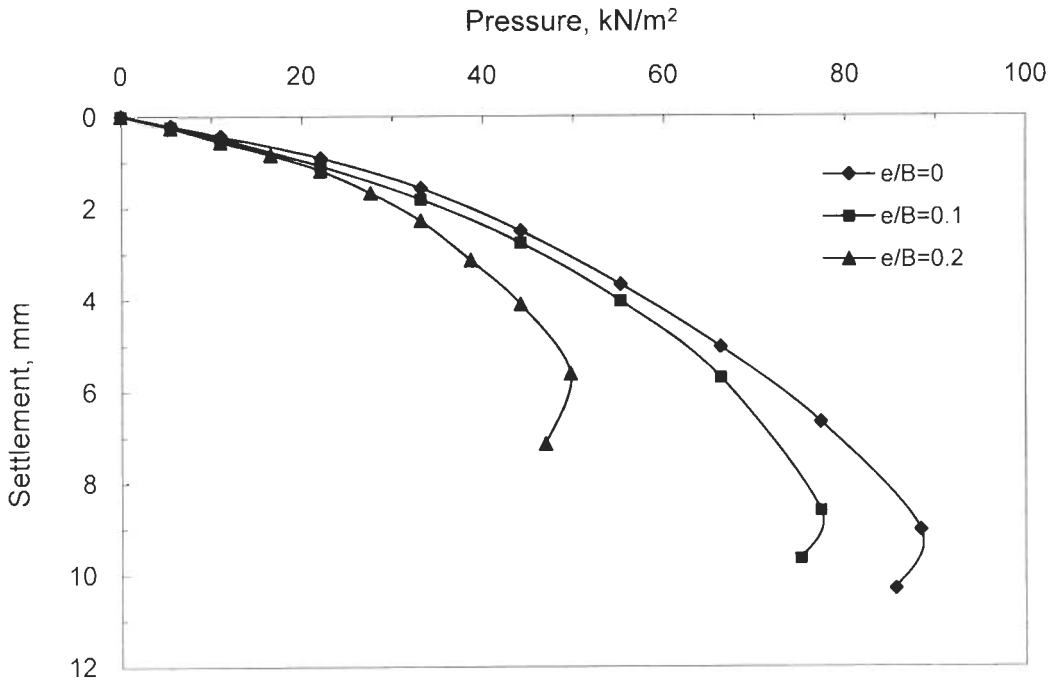

Fig. 5.25 Pressure versus Vertical Settlement Curves for Footing on a Slope (β =30° , *De/B*=2.0, *i*=0°)

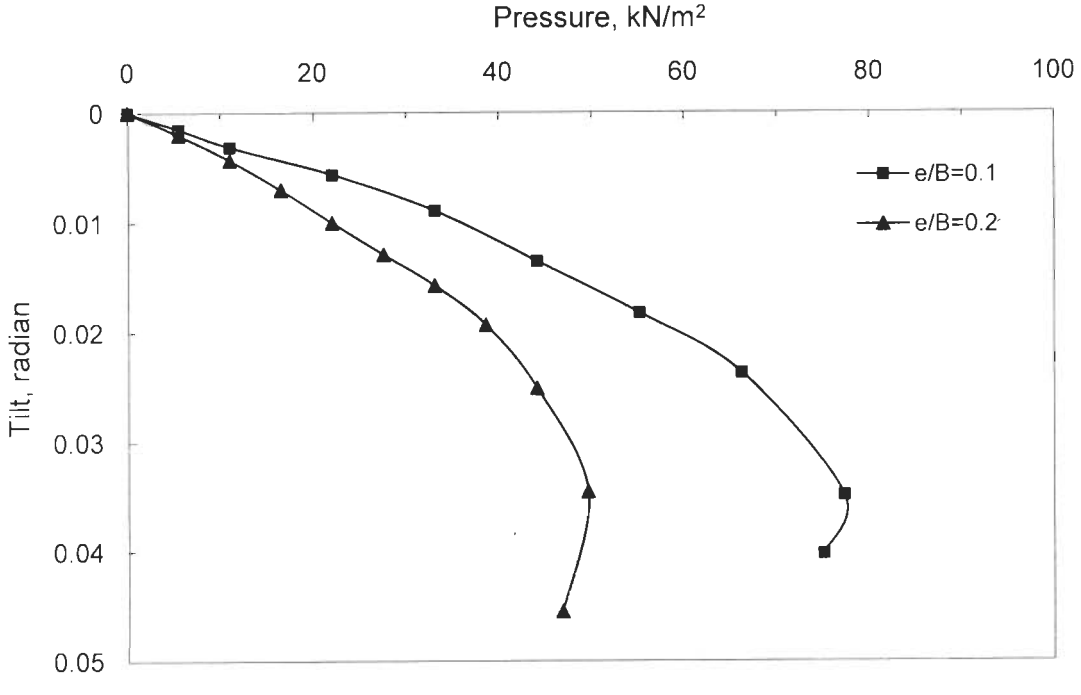

Fig. 5.26 Pressure versus Tilt Curves for Footing on a Slope (β =30° , *De/B*=2.0, *i* =0°)

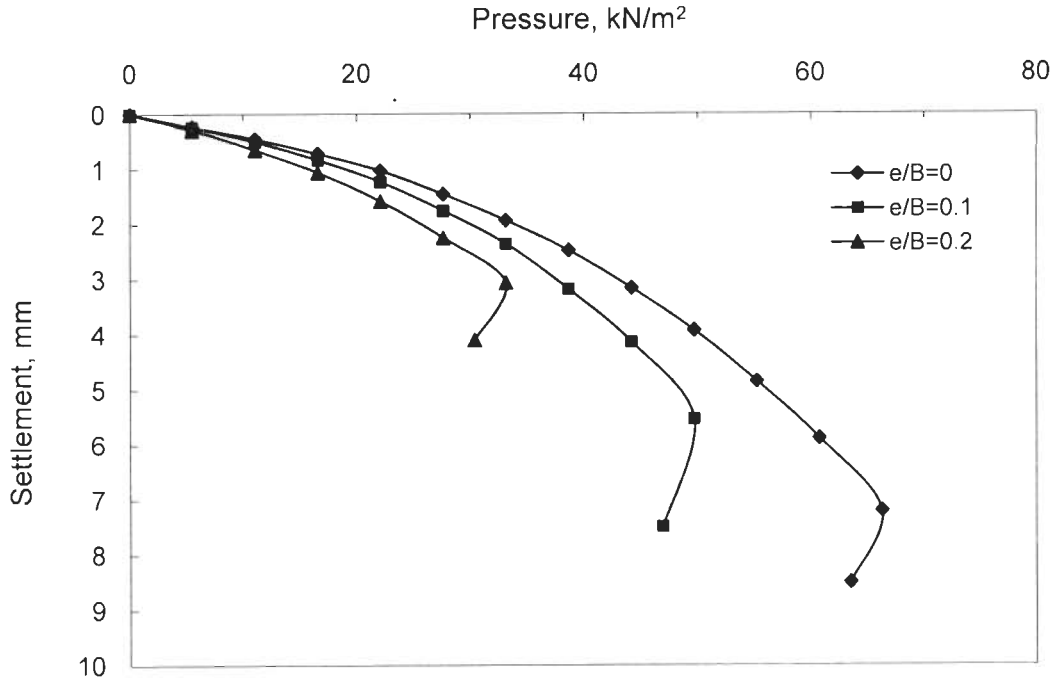

Fig. 5.27 Pressure versus Vertical Settlement Curves for Footing on a Slope (β =30°, *De/B*=2.0, *i*=10°)

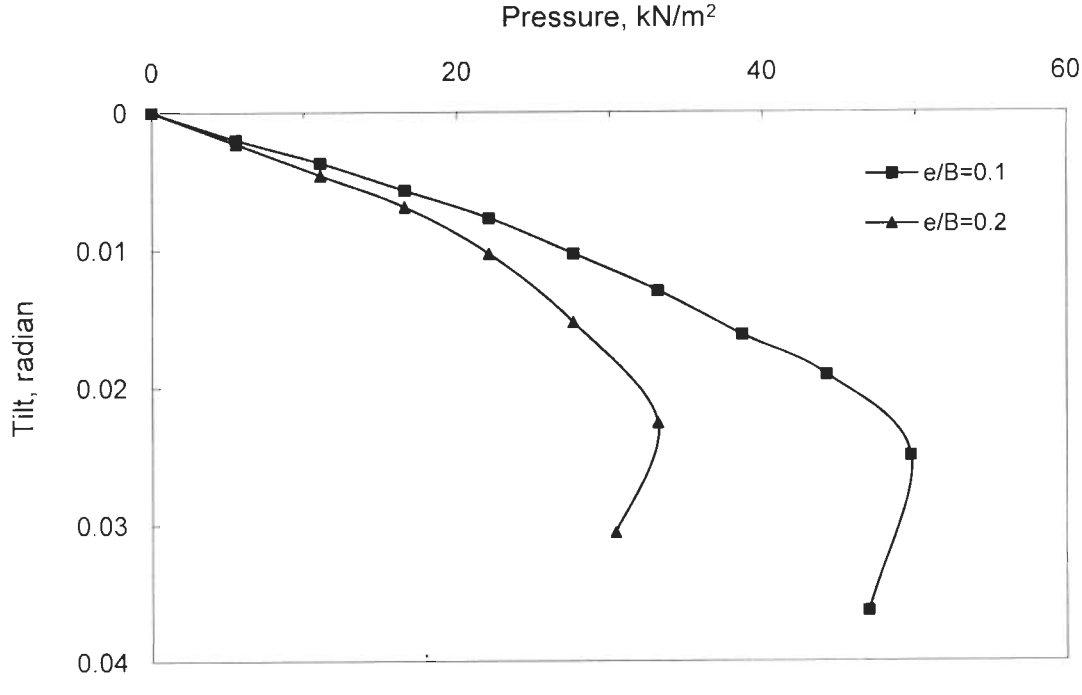

Fig. 5.28 Pressure versus Tilt Curves for Footing on a Slope (β =30° , *De/B*=2.0, *i* =10°)

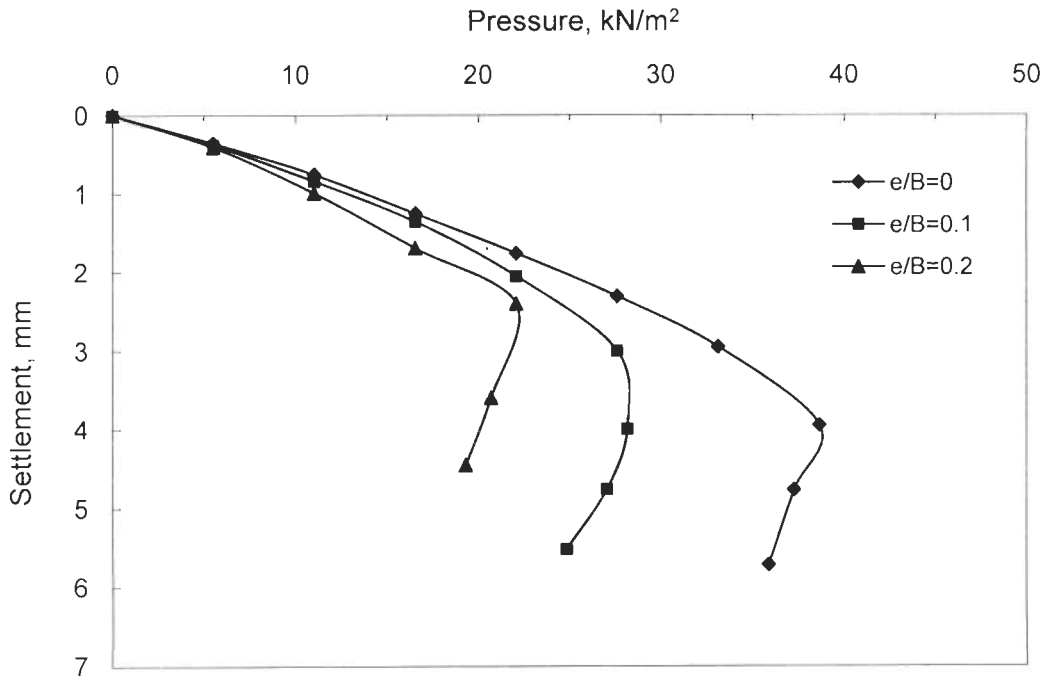

Fig. 5.29 Pressure versus Vertical Settlement Curves for Footing on a Slope (β =30°, *De/B*=2.0, *i*=20°)

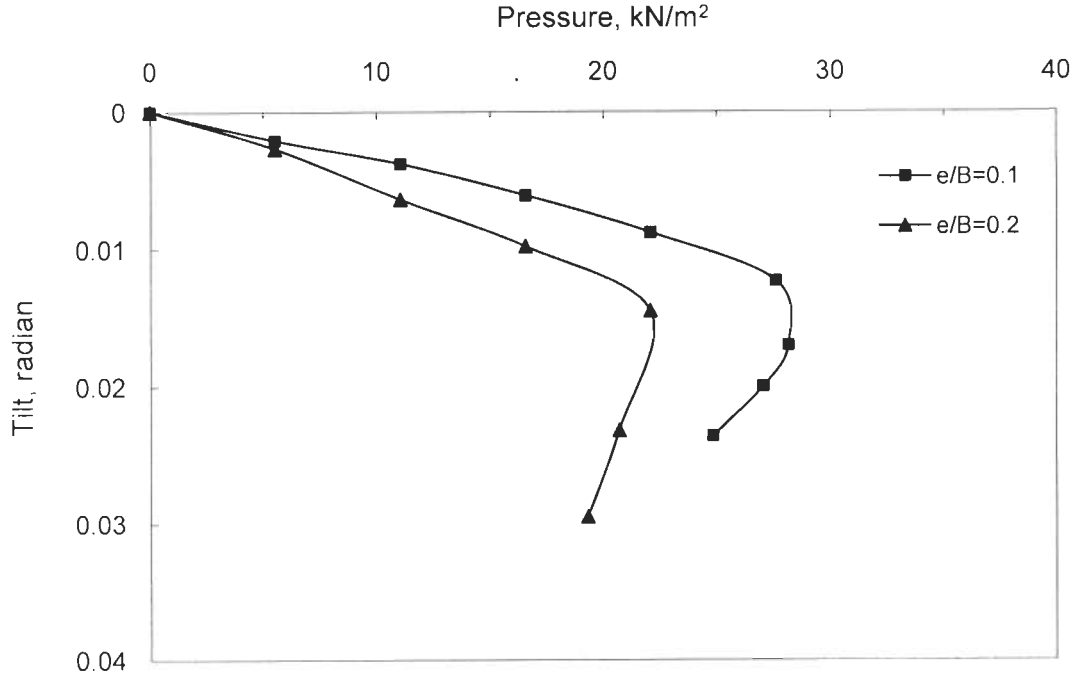

Fig. 5.30 Pressure versus Tilt Curves for Footing on a Slope (β =30° , *De/B*=2.0, *i* =20°)

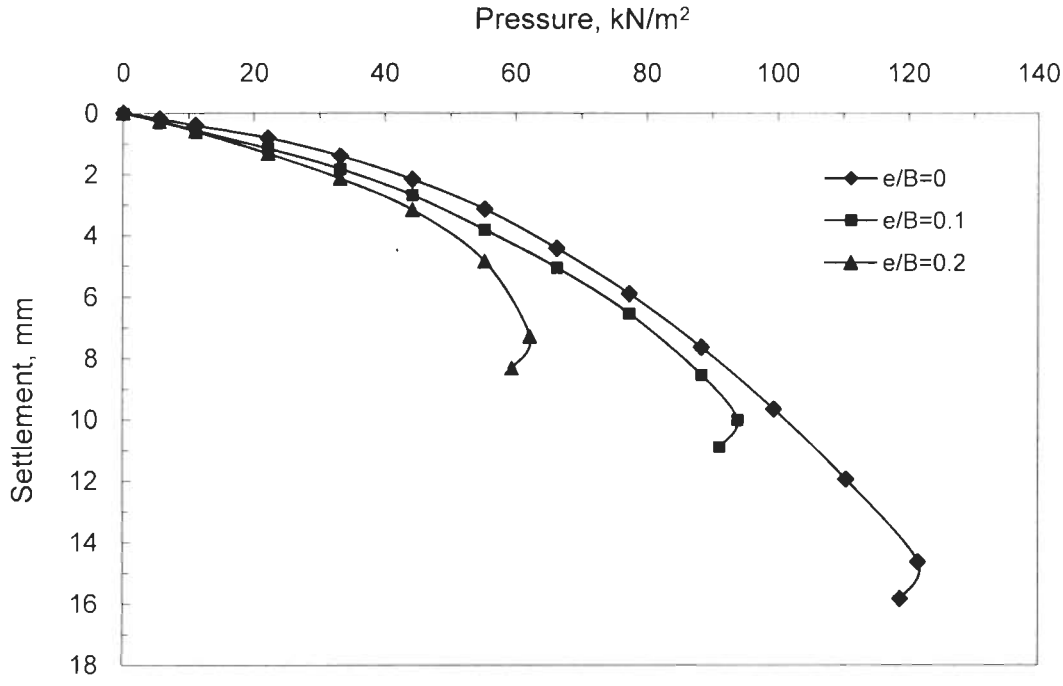

Fig. 5.31 Pressure versus Vertical Settlement Curves for Footing on a Slope (β =30° , *De/B*=3.0, *i*=0°)

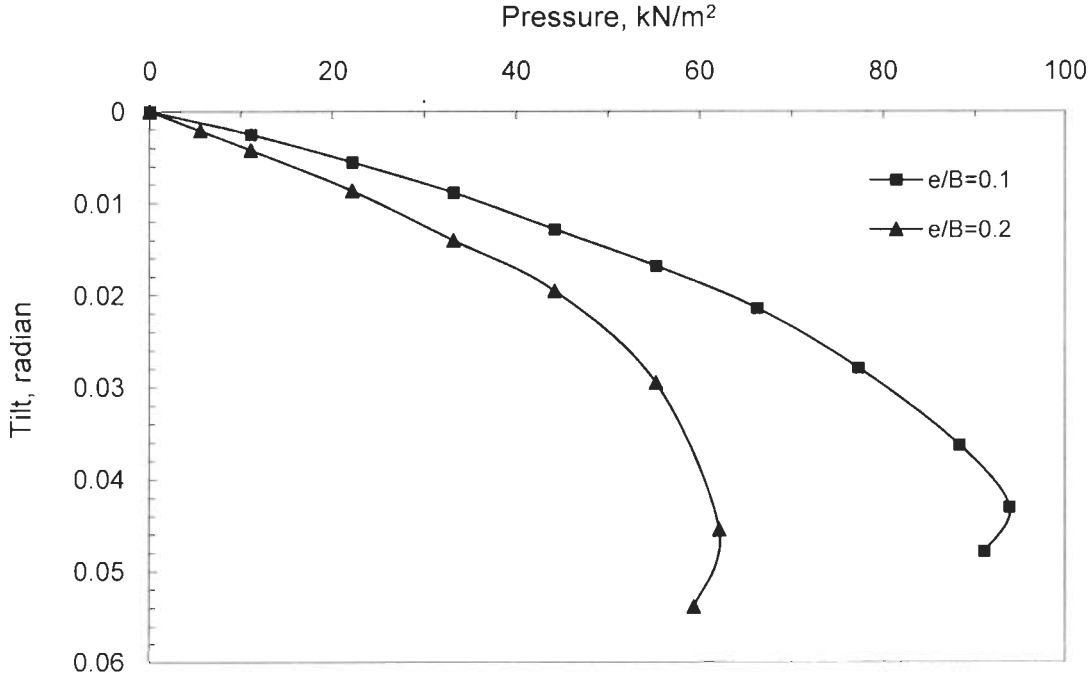

Fig. 5.32 Pressure versus Tilt Curves for Footing on a Slope (β =30° , *De/B*=3.0, *i* =0°)

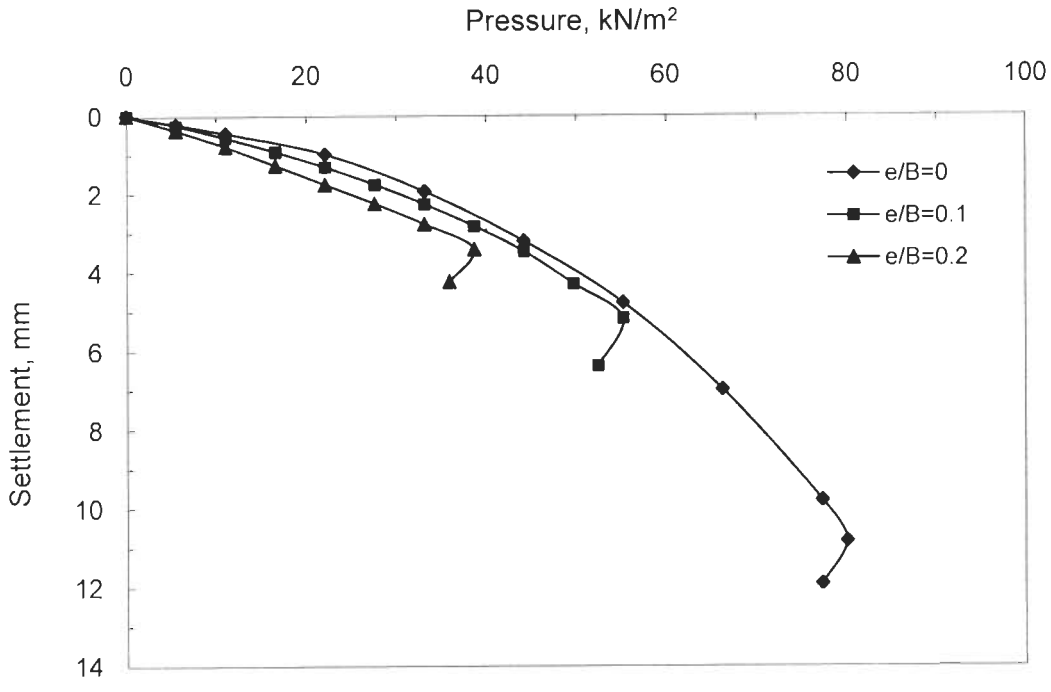

Fig. 5.33 Pressure versus Vertical Settlement Curves for Footing on a Slope (β =30°, *De/B*=3.0, *i*=10°)

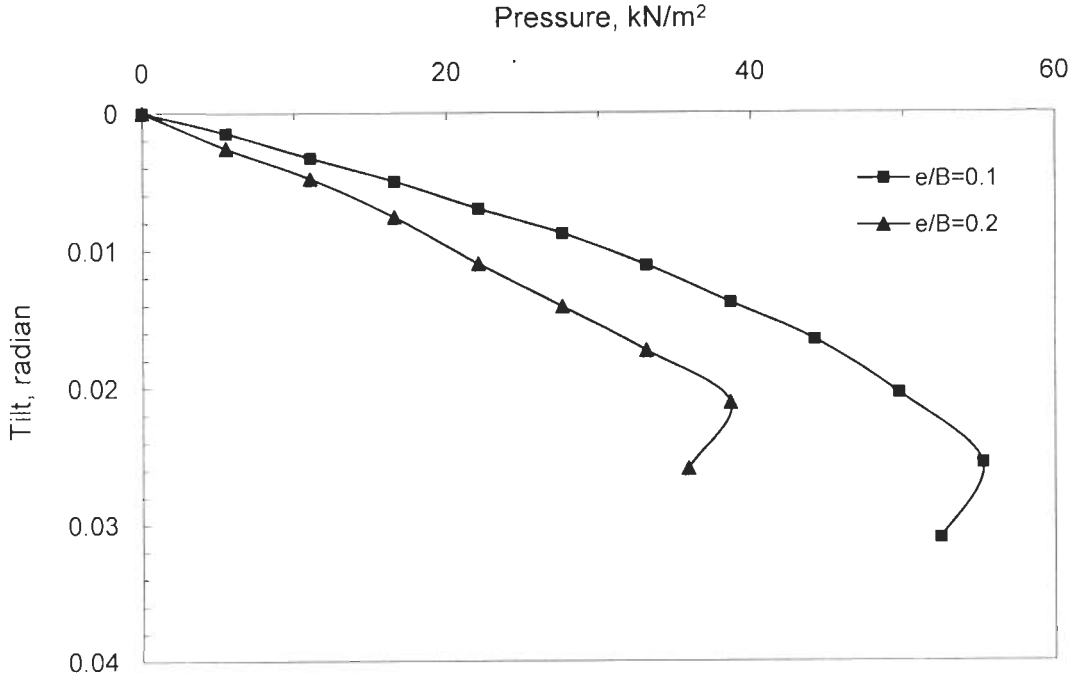

Fig. 5.34 Pressure versus Tilt Curves for Footing on a Slope (β =30°, *De/B*=3.0, *i* =10°)

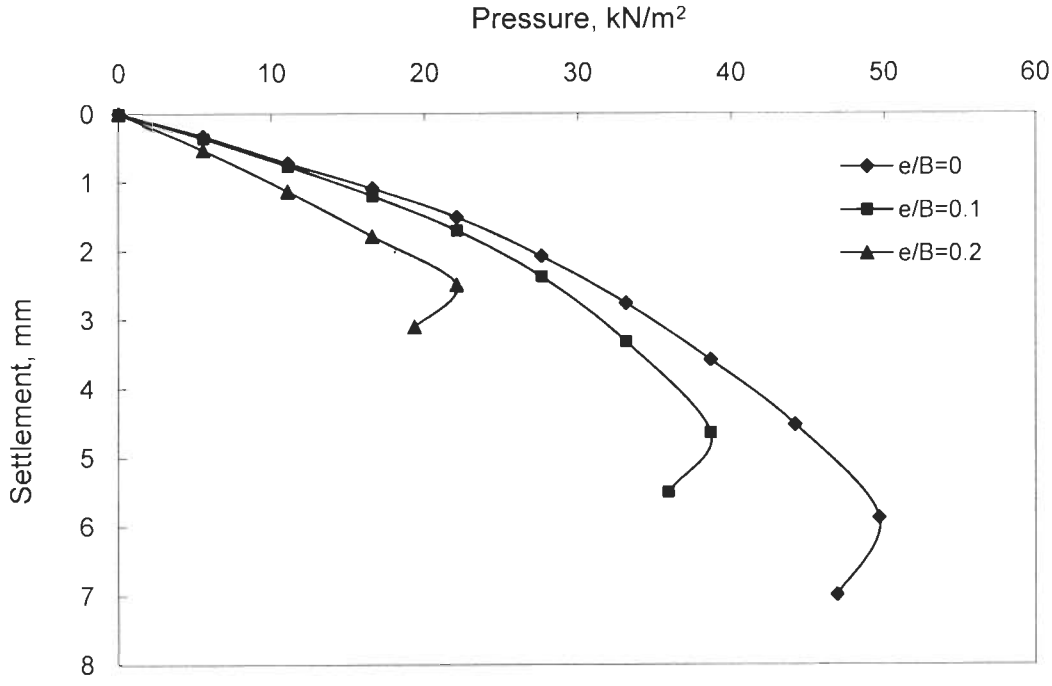

Fig. 5.35 Pressure versus Vertical Settlement Curves for Footing on a Slope (β =30°, *De/B*=3.0, *i*=20°)

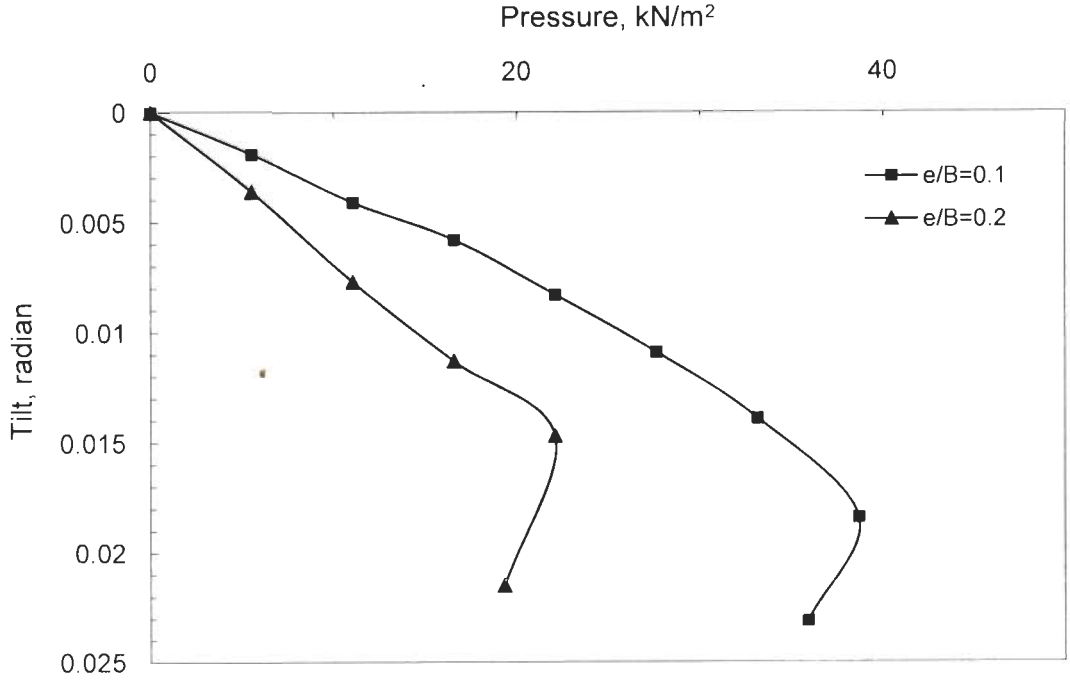

Fig. 5.36 Pressure versus Tilt Curves for Footing on a Slope (β =30° , *De/B*=3.0, *i* =20°)

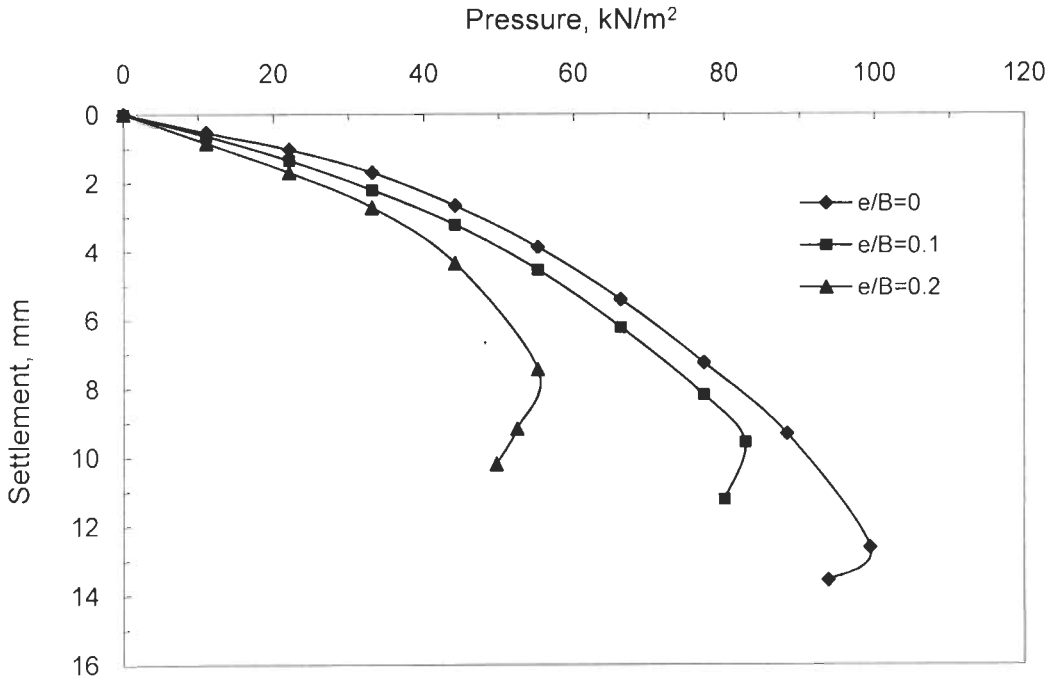

Fig. 5.37 Pressure versus Vertical Settlement Curves for Footing on a Slope (β =26.56°, *De/B*=2.0, *i*=0°)

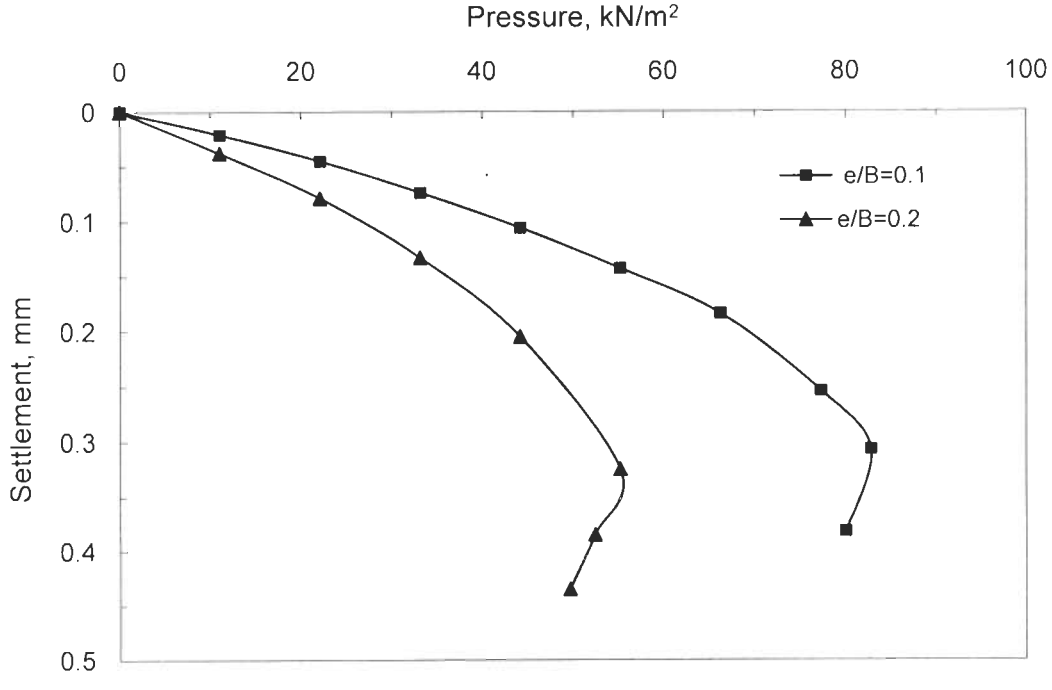

Fig. 5.38 Pressure versus Tilt Curves for Footing on a Slope (β =26.56° , *De/B*=2.0, *i* =0°)

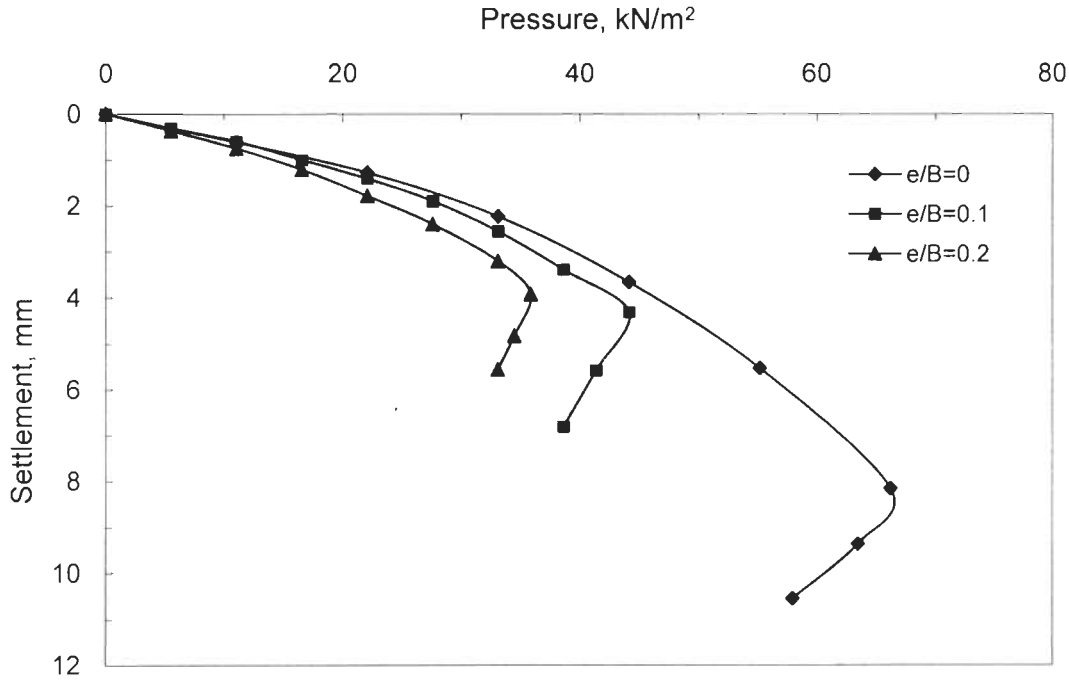

Fig. 5.39 Pressure versus Vertical Settlement Curves for Footing on a Slope (β =26.56°, *De/B*=2.0, *i*=10°)

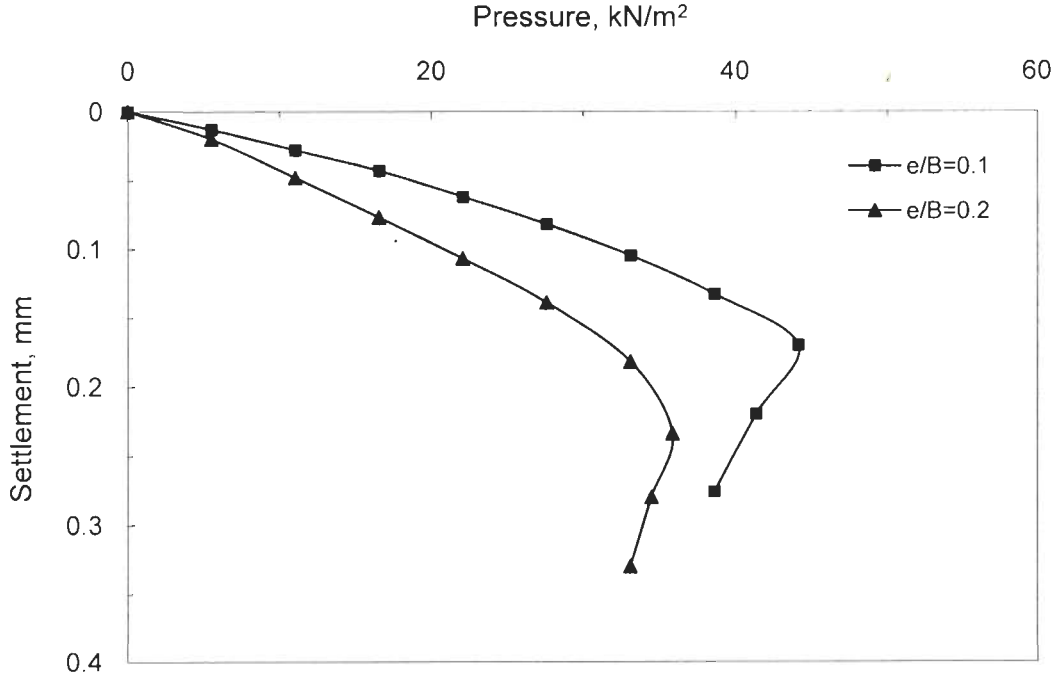

Fig. 5.40 Pressure versus Tilt Curves for Footing on a Slope (β =26.56° , *De/B*=2.0, *i* =10°)

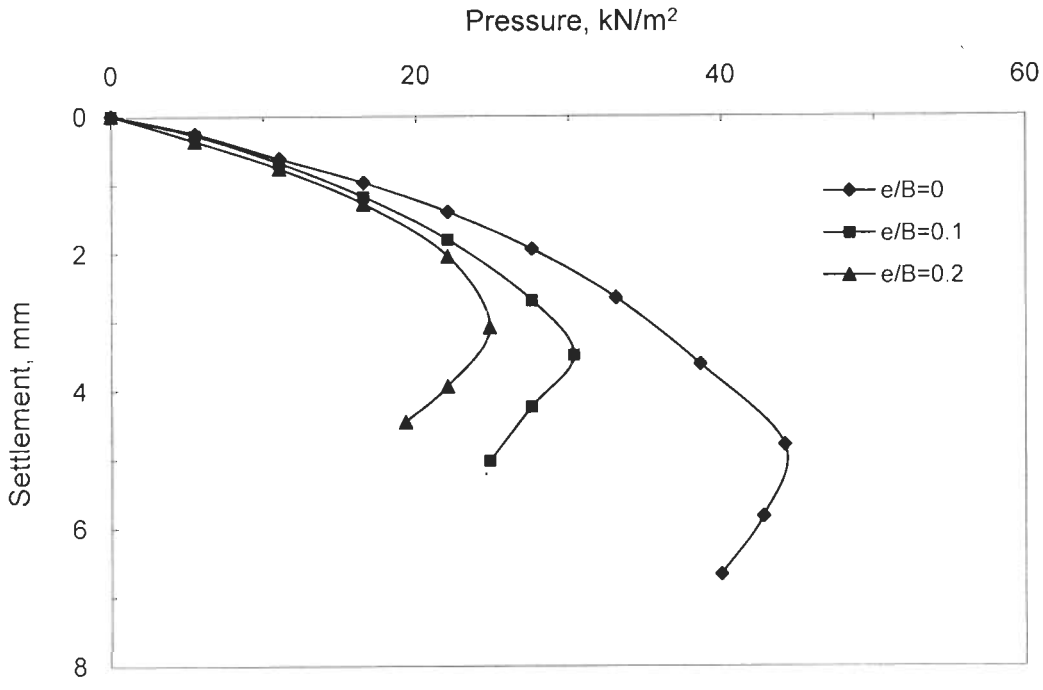

Fig. 5.41 Pressure versus Vertical Settlement Curves for Footing on a Slope (β =26.56°, De/B=2.0, i=20°)

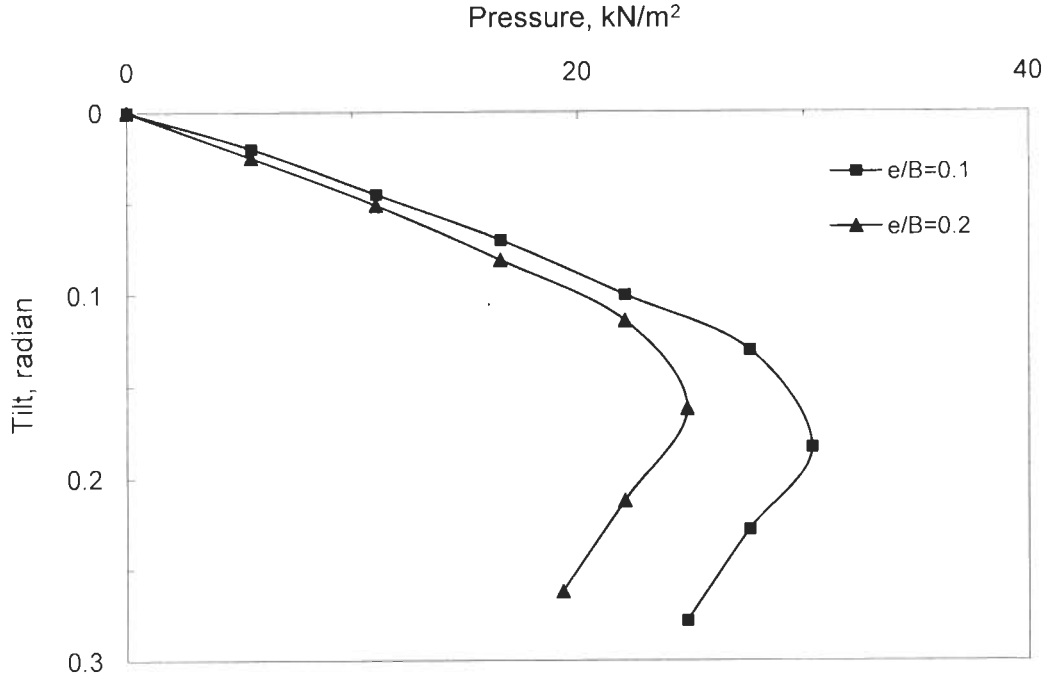

Fig. 5.42 Pressure versus Tilt Curves for Footing on a Slope (β =26.5°, *De/B*=2.0, *i* =20°)

CHAPTER-VI

RESULTS AND DISCUSSION

6.1 GENERAL

In this chapter, the results obtained from theoretically predicted values of ultimate bearing capacity and settlements have been discussed. The limit equilibrium analysis has been used to predict the ultimate bearing capacity of footings placed on upper surface of slopes and subjected to eccentric-inclined loads. The results so obtained are compared with the existing solutions and also with those obtained from the model tests.

The pressure-settlement and pressure-tilt characteristics of footings placed near the crest of a slope with eccentric-inclined loads and resting on Ranipur sand are obtained using constitutive law of the soil. The stress-strain relationship for Ranipur sand has been obtained from triaxial compression tests.

6.2 LIMIT EQUILIBRIUM ANALYSIS

The ultimate bearing capacity of footings on upper surface of slopes and subjected to eccentric-inclined load is given by the Eq. 3.25 as -

$$q_u = \frac{1}{2}\gamma B N_\gamma + \gamma D_f N_q + c N_c$$

where N_γ, N_q and N_c are the non-dimensional bearing capacity factors, which depend upon parameters, $\phi, \beta, D_e / B, D_f / B$, e/B and i. In addition to these factors the value of ultimate bearing capacity may also be limited by the overall stability of the slope. In cohesionless soils, there is always a possibility of foundation failure rather than slope failure whereas in cohesive fills, the load carrying capacity may be governed by overall stability of the slope.

To design a foundation placed on upper surface of a slope, present analysis may be used to obtain the ultimate bearing capacity of a footing due to foundation failure, and then the overall stability of the slope should be checked for this surcharge load using any slope stability method.

6.2.1 Evaluation of Assumptions

Of the six assumptions made in the development of the analysis (Ch. III), three assumptions listed at sl.nos. iii), iv) and v) in art. 3.2 of Chapter III need justification. The other assumptions are commonly made in the bearing capacity computations by limit equilibrium method.

As the length of the failure surface is smaller on the slope side, the resistance offered from this side of the footing will be less than that from the other side. Due to this fact, it seems reasonable to assume that one sided failure occurs. The observation made in the model tests performed by Peynircoiglu (1948), Mizuno et al. (1960), Shields et al. (1977) and Saran et al. (1989) have shown that the failure occurs on the side of the slope. Also in the present analysis, the load eccentricity and load inclination are assumed to be on the slope side, due to which the pressure on the base of the footing on the side of the slope will be more and the footing is likely to fail by tilting on this side. Some pressures do develop on the other side as well. At equilibrium, the resistance developed on the other side of the slope will not reach the full mobilisation value. Hence, pressure on this side has been considered at partial mobilisation of strength for computation of bearing capacity.

According to assumption iii), the centre of the log spiral has been taken at the edge of the footing. Saran (1970) has shown that for a footing on level ground, the log spiral will be tangential to the vertical only when the centre of the log spiral is on line EB (Fig. 3.1) or its extension. Agrawal (1986) has concluded that the minimum value of bearing capacity factors N_q and N_c are obtained when the centre of the log spiral coincides with the edge of the footing. Keeping this in view the centre of the log spiral was kept at the edge of the footing.

According to the assumption iv), footing loses its contact due to excessive eccentricity. The effective width of the footing is represented by $B \cdot x_1$, where x_1 is the ratio of contact width to the total width of the footing. This assumption is quite logical. However, a variation of x_1 should be considered in a proper way. In the present analysis, conventional variation has been adopted.

6.2.2 N_γ Factor

i) Mobilization factor *m*

To obtain the pressure developed on the level side, partial mobilisation, characterised by a mobilisation factor *m* as given in assumption iv), has been considered. Some values of *m* have been given in Table 6.1 for different cases. It can be seen that the value of *m* increases with increase in distance of the footing from the slope edge. It also increases with the decrease in the slope angle. For inclined loads, the value of *m* is less as compared to vertical loads and it decreases with the increase in the obliquity of the load.

Table 6.1 Mobilization Factor *m* for N_γ: $\phi = 40°$

D_e/B	β	e/B	i	m
0.0	30°	0.0	0°	0.393
1.0	30°	0.0	0°	0.733
2.0	30°	0.0	0°	0.837
3.0	30°	0.0	0°	0.914
0.5	30°	0.1	10°	0.387
0.5	20°	0.1	10°	0.470
0.5	10°	0.1	10°	0.550
1.0	30°	0.2	0°	0.471
1.0	30°	0.2	10°	0.426
1.0	30°	0.2	20°	0.291

ii) N_γ values

To study the effect of the slope angle (β), edge distance (D_e), depth of the footing (D_f), eccentricity (e) and load inclination (i), some typical plots are drawn as shown in Figs. 6.1 through 6.6. It can be observed from Figs. 6.1 and 6.2 that value of N_γ increases with increase in the edge distance and after some distance, this value becomes independent of the slope. This distance at which it becomes independent of the slope depends on all of the above parameters. Some of these distances at which N_γ values become indifferent to slope and the corresponding parameters are given in Table 6.2. The value of N_γ decreases with increase in eccentricity and obliquity of the load as can be observed in Figs. 6.3 through 6.6. This decrease is not uniform, but depends on slope angle (β), edge distance (D_e), depth of the footing (D_f), eccentricity (e) and inclination of the load (i).

Table 6.2 Minimum Edge Distance at which N_γ is Independent of Slope

ϕ	β	D_f/B	e/B	i	Minimum D_e/B	ϕ	β	D_f/B	e/B	i	Minimum D_e/B
40°	30°	0	0	0	5.56	30°	25°	0	0.2	0	1.97
40°	25°	0	0	0	5.56	30°	20°	0	0.2	0	1.97
40°	20°	0	0	0	5.56	30°	10°	0	0.2	0	1.97
40°	30°	0.5	0.1	0	4.20	30°	25°	0.5	0.1	0	1.52
40°	30°	0.5	0.2	0	3.15	30°	25°	0.5	0.2	0	0.60
40°	30°	0.5	0.3	0	1.81	30°	25°	0.5	0.3	0	0.25
40°	30°	1.0	0	10°	3.34	30°	25°	1.0	0	10°	0.84
40°	30°	1.0	0	20°	2.96	30°	25°	1.0	0	20°	0.49
35°	25°	0	0.1	0	3.57	25°	20°	0	0.3	0	0.91
35°	20°	0	0.1	0	3.57	25°	15°	0	0.3	0	0.91
35°	10°	0	0.1	0	3.57	25°	10°	0	0.3	0	0.91
35°	25°	0.5	0.1	0	2.20	25°	20°	0.5	0.1	0	0.49
35°	25°	0.5	0.2	0	1.71	25°	20°	0.5	0.2	0	0.29
35°	25°	0.5	0.3	0	0.78	25°	20°	0.5	0.3	0	0.00
35°	25°	1.0	0	10°	1.86	25°	20°	1.0	0	10°	0.00
35°	25°	1.0	0	20°	1.34	25°	20°	1.0	0	20°	0.00

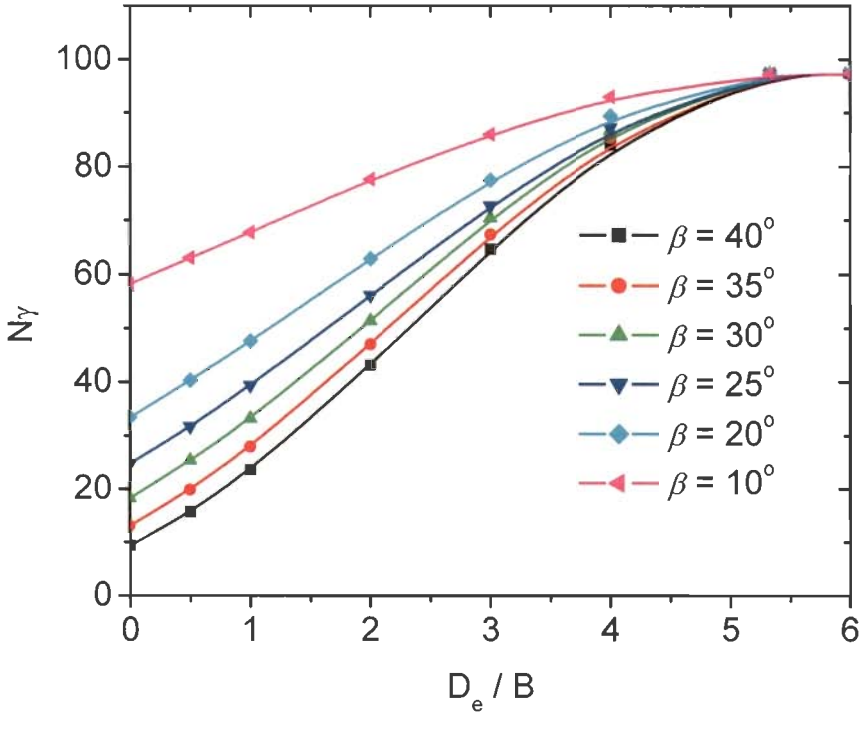

Fig. 6.1 Variation of N_γ with D_e/B for $\phi = 40°$, $D_f/B=0$, $e/B=0$, $i=10°$ for Different Slopes

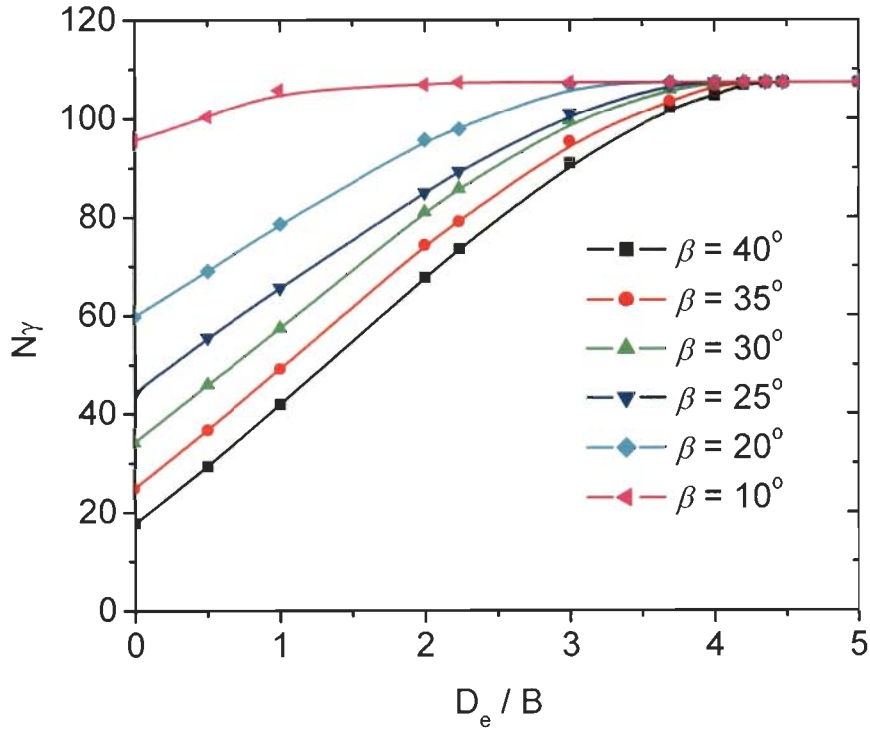

Fig. 6.2 Variation of N_γ with D_e/B for $\phi = 40°$, D_f/B=0.5, e/B=0.1, i=0° for Different Slopes

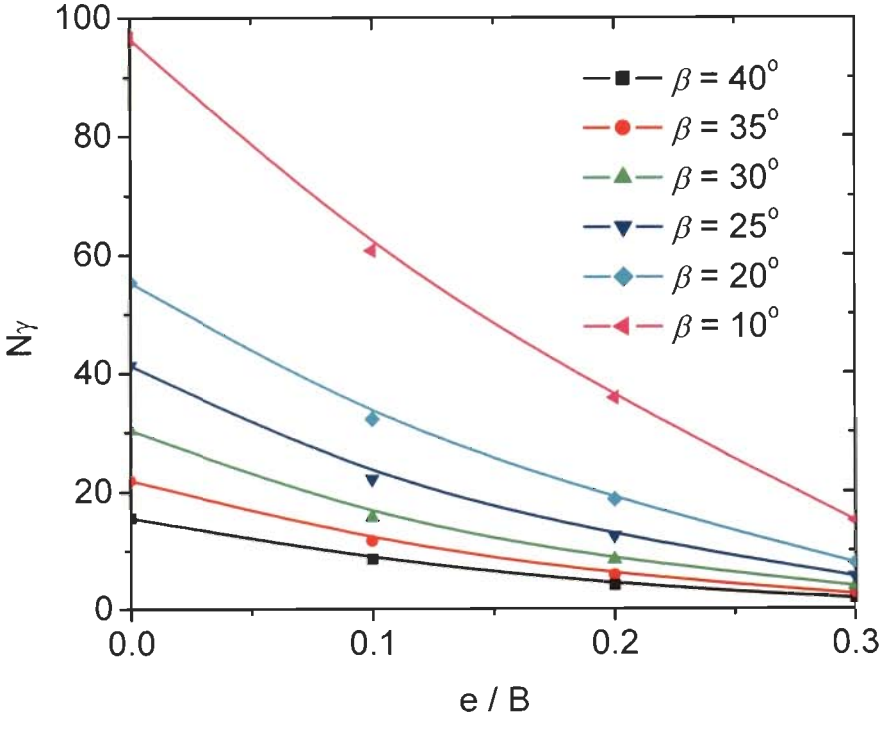

Fig. 6.3 Variation of N_γ with e/B for $\phi = 40°$, D_f/B=0, D_e/B=0, i=0° for Different Slopes

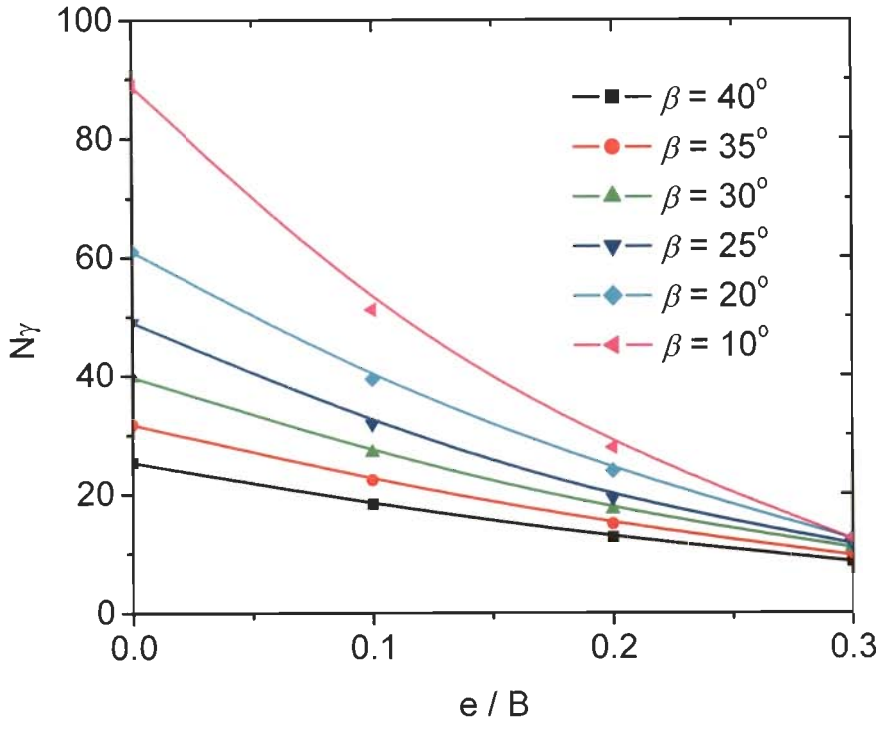

Fig. 6.4 Variation of N_γ with e/B for $\phi = 40°$, D_f/B=0.5, D_e/B=0.5, i=10° for Different Slopes

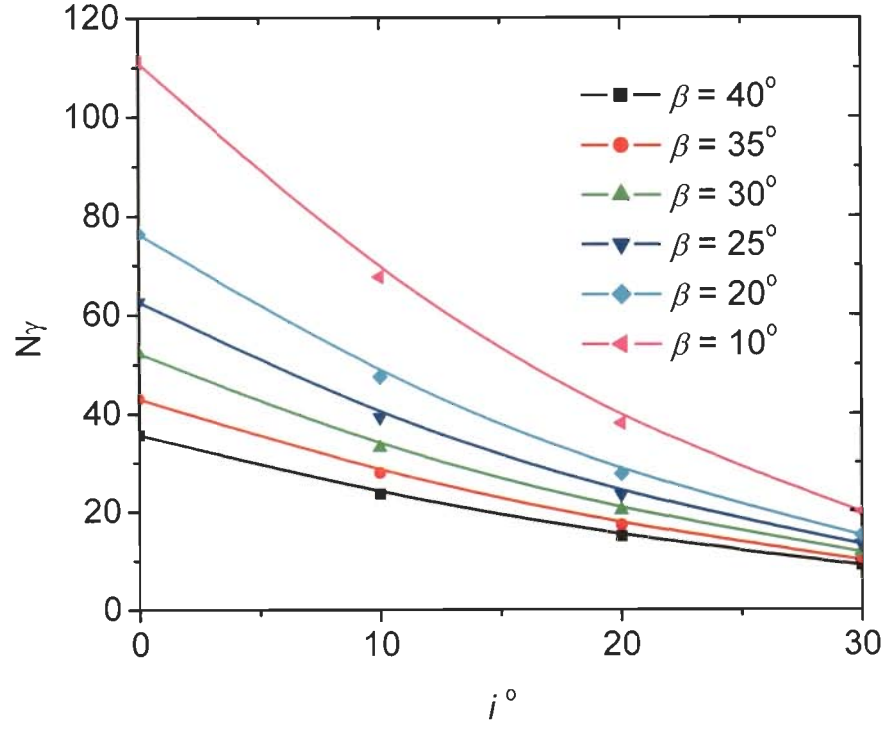

Fig. 6.5 Variation of N_γ with i for $\phi = 40°$, D_f/B=0, D_e/B=1.0, e/B=0 for Different Slopes

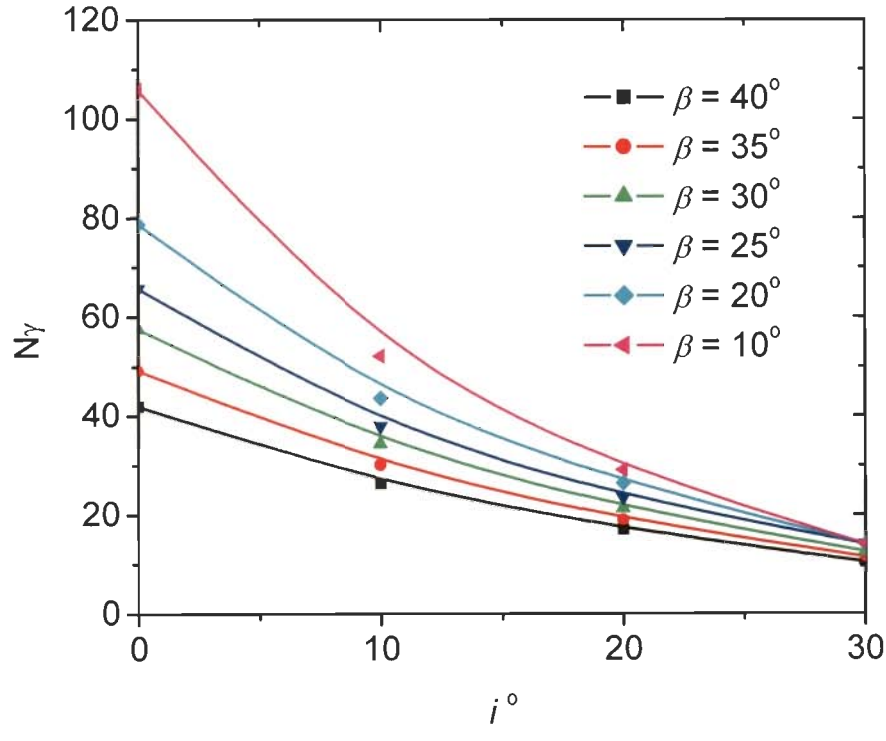

Fig. 6.6 Variation of N_γ with i for $\phi = 40°$, D_f/B=0.5, D_e/B=1.0, e/B=0.1 for Different Slopes

iii) Comparison of N_γ Values with the Analysis of Earlier Investigators

Table 6.3 shows the comparison of N_γ values obtained in the present study for footings resting on level ground (β =0) for i = 0 and e/B = 0 and those obtained by earlier investigators.

Table 6.3 Comparison of N_γ Values for Footings on Level Ground

ϕ	Terzaghi (1943)	Meyerhof (1963)	Hansen (1970)	Saran (1971)	Vesic (1973)	Ingra & Baecher (1983)*	Frydman & Burd (1997)	Dewaikar (2003)	Present Analysis
10°	1.2	0.4	0.4	1.14	1.2	1.06	-	-	1.38
20°	5.0	2.9	2.9	6.05	5.4	6.0	-	-	6.67
30°	19.7	15.7	15.1	28.89	22.4	33.9	21.7	21.4	29.76
40°	100.4	93.6	79.4	165.4	109.3	191.2	147.0	141.3	160.08

**Experimental values*

The N_γ values obtained in the present study for different values of ϕ are higher than those predicted by earlier investigators and almost same as those predicted by Saran (1970). It is generally known that Tezaghi's values give conservative estimates. Experiments performed by Feda (1961), De-Beer (1965), Balla (1962), Bolt (1982), Cichy et al. (1978), Ingra and Baecher (1983), Hartikainen and Zadroga (1994), Saran and Agarwal (1991), Shiraishi (1990) and many others have shown that Terzaghi's analysis underestimates the bearing capacity. Hence N_γ values predicted in the present study may be more realistic.

The N_γ values obtained for footings on slopes in the present investigation for the cases when $i = 0$ and $e/B = 0$ are compared with those predicted by other investigators and presented in Figs. 6.7 and 6.8. It can be observed that the N_γ values obtained in the present study are less than those given by Graham's (1988) and Saran's (1989), but higher than those given by other investigators. The difference may be attributed to the difference in the rupture surface adopted in the proposed methodology for estimating the N_γ values.

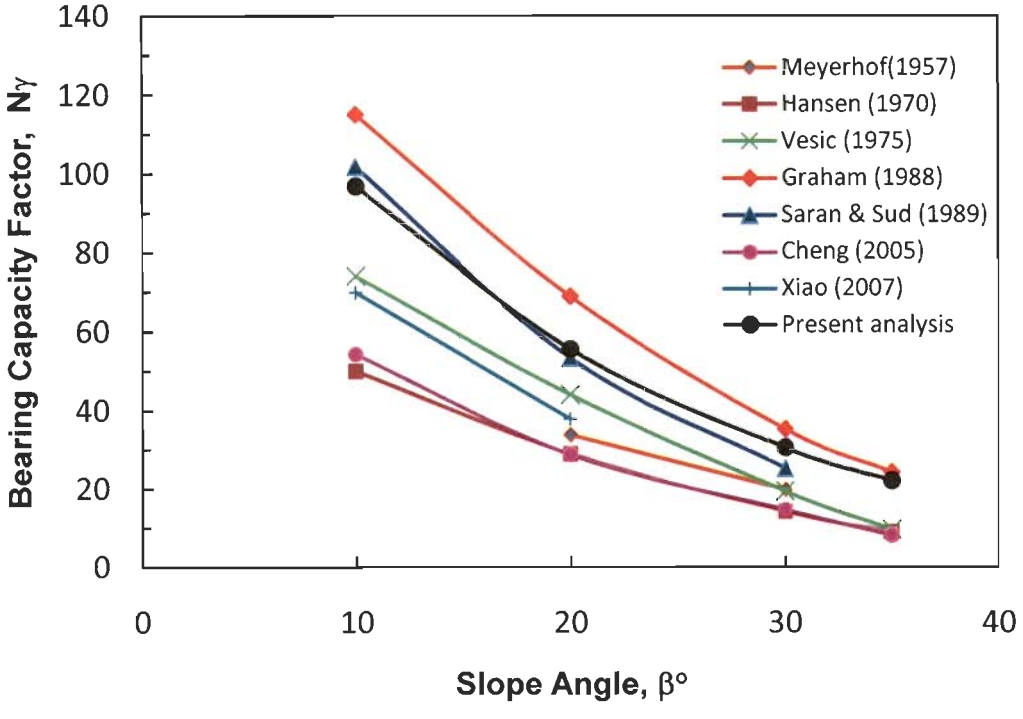

Fig.6.7 Comparison of N_γ Values for $\phi = 40°$, $D_e/B=0$, $D_f/B=0$

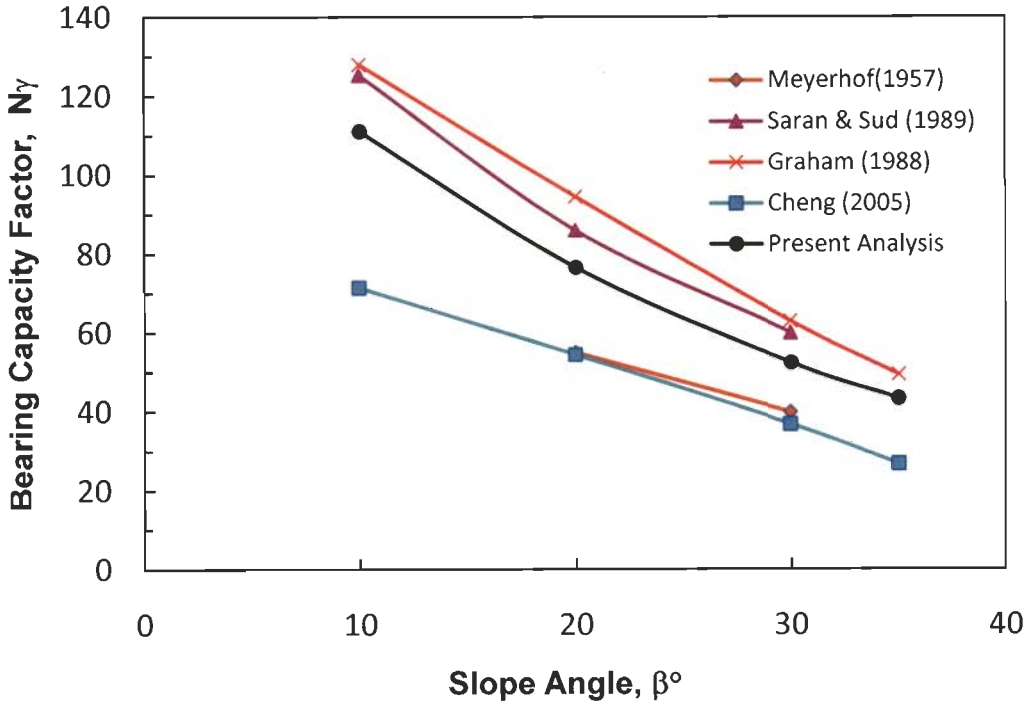

Fig.6.8 Comparison of N_γ Values for $\phi = 40°$, $D_e/B=1.0$, $D_f/B=0$

The load inclination factors, i_γ obtained in the present study for a level ground ($\beta=0$) are compared with those given by the earlier investigators and presented in Fig. 6.9 where the load inclination factor, i_γ is defined as -

$$i_\gamma = \frac{N_\gamma \ for\ inclined\ load}{N_\gamma \ for\ vertical\ load}$$

It is observed that the effect of inclination of load on N_γ values obtained in the present study compares well with those of previous investigators. Figure 6.10 compares the effect of load eccentricity factor e_γ obtained from the present analysis with those by the previous authors, where the load eccentricity factor, e_γ is defined as-

$$e_\gamma = \frac{N_\gamma \ for\ eccentric\ vertical\ load}{N_\gamma \ for\ central\ \ vertical\ load}$$

It can been seen that the proposed e_γ values tally reasonably well with those given by the previous investigators.

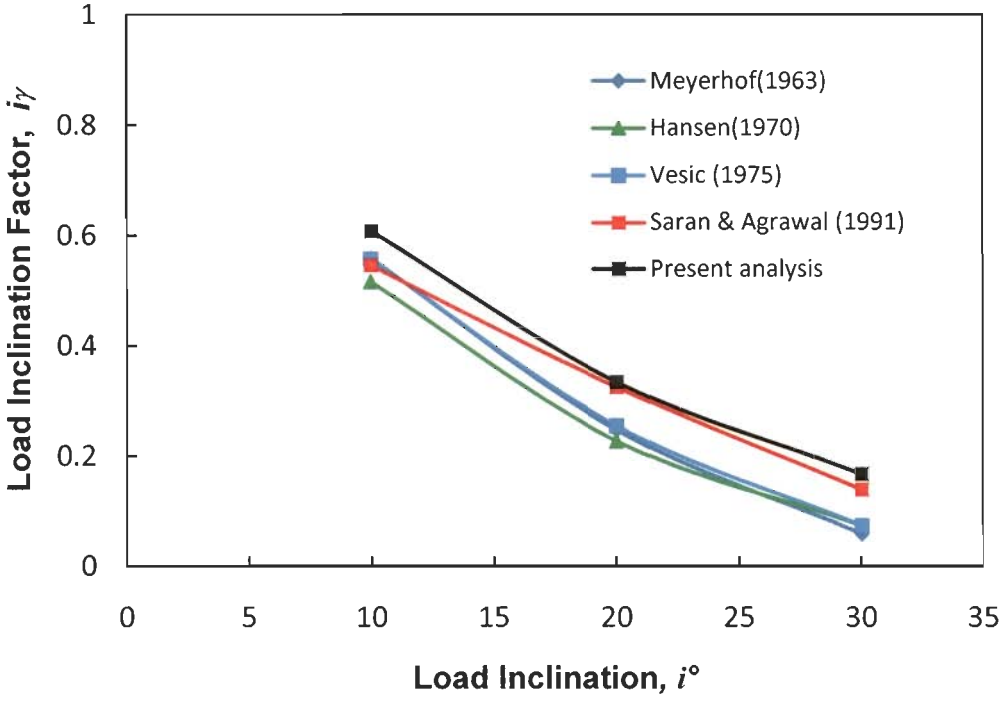

Fig.6.9 Comparison of Load Inclination Factor, i_γ for Footings on Level Ground for $\phi = 40°$, $e/B=0$

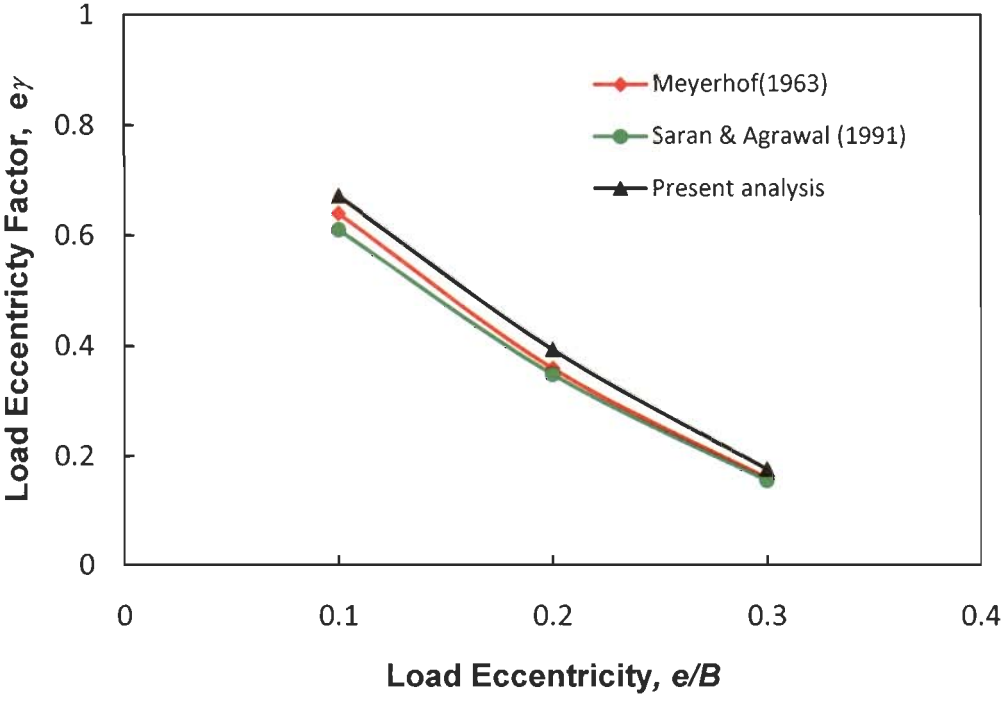

Fig.6.10 Comparison of Load Eccentricity Factor e_γ, for Footings on Level Ground for $\phi = 40°$, $i=0°$

(iv) Comparison of N_γ Values with Model Test Data

The tests were performed on sand at a relative density of 70%, and the corresponding angle of friction ϕ as determined from the triaxial compression tests was 39.5°. The details of the tests have already been presented in chapter V. Figure 6.11 shows the comparison between the ultimate bearing capacity obtained from the proposed theory and the model tests. The failure load has been taken as the peak load. It is evident from this figure that the values of ultimate bearing capacity obtained from the model tests data compare very well with the corresponding values obtained from the proposed theory.

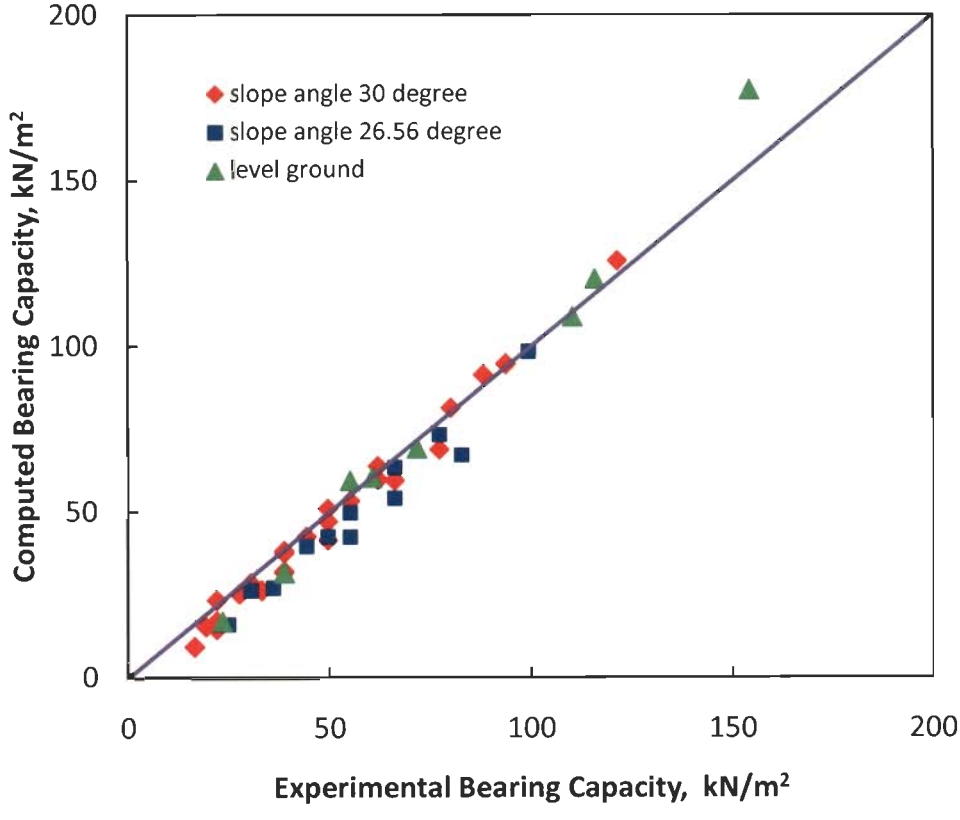

Fig.6.11 Comparison of Computed and Experimental Bearing Capacity

6.2.3 N_q Factor

i) N_q values

To study the effect of edge distance (D_e), depth of the footing (D_f), load eccentricity (e) and load inclination (i)on the bearing capacity factor, N_q, some typical plots have been presented Figs. 6.12 through 6.15. It can be observed from Figs. 6.12 and 6.13 that N_q value increases with the increase in edge distance and beyond some

distance N_q value becomes independent of the slope. It can be observed from Figs.6.14 and 6.15 that N_q value decreases with the increase in eccentricity and inclination of the load, but the rate of decrease is less as compared to the same for N_γ values.

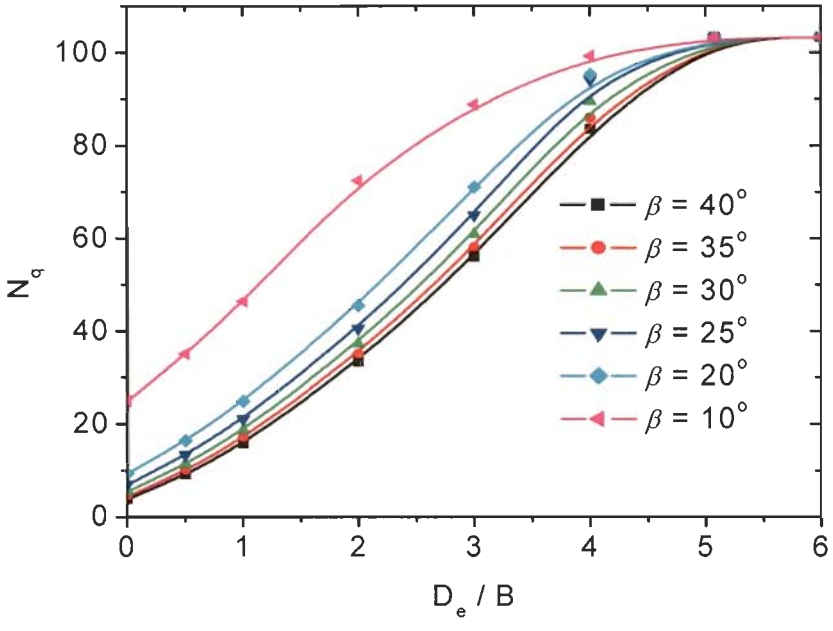

Fig. 6.12 Variation of N_q with D_e/B for $\phi = 40°$, D_f/B=0.5, e/B=0, i=0° for Different Slopes

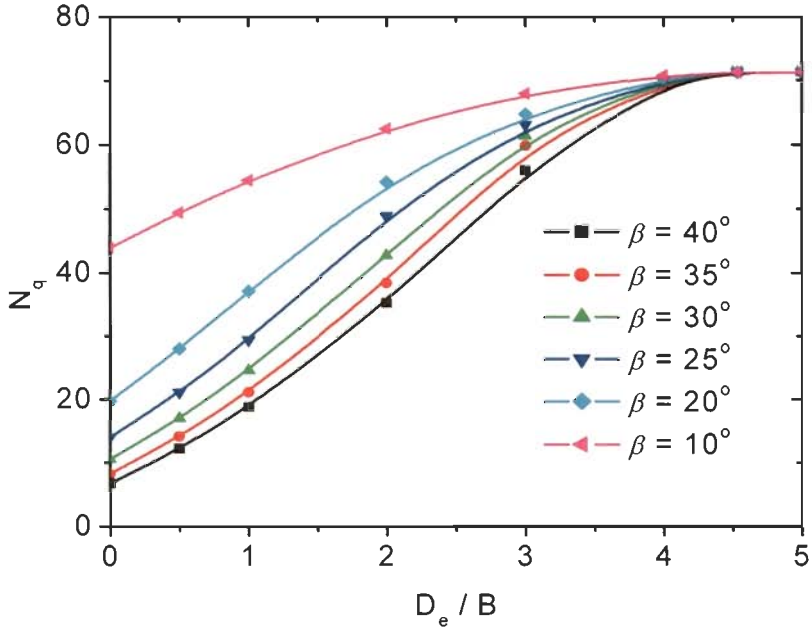

Fig. 6.13 Variation of N_q with D_e/B for $\phi = 40°$, D_f/B=1.0, e/B=0.1, i=0° for Different Slopes

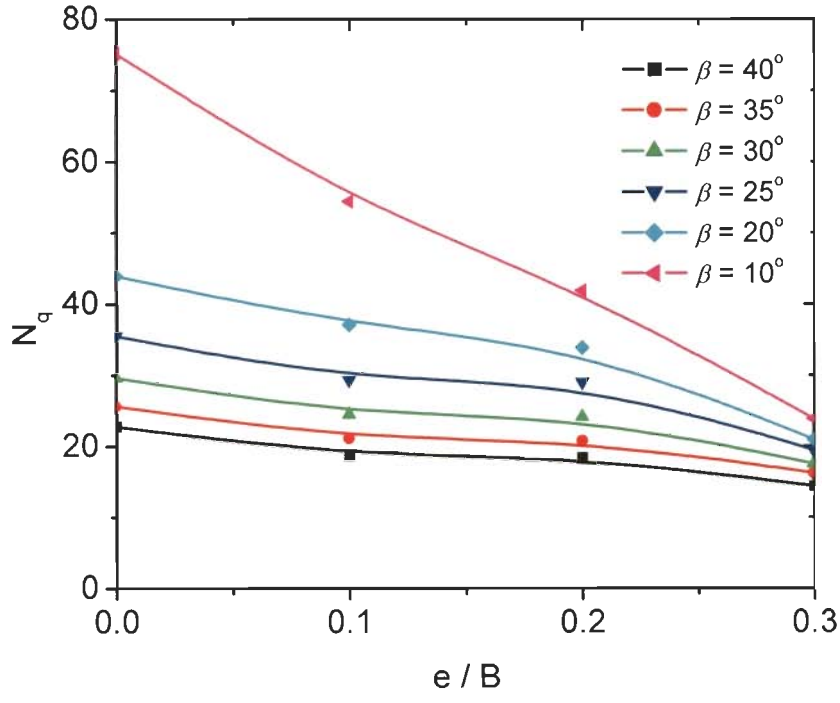

Fig. 6.14 Variation of N_q with e/B for $\phi = 40°$, D_f/B=1.0, D_e/B=1.0, i=0° for Different Slopes

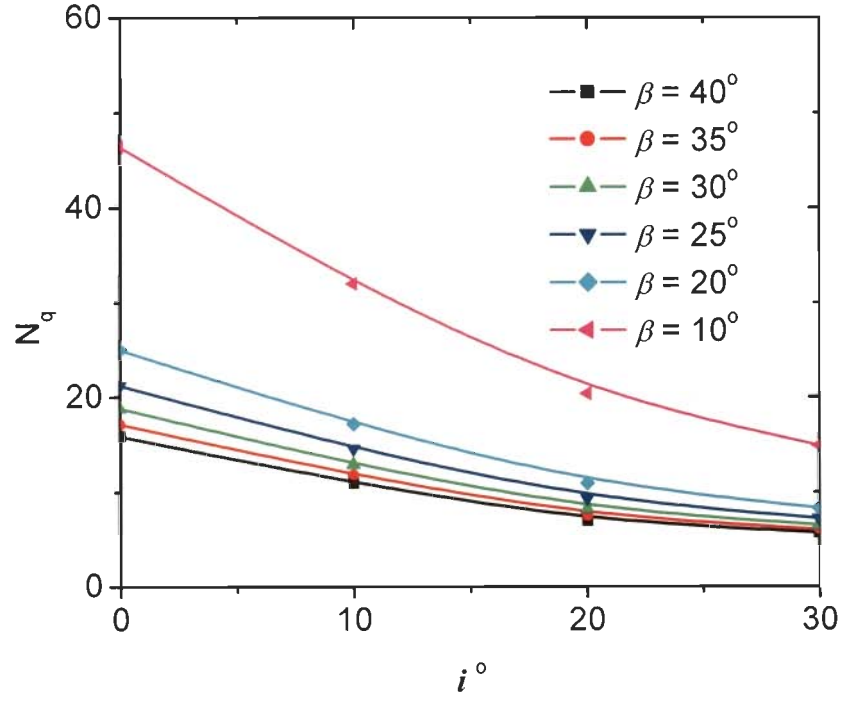

Fig. 6.15 Variation of N_q with i for $\phi = 40°$, D_f/B=0.5, D_e/B=1.0, e/B=0 for Different Slopes

ii) Comparison of N_q Values with Earlier Investigators

Table 6.4 shows the comparison of N_q values obtained from the present study for footings resting on level ground (β =0) for values of i = 0 and e/B = 0 with those obtained from earlier investigators.

Table 6.4 Comparison of N_q Values for Footings on Level Ground

ϕ	Terzaghi (1943)	Meyerhof (1963)	Hansen (1970)	Vesic (1973)	Saran (1971)	Present Analysis
10^0	2.7	2.5	2.5	2.5	2.5	2.9
20^0	7.4	6.4	6.4	6.4	7.4	8.7
30^0	22.5	18.4	18.4	18.4	22.5	27.5
40^0	81.3	64.1	64.1	64.1	81.4	103.4

The values of N_q obtained from the present analysis are higher than those predicted by all the earlier investigators, because the failure surface assumed is different from the previous investigators. In comparison to Terzaghi's (1943) and Saran's (1971) analysis, the values are about 20% higher.

The N_q values obtained for footings on slope in the present study could not be compared directly with those given by other investigators as their bearing capacity equations are different from those proposed in the present study. The bearing capacity of a footing on a cohesionless soil slope in the present case is expressed as -

$$q_u = \frac{1}{2}\gamma B N_\gamma + \gamma D_f N_q \tag{6.1}$$

which can be modified as -

$$\frac{q_u}{\gamma B} = \frac{1}{2}N_\gamma + \frac{D_f}{B}N_q \tag{6.2}$$

Similarly the bearing capacity equation used by Graham (1988) and Cheng (2005) can be modified as -

$$\frac{q_u}{\gamma B} = \frac{1}{2}N_{\gamma q} \tag{6.3}$$

The values of $q_u/\gamma B$ obtained in the present study for the case of e/B=0 and i=0 are compared with $q_u/\gamma B$ values of other investigators as shown in Figs. 6.16 and 6.17.

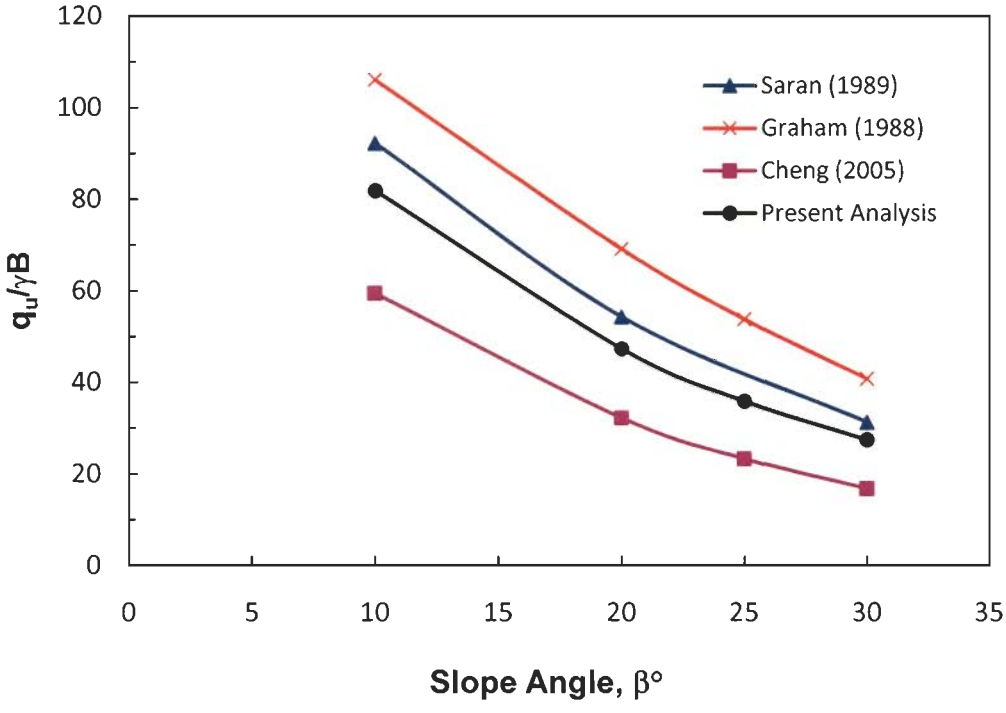

Fig.6.16 Comparison of $q_u/\gamma B$ Values for $\phi = 40°$, $D_e/B=0$, $D_f/B=0.5$

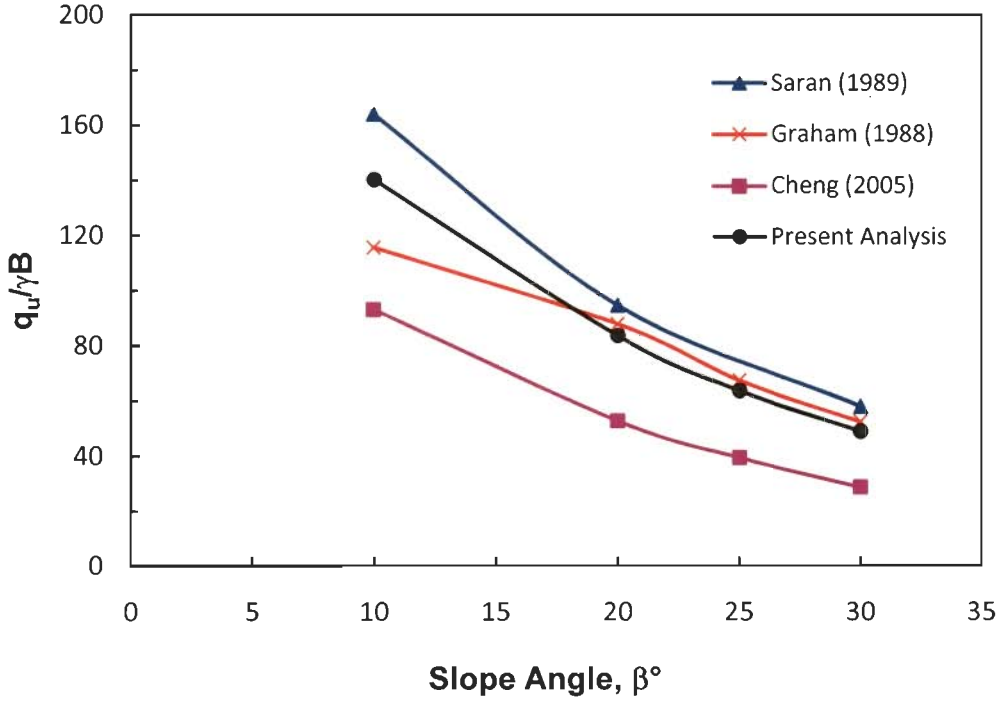

Fig.6.17 Comparison of $q_u/\gamma B$ Values for $\phi = 40°$, $D_e/B=0$, $D_f/B=1.0$

It can be observed that $q_u/\gamma B$ values predicted in the present study are higher than those given by Cheng (2005), but less than those predicted by Graham (1988) and Saran (1989).

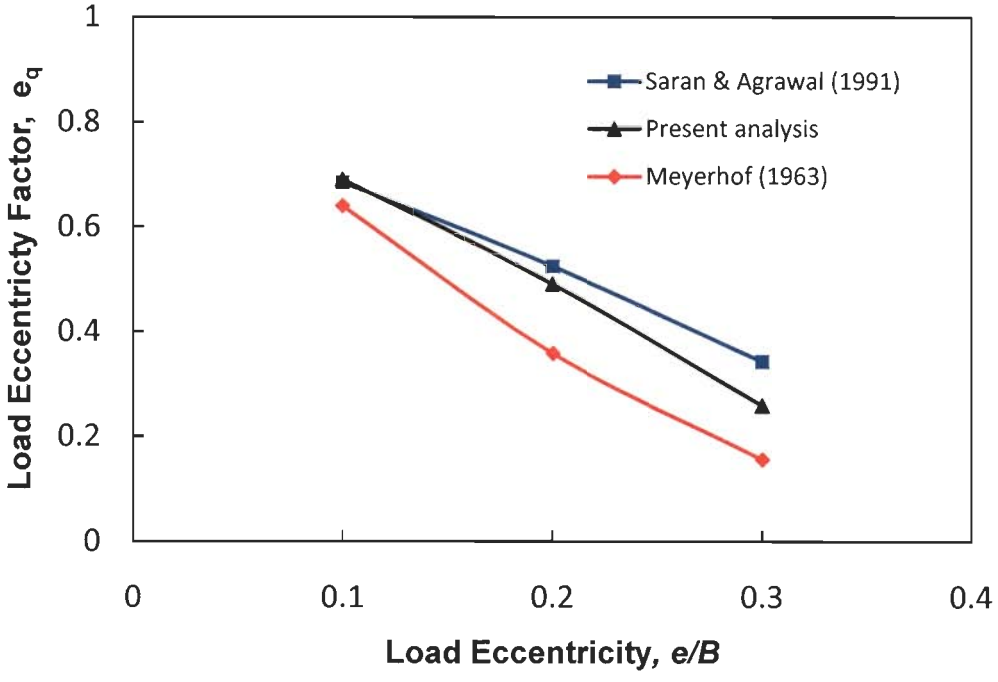

Fig.6.18 Comparison of Load Eccentricity Factor e_q for Footings on Level Ground for ϕ=40°, i=0°

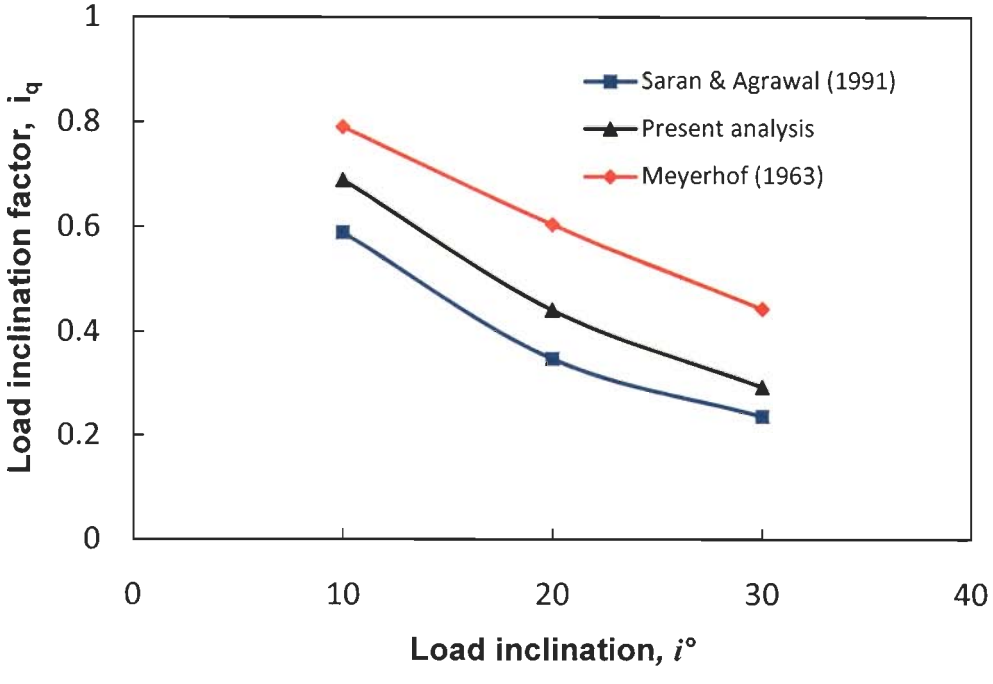

Fig.6.19 Comparison of Load Inclination Factor i_q for Footings on Level Ground for ϕ=40°, e/B=0

Figures 6.18 and 6.19 show the comparison of the reduction factor in N_q values with eccentricity and inclination of load for footings on level ground with those given by Saran & Agrawal (1991) and Meyerhof (1963). The comparison is reasonably good.

6.2.4 N_c Factor

i) N_c values

It can be observed from Figs. 6.20 through 6.23 that N_c values follow similar trend as that of N_q and N_γ . The values of N_c increase with the increase in edge distance, D_e and decrease with the increase in eccentricity, e and inclination, i of the load. The difference is that the rate of increase with D_e and the rate of decrease with eccentricity and inclination are less as compared with those for N_γ values.

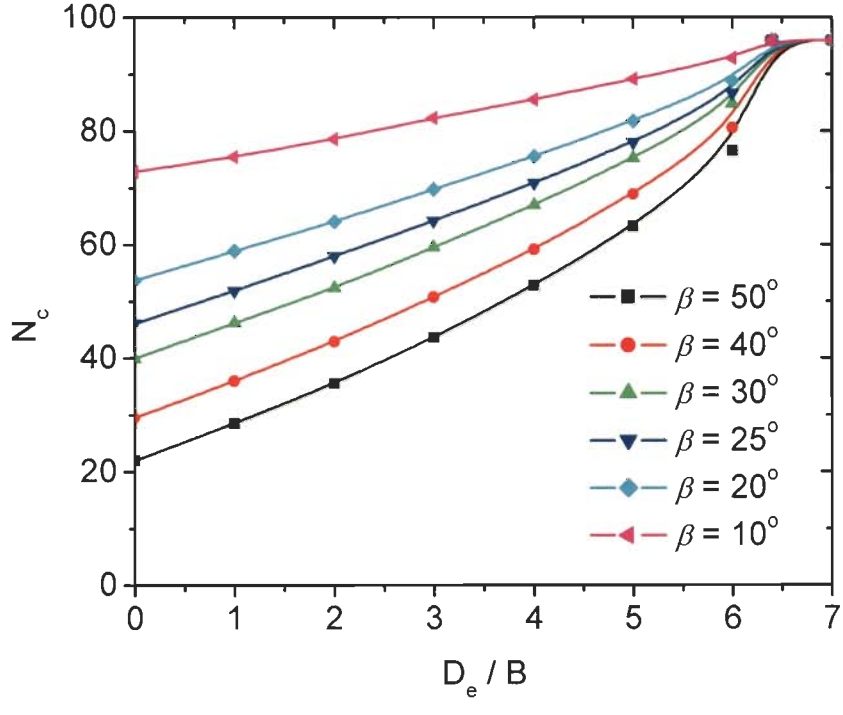

Fig. 6.20 Variation of N_c with D_e/B for $\phi = 40°$, $D_f/B=0$, $e/B=0$, $i=0°$ for Different Slopes

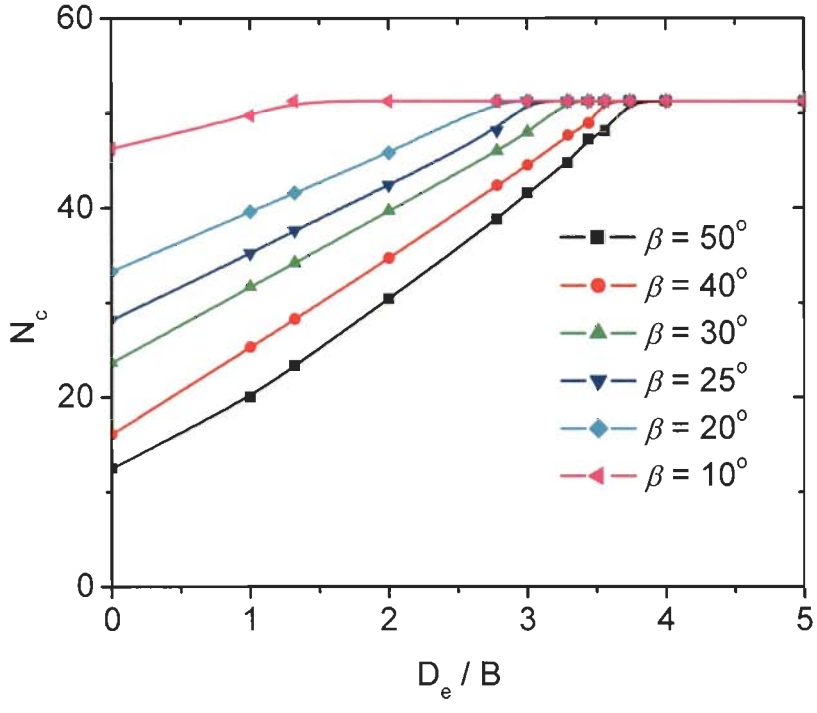

Fig. 6.21 Variation of N_c with D_e/B for $\phi = 40°$, D_f/B=0.5, e/B=0.1, i=10° for Different Slopes

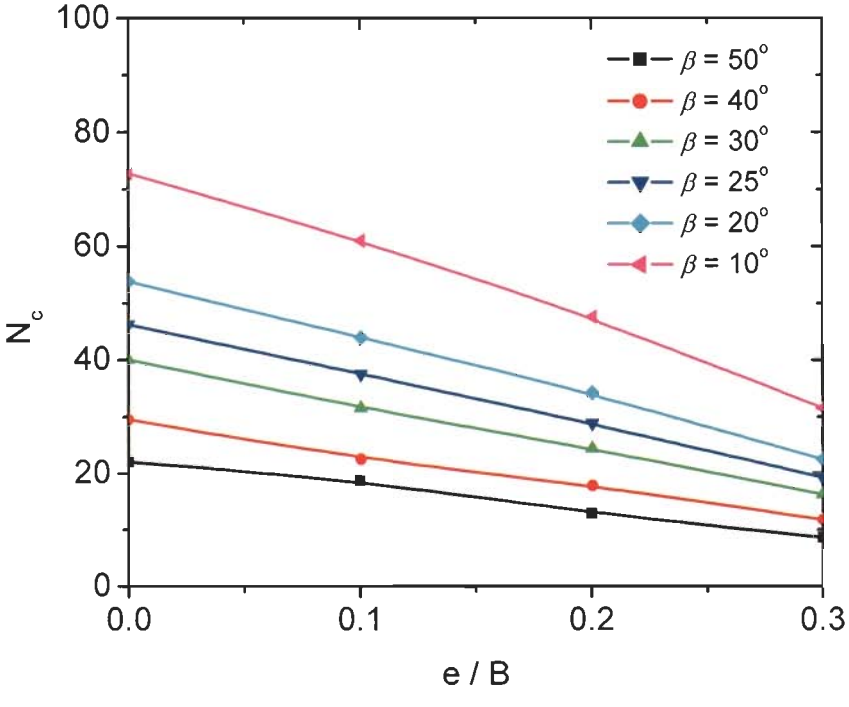

Fig. 6.22 Variation of N_c with e/B for $\phi = 40°$, D_f/B=0, D_e/B=0, i=0° for Different Slopes

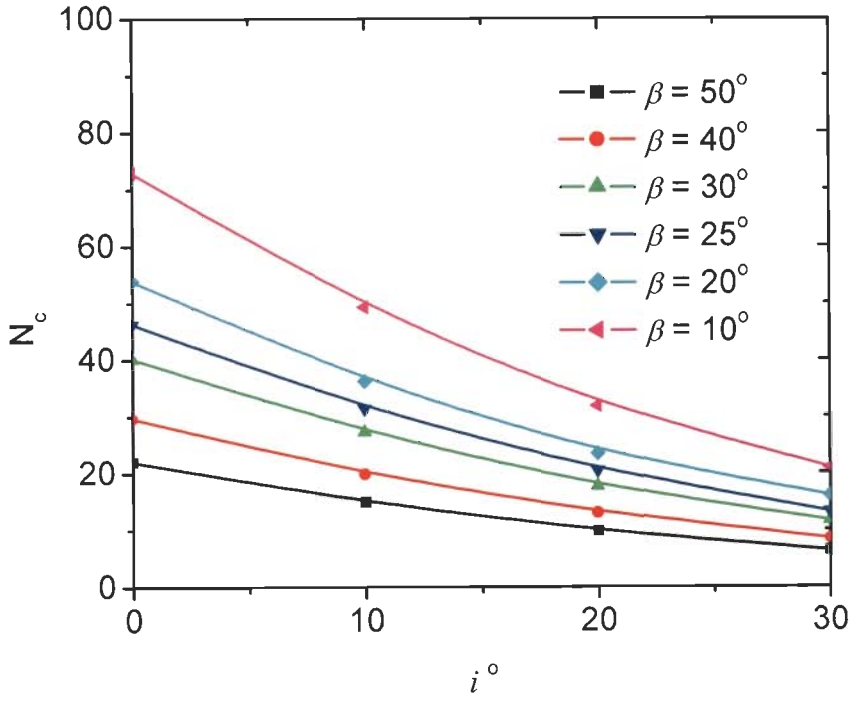

Fig. 6.23 Variation of N_c with i for $\phi = 40°$, $D_f/B=0$, $D_e/B=0$, $e=0$ for Different Slopes

iii) Comparison of N_c Values with Earlier Investigators

Table 6.5 shows the comparison of N_c values obtained in the present study for footings resting on level ground ($\beta = 0$) and for $i = 0$ and $e/B = 0$ with those obtained by previous investigators. It can be observed that the N_c values from the present analysis compare very well with Terzaghi's (1943) and Saran's (1970) values.

Table 6.5 Comparison of N_c Values for Footings on Level Ground

ϕ	Terzaghi (1943)	Meyerhof (1963)	Hansen (1970)	Vesic (1973)	Saran (1971)	Present Analysis
10^0	9.6	8.3	8.3	8.3	9.6	9.9
20^0	17.7	14.8	14.8	14.8	17.5	17.7
30^0	37.2	30.1	30.1	30.1	37.2	37.3
40^0	95.7	75.3	75.3	75.3	95.4	96.0

N_c values obtained for footings on slopes in the present investigation for the cases of $i = 0$ and $e/B = 0$ are compared with the N_c values of other investigators and are presented in Fig. 6.24. It can be observed that N_c values in the present study are on

lower side as compared with Saran's (1989) values, but higher than those given by the other investigators.

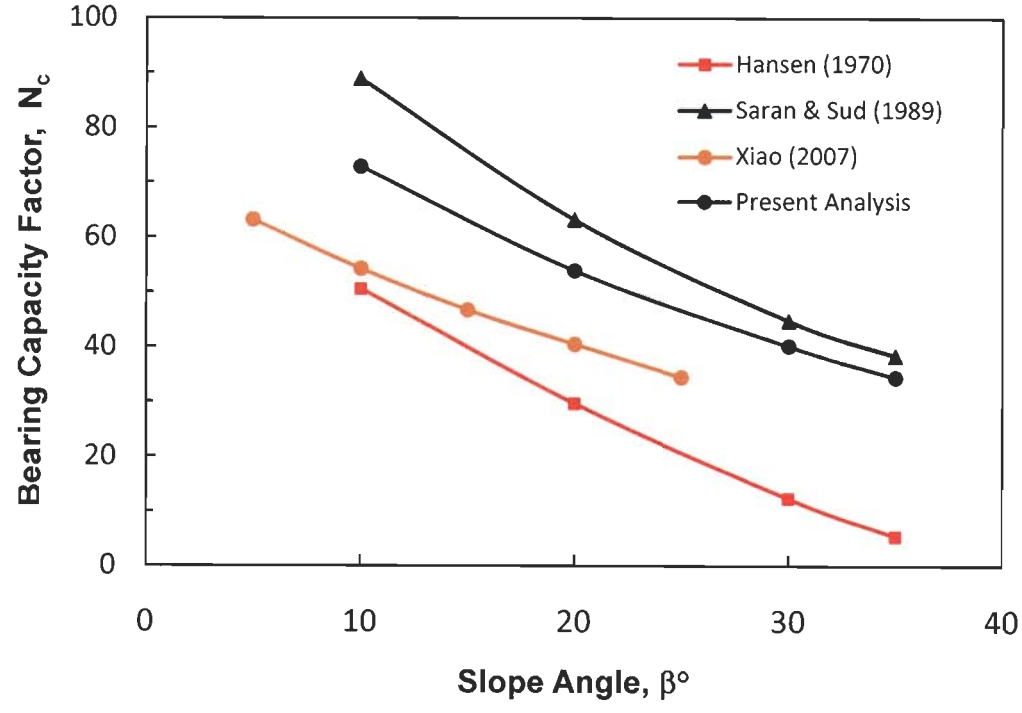

Fig.6.24 Comparison of N_c Values for $\phi = 40°$, $D_e/B=0$, $D_f/B=0$

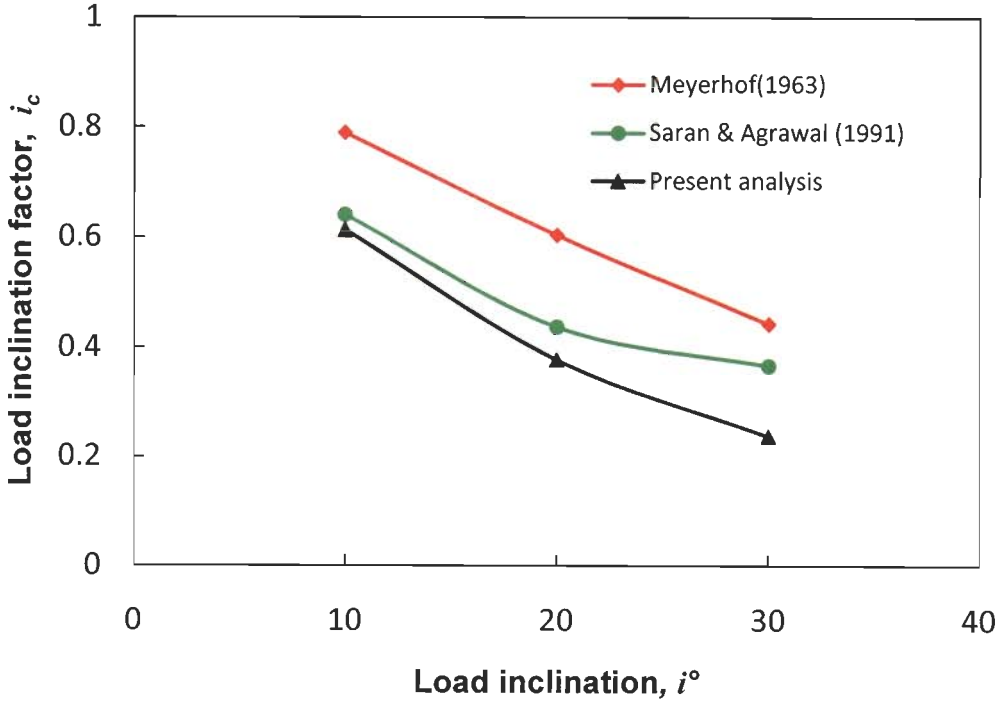

Fig.6.25 Comparison of Load Inclination Factor, i_c for Footings on Level Ground for $\phi = 40°$, $e/B=0.1$

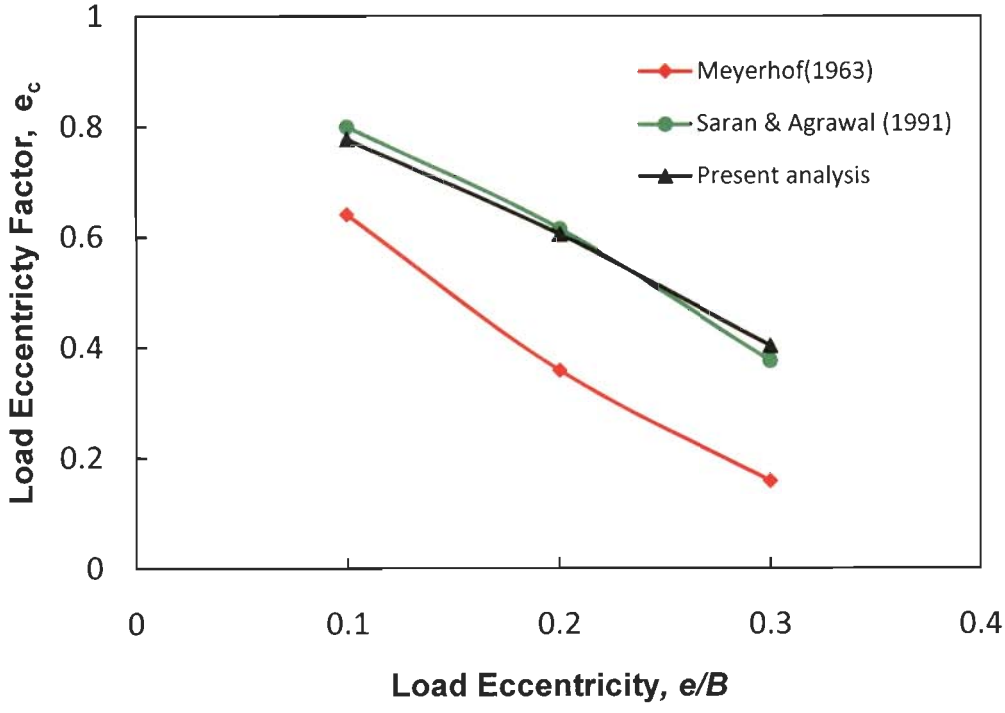

Fig.6.26 Comparison of Load Eccentricity Factor, e_c for Footings on Level Ground for $\phi = 40°$, $i=10°$

The load inclination factor i_c obtained in the present study for level ground (β =0) are compared with those by the previous investigators and presented in Fig. 6.25. Similarly the load eccentricity factors from the present analysis for footings on level ground are compared with those by previous investigators in Fig. 6.26. The results compare quite well with those presented by Saran & Agrawal (1991), but i_c is on conservative side and e_c is on higher side when compared with Meyerhof's (1963) results.

6.3 PRESSURE - SETTLEMENT CHARACTERISTICS

6.3.1 Pressure-Settlement Curves

The methodology proposed to predict the pressure-settlement and pressure-tilt characteristics of a footing placed on upper surface of a slope and subjected to eccentric-inclined load has been discussed in detail in Chapter V. The results obtained using the proposed methodology are discussed in the following sections:

The average settlements for strip footings having the width of 100 mm, 150 mm, 200 mm and 250 mm resting on Ranipur sand slope of 30° were computed. The footings were considered at an edge distance of D_e/B=2.0 and the load applied was

central vertical. The pressure versus settlement curves obtained following the proposed methodology are plotted in Fig. 6.27. These curves show that the settlement increases with applied load intensity and the rate of settlement increase also increases at higher load intensities. It can also be seen that the settlements increase with increase in footing size.

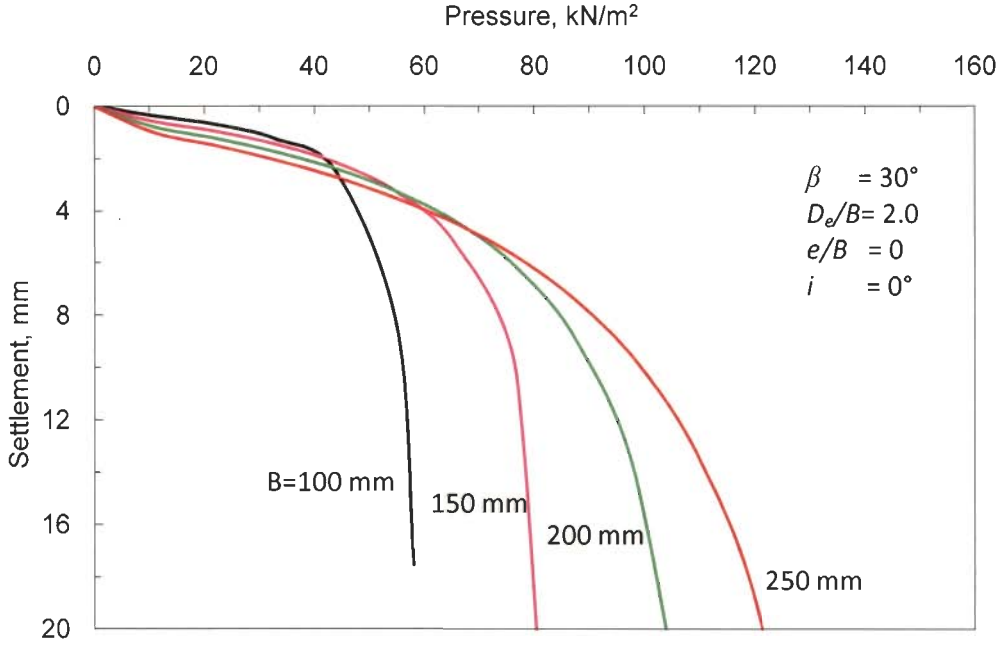

Fig.6.27 Pressure-Settlement Curves of Strip Footings of Different Widths

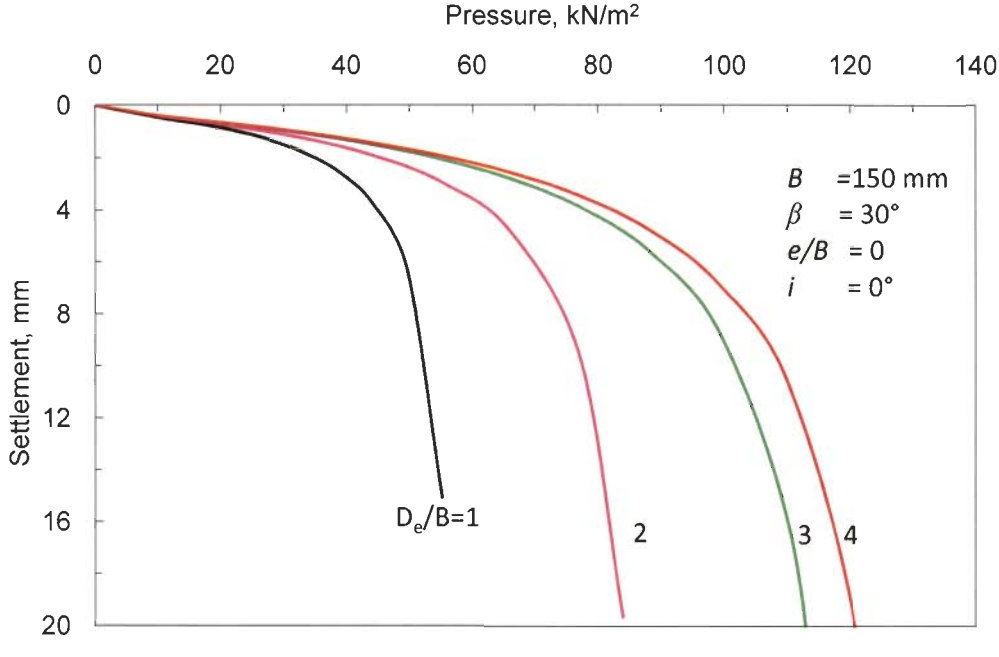

Fig.6.28 Pressure-Settlement Curves for Different D_e/B Ratios

The pressure-settlement curves for a 150 mm wide strip footing on a 30° slope have been plotted in Fig. 6.28 for an edge distance to width ratio, D_e/B=1.0, 2.0, 3.0 and 4.0 for central vertical loads. It is evident that settlement for a particular pressure decreases with the increase in edge distance.

The settlements were also computed for a 150 mm wide strip footing resting on Ranipur sand at D_e/B=2.0 for three slope angles 20°, 25° and 30°. The curves are plotted in Fig. 6.29. The figure shows that the settlement of a footing at given pressure increases as the slope becomes steeper.

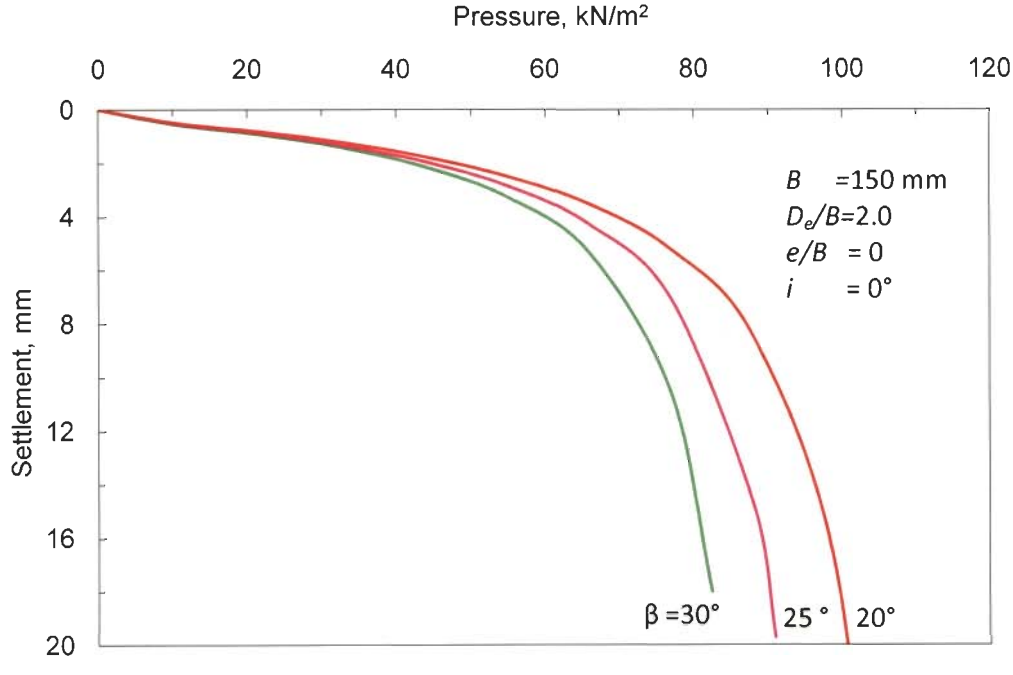

Fig.6.29 Pressure-Settlement Curves for Different Slopes

The pressure-settlement curves for a 150 mm wide strip footing resting on a 30° slope with D_e/B =2 are presented in Fig. 6.30 for different values of load eccentricity. The loads are eccentric and vertical. It can be observed that for a given pressure, the settlement increases with eccentricity. The pressure-settlement curves follow similar trend when the loads are inclined to the vertical. Figure 6.31 shows the pressure-settlement curves for a 150 mm wide strip footing resting on a 30° slope with D_e/B =2 and the loads are central and inclined at 0°, 10° and 20° to the vertical. It can be observed that for the same pressure, the settlement increases at higher values of load inclination.

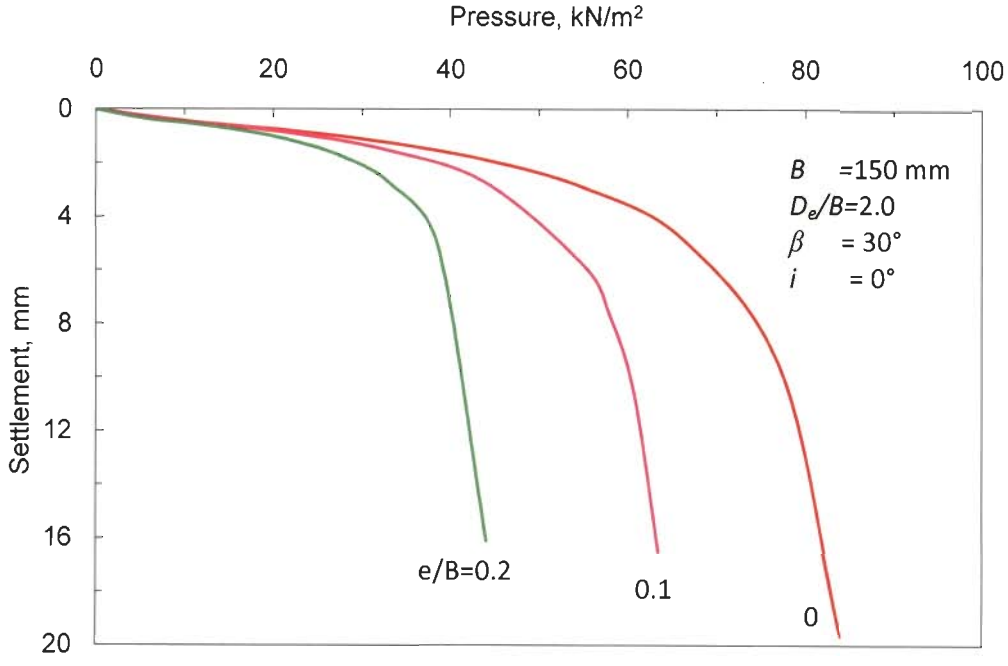

Fig.6.30 Pressure-Settlement Curves for Different Values of Load Eccentricity

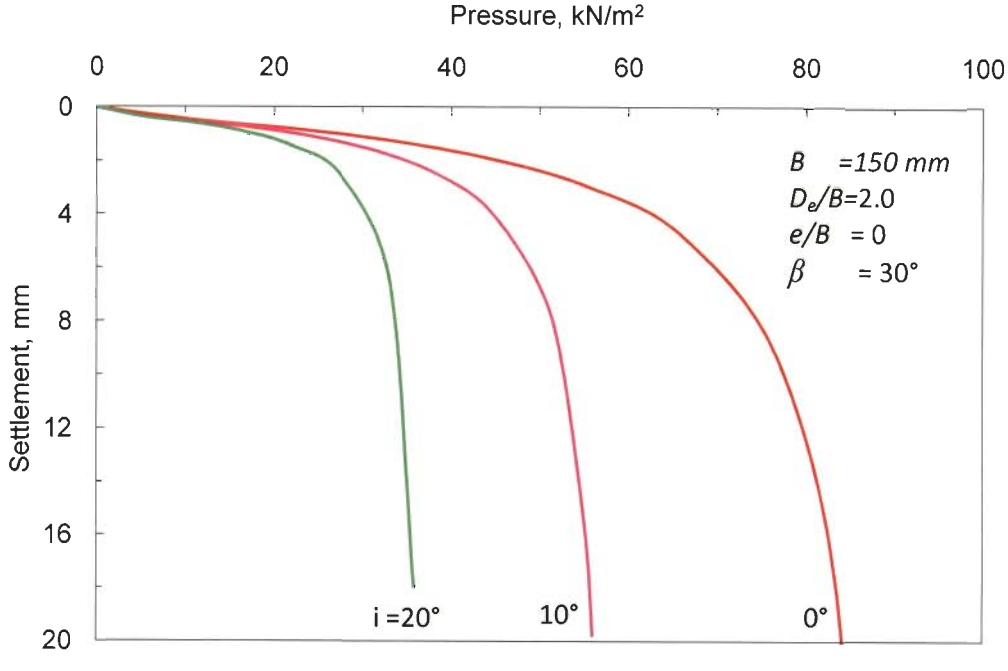

Fig.6.31 Pressure-Settlement Curves for Different Values of Load Inclination

6.3.2 Pressure-Tilt Curves

The pressure versus tilt curves obtained via the proposed methodology show similar trends as the pressure-settlement curves. Figure 6.32 shows the pressure-tilt curves for a 150 mm wide strip footing resting on a 30° slope and subjected to an eccentric-inclined load (e/B=0.1, i=10°) and for different D_e/B ratios. It is evident that tilt for a given pressure intensity reduces with increase in the edge distance. Figure 6.33 shows pressure-tilt curves for the same footing resting on slopes with different values of slope angle. The footing is subjected to an eccentric inclined load (e/B=0.1, i=10°) and placed at D_e/B ratio= 1.0. It can be observed from this plot that the tilt attains higher values for steep slope angles. Figure 6.34 shows the pressure-tilt curves for a footing placed on a 30° slope at D_e/B=1.0 and subjected to eccentric loads (e/B=0.1) with different load inclinations. It can be seen that for the same pressure intensity, the tilt of footing increases with the increase in the load inclination. Figure 6.35 shows the effect of eccentricity on the tilt of the footing. The footing is placed on a 30° slope at De/B=1.0 and subjected to inclined loads (i=10°) at different eccentricities. It can be seen that the tilt of the footing increases with the increase in the eccentricity of the applied load.

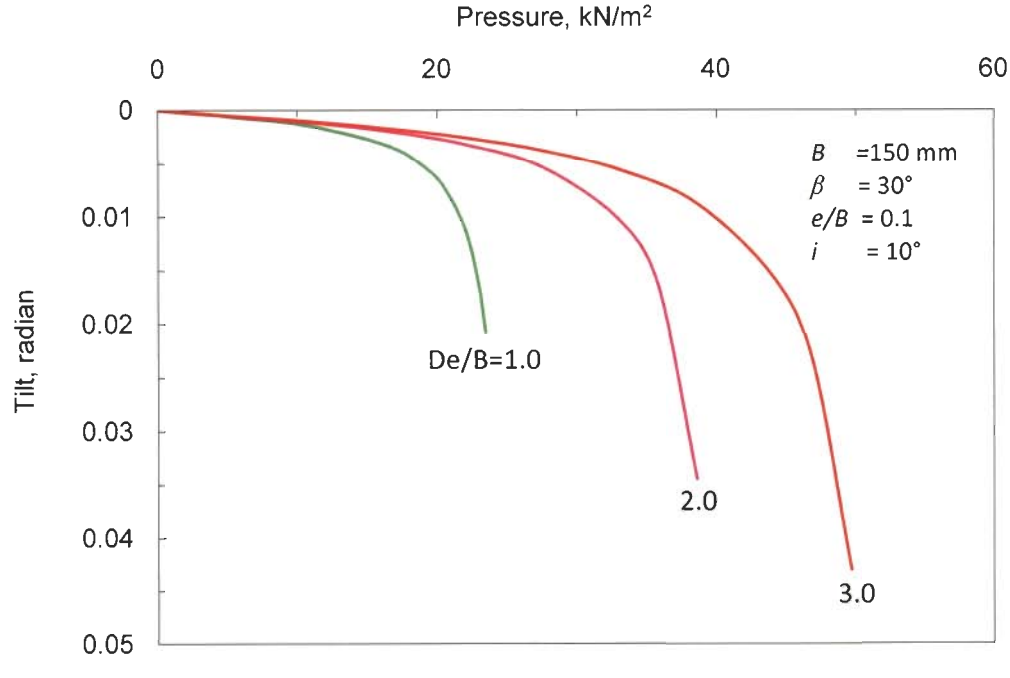

Fig.6.32 Pressure-Tilt Curves for Different D_e/B Ratios

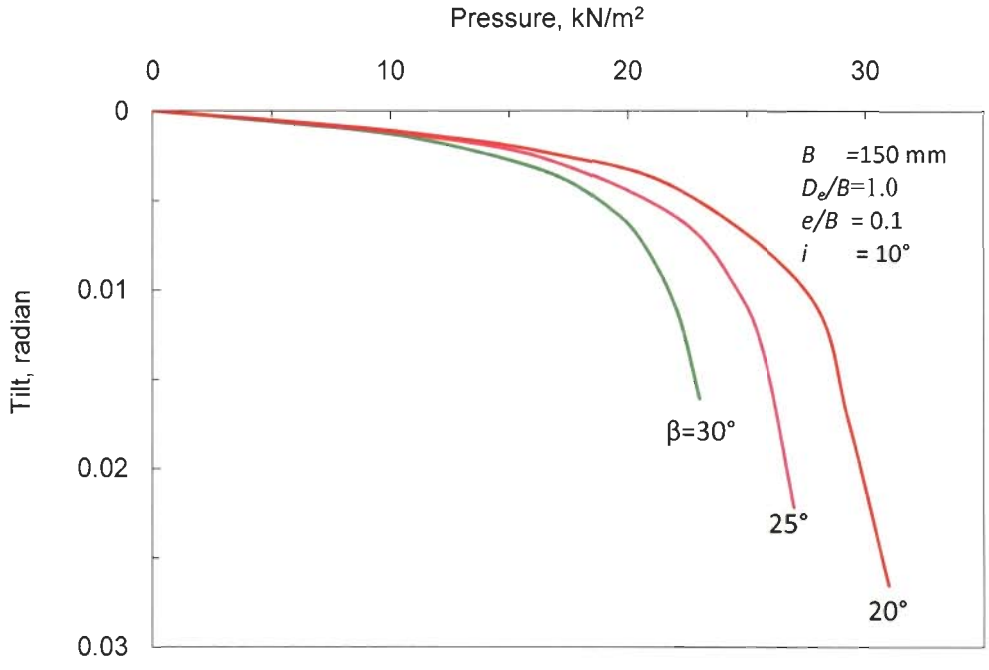

Fig.6.33 Pressure-Tilt Curves for Different Slopes

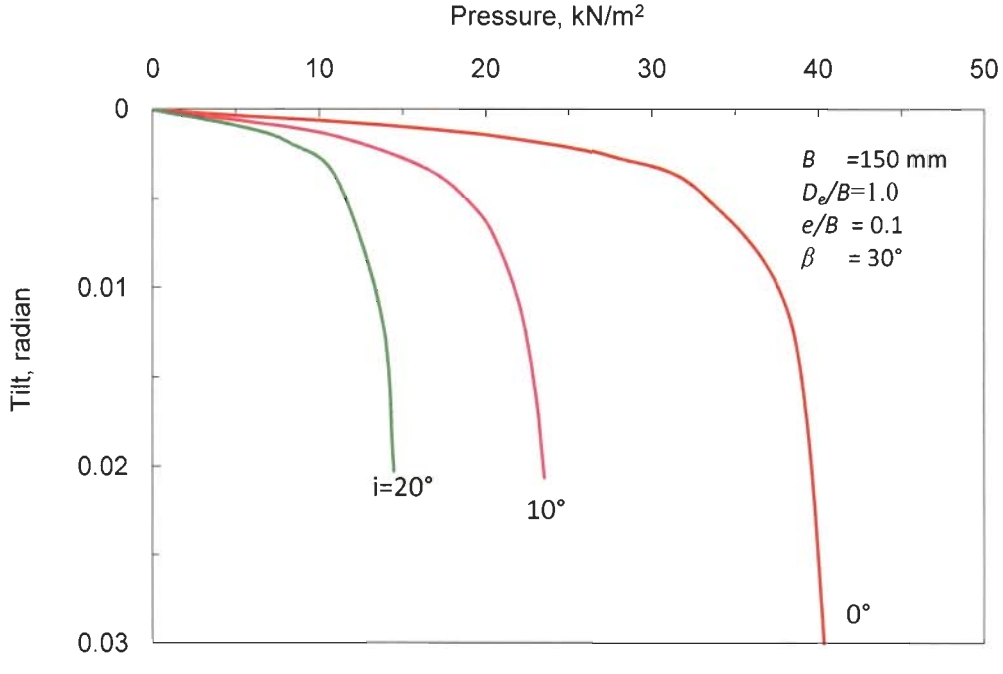

Fig.6.34 Pressure-Tilt Curves for Different Values of Load Inclination

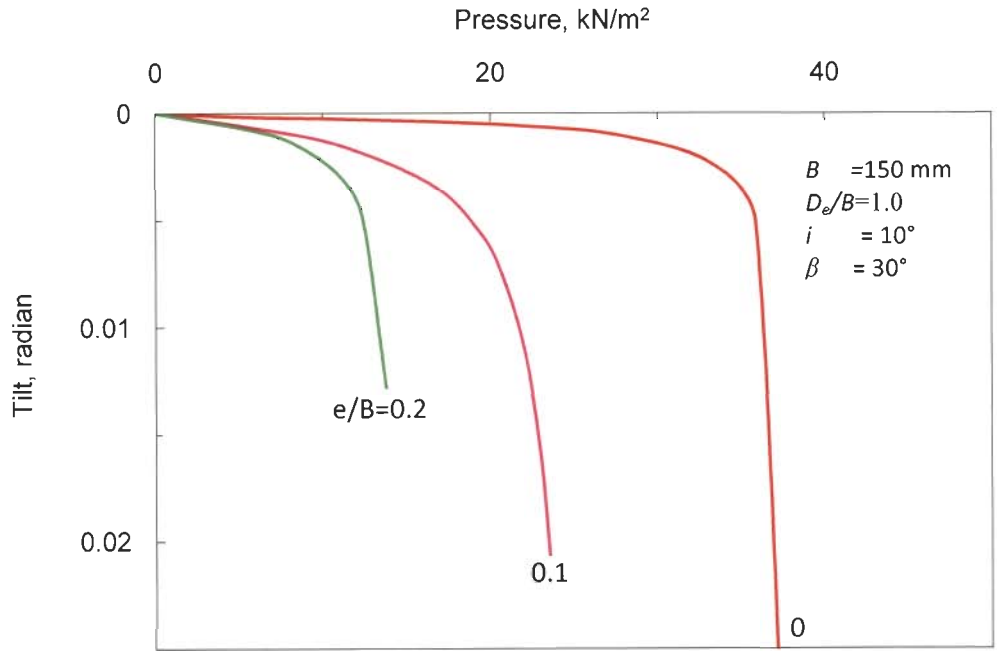

Fig.6.35 Pressure-Tilt Curves for Different Values of Load Eccentricity

6.3.3 Comparison with Test Data

Pressure-settlement curves predicted by employing the proposed methodology have been compared with the experimental curves for a 150 mm wide strip footing resting on a 30° slope placed at different edge distances and subjected to loads with different eccentricities and inclinations and are plotted in Figs. 6.36 through 6.39. The two curves are found to have the similar in nature. Upto about 50% of the failure pressure, the predicted and the experimental values tally reasonably well. The predicted values are slightly lower in this range. From the point of view of design, the settlements are usually obtained corresponding to pressure equal to one-third of the failure pressure. For this pressure, the present methodology gives the estimate of settlement almost precisely.

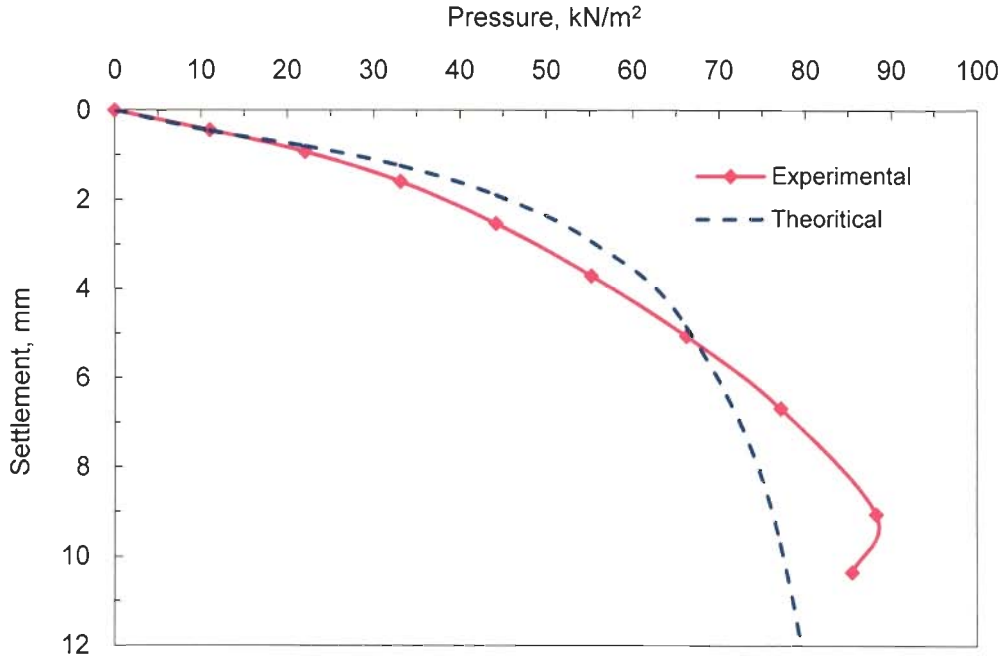

Fig.6.36 Comparison of Computed and Experimental Pressure-Settlement Curves, $\phi = 39.5°$, $\beta=30°$, $D_e/B=2.0$, $e/B=0$, $i=0°$

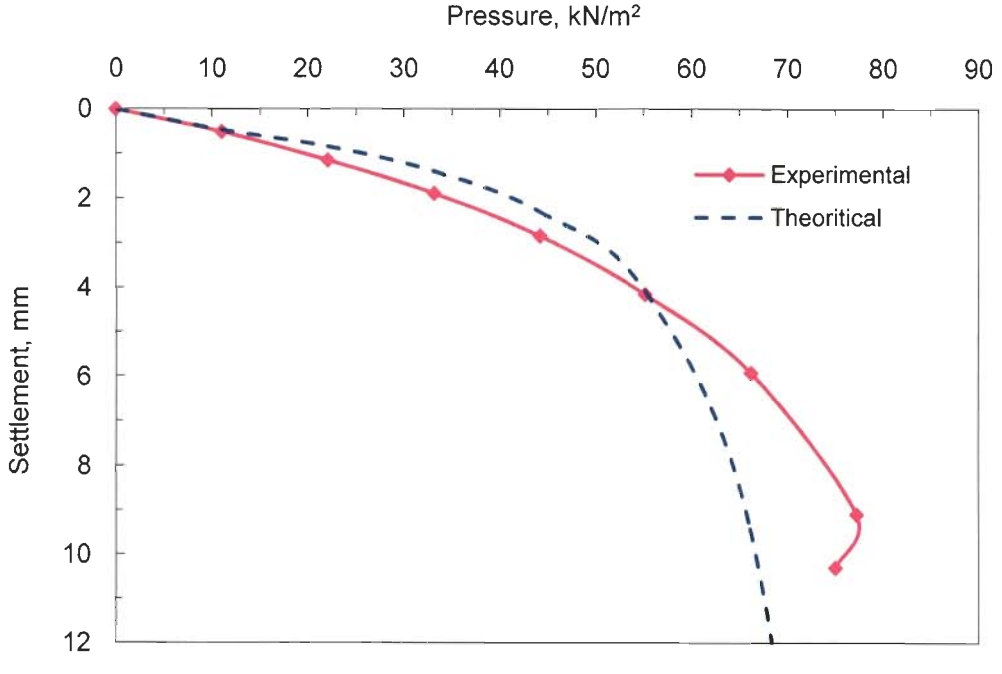

Fig.6.37 Comparison of Computed and Experimental Pressure-Settlement Curves, $\phi = 39.5°$, $\beta=30°$, $D_e/B=2.0$, $e/B=0.1$, $i=0°$

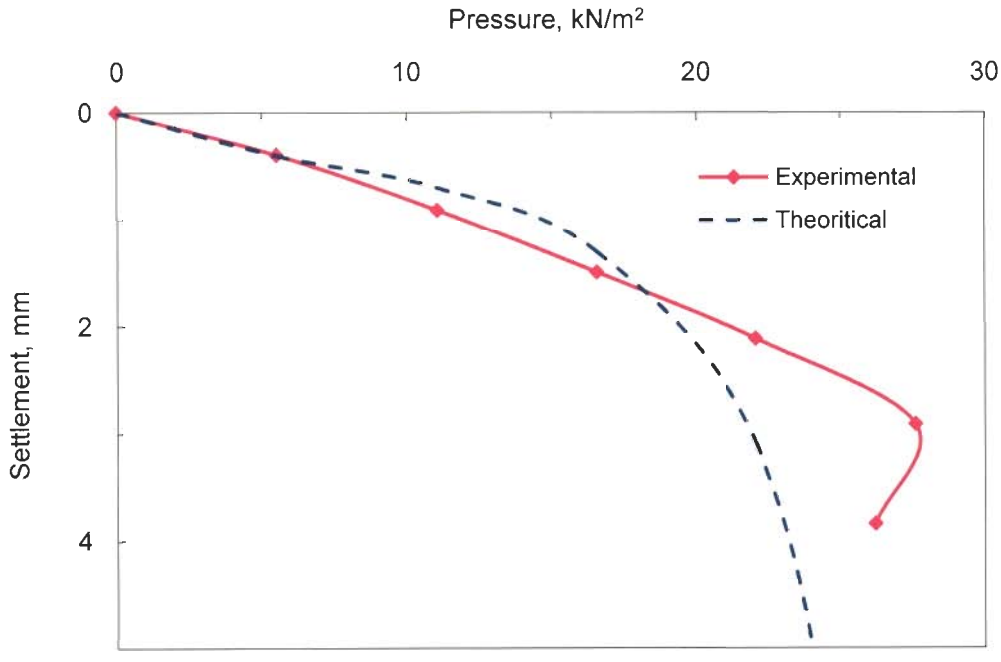

Fig.6.38 Comparison of Computed and Experimental Pressure-Settlement Curves, $\phi = 39.5°$, $\beta=30°$, $D_e/B=2.0$, $e/B=0.1$, $i=10°$

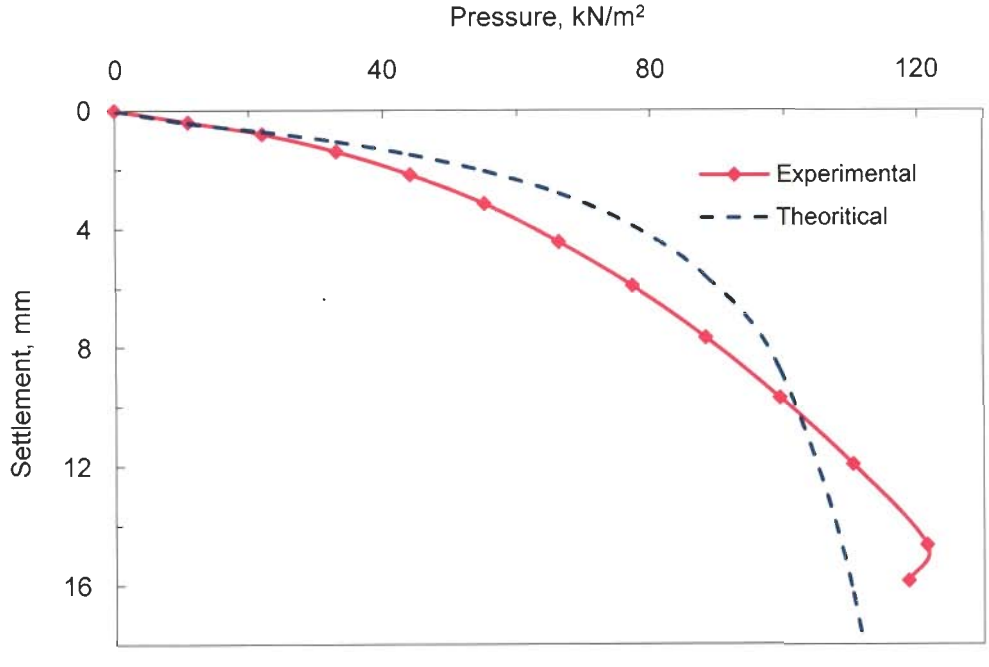

Fig.6.39 Comparison of Computed and Experimental Pressure-Settlement Curves, $\phi = 39.5°$, $\beta=30°$, $D_e/B=3.0$, $e/B=0$, $i=0°$

CHAPTER-VII

CONCLUSION AND SCOPE FOR FURTHER RESEARCH

7.1 SUMMARY

Foundations of many engineering structures are sometimes placed near the edge of a slope. Abutments of bridges and flyovers, buildings near the open section of underground railways and buildings and retaining structures constructed adjacent to ravines are some examples of foundations placed on upper surface of a slope. The footings of such structures are subjected to eccentric-inclined loads due to moments and horizontal thrusts along with vertical loads. The main criteria for a satisfactory design of foundations of such structures are the ultimate bearing capacity, permissible settlement, tilt and the overall stability of the slope.

This study is aimed at investigating the behaviour of strip footings placed near the edge of a slope and subjected to an eccentric-inclined load. Theoretical investigation forms the backbone of this study, though of course, the study also includes some experimental work which was undertaken for verification of theoretical results. The analytical work includes development of methodologies to predict the ultimate bearing capacity and the pressure-settlement and pressure-tilt characteristics of such a footing. The experimental work was aimed at obtaining the ultimate bearing capacity, the pressure-settlement and the pressure-tilt characteristics of a model strip footing placed on a sand slope and subjected to eccentric-inclined loads. This data was subsequently used for comparison with the results obtained from proposed methodologies.

7.2 CONCLUSIONS

Based on the work reported in this thesis, the following conclusions have been drawn.

7.2.1 The Ultimate Bearing Capacity

i) A theory based on limit equilibrium approach has been proposed for determining the bearing capacity of a strip footing on upper surface of a slope and subjected to an eccentric-inclined load using the concept of one sided failure. The results have been presented in terms of non-dimensional bearing capacity factors N_γ, N_q, N_c which depend upon parameters ϕ, β, D_e/B, D_f/B, e/B and i. These bearing

capacity factors have been presented in the form of charts convenient for use in design.

ii) The bearing capacity factors increase with increase in the edge distance and after a certain distance; these values become independent of the slope. The minimum edge distance at which these factors become independent of slope depend upon values of ϕ, β, e/B, i and D_f/B.

iii) The bearing capacity factors reduce with the increase in eccentricity and inclination of the load. These bearing capacity factors obtained by the proposed approach have been compared with those obtained by using the reduction factors as suggested by earlier investigators and a reasonable agreement has been found.

iv) Model tests were conducted under plane strain conditions with a strip footing resting on upper surface of a sand slope and subjected to eccentric-inclined loads. The failure loads obtained from the model tests compared very well with the corresponding values from the proposed theory.

7.2.2 Pressure-Settlement and Pressure-Tilt Characteristics

i) A procedure has been developed to predict the pressure-settlement and pressure-tilt characteristics of a strip footing resting on top of a slope and subjected to an eccentric-inclined load, using non-linear constitutive laws of soil.

ii) Comparison of results obtained by the present analysis for pressure-settlement and pressure-tilt characteristics show a good agreement with the test data.

7.3 SCOPE OF FURTHER RESEARCH

i) In the present study, the analysis has been carried out using the limit equilibrium approach. Limit analysis and finite element method may well be applied for the solution of the same problem.

ii) Model tests may be carried out on footings to obtain contact pressure distribution using sensitive pressure cells. This may help in understanding the behaviour of such footings.

iii) Model tests on clayey soils may also be conducted and the present analytical procedure may be verified by the test data on clays.

REFERENCES

1. Agrawal, R.K. (1986), Behaviour of Shallow Foundations Subjected to Eccentric-Inclined Loads. Ph.D. Thesis, University of Roorkee, Roorkee (India).
2. Agrawal, R.K. (1994), "Limit Analysis of Eccentrically Obliquely Loaded Footing", Proceedings of the 13th Int. Conf. on Soil Mech. and Found. Eng., Vol. 1, 453-456.
3. Amir, A.A.A. (1992), Interference Effect on the Behaviour of Footings. Ph.D. Thesis, University of Roorkee, Roorkee (India).
4. Arduino, P. and Macari, E. J. (1988), "Numerical Modelling of Spread Footings at Bridge–Embankment Interfaces", Transportation Research Record 1633, Paper No. 98-1473, 61-67.
5. Arduino, P., Macari, E. and Gemperline, M. (1994), "Load-Settlement Prediction of Footings on Steep Slopes", Vertical and Horizontal Deformations of Foundations and Embankments, ASCE, Vol. 2, 1385-1399.
6. Baki, A. A. and Beik, L. A. (1970), "Bearing capacity of foundations on sand", J. Soil Mech. and Found. Div., ASCE, 96(2), 545–559
7. Balla, A. (1962), "Bearing Capacity of Foundations", J. of Soil Mech. and Found. Div., ASCE, 88(5), 13-34.
8. Bathurst, R.J., Blatz, J.A. and Burger, M.H. (2003), "Performance of Instrumented Large-Scale Unreinforced and Reinforced Embankments Loaded by a Strip Footing to Failure", Can. Geotech. Journal, 40(6), 1067-1083.
9. Basudhar, P.K., Madhav, M.R. and Valsangkar, A.J. (1978), "Optimization Techniques in Bearing Capacity Analysis", Indian Geotechnical Journal, 8(2), 105-110.
10. Bauer, G. E., Shields, D. H., Scott, J. D. and Gruspier, J. E. (1981), "Bearing Capacity of Footings in Granular Slopes" Proc., 10th Int. Conf. of Soil Mech. and Found. Eng., Stockholm, Sweden, Balkema Publishers, Rotterdam, The Netherlands, Vol.2, 33–36
11. Bishop, A. W. (1955), "The Use of the Slip Circle in the Stability Analysis of Slopes", Geotechnique, 5(3), 7-17.

12. Blatz, J.A. and Bathurst, R.J. (2003), "Limit Equilibrium Analysis of Reinforced and Unreinforced Embankments Loaded by a Strip Footing", Can. Geotech. Journal, 40(6), 1084-1092.

13. Borthakur, B.C., Nambiar, M.K.C., Biswas, A. and Kalitha, U.C. (1988), "Studies on Bearing Capacity of Strip Footing on Slopes", Proc. Indian Geotechnical Conference, Vol.1, 385-389.

14. Bowles, E.J. (1977), Foundation Analysis and Design, The McGraw-Hill Companies, Inc.

15. Bransby, M.F. and Davidson, C. (2008), "The effect of shallow foundation fixity on their capacity next to slopes", Proc. of the BGA International Conference on Foundations, Dundee, Scotland, 2008. IHS BRE Press.

16. Briaud, J.L. (2007), "Spread Footings in Sand: Load Settlement Curve Approach", J. of Geotech. and Geoenviron. Engineering, 133(8), 905-920.

17. Brinkgreve, R.B.J. and Vermeer, P.A. (1988), PLAXIS Finite Element Code for Soil and Rock Analysis., Rotterdam, Balkema

18. Burland, J.B. (1965), "The Yielding and Dilation of Clay, (Correspondence)", Geotechnique, 15(2), 211-214.

19. Chen, W. F. (1975), Limit Analysis and Soil Plasticity, Elsevier Scientific Publishing Company, Amsterdam, London.

20. Cheng, Y.M. and Au, S.K. (2005), "Solution of the Bearing Capacity Problem by the Slip Line Method", Can. Geotech. Journal, 42, 1232-1241.

21. Cichy, W., Dembicki, E., Odrobinski, W., Tejchman, A. and Zadrogo, B. (1978), "Bearing Capacity of Subsoil under Shallow Foundations: Study and Model Tests", Scientific Books of Gdansk Technical University, Civil Engineering , Vol. 22, 214.

22. Das, B.M. (1981), "Bearing Capacity of Eccentrically Loaded Surface Footings on Sand", Soils and Foundation, 21(1), 115-119.

23. Das, B.M. (1981), "Eccentrically Loaded Surface Footing on Sand Layer Resting on Rough Rigid Base", Transportation Research Record No. 827, 41-44.

24. Das, B.M. and Puri, V.K. (1989), "Bearing Capacity of Strip Foundation on Top of a Clay Slope", Proc. of the 4th Int. Conf. on Civil and Structural Engineering Computing, 235-240.

25. Das, B.M. (2007), Principles of Foundation Engineering, 6th ed. Toronto, Ontario: Thomson.

26. Das, B.M. (1999), Shallow Foundations, Bearing Capacity and Settlement, CRC Press LLC.

27. Das, B.M. and Sivakugan, N. (2007), "Settlements of shallow foundations on granular soils - an overview", Int. J. of Geotech. Eng., 1 (1), 19 - 29

28. De Beer, E. E. (1965), "Bearing Capacity and Settlement of Shallow Foundations on Sand", Proc. of Symp. Bearing Capacity and Settlement of Foundations, Duke Univ., 15-34.

29. De Buhan, P. and Gaernier, D. (1998), "Three Dimensional Bearing Capacity Analysis of a Foundation near a Slope", Soils and Foundations, 38 (3), 153-163.

30. Dembicki, E. and Zadroga, B. (1974), "Model Tests on Bearing Capacity of Foundation on Slopes", Proceedings of the 4th Danube-European Conf. on Soil Mech. and Found. Eng., Vol. 1, 147-153.

31. Desai, C.S. (1971), "Non-Linear Analysis using Spline Functions", Proceedings American Society of Civil Engineers, SM: Oct. 1971:1461:8462.

32. Desai, C.S. and Wu, T.H. (1976), "A General Function for Stress-Strain Curves", Proc. 2nd Int. Conf. Numer. Methods Geomech., Blacksburg.

33. Dewaikar, D. M. and Mohapatro, B. G. (2003), "Computation of Bearing Capacity Factor N_γ-Terzaghi's Mechanism", Int. J. of Geomechanics, 3(1), 123-128.

34. Dewaikar, D. M. and Mohapatra, B. G. (2003), "Computation of Bearing Capacity Factor N_γ-Prandtl's Mechanism", Soils and Foundations, 43(3), 1-10.

35. Drucker, D.C., Prager, W. and Greenberg, H.L. (1952), "Extended Limit Design Theorems for Continuous Media", Quart. Appl. Math., Vol.9.

36. Drucker, D.C., Gibson, R.E. and Henkel, D.J. (1957), "Soil mechanics and work-hardening theories of plasticity", Transactions American Society of Civil Engineers, 122 , 338–346.

37. Duncan, J.M. and Chang, C.Y. (1970), "Nonlinear Analysis of Stress and Strain in Soils", J. of Soil Mech. and Found. Div. ASCE, 96(5), 1629-1653.

38. Feda, J. (1961), "Research on the Bearing Capacity of Loose Soil", Proc. of

the 5th Int. Conf. on Soil Mech. and Found. Eng., Vol. 1, 635-642.

39. Fellenius, W. (1927), "Erdstatishe berechmungen mit reibungund cohesion", Ernest Verlag, Berlim.

40. Finn, W.D.L. (1967), "Applications of Limit Plasticity in Soil Mechanics", J. Soil Mech. Found Div. ASCE, 93,(5),101-119.

41. Frydman, S. and Burd, H. J. (1997), "Numerical Studies of Bearing Capacity Factor N_γ ", J. Geotech. and Geoenviron. Eng., 123(1), 20–29.

42. Garnier, J., Canepa, Y., Corte, J.F. and Bakir, N.E. (1994), "Etude dela Portance de Foundations en Bord deTalus", Proceedings of the 13th Int. Conf. on Soil Mech. and Found. Eng., Vol. 2, 705-708.

43. Gemperiine, M. C. (1988), "Centrifuge Modeling of Shallow Foundations", Proc. ASCE Spring Convention, ASCE.

44. Graham, J., Andrews, M.and Shields, D.H. (1988), "Stress Characteristics for Shallow Footings in Cohesionless Slopes", Can. Geotech. Journal, 25, 238-249.

45. Giroud, J.P. and Tran, V.N. (1971), "Force Portante d'une Fondation sur une Pente. Annales de l'Institut Technique du Batiment et des Travaux Publics", Supplement, 283-284.

46. Hartikainen, J. and Zadroga, B. (1994), "Bearing Capacity of Footings and Strip Foundations: Comparison of Model Test Results with EUROCODE 7", Proc. of the 13th Int. Conf. on Soil Mech. and Found. Eng., Vol. 2, 457-460.

47. Hanna,A.M. and Meyerhof,G.G. (1981), "Experimental Evaluation of Bearing Capacity of Footing Subjected to Inclined Loads", Can. Geotech. Journal. 18, 599-603.

48. Hansen, J .B. (1963), "Discussion of Hyperbolic Stress Strain Response of Cohesive Soils", Proc. ASCE, (4), 241-242.

49. Hansen, B. (1961), "A General Formula for Bearing Capacity", Bulletin of the Danish Geotechnical Institute, No. 11.

50. Hansen, J. B. (1970), "A revised and Extended Formula for Bearing Capacity", Bull. No. 28, Danish Geotechnical Institute, Copenhagen, Denmark.

51. Ingra, S. T. and Baecher, G. B. (1983), "Uncertainty in Bearing Capacity of Sands", J. Geotech. Eng., 109(7), 899–914.

52. Janbu, N. (1954), Stability Analysis of Slopes with Dimensionless

Parameters, Cambridge, Mass., Harvard Soil Mech. Series NO.46.

53. Janbu, N. (1954), "Application of composite slip surfaces for stability analysis", Proceedings of the European Conference on Stability of Earth Slopes, Stockholm, Vol. 3, 43–49.

54. Jao, M., Agrawal, V. and Wang, M.C. (2001), "Performance of Strip Footings on Slopes", Proc., 15th Int. Conf. on Soil Mech. and Found. Eng,. Istanbul, Turkey, Vol. 1, 697-699.

55. Jao, M., Ahmedb, F., Muninarayanac, G. and Wang, M.C. (2008), "Stability of eccentrically loaded footings on slopes", Geomechanics and Geoengineering: An International Journal, 3(2), 107-111.

56. Jumikis, A.R. (1965), Soil Mechanics, D.Van Nostrand, Company, Inc. New York.

57. Krishnan Nair, K., Devdas Menon and Gandhi, S.R. (2001), "Slope Stability of Embankments - a Reliability Study", Proceedings of Eighth Intl. Conference on Structural Safety and Reliability Newport Beach, California, June 2001.

58. Kumar, J. and Khatri, V. N. (2008), "Effect of Footing Width on Bearing Capacity Factor N_γ for Smooth Strip Footings", J. of Geotech. and Geoenviron. Eng., 134(9), 1299-1310

59. Kusakabe, O., Kimura, T. and Yamaguchi, H. (1981), "Bearing Capacity of Slopes under Strip Loads on the Top Surfaces", Soils and Foundations, 21(4), 29-40.

60. Kimura, T., Kusakabe, O. and Saitoh, K. (1985), "Geotechnical Model Tests of Bearing Capacity Problems in a Centrifuge", Geotechnique, 35(1), 33–45.

61. Kondner, R.L. and Zelasko, S. (1963), "A Hyperbolic Stress-Strain Formulation for Sands", Procs. of 2nd Pan American Conf. on Soil Mech. and Found. Eng., Brazil, Vol.I, 289-324.

62. Kondner, R.L. (1963), "Hyperbolic Stress-Strain Response of Cohesive Soils", Procs. of American Society of Civil Engineers, J. of Soil Mech. and Found. Eng., 89(3),115-153.

63. Kotter, F. (1903), "Die Bestimmung des Drucks an gekru¨mmten Gleitflachen, eine Aufgabe aus der Lehre vom Erddruck., Sitzungsberichte der Akademie der Wissenschaften", Berlin, 229–233.

64. Kumbhojkar, A. S. (1993), "Numerical Evaluation of Terzaghi's N_γ", J. Geotech. Eng., 119(3), 598–607.

65. Lade, P. V. and Kim, M. K. (1988 a), "Single hardening constitutive model for frictional materials. II. Yield criterion and plastic work contours", Computers and Geotechnics, 6, 13-29.

66. Lade, P.V. and Kim, M.K. (1988 b), "Single Hardening Constitutive Model for Frictional Materials. III, Comparison with Experimental Data", Computer and Geotechnics, 6, 31-47.

67. Liu, Y., Sreng, S., Mochizuki, A. and Ueno, K. (2006), "Deformation Behaviour and Bearing Capacity of Slope due to Surface Loading and their FEM Simulation by MMX Model", Proc. of Geomechanics and Geotechnics of Particulate Media, Taylor & Francis, 403-408.

68. Marechal, O., Remaud, D., Garnier, J. and Amar, S. (1999), "Recent Advances in Design of Shallow and Deep Foundation", Geotechnics for Developing Africa: Proceedings of the Twelfth Regional Conference for Africa on Soil Mechanics and Geotechnical Engineering, Durban, South Africa, 131-134.

69. Meyerhof, G.G. (1951), "The Ultimate Bearing Capacity of Foundations", Geotechnique, 2,301-332.

70. Meyerhof, G. G. (1953), "The Bearing Capacity of Foundations under Eccentric and Inclined Loads", Proc. 3rd Int. Conf. of Soil Mechanics and Foundation Engineering, Balkema Publishers, Rotterdam, The Netherlands, Vol. 1, 440–445.

71. Meyerhof, G.G. (1957), "The Ultimate Bearing Capacity of Foundations on Slopes", Proc. 4th Int. Conf. on Soil Mech. and Found Eng., Vol.l, 384-386.

72. Meyerhof, G. G. (1963), "Some Recent Research on the Bearing Capacity of Foundations", Can. Geotech. J., 1(1), 16–26.

73. Michalowski, R.L. (1991), "Discussion of Bearing Capacity of Footings Adjacent to Slopes", J. of Geotech. Engg. ASCE, 117,(GT12),1125-1127.

74. Mizuno, Takaaki, Yoshiharll Tokumitsu, and Hiroshi Kawakami (1960), "On the Bearing Capacity of a Slope on Cohesionless Soils", Japanese Society of Soil Mech. and Found. Engg., l(2),30-37.

75. Myslivec, A. and Kysela, Z. (1978), Bearing Capacity of Building Foundations., Elsevier.

76. Narita, K. and Yamaguchi, H. (1990), "Bearing Capacity Analysis of Foundations on Slopes by Use of Log-Spiral Sliding Surfaces", Soils and Foundations, 30(3), 144-152.

77. Naylor, D.J. (1978), Stress-Strain Laws for Soil, Development of Soil Mech. 1, Edited by Scott, Applied Science Publication Ltd., London.

78. Peynircioglu, H. (1948), "Tests on Bearing Capacity of Shallow Foundations on Top Surfaces of Sand Fills", Proc. 2nd Int. Conf. on Soil Mech. and Found. Eng., Vol.3, 194.

79. Poulos,H.G. and Davis, E.H. (1974), Elastic Solutions for Soils and Rock Mechanics, John Wiley & Sons, Inc. New York.

80. Prakash,S. and Saran, S. (1971), "Bearing Capacity of Eccentrically Loaded Footings." J. Soil Mech. and Found. Div., ASCE, 97(1),95-117.

81. Prakash,S., Ranjan,G. and Saran,S. (1979), Analysis and Design of Foundations and Retaining Structures, Sarita Prakashan, N.Delhi.

82. Prakash,S., Saran,S. and Sharan,U.N. (1984), "Footings and Constitutive Laws", J. Geotech Engg., ASCE, 110(10), 1473-1488.

83. Prandtl, L. (1920), "Ueber die Haerte plastischer Koerper. Goettinger Nacher", Math.-Phys. Kl, 74–85.

84. Reissner, H. (1924), "Zum erddruckproblem", Proceedings of the 1st International Congress of Applied Mechanics, Delft, 259-3 11.

85. Saran, S. (1969), Bearing Capacity of Footings Subjected to Moments., Ph.D. Thesis, University of Roorkee, Roorkee (India)

86. Saran, S. (1970), "Fundamental Fallacy in Analysis of Bearing Capacity of Soil", J. Institution of Engineers, India,50,224-226.

87. Saran, S. and Agrawal, R.K. (1985), "Limit Equilibrium Analysis of Footings Subjected to Eccentric-Inclined Load", Proceedings of the Indian Geotechnical Conference, Vol. 1, 99-103.

88. Saran, S., Sud, V. K. and Handa, S. C. (1989), "Bearing Capacity of Footings Adjacent to Slopes", J. Geotech. Eng., ASCE, 115(4), 553-573.

89. Saran, S. and Agarwal, R.K. (1991), "Bearing Capacity of Eccentrically Obliquely Loaded Footing", J. of Geotech. Eng, ASCE, 117(11),1669-1690.

90. Scott, R.F. (1963), Principles of Soil Mechanics, Addison Wesley Pub. Co. Inc.

91. Sharan, U.N. (1977), Pressure -Settlement Characteristics of Surface

Footings from Constitutive Laws, Ph.D.Thesis, University of Roorkee, Roorkee (India).

92. Shields, D.H., Scott, J.D., Bauer, G.E., Deschenes, J.H. and Barsvary, A.K. (1977), "Bearing Capacity of Foundations near Slopes", Proc. 9th Int. Conf. on Soil Mech. and Found Engg., Tokyo, Vol. I, 715-720.

93. Shields, D.H. and Garnier, J. (1989), "Foundations at Top of Slopes", Demello Volume of the 12th Int. Conf. of the Int. Society of Soil Mech. and Found. Engineers, 411-422.

94. Shields, D.H., Chandler, N. and Garnier, J. (1990), "Bearing Capacity of Foundation in Slopes", J. of Geotech. Eng, ASCE, 116(3), 528-537.

95. Singh, D. N. and Basudhar, P. K. (1993), "Optimal Lower Bound Bearing Capacity of Strip Footing", Soils and Foundations. 33(4), 18-25.

96. Siva Reddy and Mogaliah, G. (1976), "Stability of Slopes under Foundation Load", Indian Geotechnical Journal, 6(2), 91-111.

97. Siva Reddy, and Mogaliah, G. (1975), "Bearing Capacity of Shallow Foundations on Slopes", Indian Geotechnical Journal, 5(3), 237-253.

98. Sivakugan, N. and Johnson, K. (2004), "Settlement Predictions in Granular Soils: A Probabilistic Approach", Geotechnique, 54(7), 499 – 502.

99. Sokolovski, V.V. (1960), Statics of Granular Media, 2nd Ed., Butterworths Scientific Publications, London.

100. Soriano Pena, A., Valderrama Conde, M., and Gonzalez Galindo, J. (2001), "Bearing Capacity of Shallow Foundations on Sloping Ground", Proceedings of the 15th Int. Conf. on Soil Mech. and Found. Eng., Vol. 1, 773-776.

101. Soubra, A. H. (1999), "Upper Bound Solutions for Bearing Capacity of Foundations", J. Geotech. Geoenviron. Eng., 125(1), 59–68.

102. Shiraishi, S., (1990). "Variation in Bearing Capacity Factors of Dense Sand Assessed by Model Loading Tests", Soils and Foundations, 30(1),17-27.

103. Sud,V.K. (1984), Behaviour of Shallow Foundations Adjacent to Slopes, Ph.D. Thesis, University of Roorkee, Roorkee, India.

104. Taylor, D.W. (1948), Fundamentals of Soil Mechanics, Asia Publishing House.

105. Terzaghi, K.(1943), Theoretical Soil Mechanics, Wiley, New York.

106. Vesic, A. S. (1973), "Analysis of Ultimate Loads of Shallow Foundations",

J. Geotech. Engg., 99(1), 45–73.

107. Vesic, A. (1975), Bearing Capacity of Shallow Footings., Winterkorn and Fang, eds. Foundation engineering handbook. New York, Van Nostrand Reinhold.

108. Wang, M.C., Jao, M. and Hieh, C.W. (1994), "Effect of Underground Cavity on Footing Interaction", Proceedings, 13th Int. Conf. on Soil Mech. and Found. Engg., New Delhi, India, Vol. 2, 575-578.

109. White D J, Take A and Bolton M D. (2003), "Soil Deformation Measurement using Particle Image Velocimetry (PIV) and Photogrammetry", Geotechnique, 53, 619-631.

110. Xiao, Y., Zhi-bini, W., Jin-feng, Z. and Liang, L. (2007), "Bearing Capacity of Foundation on Slope Determined by Energy Dissipation Method and Model Experiments." J. Cent. South Univ. Technol. 01–0125–04.

111. Zadroga, B. (1994), "Bearing Capacity of Shallow Foundations on Non-cohesive Soils", J. Geotech. Eng., 120(11), 1991–2008.

112. Zedan, A.J.(2004), Finite Element Analysis of Shallow Foundations for Eccentric Inclined Loads, Ph.D. Thesis, Indian Institute of Technology Roorkee, Roorkee (India).

Appendix- I

N_γ CHARTS

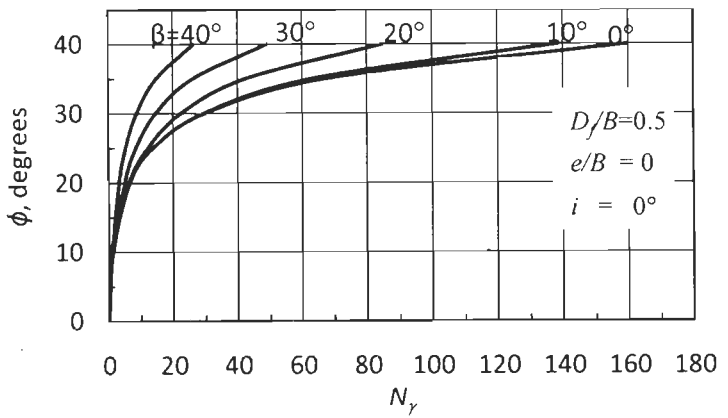

Fig. A.I.1 a (i) N_γ versus ϕ for D_e/B=0

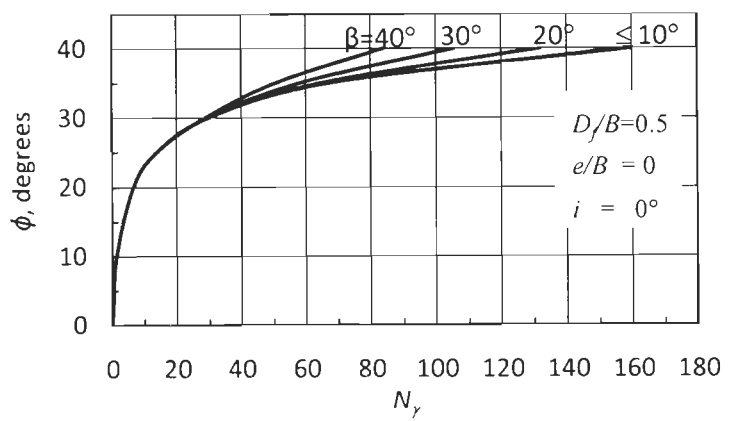

Fig. A.I.1 a (iii) N_γ versus ϕ for D_e/B=2.0

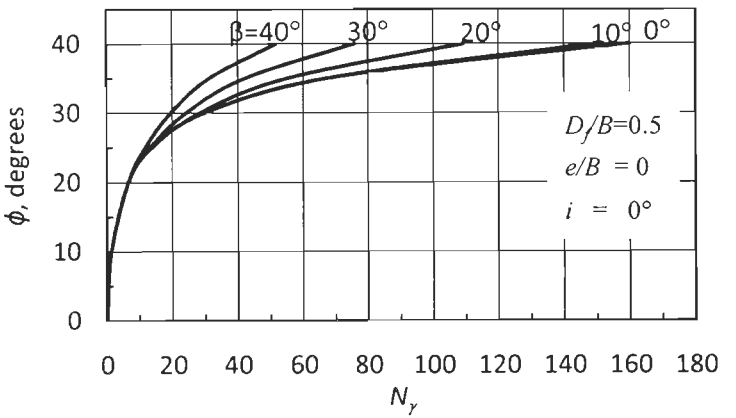

Fig. A.I.1 a (ii) N_γ versus ϕ for D_e/B=1.0

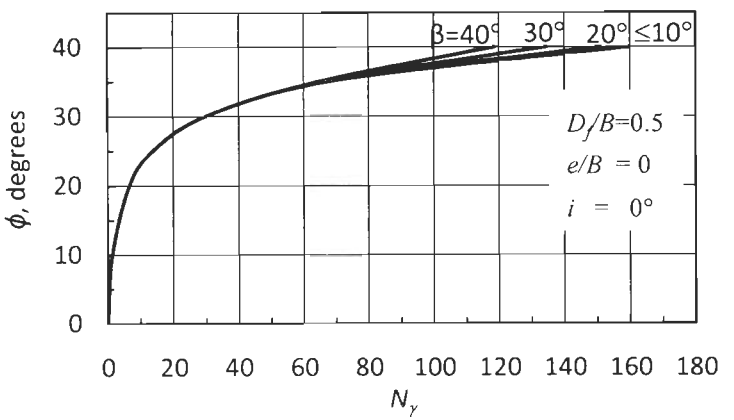

Fig. A.I.1 a (iv) N_γ versus ϕ for D_e/B=3.0

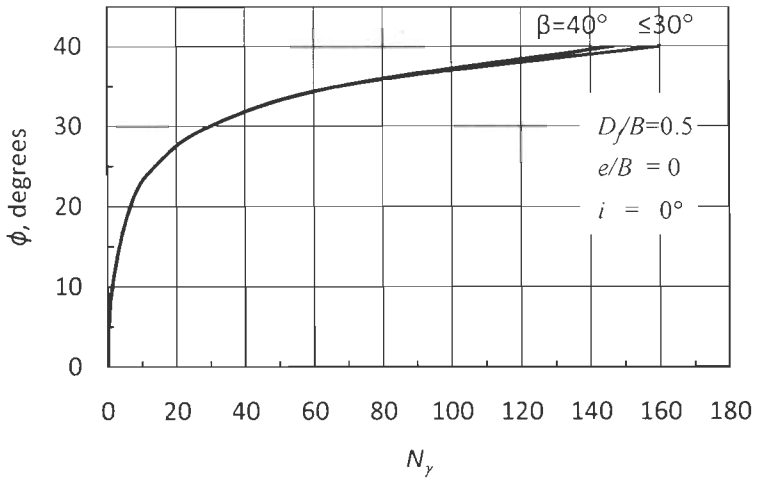

Fig. A.I.1 a (v) N_γ versus ϕ for D_e/B=4.0

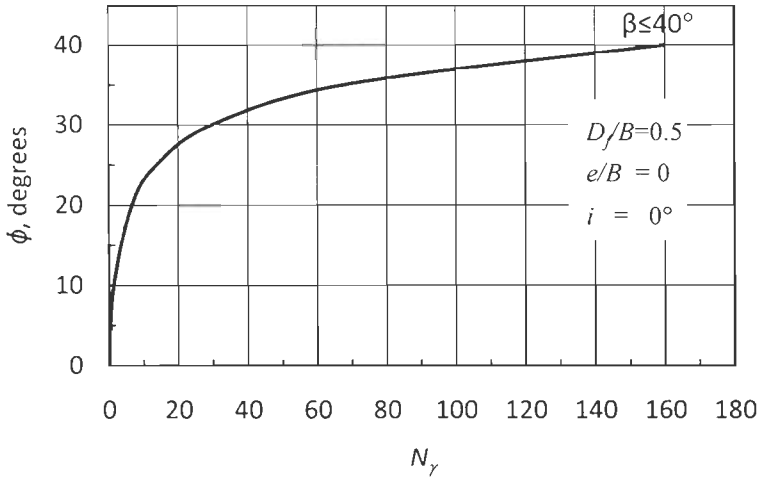

Fig. A.I.1 a (vi) N_γ versus ϕ for D_e/B=5.0

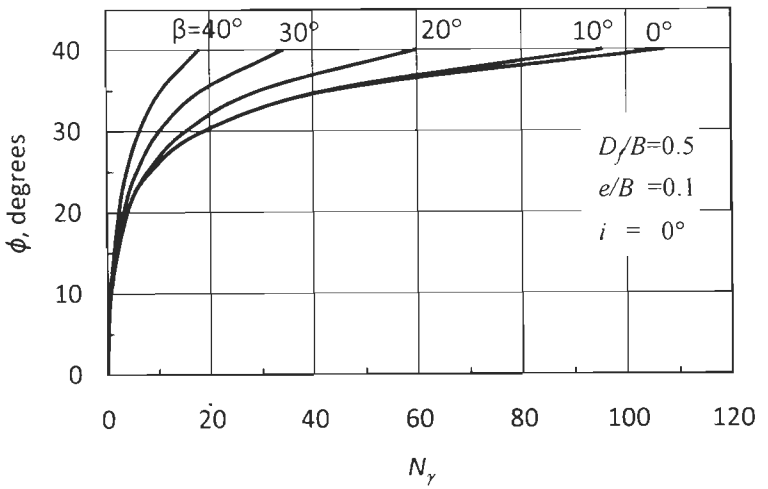

Fig. A.I.1 b (i) N_γ versus ϕ for D_e/B=0

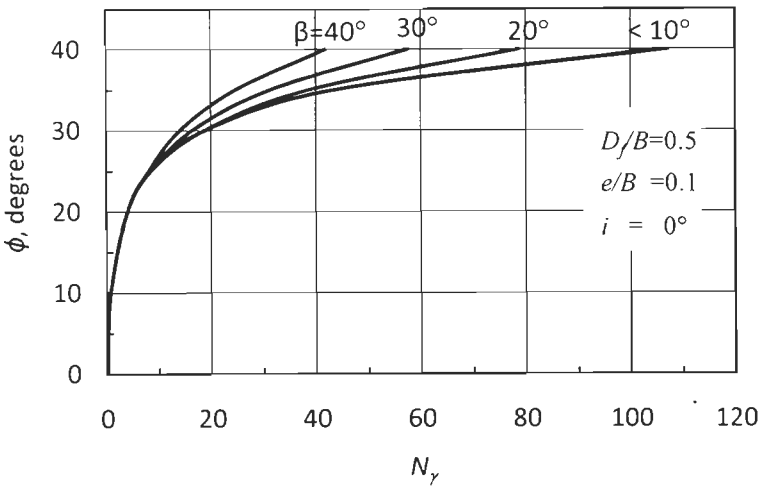

Fig. A.I.1 b (ii) N_γ versus ϕ for D_e/B=1.0

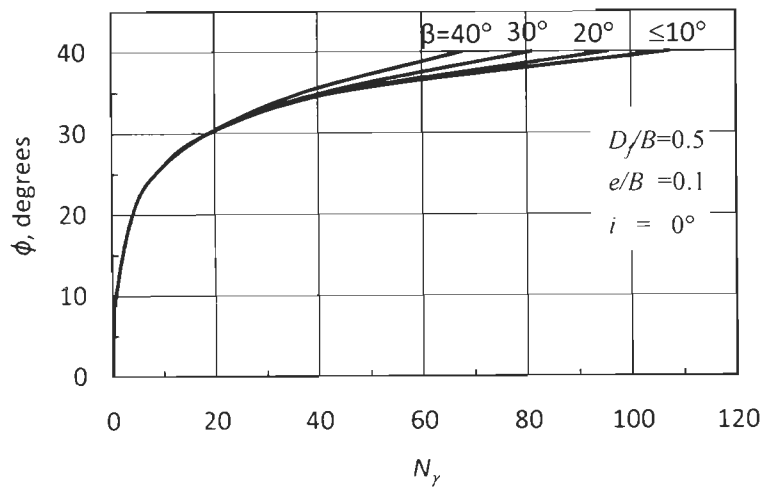

Fig. A.I.1 b (iii) N_γ versus ϕ for D_e/B=2.0

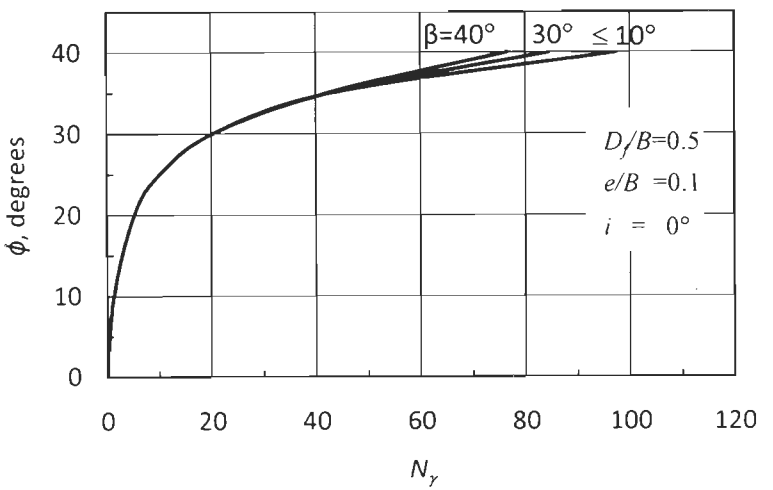

Fig. A.I.1 b (iv) N_γ versus ϕ for D_e/B=3.0

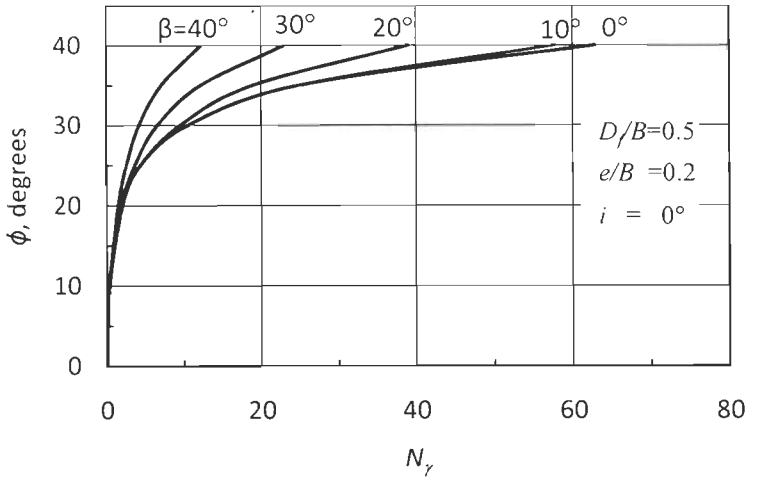

Fig. A.I.1 c (i) N_γ versus ϕ for D_e/B=0

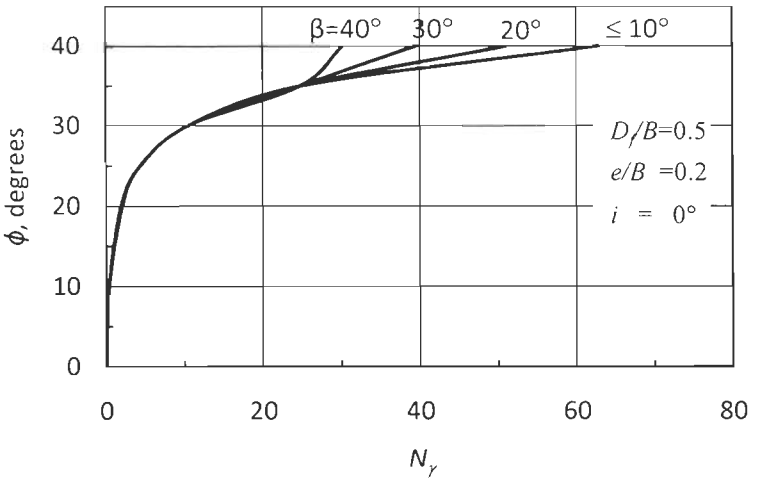

Fig. A.I.1 c (ii) N_γ versus ϕ for D_e/B=1.0

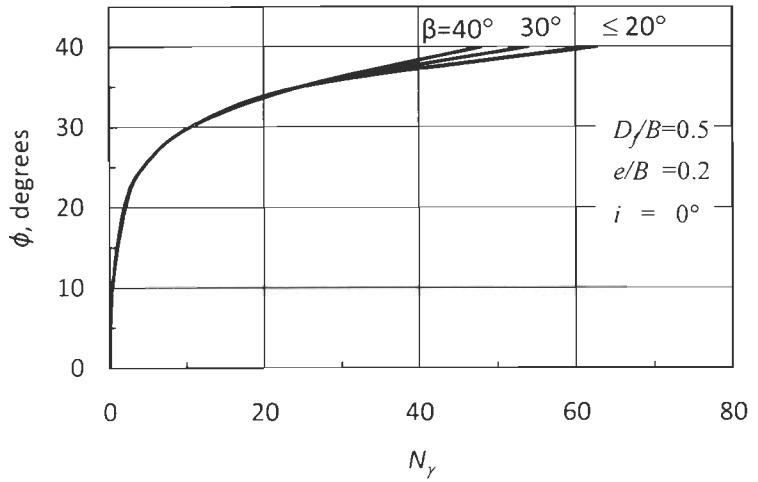

Fig. A.I.1 c (iii) N_γ versus ϕ for D_e/B=2.0

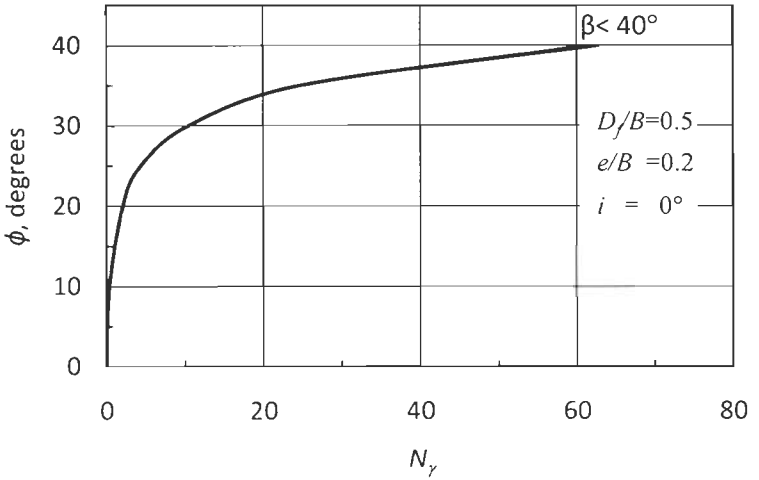

Fig. A.I.1 c (iv) N_γ versus ϕ for D_e/B=3.0

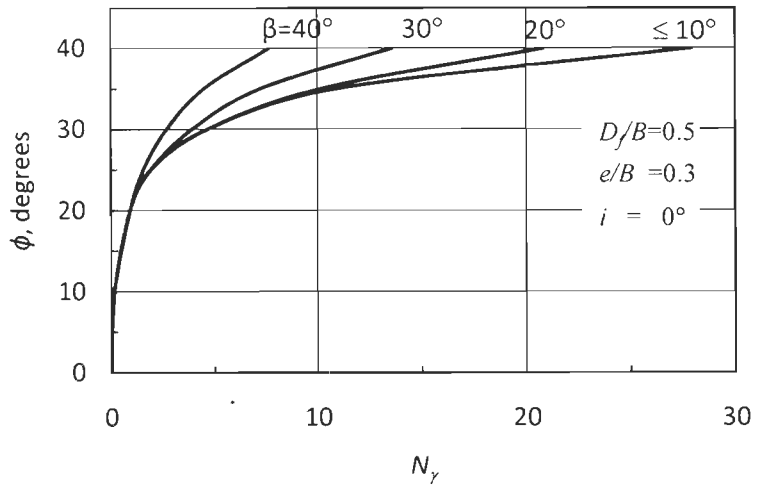

Fig. A.I.1 d (i) N_γ versus ϕ for D_e/B=0

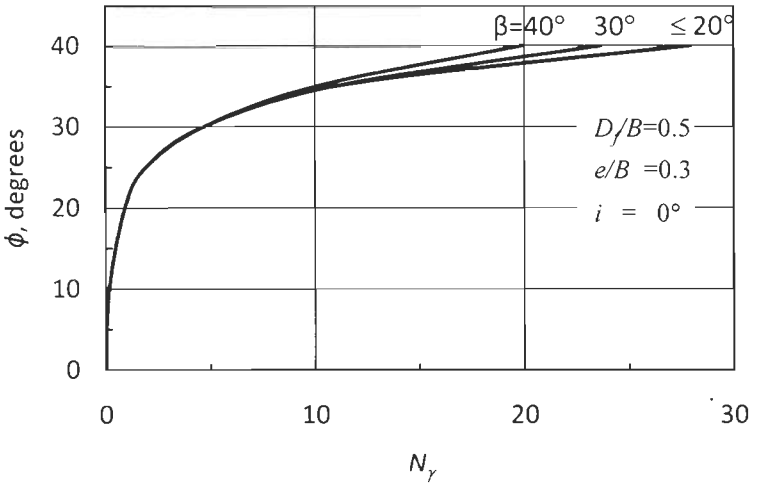

Fig. A.I.1 d (ii) N_γ versus ϕ for D_e/B=1.0

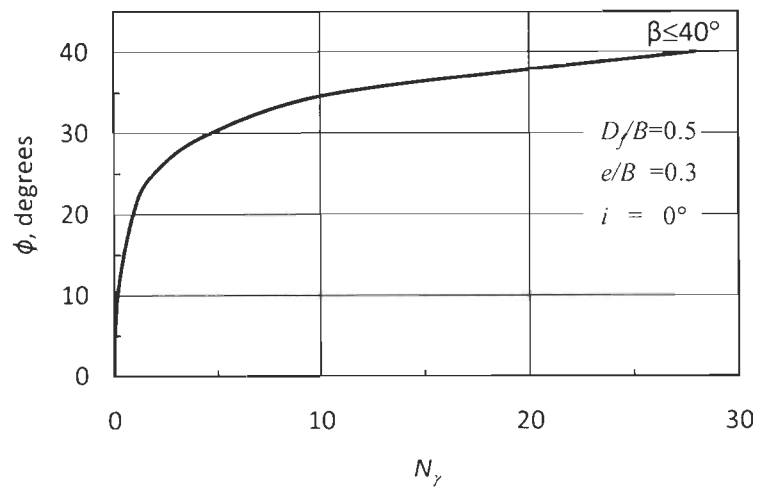

Fig. A.I.1 d (iii) N_γ versus ϕ for D_e/B=2.0

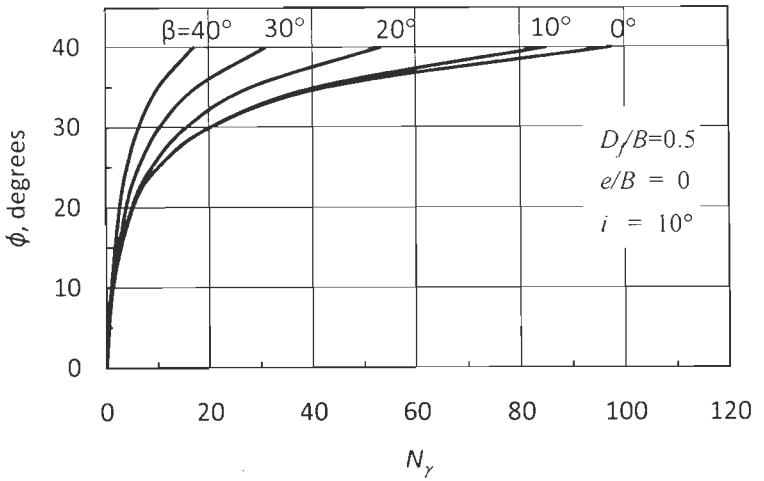

Fig. A.I.2 a (i) N_γ versus ϕ for D_e/B=0

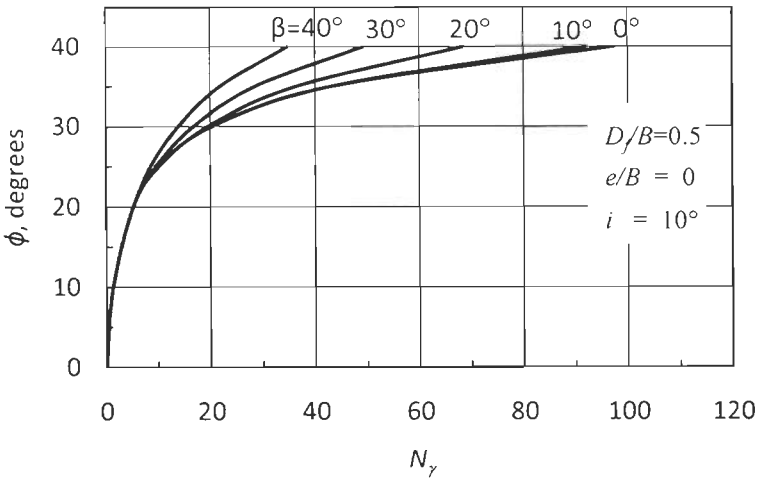

Fig. A.I.2 a (ii) N_γ versus ϕ for D_e/B=1.0

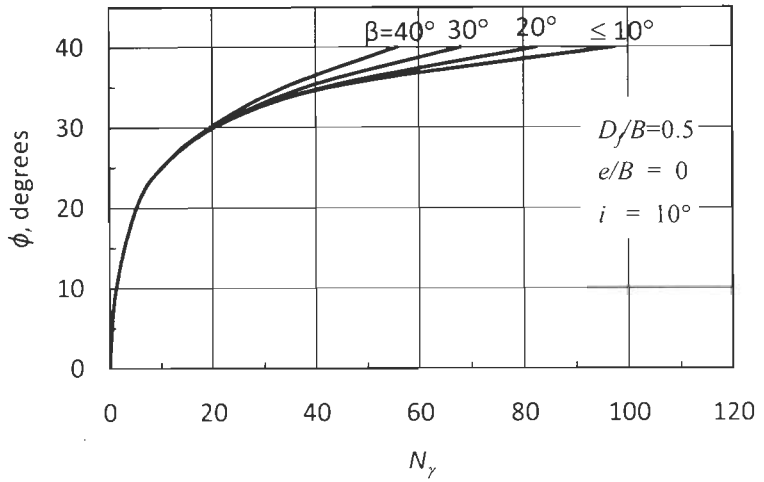

Fig. A.I.2 a (iii) N_γ versus ϕ for D_e/B=2.0

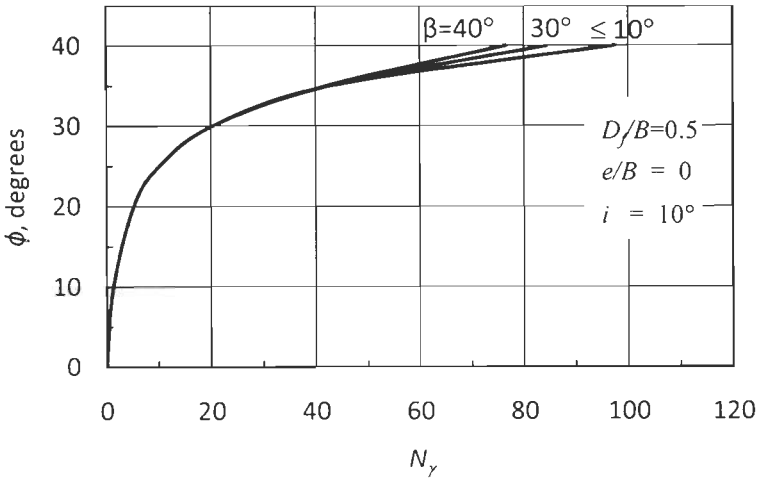

Fig. A.I.2 a (iv) N_γ versus ϕ for D_e/B=3.0

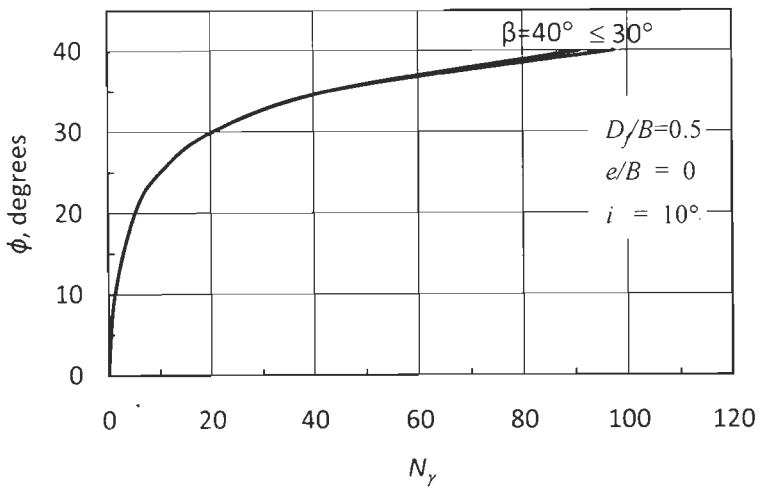

Fig. A.I.2 a (v) N_γ versus ϕ for D_e/B=4.0

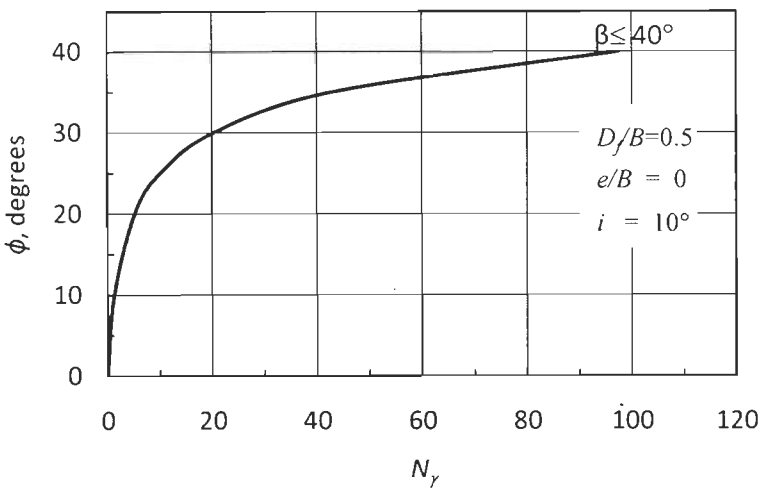

Fig. A.I.2 a (vi) N_γ versus ϕ for D_e/B=5.0

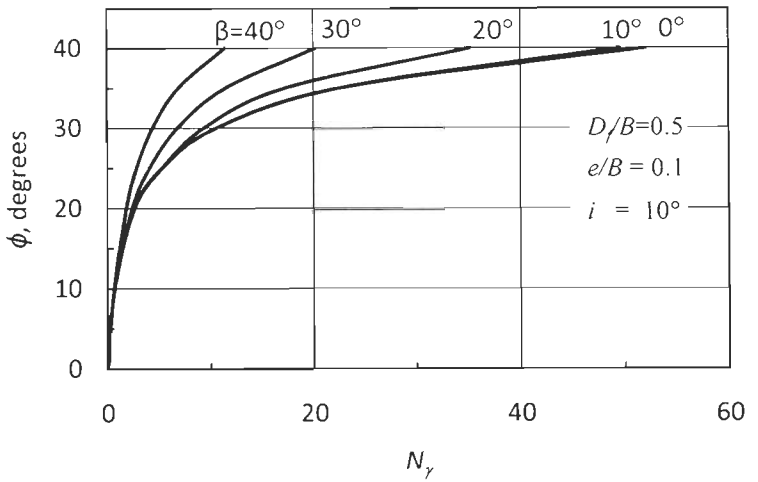

Fig. A.I.2 b (i) N_γ versus ϕ for D_e/B=0

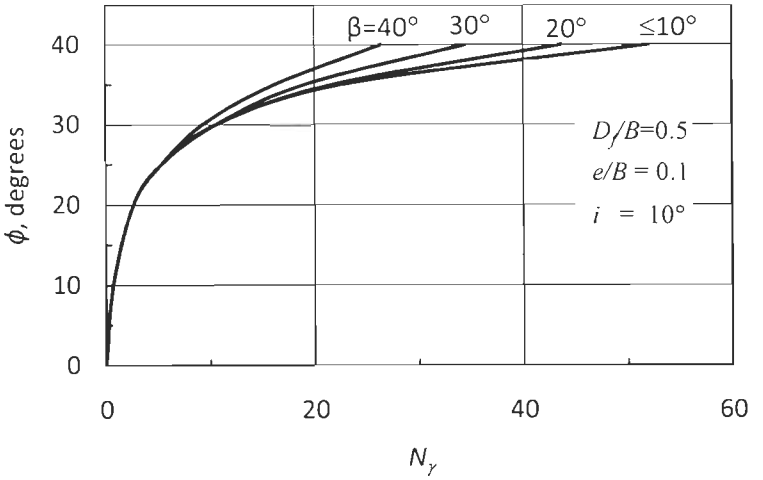

Fig. A.I.2 b (ii) N_γ versus ϕ for D_e/B=1.0

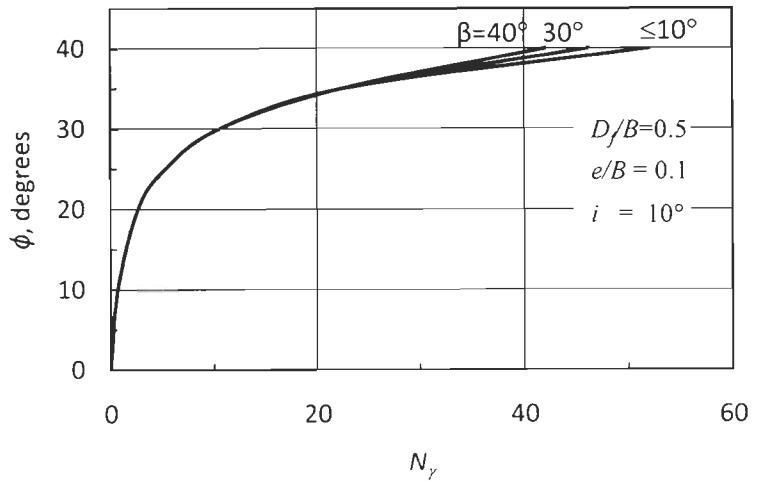

Fig. A.I.2 b (iii) N_γ versus ϕ for D_e/B=2.0

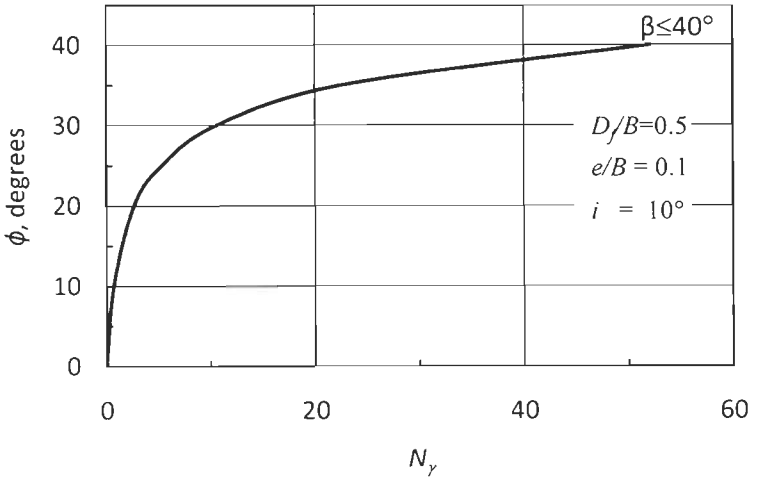

Fig. A.I.2 b (iv) N_γ versus ϕ for D_e/B=3.0

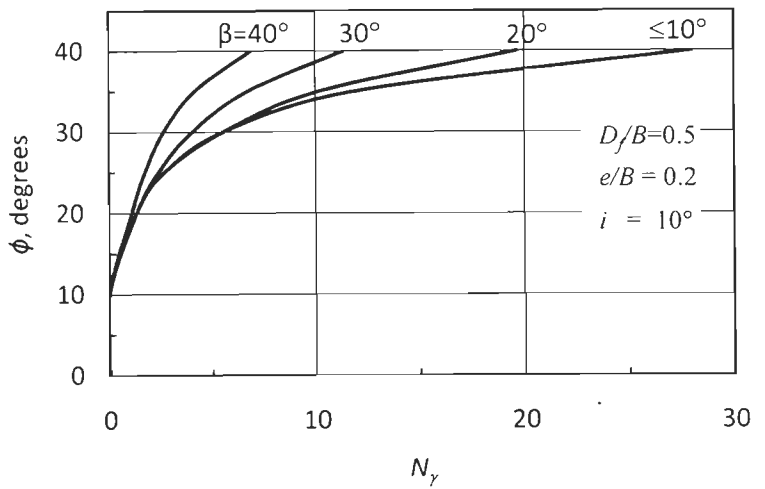

Fig. A.I.2 c (i) N_γ versus ϕ for D_e/B=0

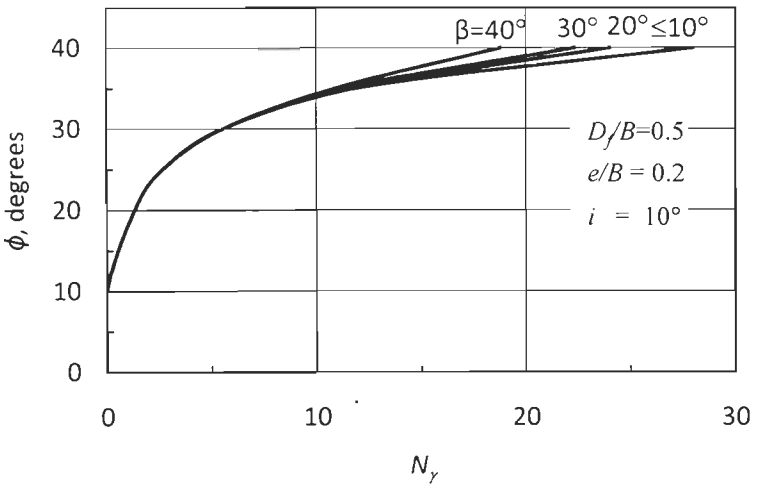

Fig. A.I.2 c (ii) N_γ versus ϕ for D_e/B=1.0

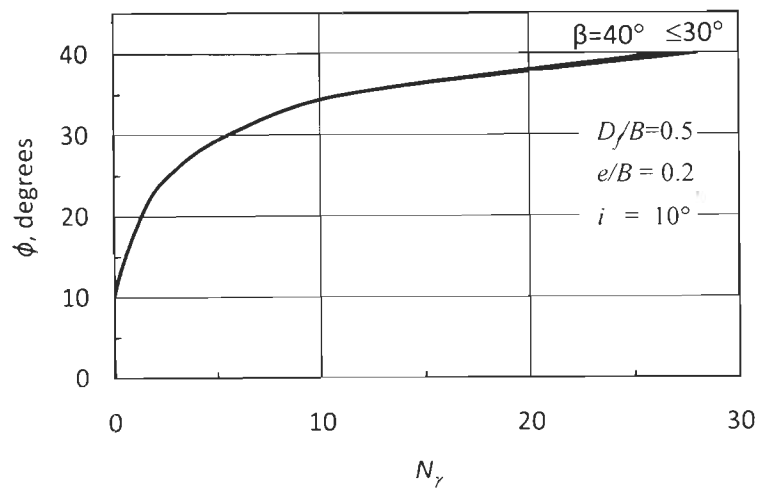

Fig. A.I.2 c (iii) N_γ versus ϕ for D_e/B=2.0

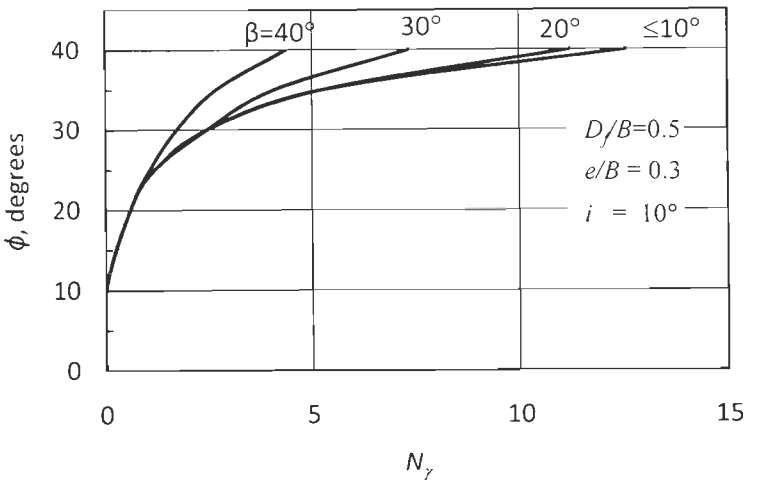

Fig. A.I.2 d (i) N_γ versus ϕ for D_e/B=0

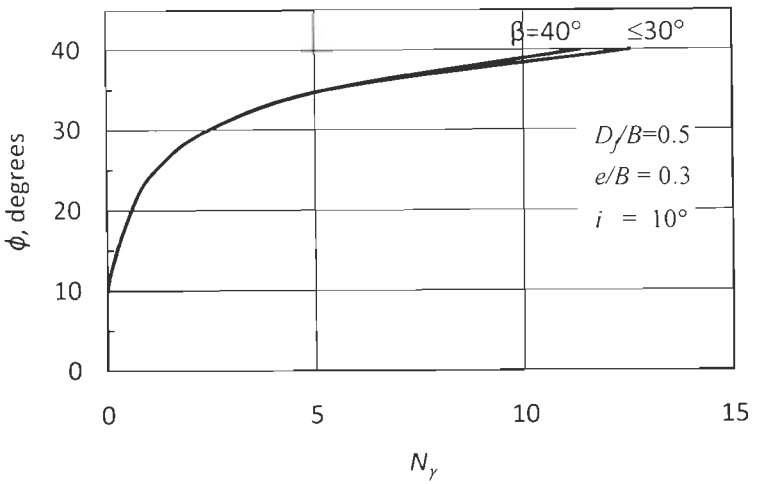

Fig. A.I.2 d (ii) N_γ versus ϕ for D_e/B=1.0

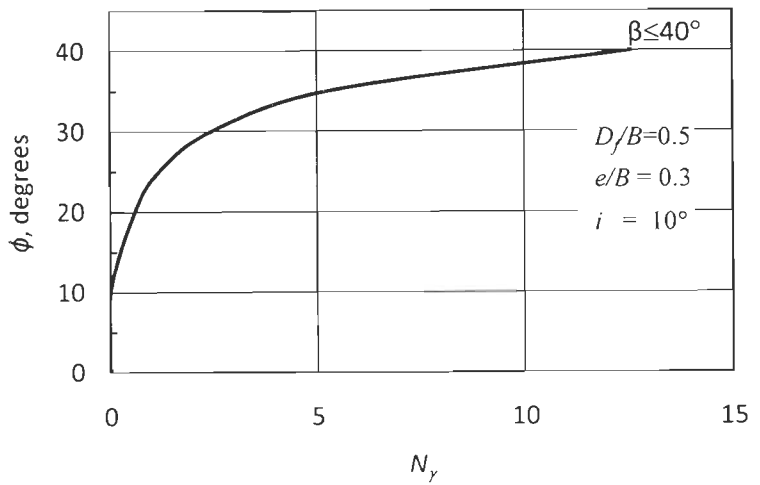

Fig. A.I.2 d (iii) N_γ versus ϕ for D_e/B=2.0

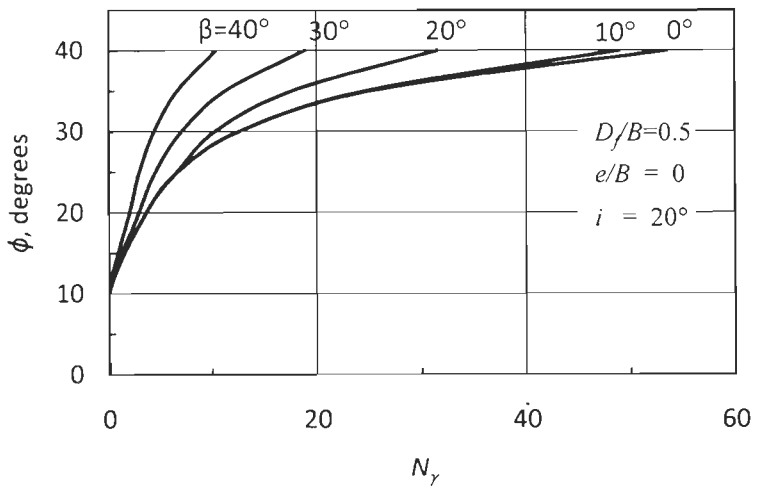

Fig. A.I.3 a (i) N_γ versus ϕ for D_e/B=0

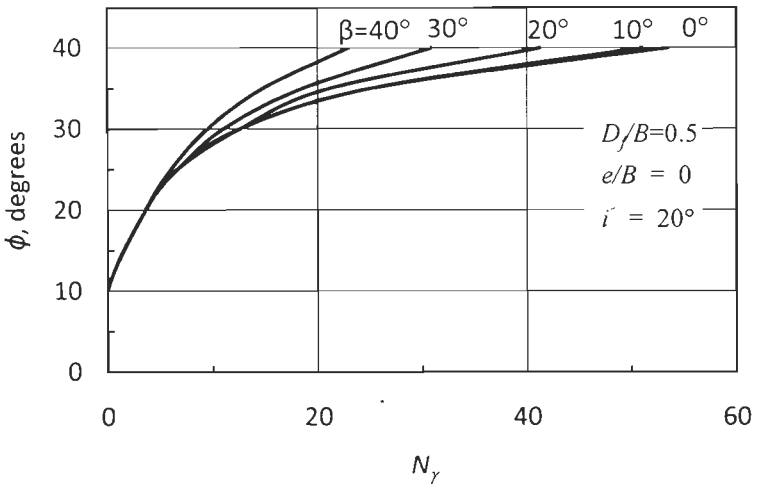

Fig. A.I.3 a (ii) N_γ versus ϕ for D_e/B=1.0

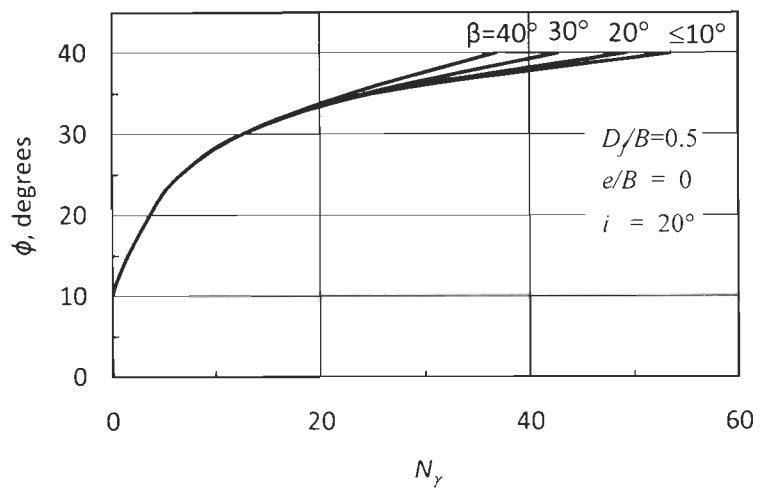

Fig. A.I.3 a (iii) N_γ versus ϕ for D_e/B=2.0

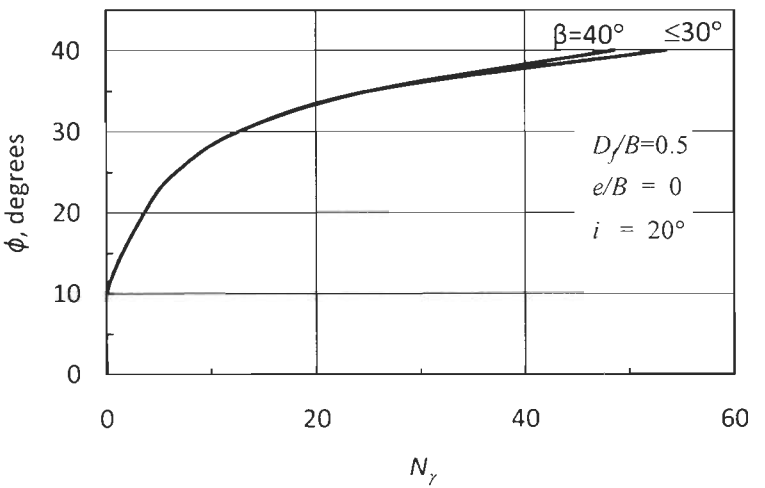

Fig. A.I.3 a (iv) N_γ versus ϕ for D_e/B=3.0

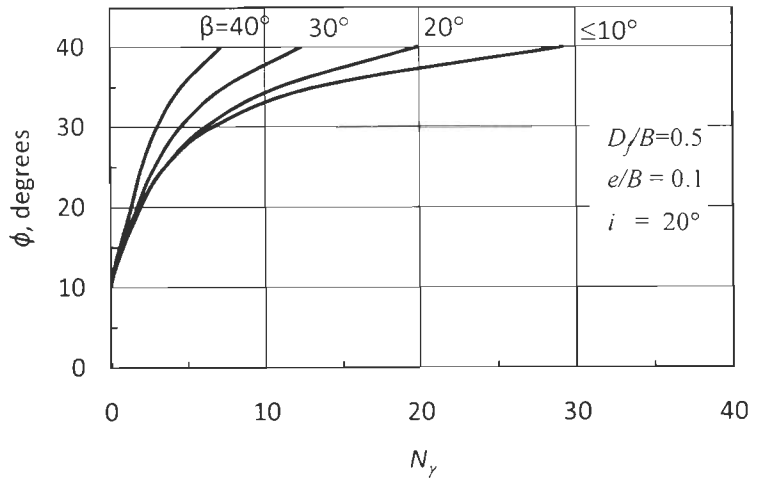

Fig. A.I.3 b (i) N_γ versus ϕ for D_e/B=0

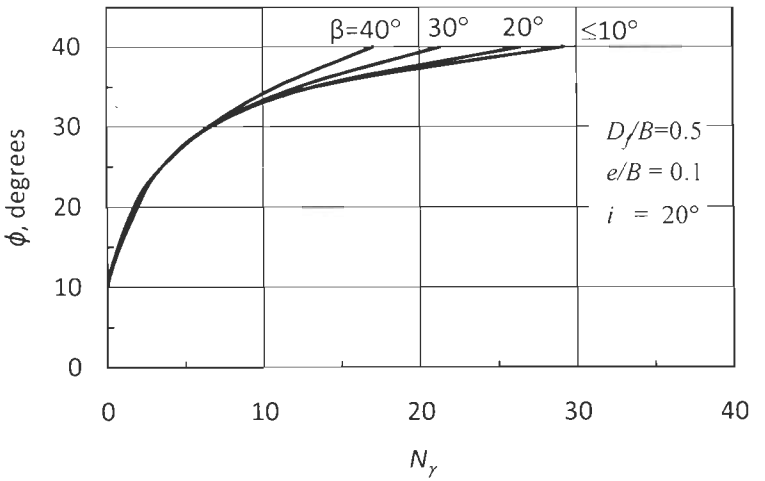

Fig. A.I.3 b (ii) N_γ versus ϕ for D_e/B=1.0

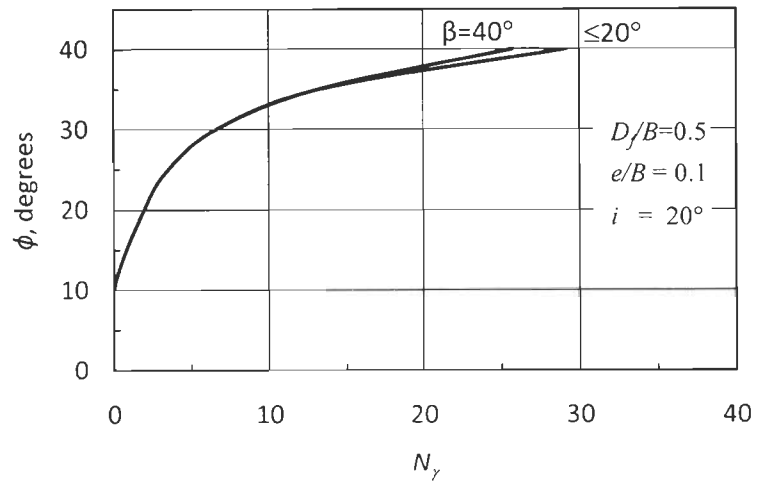

Fig. A.I.3 b (iii) N_γ versus ϕ for D_e/B=2.0

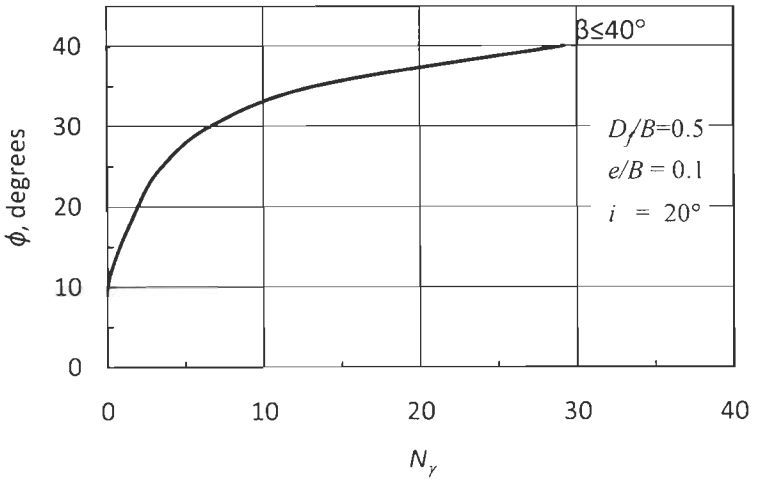

Fig. A.I.3 b (iv) N_γ versus ϕ for D_e/B=3.0

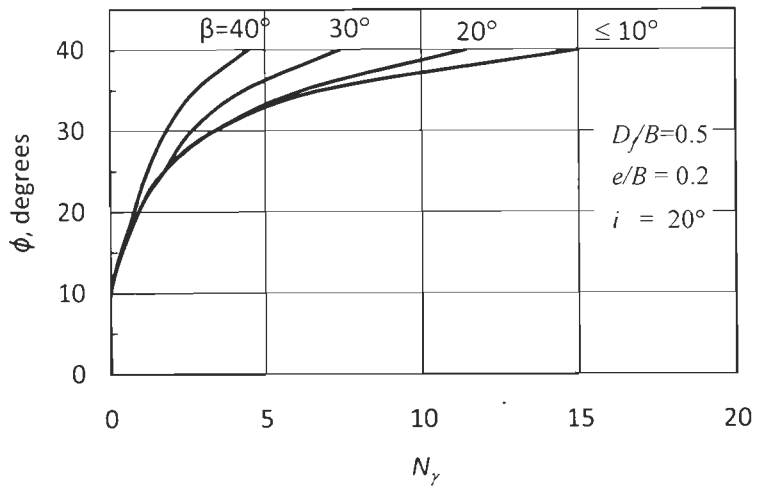

Fig. A.I.3 c (i) N_γ versus ϕ for D_e/B=0

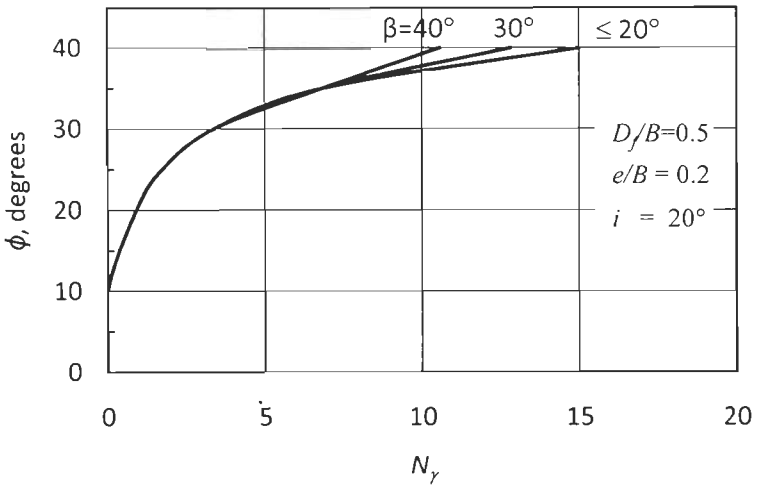

Fig. A.I.3 c (ii) N_γ versus ϕ for D_e/B=1.0

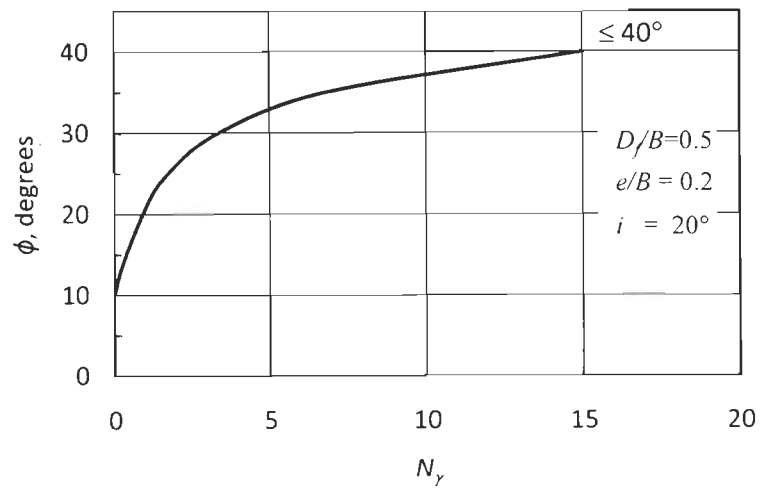

Fig. A.I.3 c (iii) N_γ versus ϕ for D_e/B=2.0

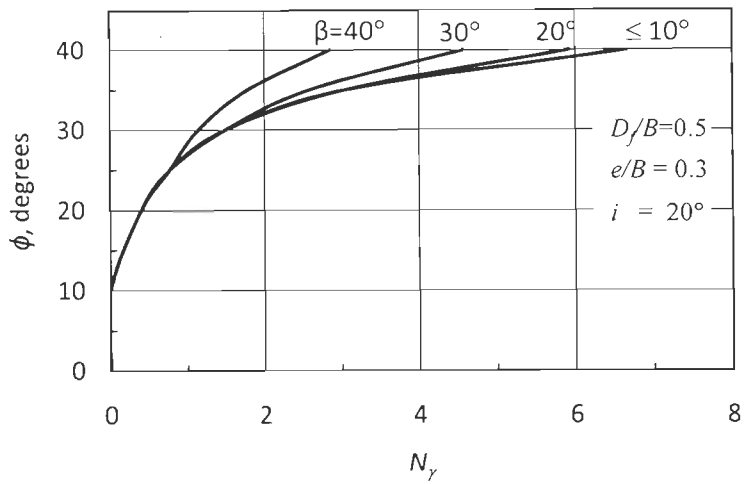

Fig. A.I.3 d (i) N_γ versus ϕ for D_e/B=0

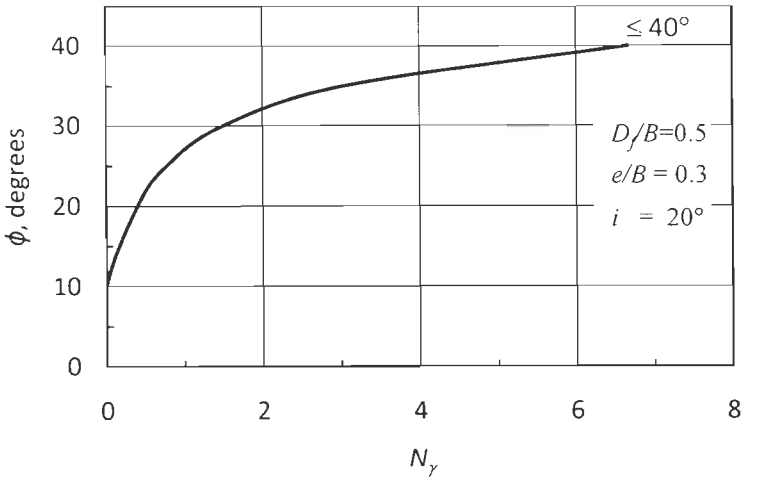

Fig. A.I.3 d (ii) N_γ versus ϕ for D_e/B=1.0

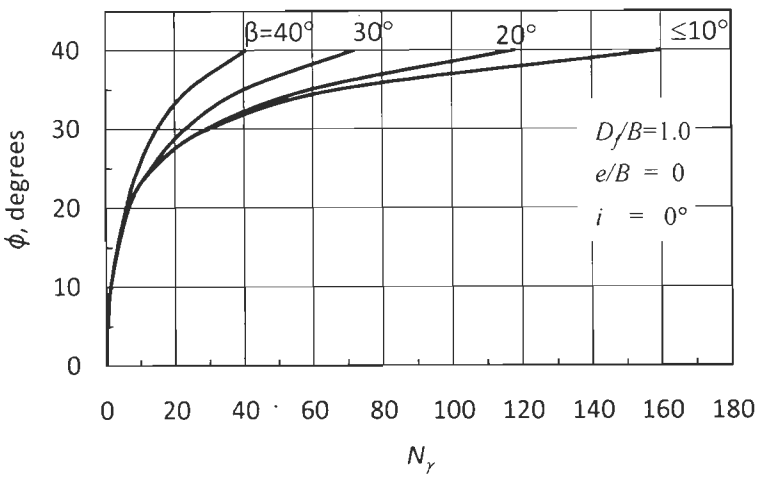

Fig. A.I.4 a (i) N_γ versus ϕ for D_e/B=0

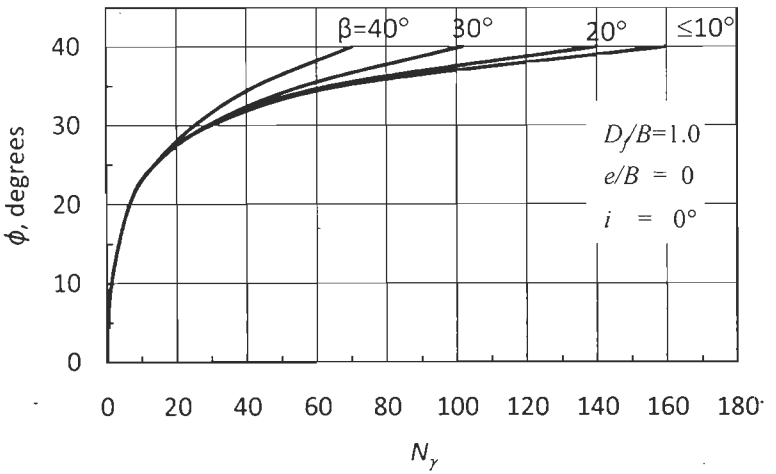

Fig. A.I.4 a (ii) N_γ versus ϕ for D_e/B=1.0

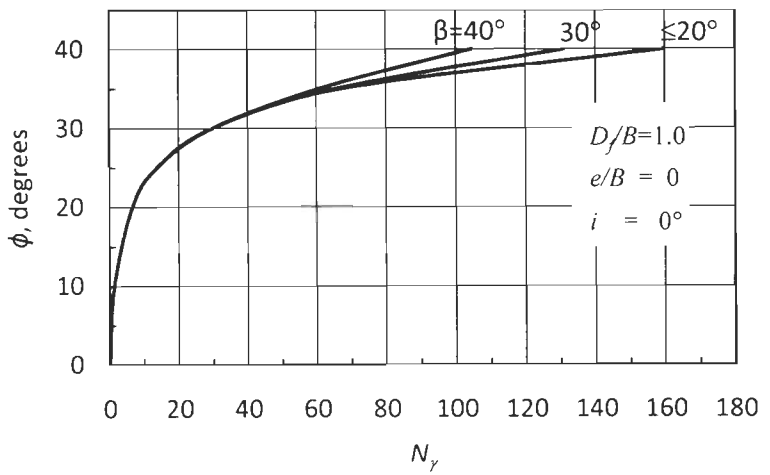

Fig. A.I.4 a (iii) N_γ versus ϕ for D_e/B=2.0

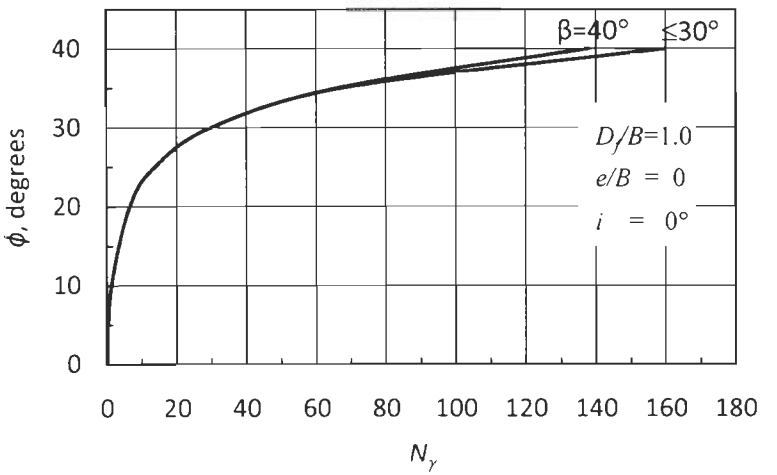

Fig. A.I.4 a (iv) N_γ versus ϕ for D_e/B=3.0

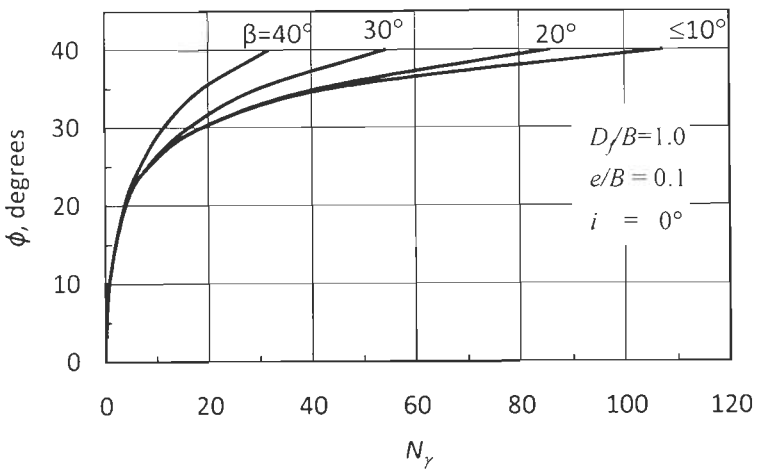

Fig. A.I.4 b (i) N_γ versus ϕ for D_e/B=0

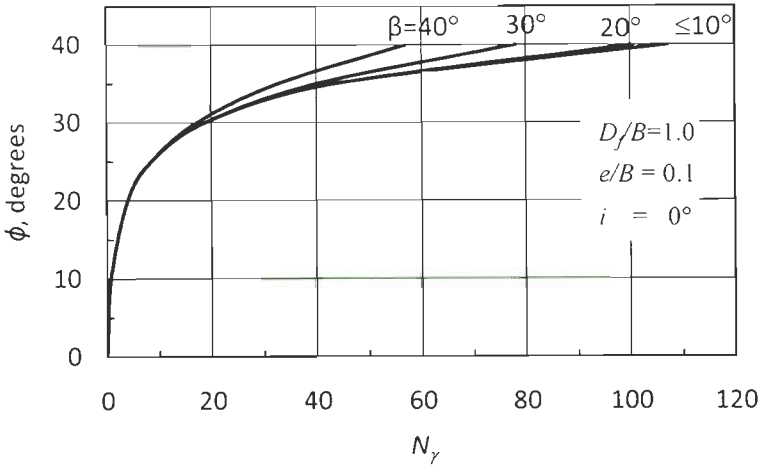

Fig. A.I.4 b (ii) N_γ versus ϕ for D_e/B=1.0

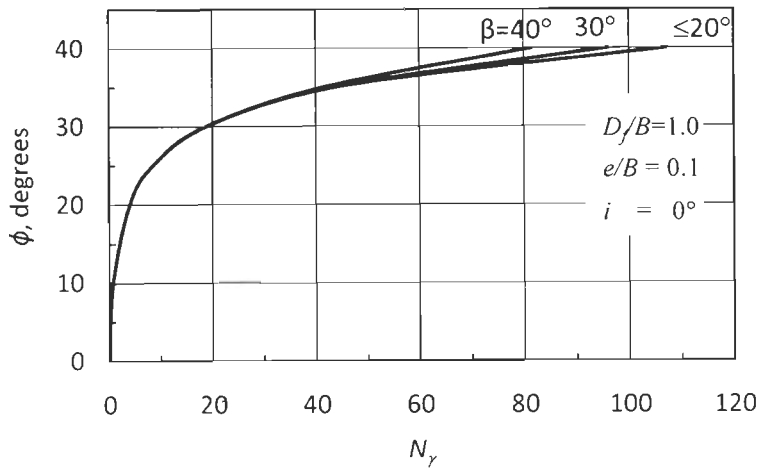

Fig. A.I.4 b (iii) N_γ versus ϕ for D_e/B=2.0

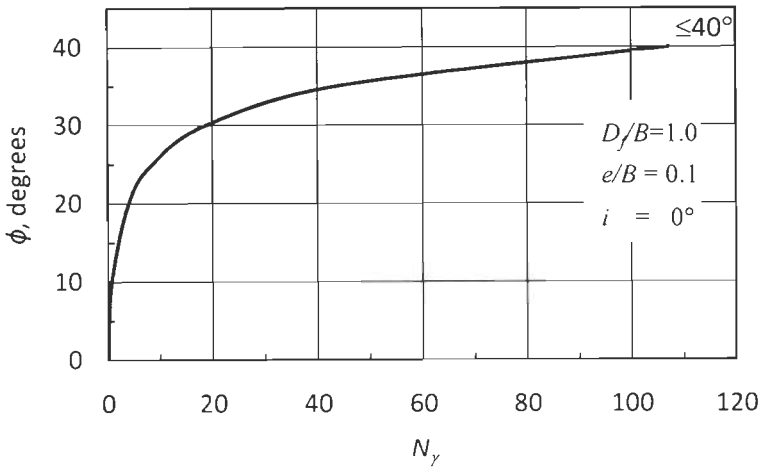

Fig. A.I.4 b (iv) N_γ versus ϕ for D_e/B=3.0

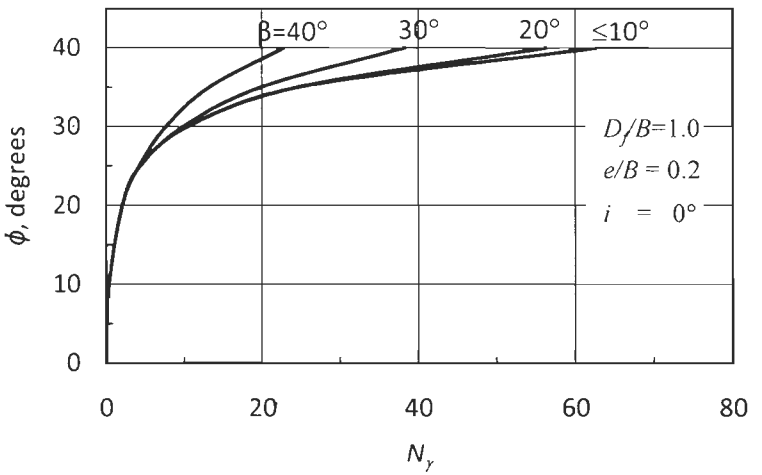

Fig. A.I.4 c (i) N_γ versus ϕ for D_e/B=0

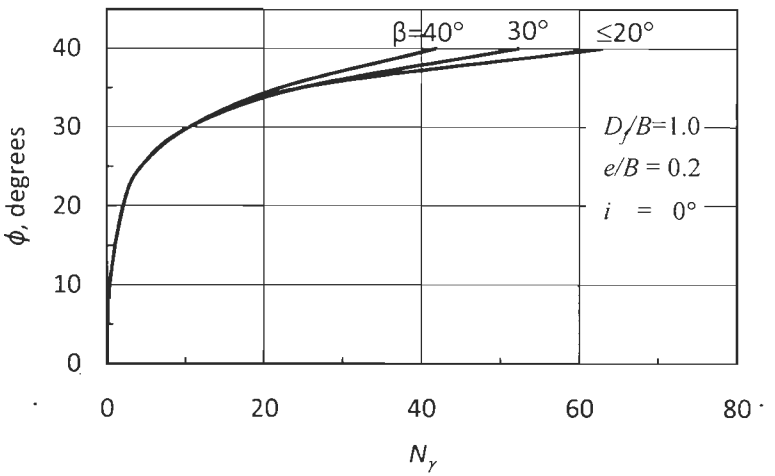

Fig. A.I.4 c (ii) N_γ versus ϕ for D_e/B=1.0

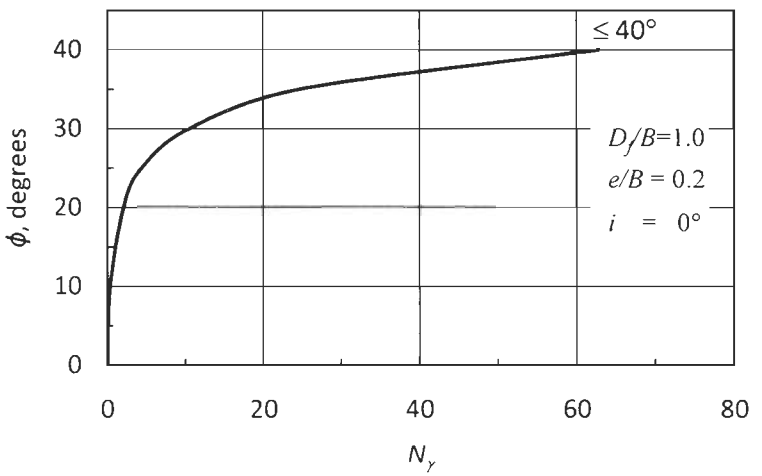

Fig. A.I.4 c (iii) N_γ versus ϕ for D_e/B=2.0

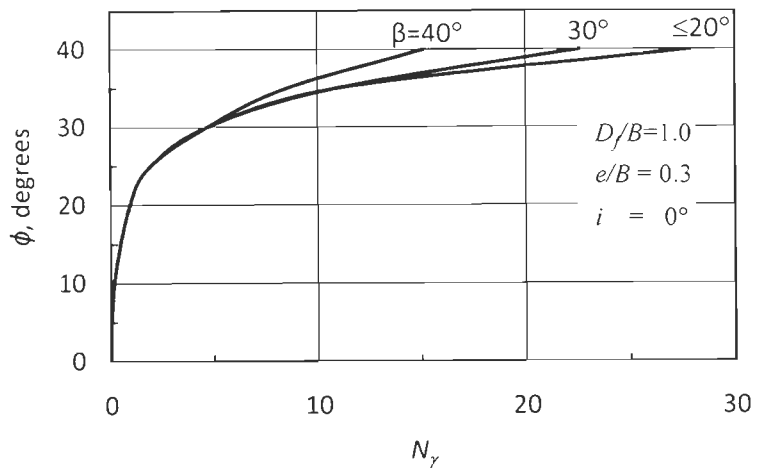

Fig. A.I.4 d (i) N_γ versus ϕ for D_e/B=0

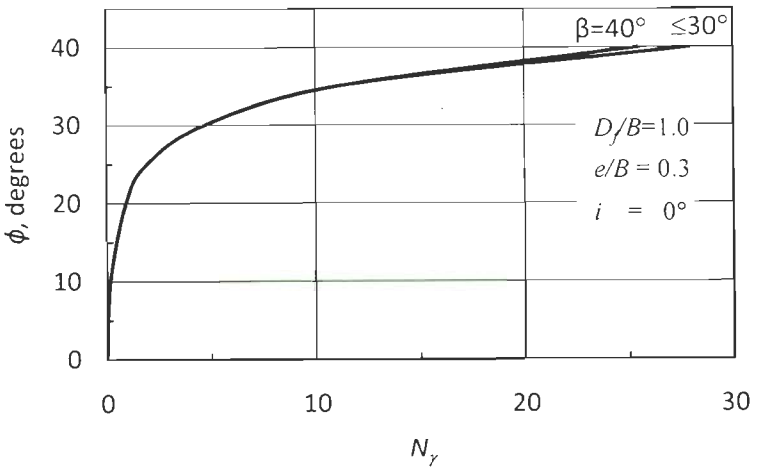

Fig. A.I.4 d (i) N_γ versus ϕ for D_e/B=1.0

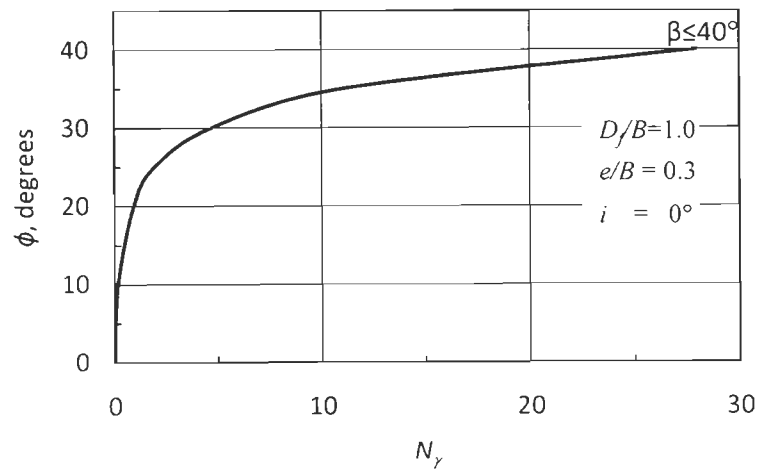

Fig. A.I.4 d (iii) N_γ versus ϕ for D_e/B=2.0

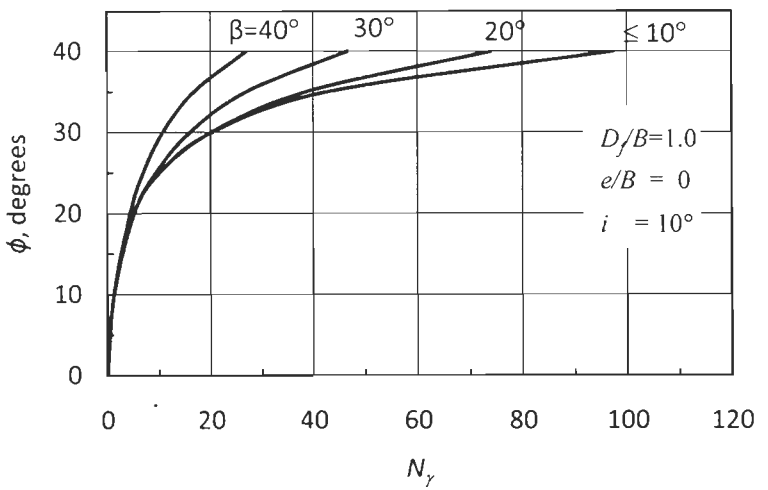

Fig. A.I.5 a (i) N_γ versus ϕ for D_e/B=0

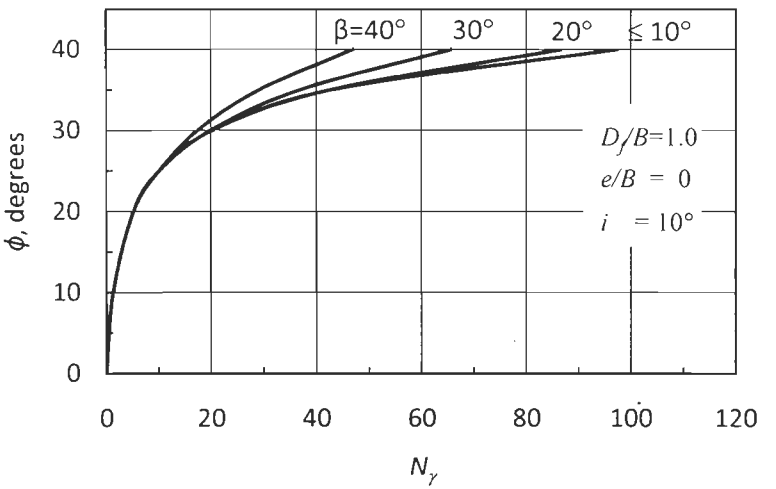

Fig. A.I.5 a (ii) N_γ versus ϕ for D_e/B=1.0

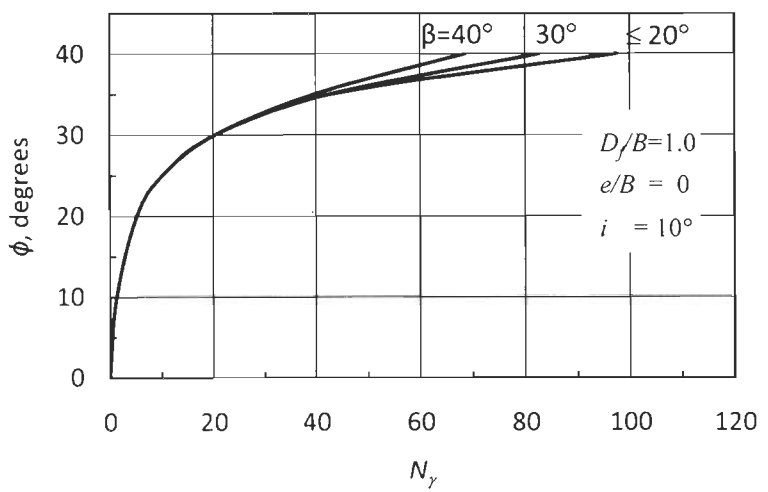

Fig. A.I.5 a (iii) N_γ versus ϕ for D_e/B=2.0

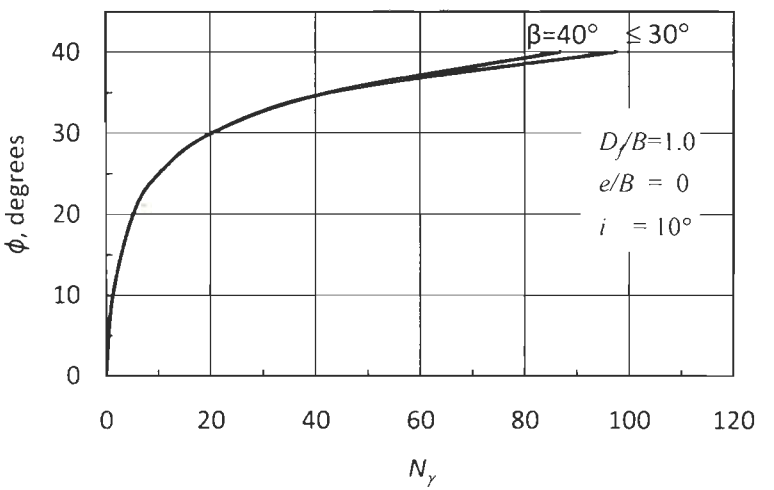

Fig. A.I.5 a (iv) N_γ versus ϕ for D_e/B=3.0

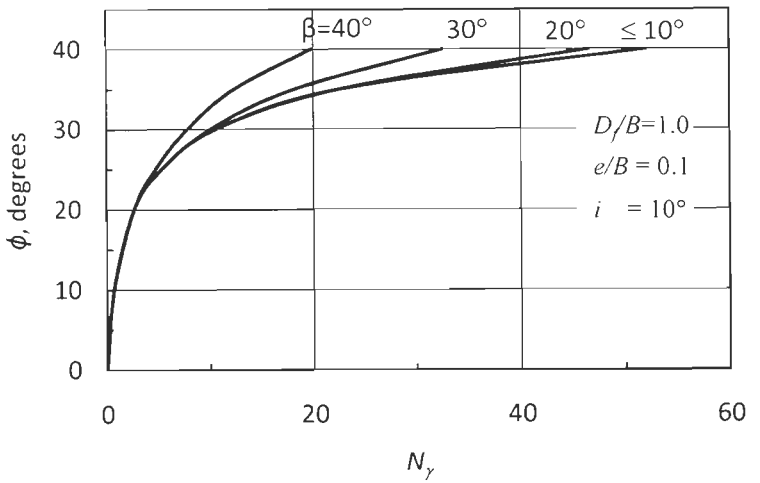

Fig. A.I.5 b (i) N_γ versus ϕ for D_e/B=0

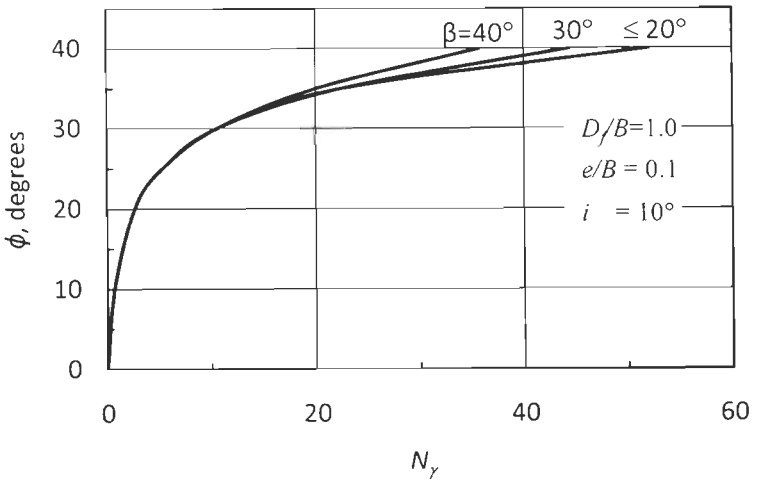

Fig. A.I.5 b (ii) N_γ versus ϕ for D_e/B=1.0

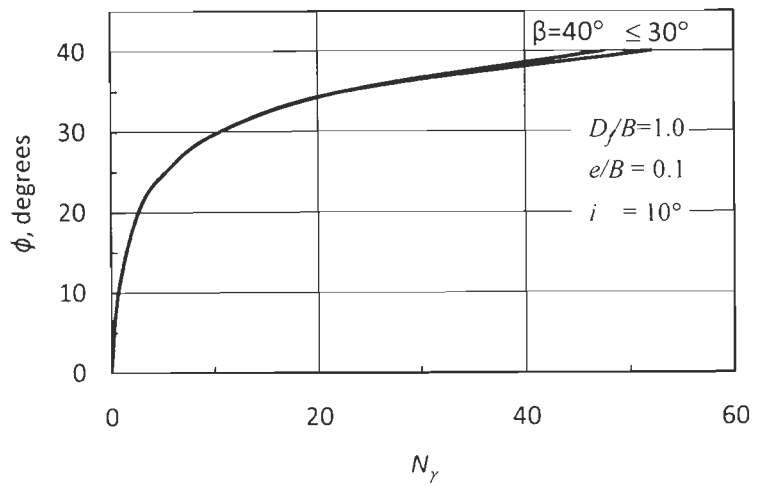

Fig. A.I.5 b (iii) N_γ versus ϕ for D_e/B=2.0

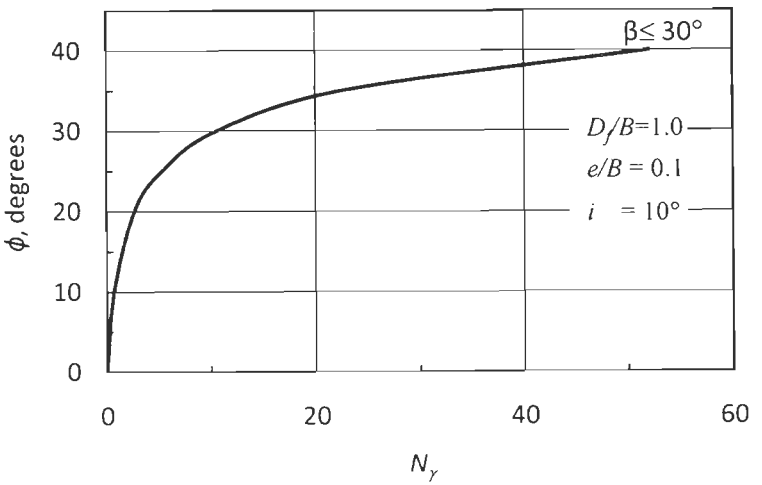

Fig. A.I.5 b (iv) N_γ versus ϕ for D_e/B=3.0

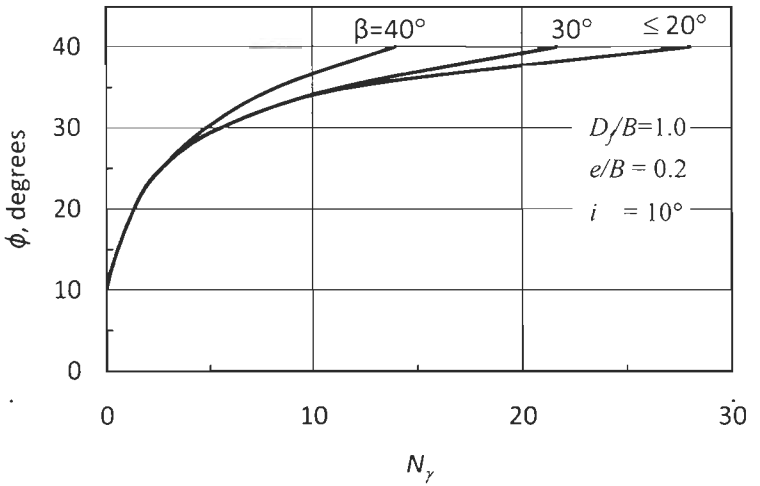

Fig. A.I.5 c (i) N_γ versus ϕ for D_e/B=0

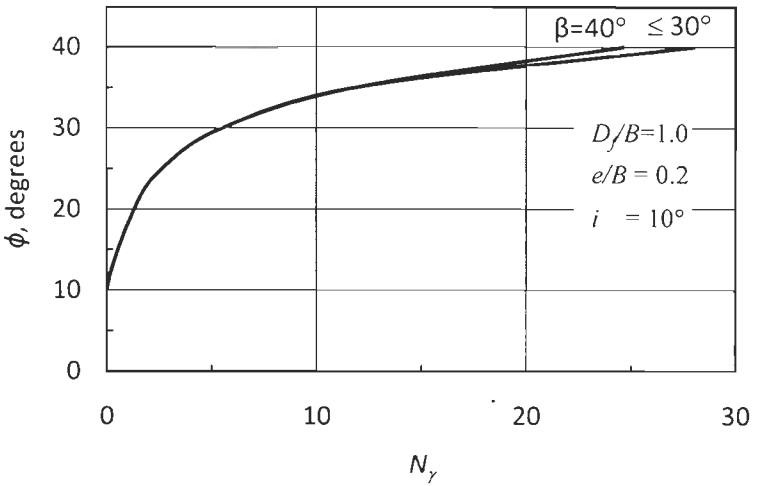

Fig. A.I.5 c (ii) N_γ versus ϕ for D_e/B=1.0

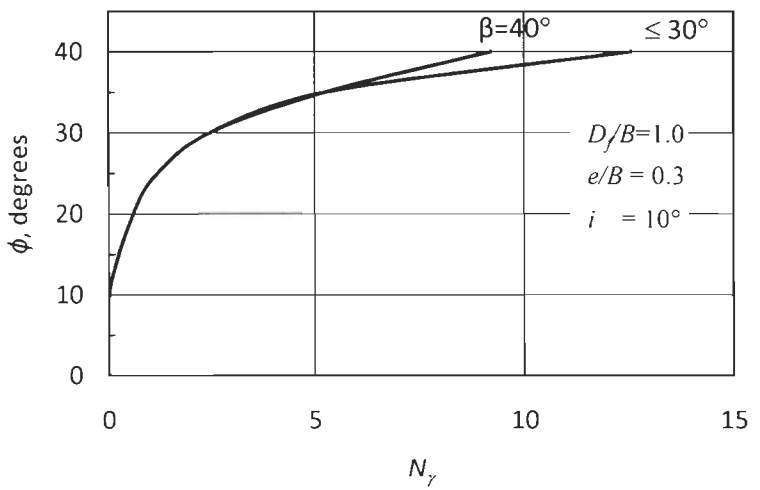

Fig. A.I.5 d (i) N_γ versus ϕ for D_e/B=2.0

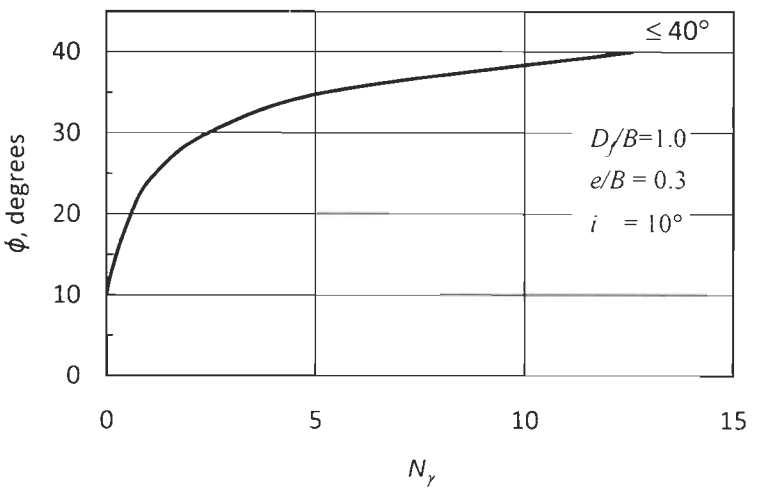

Fig. A.I.5 d (ii) N_γ versus ϕ for D_e/B=3.0

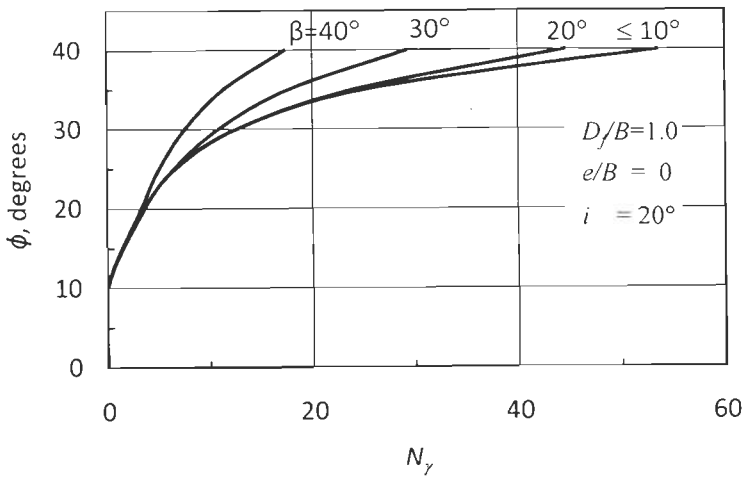

Fig. A.I.6 a (i) N_γ versus ϕ for D_e/B=0

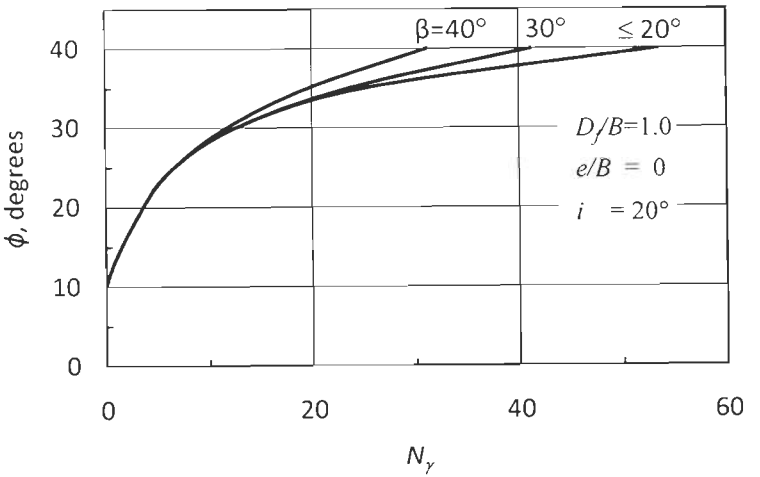

Fig. A.I.6 a (ii) N_γ versus ϕ for D_e/B=1.0

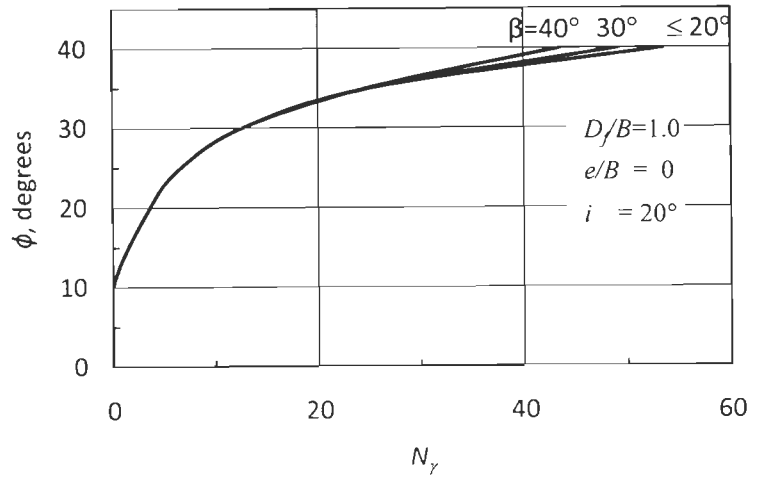

Fig. A.I.6 a (iii) N_γ versus ϕ for D_e/B=2.0

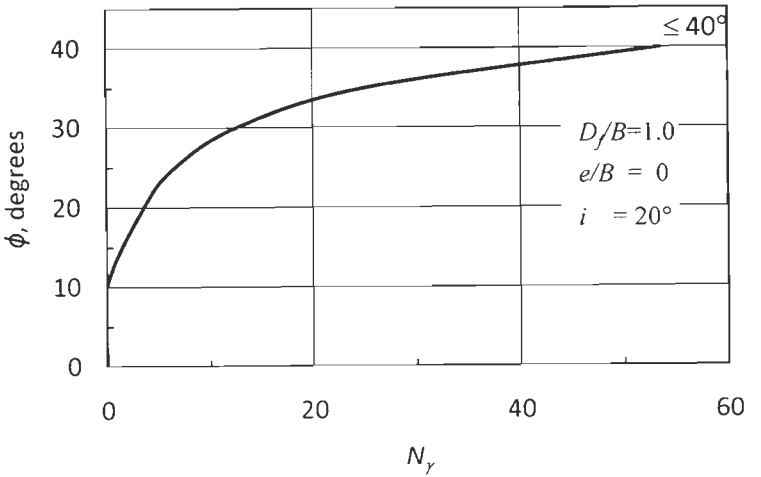

Fig. A.I.6 a (iv) N_γ versus ϕ for D_e/B=3.0

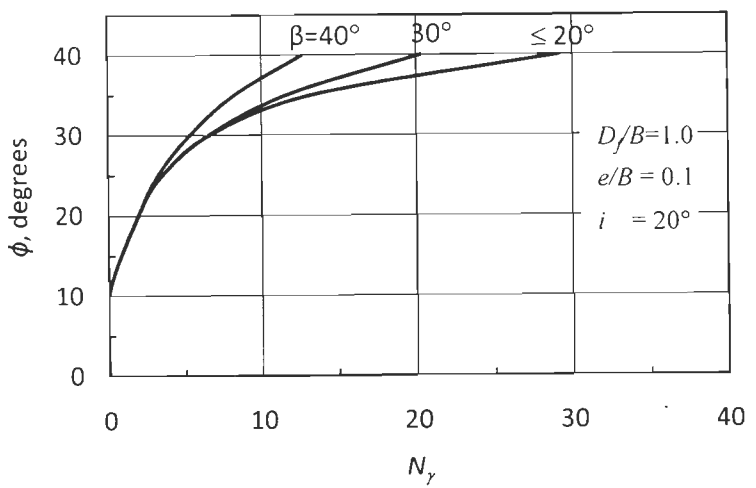

Fig. A.I.6 b (i) N_γ versus ϕ for D_e/B=0

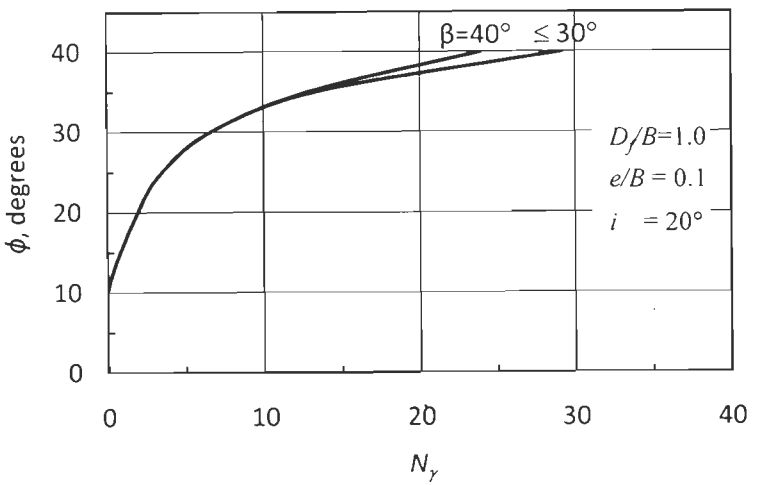

Fig. A.I.6 b (ii) N_γ versus ϕ for D_e/B=1.0

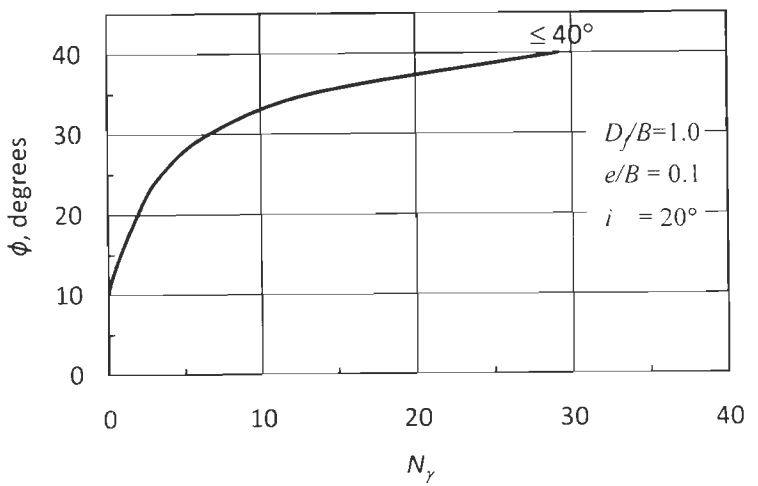

Fig. A.I.6 b (iii) N_γ versus ϕ for D_e/B=2.0

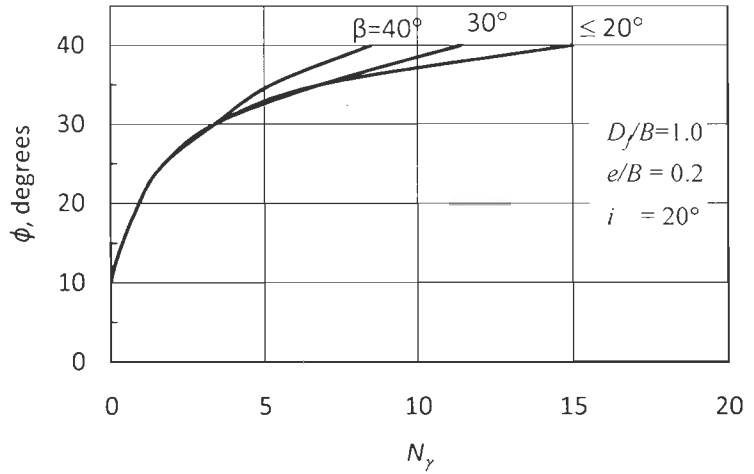

Fig. A.I.6 c (i) N_γ versus ϕ for D_e/B=0

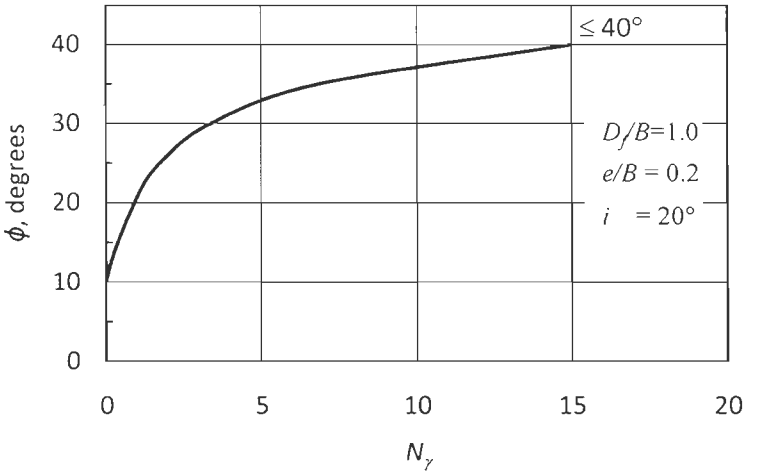

Fig. A.I.6 c (ii) N_γ versus ϕ for D_e/B=1.0

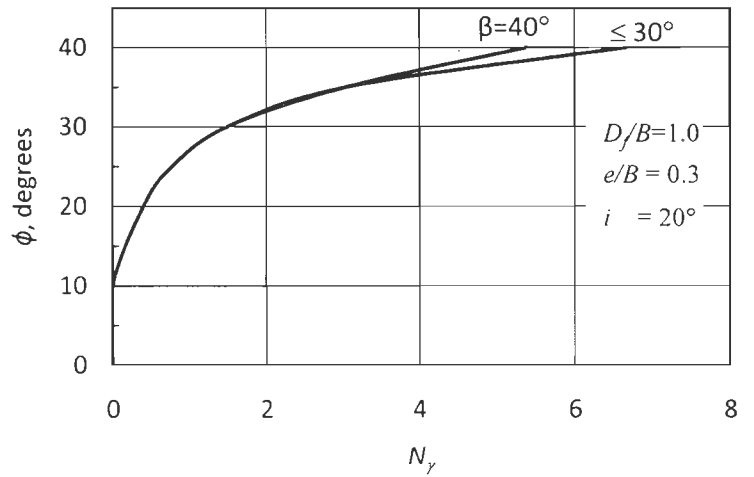

Fig. A.I.6 d (i) N_γ versus ϕ for D_e/B=0

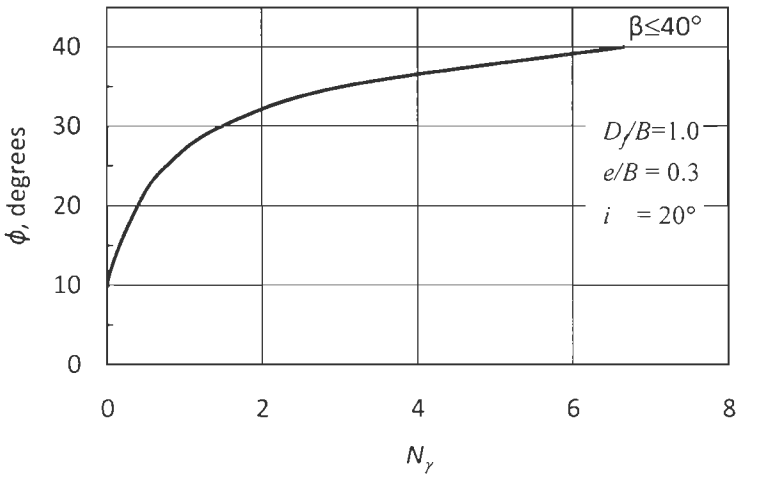

Fig. A.I.6 d (ii) N_γ versus ϕ for D_e/B=1.0

Appendix- II

N_q CHARTS

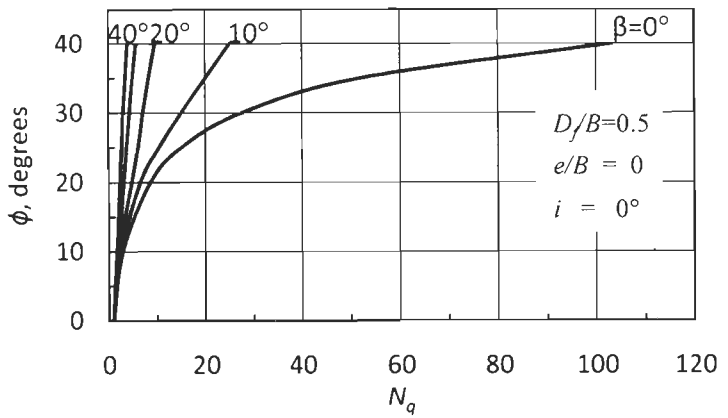

Fig. A.II. 1 a (i) N_q versus ϕ for D_e/B=0

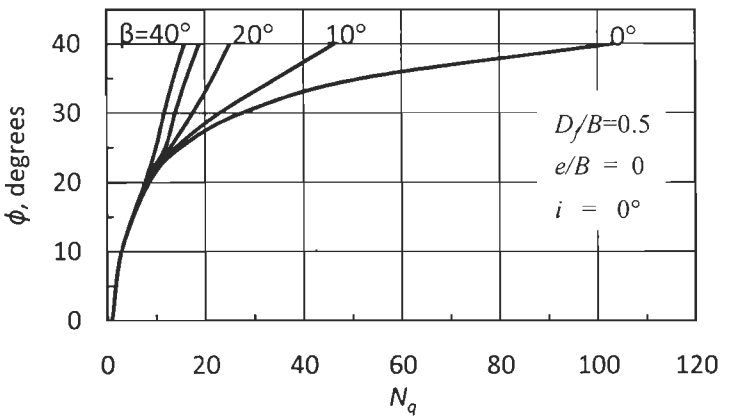

Fig. A.II. 1 a (ii) N_q versus ϕ for D_e/B=1.0

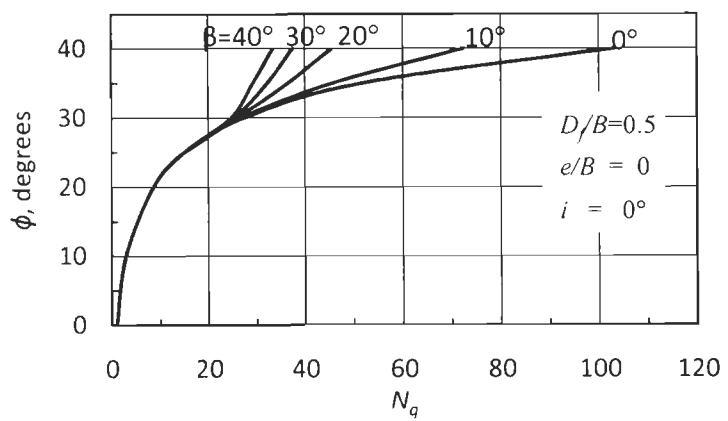

Fig. A.II. 1 a (iii) N_q versus ϕ for D_e/B=2.0

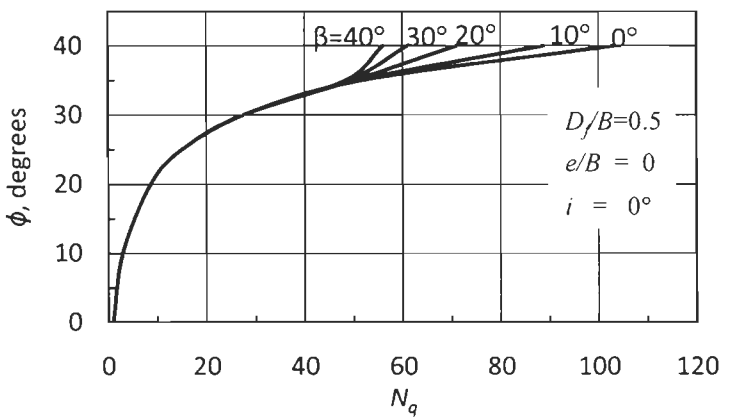

Fig. A.II. 1 a (iv) N_q versus ϕ for D_e/B=3.0

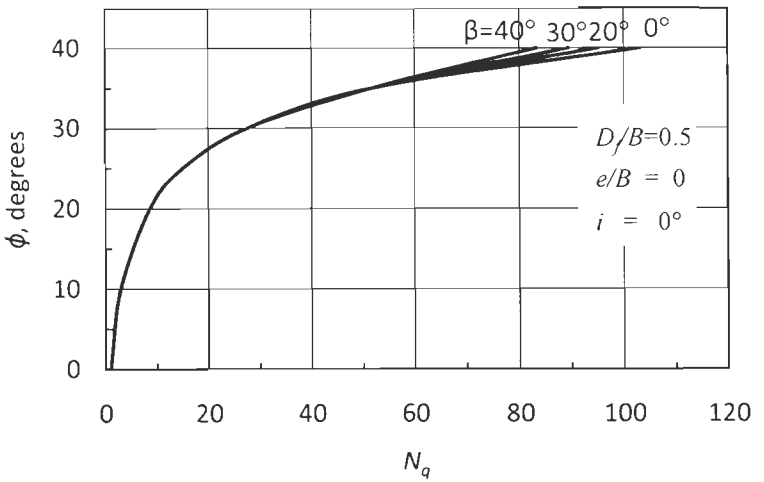

Fig. A.II. 1 a (v) N_q versus ϕ for D_e/B=4.0

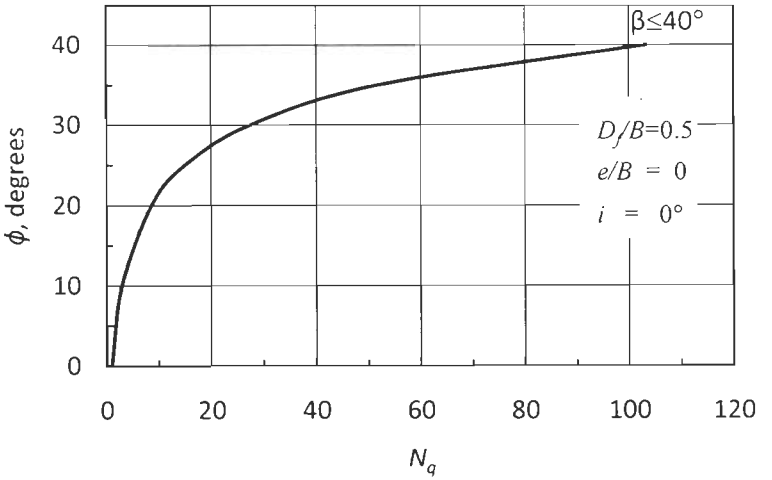

A.II. 1 a (vi) N_q versus ϕ for D_e/B=5.0

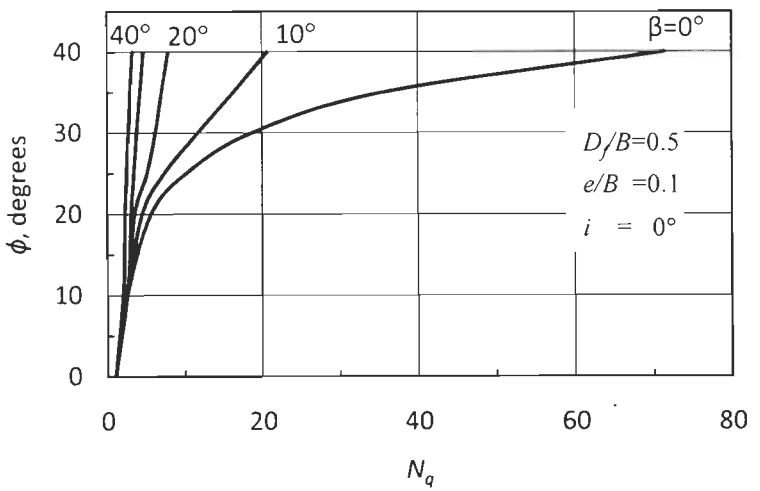

Fig. A.II. 1 b (i) N_q versus ϕ for D_e/B=0

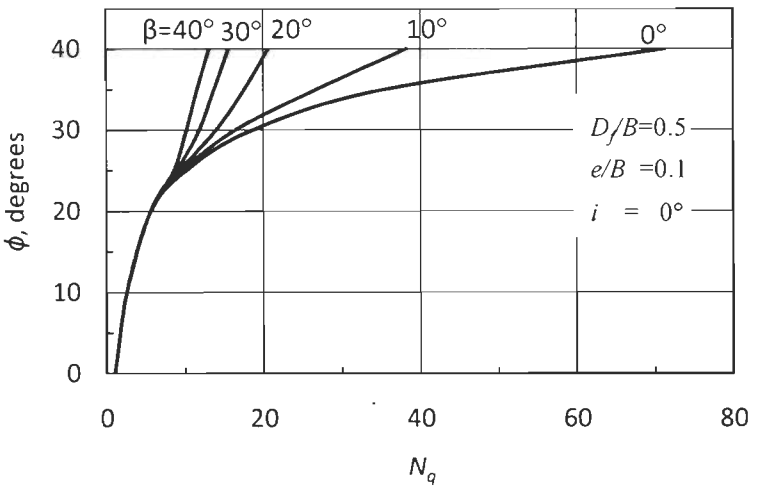

Fig. A.II. 1 b (ii) N_q versus ϕ for D_e/B=1.0

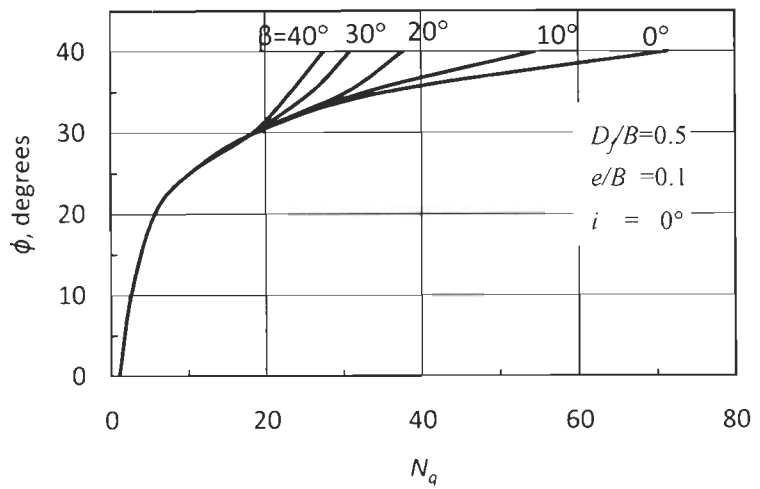

Fig. A.II. 1 b (iii) N_q versus ϕ for D_e/B=2.0

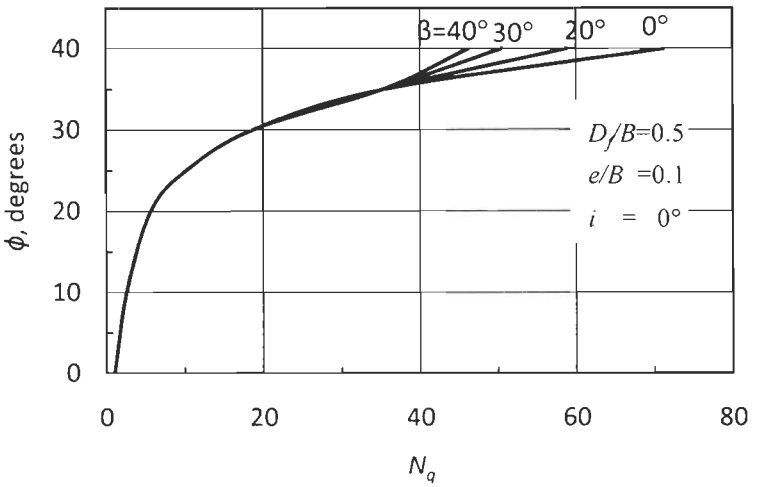

Fig. A.II. 1 b (iv) N_q versus ϕ for D_e/B=3.0

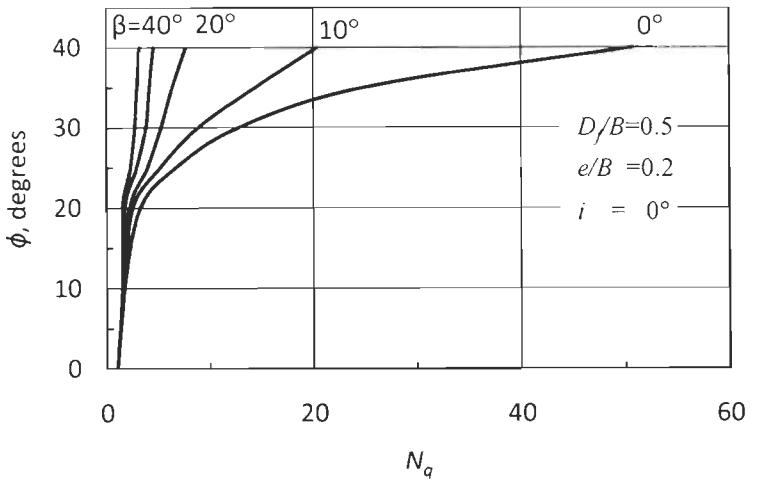

Fig. A.II. 1 c (i) N_q versus ϕ for D_e/B=0

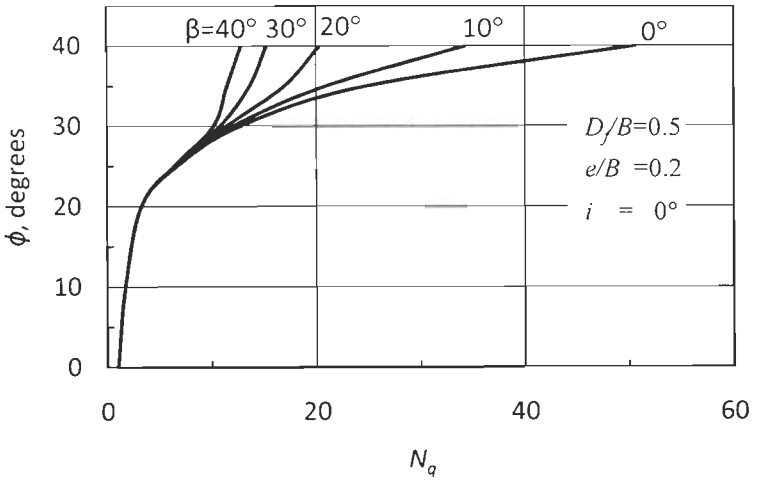

Fig. A.II. 1 c (ii) N_q versus ϕ for D_e/B=1.0

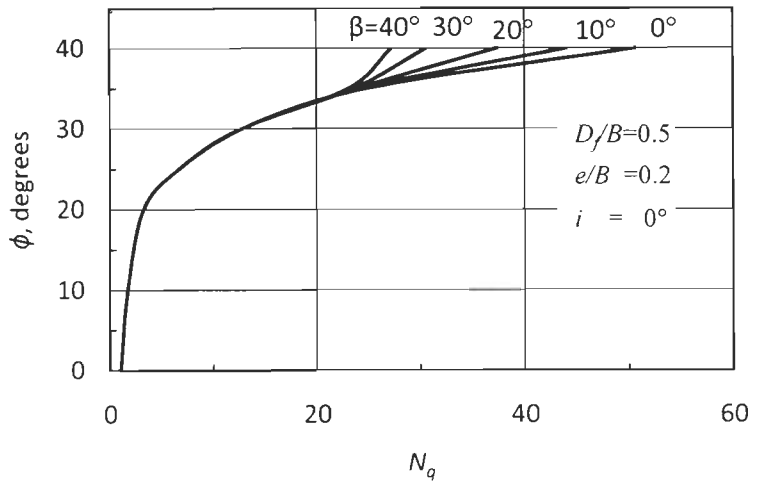

Fig. A.II. 1 c (iii) N_q versus ϕ for D_e/B=2.0

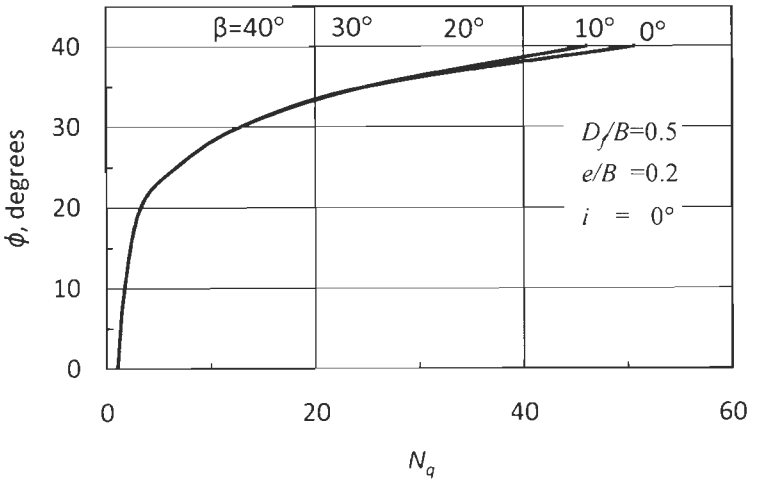

Fig. A.II. 1 c (iv) N_q versus ϕ for D_e/B=3.0

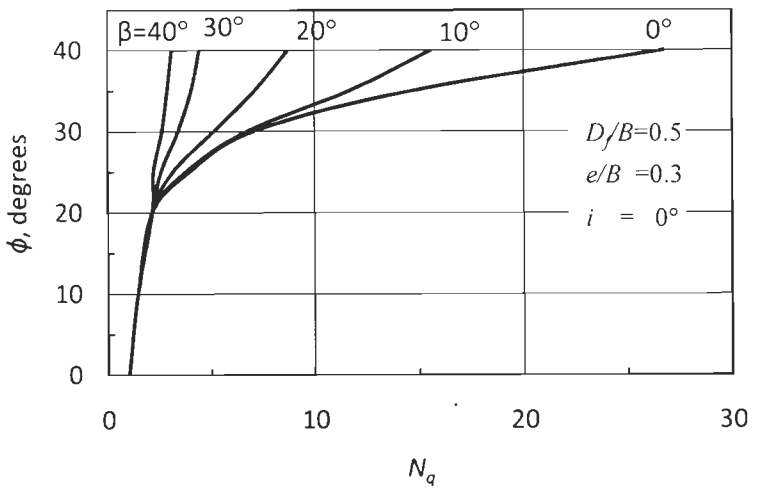

Fig. A.II. 1 d (i) N_q versus ϕ for D_e/B=0

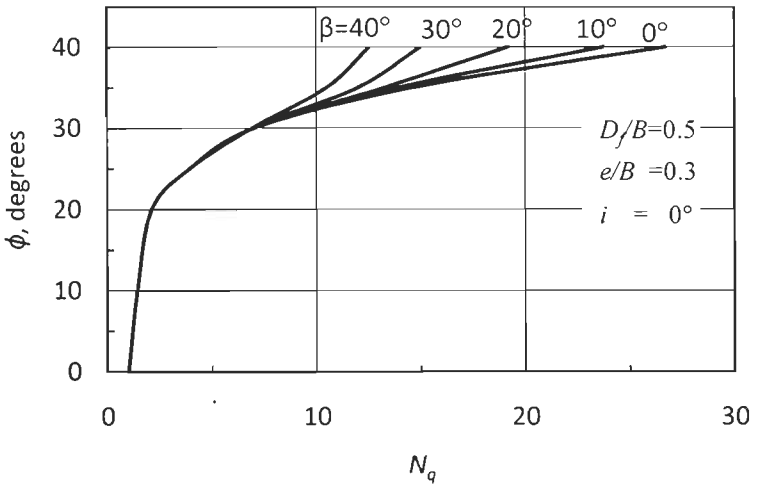

Fig. A.II. 1 d (ii) N_q versus ϕ for D_e/B=1.0

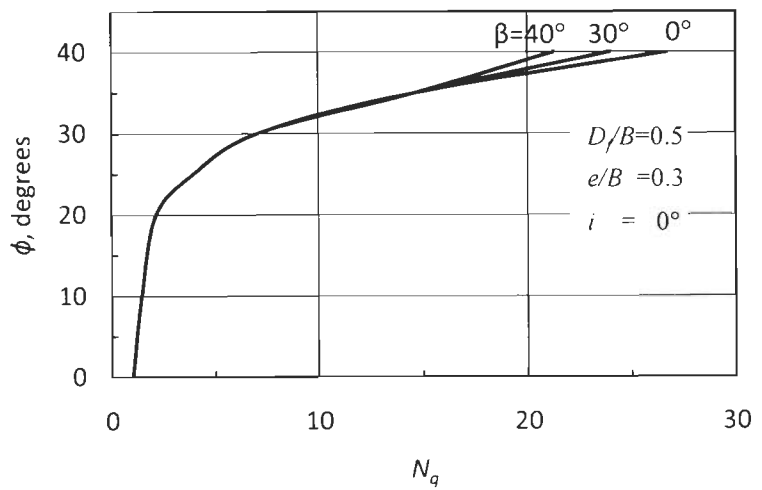

Fig. A.II. 1 d (iii) N_q versus ϕ for D_e/B=2.0

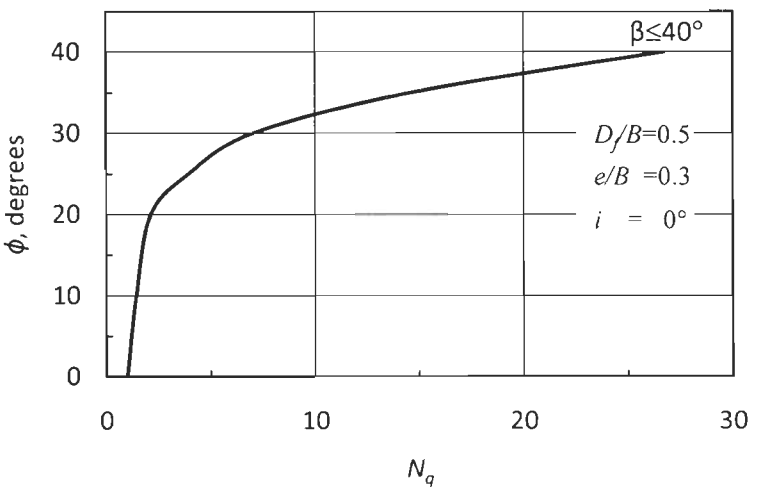

Fig. A.II. 1 d (iv) N_q versus ϕ for D_e/B=3.0

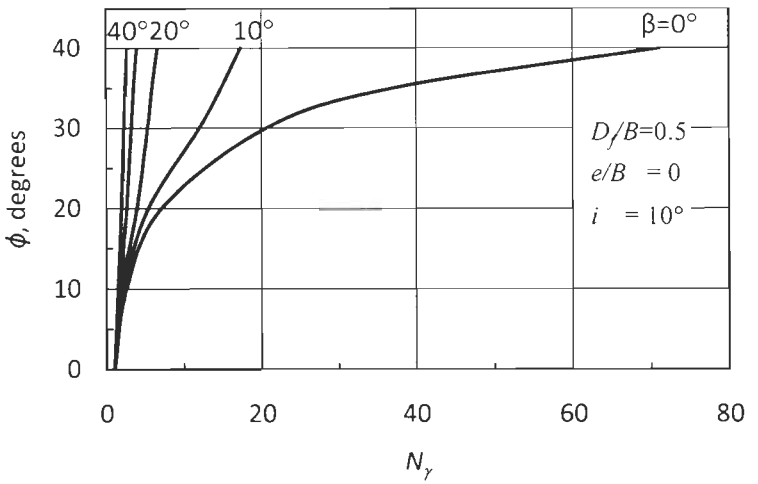

Fig. A.II. 2 a (i) N_q versus ϕ for D_e/B=0

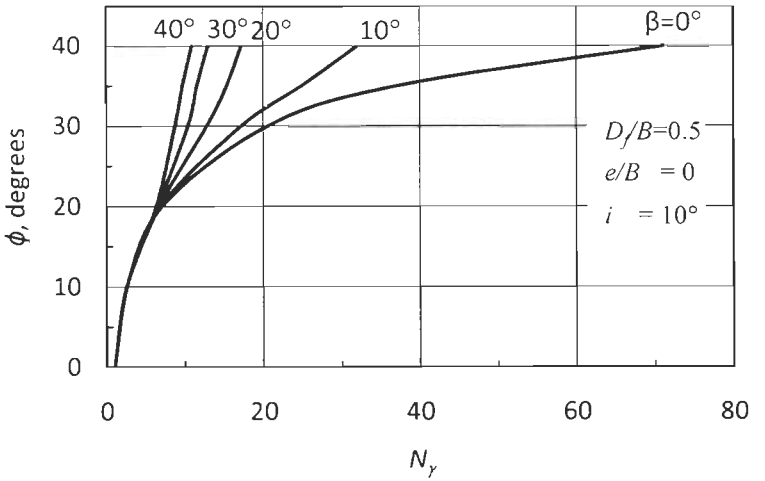

Fig. A.II. 2 a (ii) N_q versus ϕ for D_e/B=1.0

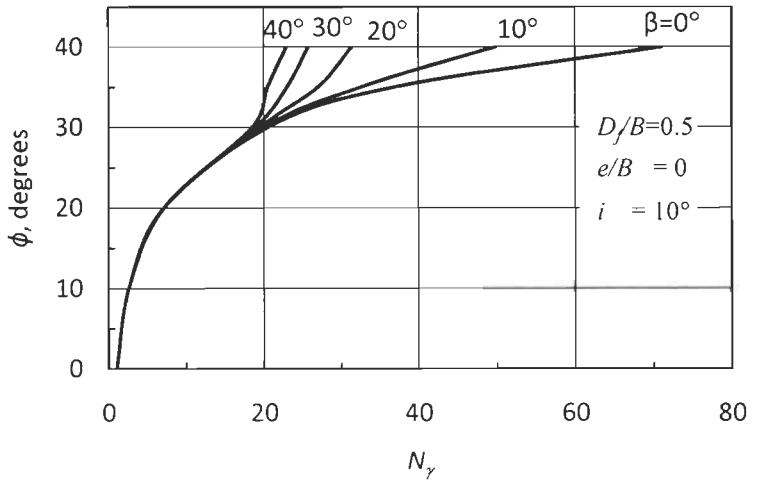

Fig. A.II. 2 a (iii) N_q versus ϕ for D_e/B=2.0

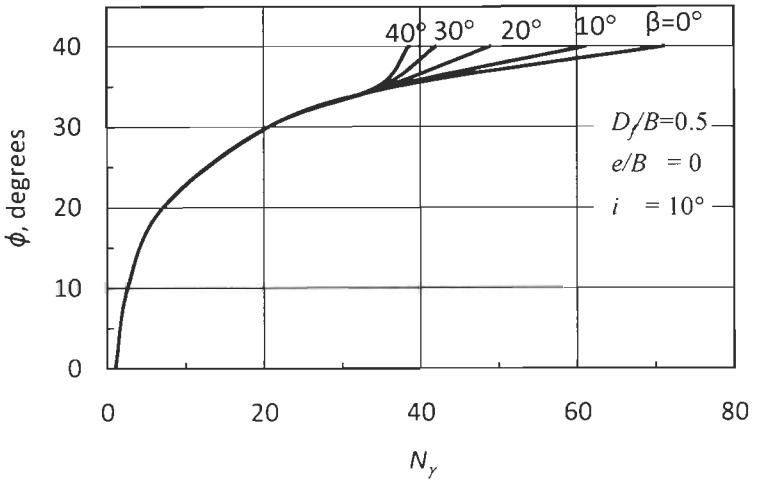

Fig. A.II. 2 a (iv) N_q versus ϕ for D_e/B=3.0

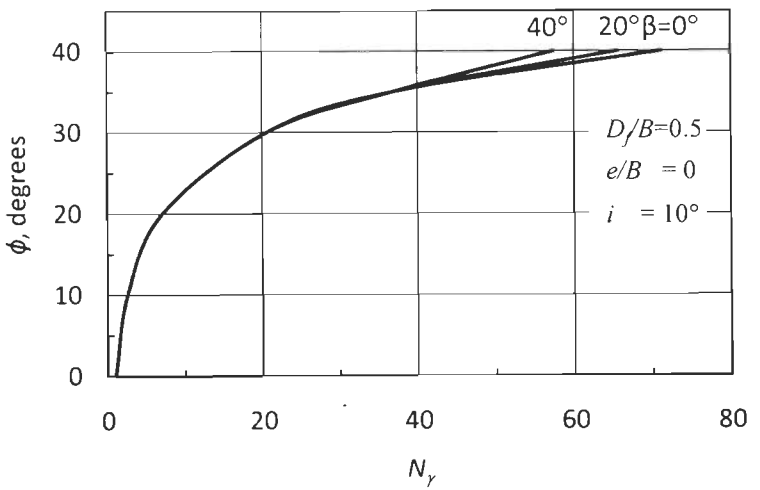

Fig. A.II. 2 a (v) N_q versus ϕ for D_e/B=4.0

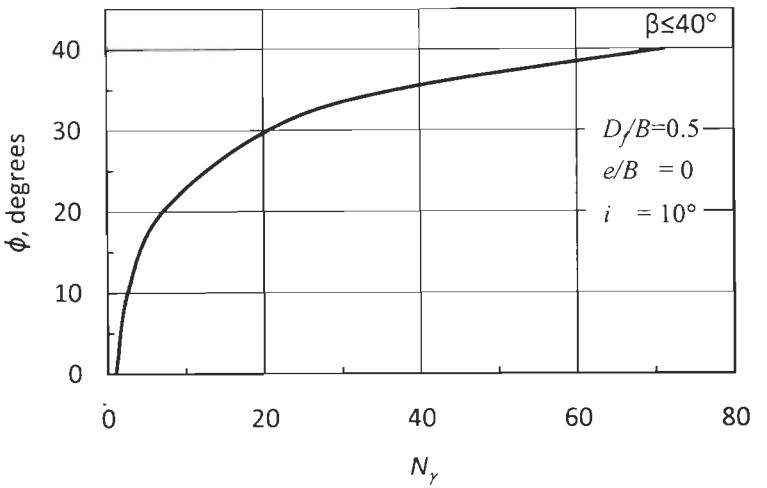

Fig. A.II. 2 a (vi) N_q versus ϕ for D_e/B=5.0

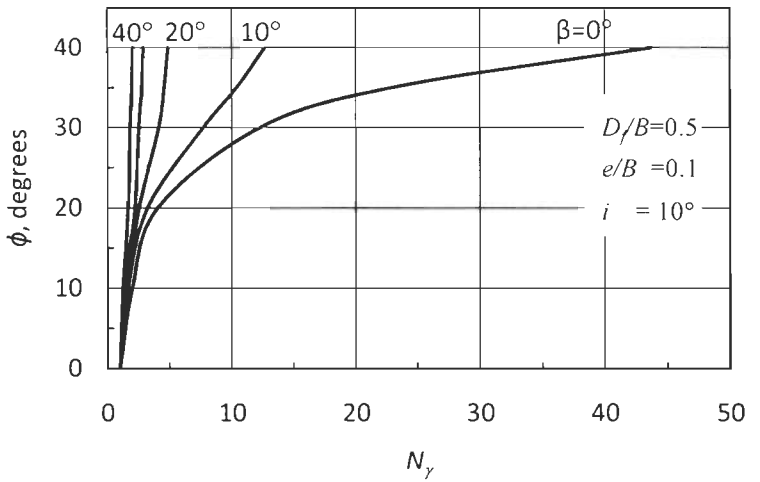

Fig. A.II. 2 b (i) N_q versus ϕ for D_e/B=0

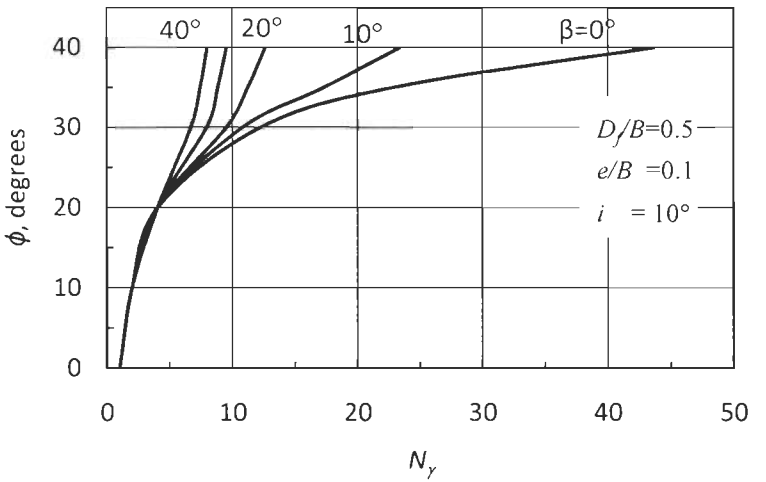

Fig. A.II. 2 b (ii) N_q versus ϕ for D_e/B=1.0

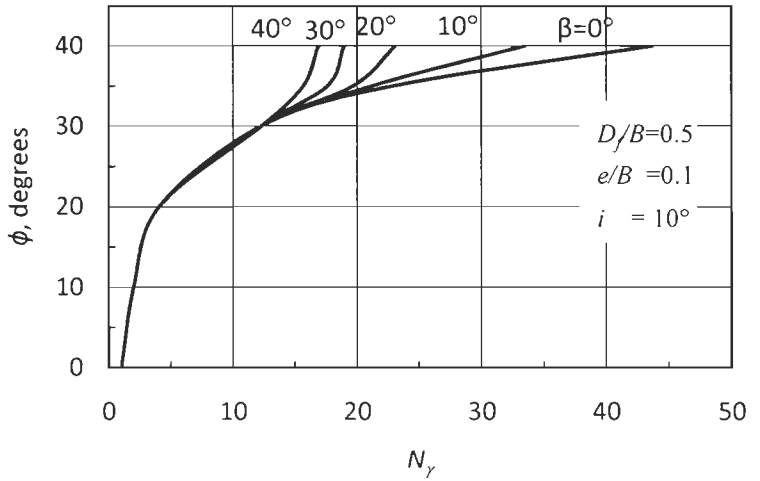

Fig. A.II. 2 b (iii) N_q versus ϕ for D_e/B=2.0

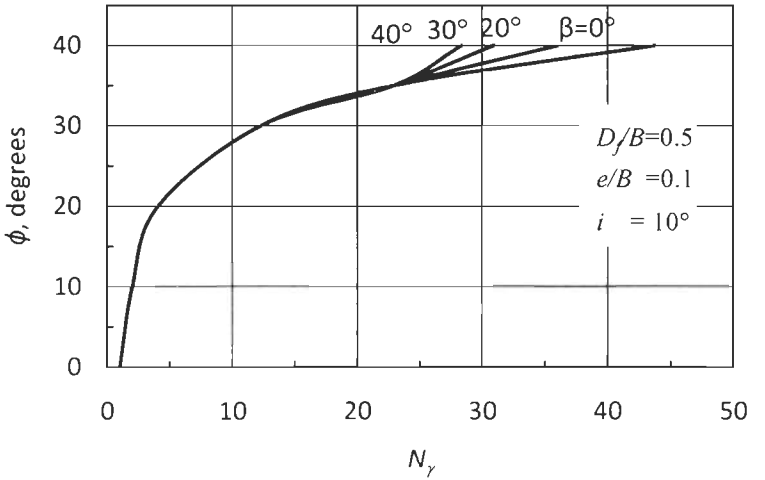

Fig. A.II. 2 b (iv) N_q versus ϕ for D_e/B=3.0

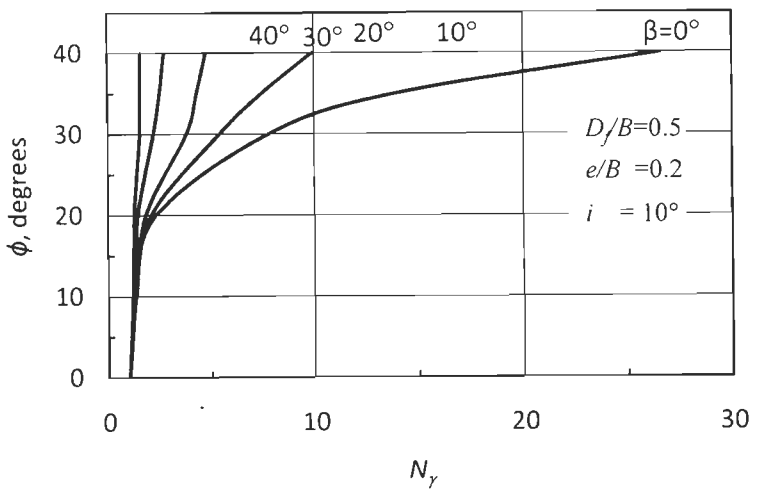

Fig. A.II. 2 c (i) N_q versus ϕ for D_e/B=0

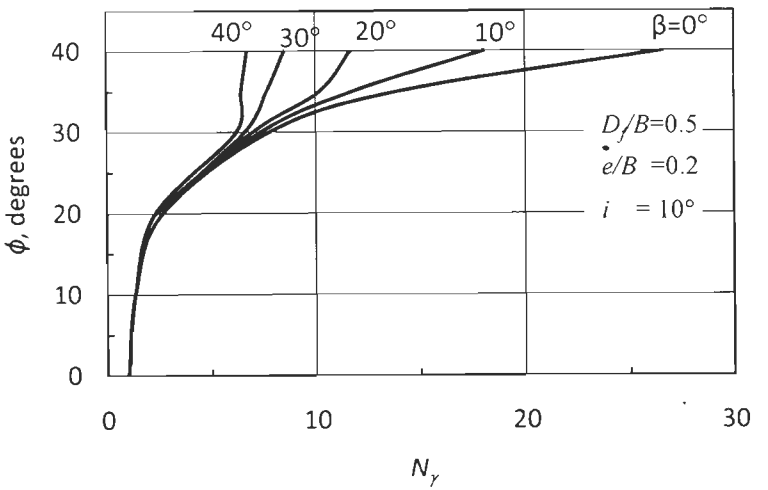

Fig. A.II. 2 c (ii) N_q versus ϕ for D_e/B=1.0

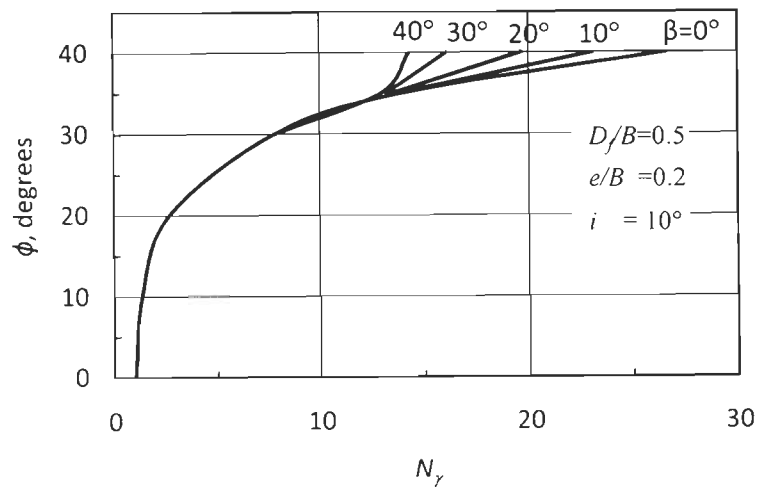

Fig. A.II. 2 c (iii) N_q versus ϕ for D_e/B=2.0

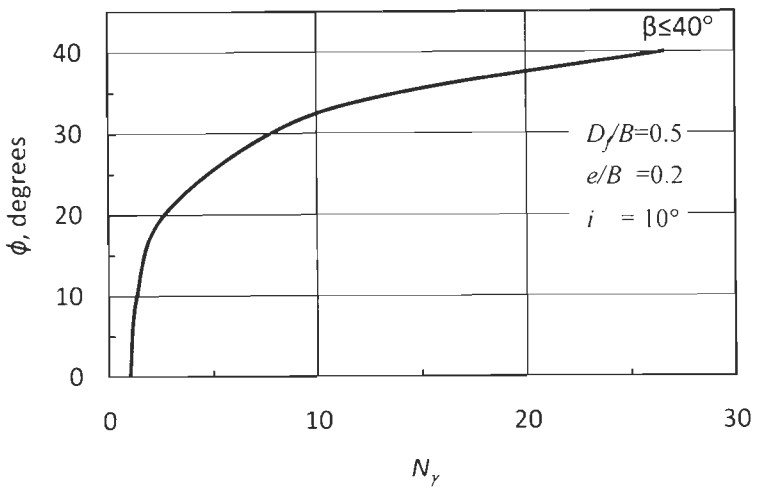

Fig. A.II. 2 c (iv) N_q versus ϕ for D_e/B=3.0

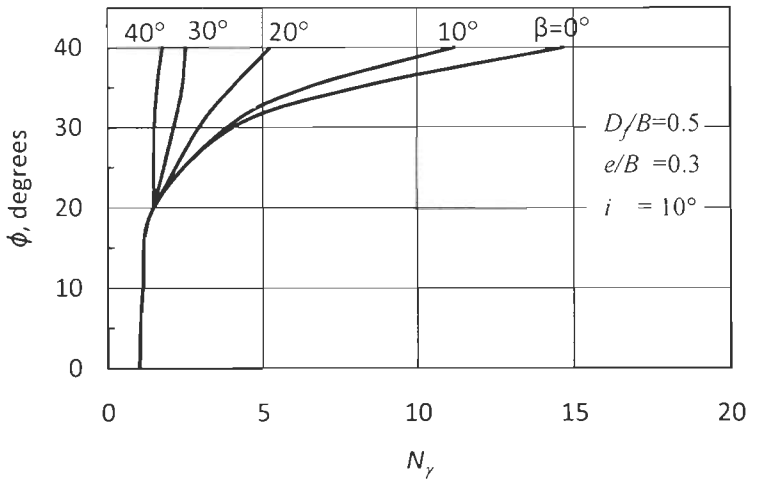

Fig. A.II. 2 d (i) N_q versus ϕ for D_e/B=0

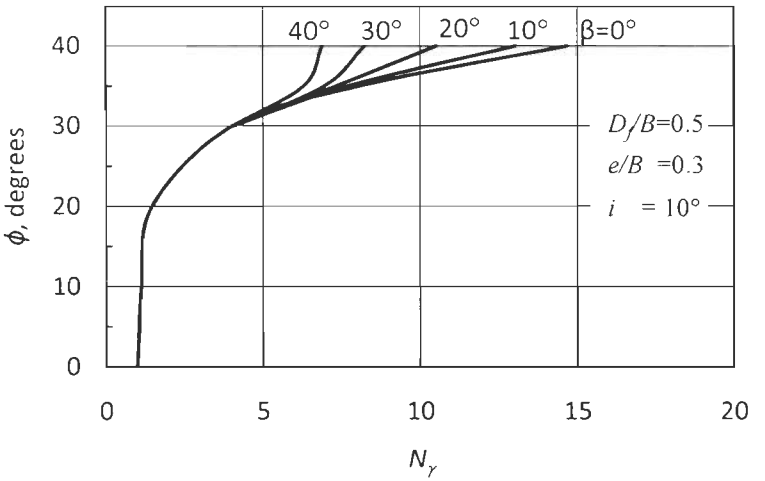

Fig. A.II. 2 d (ii) N_q versus ϕ for D_e/B=1.0

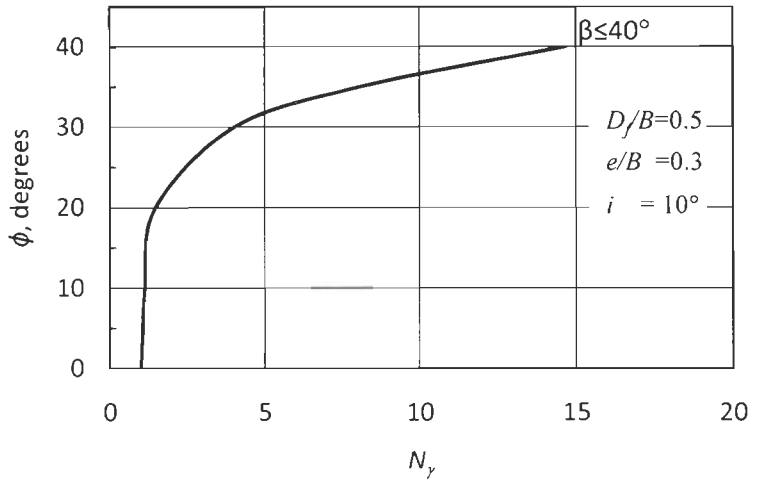

Fig. A.II. 2 d (iii) N_q versus ϕ for D_e/B=2.0

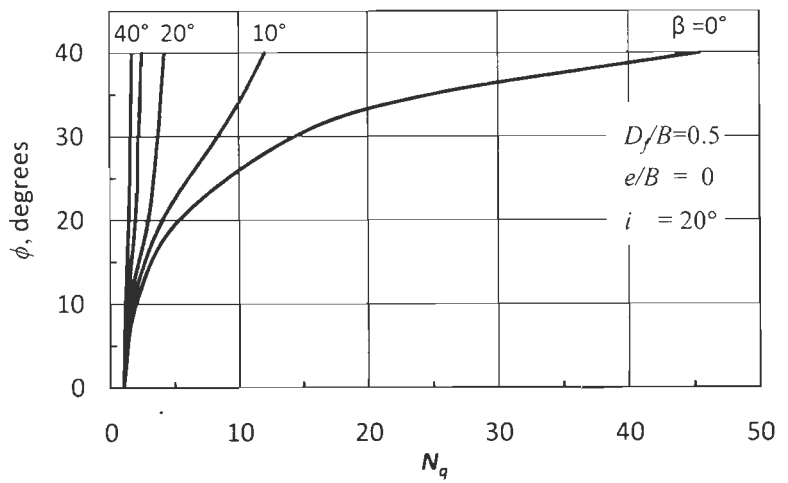

Fig. A.II. 3 a (i) N_q versus ϕ for D_e/B=0

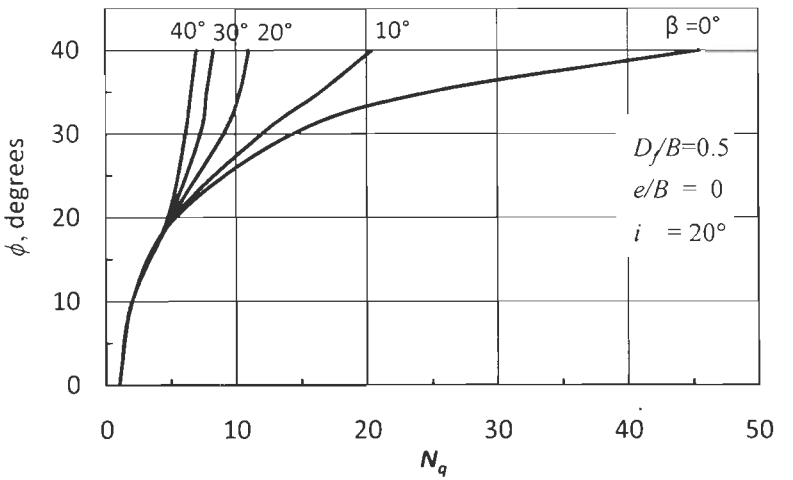

Fig. A.II. 3 a (ii) N_q versus ϕ for D_e/B=1.0

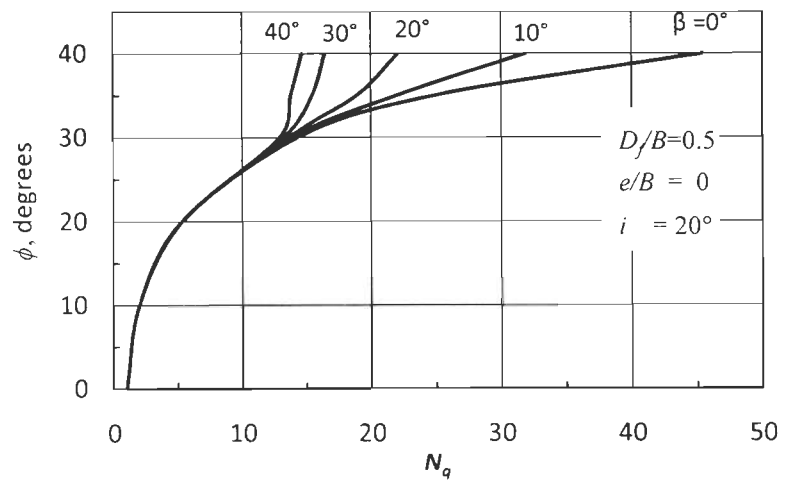

Fig. A.II. 3 a (iii) N_q versus ϕ for D_e/B=2.0

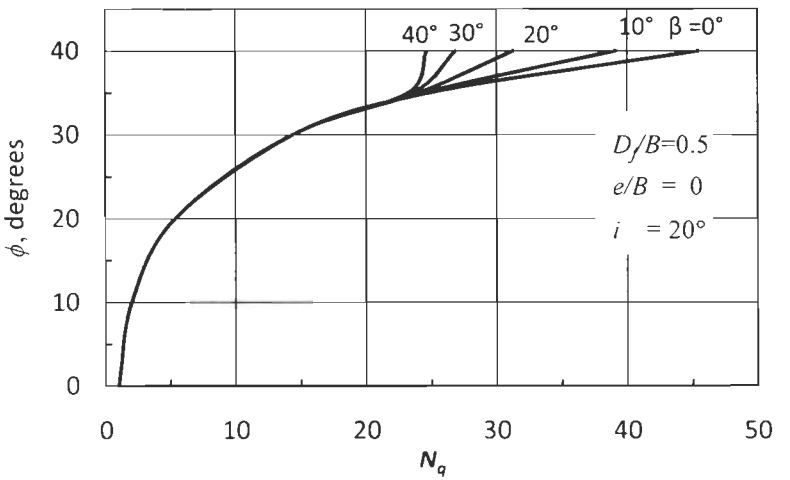

Fig. A.II. 3 a (iv) N_q versus ϕ for D_e/B=3.0

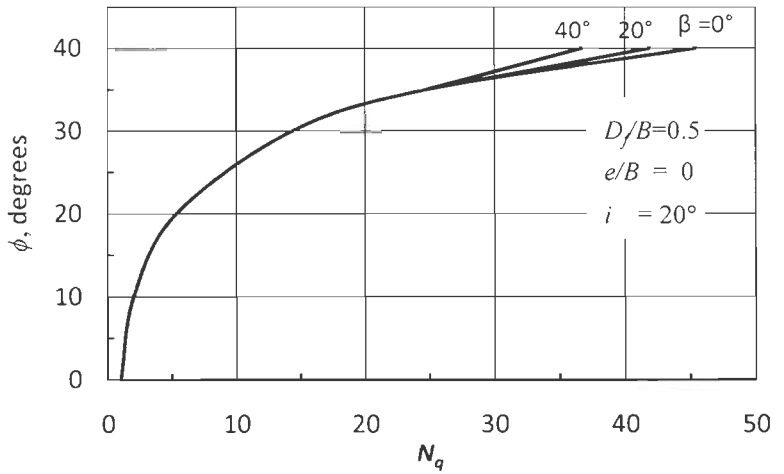

Fig. A.II. 3 a (v) N_q versus ϕ for D_e/B=4.0

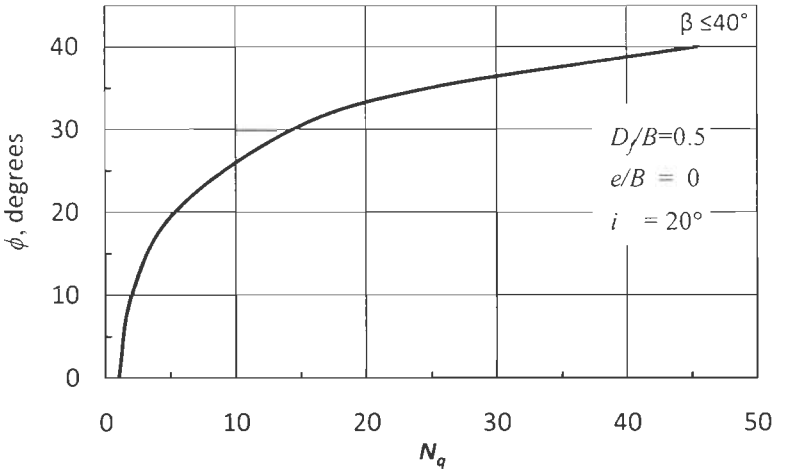

Fig. A.II. 3 a (vi) N_q versus ϕ for D_e/B=5.0

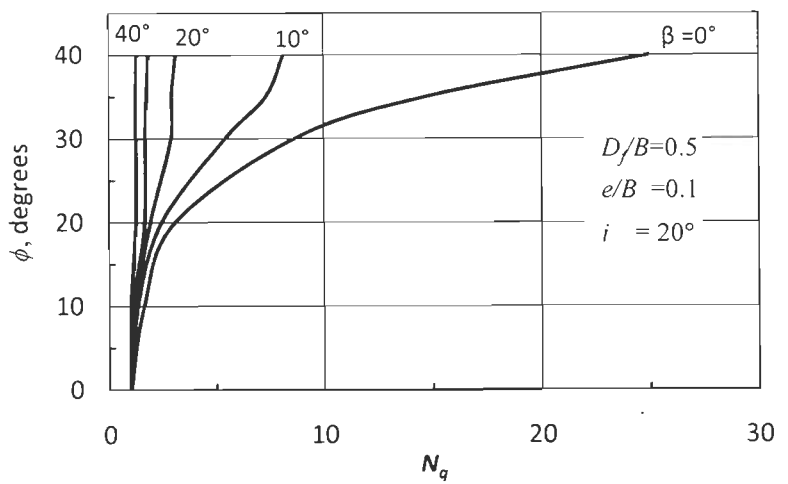

Fig. A.II. 3 b (i) N_q versus ϕ for D_e/B=0

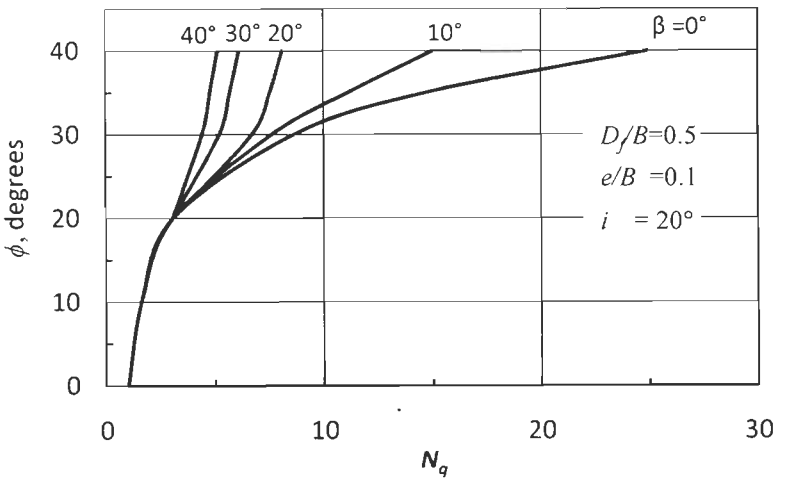

Fig. A.II. 3 b (ii) N_q versus ϕ for D_e/B=1.0

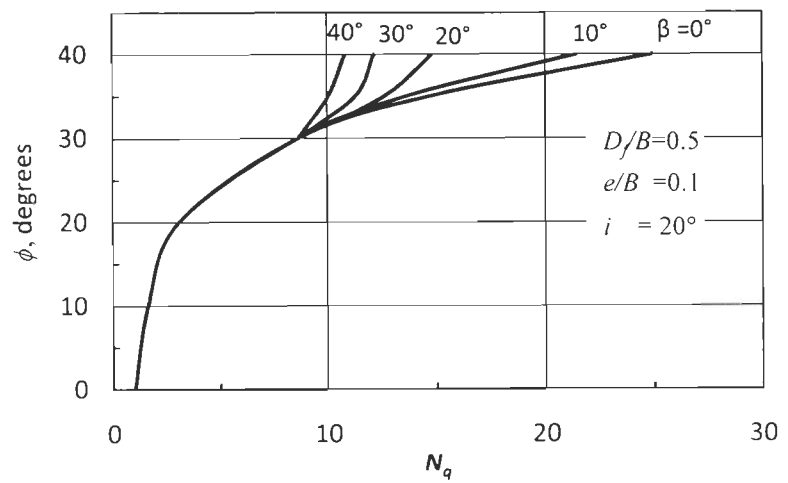

Fig. A.II. 3 b (iii) N_q versus ϕ for D_e/B=2.0

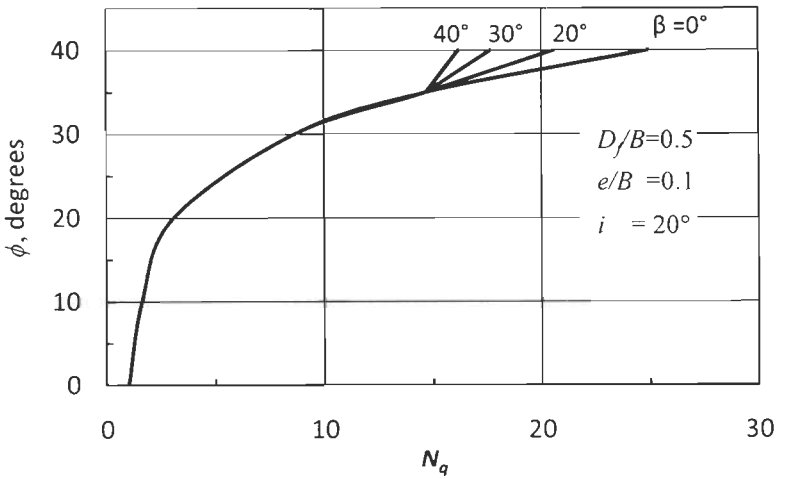

Fig. A.II. 3 b (iv) N_q versus ϕ for D_e/B=3.0

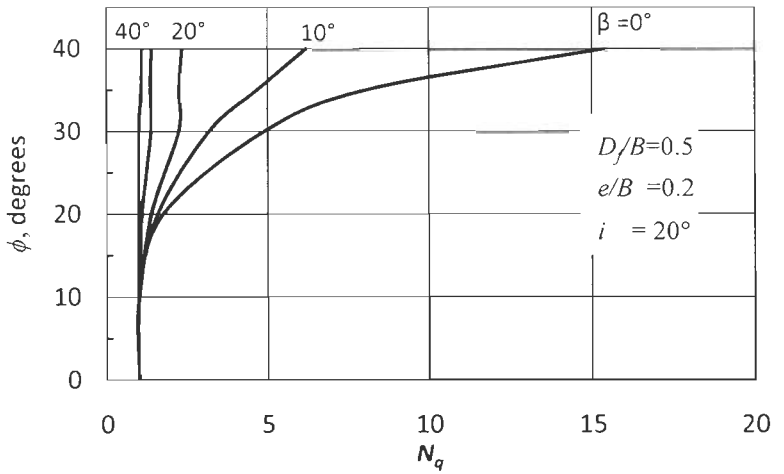

Fig. A.II. 3 c (i) N_q versus ϕ for D_e/B=0

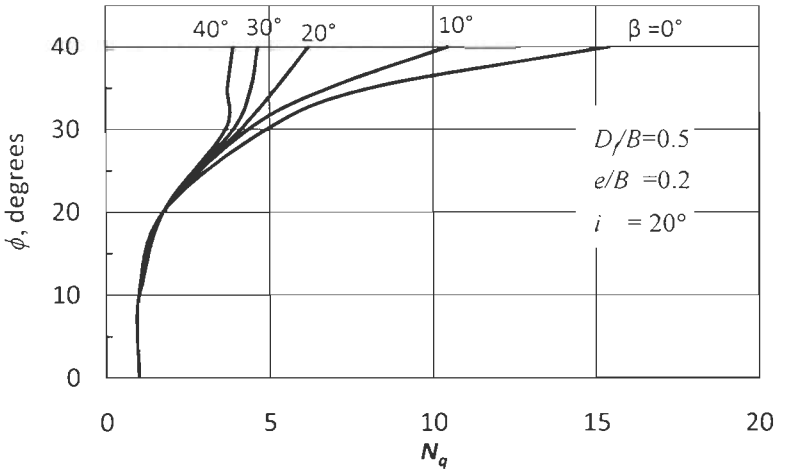

Fig. A.II. 3 c (ii) N_q versus ϕ for D_e/B=1.0

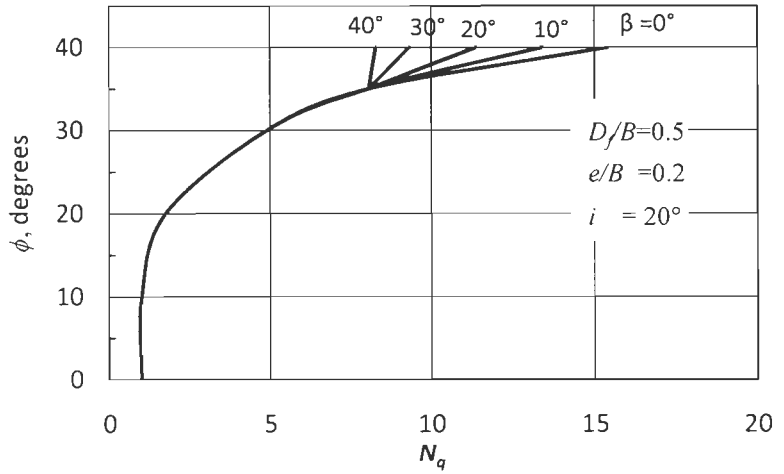

Fig. A.II. 3 c (iii) N_q versus ϕ for D_e/B=2.0

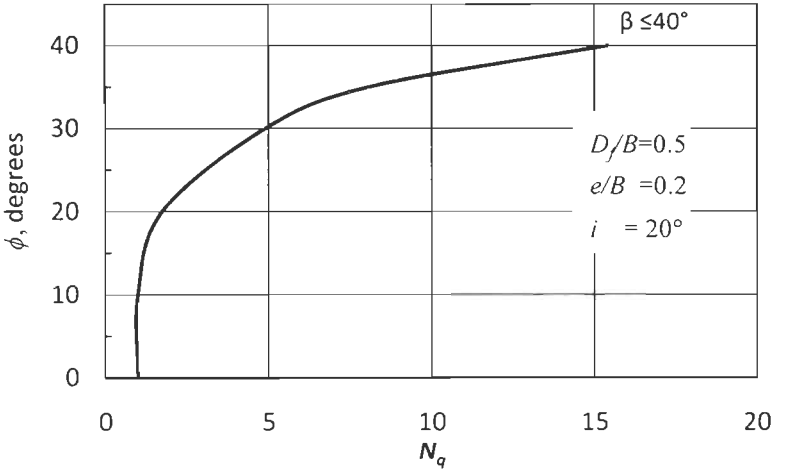

Fig. A.II. 3 c (iv) N_q versus ϕ for D_e/B=3.0

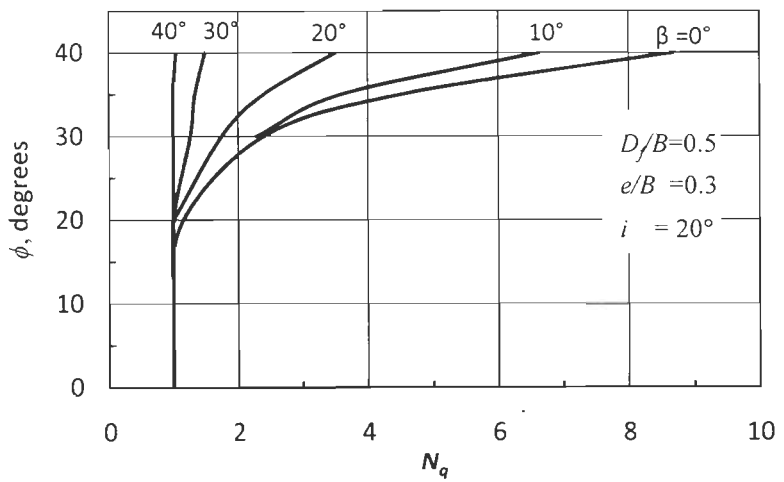

Fig. A.II. 3 d (i) N_q versus ϕ for D_e/B=0

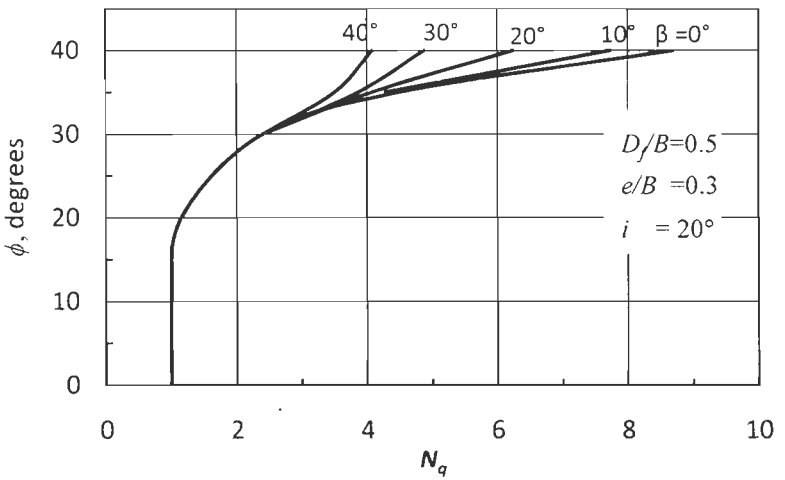

Fig. A.II. 3 d (ii) N_q versus ϕ for D_e/B=1.0

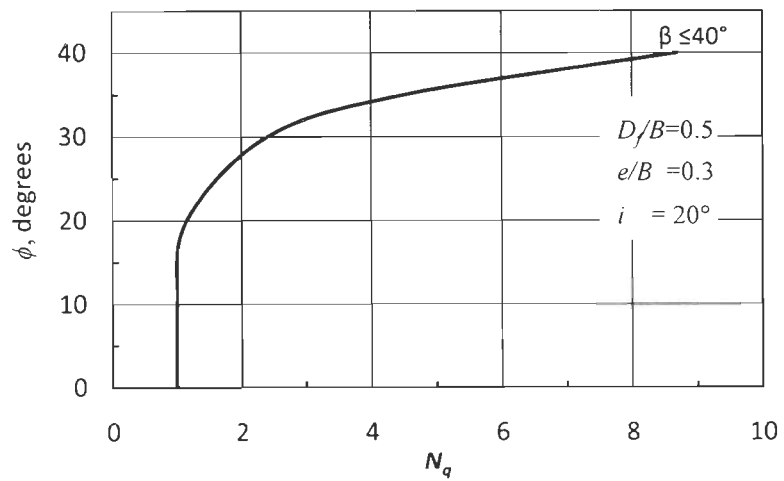

Fig. A.II. 3 d (iii) N_q versus ϕ for D_e/B=2.0

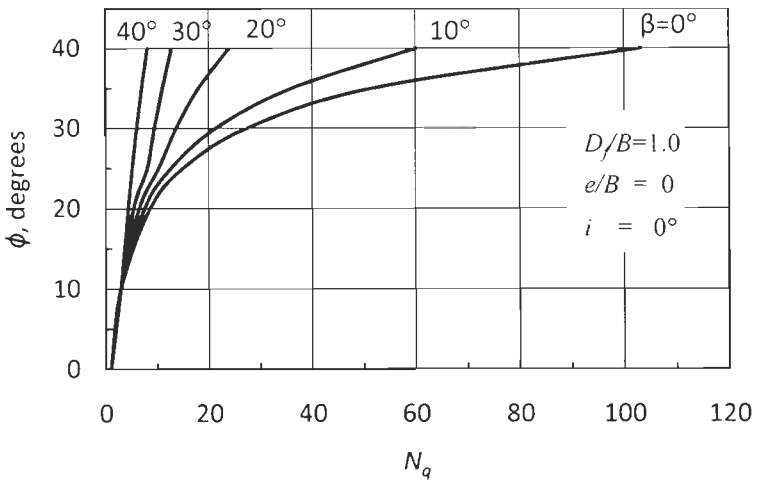

Fig. A.II. 4 a (i) N_q versus ϕ for D_e/B=0

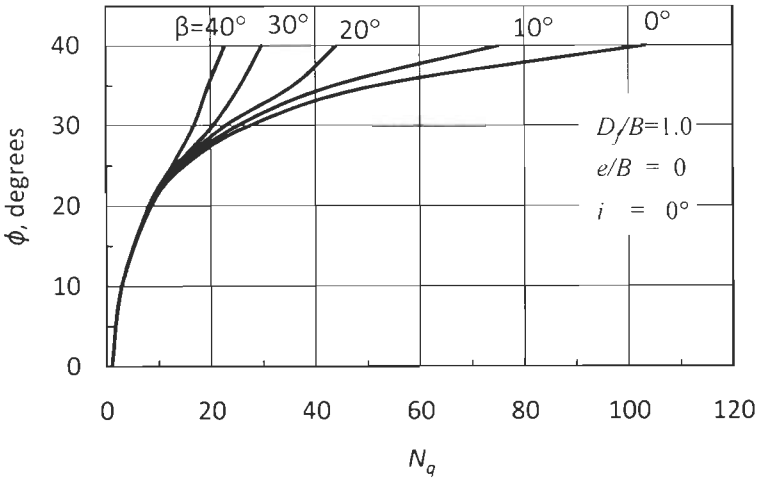

Fig. A.II. 4 a (ii) N_q versus ϕ for D_e/B=1.0

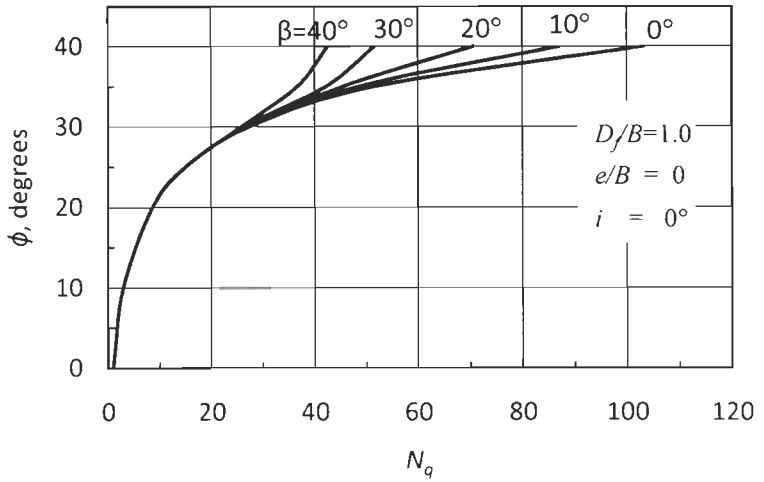

Fig. A.II. 4 a (iii) N_q versus ϕ for D_e/B=2.0

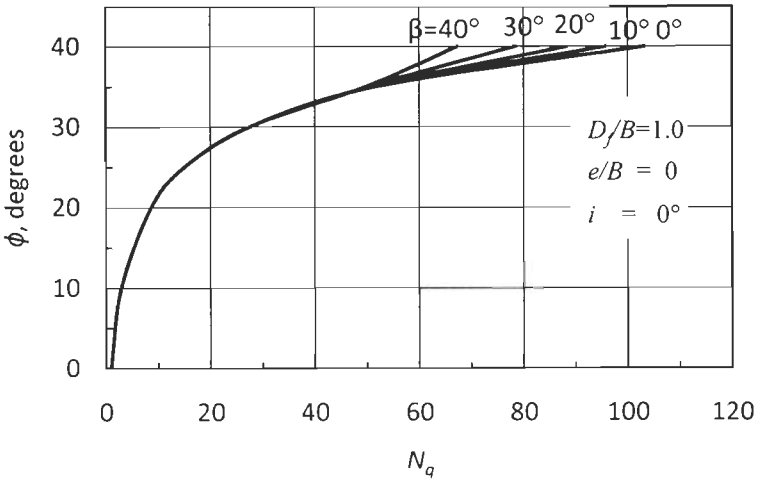

Fig. A.II. 4 a (iv) N_q versus ϕ for D_e/B=3.0

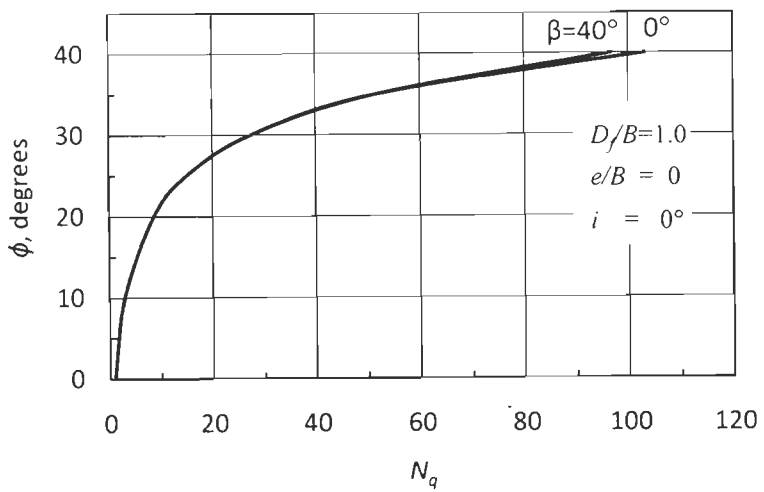

Fig. A.II. 4 a (v) N_q versus ϕ for D_e/B=4.0

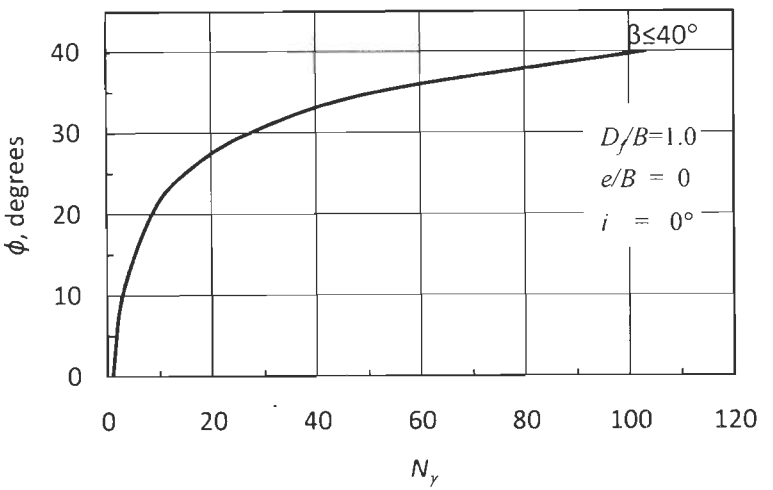

Fig. A.II. 4 a (vi) N_q versus ϕ for D_e/B=5.0

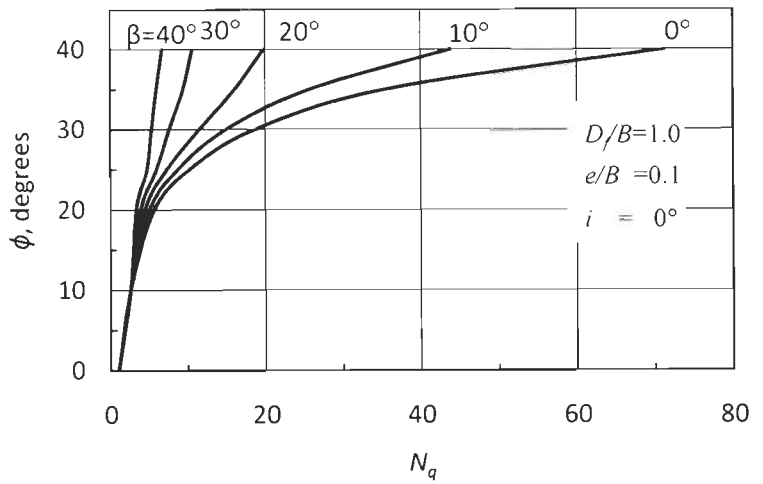

Fig. A.II. 4 b (i) N_q versus ϕ for D_e/B=0

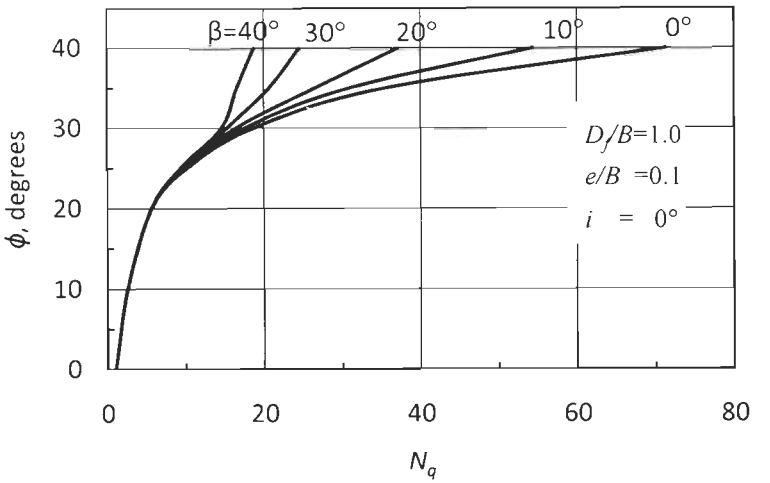

Fig. A.II. 4 b (ii) N_q versus ϕ for D_e/B=1.0

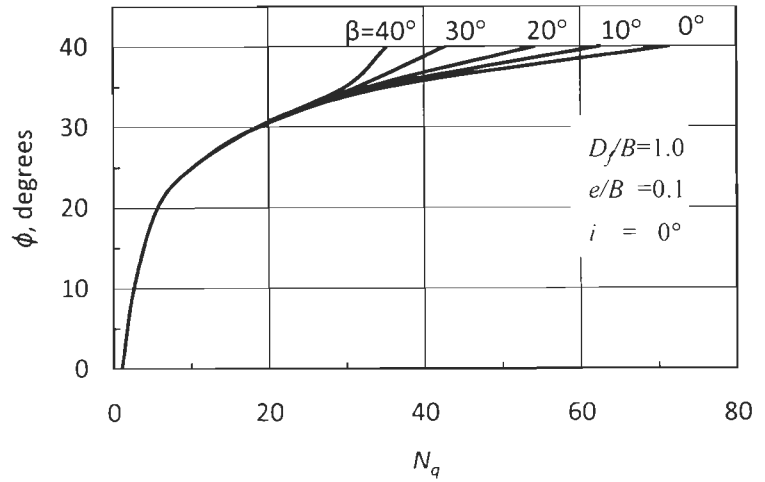

Fig. A.II. 4 b (iii) N_q versus ϕ for D_e/B=2.0

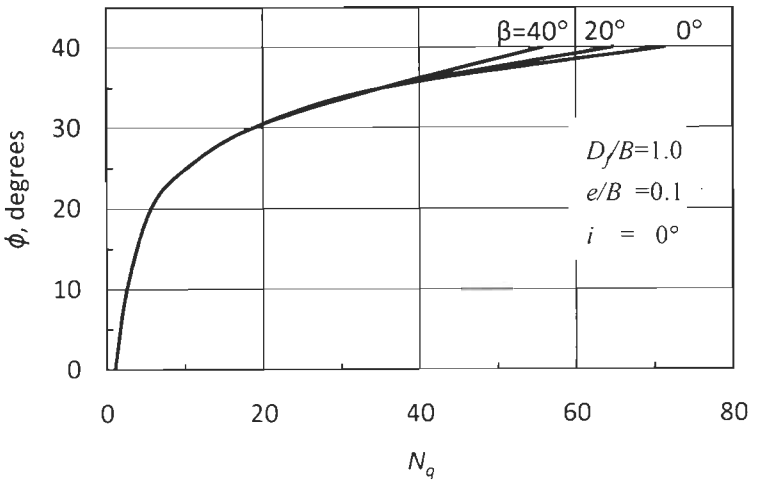

Fig. A.II. 4 b (iv) N_q versus ϕ for D_e/B=3.0

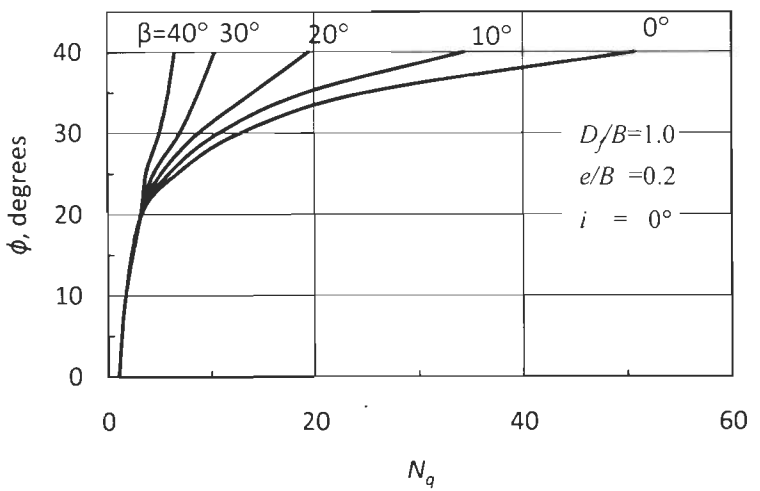

Fig. A.II. 4 c (i) N_q versus ϕ for D_e/B=0

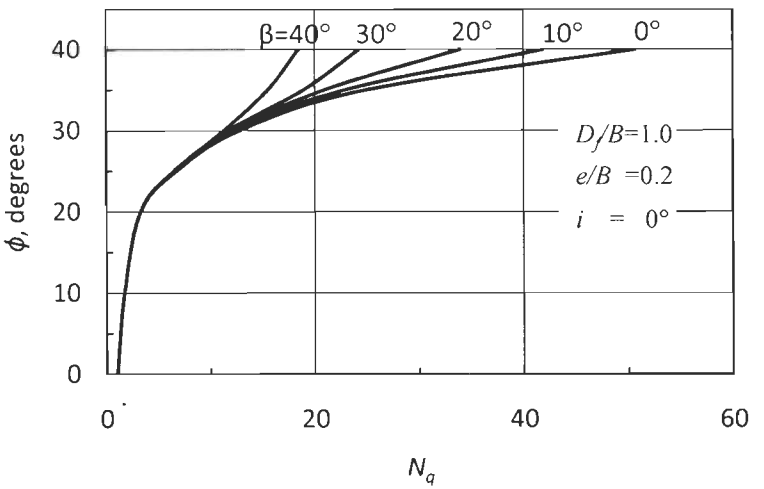

Fig. A.II. 4 c (ii) N_q versus ϕ for D_e/B=1.0

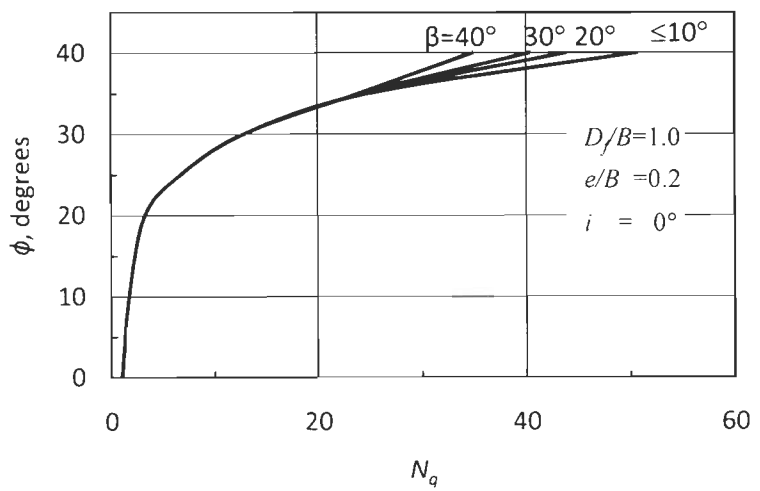

Fig. A.II. 4 c (iii) N_q versus ϕ for D_e/B=2.0

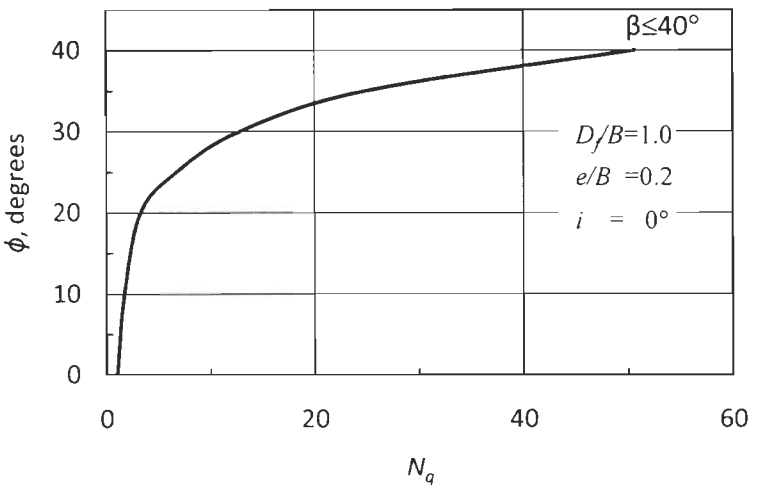

Fig. A.II. 4 c (iv) N_q versus ϕ for D_e/B=3.0

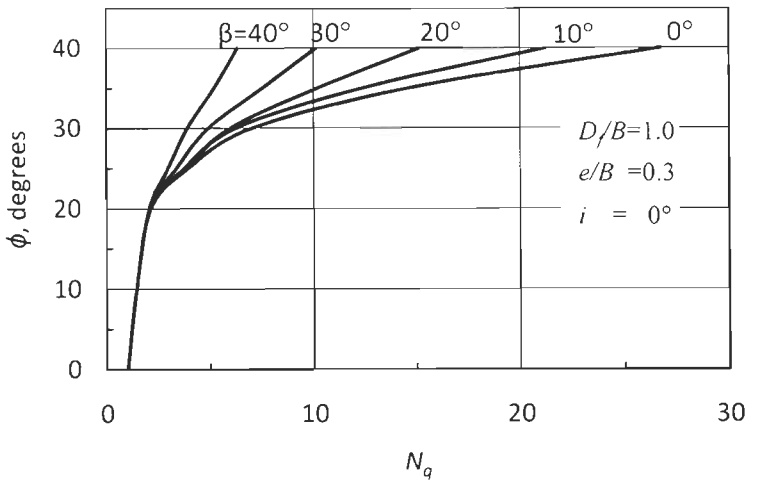

Fig. A.II. 4 d (i) N_q versus ϕ for D_e/B=0

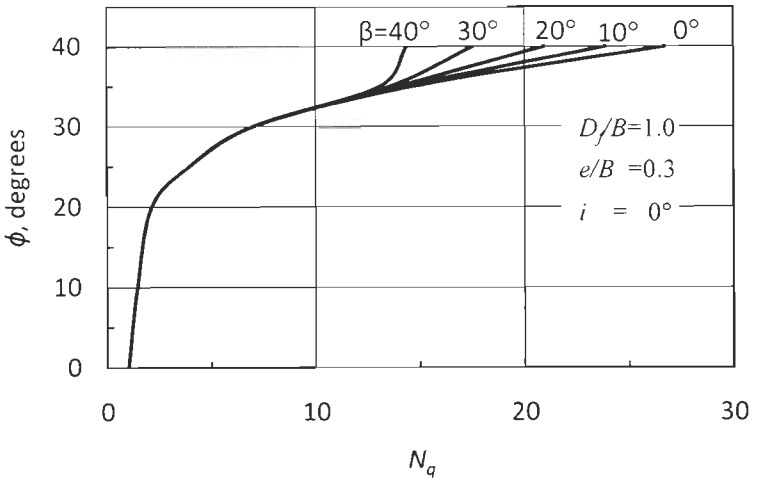

Fig. A.II. 4 d (ii) N_q versus ϕ for D_e/B=1.0

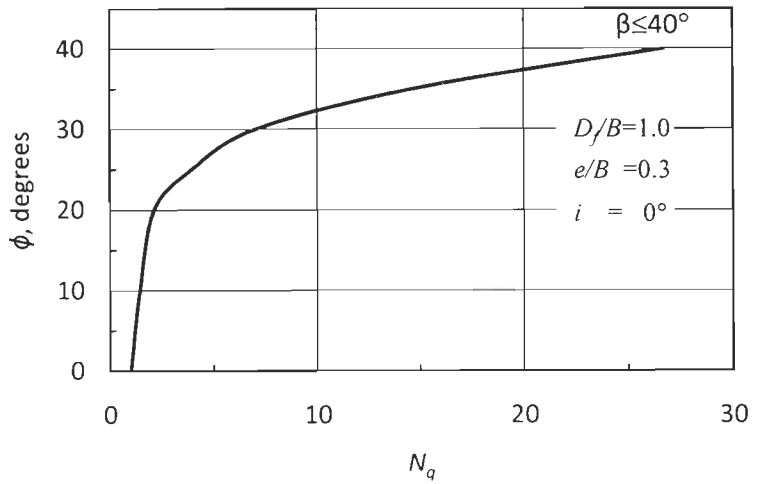

Fig. A.II. 4 d (iii) N_q versus ϕ for D_e/B=2.0

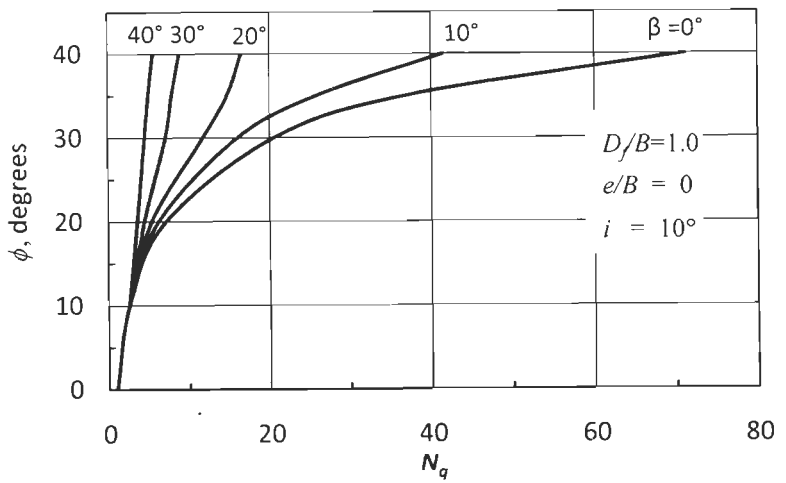

Fig. A.II. 5 a (i) N_q versus ϕ for D_e/B=0

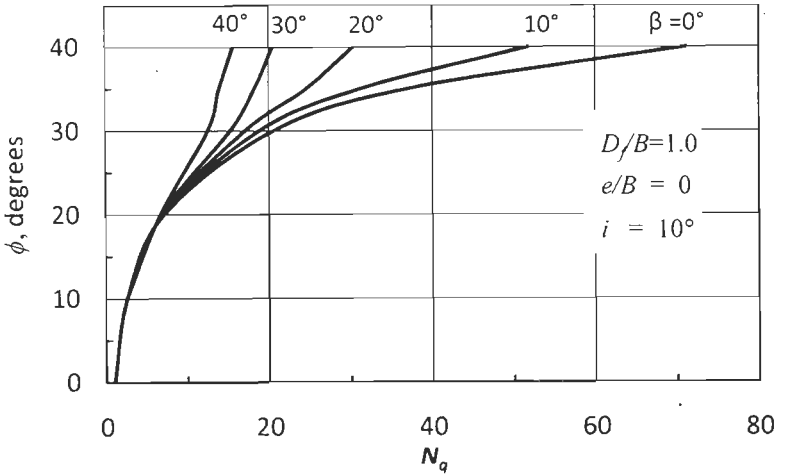

Fig. A.II. 5 a (ii) N_q versus ϕ for D_e/B=1.0

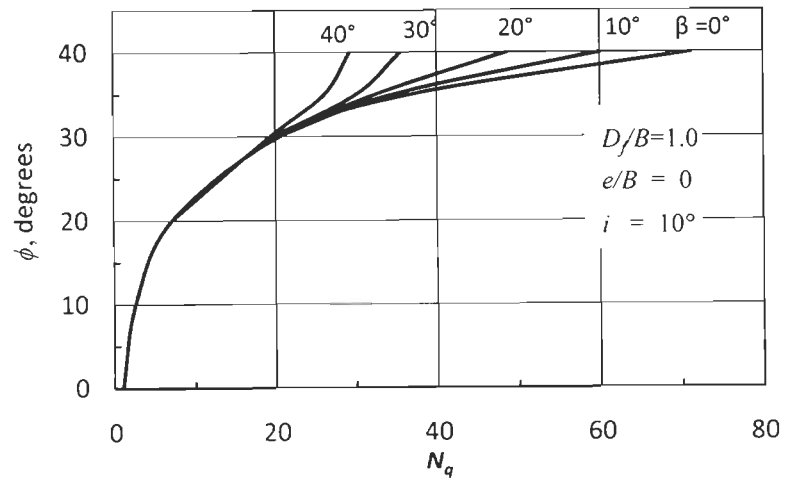

Fig. A.II. 5 a (iii) N_q versus ϕ for D_e/B=2.0

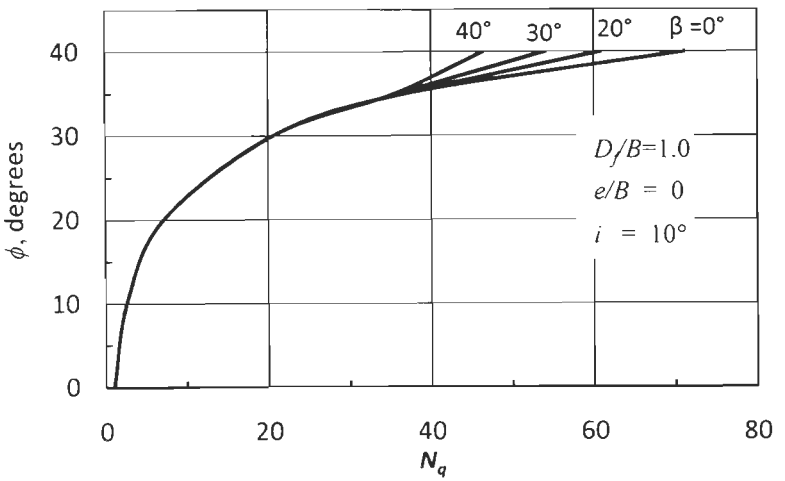

Fig. A.II. 5 a (iv) N_q versus ϕ for D_e/B=3.0

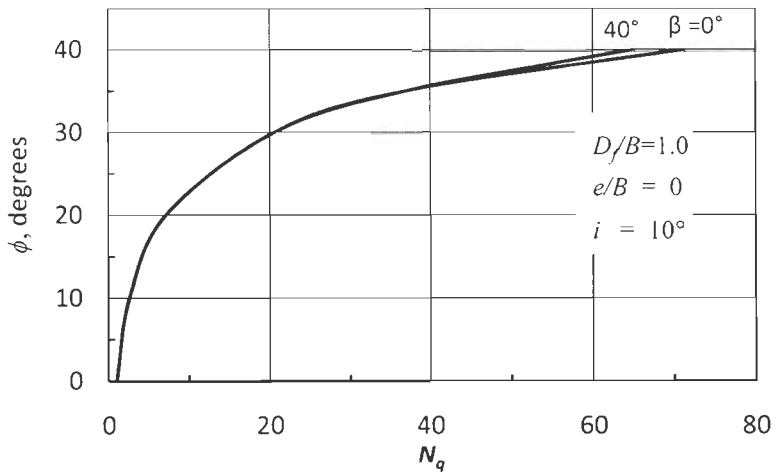

Fig. A.II. 5 a (v) N_q versus ϕ for D_e/B=4.0

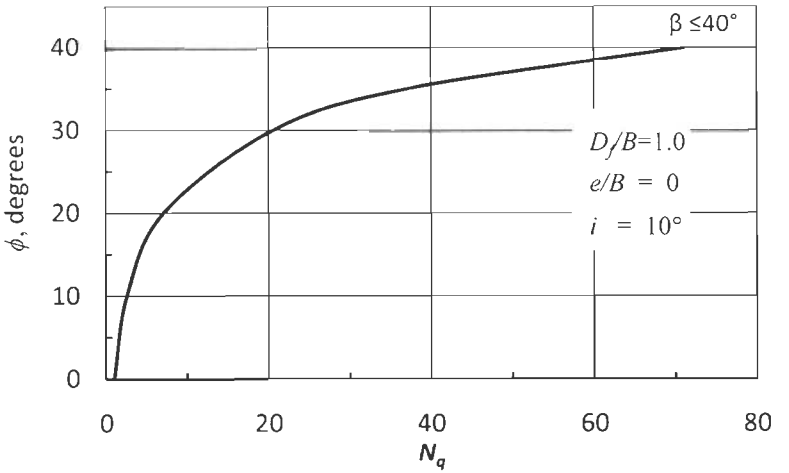

Fig. A.II. 5 a (vi) N_q versus ϕ for D_e/B=5.0

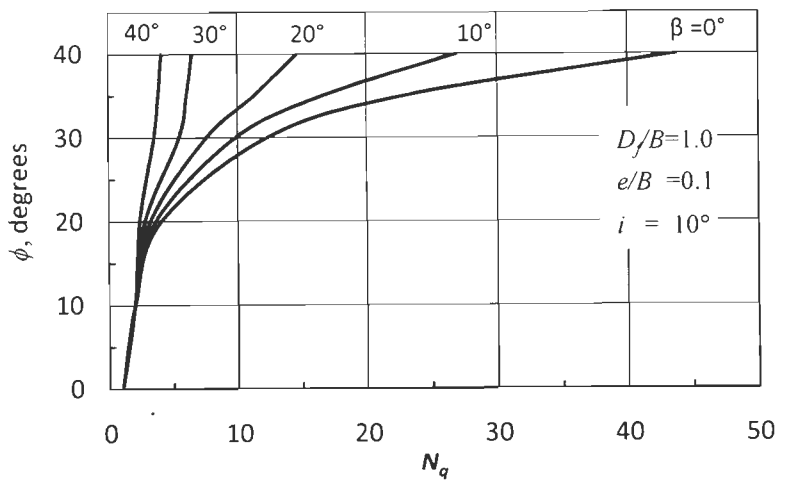

Fig. A.II. 5 b (i) N_q versus ϕ for D_e/B=0

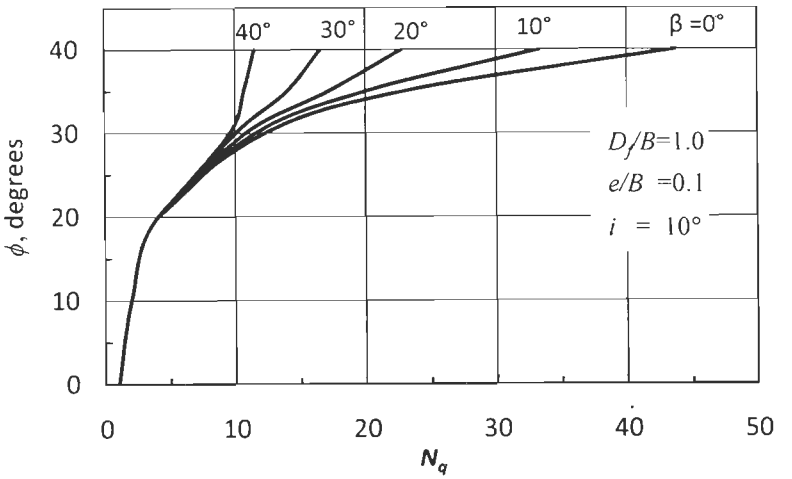

Fig. A.II. 5 b (ii) N_q versus ϕ for D_e/B=1.0

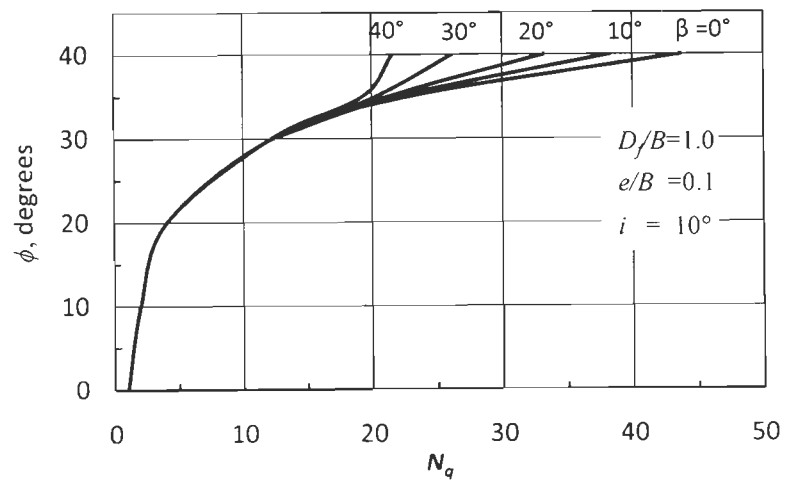

Fig. A.II. 5 b (iii) N_q versus ϕ for D_e/B=2.0

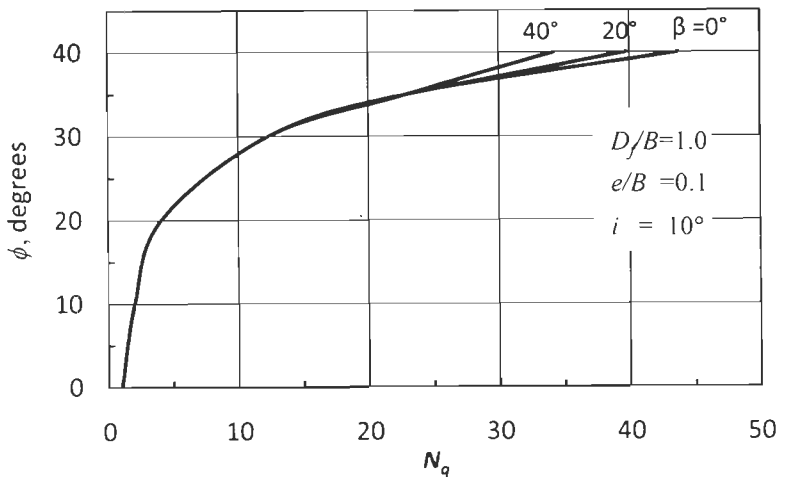

Fig. A.II. 5 b (iv) N_q versus ϕ for D_e/B=3.0

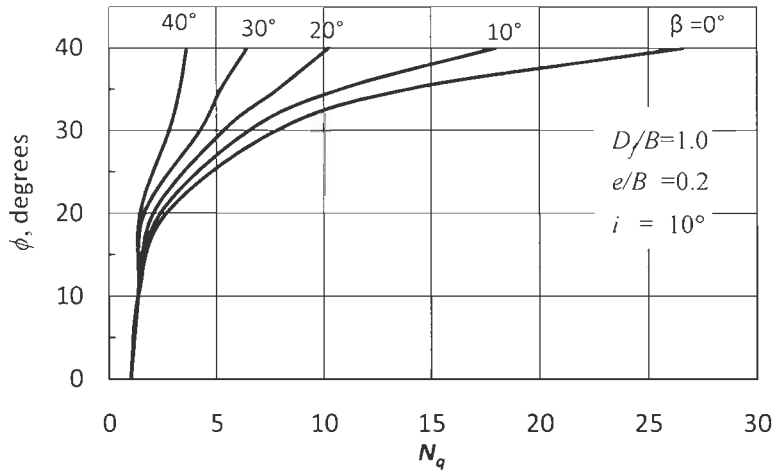

Fig. A.II. 5 c (i) N_q versus ϕ for D_e/B=0

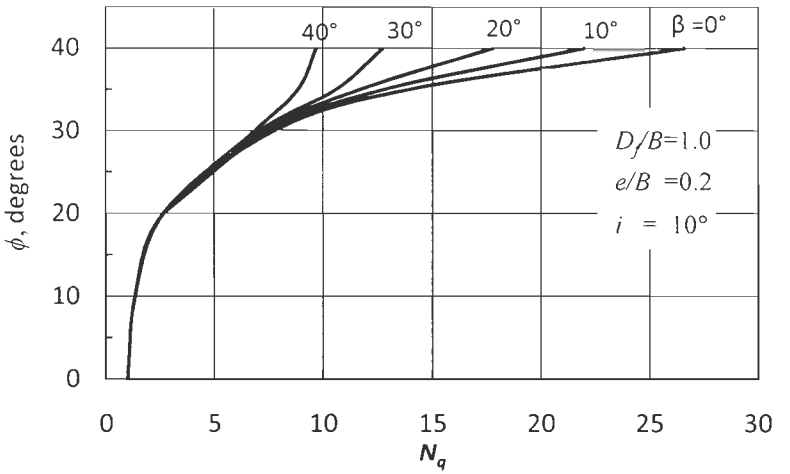

Fig. A.II. 5 c (ii) N_q versus ϕ for D_e/B=1.0

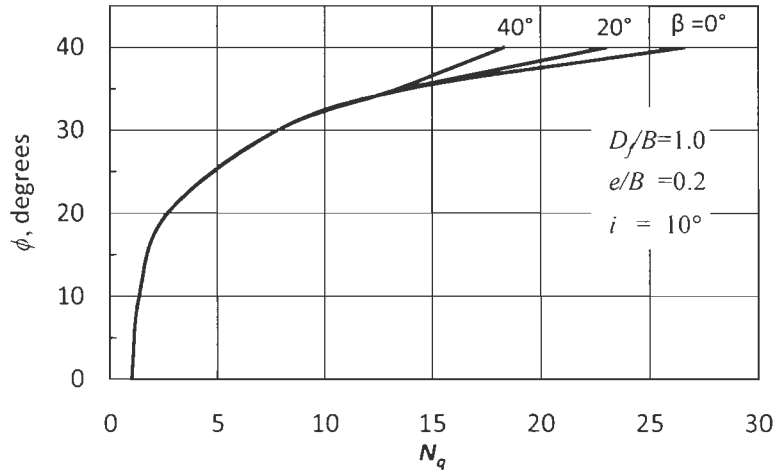

Fig. A.II. 5 c (iii) N_q versus ϕ for D_e/B=2.0

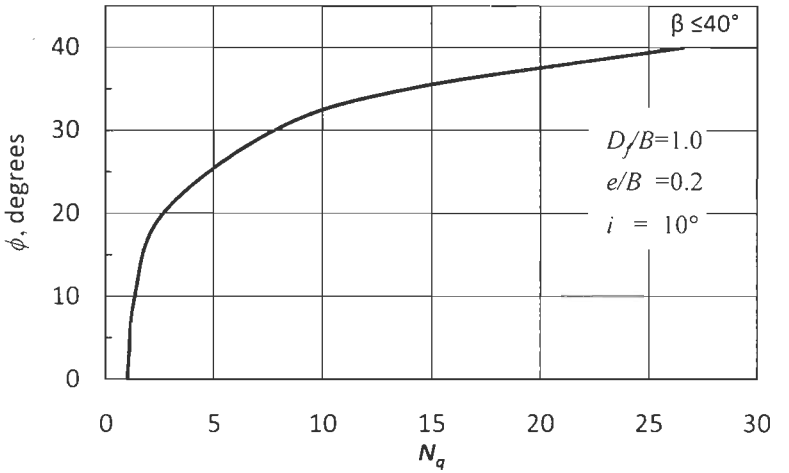

Fig. A.II. 5 c (iv) N_q versus ϕ for D_e/B=3.0

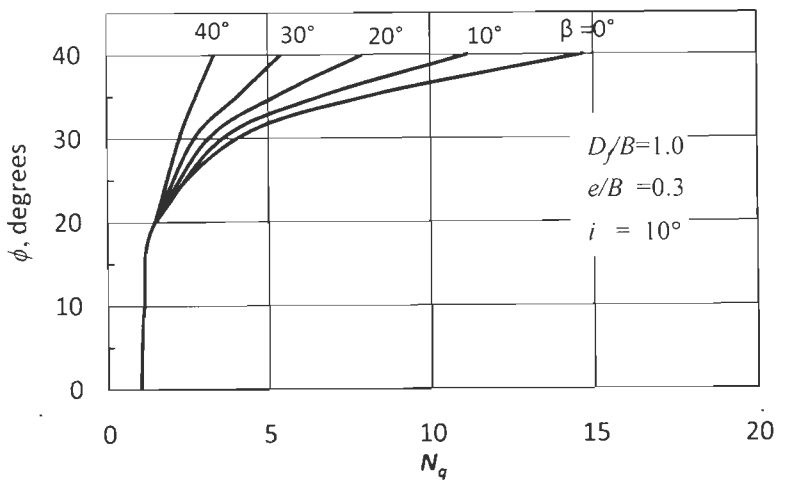

Fig. A.II. 5 d (i) N_q versus ϕ for D_e/B=0

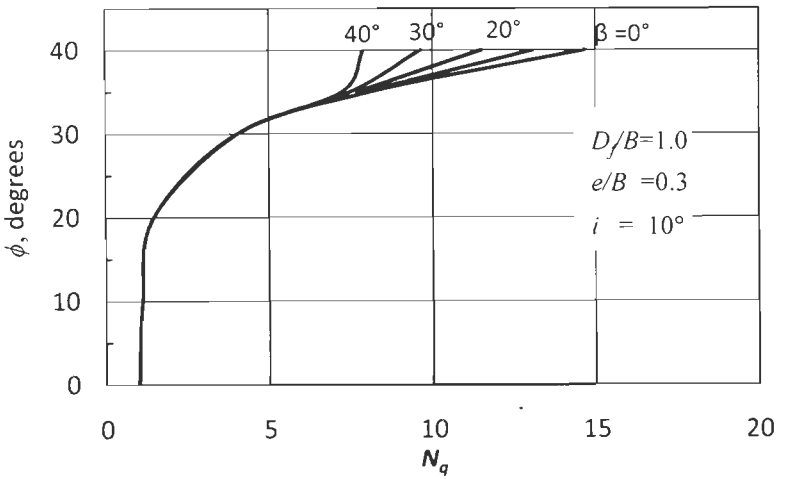

Fig. A.II. 5 d (ii) N_q versus ϕ for D_e/B=1.0

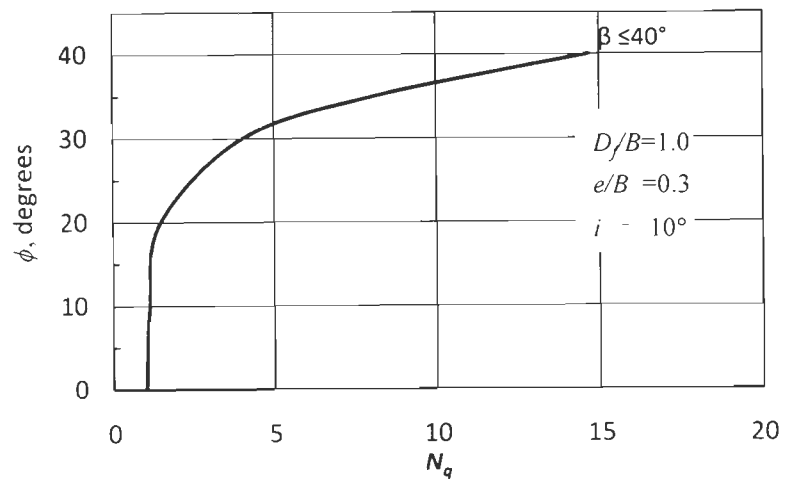

Fig. A.II. 5 d (iii) N_q versus ϕ for D_e/B=2.0

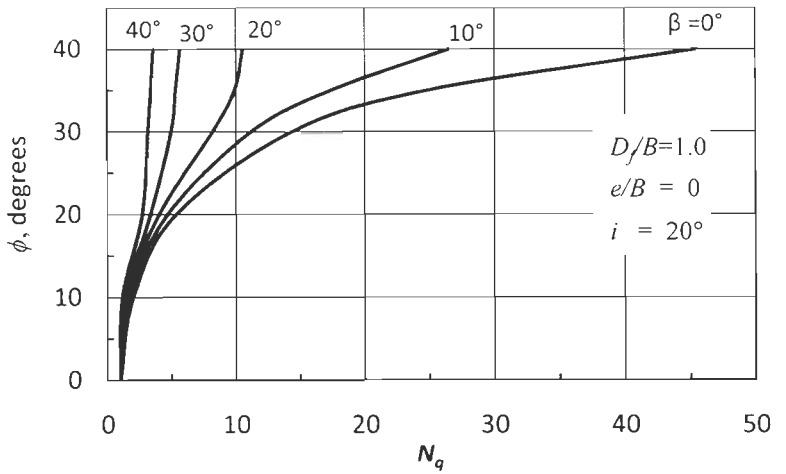

Fig. A.II. 6 a (i) N_q versus ϕ for D_e/B=0

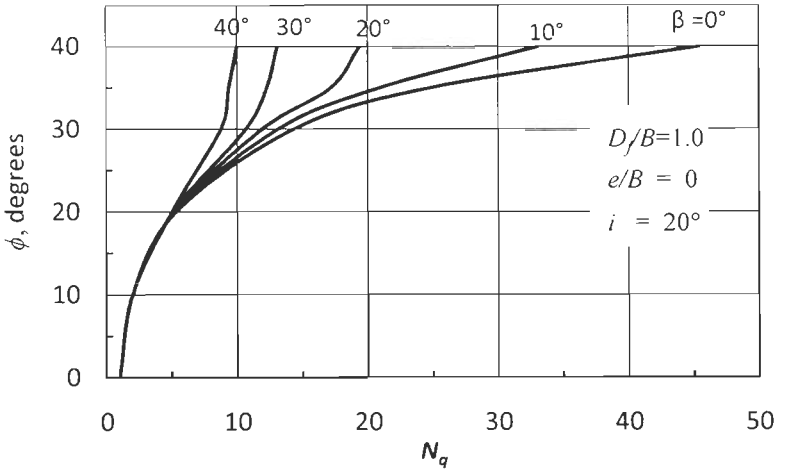

Fig. A.II. 6 a (ii) N_q versus ϕ for D_e/B=1.0

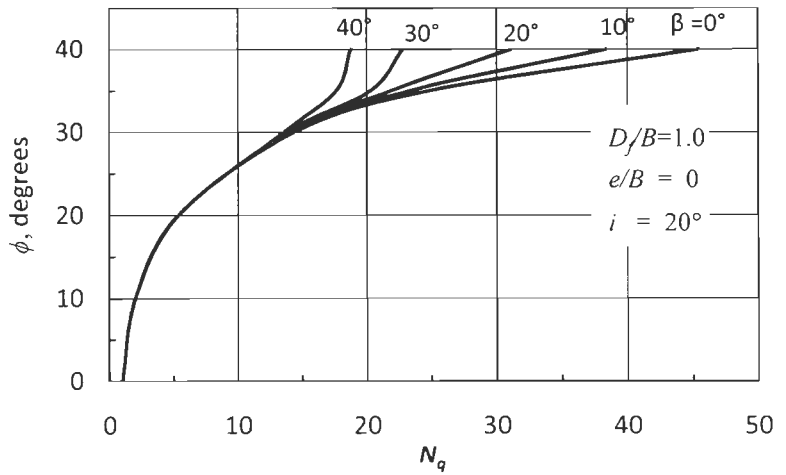

Fig. A.II. 6 a (iii) N_q versus ϕ for D_e/B=2.0

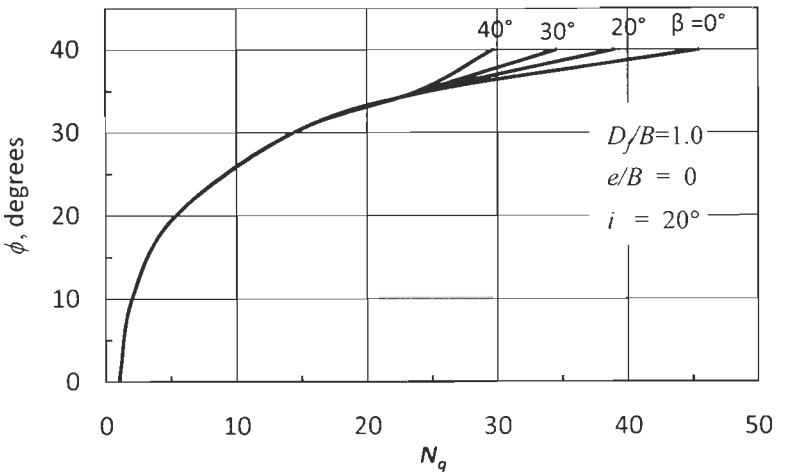

Fig. A.II. 6 a (iv) N_q versus ϕ for D_e/B=3.0

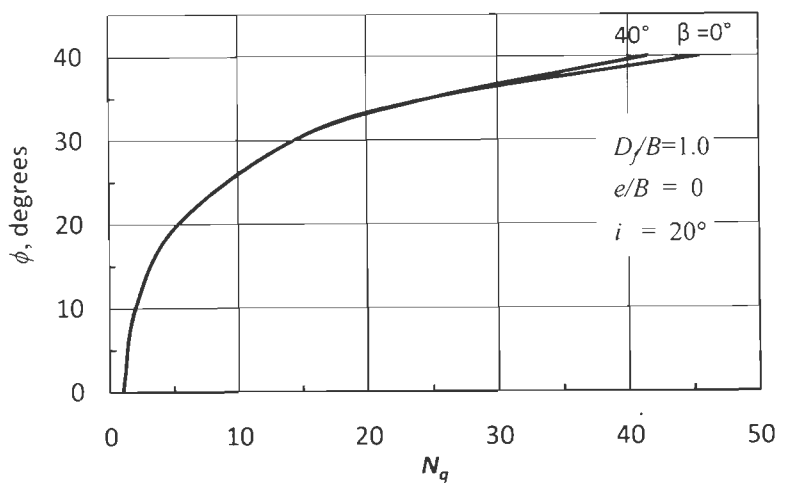

Fig. A.II. 6 a (v) N_q versus ϕ for D_e/B=4.0

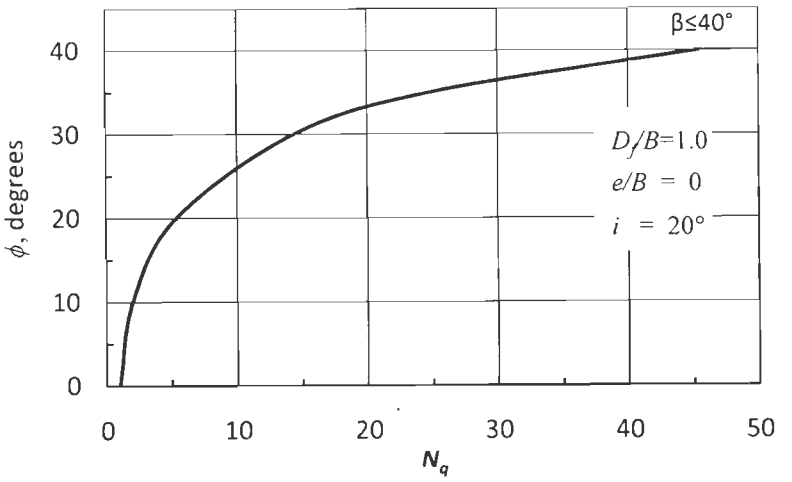

Fig. A.II. 6 a (vi) N_q versus ϕ for D_e/B=5.0

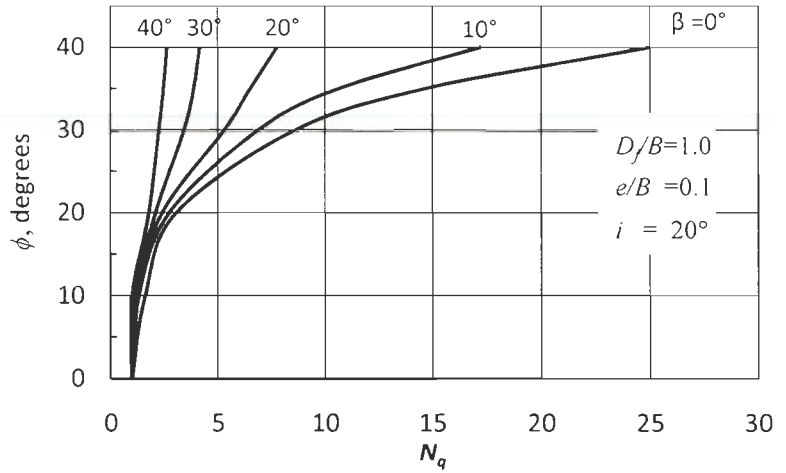

Fig. A.II. 6 b (i) N_q versus ϕ for D_f/B=0

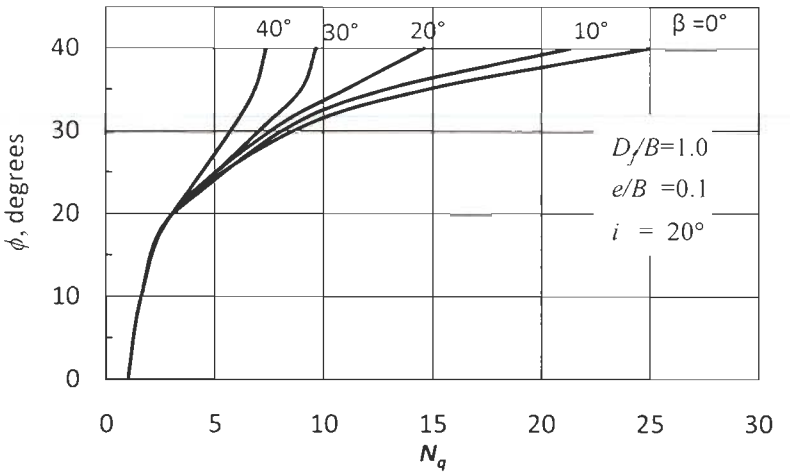

Fig. A.II. 6 b (ii) N_q versus ϕ for D_e/B=1.0

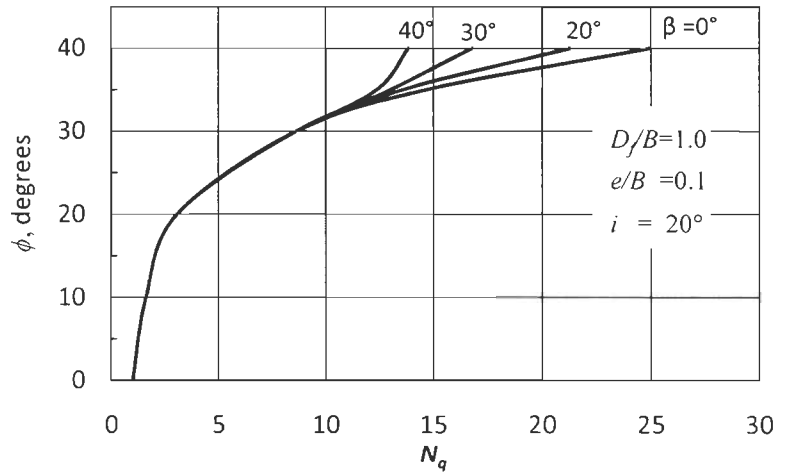

Fig. A.II. 6 b (iii) N_q versus ϕ for D_e/B=2.0

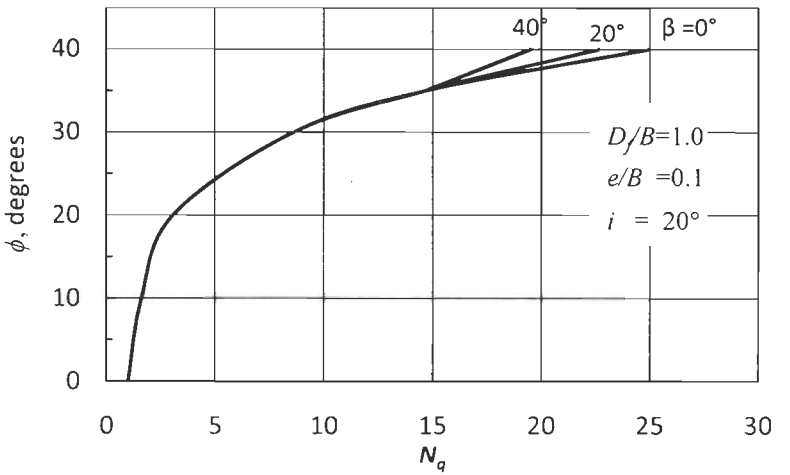

Fig. A.II. 6 b (iv) N_q versus ϕ for D_e/B=3.0

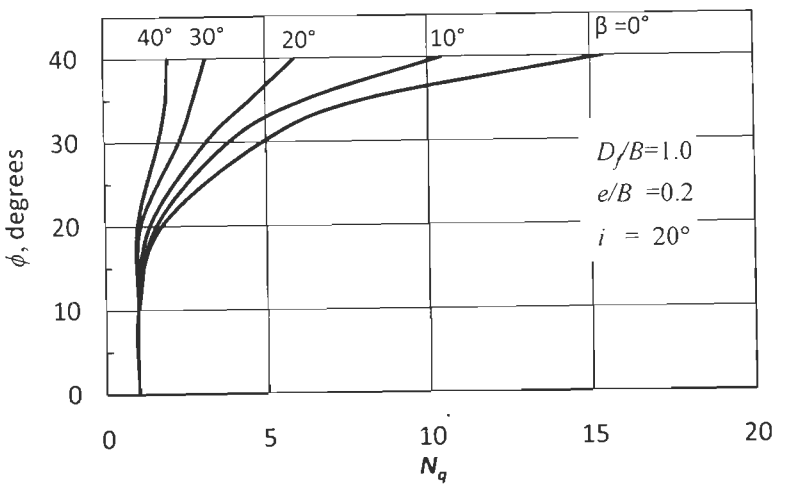

Fig. A.II. 6 c (i) N_q versus ϕ for D_e/B=0

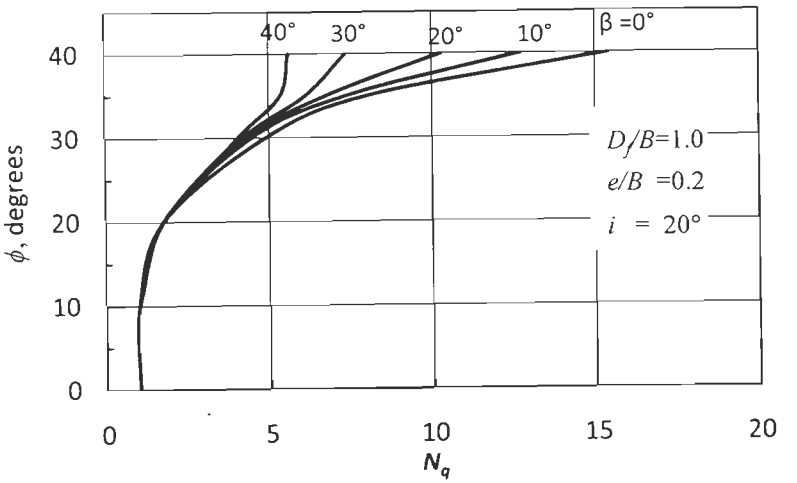

Fig. A.II. 6 c (ii) N_q versus ϕ for D_e/B=1.0

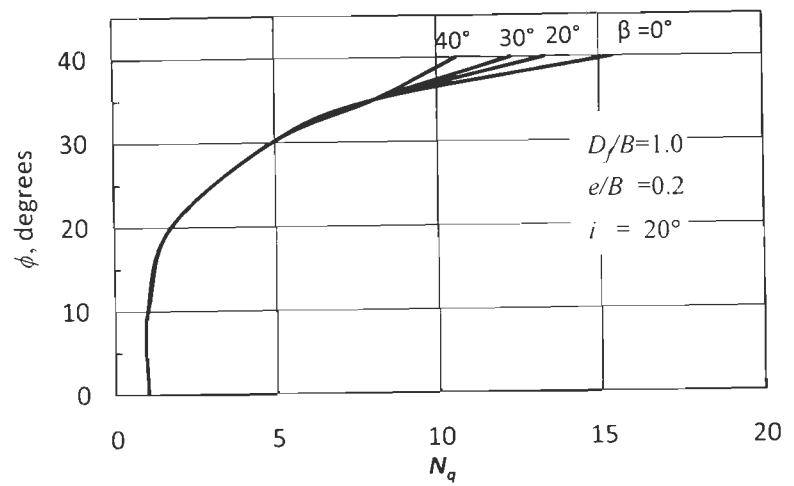

Fig. A.II. 6 c (iii) N_q versus ϕ for D_e/B=2.0

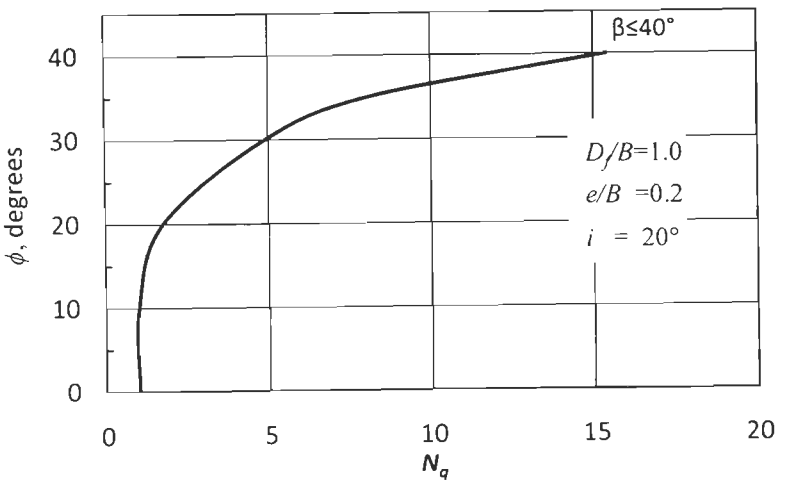

Fig. A.II. 6 c (iv) N_q versus ϕ for D_e/B=3.0

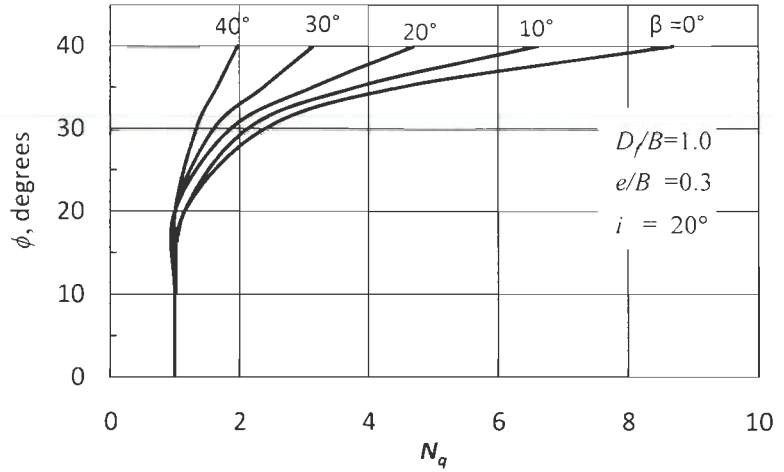

Fig. A.II. 6 d (i) N_q versus ϕ for D_e/B=0

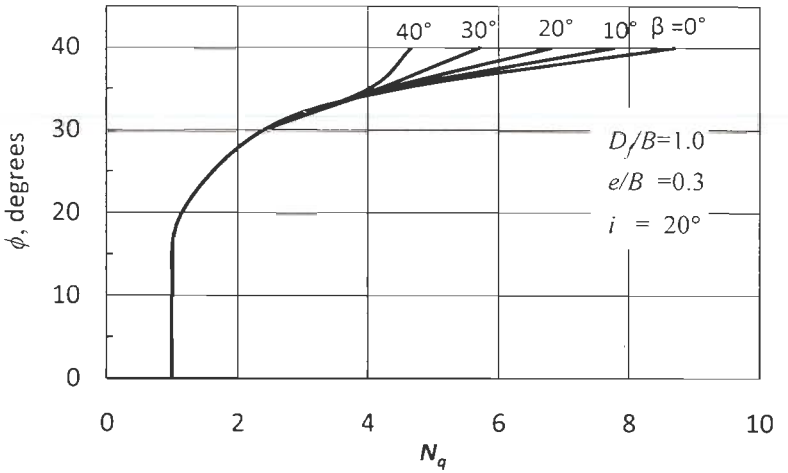

Fig. A.II. 6 d (ii) N_q versus ϕ for D_e/B=1.0

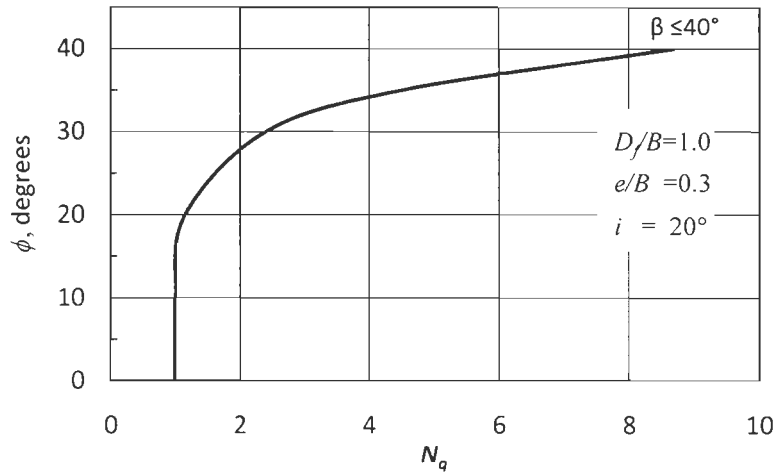

Fig. A.II. 6 d (iii) N_q versus ϕ for D_e/B=2.0

Appendix- III

N_c CHARTS

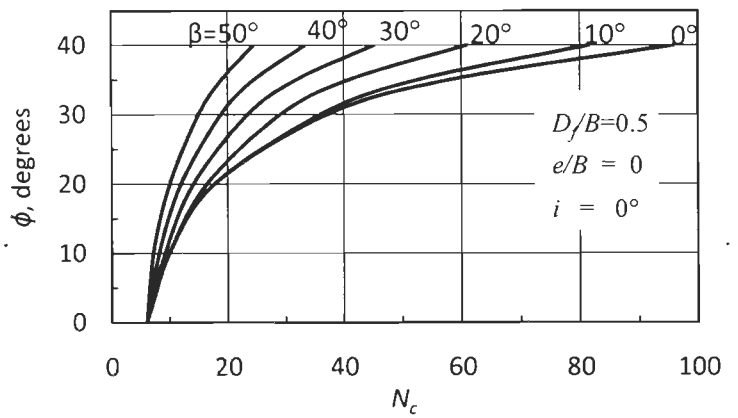

Fig. A.III. 1 a (i) N_c versus ϕ for D_e/B=0

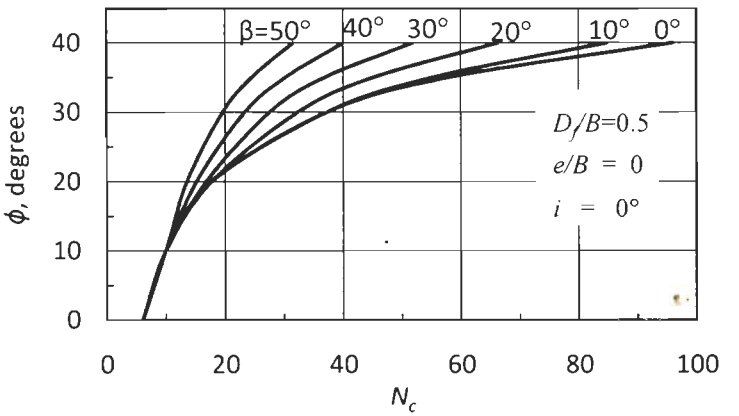

Fig. A.III. 1 a (ii) N_c versus ϕ for D_e/B=1.0

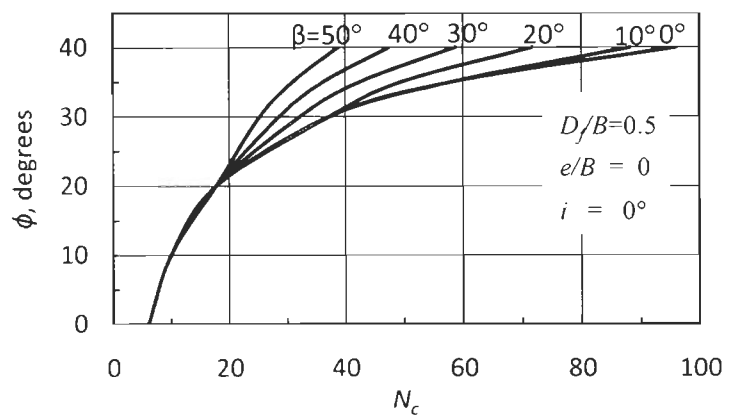

Fig. A.III. 1 a (iii) N_c versus ϕ for D_e/B=2.0

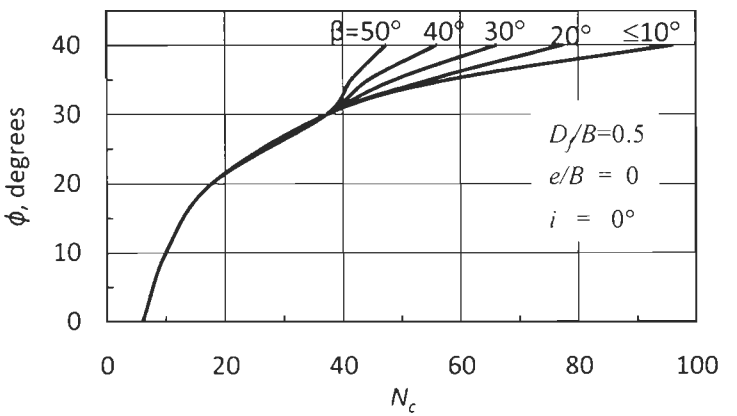

Fig. A.III. 1 a (iv) N_c versus ϕ for D_e/B=3.0

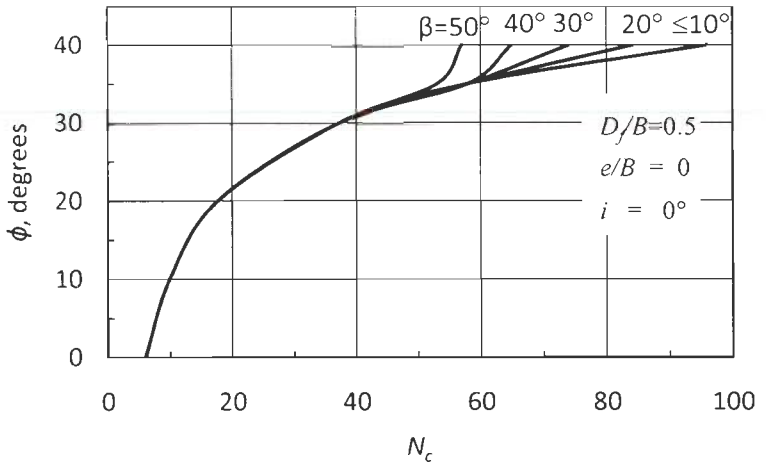

Fig. A.III. 1 a (v) N_c versus ϕ for D_e/B=4.0

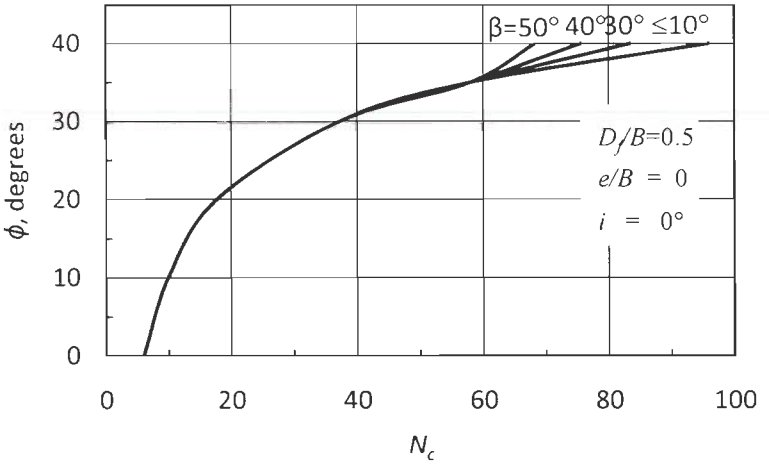

Fig. A.III. 1 a (vi) N_c versus ϕ for D_e/B=5.0

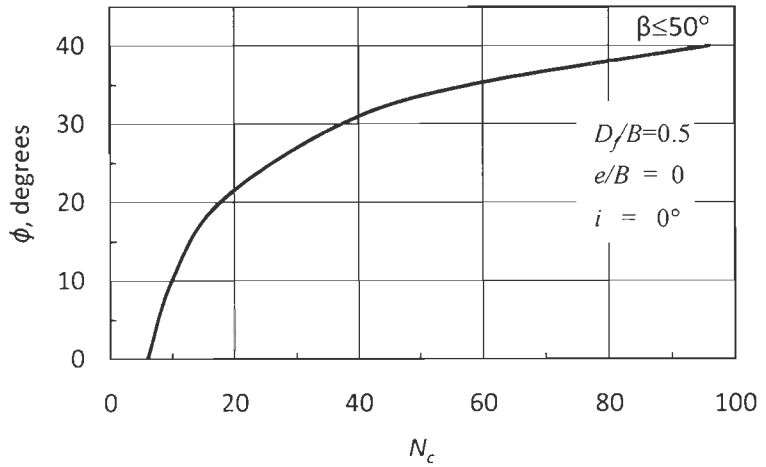

Fig. A.III. 1 a (vii) N_c versus ϕ for D_e/B=6.0

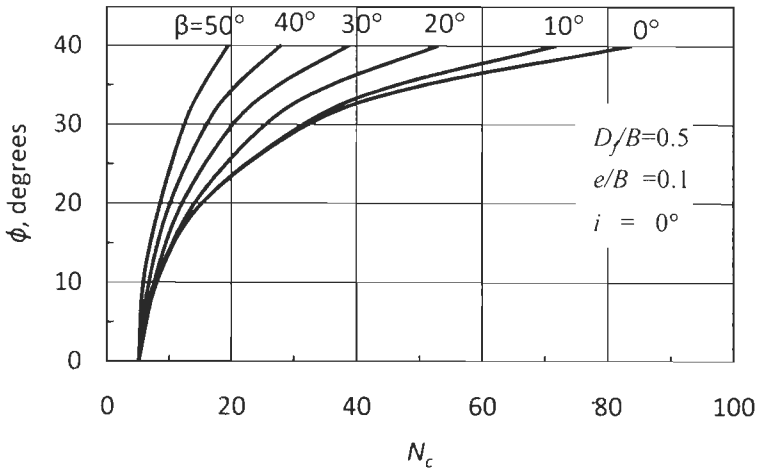

Fig. A.III. 1 b (i) N_c versus ϕ for D_e/B=0

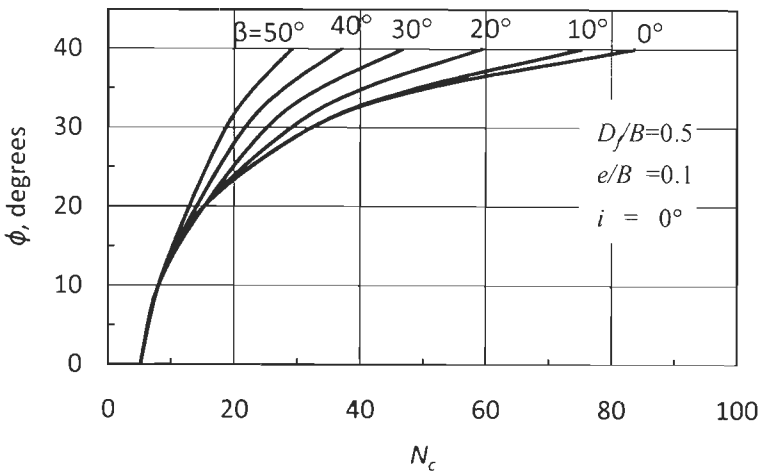

Fig. A.III. 1 b (ii) N_c versus ϕ for D_e/B=1.0

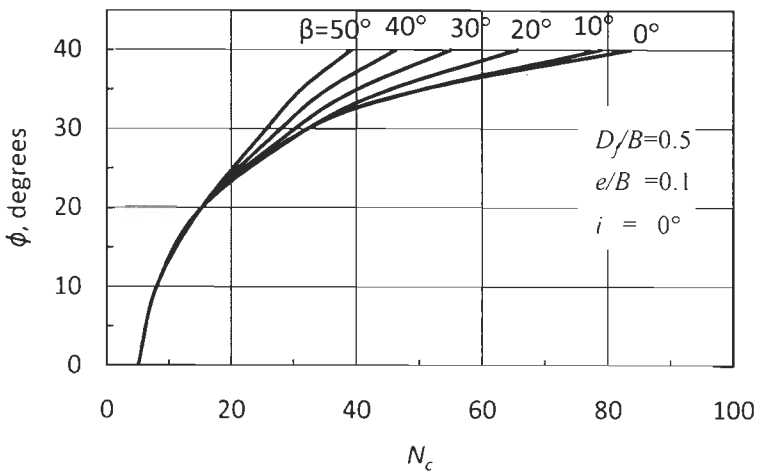

Fig. A.III. 1 b (iii) N_c versus ϕ for D_e/B=2.0

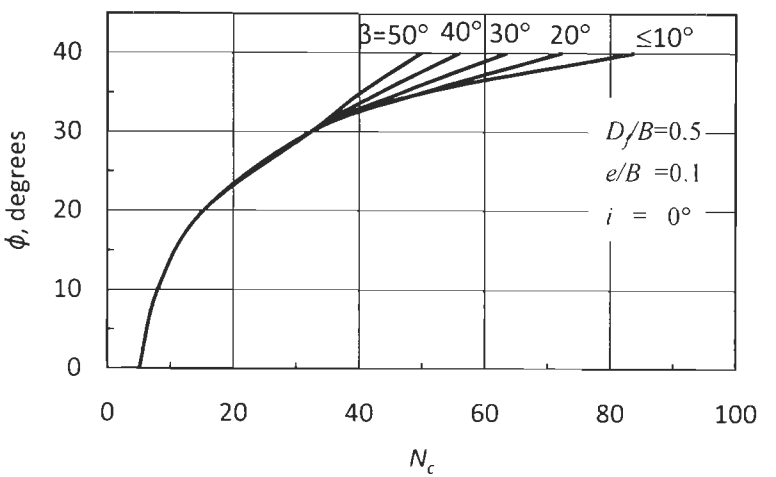

Fig. A.III. 1 b (iv) N_c versus ϕ for D_e/B=3.0

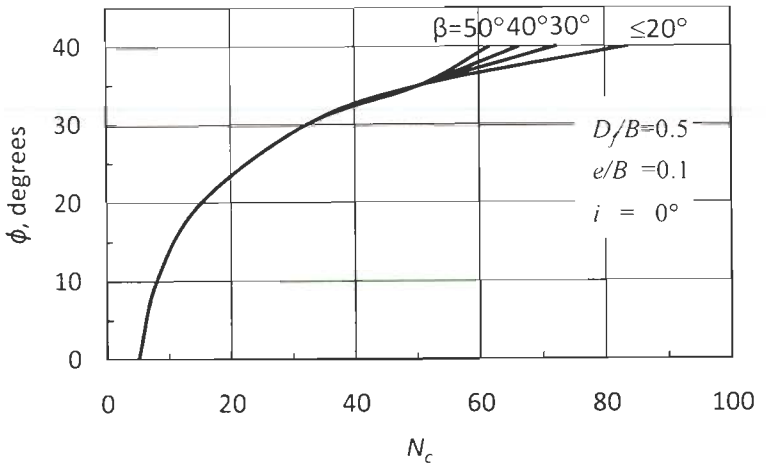

Fig. A.III. 1 b (v) N_c versus ϕ for D_e/B=4.0

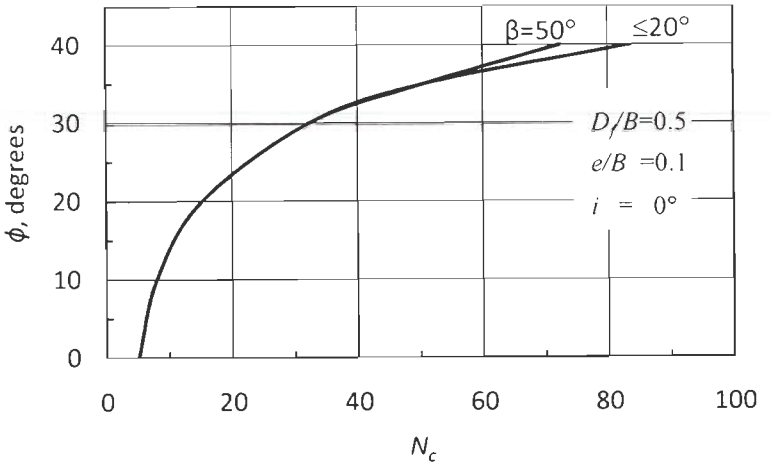

Fig. A.III. 1 b (vi) N_c versus ϕ for D_e/B=5.0

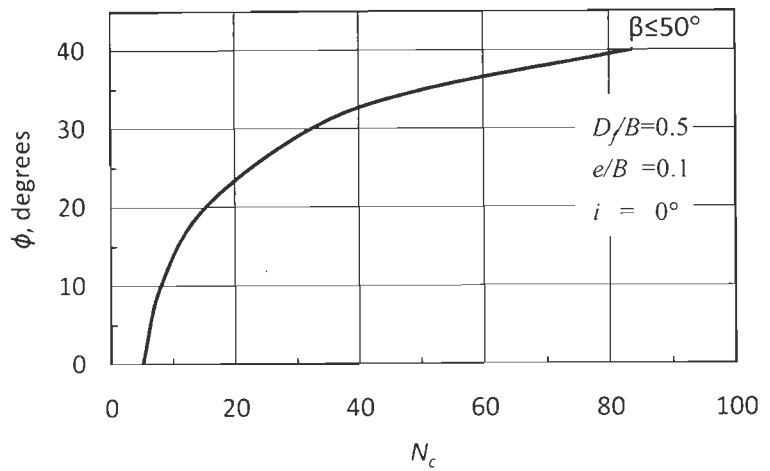

Fig. A.III. 1 b (vii) N_c versus ϕ for D_e/B=6.0

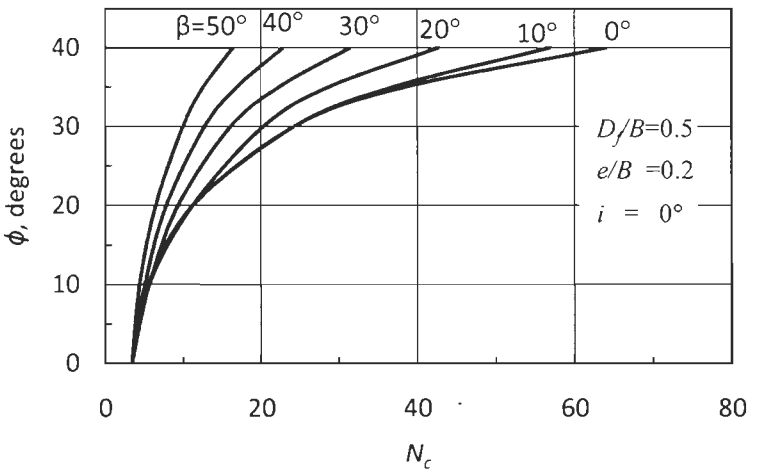

Fig. A.III. 1 c (i) N_c versus ϕ for D_e/B=0

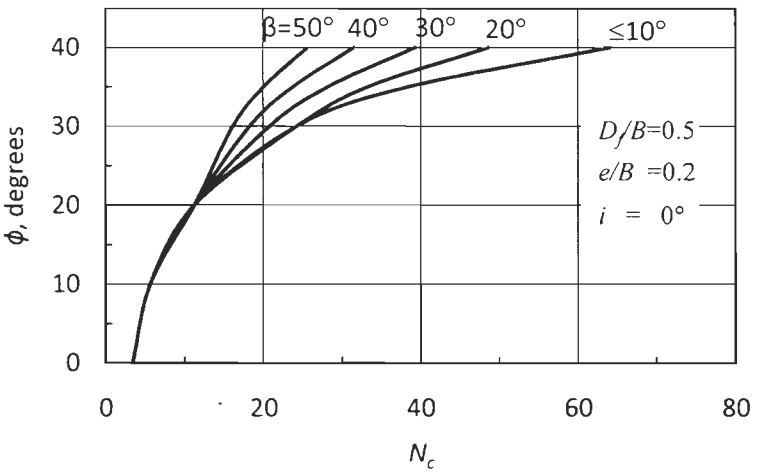

Fig. A.III. 1 c (ii) N_c versus ϕ for D_e/B=1.0

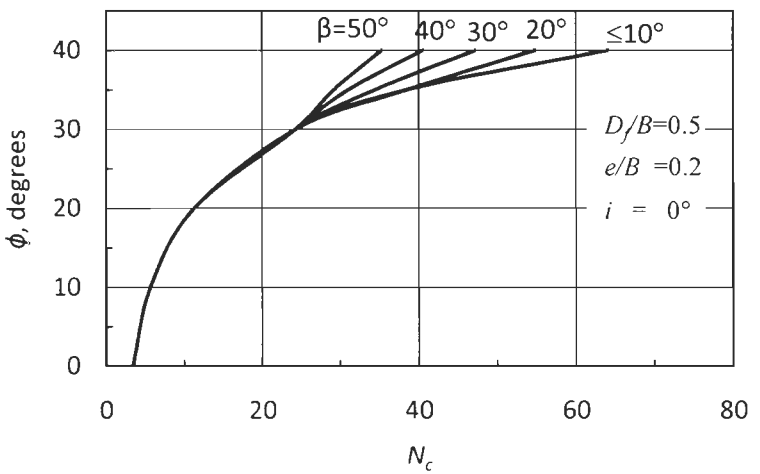

Fig. A.III. 1 c (iii) N_c versus ϕ for D_e/B=2.0

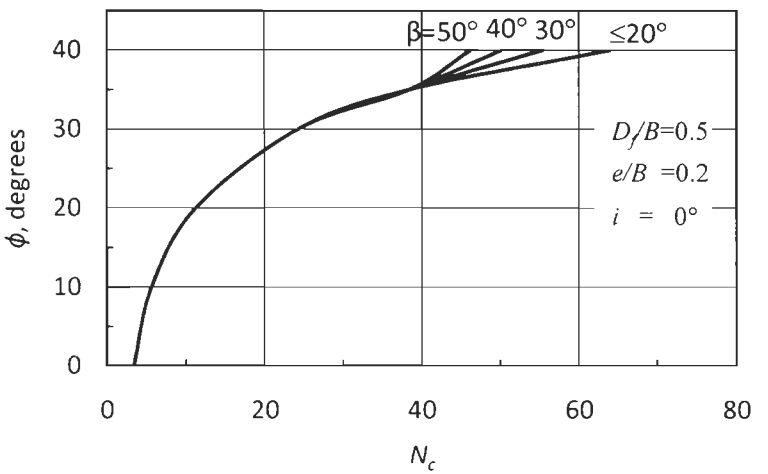

Fig. A.III. 1 c (iv)N_c versus ϕ for D_e/B=3.0

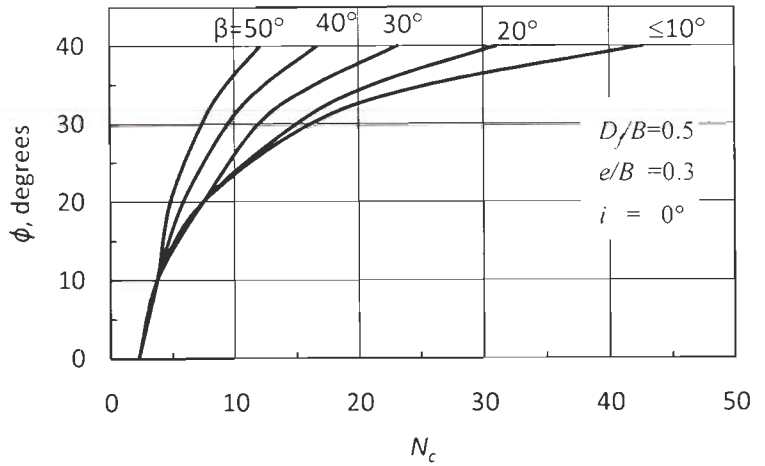

Fig. A.III. 1 d (i) N_c versus ϕ for D_e/B=0

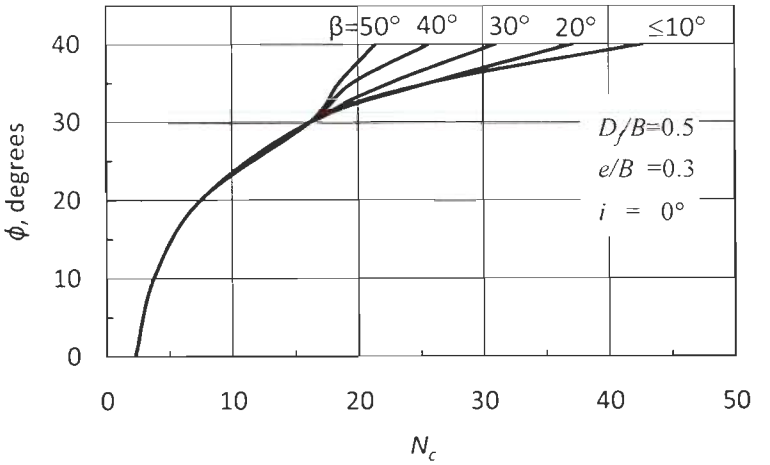

Fig. A.III. 1 d (ii) N_c versus ϕ for D_e/B=1.0

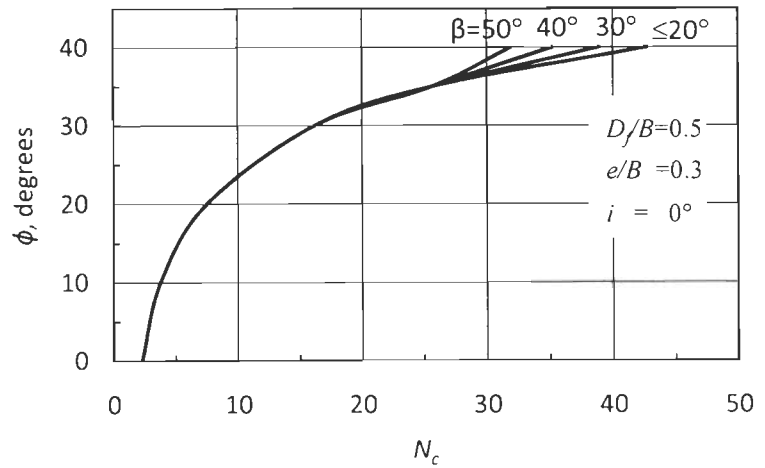

Fig. A.III. 1 d (iii) N_c versus ϕ for D_e/B=2.0

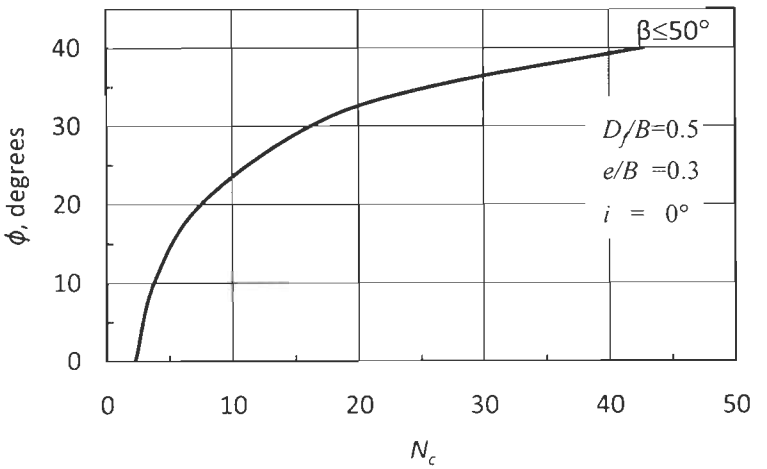

Fig. A.III. 1 d (iv) N_c versus ϕ for D_e/B=3.0

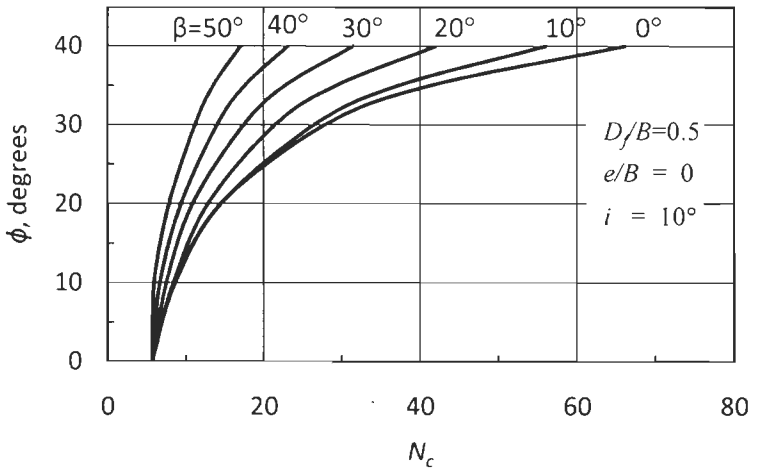

Fig. A.III. 2 a (i) N_c versus ϕ for D_e/B=0

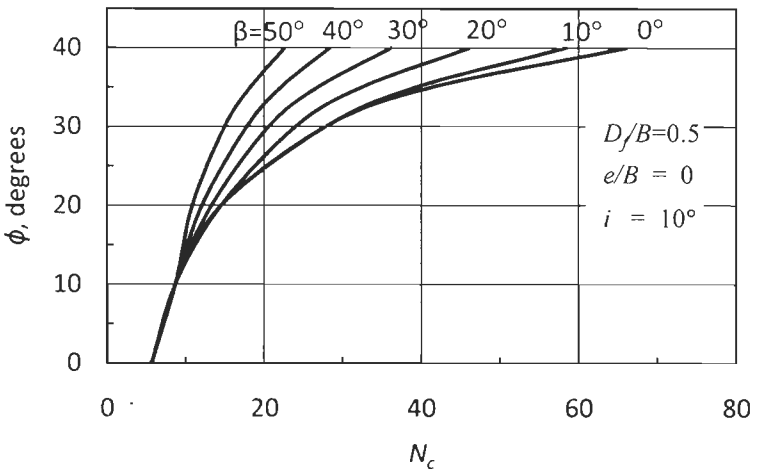

Fig. A.III. 2 a (ii) N_c versus ϕ for D_e/B=1.0

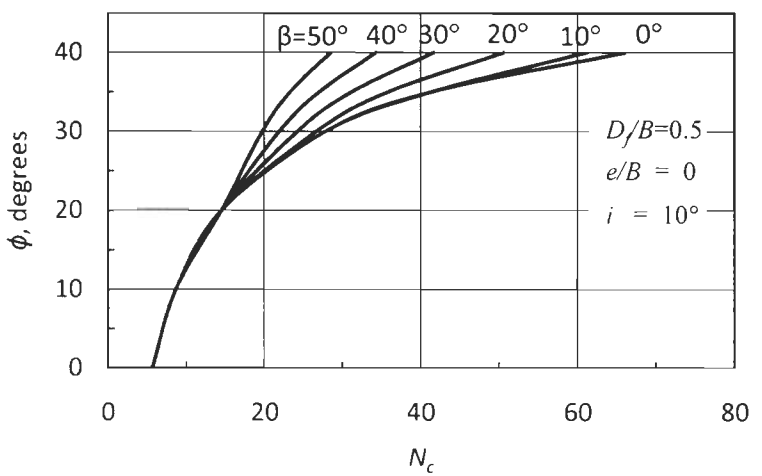

Fig. A.III. 2 a (iii) N_c versus ϕ for D_e/B=2.0

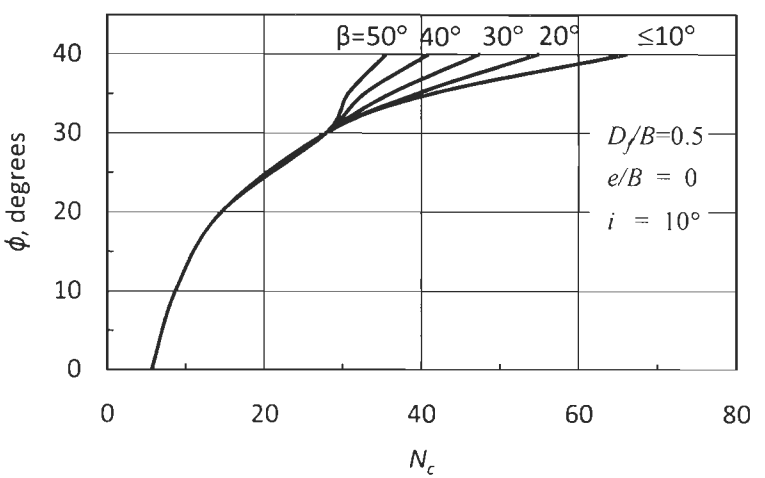

Fig. A.III. 2 a (iv) N_c versus ϕ for D_e/B=3.0

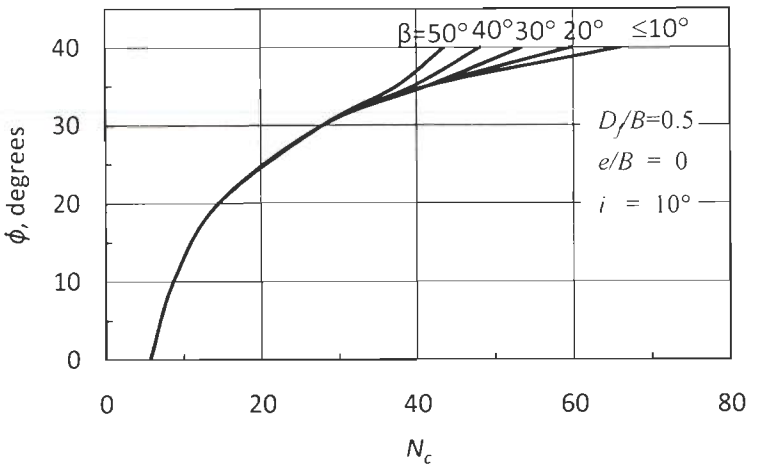

Fig. A.III. 2 a (v) N_c versus ϕ for D_e/B=4.0

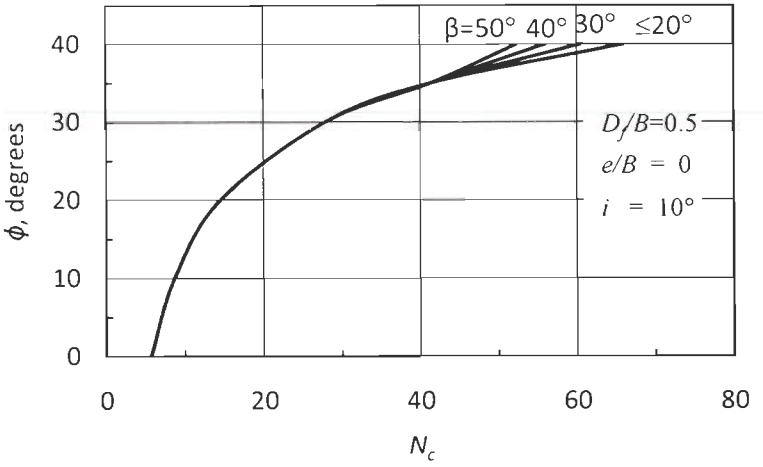

Fig. A.III. 2 a (vi) N_c versus ϕ for D_e/B=5.0

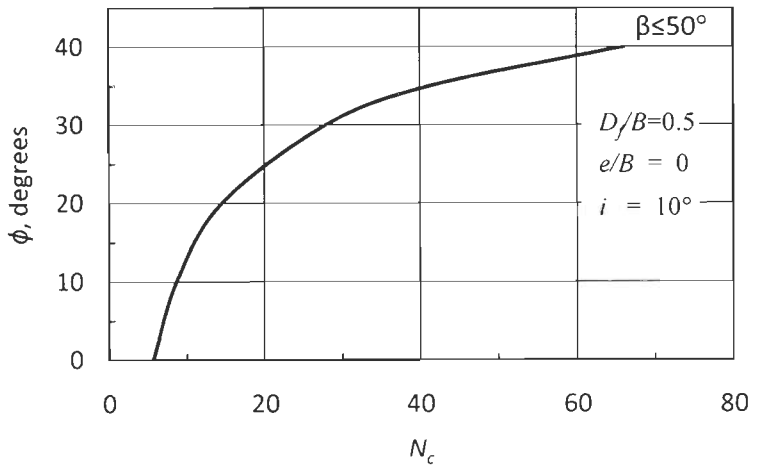

Fig. A.III. 2 a (vii) N_c versus ϕ for D_e/B=6.0

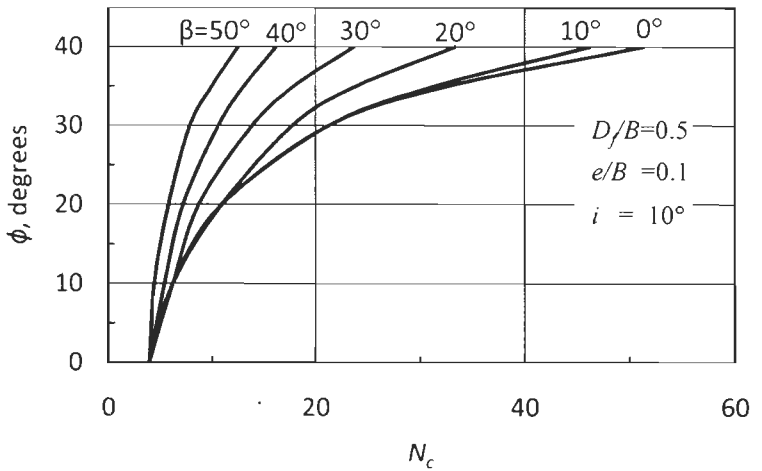

Fig. A.III. 2 b (i) N_c versus ϕ for D_e/B=0

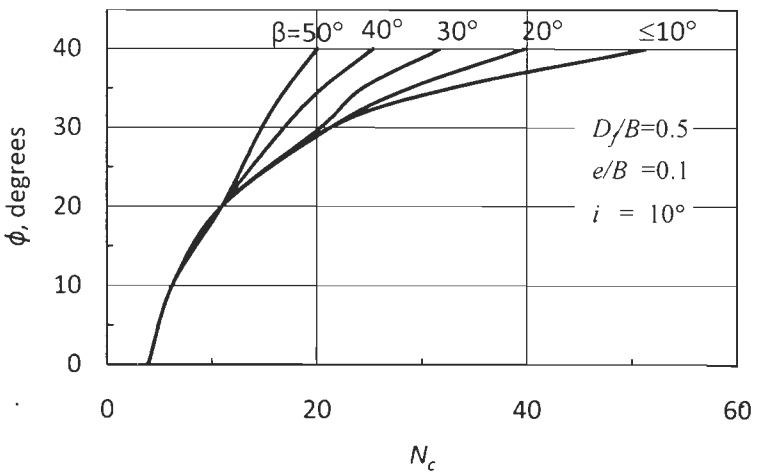

Fig. A.III. 2 b (ii) N_c versus ϕ for D_e/B=1.0

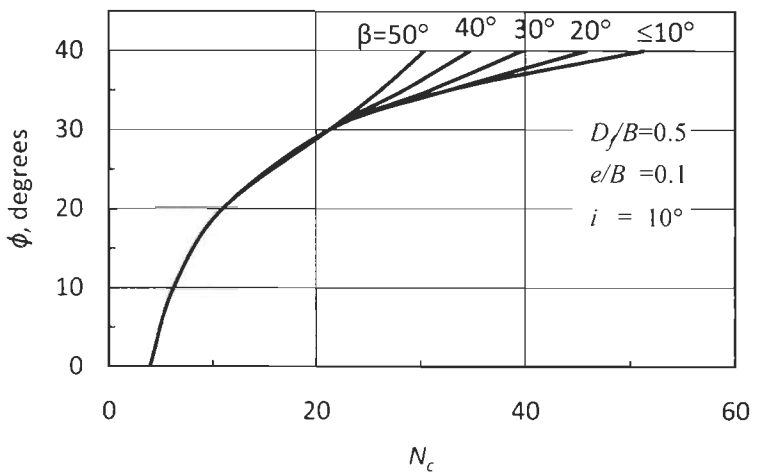

Fig. A.III. 2 b (iii) N_c versus ϕ for D_e/B=2.0

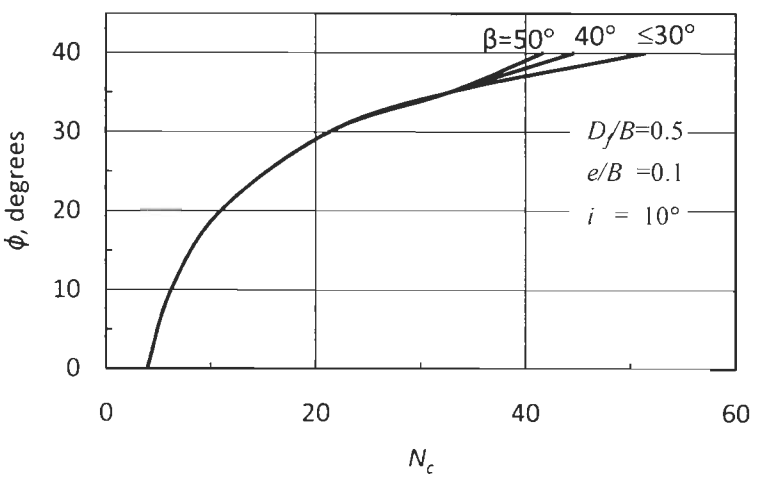

Fig. A.III. 2 b (iv) N_c versus ϕ for D_e/B=3.0

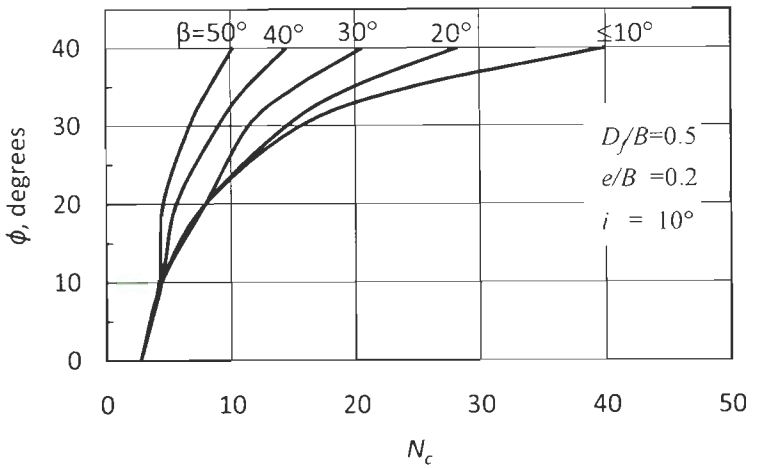

Fig. A.III. 2 c (i) N_c versus ϕ for D_e/B=0

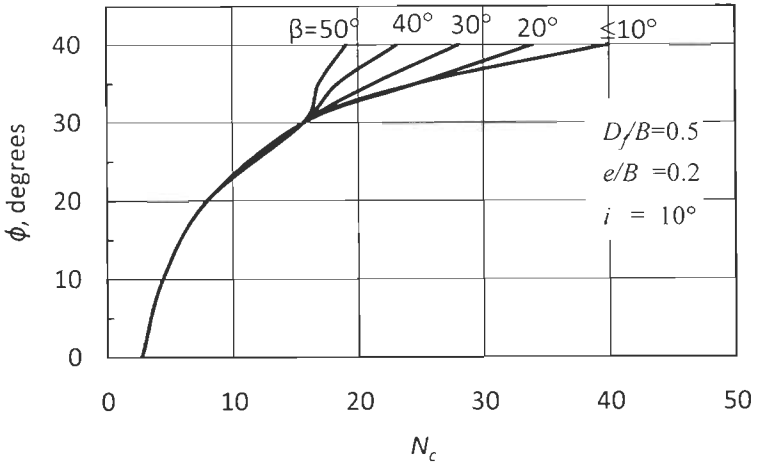

Fig. A.III. 2 c (ii) N_c versus ϕ for D_e/B=1.0

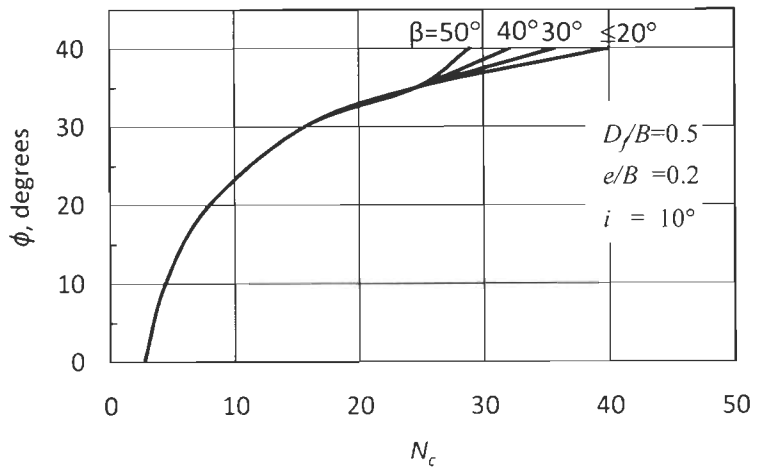

Fig. A.III. 2 c (iii) N_c versus ϕ for D_e/B=2.0

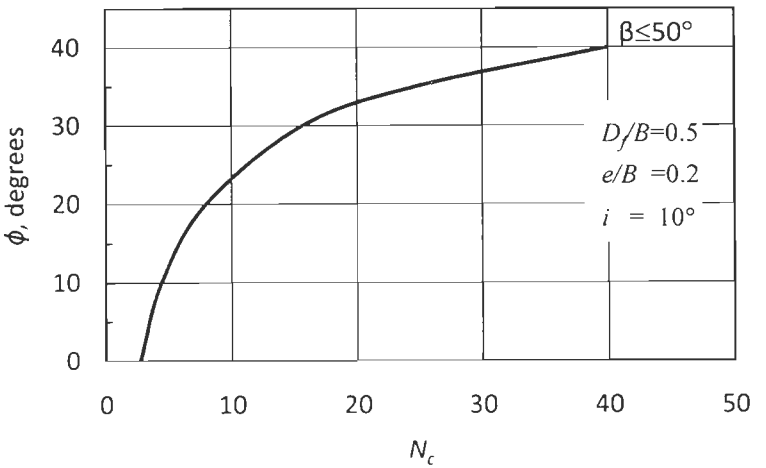

Fig. A.III. 2 c (iv) N_c versus ϕ for D_e/B=3.0

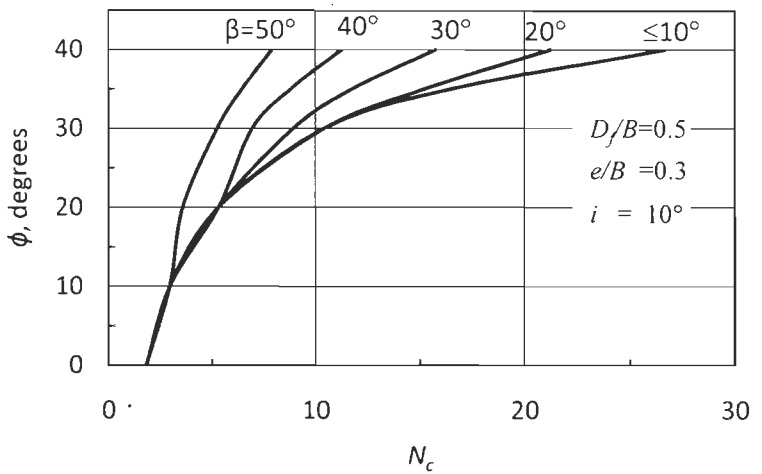

Fig. A.III. 2 d (i) N_c versus ϕ for D_e/B=0

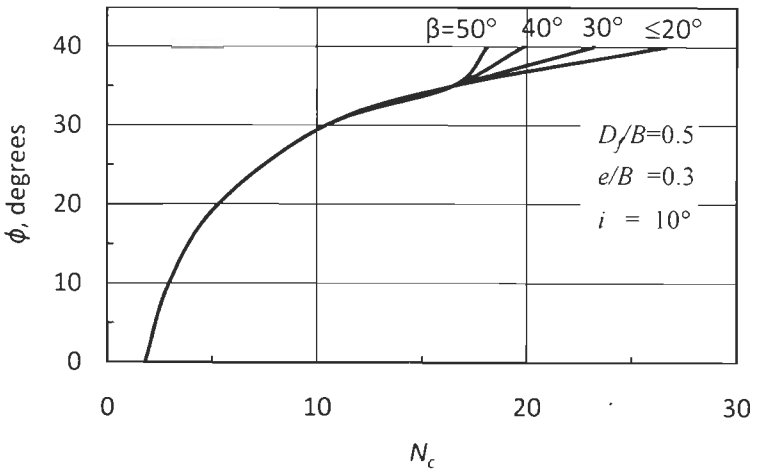

Fig. A.III. 2 d (ii) N_c versus ϕ for D_e/B=1.0

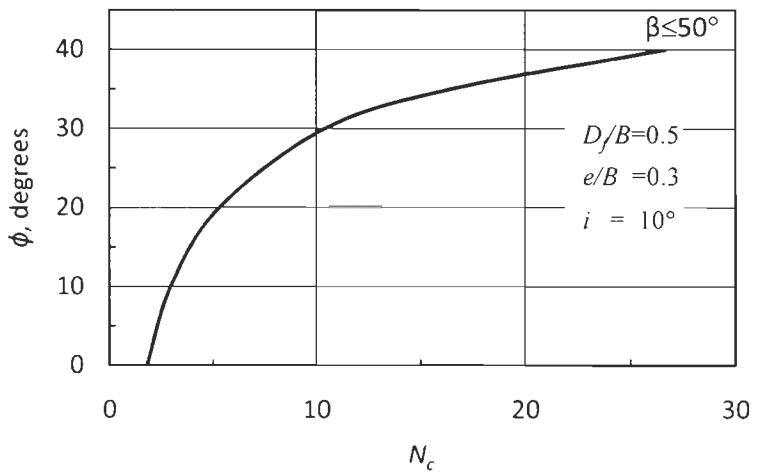

Fig. A.III. 2 d (iii) N_c versus ϕ for D_e/B=2.0

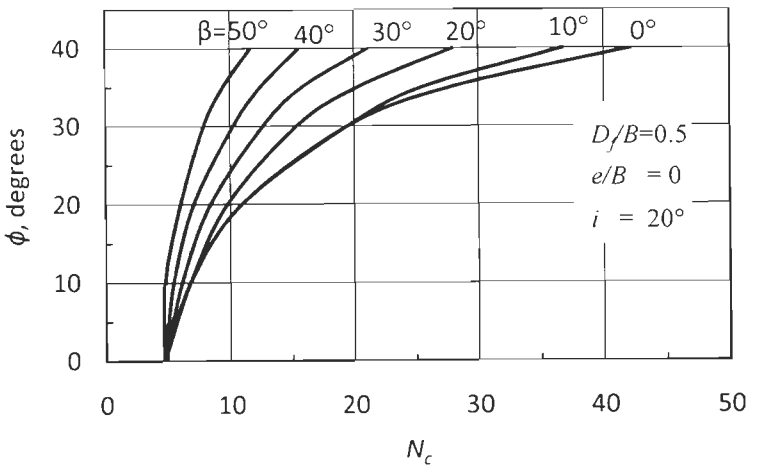

Fig. A.III. 3 a (i) N_c versus ϕ for D_e/B=0

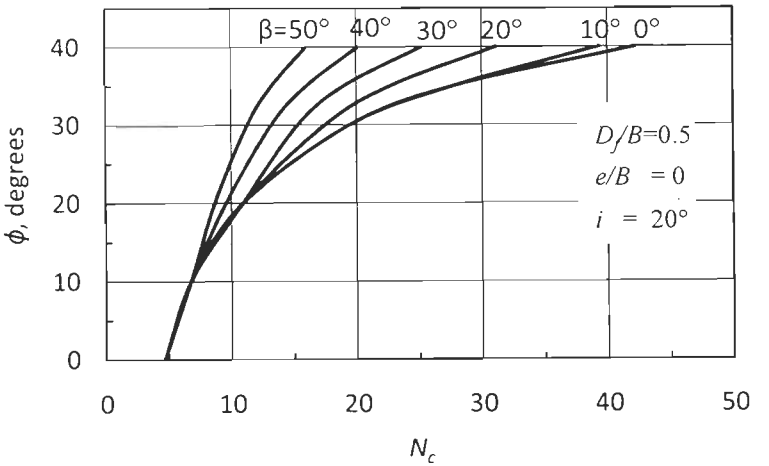

Fig. A.III. 3 a (ii) N_c versus ϕ for D_e/B=1.0

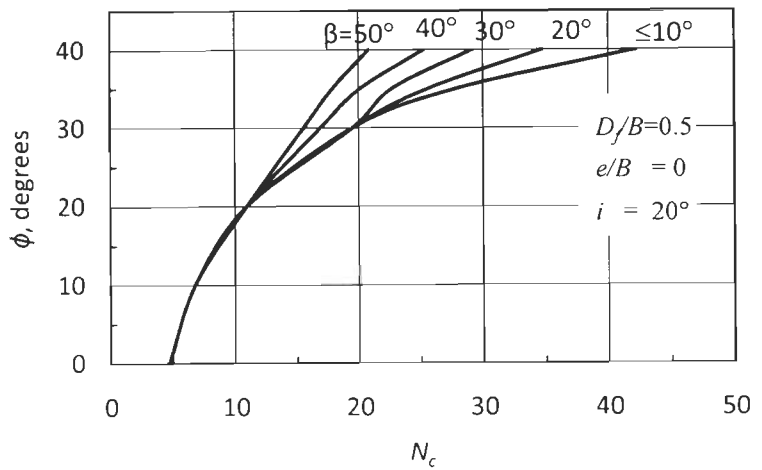

Fig. A.III. 3 a (iii) N_c versus ϕ for D_e/B=2.0

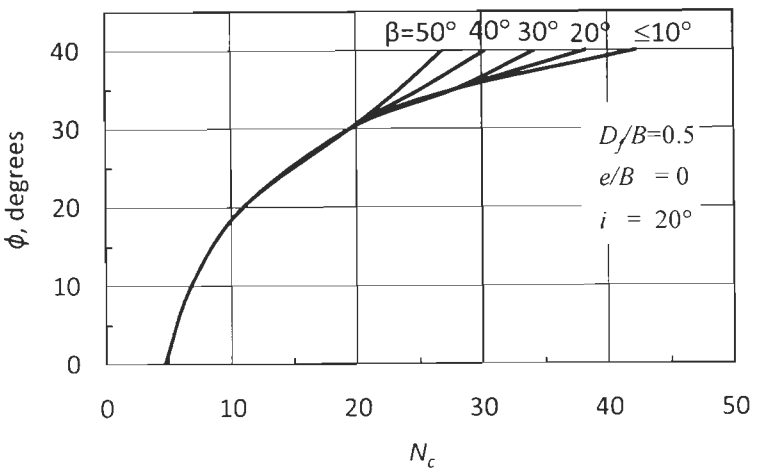

Fig. A.III. 3 a (iv) N_c versus ϕ for D_e/B=3.0

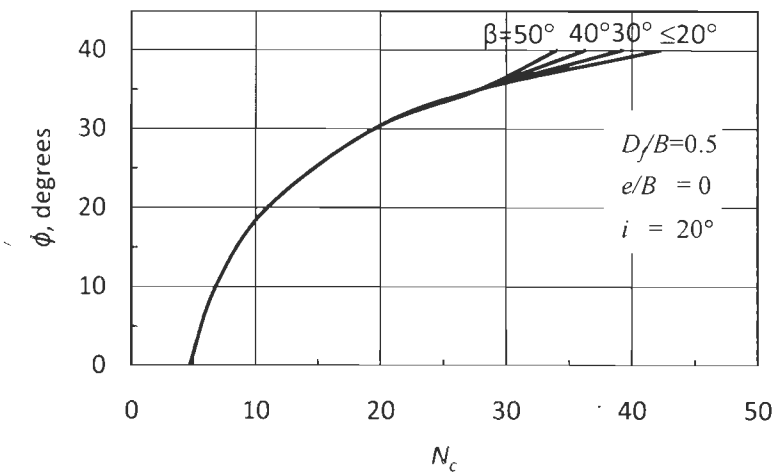

Fig. A.III. 3 a (v) N_c versus ϕ for D_e/B=4.0

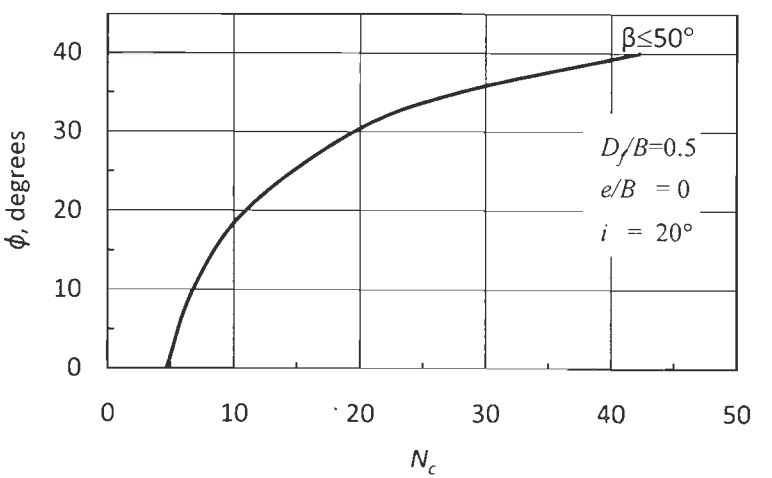

Fig. A.III. 3 a (vi) N_c versus ϕ for D_e/B=5.0

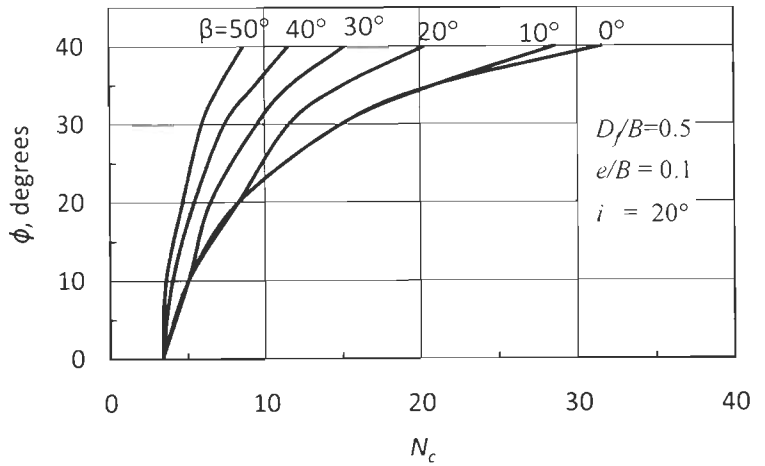

Fig. A.III. 3 b (i) N_c versus ϕ for D_e/B=0

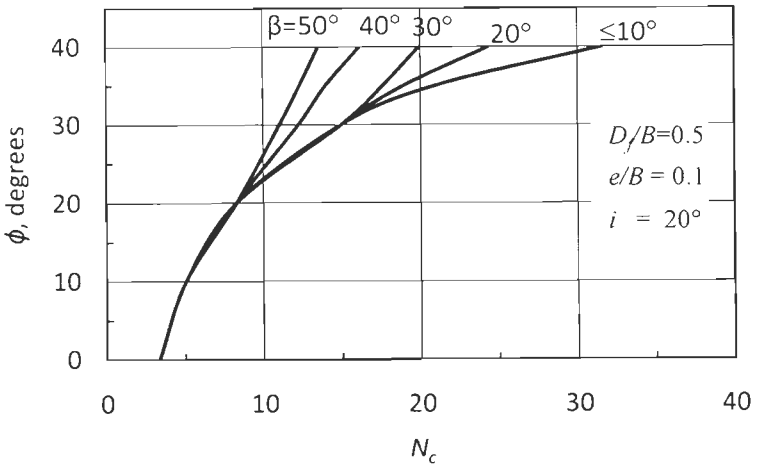

Fig. A.III. 3 b (ii) N_c versus ϕ for D_e/B=1.0

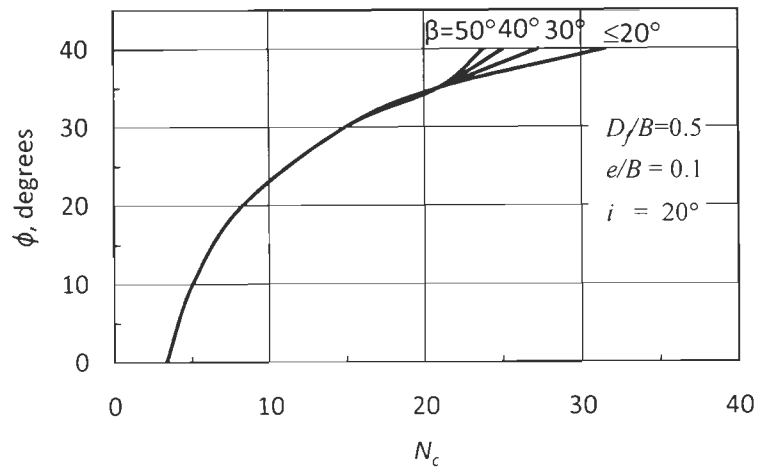

Fig. A.III. 3 b (iii) N_c versus ϕ for D_e/B=2.0

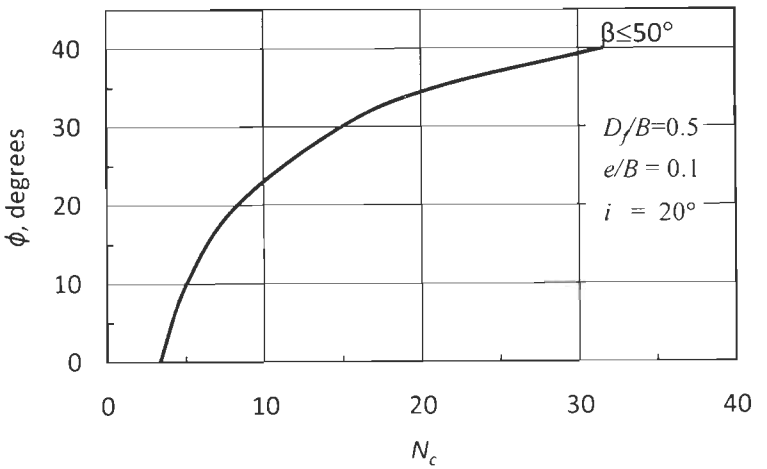

Fig. A.III. 3 b (iv) N_c versus ϕ for D_e/B=3.0

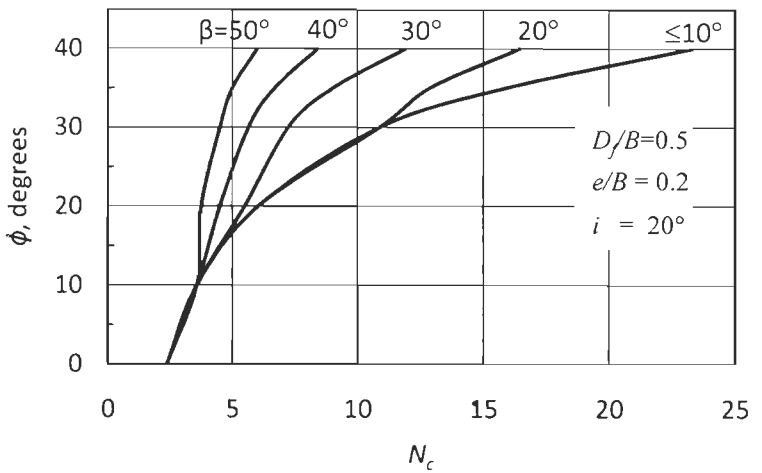

Fig. A.III. 3 c (i) N_c versus ϕ for D_e/B=0

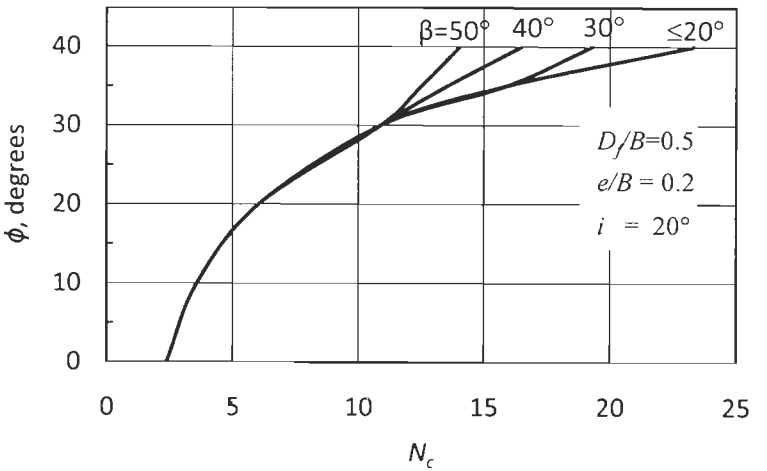

Fig. A.III. 3 c (ii) N_c versus ϕ for D_e/B=1.0

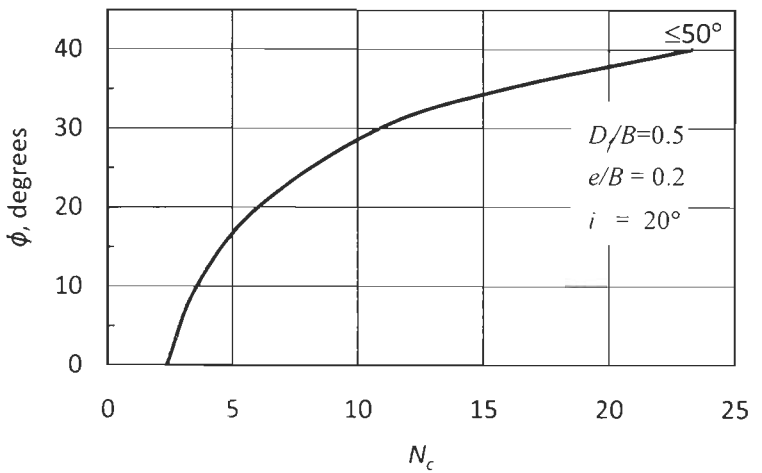

Fig. A.III. 3 c (iii) N_c versus ϕ for D_e/B=2.0

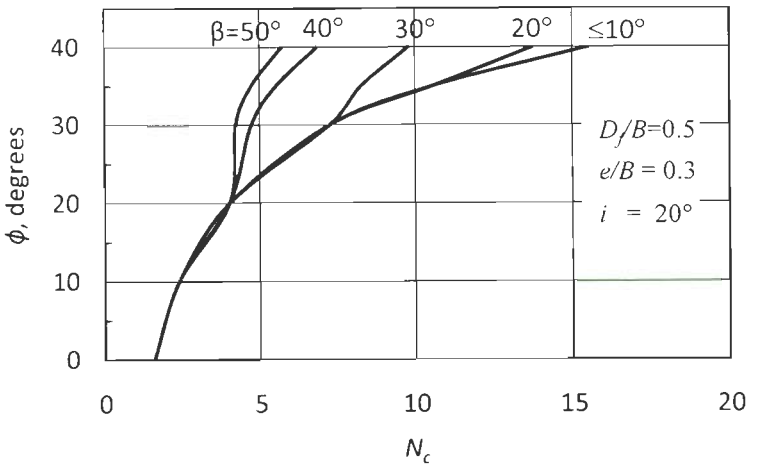

Fig. A.III. 3 d (i) N_c versus ϕ for D_e/B=0

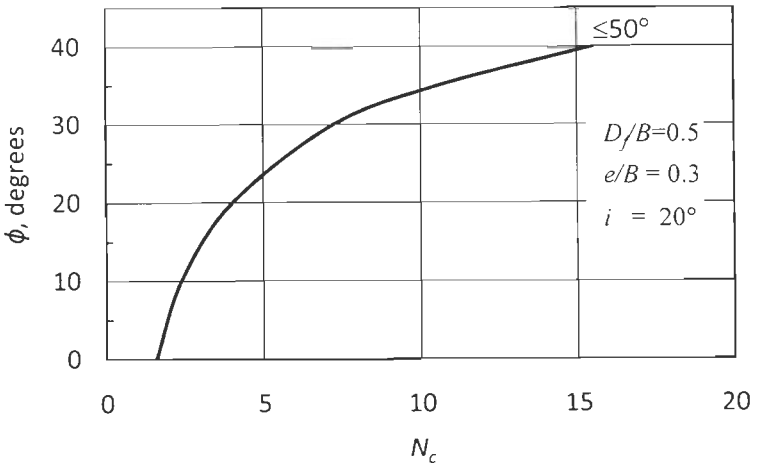

Fig. A.III. 3 d (ii) N_c versus ϕ for D_e/B=1.0

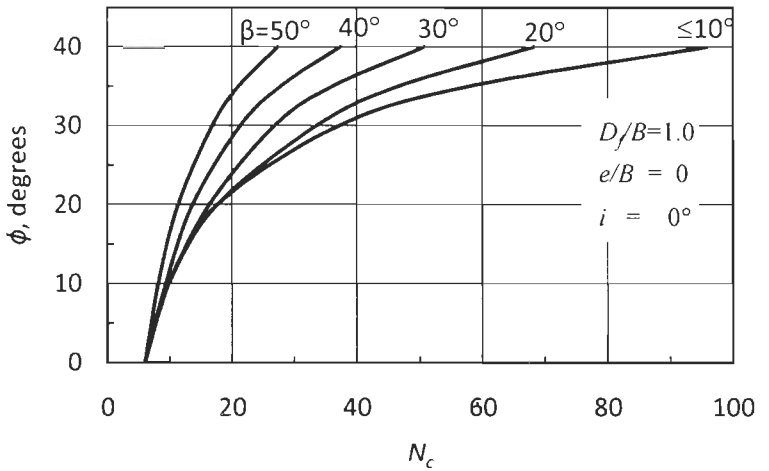

Fig. A.III. 4 a (i) N_c versus ϕ for D_e/B=0

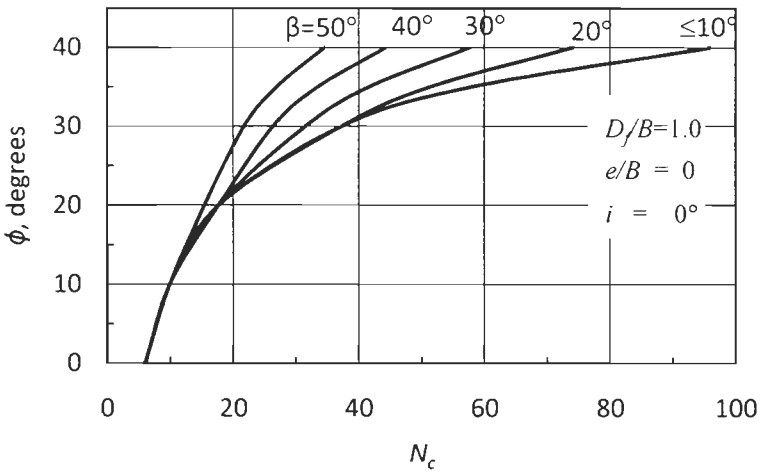

Fig. A.III. 4 a (ii) N_c versus ϕ for D_e/B=1.0

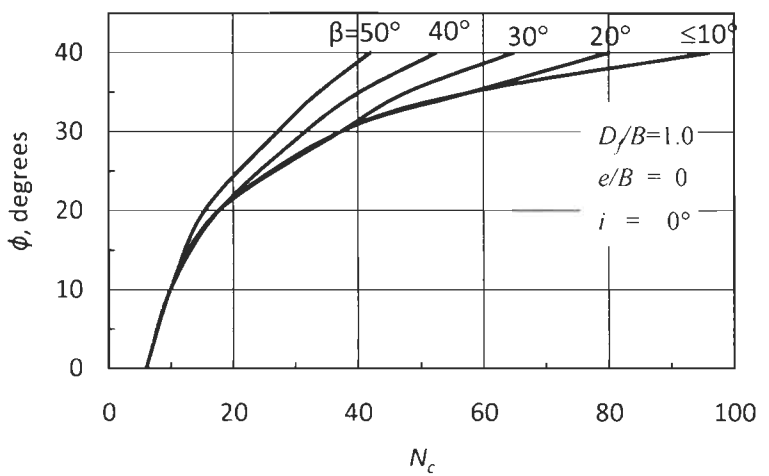

Fig. A.III. 4 a (iii) N_c versus ϕ for D_e/B=2.0

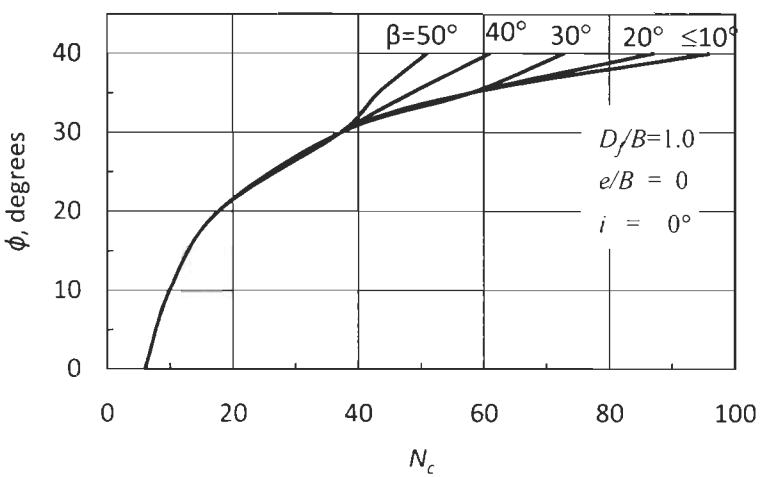

Fig. A.III. 4 a (iv) N_c versus ϕ for D_e/B=3.0

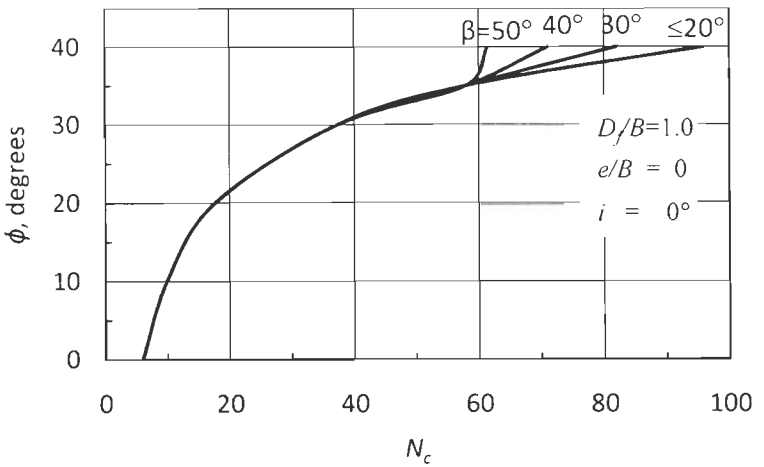

Fig. A.III. 4 a (v) N_c versus ϕ for D_e/B=4.0

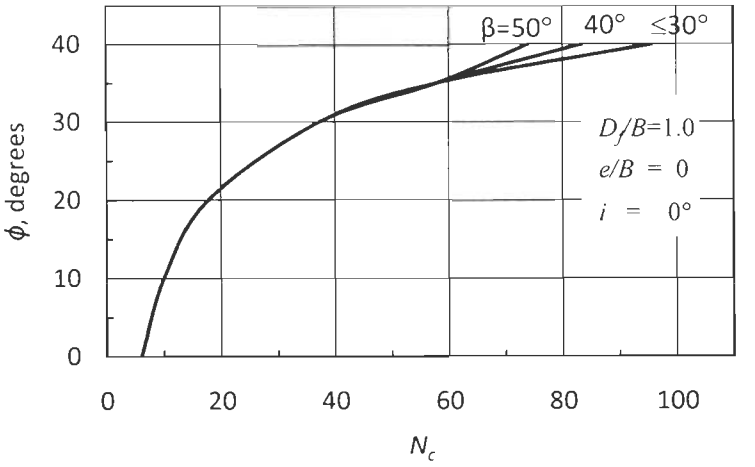

Fig. A.III. 4 a (vi) N_c versus ϕ for D_e/B=5.0

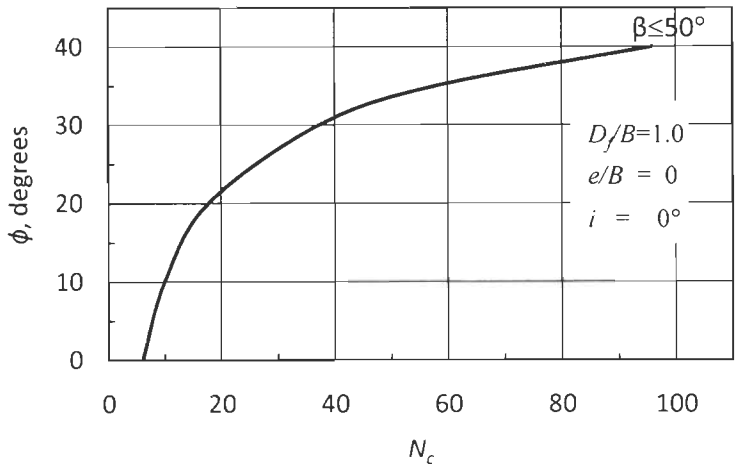

Fig. A.III. 4 a (vii) N_c versus ϕ for D_e/B=6.0

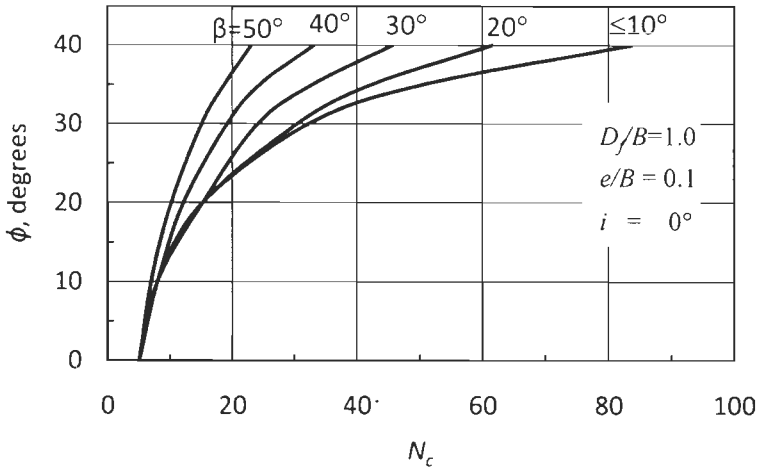

Fig. A.III. 4 b (i) N_c versus ϕ for D_e/B=0

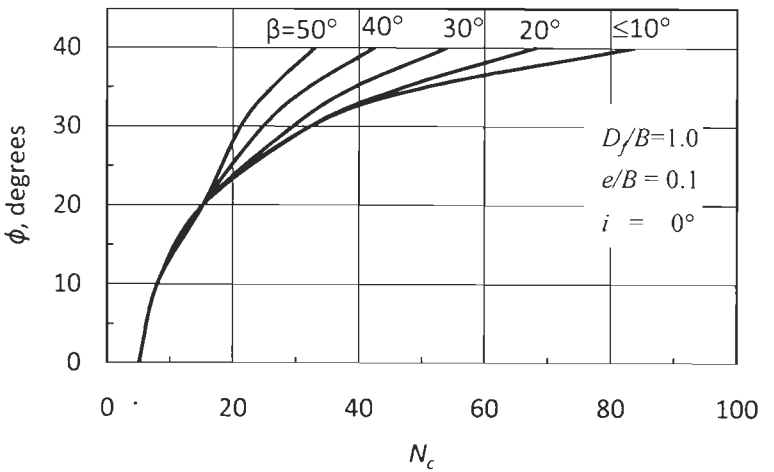

Fig. A.III. 4 b (ii) N_c versus ϕ for D_e/B=1.0

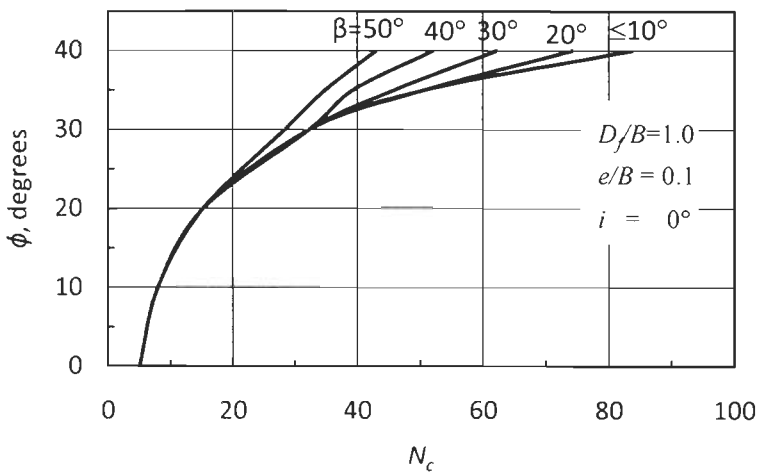

Fig. A.III. 4 b (iii) N_c versus ϕ for D_e/B=2.0

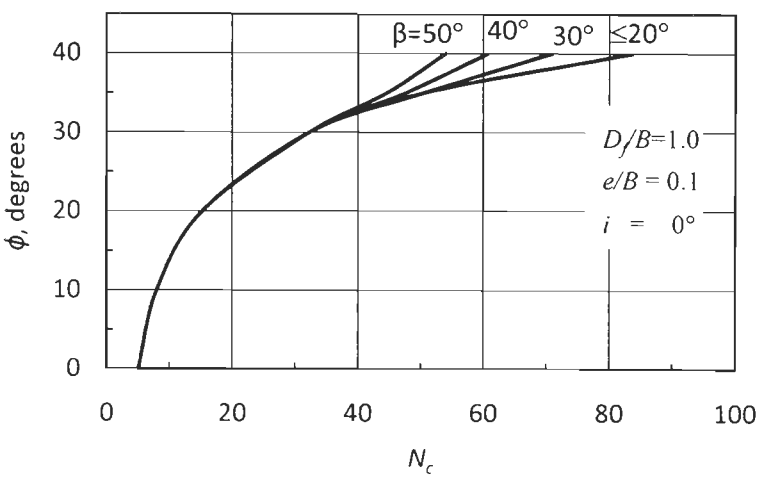

Fig. A.III. 4 b (iv) N_c versus ϕ for D_e/B=3.0

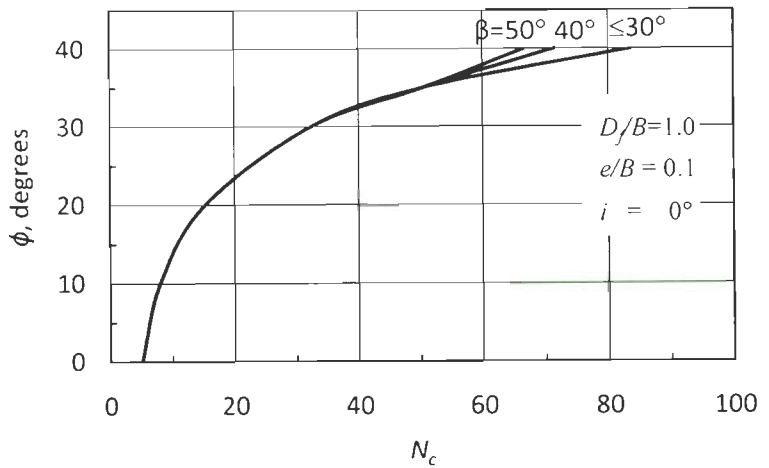

Fig. A.III. 4 b (v) N_c versus ϕ for D_e/B=4.0

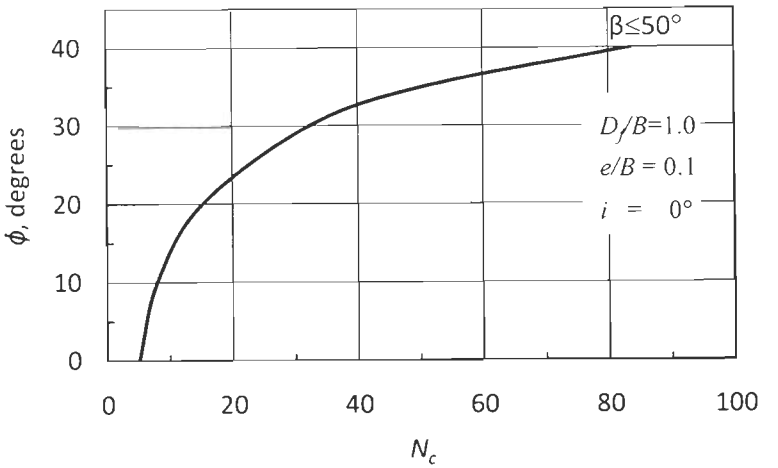

Fig. A.III. 4 b (vi) N_c versus ϕ for D_e/B=5.0

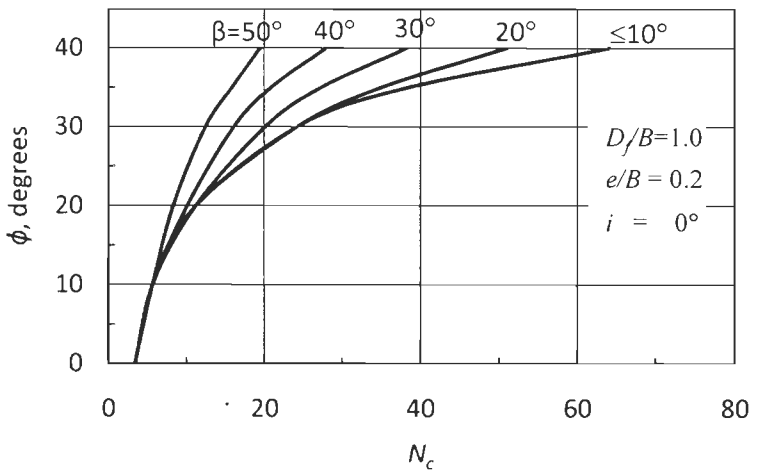

Fig. A.III. 4 c (i) N_c versus ϕ for D_e/B=0

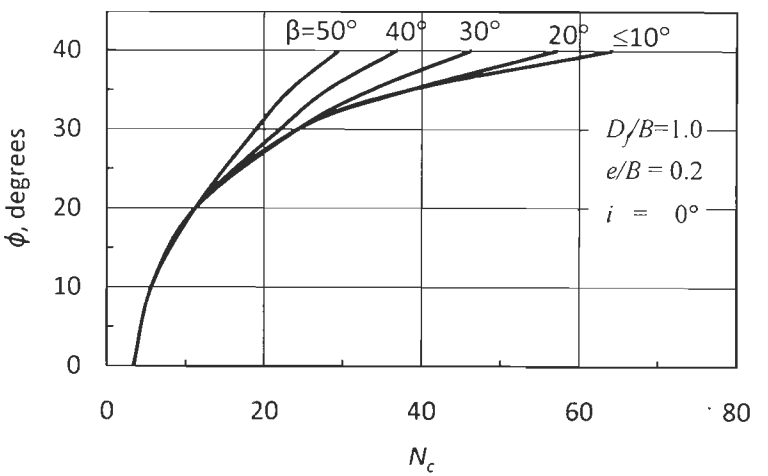

Fig. A.III. 4 c (ii) N_c versus ϕ for D_e/B=1.0

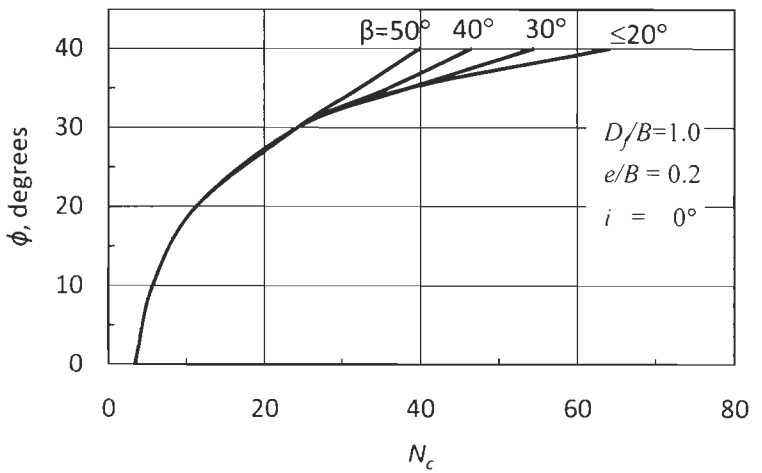

Fig. A.III. 4 c (iii) N_c versus ϕ for D_e/B=2.0

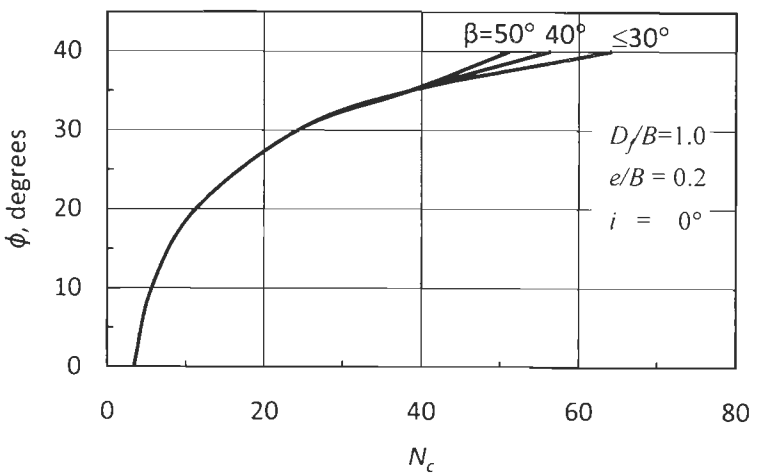

Fig. A.III. 4 c (iv) N_c versus ϕ for D_e/B=3.0

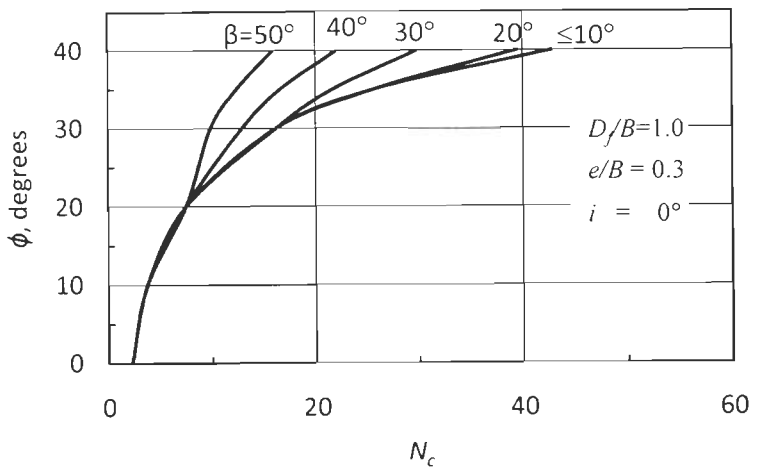

Fig. A.III. 4 d (i) N_c versus ϕ for D_e/B=0

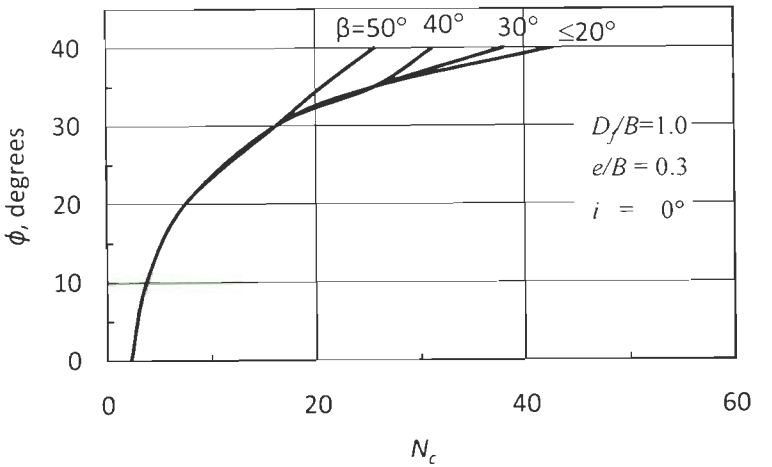

Fig. A.III. 4 d (ii) N_c versus ϕ for D_e/B=1.0

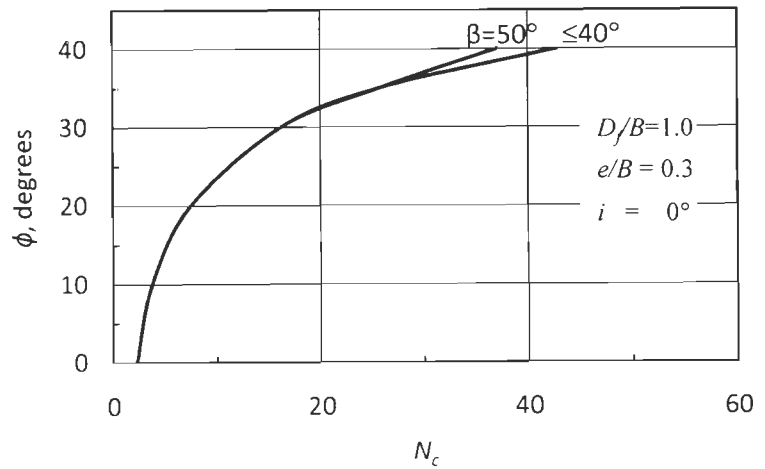

Fig. A.III. 4 d (iii) N_c versus ϕ for D_e/B=2.0

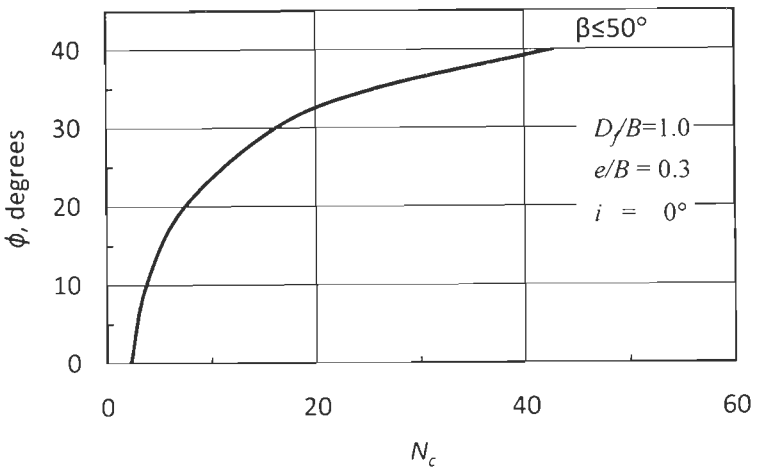

Fig. A.III. 4 d (iii) N_c versus ϕ for D_e/B=3.0

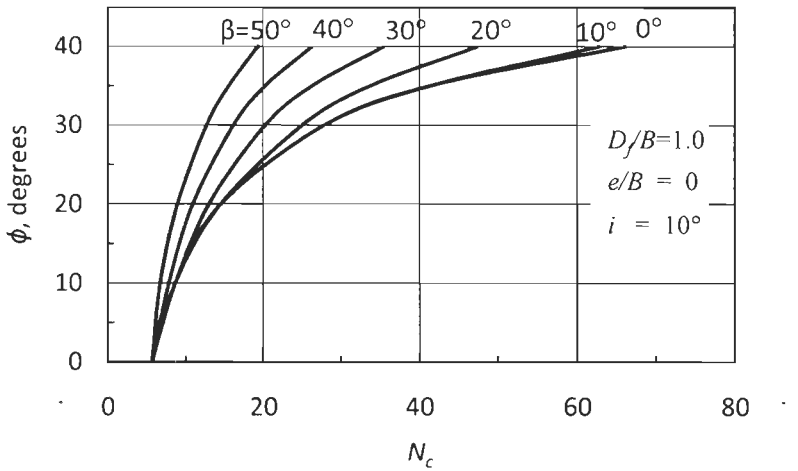

Fig. A.III. 5 a (i) N_c versus ϕ for D_e/B=0

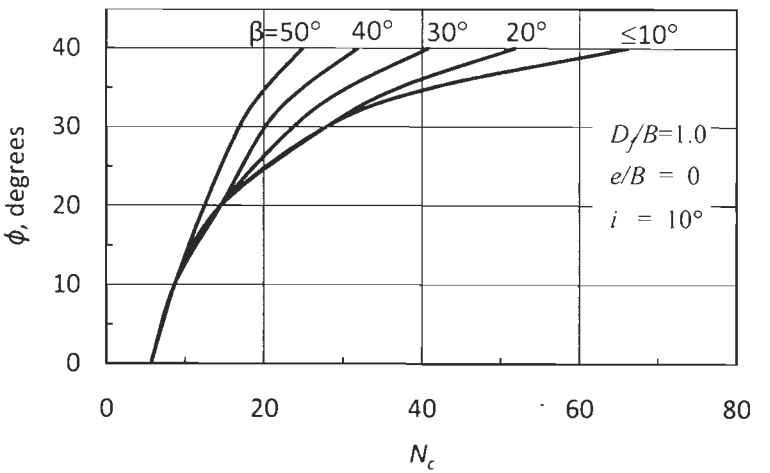

Fig. A.III. 5 a (ii) N_c versus ϕ for D_e/B=1.0

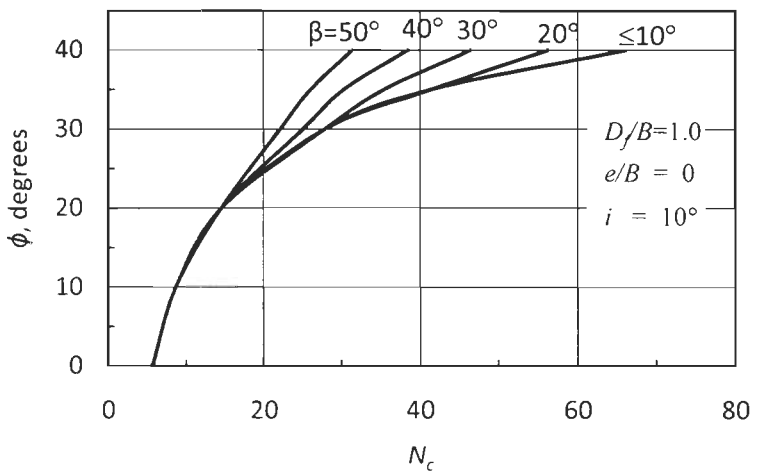

Fig. A.III. 5 a (iii) N_c versus ϕ for D_e/B=2.0

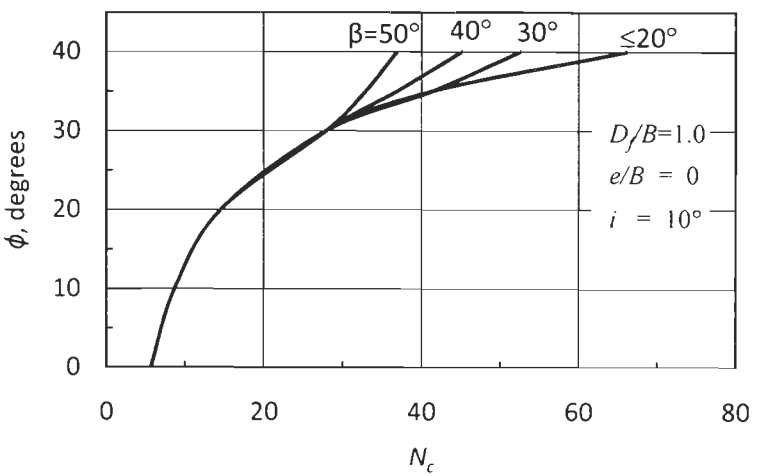

Fig. A.III. 5 a (iv) N_c versus ϕ for D_e/B=3.0

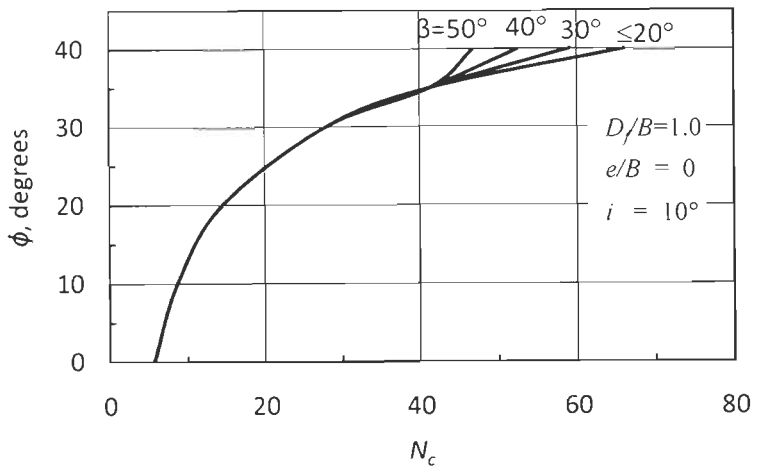

Fig. A.III. 5 a (v) N_c versus ϕ for D_e/B=4.0

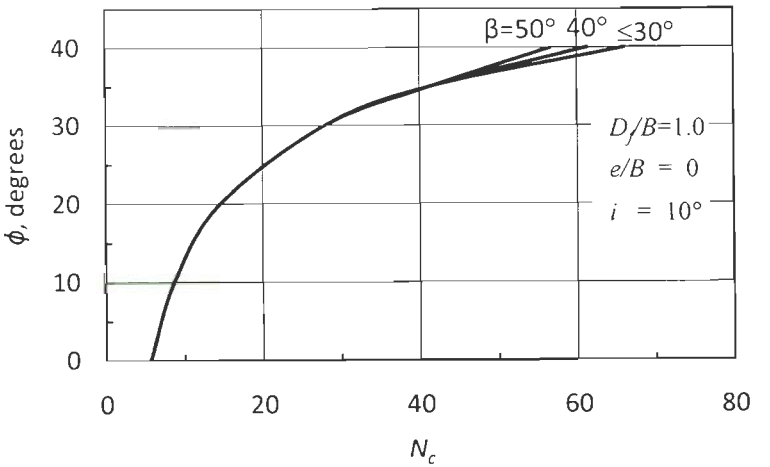

Fig. A.III. 5 a (vi) N_c versus ϕ for D_e/B=5.0

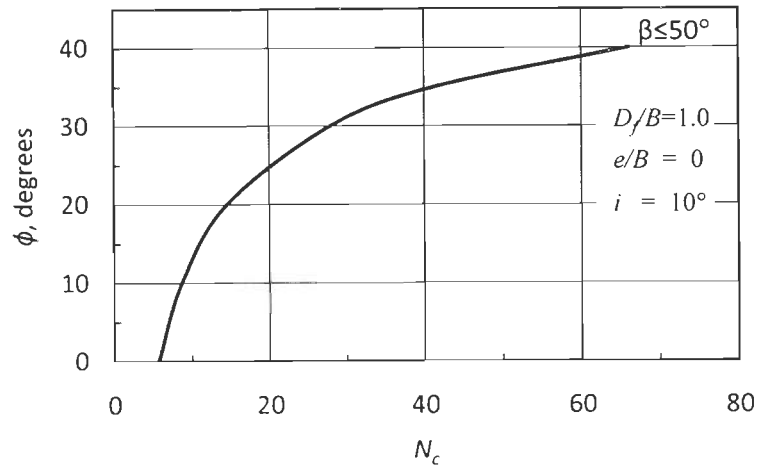

Fig. A.III. 5 a (vii) N_c versus ϕ for D_e/B=6.0

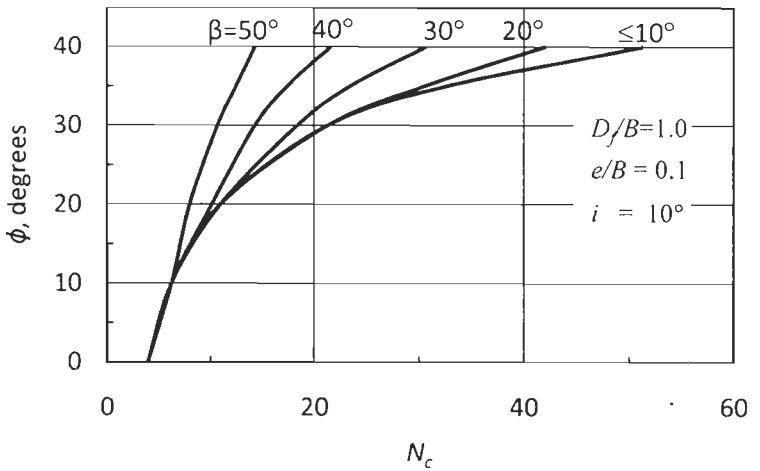

Fig. A.III. 5 b (i) N_c versus ϕ for D_e/B=0

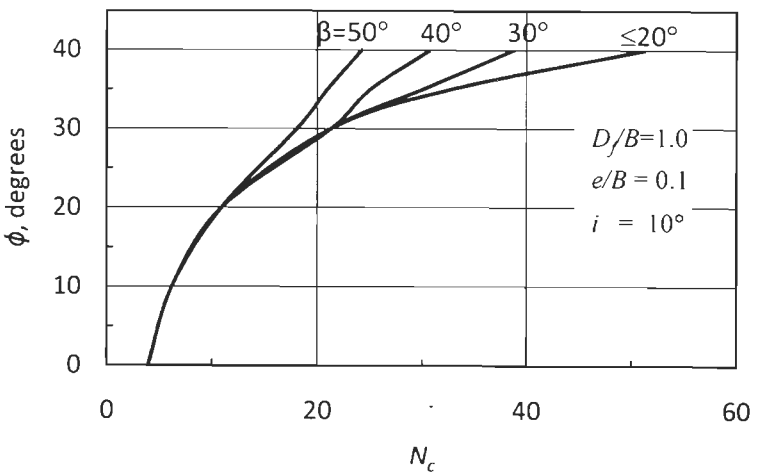

Fig. A.III. 5 b (ii) N_c versus ϕ for D_e/B=1.0

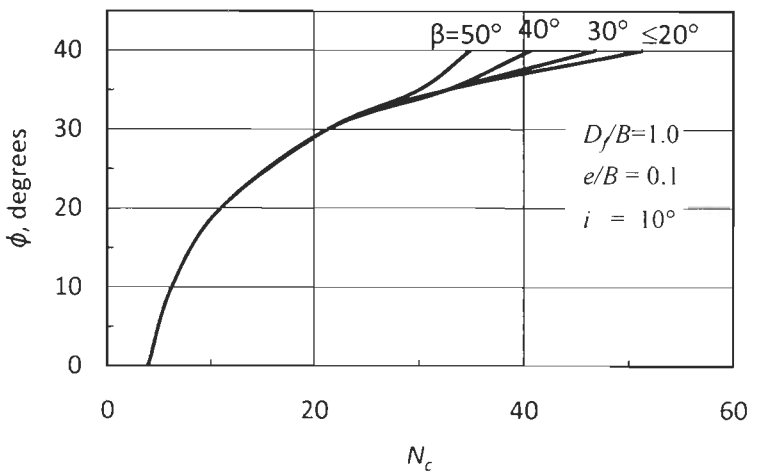

Fig. A.III. 5 b (iii) N_c versus ϕ for D_e/B=2.0

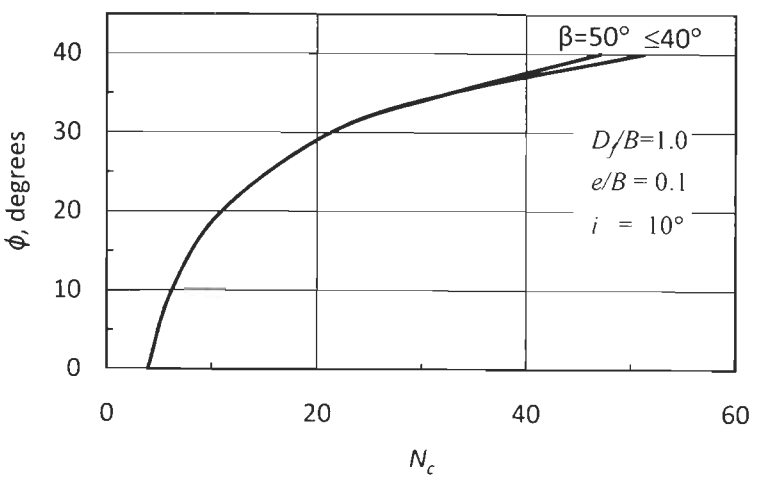

Fig. A.III. 5 b (iv) N_c versus ϕ for D_e/B=3.0

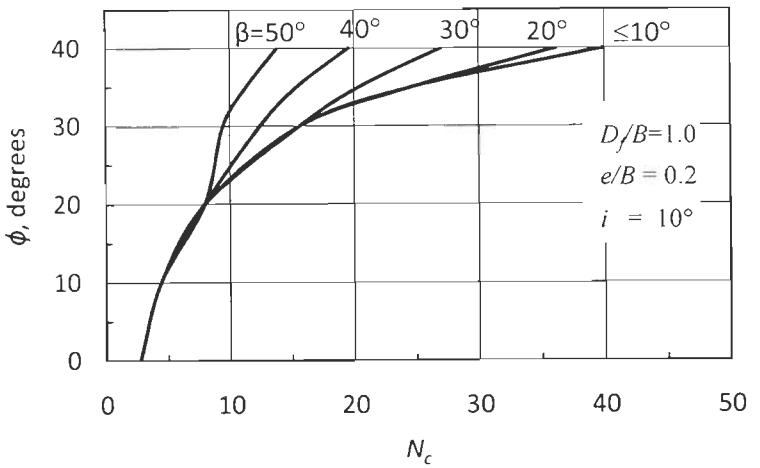

Fig. A.III. 5 c (i) N_c versus ϕ for D_e/B=0

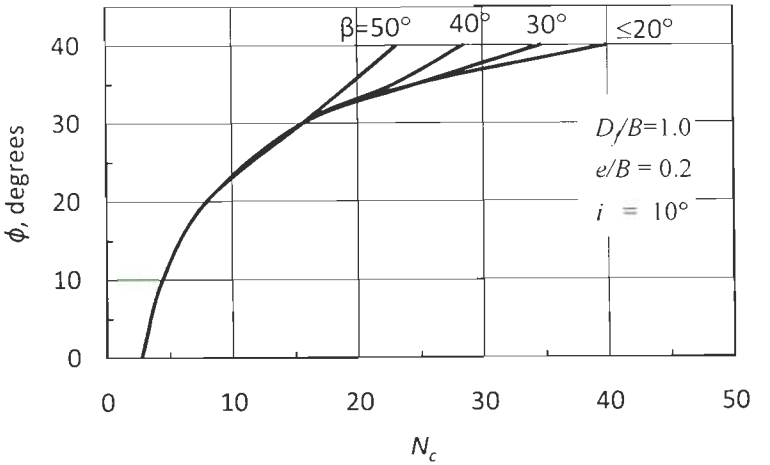

Fig. A.III. 5 c (ii) N_c versus ϕ for D_e/B=1.0

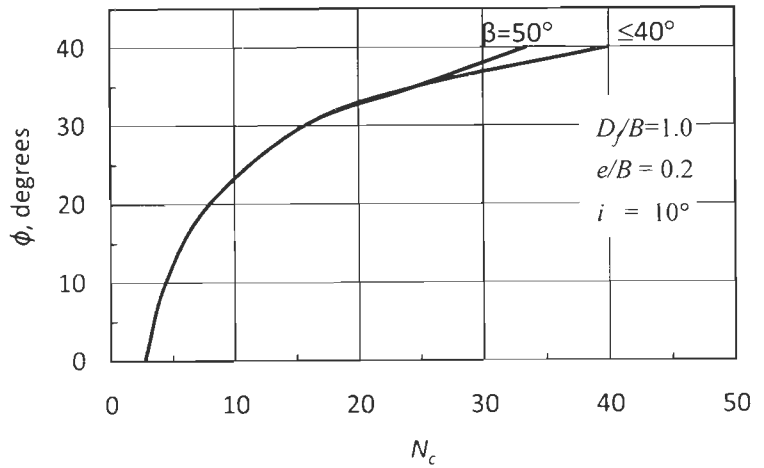

Fig. A.III. 5 c (iii) N_c versus ϕ for D_e/B=2.0

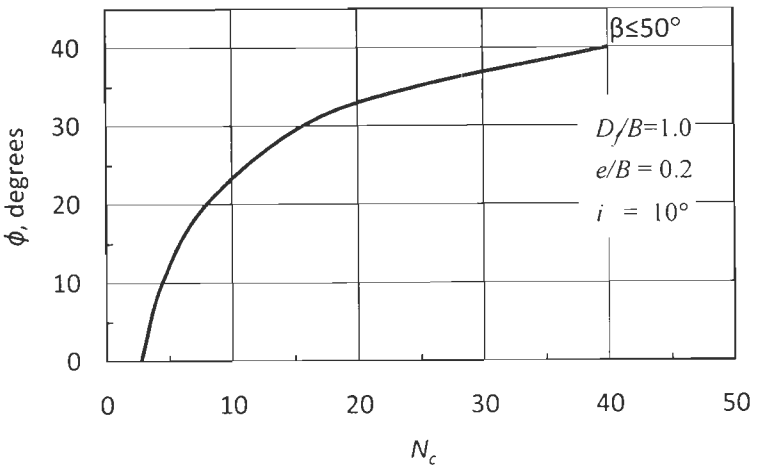

Fig. A.III. 5 c (iv) N_c versus ϕ for D_e/B=3.0

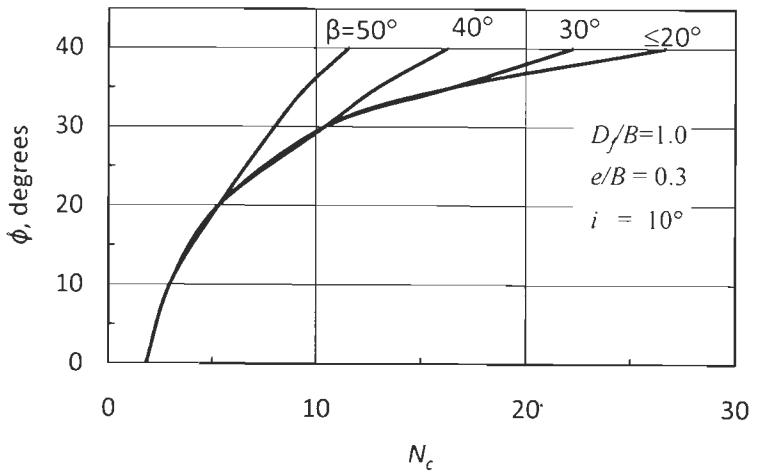

Fig. A.III. 5 d (i) N_c versus ϕ for D_e/B=0

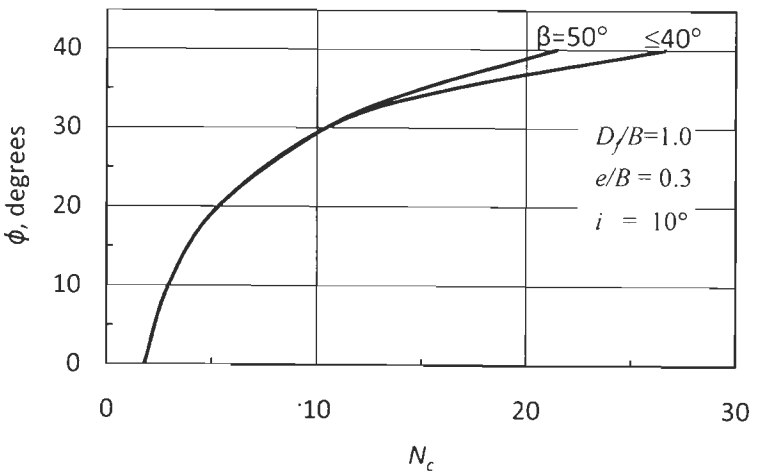

Fig. A.III. 5 d (ii) N_c versus ϕ for D_e/B=1.0

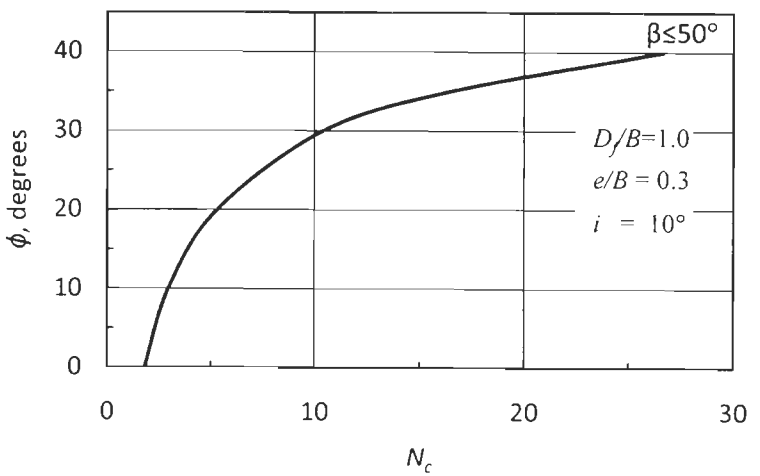

Fig. A.III. 5 d (iii) N_c versus ϕ for D_e/B=2.0

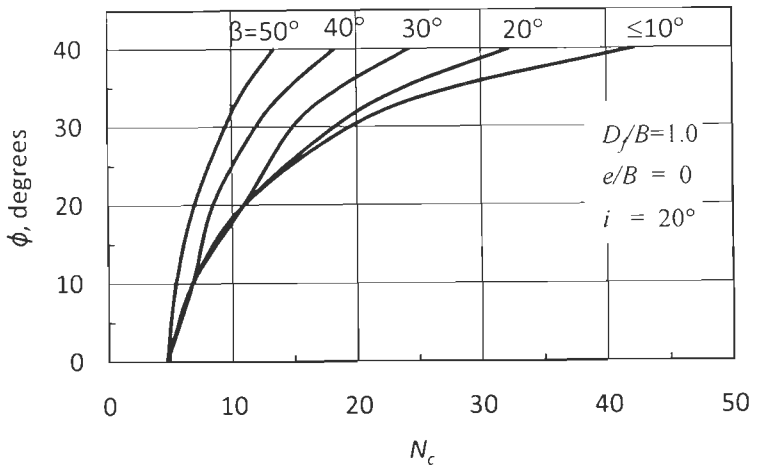

Fig. A.III. 6 a (i) N_c versus ϕ for D_e/B=0

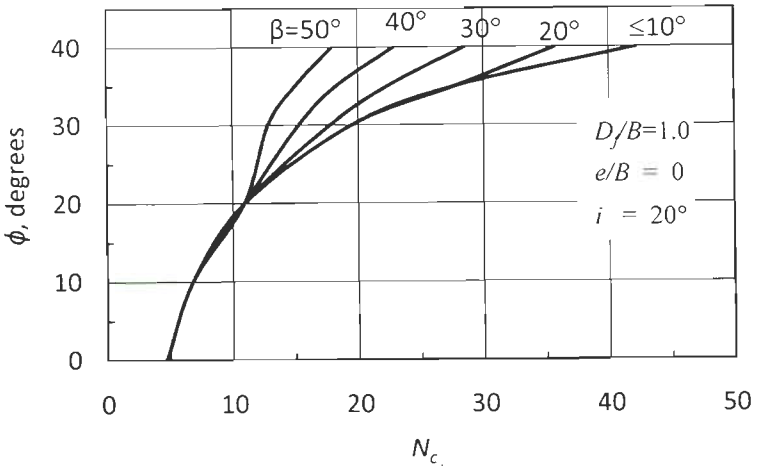

Fig. A.III. 6 a (ii) N_c versus ϕ for D_e/B=1.0

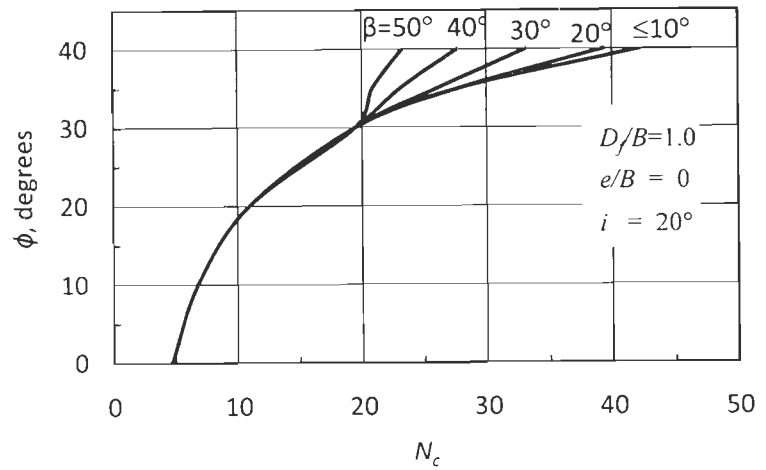

Fig. A.III. 6 a (iii) N_c versus ϕ for D_e/B=2.0

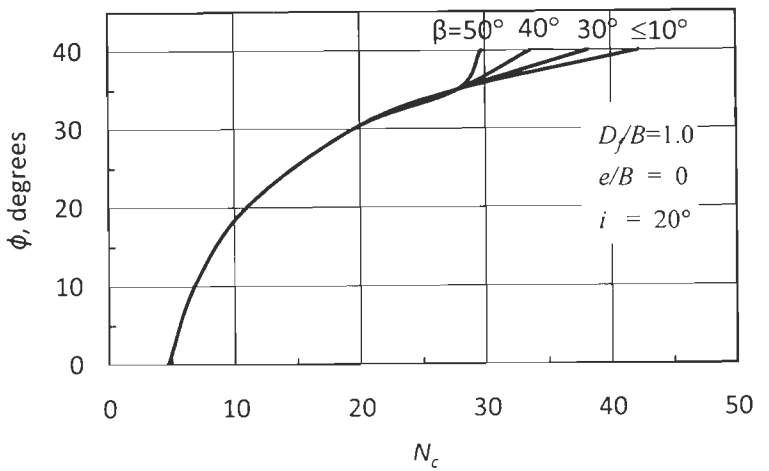

Fig. A.III. 6 a (iv) N_c versus ϕ for D_e/B=3.0

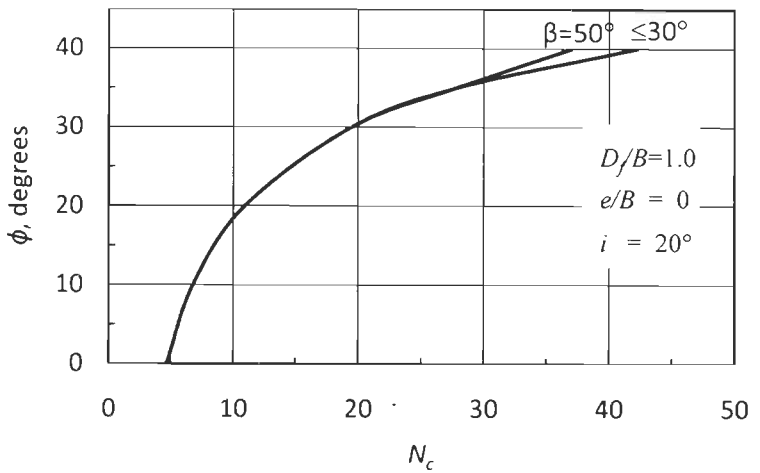

Fig. A.III. 6 a (v) N_c versus ϕ for D_e/B=4.0

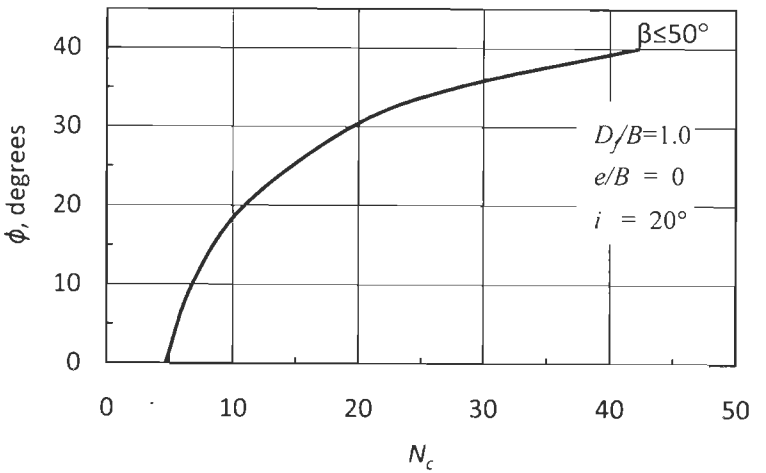

Fig. A.III. 6 a (vi) N_c versus ϕ for D_e/B=5.0

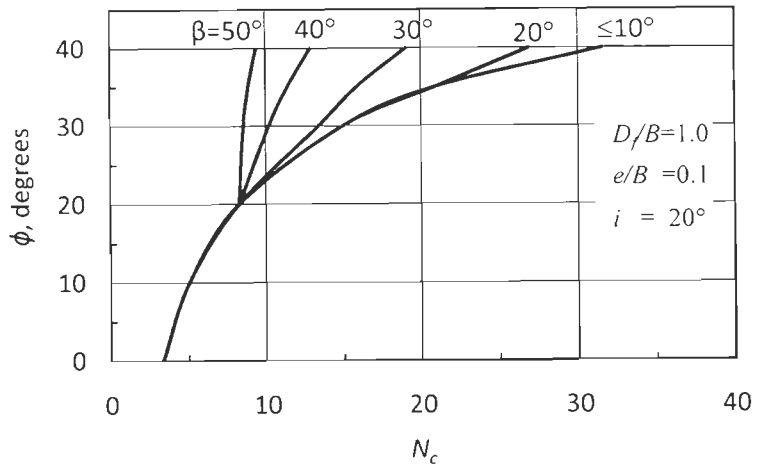

Fig. A.III. 6 b (i) N_c versus ϕ for D_e/B=0

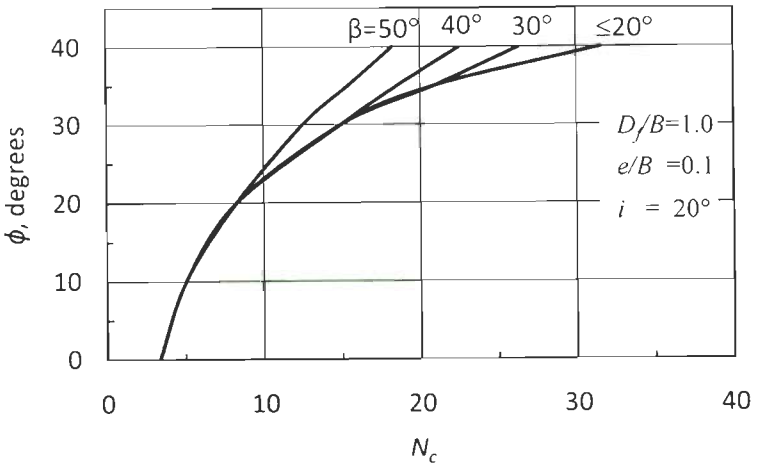

Fig. A.III. 6 b (ii) N_c versus ϕ for D_e/B=1.0

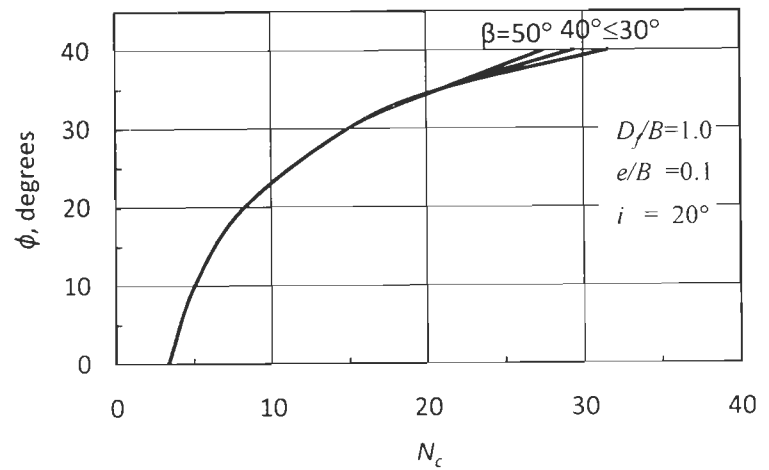

Fig. A.III. 6 b (iii) N_c versus ϕ for D_e/B=2.0

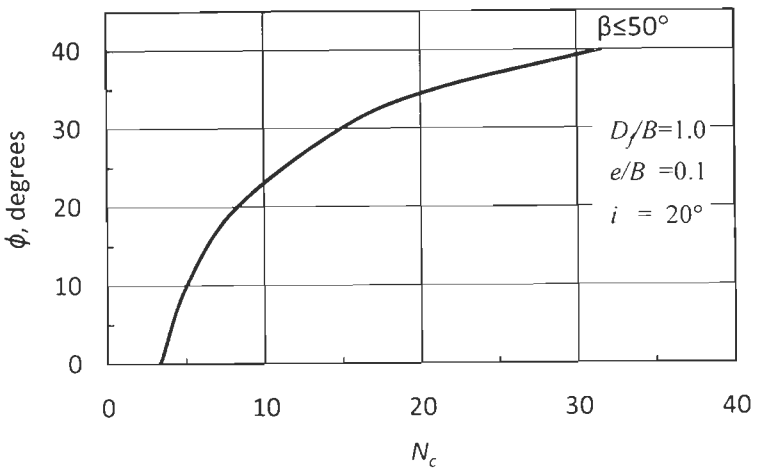

Fig. A.III. 6 b (iv) N_c versus ϕ for D_e/B=3.0

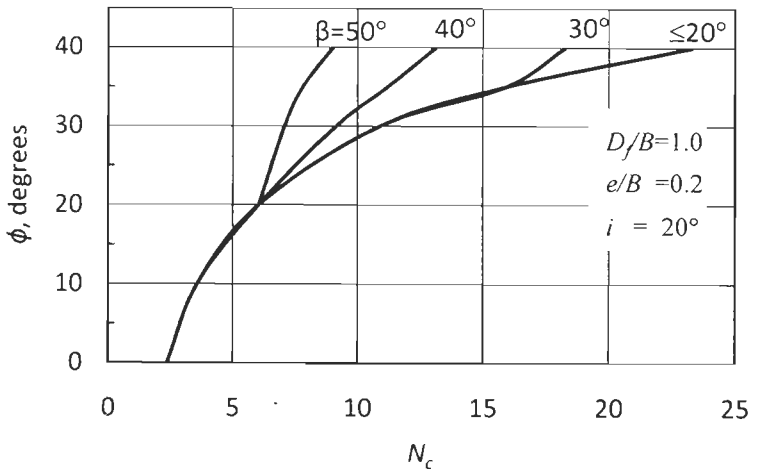

Fig. A.III. 6 c (i) N_c versus ϕ for D_e/B=0

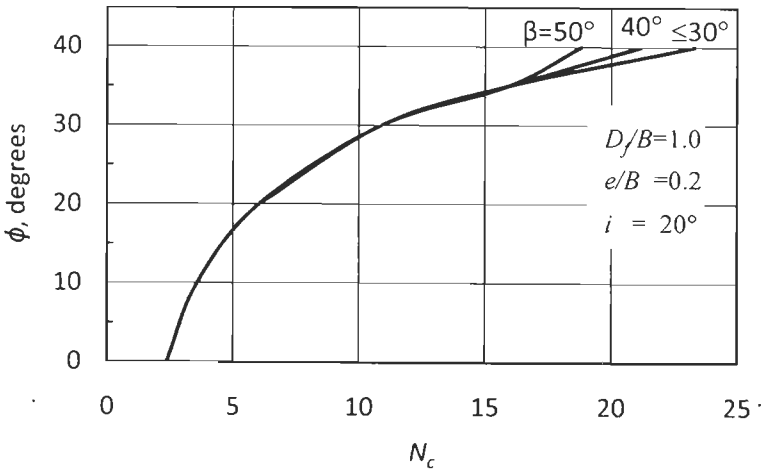

Fig. A.III. 6 c (ii) N_c versus ϕ for D_e/B=1.0

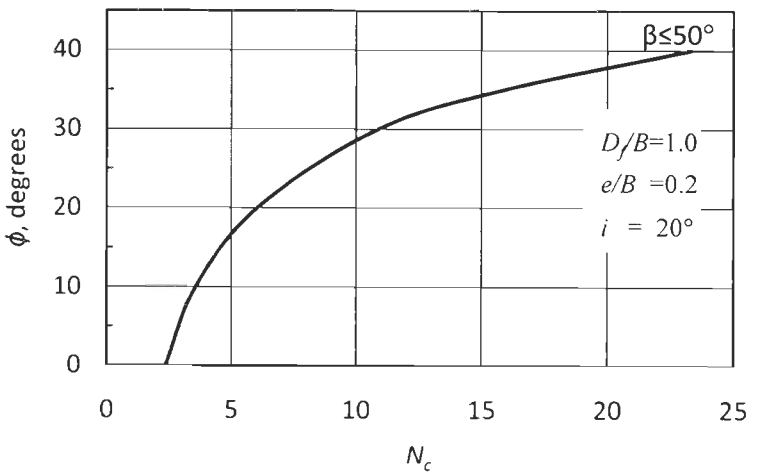

Fig. A.III. 6 c (iii) N_c versus ϕ for D_e/B=2.0

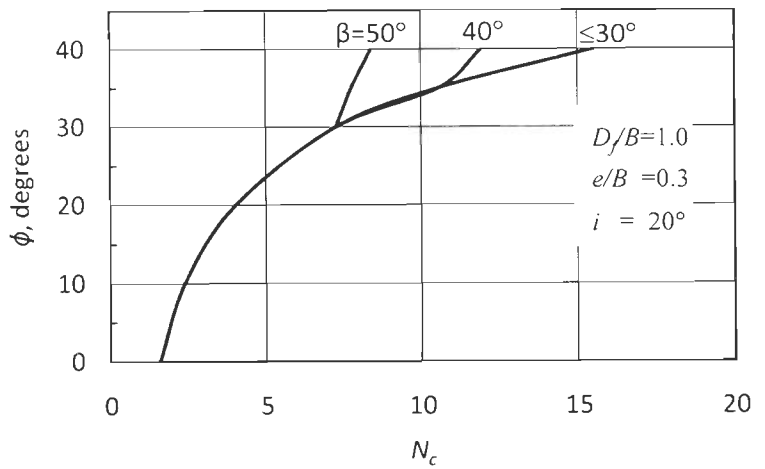

Fig. A.III. 6 d (i) N_c versus ϕ for D_e/B=0

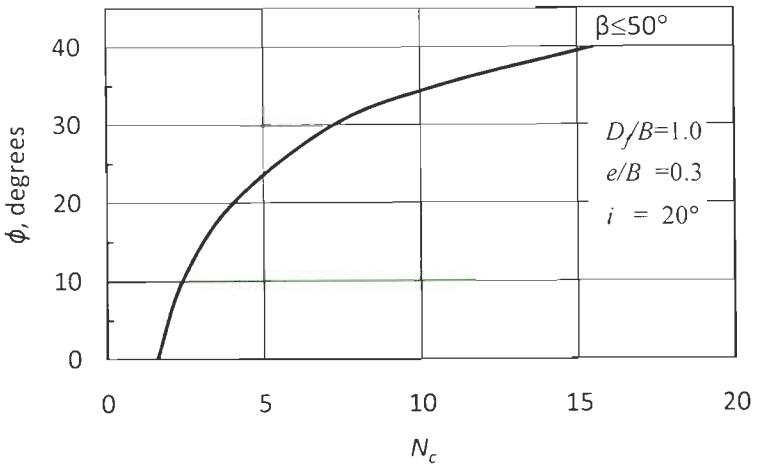

Fig. A.III. 6 d (ii) N_c versus ϕ for D_e/B=1.0